

QA: QA

**Civilian Radioactive Waste Management System  
Management & Operating Contractor**

**Near Field Environment Process Model Report**

**TDR-NBS-MD-000001 REV00 ICN 03**

**November 2000**

Prepared for:

U.S. Department of Energy  
Yucca Mountain Site Characterization Office  
P.O. Box 30307  
North Las Vegas, Nevada 89036-0307

Prepared by:

TRW Environmental Safety Systems Inc.  
1180 Town Center Drive  
Las Vegas, Nevada 89144

**INFORMATION COPY  
LAS VEGAS DOCUMENT CONTROL**

Under Contract Number  
DE-AC08-91RW00134

WM-11  
NBS07

Enclosure 1

#### **DISCLAIMER**

This report was prepared as an account of work sponsored by an agency of the United States Government. Neither the United States Government nor any agency thereof, nor any of their employees, nor any of their contractors, subcontractors or their employees, makes any warranty, express or implied, or assumes any legal liability or responsibility for the accuracy, completeness, or any third party's use or the results of such use of any information, apparatus, product, or process disclosed, or represents that its use would not infringe privately owned rights. Reference herein to any specific commercial product, process, or service by trade name, trademark, manufacturer, or otherwise, does not necessarily constitute or imply its endorsement, recommendation, or favoring by the United States Government or any agency thereof or its contractors or subcontractors. The views and opinions of authors expressed herein do not necessarily state or reflect those of the United States Government or any agency thereof.



**Civilian Radioactive Waste Management System  
Management & Operating Contractor**

**Near Field Environment Process Model Report**

**TDR-NBS-MD-000001 REV00 ICN 03**

**November 2000**

Prepared by:

Ralph A. Wagner  
R.A. Wagner

14 Nov 00  
Date

Checked by:

G.E. Barr  
G.E. Barr

14 Nov 2000  
Date

Approved by:

S.A. Orrell  
S.A. Orrell  
Responsible Manager, NFE PMR Department Manager

14 Nov 00  
Date

**Civilian Radioactive Waste Management System  
Management & Operating Contractor**

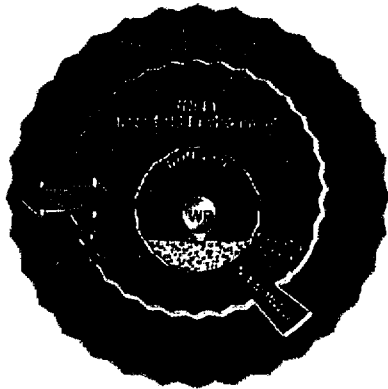
**Near Field Environment Process Model Report**

**TDR-NBS-MD-000001 REV00 ICN 03**

**November 2000**

**Editor:** D.G. Wilder

**Technical Editors:** J.A. Blink  
S.D. Crawford  
G.S. Siemering



**Authors:**

S.C. Blair	K. Lee
T.A. Buscheck	W. Lin
G. Carrigan	C.E. Palmer
N.D. Francis	E.L. Sonnenthal
P.C. Gaillard	Y. Tsang
M.T. Itamura	R.A. Wagner

**Reviewers:**

R.W. Andrews  
G.S. Bodvardsson  
J. Case  
J.D. Frey  
J.E. Gebhart  
G.T. Hanson  
J.E. Houseworth  
J.T. Kam  
J.L. King  
M.A. Lugo  
S.E. Saterlie  
M.L. Scott  
D. Stahl  
D.E. Watkins

**Production:**

J.E. Barboa  
S.A. Barnett  
S.E. Boelter  
M. Capobianco  
J.B. Cho  
M. Coatsworth  
K.K. Fong  
T. Gibson  
L.C. Grisham  
Y.L. Larkin  
H.H. Miller  
V.A. Obrad  
C.J. Passos  
C.A. Stewart  
T.J. Vogt

**Checking:**

G.E. Barr  
J.R. Beesley  
N.E. Biggar  
C.L. Lum  
G.H. Nieder-Westerman

**Illustrations:**

T.J. Carey  
R.J. Danat  
P.M. Harding

INTENTIONALLY LEFT BLANK

## CHANGE HISTORY

<u>Revision Number</u>	<u>Interim Change Number (ICN)</u>	<u>Description of Change</u>
00	00	Initial issue
00	01	ICN 01 incorporates DOE comments and editorial changes. Changes are designated by a change bar in the right margin.
00	02	ICN 02 incorporates DOE comments. Changes are designated by a change bar on the right margin. Changes from ICN 01 were accepted and change bars from ICN 01 were removed.
00	03	ICN 03 incorporates DOE comments. Changes are designated by a change bar on the right margin except where approximately two pages were deleted preceding the change bar that appears on the current page 2-30. Changes from ICN 02 were accepted and change bars from ICN 02 were removed.

INTENTIONALLY LEFT BLANK

## EXECUTIVE SUMMARY

Waste emplacement and activities associated with construction of a repository system potentially will change environmental conditions within the repository system. These environmental changes principally result from heat generated by the decay of the radioactive waste, which elevates temperatures within the repository system. Elevated temperatures affect distribution of water, increase kinetic rates of geochemical processes, and cause stresses to change in magnitude and orientation from the stresses resulting from the overlying rock and from underground construction activities. The recognition of this evolving environment has been reflected in activities, studies and discussions generally associated with what has been termed the Near-Field Environment (NFE).

The NFE interacts directly with waste packages and engineered barriers as well as potentially changing the fluid composition and flow conditions within the mountain. As such, the NFE defines the environment for assessing the performance of a potential Monitored Geologic Repository at Yucca Mountain, Nevada. The NFE evolves over time, and therefore is not amenable to direct characterization or measurement in the ambient system. Analysis or assessment of the NFE must rely upon projections based on tests and models that encompass the long-term processes of the evolution of this environment. This NFE Process Model Report (PMR) describes the analyses and modeling based on current understanding of the evolution of the near-field within the rock mass extending outward from the drift wall.

The NFE PMR is one of nine PMRs that address the technical basis supporting the Total System Performance Assessment. The PMRs are supported by Analysis Model Reports. The NFE PMR is supported by four Analysis Model Reports and one Calculation, which provide detailed descriptions of the various near-field models. The Analysis Model Reports summarize thermal test results, thermal-hydrological-chemical (THC) processes and their abstraction, and features, events and processes (FEPs) used in Total System Performance Assessment. The Calculation summarizes thermal-hydrological-mechanical (THM) processes. Direct inputs to Total System Performance Assessment from the NFE PMR include the near-field host rock water and gas composition and the percolation flux above the crown of the emplacement drift. These serve as inputs for the Total System Performance Assessment in-drift geochemical environment model and the Total System Performance Assessment seepage model. Inputs to Total System Performance Assessment also include the drift wall temperature and relative humidity. Repository heat driven variability of each performance driver listed above is inherently included since the supporting process models used to characterize the heat and fluid flow processes occurring in the near-field host rock include repository heating as a model input.

In addition to description of the process models and abstraction models, this PMR also addresses the *Evolution of the Near-Field Environment* Key Technical Issue, and the related Issue Resolution Status Report that the Nuclear Regulatory Commission considers important to repository performance. The PMR also addresses issues related to the NFE that have been identified by the Nuclear Waste Technical Review Board and by peer-review panels.

The NFE evolves as a result of the coupling of thermal, hydrological, chemical, and mechanical processes. This environment develops principally in response to heat generated by decay of the radioactive waste. The resulting elevated temperatures drive coupled processes that cause

changes in the environment to occur. The elevated temperatures affect distribution of water, increase kinetic reaction rates of geochemical processes (resulting in potential for changes in water and gas chemistry), and cause stresses to change in magnitude and orientation. Heat from the emplaced waste results in enhanced coupled thermal-hydrological-chemical processes in the near-field rock mass that may extend for time periods of up to 10,000 years (driftwall temperatures have decreased below  $\sim 50^{\circ}\text{C}$  by 10,000 years).

The major issues discussed in this PMR are: evolution of water and gas chemistry, thermally induced changes in hydrological conditions (such as saturation) that can influence seepage or percolation flux, changes in hydrological properties (such as fracture permeability) due to chemical processes, and changes in fracture hydrological properties due to mechanical responses.

The PMR discusses the coupling in terms of:

- *thermal-hydrological* responses (temperature regime evolution, moisture redistribution, relative humidities)
- THC responses (water chemistry, gas composition, mineralogy changes, and changes in hydrological properties, such as fracture-plugging potential), and
- THM responses, mainly in terms of changes in water flow patterns or hydrologic properties.

*Thermal-hydrological* models have been used to determine the hydrological responses of the system. The models consider three infiltration cases, and three climates provided by activities from the Unsaturated Zone Flow and Transport PMR. The current best estimate of average (over the potential repository footprint) net-infiltration is 4.6 mm/yr, which is projected to be the net-infiltration rate for the next 600 years. This is then projected to be followed for the next 1,400 years (until 2,000 years from present) by a warmer and wetter climate with net-infiltration of 12.2 mm/yr. For the next 8,000 years (the remainder of the 10,000 year compliance period), net-infiltration is estimated to be 17.8 mm/yr. These averages are as reported in the Unsaturated Zone Flow and Transport PMR; however, the models used to evaluate the near-field incorporated the detailed Unsaturated Zone Flow and Transport infiltration estimates for individual chimneys or cells evaluated in the model. This, therefore, considered the variations of infiltration over the footprint. As a result, the average infiltration values used in these models were higher than the overall footprint averages. The average of the infiltration values used were 6, 16, and 25 mm/yr, respectively.

The NFE models incorporate the repository layout of Enhanced Design Alternative II(EDA II), which has greater drift spacing and is expected to result in lower temperatures below those of previous designs upon which NFE calculations were based, including the DOE's 1998 Viability Assessment of the Yucca Mountain site. The results of the NFE model analyses indicate that temperature increases within the rock mass may extend 600 m laterally from the potential repository footprint, with estimated temperature increases of 30 to 35°C at the water table, and up to 5°C at the ground surface. The temperatures do not entirely return to ambient levels for 50,000 to 100,000 years.

With the assumed design options (Enhanced Design Alternative II and 50-year ventilation, currently under revision), boiling will occur around the drifts; and the region experiencing the boiling temperature (~96°C) will extend to a maximum diameter of about 24 meters with a zone of dryout that extends to 34 meters diameter. The above boiling temperature and dryout regions are not symmetrical around the drifts. The dryout zone extends about 17 meters into the pillars from the drift centerline and 10 and 22 meters above and below the drift centerline, respectively. Temperatures in the middle of the regions (pillars) between the waste emplacement drifts (tunnels) will increase to 80 to 85°C.

It should be noted that the Enhanced Design Alternative II design used in these analyses included backfilled drifts. The current design does not include backfill. This document (ICN 01) includes *thermal-hydrological* analyses of the no-backfill design, and THC and THM analyses are ongoing. These results will be included in Total System Performance Assessment modeling that supports the Site Recommendation.

Additionally, a three-dimensional mountain-scale *thermal-hydrological* model indicates that temperatures above boiling are primarily located near the repository horizon. Rock drying is also limited to regions around the repository horizon specifically in locations with low infiltration rates. The models indicate that condensate from mobilized waters should drain through the pillar regions, although they also indicate regions of increased saturation that extend from a region in the pillar at the repository elevation, to include the rock above the drifts in the higher infiltration case. Sufficient drainage of condensate is predicted by the Unsaturated Zone Flow and Transport PMR analyses such that matrix saturation above the drifts during the thermal period will not be greatly or persistently increased for most locations within the potential repository. The drainage capacity is due to the relatively high fracture permeabilities of the potential repository hydrogeological units. The multiscale thermohydrologic model used as the basis for Total System Performance Assessment abstraction of the emplacement drift thermodynamic environment and near-field host rock percolation flux also indicates significant condensate drainage during the early heating period. An analogous response for each of the analyses (Unsaturated Zone Flow and Transport PMR and NFE PMR) is expected since both process models apply the same hydrologic property sets, infiltration rate boundary conditions, and conceptual flow models used to determine the flow of water through the fractures and rock matrix.

The thermal test results to date are generally consistent with temperatures and saturations calculated by NFE models. The local and temporary differences observed are likely due to heterogeneity of the natural system which is not fully included in current models.

The THC models, which are consistent with observations in thermal tests, indicate that the chemistry of water in the NFE will have relatively neutral pH values, ranging from 7 to 9, and total chloride concentrations that increase to a maximum of about four times the concentrations in the ambient pore water. The pH of the water decreases during the period from closure until around 10,000 years, when the pH begins to slowly return to higher values. Most of the chemical constituents return to values that are similar to those prior to waste emplacement. This implies that there are no long-term perturbations in water chemistry, with the possible exception of bicarbonate ( $\text{HCO}_3^-$ ), and silica ( $\text{SiO}_2$ ). There is a significant decrease in carbon dioxide

(CO<sub>2</sub>) concentration in fractures during drying period. The models indicate an increase in CO<sub>2</sub> gas and carbonate concentrations around the drift during rewetting.

Changes to hydrologic properties were evaluated using the THC model, based on interaction of the constituents in the water with the rock, in response to temperatures. Specifically, the models were used to calculate dissolution and precipitation of minerals that would change the porosity and permeability of the fracture system. These analyses were done using revised estimates of fracture porosity (approximately 100 times the porosities used in past analyses) to assess the potential for changes to hydrologic properties. Given the current understanding of fracture porosities, the precipitation or dissolution of various chemical species or minerals was found to have negligible effects on fracture and matrix hydrological properties, for the 1% fracture porosity used as an initial condition.

Because of the complexity of THC coupling, there are differences in approaches or views regarding how to address this coupling. The Total System Performance Assessment –Viability Assessment peer review expressed concern about the basis for accepting the results as indicative of repository behavior. Further, analyses of CO<sub>2</sub> and water pH for the Drift Scale Test matched the data better when using a less complete suite of minerals. Possible reasons that the more complex model, which might be expected to more closely match the data, did not match the data as well include: uncertainties in rate parameters and thermodynamic properties, and the short duration of the test. Further, there is limited geochemical data for high ionic strength solutions at elevated temperatures. However, for the potential repository model, results have shown that higher ionic strengths are reached only when the liquid saturations are typically less than 1% and are therefore basically immobile and less important to fundamental changes in seepage chemistry and permeability modification.

The Yucca Mountain Site Characterization Project has changed the repository design to lower the temperatures, in an attempt to reduce some of the uncertainty caused by elevated temperatures. The concern regarding uncertainty is based, in part, upon the fact that increased temperatures increases the rates of chemical reactions and introduces additional complexity of vapor phase reactions and transport.

While some of the uncertainties may be reduced by lower temperatures, other uncertainties may not be reduced or may even be increased. The higher chemical reaction rates will lower kinetic barriers to reach equilibrium for all kinetically inhibited reactions. Although there may be increased uncertainty for kinetic rate parameters due to a lack of data, much of the data collected on kinetic rates was obtained in experiments that were necessarily at higher rather than lower temperatures (to shorten the time for reactions to be observed). Furthermore, because of the higher rates of reaction, the divergence of the system from equilibrium is smaller at higher temperatures and the length of time to reach equilibrium is smaller. There is much less uncertainty in assessing equilibrium chemical processes than kinetic processes. Even with the uncertainties noted, the THC models have matched the field data sufficiently that the models are considered appropriate for use in analyses of THC processes associated with the NFE.

The final topic of concern for the NFE is that of the geomechanical responses and how they couple to other processes within the NFE. Based on the calculated deformations, permeability increases of about 40 percent might be experienced above the drifts due to normal (widening or

narrowing) deformations of the fractures, and larger increases of 3 to 6.5 times preheat values due to shear (slip) displacements, during the peak of the thermal pulse. After 1,000 years, the permeability in the regions above the drifts is approximately twice the pre-emplacement value, due to normal deformations, and about an order of magnitude higher due to shear displacements.

Assessment of model confidence indicates that the models are appropriate for the analyses. The models have produced *thermal-hydrological* projections that compare well with the results of three field tests that have considerably varied geometry. The THC models used calculated trends of chemistry that were consistent with field tests, although the actual concentrations of constituents did not match field results as closely as did the temperature and saturation results of the *thermal-hydrological* models. In considering uncertainties with respect to field-test comparison, the greatest uncertainty was with the less mature THM model results. However, the THM responses are not currently linked as directly to performance as are the *thermal-hydrological* and THC models.

Based on these analyses, it is concluded that the model results are suitable for input to the site recommendation decision process and, further, that the models are appropriate for Total System Performance Assessment. Ongoing work to refine and test the models is expected to reduce uncertainty and increase confidence in performance assessment results.

INTENTIONALLY LEFT BLANK

# CONTENTS

	Page
ACRONYMS .....	xxvii
1. INTRODUCTION .....	1-1
1.1 BACKGROUND .....	1-1
1.2 DEFINITION OF NEAR-FIELD ENVIRONMENT .....	1-2
1.2.1 Definition of the Near-Field Environment .....	1-2
1.2.2 The Host-Rock Portions of the Near-Field Environment (this PMR) .....	1-3
1.2.3 The In-Drift Portions of the NFE as Covered in the EBS PMR .....	1-6
1.3 OBJECTIVE .....	1-6
1.4 SCOPE .....	1-6
1.4.1 Organization of this Process Model Report .....	1-7
1.4.2 Analysis Model Reports and Calculation Directly Supporting this Process Model Report .....	1-8
1.4.3 Near-Field Environment Issues and Processes .....	1-10
1.5 QUALITY ASSURANCE .....	1-12
1.6 RELATIONSHIP TO OTHER PROCESS MODEL REPORTS AND KEY PROJECT DOCUMENTS .....	1-13
1.6.1 Process Model Report Interfaces .....	1-15
1.6.1.1 Integrated Site Model Process Model Report .....	1-15
1.6.1.2 Unsaturated-Zone Flow and Transport Process Model Report .....	1-16
1.6.1.3 Engineered Barrier System Degradation, Flow and Transport Process Model Report .....	1-16
1.6.1.4 Disruptive Events Process Model Report .....	1-17
1.6.2 Process Model Report Inputs/Outputs .....	1-17
1.6.3 Relationship to the Repository Safety Strategy .....	1-19
1.7 REGULATORY FRAMEWORK .....	1-20
2. EVOLUTION OF THE NEAR-FIELD ENVIRONMENT PROCESS MODEL .....	2-1
2.1 THE NEAR-FIELD ENVIRONMENT PROCESS MODEL DEVELOPMENT PHILOSOPHY .....	2-6
2.2 PREVIOUS NEAR-FIELD MODELING .....	2-13
2.2.1 Thermal-Hydrological Models of Near-Field Processes .....	2-14
2.2.2 Past THC Modeling .....	2-18
2.2.3 Past THM Modeling .....	2-19
2.3 THERMAL HYDROLOGY AND COUPLED PROCESSES WORKSHOP SUMMARY .....	2-22
2.4 SUMMARY OF OTHER VIEWS AND ALTERNATIVE CONCEPTUAL MODELS .....	2-25
2.4.1 TH Alternative Models .....	2-26
2.4.2 TH/THC Alternative Models .....	2-28
2.4.3 THM Alternative Models .....	2-32
2.4.4 TSPA Peer Review Panel .....	2-32

## CONTENTS (Continued)

	Page
2.4.5 Expert Elicitation .....	2-33
2.4.6 Summary of Issues from Affected Organizations.....	2-33
2.5 FEATURES, EVENTS, AND PROCESSES .....	2-34
3. PROCESS MODELS, ABSTRACTIONS AND CONFIDENCE BUILDING .....	3-1
3.1 INTRODUCTION .....	3-1
3.1.1 Overview Description and Results of Models and Abstractions .....	3-1
3.1.2 Thermal Testing AMR.....	3-3
3.1.3 The THC Process AMR.....	3-4
3.1.4 The THC Abstraction AMR .....	3-5
3.1.5 Thermally Perturbed Percolation Flux in the Near-Field Host Rock .....	3-8
3.2 THERMAL-HYDROLOGICAL PROCESSES AND MODELS.....	3-12
3.2.1 Thermal-Hydrological (TH) Processes Affecting TH Behavior.....	3-12
3.2.1.1 The Thermal-Hydrological Near-Field State: General Observations.....	3-14
3.2.1.2 Key Factors Influencing Thermal-Hydrological Conditions in the NFE .....	3-18
3.2.2 Thermal-Hydrological Models .....	3-18
3.2.2.1 Multi-scale Thermohydrologic Model .....	3-19
3.2.2.2 Unsaturated-Zone Mountain-Scale TH Model.....	3-24
3.2.3 Thermal-Hydrological-Model Results .....	3-27
3.2.3.1 Multi-scale Thermohydrologic Model Calculations for the Site- Recommendation Design with No Backfill .....	3-28
3.2.3.2 Thermal-Hydrological Results for the EDA-II Design with Backfill.....	3-40
3.2.3.3 LDTH Calculations of Point and Line Loads .....	3-53
3.2.3.4 Comparison of Results from TH and THC Models .....	3-64
3.3 DRIFT-SCALE THERMAL-HYDROLOGICAL-CHEMICAL PROCESSES AND MODELS .....	3-76
3.3.1 Thermal-Hydrological-Chemical Conceptual Model .....	3-76
3.3.1.1 TH Processes .....	3-77
3.3.1.2 Effects of TH Processes (Boiling, Condensation, and Drainage) on Water and Gas Chemistry and Mineral Evolution .....	3-79
3.3.1.3 Effects of Infiltration and Climate Changes on THC Processes .....	3-80
3.3.1.4 Hydrologic Property Changes in Fractures and Matrix .....	3-81
3.3.2 Modeling Approach, Assumptions, Inputs and Outputs.....	3-81
3.3.2.1 Dual-Permeability Model for Reaction-Transport Processes .....	3-83
3.3.2.2 Active Fracture Model for Reaction-Transport Processes .....	3-83
3.3.2.3 Equilibrium and Kinetic Models for Mineral-Water-Gas Reactions.....	3-83
3.3.2.4 Initial and Infiltrating Water and Gas Chemistry and Mineralogy .....	3-84
3.3.2.5 Relations for Mineral Reactive Surface Areas.....	3-85
3.3.2.6 Relations for Hydrological Property Changes .....	3-85

## CONTENTS (Continued)

		Page
	3.3.2.7 Basis for Numerical Code TOUGHREACT V2.2.....	3-86
3.3.3	THC Process Model.....	3-87
	3.3.3.1 THC Process-Model Description.....	3-88
	3.3.3.2 TH Effects.....	3-88
	3.3.3.3 Gas-Phase CO <sub>2</sub> Evolution.....	3-88
	3.3.3.4 Water-Chemistry Evolution.....	3-90
	3.3.3.5 Porosity and Permeability Changes and Assessment of Precipitation "Cap" Formation.....	3-93
	3.3.3.6 Zeolite and Water Table Impacts.....	3-96
3.3.4	Uncertainties and Limitations.....	3-96
3.3.5	Summary and Conclusions.....	3-98
3.4	THC MODEL ABSTRACTION.....	3-99
	3.4.1 Inputs to the Abstraction.....	3-100
	3.4.2 Abstraction of THC Results.....	3-100
	3.4.2.1 Mean Infiltration Flux Case.....	3-101
	3.4.2.2 Low and High Infiltration-Flux Cases.....	3-104
3.5	THERMAL-HYDROLOGIC-MECHANICAL CALCULATIONS.....	3-106
	3.5.1 Approach to Coupling TM to TH Behavior.....	3-107
	3.5.2 Distinct-Element Calculation of TM Effect on Permeability – EDA-II Design.....	3-107
	3.5.2.1 Thermal Field.....	3-108
	3.5.2.2 Fracture Deformation.....	3-111
	3.5.2.3 Calculation of Permeability Change.....	3-112
	3.5.2.4 Results of Distinct-Element Calculation.....	3-113
	3.5.3 Summary of Thermal-mechanical Models.....	3-114
3.6	VALIDATION OF NFE MODELS FOR USE ON YUCCA MOUNTAIN.....	3-117
	3.6.1 Model Confidence Building through Field Thermal Testing.....	3-131
	3.6.1.1 Large-Block Test.....	3-133
	3.6.1.2 Single Heater Test.....	3-147
	3.6.1.3 Drift Scale Test.....	3-164
	3.6.2 Confidence Building through Use of Natural Analogs.....	3-195
	3.6.2.1 Thermohydrological Analogs.....	3-197
	3.6.2.2 THC Analogs.....	3-198
	3.6.3 Summary of Laboratory Tests.....	3-203
	3.6.3.1 Hydrological Properties.....	3-203
	3.6.3.2 Chemical and Transport Properties.....	3-203
	3.6.3.3 Laboratory-Scale TH Processes.....	3-203
	3.6.4 Summary of Model Validation and Confidence Building.....	3-208
	3.6.4.1 Validation of TH Models.....	3-208
	3.6.4.2 Validation of THC Models.....	3-217
	3.6.4.3 Validation of TM and THM Models.....	3-221
	3.6.4.4 Summary of Validation from Analog Studies.....	3-226

## CONTENTS (Continued)

	Page
4. RELATIONSHIP TO NRC ISSUE RESOLUTION STATUS REPORTS .....	4-1
4.1 SUMMARY OF THE KEY TECHNICAL ISSUES.....	4-1
4.2 RELATIONSHIP OF THE NEAR-FIELD ENVIRONMENT PMR TO THE KTIs .....	4-2
4.2.1 Evolution of the Near-Field Environment .....	4-4
4.2.1.1 ENFE IRSR Subissue 1 .....	4-4
4.2.1.2 ENFE IRSR Subissue 2 .....	4-5
4.2.1.3 ENFE IRSR Subissue 3 .....	4-5
4.2.1.4 ENFE IRSR Subissue 4 .....	4-6
4.2.2 Thermal Effects on Flow (TEF).....	4-6
4.2.2.1 TEF IRSR Subissue 1 .....	4-7
4.2.2.2 TEF IRSR Subissue 2 .....	4-7
4.2.3 Repository Design and Thermal-Mechanical Effects .....	4-7
4.2.4 Total System Performance Assessment and Integration (TSPAI).....	4-8
4.2.4.1 TSPAI IRSR Subissue 1 .....	4-8
4.2.4.2 TSPAI IRSR Subissue 2 .....	4-9
5. SUMMARY AND CONCLUSIONS .....	5-1
5.1 THE UZ FLOW AND TRANSPORT INPUTS AND THE NFE MODELS .....	5-1
5.2 THE REPOSITORY DESIGN INPUTS AND THE NFE PMR.....	5-1
5.3 THE EBS INPUTS AND THE NFE PMR.....	5-2
5.4 VALIDITY OF COUPLED PROCESS MODELS FOR THE NEAR-FIELD ENVIRONMENT .....	5-2
5.5 MODEL CONFIDENCE.....	5-10
5.6 CONCLUSION.....	5-14
6. REFERENCES .....	6-1
6.1 DOCUMENTS CITED.....	6-1
6.2 CODES, STANDARDS, REGULATIONS, AND PROCEDURES .....	6-18
6.3 SOURCE DATA, LISTED BY DATA TRACKING NUMBER .....	6-18
APPENDIX A - STATUS OF TH MODELS IMPLEMENTED BY THE NUFT COMPUTER CODE .....	A-1
APPENDIX B - ISSUES IDENTIFIED BY REVIEW GROUPS, AND PMR APPROACH FOR RESOLUTION.....	B-1
APPENDIX C - NEAR-FIELD ENVIRONMENT FEATURES, EVENTS, AND PROCESSES .....	C-1
APPENDIX D - ISSUE RESOLUTION STATUS REPORTS, SUBISSUES, TECHNICAL ACCEPTANCE CRITERIA, AND PMR APPROACH .....	D-1

## FIGURES

		<b>Page</b>
1-1.	Schematic Representation of the Near-Field Environment, Altered Zone, and Far-Field Environment, used in the Viability Assessment .....	1-4
1-2.	Schematic Representation (Not to Scale) of the Near-Field Environment.....	1-5
1-3.	Flow of Information through the Nominal Case Near-Field Environment Models .....	1-10
1-4.	Flow of Information through Site Recommendation Process and the Nominal Case Total System Performance Assessment Models.....	1-14
1-5.	Spatial Relationships of Processes and Interactions Among Three Process Model Reports .....	1-15
2-1.	Schematic View of the Potential Repository Layout, Drift Connections and Representative Waste Package Types within an Emplacement Drift.....	2-4
2-2.	Schematic Cross Section of an Emplacement Drift Containing a 21-PWR Waste Package, Showing Major Elements of the Engineered Design Alternative II Design for the Engineered Barrier System .....	2-5
2-3.	Schematic Representation of Thermal Hydrological Processes in an Unsaturated, Fractured Geological Medium .....	2-8
2-4.	Coupling Between Thermal, Hydrological, Chemical, and Mechanical Processes.....	2-10
3-1.	The Location-Dependent Data in the Different Infiltration Bins for the Low Glacial Infiltration Map .....	3-10
3-2.	The Location-Dependent Data in the Different Infiltration Bins for the Mean Glacial Infiltration Map.....	3-11
3-3.	The Location-Dependent Data in the Different Infiltration Bins for the High Glacial Infiltration Map .....	3-11
3-4.	DS Schematic Showing Decay-Heat-Driven TH Flow and Transport Processes Fracture Flow is Shown with Solid Arrows, Water Vapor Flow with Dashed Arrows, and Heat Flow with Oscillatory Arrows.....	3-16
3-5.	Mountain-Scale Schematic Showing Decay-Heat-Driven TH Flow and Transport Processes that Influence Moisture Redistribution and the Moisture Balance in the UZ.....	3-17
3-6.	The Submodels of the Multi-Scale Thermal Hydrologic Model.....	3-22
3-7.	Perimeter-Averaged Temperature on the Drift Wall for a 21-PWR WP for the Mean Infiltration-Flux Case for the Indicated Times.....	3-30
3-8.	Temperature 5 m above the Crown of the Drift in the Vicinity of a 21-PWR WP for the Mean Infiltration-Flux Case for the Indicated Times .....	3-32
3-9.	Temperature 7.39 m Laterally away from the Springline of the Drift in the Vicinity of a 21-PWR WP for the Mean Infiltration-Flux Case for the Indicated Times .....	3-33
3-10.	Temperature History at the Indicated Locations at (a) the Geographical Center of the Repository and (b) a Location 27.5 m from the Eastern Edge of the Repository .....	3-34

## FIGURES (Continued)

	Page
3-11. (a) The Complementary Cumulative Distribution Function (CCDF) for the Peak Temperature on Waste Packages and for the Peak Perimeter-Averaged Drift-Wall Temperature. (b) The CCDF of the Maximum Lateral Extent of the Boiling Point ( $T = 96^{\circ}\text{C}$ ).....	3-36
3-12. Perimeter-Averaged Drift-Wall Relative Humidity for a 21-PWR WP for the Mean Infiltration-Flux Case for the Indicated Times.....	3-37
3-13. Perimeter-Averaged Drift-Wall Liquid-Phase Matrix Saturation History (a) and Relative Humidity History (b) at the Geographical Center of the Repository and a Location 27.5 m from the Eastern Edge of the Repository.....	3-38
3-14. Evaporation Rate History in the Host Rock at the Crown of the Drift at the Geographical Center of the Repository and a Location 27.5 m from the Eastern Edge of the Repository.....	3-39
3-15. Capillary Pressure History in (a) the Fractures and in (b) the Matrix Averaged Around the Perimeter of the Drift Wall at the Geographical Center of the Repository and a Location 27.5 m from the Eastern Edge of the Repository.....	3-41
3-16. Liquid-Phase Flux 5 m and 3 m above the Crown of the Drift and in the Vicinity of a 21-PWR WP for the Mean Infiltration-Flux Case for the Indicated Times.....	3-42
3-17. Liquid-Phase Flux at the Upper Drift Wall in the Vicinity of a 21-PWR WP for the Mean Infiltration-Flux Case for the Indicated Times.....	3-44
3-18. Liquid-Phase Flux History at the Indicated Locations above the Drift at (a) the Geographical Center of the Repository and (b) a Location 27.5 m from the Edge of the Repository.....	3-45
3-19. Peak Temperature on the Lower Drift Wall (Below the Invert) for the Low, Mean, and High Infiltration-Flux Cases.....	3-46
3-20. Liquid-Phase Flux 5 m above the Crown of the Drift for the Mean Infiltration Flux Case for the Indicated Times.....	3-48
3-21. Liquid-Phase Flux 0.2 m above the Crown of the Drift for the Mean Infiltration-Flux Case for the Indicated Times.....	3-50
3-22. Liquid-Phase Flux History at Indicated Drift-Scale Locations for the Mean Infiltration Flux Case at (top) the Geographic Center of the Repository, and (bottom) a Location 27.5 m from the Eastern Edge of the Repository.....	3-52
3-23. Vertical Cross Section of the Emplacement Drift in the DDT and LDTH Model Showing the Thermal Radiation Connections Among the Surfaces in the Drift that are used in Thermal Simulations.....	3-56
3-24. Temperature and Liquid-Phase Saturation Distributions for <i>Point Loading</i> of 28 m-Spaced Drifts.....	3-60
3-25. Temperature and Liquid-Phase Saturation Distributions for <i>Line Loading</i> of 56.6 m-Spaced Drifts.....	3-62
3-26. Host-Rock Fracture Liquid Flux at the Emplacement-Drift Crown.....	3-71
3-27. Comparison of Drift Crown Temperatures Using the THC Model Multiscale TH Model.....	3-72

## FIGURES (Continued)

	Page
3-28. Temperature Distribution Calculated at 1,000 Years in a 2-D Mountain-Scale TH Model.....	3-73
3-29. Schematic Diagram of THC Processes Around a Potentially Heated Drift .....	3-78
3-30. Schematic Diagram Showing Relation Between TH Processes and THC Processes.....	3-80
3-31. Model Diagram Relating Inputs and Outputs for the THC Process Model (labeled THC) and THC Drift Scale Test Model (labeled THC DST).....	3-82
3-32. THC Process Model Mesh Showing Hydrogeologic Units in Proximity of the Drift.....	3-89
3-33. Contour Plot of Modeled Liquid Saturations in the Matrix at 600 Yr (Near Maximum Dryout) for Three Climate-Change Scenarios .....	3-90
3-34. Time Profiles of Modeled CO <sub>2</sub> Concentrations in the Gas Phase in Fractures at Three Drift Wall Locations for Different Climate-Change Scenarios ( <i>Less Complex Calcite-Silica-Gypsum System</i> ) .....	3-91
3-35. Time Profiles of Modeled Total Aqueous Chloride Concentrations in Fracture Water at Three Drift-Wall Locations for Different Climate-Change Scenarios ( <i>Complex Mineral Assemblage</i> ).....	3-92
3-36. Time Profiles of the Modeled pH of Fracture Water at Drift-Wall Locations for Different Climate-Change Scenarios ( <i>Less Complex System</i> ) .....	3-94
3-37. Time Profiles of Modeled Total Aqueous Carbonate Concentrations (as HCO <sub>3</sub> <sup>-</sup> ) in Fracture Water at Drift-Wall Locations for Different Climate-Change Scenarios ( <i>Less Complex System</i> ).....	3-95
3-38. Contour Plot of Calculated Total Fracture Porosity Change at 10,000 Yr for Three Climate-Change Scenarios ( <i>Less Complex</i> ) .....	3-97
3-39. Simulated Rock Mass for TM Coupled Effects Showing Three Sets of Fractures and Two Fracture Densities for Each Set .....	3-109
3-40. Schematic of Heater Layout for Simulation .....	3-110
3-41. Thermal Power History for Simulation .....	3-111
3-42. 55-year Estimate of Permeability Change Due to Normal Displacement.....	3-115
3-43. Permeability Multiplier Values Due to Shear Displacement at 55 Years .....	3-115
3-44. Permeability Multiplier Values Due to Normal Displacement at 1,000 Years .....	3-116
3-45. Permeability Multiplier Values Due to Shear Displacement at 1,000 Years .....	3-116
3-46. Hierarchy of Models .....	3-118
3-47. Hierarchy of NF Models and Relationship to Data Inputs and to TSPA .....	3-119
3-48. Photograph of Large Block Test Site .....	3-130
3-49. LBT Instrument Holes.....	3-136
3-50. Temperature Measured in Borehole TT1-14 of the LBT as a Function of Elapsed Time .....	3-137
3-51. Temperature Measured in Borehole TT2-14 of the LBT as a Function of Elapsed Time .....	3-137
3-52. Snapshots of the Temperature in NT3 of the LBT at the Location of each RTD Sensor in the Borehole.....	3-138

## FIGURES (Continued)

	Page
3-53. Snapshots of the Temperature in WT3 of the LBT at the Location of each RTD Sensor in the Borehole.....	3-138
3-54. Temperatures at Several RTDs in TT1 Show Fluctuations Due to a Thermal-Hydrological Event on June 13, 1997.....	3-139
3-55. Temperatures at Several RTDs in TT1 Show the Fluctuations Due to a Thermal-Hydrological Event on September 2, 1997.....	3-140
3-56. Temperature and the Electrical-Resistance Tomograph of an East-West Cross Section of the LBT .....	3-142
3-57. Difference Volume-Fraction Water in TN3 of the LBT as a Function of Depth, up to 103 Days of Heating .....	3-143
3-58. Difference Volume-Fraction Water in TN3 as a Function of Depth, from 103 to 565 Days of Heating.....	3-144
3-59. Thermal and Deformation History for the Large Block Test .....	3-145
3-60. Simulated Temperature Profile Along Borehole TT1 in the LBT Computed Using the DS and MS Rock Property Data Set, Compared to Measured Data .....	3-148
3-61. Statistical Measures for LBT Thermal Analyses.....	3-149
3-62. Simulated Versus Measured Temperature Histories for Sensors TT1-14 (Top) and TT1-19 (Bottom) in Borehole TT1 of the LBT. The DS Property Set was Used in the Simulation. ....	3-150
3-63. Liquid-Saturation Profile Along Borehole TN3 for the LBT. The DS Property Set was Used in the Simulation .....	3-151
3-64. Comparison of Liquid Saturation Along Borehole TN3 in the LBT for the DS and MS Rock Property Data Sets .....	3-152
3-65. Borehole Layout for the Single Heater Test.....	3-154
3-66. Displacement History for ESF-TMA-MPBX-2 (Corrected for Rod Thermal Expansion; Extension Positive).....	3-156
3-67. Pretest Predicted MPBX-2 Anchor-to-Ancor Displacement History Relative to the Borehole Collar .....	3-157
3-68. Synthesis of ERT and Neutron Logging Measurements of the Single Heater Test .....	3-158
3-69. Comparison of the DKM/TOUGH2 Simulation Using the Drift-Scale Property Set and the SHT Measured Temperatures at Thermocouple Location TMA-TC-4A-6 (73 cm below the heater center) .....	3-159
3-70. Comparison of the DKM/TOUGH2 Simulation Using the Drift-Scale Property Set and the SHT Measured Temperatures at Thermocouple Location TMA-TC-5A-7 (66 cm above the Heater Center).....	3-160
3-71. Comparison of the DKM/TOUGH2 Simulation Using the Drift-Scale Property Set and the SHT Temperatures Measured Radially Around Heater Mid-Length.....	3-160
3-72. Comparison of Three SHT DKM/TOUGH2 Simulations (Property Sets: DS, Median $k_b$ , and TSPA-VA) and Measured SHT Temperatures at Thermocouple Location TMA-TC-1A-7.....	3-161

## FIGURES (Continued)

		Page
3-73.	Comparison of Three SHT DKM/TOUGH2 Simulations (Property Sets: DS, Median $k_b$ , and TSPA-VA) and Measured SHT Temperatures at Thermocouple Location TMA-TC-5A-7 .....	3-161
3-74.	Statistical Measures for SHT Thermal Analyses.....	3-162
3-75.	Plan View of the DST.....	3-166
3-76.	Cross Section (A-A') Parallel to the Heated Drift in the DST .....	3-167
3-77.	Cross Section (B-B') Orthogonal to the Heated Drift in the DST.....	3-168
3-78.	Temperature at a Depth of 2 m from Collar of Holes #137 To 141 as a Function of Elapsed Time.....	3-171
3-79.	Temperature at a Depth of 2 m from Collar of Holes #158 to 162 of the DST as a Function of Elapsed Time.....	3-172
3-80.	Temperature at About 0.4 m from the HD Wall in All Vertical Temperature Holes of the DST, as a Function of Distance from the Bulkhead .....	3-174
3-81.	Temperature Snapshots along Hole #80 of the DST, as a Function of Distance from the Bulkhead .....	3-174
3-82.	Difference Volume-Fraction Water in Hole #50 of the DST, as a Function of Depth from Collar .....	3-175
3-83.	Comparison of Distributions of Measured and Simulated (NUFT) Water Saturation at 547 Days for the DST, Using the DS Property Set .....	3-176
3-84.	Tomogram Showing Saturation Change from Pre-Heat Ambient Values Derived from a Cross-Hole Radar Survey Taken in January of 1999 (~13 months of heating) in the Plane of DST Boreholes 64-68 .....	3-177
3-85.	Difference Volume-Fraction Water in Hole #67 of the DST, as a Function of Depth from Collar .....	3-178
3-86.	Difference Volume-Fraction Water in Hole #68 of the DST, as a Function of Depth from Collar .....	3-178
3-87.	Difference Volume-Fraction Water in Hole #80 of the DST, as a Function of Depth from Collar .....	3-179
3-88.	Measured (top) and DKM/TOUGH2 Simulated (bottom) DST Temperatures, as a Function of Distance of Sensor Locations from Borehole Collars in RTD Boreholes 137-144, after 18 Months of Heating .....	3-182
3-89.	DKM/TOUGH2 Simulated Temperatures along RTD Boreholes 137-144 after 18 Months of DST Heating.....	3-183
3-90.	Statistical Measures for DST DKM/TOUGH2 Thermal Analyses .....	3-184
3-91.	Measured (top) and DKM/TOUGH2 Simulated (bottom) DST Temperatures, as a Function of Time at Selected Sensor Locations in Borehole 160 (Horizontal, near the Wing Heaters).....	3-185
3-92.	Comparison of DKM/NUFT Simulated and Measured Temperatures from the DST, Along Borehole 137 (Vertical-Upward) at (a) 12 Months and (b) 18 Months .....	3-186

## FIGURES (Continued)

	Page
3-93. Comparison of DKM/NUFT Simulated and Measured Temperature Histories for Sensors No. 2, 5, 10, 40, and 67 Over 18 Months of Heating in Borehole 160 (Horizontal, near the Wing Heaters) for the DST, Using the DS Property Set .....	3-187
3-94. Statistical Measures for DST DKM/NUFT Thermal Analyses.....	3-188
3-95. TOUGH2 Simulated Matrix Liquid Saturation in the Plane of DST Boreholes 64-68 After 12 Months of Heating, Using the DS/AFM-UZ99 Properties.....	3-189
3-96. Fraction-Volume of Water Content in DST Boreholes as Measured by Neutron Logging Boreholes 64 to 68 for Nominal Heating Duration of 12 Months.....	3-190
3-97. Comparison of Modeled CO <sub>2</sub> Concentrations ( <i>Less Complex</i> ) in Fractures and Matrix Over Time to Measured Concentrations in Boreholes (a) Borehole Interval 74-3 at Nodes Above and Below (upper left); (b) Borehole Interval 75-3 (upper right); (c) Borehole Interval 76-3 (lower left); and (d) Borehole Interval 78-3 at Nodes Near Center and End (lower right). .....	3-193
3-98. Distribution of pH and Temperature at 12 Months (Fracture –13a, Matrix – 13b) and at 20 Months (Fracture – 13c, Matrix – 13d) .....	3-194
3-99. Yucca Mountain Mineralogy, an analog for potential Mineral Alteration.....	3-200
3-100. Volume of Silica Polymorphs Precipitated in Fracture as a Function of Volume Fraction for a 10 Percent Matrix Porosity .....	3-202
3-101. Permeability of a Single Fracture in a Core Sample of Topopah Spring Welded Tuff, Which Varied as a Function of Time and Exposure to Flowing Water .....	3-204
3-102. Difference X-Ray Radiography Images of 7.2 (Left) and 0.67 (Right) Hours after Flow was Initiated .....	3-205
3-103. Physical Model of Water Flow in an Unsaturated Fracture Consisting of Parallel Plates of Acrylic Plastic .....	3-206
3-104. Pentane Visualization (Left) and Temperature Distribution (Right) Showing a Heat Pipe.....	3-207
3-105. Comparison of DKM Simulated (NUFT) and Measured Temperature Histories for Sensor #10 in Borehole 160 (Horizontal, Near the Wing) for All Property Sets in the DST .....	3-214
3-106. Simulated CO <sub>2</sub> Volume-Fractions in Fractures and Matrix, After 6 and 20 Months of Heating, During the Drift-Scale Test ( <i>Less Complex</i> case) .....	3-220
3-107. Comparison of Two Simulations with Temperatures Measured During the Large Block Test. Increasing Fracture Permeability at 122 Days Causes Temperatures to Drop to Values Closer to Those Observed. ....	3-225
5-1. Interaction Matrix Showing Coupling of NFE Processes .....	5-4
5-2. Interaction Matrix Showing TH Coupling .....	5-5
5-3. Interaction Matrix Showing THC Coupling.....	5-7
5-4. Interaction Matrix Showing THM Coupling.....	5-9

## TABLES

		Page
1-1.	Near-Field Environment Analysis Model Report Identification .....	1-9
1-2.	Summary of Relationships Between the Near-Field Environment Process Model Report and Other Process Model Reports .....	1-17
1-3.	Factors Potentially Important to Postclosure Safety .....	1-20
3-1.	Uncertainty in Major AMRs used in the Near-Field Environment PMR .....	3-2
3-2.	Distribution of Process-Level Model Results within Infiltration Bins .....	3-12
3-3.	Summary of TH and T Model (or Submodel) Types, Including Those Used in the Multi-scale Thermal Hydrological Model .....	3-20
3-4.	List of NFE and EBS TH Parameters Calculated with the MSTHM for the TSPA-VA and for the TSPA-LADS .....	3-24
3-5.	List of NFE and EBS TH Variables Calculated with the MSTHM at 623 Repository Subdomains for Backfill-Runs of the TSPA-SR .....	3-25
3-6.	List of NFE and EBS TH Variables Calculated with the MSTHM at 610 Repository Subdomains for No Backfill-Runs Rev 00 of the TSPA-SR .....	3-26
3-7.	Major Hydrogeological Unit, Lithostratigraphic Unit, Detailed Hydrogeological Unit, and UZ Model Layer Nomenclatures .....	3-54
3-8.	TSw Pore Water Composition and CO <sub>2</sub> Partial Pressure .....	3-84
3-9.	Model Mineral Assemblage, Aqueous and Gaseous Species .....	3-87
3-10.	Comparison of Fracture Porosities Used in Analyses of Potential Fracture Plugging .....	3-99
3-11.	THC Abstraction for the Mean Infiltration Rate Case with Climate Change .....	3-102
3-12.	List of NFE Models, by Hierarchy, Showing Details Pertinent to Validation .....	3-120
3-13.	Thermal-Hydrological Property Sets Used in TH Models in the NFE PMR .....	3-127
3-14.	Test Strategy .....	3-129
3-15.	Borehole Numbers, Types, and Locations for the Single Heater Test .....	3-155
3-16.	Measured Concentrations in TSw Pore Water from Alcove 5 and Chemistry of Water Taken from Hydrology Boreholes .....	3-192
3-17.	Application of Geothermal Field Information as Analogs to Coupled Processes Anticipated at a Potential Yucca Mountain Repository .....	3-196
3-18.	Similarity of Analog Sites to Yucca Mountain .....	3-197
4-1.	Issue Resolution Status Report/Key Technical Issues Related to the NFE PMR .....	4-2
4-2.	PMRs Related to ENFE Issue Resolution Status Report/Key Technical Issue Subissues .....	4-3

INTENTIONALLY LEFT BLANK

## ACRONYMS

ACNW	Advisory Committee for Nuclear Waste
AFM	active fracture model
AML	areal mass loading
AMR	Analysis Model Report
AOD	Access/Observation Drift
AZ	Altered Zone
C	chemical
CD	Connecting Drift
CDTT	Cross Drift Thermal Test
CPM	Calibrated Properties Model
CSNF	commercial spent nuclear fuel
DDT	Discrete-heat-source, Drift-scale, Thermal-conduction
DE	Disruptive Events (PMR)
DFM	Discrete Fracture Model
DK	Dual-Permeability
DKM	Dual-Permeability Model
DOE	United States Department of Energy
DS	drift scale
DSCP	Drift-Scale Coupled Processes
DSNF	DOE-owned spent nuclear fuel
DST	Drift Scale Test
EBS DFT	Engineered Barrier System Degradation, Flow, and Transport Process Model Report
EBS	Engineered Barrier System
ECM	equivalent-continuum model
EDA	Enhanced Design Alternative
ENFE	Evolution of the Near-Field Environment
ERT	electrical-resistance tomography
ESF	Exploratory Studies Facility
FEPs	features, events, and processes
FMX	fracture-matrix interaction
GPR	ground-penetrating radar

## ACRONYMS (Continued)

H	hydrological
HD	Heater Drift
IRSR	Issue Resolution Status Reports
ISM	Integrated Site Model
KTI	Key Technical Issue
LA	License Application
LADS	License Application Design Selection
LBT	Large Block Test
LDTH	Line-averaged-heat-source Drift-scale Thermal-Hydrological
M	mechanical
MD	mean difference
MPBX	multiple-point borehole extensometers
MS	mountain scale
MSTHM	Multi-scale Thermohydrologic Model
NAMD	normalized-absolute-mean-difference
NF	Near-Field
NF/AZ	near field and altered zone
NFE	Near-Field Environment
NFER	Near-Field Environment Report
NFGE	near-field geochemical environment
NRC	Nuclear Regulatory Commission
NUFT	Nonisothermal Unsaturated-saturated Flow and Transport
NWPA	Nuclear Waste Policy Act
NWTRB	Nuclear Waste Technical Review Board
PA	Performance Assessment
PAO	Performance Assessment Operations
PAPR	Performance Assessment Peer Review Panel
PEBSFT	Prototype Engineered Barrier System Field Tests
PMR	Process Model Report
QARD	Quality Assurance Requirements and Description
RDTME	Repository Design and Thermal-Mechanical Effects
RH	relative humidity
RMSD	root-mean-squared difference
RN	radionuclide
RSS	Repository Safety Strategy
RTD	resistance temperature devices

## ACRONYMS (Continued)

SCP	Site Characterization Plan
SDT	smear-heat-source, Drift-scale, Thermal-conduction
SEAMIST	Science and Engineering Associates Membrane In-site Sampling Technology
SHT	Single Heater Test
SMT	Smear-heat-source, Mountain-scale, Thermal-conduction
SR	site recommendation
SRR	Site Recommendation Report
T	thermal or temperature
TC	thermal-chemical
THCM	thermal-hydrological-chemical-mechanical
TDMS	Technical Database Management System
TEF	Thermal Effects on Flow
TH	thermal-hydrological
THC	thermal-hydrological-chemical
THCP	thermal hydrology and coupled process
THM	thermal-hydrological-mechanical
TM	thermal-mechanical
Tpt	Topopah Spring Tuff
Tptpll	crystal-poor lower lithostratigraphic unit of the Topopah Spring Welded Tuff (TSW) hydrologic unit
TSPA	Total System Performance Assessment
TSPA-I	Total System Performance Assessment and Integration
TSPA-SR	Total System Performance Assessment for Site Recommendation
TSPA-VA	Total System Performance System Assessment - Viability Assessment
TSW	Topopah Spring Welded Tuff
TTTH	Thermal Tests Thermal-Hydrological
UZ F&T	Unsaturated-Zone Flow and Transport Model
UZ	Unsaturated Zone
VA	Viability Assessment
WF	Waste Form
WFD	Waste Form Degradation
WP	Waste Package
WPD	Waste Package Degradation
YM	Yucca Mountain
YMP	Yucca Mountain Site Characterization Project

INTENTIONALLY LEFT BLANK

## 1. INTRODUCTION

This Chapter presents the purpose of this report, its basic organization, and related issues. This section also provides a high-level summary of how the NFE Process Model Report (PMR) relates to technical topics presented in the other PMRs, and other key Yucca Mountain Site Characterization Project (YMP) documents.

### 1.1 BACKGROUND

The U.S. Department of Energy (DOE) is investigating the suitability of Yucca Mountain as a potential site for the nation's first high-level nuclear waste repository. If the site is found suitable, the goal is to seek a license to construct, subsequently to operate, and eventually close a high-level waste disposal facility. The determination of suitability relies on evaluations of performance of the repository engineered barrier system (EBS) and natural barrier characteristics of the site.

To evaluate or assess the postclosure performance of a potential repository at Yucca Mountain, a series of Total System Performance Assessments (TSPAs) are being conducted. A set of nine PMRs, of which this is one, is being developed to summarize the technical basis for each of the process models supporting the TSPA model for the Site Recommendation (SR). These reports cover the following topics:

- Integrated Site Model (ISM)
- Unsaturated-Zone Flow and Transport (UZ F&T)
- Near Field Environment (NFE, this PMR)
- EBS Degradation, Flow, and Transport
- Waste Package (WP) Degradation
- Waste Form (WF) Degradation
- Saturated-Zone Flow and Transport
- Biosphere
- Disruptive Events (DE).

These PMRs are supported by Analysis Model Reports (AMRs) that contain the more detailed technical information for input into each PMR and the TSPA. This technical information consists of data, analyses, models, software, and supporting documentation that will be used to describe the applicability of each process model for its intended purpose of evaluating the postclosure performance of the potential Yucca Mountain repository system. The PMR process will ensure the traceability of this information from its source through the AMRs, PMRs, and eventually to the uses of that information in the TSPA.

Favorable aspects of YM as a potential repository site include its isolated location, arid nature, and the sorptive properties of the rock materials. The arid environment results in unsaturated conditions at the potential emplacement horizon, the Topopah Spring Tuff (Tpt) of the Paintbrush Group. The major advantage of unsaturated conditions is minimization of water contact that can contribute to container corrosion, waste-form leaching, and radionuclide transport.

The emplacement of waste and the activities associated with construction of a repository system have the potential to change the environmental conditions within the repository system, specifically those that affect the WP and WF, and engineered barriers within the drifts. These environmental changes are principally a result of heat generated by decay of the radioactive waste that elevates temperatures within the repository system. The elevated temperatures affect distribution and chemistry of NF water, increase kinetic rates of geochemical processes, and cause stresses to change, in magnitude and orientation, from stresses resulting from the overlying rock and from underground construction activities. As described in the EBS PMR (CRWMS M&O 2000g), within the drifts themselves, thermally driven reactions of the altered NF water and the materials introduced into the drifts by construction can have strong influence on WP corrosion and WF degradation. Furthermore, ventilation associated with construction can cause significant drying of the rock immediately surrounding the drifts. Recognition of this evolving environment has been reflected in activities, studies and discussions generally associated with what has been termed the NFE.

The NFE evolves over time in response to construction and heat-producing waste, as well as changes in the natural environment (e.g. changed climates). Therefore, it is impossible to directly characterize the NFE by measurements, as that environment does not currently exist. Characterization of the NFE must rely on projections based on tests and models that encompass the long-term processes of the evolution of that environment. NFE characterization must rely on models that include detailed process evaluations as well as those that include simplifications and abstractions. The combination of detailed and abstracted-model assessments supports the site recommendation.

There have been modifications in design (as discussed in the Introduction to Chapter 2), operational concepts, and in development of the Repository Safety Strategy (CRWMS M&O 2000s; Sections 1.2 and 1.3). Earlier reports on the NFE which are based on earlier designs are useful, but may be limited by all of these factors. They are referenced for historical purposes, because they were part of the basis for many issues that are addressed in this PMR, and to provide corroborative evidence for the model analyses reported here.

## **1.2 DEFINITION OF NEAR-FIELD ENVIRONMENT**

This section reviews the definition of NFE and how this relates to this PMR.

### **1.2.1 Definition of the Near-Field Environment**

The Site Characterization Plan (DOE 1988, Volume III, Part A, Sections 7.1 and 7.4.1) associates the NFE with the WP Environment and with environmental-condition changes in the rock surrounding boreholes (borehole emplacement was the design being considered at that time). A distinction in definitions between near- and far-field environments was made based on whether analyses needed to consider specifics of the design (NF) or merely the overall mass loading of the waste (far-field) (DOE 1988, Volume VIII, Part B, Glossary, pp. G-38 and G-68). Subsequent to the Site Characterization Plan, design changes as well as changes in the organization of effort have evolved the definition.

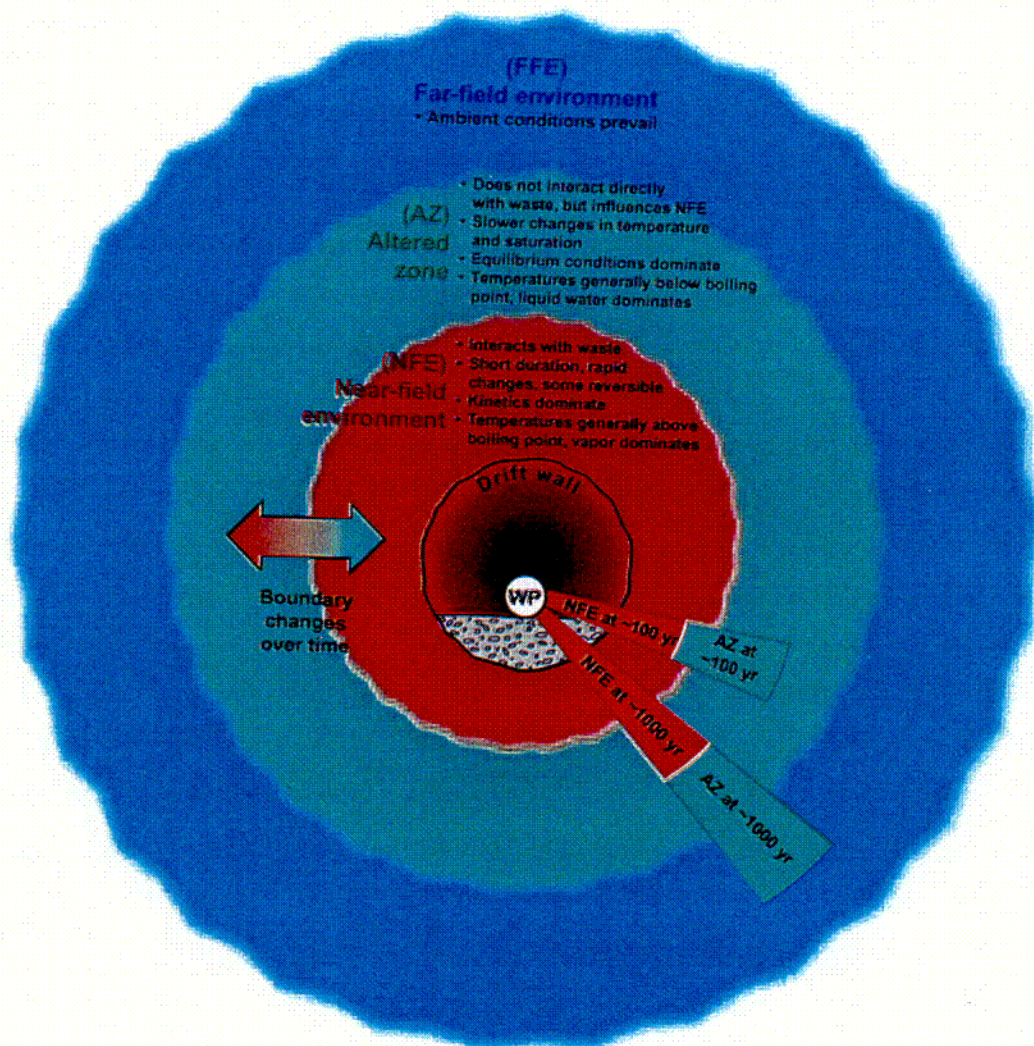
The NFE Report was identified in the *Waste Package Plan* (Harrison-Giesler et al. 1991) as the formal means for transmitting and documenting information regarding the NFE. As defined in the *Preliminary Near-Field Environment Report* (Wilder 1993), it included the in-drift environment that contacted the WPs and WFs, all of the materials within the drifts, and the environment that developed within the rock mass and extended into the rock mass a distance that depended on the physical process being considered. The extent of the NFE, for some processes, was as large as tens of meters (e.g., saturation changes in response to heat) or limited to a few centimeters into the rock (e.g., radiation effects). Furthermore, the extent of the NFE for any given process was a function of time and depended very strongly on repository design and operational parameters. Thus, the NFE was defined based upon impacts or changes in the environmental parameters that were significant to performance of the repository system. The issues related to the NFE were reported to be more of processes and how they related to various designs than of the more typical environmental descriptions associated with site characterization.

Subsequent to the *Preliminary Near-Field Environment Report*, and within the Viability Assessment (VA), the NF has been described as being limited to the environment within the drifts and the region of rock in close proximity to the drifts where the temperatures exceed boiling. The evolving environment within the surrounding rock mass was described as the Altered Zone (AZ) (Wilder 1997, Figure 1-2), and the rock beyond the AZ with only small heat-driven changes was termed the Far-Field. Potential far-field thermal effects include chemical reaction zones in the heated part of the saturated zone, and in the capillary fringe area just above the water table, and a convection cell in the heated part of the saturated zone. These effects for the EDA-II design, are expected to be both temporary and small in magnitude. Rock-water interactions are quite efficient at temperatures just below boiling (and are far more efficient at any temperature above the ambient). This report does not address these issues. For high thermal load repository designs, the AZ may extend throughout the unsaturated zone (UZ) above and below the repository horizon (Hardin 1998, p. 1-1). Figure 1-1 depicts the time-dependent locations of these regions, as defined at the time of the Viability Assessment (VA).

### **1.2.2 The Host-Rock Portions of the Near-Field Environment (this PMR)**

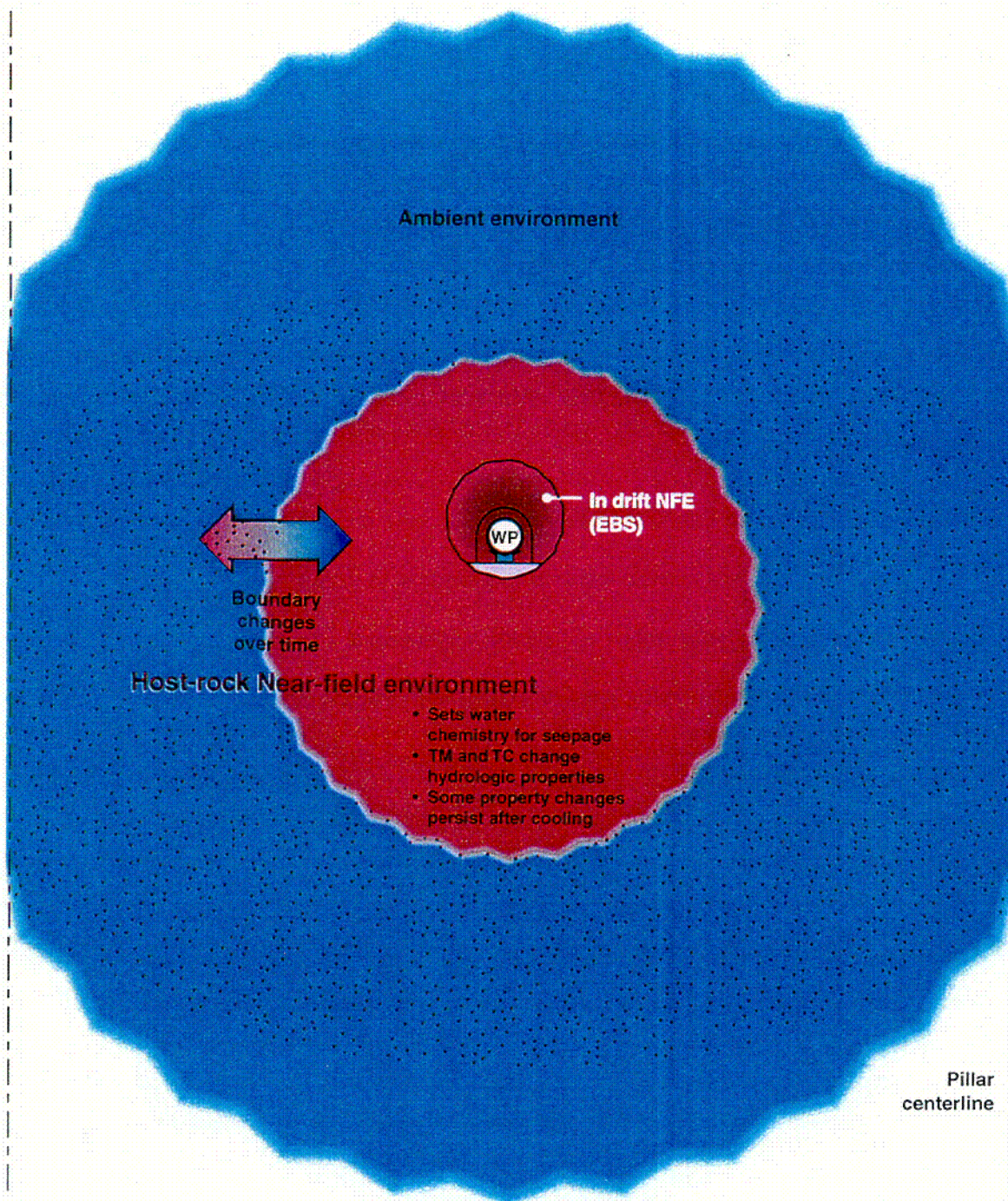
The definition of the NFE continues to include the in-drift environment and immediately surrounding host rock. However, the increased emphasis on engineered barriers created a need to consolidate discussions related directly to the EBS into a separate PMR. Thus, this PMR describes models used to evaluate the rock part of the NFE, while the Engineered Barrier System Degradation, Flow, and Transport (EBS DFT) PMR (CRWMS M&O 2000g) describes models used to evaluate the in-drift part of the NFE. In this PMR, the term "NFE" refers to the environment that develops within the rock extending from the drift walls, outward to a distance where heat or excavation-driven changes in the properties or processes within the rock affect performance assessment parameters, such as water flow paths and water chemistry. Figure 1-2 depicts the part of the NFE described in this PMR. As can be observed by comparing Figures 1-1 and 1-2, the overall region of perturbation is similar (design and operational modifications result in a somewhat smaller region of perturbation, ignoring heterogeneity). The differences relate to which PMR discusses the various portions of the NFE. As noted, a distinction is no longer made between NF and AZ in this PMR. The NFE as described in this PMR subsumes what had been separately identified as the AZ. This description of the NFE reflects the current organization of effort within the YMP.

The basic characteristic of the NFE is that it is an environment that evolves within the rock mass due to coupled processes involving heat transfer, fluid mobilization and phase changes, chemical interactions, and mechanical deformations and stresses. It is thus characterized by coupled processes, that is coupling between thermal, hydrological, geochemical and geomechanical processes. This coupling is sometimes binary, but can involve all four processes and can include feedback. For example, heat from the waste (thermal process) can mobilize water (hydrological process), which can dissolve and precipitate minerals (geochemical processes), which can affect flow paths (hydrological process). This is referred to as coupled thermal-hydrological-chemical (THC) processes.



Source: Wilder 1997, Figure 1-2

Figure 1-1. Schematic Representation of the Near-Field Environment, Altered Zone, and Far-Field Environment, used in the Viability Assessment



NOTE: The red portions represent regions of extensive dryout. The stippled portions represent regions of significantly increased temperatures and decreased saturation. The Host-Rock portions of the NFE (red and stippled) are those reported in this Process Model Report.

Figure 1-2. Schematic Representation (Not to Scale) of the Near-Field Environment

C-2

### **1.2.3 The In-Drift Portions of the NFE as Covered in the EBS PMR**

As noted, the EBS PMR discusses the portion of the NFE that resides within the drifts. Therefore, issues related to evolution of water and gas chemistry within the drift that interacts with the waste packages and with the waste form are covered within that PMR. Further, issues of water distribution within the drift, of relative humidity and temperature distributions within the drift, and the interactions with introduced materials are all within the scope of the EBS PMR. As a result, much of the discussion of engineering design options on the NFE (such as backfill options) are within the scope of the EBS PMR.

### **1.3 OBJECTIVE**

The overall objective of the NFE PMR is to synthesize the necessary and sufficient technical information that the YMP will rely upon to make its site suitability evaluation and licensing arguments pertaining to the NFE.

The detailed objectives of the NFE PMR are to

- 1) Describe and summarize processes important to performance in the NFE
- 2) Describe the models that simulate these processes
- 3) Summarize the technical bases for these NF process models
- 4) Abstract the detailed NF process models for use by TSPA
- 5) Evaluate uncertainties inherent in the NFE modeling results
- 6) Address resolution of the U.S. Nuclear Regulatory Commission's (NRC's) ENFE Key Technical Issue (KTI) and related Issue Resolution Status Reports (IRSRs).
- 7) Provide results of NFE analyses to other PMRs, particularly EBS and UZ PMRs. Information provided includes, but is not limited to, changes in porosity and permeability, evolved water chemistry and mineralogy, thermal mobilization of water, and geomechanical condition changes (see Figure 1-5).

In addition, because discussion of the NFE is not contained within a single PMR, there is a need to provide continuity with past reports or documents such as the NRC's ENFE IRSR (NRC 1999a). Thus, one of the functions of this PMR is to provide a mapping function between the current documents that discuss NF processes and past documents (see Chapter 4).

This PMR supports key YMP milestone documents, including the Site Recommendation Consideration Report (SRCR), Site Recommendation Report (SRR), and the LA.

### **1.4 SCOPE**

The major issues regarding the NFE in this PMR are thermally-driven changes in the rock-mass hydrological properties that determine flow of fluids in the rock, and mineral changes or salt

depositions that potentially impact water chemistry. The hydrologic properties can be affected by both THC and THM processes.

This PMR summarizes:

- The coupled thermal-hydrological-chemical (THC) processes and the coupled thermal-hydrological-mechanical (THM) processes that occur within the NF
- The technical bases for evaluations made to identify the features, events, and processes (FEPs) associated with the NF and that might affect performance of the geologic repository
- The use of analysis and modeling results developed in the AMRs to support the TSPA
- The thermal-hydrological (TH) model evaluation and validation (model confidence assessment) activities associated with thermal testing in the Exploratory Studies Facility (ESF)
- Issues related to changes in properties and water chemistry within the rock mass due to excavation or heat.
- Issues associated with the NFE that are not discussed in detail in the NFE PMR but are discussed in other PMRs.

Because of the coupling of processes, the discussion of the processes models used to evaluate the NFE must be in the context of the coupled processes. The forward-and-back coupling of processes makes the NFE an environment typified by interrelated interactions. There are multiple and complex ways in which coupling between processes can occur. The approach often used is to analyze only partially or singly coupled processes, then determine these responses before adding the other coupling. The scope of this PMR includes discussion of the TH, THC and THM coupled processes separately, synthesizes the NF THCM behavior from consideration of the TH, THC, and THM separate results.

The scope of this PMR is limited to considerations of coupling that impact seepage into drifts, water chemistry, mineralogy and rock-property changes, as well as geomechanical responses based on ambient-property inputs from the Unsaturated-Zone Flow and Transport Model (UZ F&T) PMR. Ongoing work will incorporate additional complexity in coupling as well as potential changes in water chemistry and flow returned to the NF from the drifts. THMC processes in the NFE may also influence the stability of the rock surrounding the emplacement drifts, especially in the region within 1 drift diameter of the drift walls. A thermal-mechanical analysis of drift stability is presented in the EBS PMR (CRWMS M&O 2000g).

#### **1.4.1 Organization of this Process Model Report**

This report is divided into five chapters.

Chapter 1 defines the NFE and relationships between this PMR and other PMRs and regulatory documents.

Chapter 2 provides a perspective against which the NFE PMR was developed. The section provides a general description of the background, evolution of the conceptual approach, past modeling efforts, the objectives and outcome of a performance assessment NFE workshop, and a discussion of the NFE FEP.

Chapter 3 describes the process-level models, model abstractions, and supporting analyses that address the NFE processes. Discussions include the relationships among the process-level models, model abstractions, data, and supporting analyses. Chapter 3 also describes activities that relate to model confidence building or validation, including discussion of applicable natural analogs.

Chapter 4 describes the relationship with the NRC IRSRs and how acceptance criteria in the IRSRs relevant to the NFE PMR have been addressed.

Chapter 5 summarizes the conclusions of this PMR.

#### **1.4.2 Analysis Model Reports and Calculation Directly Supporting this Process Model Report**

This PMR summarizes the detailed analyses of constituent submodels from the following four AMRs and one calculation:

AMR N0080: *Features, Events, and Processes in Thermal Hydrology and Coupled Processes* (CRWMS M&O 2000e) identifies and examines the effects of features, processes, and events that are related to the NFE on repository performance and provides the technical basis for evaluation of those FEPs. This AMR is referred to as the *NFE FEPs AMR* throughout this PMR.

AMR N0000: *Thermal Tests Thermal-Hydrological Analysis/Model Report* (CRWMS M&O 2000a) has a primary purpose that relates to building confidence in the models that describe thermal-hydrological (TH) processes in the potential repository system. The AMR tests the various property sets proposed for use in design and TSPA to characterize the potential repository geologic setting. The AMR compares measurements from field tests to calculated temperatures and saturations using these property sets. The evaluation of the TH property sets inherently involves the evaluation of the coupled TH processes that are both numerically-simulated and field-measured. This AMR is referred to as the *Thermal Test AMR* throughout this PMR.

AMR N0120: *Drift-Scale Coupled Processes (DST and THC Seepage) Models Report* (CRWMS M&O 2000b) discusses coupled THC processes. This AMR supports both this PMR and the UZ F&T PMR (and thus carries a second designation, U0110). The AMR focuses on the impact of coupled processes on fracture and rock hydrological-property changes, and on mineral-water-gas reactions that drive changes to water and gas compositions that may enter the potential drifts. This AMR is referred to as the *THC Process AMR* throughout this PMR.

AMR N0125: *Abstraction of Drift-Scale Coupled Processes* (CRWMS M&O 2000c) provides the technical basis for the TSPA abstraction of THC processes. It abstracts water and gas compositions in the rock and fractures outside of the drifts from the *THC Process AMR* for use in

TSPA. It also compares the TH results for process-level and abstracted TH and THC models. This AMR is referred to as the *THC Abstraction AMR* throughout this PMR.

Calculation N0C30: *Calculation of Permeability Change due to Coupled Thermal-Hydrological-Mechanical Effects* (CRWMS M&O 2000d) discusses mechanical responses to the thermal pulse and the effects of consequent fracture closure or opening on the hydrological properties of the rock mass. This calculation is referred to as the *THM Calculation* throughout this PMR.

Table 1-1 lists the reports that directly support the NFE PMR.

Table 1-1. Near-Field Environment Analysis Model Report Identification

AMR Title	ID Number	Abbreviated Designator	DI Number and Reference	PMR Section
<i>Features, Events, and Processes in Thermal Hydrology and Coupled Processes</i>	N0080	<i>NFE FEPs AMR</i>	ANL-NBS-MD-000004 CRWMS M&O 2000e	2.5
<i>Thermal Tests Thermal-Hydrological Analysis/Model Report</i>	N0000	<i>Thermal Test AMR</i>	ANL-NBS-TH-000001 CRWMS M&O 2000a	3.2, 3.6
<i>Drift-Scale Coupled Processes (DST and THC Seepage) Models</i>	N0120	<i>THC Process AMR</i>	MDL-NBS-HS-000001 CRWMS M&O 2000b	3.3
<i>Abstraction of Drift-Scale Coupled Processes</i>	N0125	<i>THC Abstraction AMR</i>	ANL-NBS-HS-000029 CRWMS M&O 2000c	3.4
<i>Draft Calculation of Permeability Change due to Coupled Thermal-Hydrological-Mechanical Effects</i>	N0C30	<i>THM Calculation</i>	CAL-NBS-MD-000002 CRWMS M&O 2000d	3.5

In addition to summarizing the above documents, Section 3.6 of this PMR summarizes other pertinent YMP work, including results from laboratory and field thermal tests that were not discussed in the limited scope of the *Thermal Test AMR*. Laboratory tests deal with relatively simple processes and one medium at a time. For example, a laboratory test may study fracture healing in a rock sample with one single fracture. Therefore data from laboratory tests can only be used to build confidence on certain processes of a complex model that is used to predict the behaviors of the rock mass in a potential repository. Laboratory tests are summarized in Section 3.6.3.

The following submodels are described in the indicated sections of this PMR and associated AMRs:

- TH Sections 2.2.1, 3.2, 3.6.1, and 3.6.4.1;  
The *THC Abstraction AMR* (CRWMS M&O 2000c) and the *Multiscale Thermohydrologic Model* (CRWMS M&O 2000k) which supports the EBS PMR

- **THC** Sections 2.2.2, 3.3, 3.4 and 3.6.4.2;  
The *THC Process AMR* (CRWMS M&O 2000b) and the *THC Abstraction AMR* (CRWMS M&O 2000c)
- **THM** Sections 2.2.3, 3.5, and 3.6.4.3;  
The *THM Calculation* (CRWMS M&O 2000d)

Figure 1-3 shows the flow of information through the NFE submodels. Models are shown in bold rectangles, circled boxes are inputs, hexagonal boxes are output, and information categories label the flow-arrows. The TH submodel is shared by the NFE and EBS models, with the rock temperatures (T) and saturations being used by the NFE model and the in-drift temperatures and relative humidities (RH) being used by the EBS model.

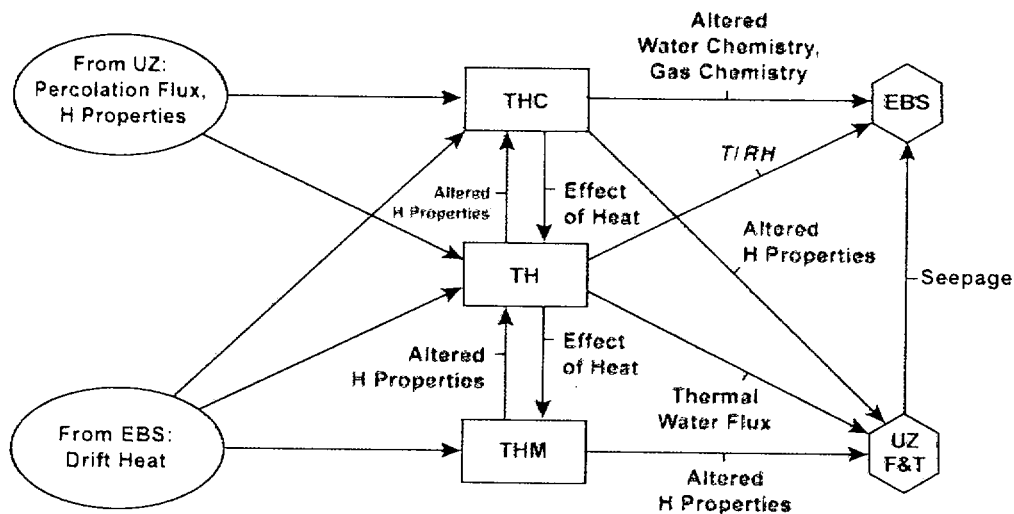


Figure 1-3. Flow of Information through the Nominal Case Near-Field Environment Models

### 1.4.3 Near-Field Environment Issues and Processes

The issues dealt with specifically in the PMR are:

- Evolution of the NFE and how that evolution relates to the amount of water that can enter the drifts or potentially leave the drifts. This specifically includes an evaluation of changes to the porosity and permeability of the zone of rock surrounding the drifts and extends outward until there are no significant changes in those parameters. The changes may result from geochemical interactions between the rock and fluids that are a result of the elevated temperatures. They may also result from geomechanical processes related to excavation or elevated temperatures.
- The impacts on NF water chemistry that may result from changes in mineralogy, dissolution and precipitation of minerals, vaporization and condensation of water in the matrix and fractures, and changes in gas chemistry.

- Strongly coupled effects in which one process has a major impact on another process. Much of the coupling is the consequence of the thermal output from the waste and resulting temperature distribution. Therefore, the NFE is affected directly by the repository system design and operation, particularly the repository layout (thermal loading) and the preclosure ventilation. In this PMR, the analyses consider the Enhanced Design Alternative (EDA) II design (see the Introduction to Chapter 2). This design includes titanium drip shields, no concrete drift liners, and backfill between the drip shield and drift walls. EDA II uses line-loading (close spacing of WPs) in widely spaced drifts. These design characteristics contribute to the spatial and temporal thermal regime that develops within the NFE.

During development of this PMR, decisions have been made by YMP management to eliminate backfill from the design and to alter the orientation of the drifts. These modifications to the design have not been completely incorporated into the AMRs and PMR at this point.

From a thermal perspective, backfill insulates the heat source (waste packages) from the NF heat sink; the consequence of a backfilled design (after a short period during which the backfill temperature equilibrates) is higher waste package temperatures with little overall change in NF rock temperatures. Depending on the backfill geometry and hydrological properties, there can be differences in distribution of temperature and saturation around the periphery of the drift for backfilled versus non-backfilled designs.

Drift orientation (with respect to the orientation of major fracture sets) can change shear stresses at rock contact points and the size of key blocks for rock fall. The models described in this PMR are applicable to the initial SR design (backfill drifts oriented as in the viability assessment) and to the evolving SR design (no backfill and drifts oriented to reduce rock fall loads on the drip shield). TH analyses for the no-backfill option is described in this PMR.

This PMR is focused on processes that occur during the period of time when the thermal processes are active, and on the effects that may extend beyond the thermal period. Changes that occur either outside the region or time frame thus described are included in other PMRs; for example, climate change is included in the UZ F&T PMR (CRWMS M&O 2000f). Those changes in the environment that occur within the thermal period, but are long lasting or permanent, are identified in the NFE PMR. However, impacts on performance beyond the approximately 10,000 years limit for thermal processes are also considered in the UZ F&T PMR (see Section 3.12 of that document); these impacts are primarily related to seepage and transport.

To provide continuity with past reports or documents such as the NRC's ENFE IRSR (NRC 1999a), issues that have been identified in the past as associated with the NFE are identified here, with references to the appropriate PMR. This PMR also discusses model validation or confidence building for models that support the NFE (see Section 3.6.4). This is critical because it is impossible, during the evaluation and licensing process, to directly measure the NFE environment that will develop over long periods of time. Therefore, evaluations of the NFE evolution, by necessity, will involve use of complex predictive models that are based on detailed mechanistic models of the processes involved in that evolution. Confidence that the predictive models are appropriate is established by comparison of the model results to a series of accelerated field and laboratory tests. This PMR reports results of the underground (in situ)

Single Heater Test (SHT) and Drift Scale Test (DST) performed as part of the ESF studies, as well as results of the Large Block Test (LBT) located on the surface near Yucca Mountain (see Section 3.6.1). The results of laboratory tests are discussed in Section 3.6.3. This PMR focuses on the thermal-hydrological aspects of the DST. Analyses and calculations are ongoing to investigate the fully coupled thermal-hydrological-chemical-mechanical (THCM) processes in the test, including processes that are expected to occur in the cool-down phase. The cool-down phase of the test has not yet begun and confidence building will, therefore, not be fully addressed for several years. In spite of the uncertainties and also the incomplete testing of the models, as discussed in Section 3.6, there has been good agreement between model predictions of the coupled process responses (particularly for the critical processes of TH and THC) for the field tests with the actual responses monitored.

Additional testing of model appropriateness can also be achieved through evaluations of comparable natural analogs. This PMR contains information regarding use of natural analogs to gain insight into coupled NF processes (see Section 3.6.2). Expert judgment and technical reviews have also been used to further assist in determining appropriateness of the models (see Sections 2.3 and 2.4). This information was obtained formally through use of Expert Elicitation and Technical Peer Review.

## 1.5 QUALITY ASSURANCE

The activities documented in this technical report were evaluated in accordance with procedure QAP-2-0, *Conduct of Activities*, and determined to be subject to the requirements of the Quality Assurance Requirements and Description (QARD) document (DOE 2000). This is documented in the activity evaluation for the NFE PMR Work Package Plan (CRWMS M&O 1999b). The NF environment is also identified on the Q-list (DOE 1988) as important to waste isolation.

This document was prepared in accordance with AP-3.11Q, *Technical Reports*. The Technical Development Plan for the PMR (CRWMS M&O 2000x) was prepared in accordance with AP-2.13Q, *Technical Product Development Planning*. The AMRs that support this PMR were prepared in accordance with AP-3.10Q, *Analyses and Models*. The calculation that supports this PMR was prepared in accordance with AP-3.12Q, *Calculations*.

The qualification status of input data and references are tracked in the electronic Document Input Reference System (DIRS) in accordance with AP-3.15Q, *Managing Technical Product Inputs*. Data qualification was performed in accordance with procedure AP-SIII.2Q, *Qualification of Unqualified Data and the Documentation of Rationale for Accepted Data*.

This document summarizes the major results and conclusions from AMRs and abstractions. Word-processing and graphic-illustration applications were used in the development of this document.

This PMR includes results from the following software codes used for thermal, hydrological, chemical, and mechanical analyses, as documented in the supporting AMRs (Section 1.4.2). However, no software codes were used in the development of this PMR. The following statements listing software codes are presented for information only. Their qualification status is

documented in the Configuration Management Database and DIRS database for the AMRs where used.

- NUFT, Version 3.0.1s (LLNL 1999), which is a heat and mass-transfer code used for thermal-hydrological (TH) modeling. Appendix A is an evaluation of the status of NUFT, with respect to known physical data and processes.
- TOUGH2, Version 1.4 (LBNL 2000) is a heat and mass-transfer code used for TH modeling. The UZ F&T PMR and supporting documents discuss the validation status of the TOUGH2 code.
- TOUGHREACT, Version 2.2 (LBNL 1999), is a heat transfer, mass transfer, and reactive-transport code used for THC analyses. Section 3.3 of this report and the *THC Process AMR* discuss the validation status of the TOUGHREACT code.
- 3DEC, Version 2.00 (Itasca Consulting Group 1998), is a heat transfer and distinct element stress-analysis code used for TM analyses. This code is commercial software that has been qualified for use on YMP. The validation of the models it implements is ongoing.

These software codes are managed in accordance with procedure AP-SI.1Q, *Software Management*.

This document may be affected by technical product input information that requires confirmation. Any changes to the document that may occur as a result of completing the confirmation activities will be reflected in subsequent revisions. The status of the input information quality may be confirmed by review of the Document Input Reference System database.

## 1.6 RELATIONSHIP TO OTHER PROCESS MODEL REPORTS AND KEY PROJECT DOCUMENTS

Section 1.1 listed the nine process models that support Site Recommendation (SR) and TSPA-SR. Figure 1-4 shows the flow of information through the eight process models that analyze scenarios with no disruptive events. This flow takes place at both the process-model level (between PMRs) and in TSPA abstractions. The boundaries between process models sometimes overlap for calculational convenience. The two circled models (ISM and WF) are starting points for PA calculations, and the hexagonal model (biosphere) is the end point for PA. Arrows represent the flow of information, with specific information categories shown as labels. The blue labels identify output information from the NFE PMR.

The effects of coupled processes that occur within the emplacement drifts are discussed within the EBS PMR. Therefore, the environmental conditions that interact directly with the waste packages are described in the EBS PMR. The issues of coupling between the WP and the environment that help to determine the evolution of the environment (e.g., impact of corrosion products on water chemistry within the drift) are covered jointly within the EBS and WPD PMRs. Interactions between the environment within the drifts and the waste are less

direct, in that the waste package materials or corrosion products are also involved. Therefore, these interactions are discussed in the EBS, WP, and WFD PMRs. Each of these PMRs depends on the thermal-hydrological conditions in the NF rock, as defined in the NFE PMR.

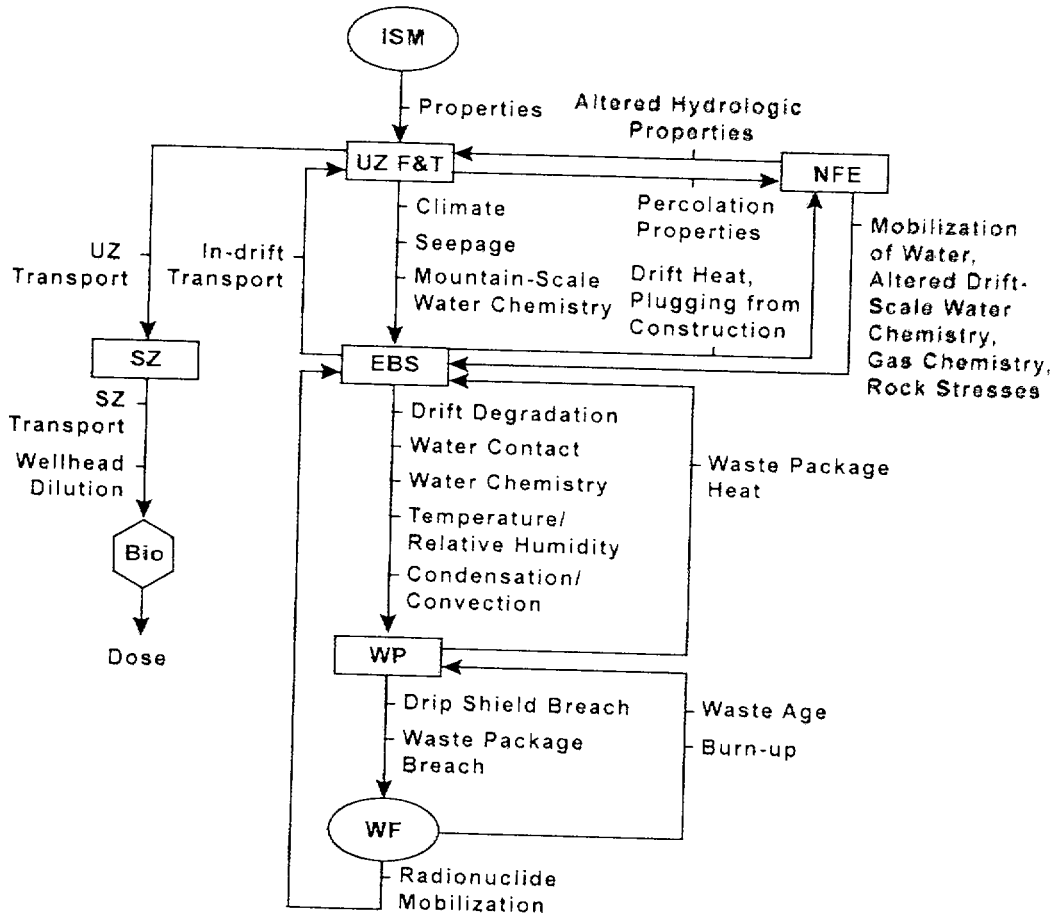


Figure 1-4. Flow of Information through Site Recommendation Process and the Nominal Case Total System Performance Assessment Models

Coupled processes that occur outside of the drifts are discussed in this PMR and the UZ F&T PMR. Saturated-zone flow and transport is also subject to coupled processes, but much less significantly than in the unsaturated zone. In general, changes in UZ hydrological properties, moisture or fluid redistribution in response to coupled processes, geochemical changes in fluids and minerals due to coupled processes, and changes to the permeability, porosity or fracture characteristics as result of mechanical coupling are all discussed within the NFE PMR. Seepage into emplacement drifts and changes in the seepage that result from coupled processes are discussed in the UZ F&T PMR. Chemistry of ambient fluids within the mountain is discussed in the UZ F&T PMR. The UZ F&T PMR also discusses changes of mineralogy as it relates to transport, including changes in sorption or retardation capacity of the minerals.

Figure 1-5 shows the spatial relationship between the processes reported by the NFE PMR and the EBS and UZ F&T PMRs as well as the interactions between those models.

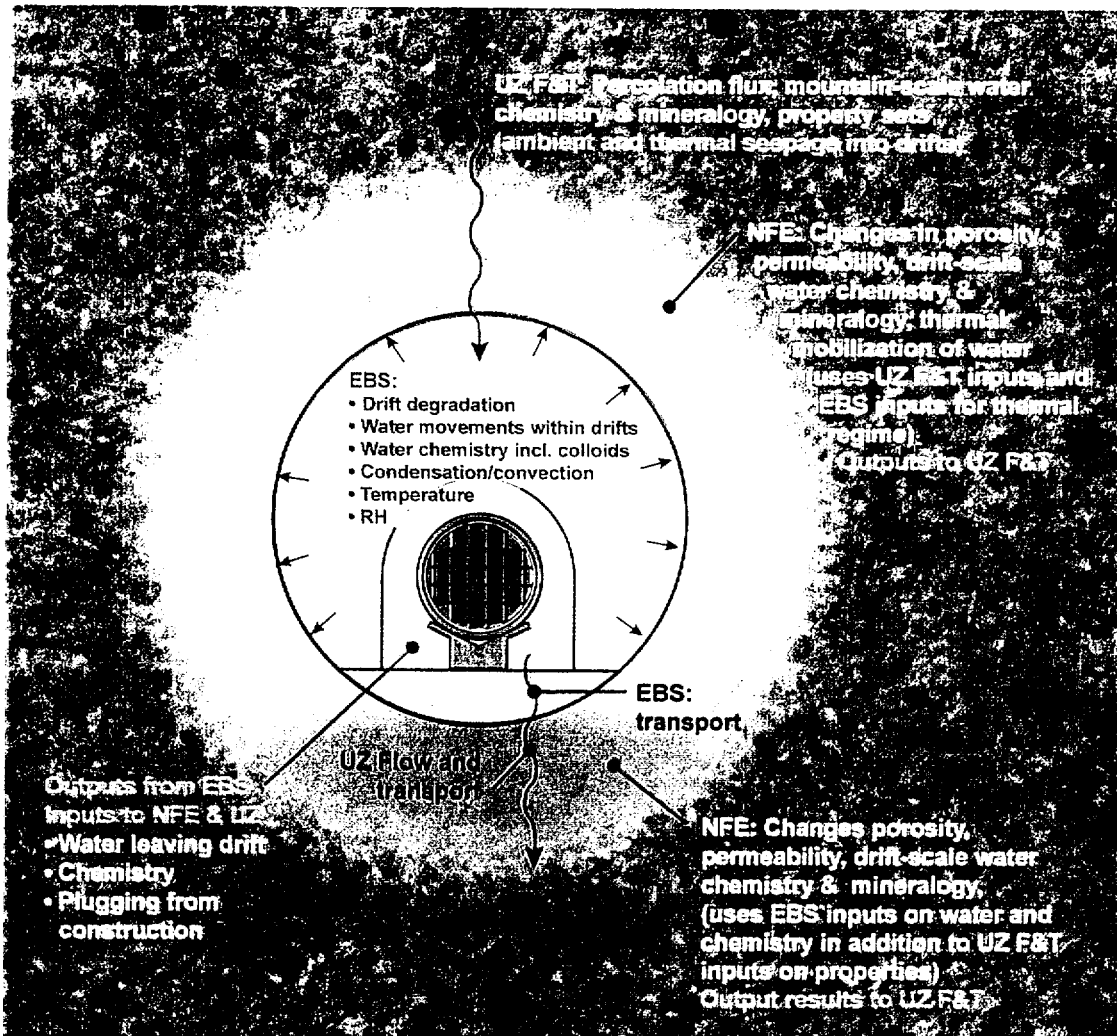


Figure 1-5. Spatial Relationships of Processes and Interactions Among Three Process Model Reports

The ENFE KTI (NRC 1999a) assesses all aspects of the evolution of the NFE that have the potential to affect the performance of the proposed repository. The ENFE KTI subissues are addressed in various PMRs. Section 4.2 presents a correlation between the ENFE KTI subissues and the PMRs that address them. Chapter 4 and Appendix D of this PMR provide detailed explanations describing how the acceptance criteria relevant to the NFE PMR have been addressed.

**1.6.1 Process Model Report Interfaces**

The following sections summarize the PMRs with interfaces to the NFE PMR.

**1.6.1.1 Integrated Site Model Process Model Report**

The ISM PMR (CRWMS M&O 2000y) describes the geologic framework models of the site (e.g., stratigraphy, structural characteristics, rock properties, and mineralogy). This PMR describes how geological, geophysical and hydrological property information has been used to

model the geological properties of the site. The geological framework is used in the calculation and AMRs supporting the NFE PMR.

#### **1.6.1.2 Unsaturated-Zone Flow and Transport Process Model Report**

The UZ F&T PMR (CRWMS M&O 2000f) describes the processes affecting the amount of water entering the unsaturated zone above the potential repository and the subsequent seepage into emplacement drifts. It also describes the movement of water with dissolved radionuclides or colloidal particles through the unsaturated zone below the potential repository. The flow fields calculated by the UZ F&T PMR and supporting AMRs are used in the NFE PMR supporting analyses. Further, the mountain scale (MS) TH model, developed as part of the UZ effort and reported within the UZ F&T PMR, is an integral part of the THC model, the results of which are reported within the NFE PMR. Changes to hydrologic properties calculated by use of the THC model are reported in the NFE AMRs and are fed directly back to the UZ F&T analyses.

#### **1.6.1.3 Engineered Barrier System Degradation, Flow and Transport Process Model Report**

The EBS PMR (CRWMS M&O 2000g) describes how the in-drift processes and environments change with time after emplacement of nuclear waste in a potential repository, as affected or controlled by the EBS design. The processes in the EBS PMR include:

- Evolution of heat by radioactive decay, and its removal by preclosure ventilation
- Drift degradation by rockfall
- Flow of water within the drift
- Evaporation and condensation within the drift
- Deposition of salts and precipitates within the drift
- Gas exchange between the drifts and the surrounding rock
- Chemical reactions between water, rock, and introduced materials (in the drift)
- Colloids formed by corrosion products with high sorptive capacity for radionuclides
- Growth and activity of microbes in the EBS
- Transport of radionuclides through the invert by advection and diffusion
- Chemistry of effluent leaving the drift, including colloids
- Production of fine particles that could affect drift change through the NF rock

A primary interface between the NFE and EBS PMRs involves the chemistry of seepage water from the NFE that enters the drift. This seepage interacts with such components as steel or cements within the drift. It affects the degree to which salts and precipitates form on EBS components during repository heating, and dissolution of such salts and precipitates during repository cooling.

Another primary interface is the thermal source distribution from waste heating. The Multi-scale Thermohydrologic Model (MSTHM) (CRWMS M&O 2000k) describes the thermal-hydrologic (TH) evolution throughout the potential repository and is used by the NFE and EBS PMRs, and directly by TSPA. The model evaluates the period of reduced relative humidity on the WP surface and the extent to which the repository pillars remain below boiling, for example.

### 1.6.1.4 Disruptive Events Process Model Report

The DE PMR summarizes the consequences of volcanic and seismic events that potentially could affect a potential geologic repository at Yucca Mountain. The consequence analyses rely on inputs from the probabilistic volcanic and probabilistic seismic hazard analyses to describe the frequency of disruptive events. Effects of igneous activity on drifts, waste packages, and the waste forms are also discussed in this PMR, and modes of radionuclide release resulting from igneous events are characterized. Incremental effects of seismic ground motion on rockfall are described. The consequences of fault displacement for the EBS and waste packages are also summarized. Finally, the potential effects of seismic activity on the hydrologic system are discussed.

The NFE and DE PMRs both consider thermal and mechanical perturbation of NF rock, but the DE PMR uses bounding analyses to describe the effects on WPs of the thermal pulse generated by an intrusive dike.

### 1.6.2 Process Model Report Inputs/Outputs

The relationships between the PMRs are illustrated in Table 1-2. The PMRs are interrelated not only in overlapping issues, but also in exchanging information. The UZ F&T PMR and associated AMRs report information on the amount of water flowing through the mountain (percolation flux), pore and fracture-water chemistries, mineralogy, and hydrologic and mineralogic property sets. This information (some of which was assimilated from other PMRs, such as geological information from the ISM PMR) is used as inputs to the NFE models and analyses. The EBS PMR provides information regarding the impact of EBS design on the thermal source and temperature distributions within the drifts. The EBS PMR also documents the amount and spatial distribution of water that is expected to leave the drifts, the chemistry of that water, and colloid generation. EBS PMR determinations of water chemistry and colloid generation are made considering corrosion products identified in the WPD PMR (CRWMS M&O 2000c) and waste form dissolution products identified in the WFD PMR (CRWMS M&O 2000ab). Finally, the EBS PMR considers the potential consequences of fracture plugging below the drift invert resulting from construction and emplacement activities.

Table 1-2. Summary of Relationships Between the Near-Field Environment Process Model Report and Other Process Model Reports

Other Process Model Reports	Inputs Provided to the NFE PMR	Input Provided by the NFE PMR
ISM	Stratigraphic data (through UZ F&T PMR)	None
Unsaturated Zone	Percolation flux (amount of water) Hydrologic property sets Ambient water chemistry (pore and fracture)	Porosity and permeability changes from THC Porosity and permeability changes from THM Mineralogy changes and precipitates Thermally altered water chemistry
EBS	In-drift gaseous- and aqueous-phase compositions Chemistry of water leaving drifts Spatial distribution of water leaving drifts EBS thermal source term	Thermally altered seepage water chemistry

The NF AMRs and PMR use this information to determine changes to properties and conditions within the NFE. This information is then used by the UZ F&T PMR to determine any impacts on percolation and seepage, and on transport. Inputs of NFE information to other PMR activities are through the UZ F&T PMR.

The thermal-hydrological models used to support TSPA are shared by the NFE and EBS PMRs. The EBS primarily uses the TH models to determine in-drift conditions, while the NFE PMR focuses on conditions in the NF rock, to include chemical and mechanical coupling effects. The multi-scale TH models are discussed in the *Multiscale Thermohydrological Model* (CRWMS M&O 2000k).

The inputs to TSPA, from the TH process-level models and abstractions, include the in-drift thermodynamic environment. The abstractions used in the TSPA model include direct input from the process-level model and appropriately averaged inputs based on representative infiltration rate bins defined by TSPA. The directly-applied input to the TSPA model is based on the location-dependent results described in detail in the Multiscale TH Model and In-Drift Environment Abstraction AMRs (CRWMS M&O 2000k and CRWMS M&O 2000m). Direct EBS inputs from the TH models to TSPA include:

- Waste package surface temperature
- Drip shield temperature distribution
- Waste package relative humidity
- Drip shield relative humidity
- Top of drip shield evaporation rate
- Volume flow rate at top of drip shield
- Maximum waste package surface temperature

The appropriately averaged EBS inputs from the TH models to TSPA include:

- Waste package surface temperature
- Invert liquid saturation
- Invert temperature
- Invert relative humidity
- Invert evaporation rate
- Absolute invert volume flow rate

The inputs to TSPA, from the TH and THC process-level models and abstractions, also include the NF host rock environment. The abstractions used in the TSPA model include direct input from the process-level models and appropriately averaged input based on representative infiltration rate bins and time periods defined by TSPA. The directly-applied input to the TSPA model is based on the location-dependent results described in detail in *THC Process*, *THC Abstraction*, *Multiscale TH*, and *In-Drift Environment Abstraction* AMRs (CRWMS M&O 2000b, CRWMS M&O 2000c, CRWMS M&O 2000k, and CRWMS M&O 2000m). Direct NFE inputs to the TSPA include:

- Percolation flux at 5 m above the drift crown
- Water and gas compositions in the fractures above the drift crown

The appropriately averaged NFE inputs to TSPA include:

- Drift wall temperature
- Drift wall relative humidity

### **1.6.3 Relationship to the Repository Safety Strategy**

The Repository Safety Strategy (RSS) (CRWMS M&O 2000s) guides development of the postclosure safety case. One purpose of the RSS is to identify factors that contribute to the safety case, in order to identify additional information needs or simplifications that can be made. Performance Assessment (PA) models and detailed process models support the RSS development.

The RSS does not discuss details of the models and analyses regarding factors in the safety case. As noted in the RSS, "Information relevant to the principal factors of the postclosure safety case to support the site recommendation (SR) and LA considerations will be provided in process model reports" (CRWMS M&O 2000s, Section 3.6).

Through a process of reviews and performance model analyses, the RSS identified (CRWMS M&O 2000s, Section 3.1) the principal factors that are central to determining and demonstrating the long-term safety of the repository system. In addition to these principal factors, the RSS also reviewed other factors (CRWMS M&O 2000s, Sections 3.3 and 3.4) that could potentially improve the long-term safety of the repository system or that must be specified to complete the TSPA analyses. Among the "other" factors considered in the RSS are the coupled-process effects on unsaturated-zone flow (CRWMS M&O 2000s, Section 3.3.2) and coupled-process effects on seepage (CRWMS M&O 2000s, Section 3.3.3). Ambient Seepage into drifts is a principal factor (CRWMS M&O 2000s, Section 3.2.1). Although other issues related to coupling were discussed in the RSS, they are covered in other PMRs, as noted in Sections 1.6 through 1.6.2. The seven principal factors and twenty other factors of second-order importance identified in the RSS (CRWMS M&O 2000s, Table 3-1) are listed in Table 1-3.

The NFE affects seepage into drifts in two ways. First, the thermal pulse can mobilize large quantities of water that could, in some locations, temporarily cause seeps. Secondly, changes to hydrologic properties could permanently alter seepage locations and seepage flux. Analyses of the principal factor of Seepage into Drifts are performed and reported by the UZ F&T PMR and its associated AMRs. The effects of the NFE on thermal perturbations to flux and on changes to hydrologic properties are considered in the NFE PMR, as direct effects on seepage into the drifts. NFE processes influence other factors including: Coupled Processes-Effects on UZ Flow, Coupled Processes-Effects on Seepage, Environments on Drip Shield, Environments on Waste Package (WP), and Coupled Processes-Effects on UZ Transport.

Table 1-3. Factors Potentially Important to Postclosure Safety

	Factors for the Enhanced Repository System	Factors Directly Affected by NFE Processes
<b>Principal Factors</b>	Seepage into Drifts	(indirect)
	Performance of Drip Shield	
	Performance of Waste Package (WP) Barriers	
	Solubility Limits of Dissolved Radionuclides	
	Retardation of Radionuclide Migration in the UZ	
	Retardation of Radionuclide Migration in the Saturated Zone (SZ)	
	Dilution of Radionuclide Concentrations During Migration	
<b>Other Factors</b>	Climate	
	Infiltration	
	Unsaturated-Zone (UZ) Flow above Repository	
	Coupled Processes-Effects on UZ Flow	X
	Coupled Processes-Effects on Seepage	X
	Environments on Drip Shield	X
	Environments on WP	X
	Environments within WP	
	Commercial Spent Nuclear Fuel (CSNF) Waste Form (WF) Performance	
	DOE-Owned Spent Nuclear Fuel (DSNF), Navy Fuel, and Plutonium Disposition WF Performance	
	Defense High-Level Waste (DHLW) WF Performance	
	Colloid Associated Radionuclide Concentrations	
	In-Package Radionuclide Transport	
	Transport through Drift Invert	
	Advective Pathways in the UZ	
	Colloid-Facilitated Transport in the UZ	
	Coupled Processes-Effects on UZ Transport	
	Advective Pathways in the Saturated Zone (SZ)	
	Colloid-Facilitated Transport in the SZ	
	Biosphere Transport and Uptake	

## 1.7 REGULATORY FRAMEWORK

This Section summarizes discussion of the NFE in the NRC proposed rule 10 CFR Part 63 (64 FR 8640) and the DOE proposed rule 10 CFR Part 963 (64 FR 67054).

The NRC's proposed rule on *Disposal of High-Level Radioactive Wastes in a Proposed Geologic Repository at Yucca Mountain, Nevada*, 10 CFR Part 63 (64 FR 8640) lists licensing criteria that will address performance of the repository system. As part of the proposed rule, the NRC states that "...Demonstrating compliance, by necessity, will involve the use of complex

predictive models that are supported by limited data from field and laboratory tests, site-specific monitoring, and natural analog studies that may be supplemented with prevalent expert judgment....” (64 FR 8640, p. 8650). The *THC Process AMR*, *THC Abstraction AMR*, and *THM Calculation* described in Section 1.4.2 of this PMR, are documentation of the use of those models (CRWMS M&O 2000b, 2000c, 2000d). The *Thermal Test AMR* (CRWMS M&O 2000a) meets the further requirement stated in the same section of the proposed rule “The performance assessment will rely...on computer modeling.... In most applications, it [modeling] is accompanied by a rigorous testing program, involving model validation and verification....”.

The proposed rule, 10 CFR 63 (64 FR 8640, p. 8650), also defines the need for the evaluation reported in the *NFE FEPs AMR* (CRWMS M&O 2000e). It states “...A defensible performance should contain a technical rationale for those FEP that have been included in the performance calculation, as well as those that have been considered but were excluded....”. Further, the proposed rule states (64 FR 8640, Part 63.2) that “Performance Assessment means a probabilistic analysis that:

- 1) Identifies the features, events and processes that might affect the performance of the geologic repository, and
- 2) Examines the effects of such FEP on the performance of the geologic repository; and...”

The proposed rule, 10 CFR Part 63 (64 FR 8640, Part 63.21[c]), discusses the need for assessment of the coupled processes associated with the NFE, although it does not identify the NF by name. It states “The Safety Analysis Report shall include:... (6) An assessment of the anticipated response of the geomechanical, hydrogeologic, and geochemical systems to the range of design thermal loadings under consideration, given the pattern of fractures and other discontinuities and the heat transfer properties of the rock mass and groundwater.”

The proposed rule, 10 CFR Part 63 (64 FR 8640, Part 63.114), defines the scope of the PMR report on model testing. It states “(e) Provide the technical basis for either inclusion or exclusion of specific FEP of the geologic setting in the performance assessment...” and “(g) Provide the technical basis for models used in the performance assessment such as comparisons made with outputs of detailed process-level models and/or empirical observations (e.g., laboratory testing, field investigations, and natural analogs).”

The DOE, in rule 10 CFR Part 960 and proposed rule 10 CFR Part 963 (Parts 960 and 963 combined in 64 FR 67054, page 67054), proposed “...criteria and methodology to be used for evaluating relevant geological and other related aspects of the Yucca Mountain site...” Within these rules (64 FR 67054, Part 963.17[a]), the function of the PMRs is identified: “Postclosure...suitability criteria reflect both the processes and the models used to simulate those processes...”.

As noted in Sections 1.1 and 1.4.3 of this report, the PMR provides the technical basis for models used in the TSPA. This is consistent with 10 CFR 963, which notes “...the postclosure suitability criteria largely represent the process model components of the TSPA that DOE will

use to evaluate the performance of the repository during the postclosure period.” (64 FR 67054, page 67081).

Nine postclosure suitability criteria related to the Nuclear Waste Policy Act as Amended (NWPA, Section 112[a]) factors are identified in the proposed rule (64 FR 67054, Table 2). These factors are specific processes pertinent to total system performance. Four additional postclosure suitability criteria are related to disruptive processes and events. These thirteen criteria correspond to the nine PMR reports. Two of the criteria in the proposed rule are combined in the UZ F&T PMR, and the four disruptive-event criteria are combined in the DE PMR. The other seven criteria in the proposed rule are one-to-one matches with the remaining seven PMRs “Near-field environment characteristics” is criterion 3, which corresponds to the NFE PMR.

The proposed rule, 10 CFR 963 (64 FR 67054, page 67082), notes that the “...near-field environment characteristics, also relates to processes important to limiting the amount of water that could contact wastes. This criterion includes: (a) Thermal hydrology...(b) near-field geochemical environment...”. These issues are discussed within the context of this PMR.

The definition of the NF, in proposed rule 10 CFR Part 963 (64 FR 67054, Part 963.2), states “Near-Field means the region where the adjacent natural geohydrological system has been significantly impacted by the excavation of the repository and the emplacement of the waste.” The proposed rule continues in Part 963.17 “... and the temperature and humidity at the engineered barriers ... and ... water contacting the waste and the engineered materials”. This definition is consistent with the overall definition of NFE used by the Project, with the rock part being described in this PMR and the in-drift part being described in the EBS PMR (CRWMS M&O 2000g).

Chapter 4 of this PMR describes the NRC’s KTIs and the subissues relevant to the NFE PMR. Section 4.2 lists the KTIs that contain subissues relevant to the NFE PMR. The relevant subissues are shown in italics. Appendix D lists the acceptance criteria relevant to the NFE PMR and provides a description of the PMR approach. In many cases, a given PMR may only partially address acceptance criteria. For acceptance criteria that are addressed in more than one PMR, cross-references to other PMRs are provided. For all acceptance criteria in the NRC’s ENFE IRSR, pointers to other PMRs that contain details relevant to ENFE IRSR acceptance criteria are provided.

## 2. EVOLUTION OF THE NEAR-FIELD ENVIRONMENT PROCESS MODEL

This chapter includes a general description of the background, the conceptual approach and evolution of the NFE process model; past modeling efforts; the performance assessment NFE workshop; and the NFE FEP.

The NFE evolves in response to excavation and ventilation of the repository, and to emplacement of heat-producing waste and other materials, as well as to changes in the ambient site, such as climate change. Consequently, it is impossible to measure or characterize the NFE, because that environment does not currently exist. Therefore, the NFE must be projected by the use of models. Evolution of the NFE Process Models reflects increased understanding of the coupled processes and material properties, improvements in computer-code capabilities, and evolution of the repository design. Revisions to design or parameter values may influence projections of the NFE. However, they also impact the models used to evaluate performance or make those projections. At present, the advances in computational capabilities are insufficient to rigorously and simultaneously evaluate all processes and how they couple. Therefore, judgment decisions are required as to assumptions, approximations and simplifications that can be made.

Changes in design result in changes to the models used to evaluate the processes. An example is the shift in model emphasis that occurred with change in drift spacing from 28 m in the Viability Assessment (VA) design to the current value of 81 m (CRWMS M&O 1999a, Table 6-3). One of the issues evaluated in the past was the potential to build-up significant volumes of condensate that might be "thermally perched" by the coalescence of boiling fronts in the pillars between emplacement drifts (CRWMS M&O 1999a, Section 7.2). Because of the wider pillars and lower temperatures in the current design, impacts of condensate perching in the pillar areas, refluxing above the condensate zone, and accompanying two-phase flow conditions have been reduced (CRWMS M&O 1999a, Section 7.2). The consequent issues of mass transport of minerals (dissolution and precipitation) are of less import due to the shorter duration and limited extent of near-boiling conditions. For the current design, the issues of greatest importance are thermal-hydrological-chemical (THC) effects (rock-water interactions), particularly in the pillar region where dry-out is not expected to be extensive and temperatures are sub-boiling. This contrasts with the analyses for the VA design, where part of the NFE THC response was dominated by refluxing. For that reason, the emphasis in this report is placed on expected conditions and on the coupled processes that may cause permanent changes in the environmental conditions.

Details of the current understanding of the processes and models are contained in the supporting Analysis Model Reports (AMRs) and the calculation listed in Section 1.4.2. This understanding has evolved significantly over the years. Examples of this evolution include model revisions to include incorporation of condensate drainage, approaches to account for channelized flow in fractures and impacts on FMXs (FMXs) (AFM), improved or updated property sets and understanding, conceptual models of mechanical interactions with hydrological processes, and laboratory identification of chemical and mechanical processes and property measurements. In addition, the current understanding as reported in the AMRs and calculation is focused on current designs, and therefore includes analyses of processes that were not identified in earlier studies. Models used in previous analyses that focused on the VA design were reported in the *Near-field Altered Zone (NF/AZ) Models Report* (Hardin 1998) and in the Total System

Performance Assessment-Viability Assessment (TSPA-VA) Technical Basis Document (CRWMS M&O 1998b, Chapters 3 and 4).

The *License Application Design Selection* (LADS) process (CRWMS M&O 1999a, Sections 4, 5, and 6) considered a number of alternative conceptual designs to improve the projected total system performance beyond that presented in the *Total System Performance Assessment-Viability Assessment* (TSPA-VA) (DOE 1998, Volume 3, Figure 4-26). Although the site characteristics alone are expected to prevent release of most radionuclides to the accessible environment (CRWMS M&O 2000s, Figure 2-1), engineered barriers were added in LADS to reduce uncertainty and to provide defense in depth (CRWMS M&O 1999a, Section O.2.1.4). The LADS effort resulted in adoption, in June 1999, of (EDA-II) (Wilkins and Heath 1999). The EDA-II design (Figures 2-1 and 2-2) includes the following (CRWMS M&O 1999a, Sections 6.5 and 7):

- Blending of high and low thermal output waste in waste packages (WPs), to limit peak WP temperatures
- Use of preclosure ventilation to remove heat before closure, limiting peak rock and WP temperatures
- Line-loading of WPs in widely spaced drifts to enable drainage of ambient and mobilized percolation flux through the pillars between the drifts
- Use of drip shields and backfill to protect WPs from water contact and rockfall
- Reduction of the amount of concrete in the drifts, to reduce in-drift chemical processes
- Use of a long-lived invert and WP-support to enhance drainage and limit water contact with the drip shields and WPs.

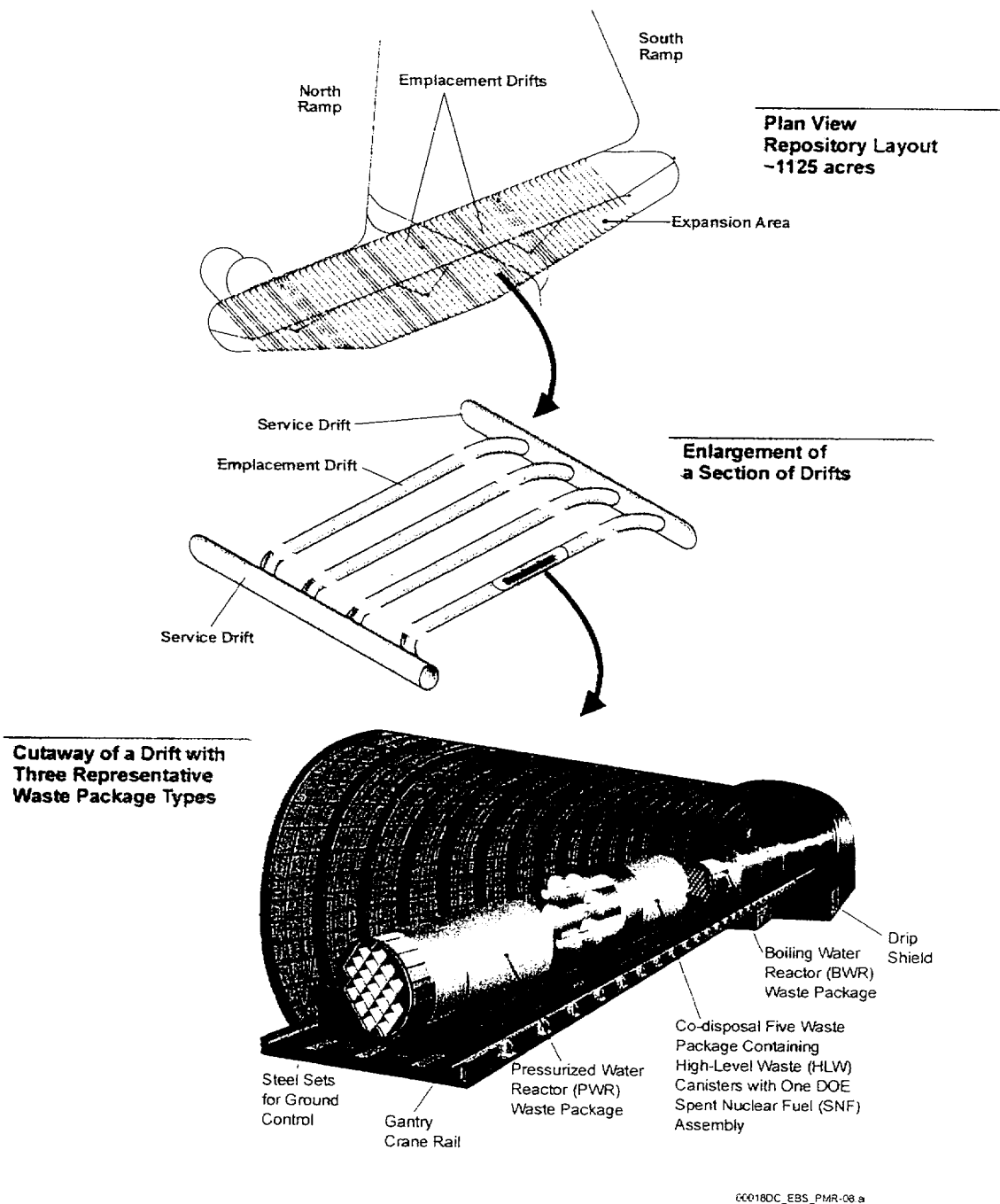
As the Site Recommendation (SR) design work has progressed, additional changes have been made in the design. During development of this Process Model Report (PMR), decisions have been made by YMP management to eliminate backfill from the design. This change places more emphasis on understanding NF rock stresses and their contribution to rockfall. Within the EBS, elimination of backfill changes the seepage situation (the air gap extends around much of the periphery), increases the potential mechanical loading of the drip shields, and reduces peak WP and Waste Form (WF) temperatures. These modifications to the design and process models have not been completely incorporated into the AMRs and PMRs at this point. TH analyses for the no-backfill option are included in this PMR and THC and THM analyses are ongoing. For the NFE PMR, elimination of backfill is not expected to significantly change the conclusions of the report. Section 1.4.3 discusses the overall influence of backfill on the NFE. On an AMR by AMR basis the effect of backfill removal from the design is discussed below:

- The *Thermal Test AMR* is unaffected by changes in repository design since the purpose of this AMR is to provide hydrologic and thermal property set testing and conceptual flow model validation with respect to a controlled heat input to the NF host rock.

- The *THC Process AMR* characterizes the chemical evolution of the NF host rock using the emplacement drift environment as a heat transfer boundary condition only. Any potential changes in the introduced chemical environment (either by including or not including backfill) and how they may influence the evolution of the host rock chemical environment are not considered in the process model. Consequently, only changes in the thermal (temperature) history at the drift wall will have an impact on the water and gas compositions there. These changes should primarily be limited to early times (after closure) since the peak and time-to-peak-temperature are affected by the inclusion or exclusion of an engineered backfill material. In the case without backfill, it is expected that the peak temperature at the crown of the emplacement drift will be slightly higher since it occurs earlier, the resistance to heat transfer is reduced, and the heat flow will be more isotropic, because the backfilled design has a higher fraction of the heat flow in the downward direction (CRWMS M&O 2000k, Sections 6.11.1.1 and 6.11.1.4). At times shortly after closure (possibly within 100 or 200 years), it is expected that the two design cases will exhibit nearly identical thermal histories at the drift wall and hence identical chemical histories in the host rock.
- The *THC Abstraction AMR* is affected similarly to the *THC Process AMR*.
- The *NFE FEPs AMR* may require modifications to FEPs excluded based on the emplacement-of-backfill screening argument. However, since these FEPs primarily impact the in-drift thermodynamic environment (by changing the environment near the drip shield and waste packages), it is expected that they will have less influence on the processes occurring within the NF host rock. Consequently, the FEPs associated with the NFE PMR are less affected by the removal of backfill from the repository design.
- The *THM Calculation* is largely restricted to the host rock and will be affected primarily by changes in the thermal history as described above for the *THC Process AMR*.

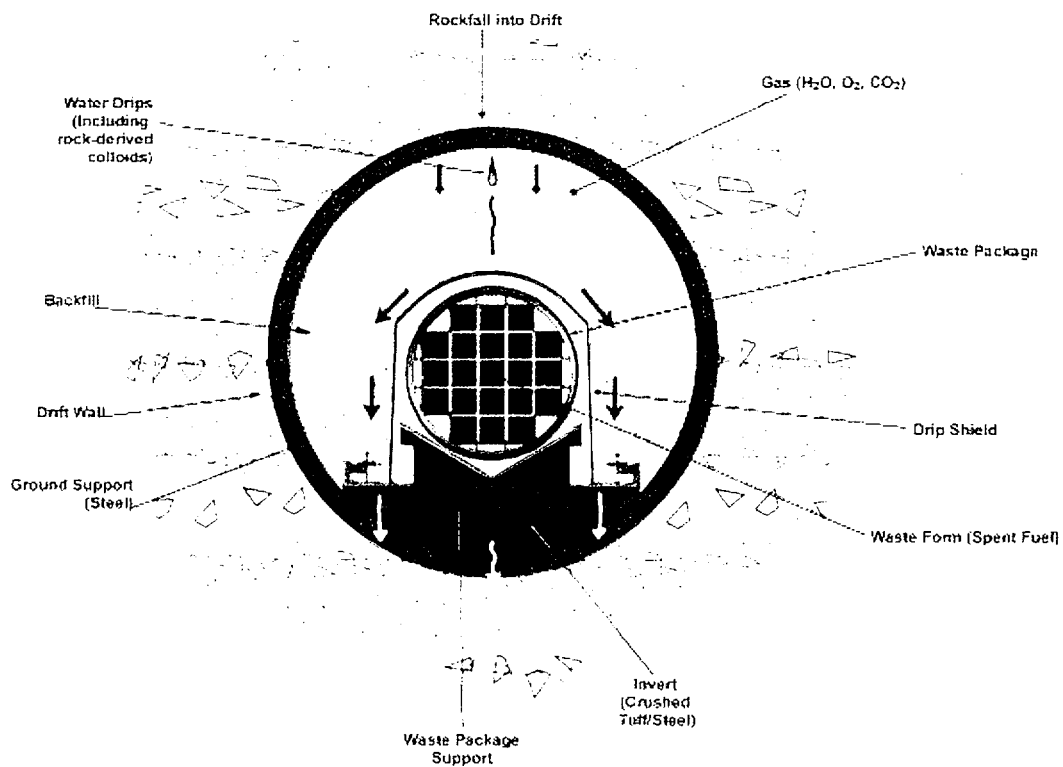
The design of the potential repository is controlled by a series of hierarchical design requirement documents. The lowest level of these documents is termed Subsystem Design Descriptions (SDDs). Five of these SDDs have been identified that have interfaces with the NFE PMR, as follows:

- Subsurface Facility SDD (CRWMS M&O 2000aa)
- Emplacement Drift SDD (CRWMS M&O 2000ad) (includes the invert)
- Backfill Emplacement SDD (CRWMS M&O 2000ae)
- Subsurface Ventilation SDD (CRWMS M&O 2000af)
- Ground Control SDD (CRWMS M&O 2000ag).



Source: CRWMS M&O 2000g, Figure 1-2

Figure 2-1. Schematic View of the Potential Repository Layout, Drift Connections and Representative Waste Package Types within an Emplacement Drift



Source: CRWMS M&O 2000g, Figure 1-3

Figure 2-2. Schematic Cross Section of an Emplacement Drift Containing a 21-PWR Waste Package, Showing Major Elements of the Engineered Design Alternative II Design for the Engineered Barrier System

The Subsurface Facility SDD establishes the requirements for the location of emplaced waste. The SDD limits the minimum thickness of rock above the emplacement drifts, the minimum unsaturated-rock thickness below the drifts, and the standoff from the main trace of Type 1 faults (those with movement in the Quaternary period, the last two million years, such as the Solitario Canyon fault). These criteria are being applied to the repository design in parallel with development of the TSPA-SR and its supporting PMRs. The design organization has recently changed the design from a plane with the highest elevations at the south end to a plane with a grade downward in the north and south directions from a selected (nominally east-west) emplacement drift (CRWMS M&O 2000i). Both designs include a ½ % grade downward from each drift midpoint, for drainage. This design change allows the emplacement area to extend farther to the south without exceeding the rock-cover minimum, and increases the potential emplacement area. This change will affect the detailed coupled process calculations for the NFE, but likely would not change overall conclusions about site suitability or performance, as discussed in Section 1.4.3, because NFE processes are more sensitive to thermal loading than to footprint and because the rock properties in the new area are similar to the original region.

Examples of the Subsurface Facility SDD (CRWMS M&O 2000aa) criteria that are direct inputs into NFE models include:

- 1.2.1.4: The system shall provide emplacement space to allow for an average waste package spacing of TBD-3791.

- 1.2.1.5: The system shall space the emplacement drifts 81 m center to center.
- 1.2.1.7: The system shall orient emplacement drifts at least 30 degrees from dominant rock-joint orientations
- 1.2.2.1.4 to 1.2.2.1.6: Standoff distances (these are the criteria discussed above)
- 1.2.2.1.8 and 1.2.2.1.9: Location of the repository

As the design organization selects design parameters in accordance with these criteria, some of the details in the TSPA abstracted and process models will change. The models have been developed with this process in mind, and are intended to be suitably robust to permit such changes without extensive model redevelopment.

The Subsurface Facility SDD criterion for emplacement-drift orientation (1.2.1.7) is being used to select the orientation of the drifts with respect to rock joints. The design organization recently changed the drift orientation from the generally east-west orientation of the VA design (CRWMS M&O 2000i). This change will have an effect on the representation of rock displacements and slip in NFE models (NFE PMR) and rock-fall calculations (EBS PMR). Since the purpose of such a change would be to improve performance and the orientation is based on analysis of mapped fractures, it is expected that the overall effects would be favorable.

The Emplacement Drift SDD includes criteria regarding drift-wall temperatures, line-loading, drip shield, and invert. These criteria have been factored into TSPA abstracted and process models.

The NFE coupled processes that have been studied for the VA design also occur in the EDA-II design, but for a shorter duration and a smaller spatial domain. The major element of the VA design that does not occur in the EDA-II design is large-scale boiling and dry-out of the pillars between the emplacement drifts; in the EDA-II design the capacity to drain percolation flux between the drifts is expected to be available at all times.

## **2.1 THE NEAR-FIELD ENVIRONMENT PROCESS MODEL DEVELOPMENT PHILOSOPHY**

Activities associated with the NFE have historically focused on how the evolving environment would impact repository performance. As stated earlier, the NFE does not presently exist, and therefore cannot be directly measured. Of necessity, evaluation of NFE impacts on performance must be based on model projections to first define the NFE. As such, although these activities are associated with site characterization, they have been dominated by model development, defining parameters and input to models, and obtaining measurements to provide testing of and insight into the physical processes that are to be modeled.

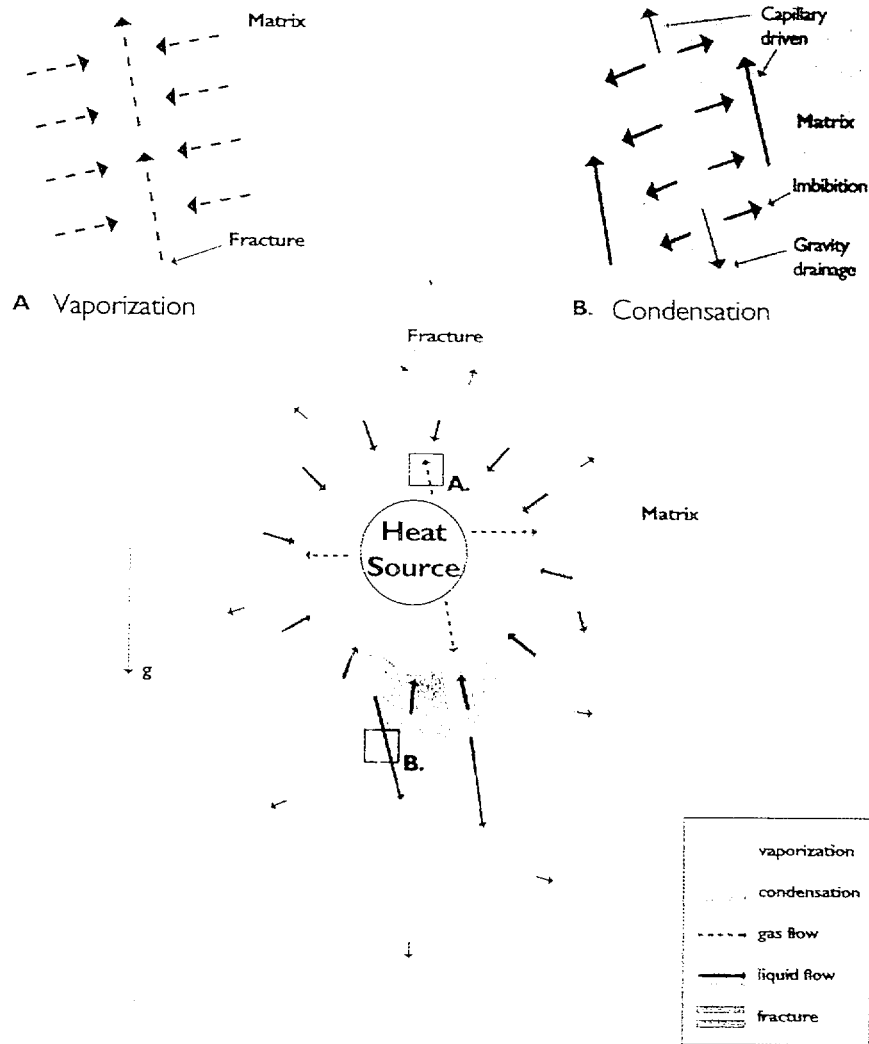
Development of the NF process models (Section 1.4.2) was based on a series of laboratory and field tests, as well as fundamental principles of heat and mass transfer, and of chemical equilibrium and kinetics. Conceptual process models using these scientific principles were implemented in numerical models, as computer software (codes). In some cases, these

implemented models were benchmarked to laboratory and field test data, to validate selection of the conceptual processes and to calibrate input parameters, such as rock properties.

The processes of the NFE are primarily driven by or coupled to the generation of heat from the waste. The laboratory work and early field studies that were related to development of the NFE models were reported in the *Synthesis Report on Thermally Driven Coupled Processes* (Hardin and Chesnut 1997).

The emplacement of high-level radioactive waste, especially CSNF, in Yucca Mountain will release a large amount of heat into the rock adjacent to the repository. The heating rate will decrease with time, creating a thermal pulse. There is an imbalance between the declining heat source and the outward loss of heat from the volume of rock heated to a given temperature. Because the initial heat dissipation area is small, this imbalance initially favors increasing temperatures and an expanding volume of heated rock, with the drift wall reaching its peak temperature within several decades after repository closure. Thereafter, the imbalance favors decreasing temperatures at the drift wall; however, because of the thermal inertia of the heated rock and the continuing (though declining) heat source, the return to near-ambient temperatures takes many thousands of years. Percolating water can hasten the cooling process, but temperatures at the drift wall are calculated to remain above 50°C for at least several thousands of years (see Section 3.2.3.1.3).

In addition to raising the rock temperature through the relatively slow process of heat conduction, heat can be transported more effectively by the sensible (single-phase) heat process accompanied by advective transport of water, and by latent heat associated with vaporization of water accompanied by vapor transport. The latter can result in either escape of vapor from the NFE and EBS, or in gravity-driven heat-pipes in the fractured rock of the NF. In such a heat-pipe, water present within the porous rock matrix near the heat source will absorb heat and vaporize. The vapor will be expelled into nearby fractures, and will flow through the fractures to a cooler location (e.g., upward above the drift, but downward below the drift). Eventually, the water vapor will condense into liquid water, releasing its latent heat. The condensate can be imbibed into the nearby matrix, can flow downward in the fracture system, or can move back toward the hotter, dryer region due to capillary forces. Depending on the condensation location, the fracture-system geometry, and the competition between imbibition, capillary movement in fractures, and gravity-driven movement in fractures, the water may drain below the repository horizon, or it may return to the heated region. The latter water can repeat the cycle, which is known as refluxing, greatly enhancing the rate of heat transfer away from the emplacement drifts. These processes are schematically illustrated in Figure 2-3 (CRWMS M&O 2000a, Figure 26).



Source: CRWMS M&O 2000a, Figure 26

Figure 2-3. Schematic Representation of Thermal Hydrological Processes in an Unsaturated, Fractured Geological Medium

When the water vaporization and condensate return (reflux) cycle is active, the heat pipe transports heat, in the form of the latent heat of vaporization of water, rapidly from the heat source into the surrounding rock. The mobilization of water temporarily (for decades to centuries) increases the percolation flux in the NF by a large amount. This creates the possibility that water may quickly drain back onto the drifts or that it may “shed” through the pillars between emplacement drifts. The thermal-hydrological aspects of models discussed in Sections 2.2.1, 3.2, 3.3, 3.4, and 3.6 include consideration of refluxing for both temperature and saturation distribution in the NF rock.

Other effects, such as coupled chemical and mechanical processes (described in Sections 2.2.2, 2.2.3, 3.3, 3.4, 3.5 and 3.6), may also influence the movement of water above, within, and below

the emplacement drifts. For example, the rapid movement of water generated by heat pipes, and the temperature changes experienced by the water in heat pipes, have the potential to create "stills" in which water deposits its dissolved minerals in the boiling region and aggressively dissolves new minerals in the condensation region. This THC process can affect seepage water chemistry and the hydrological pathways and properties. These processes are most intense when above boiling temperatures are present, but they operate to a lesser degree at sub-boiling temperatures, because the vapor pressure of water increases with temperature. Coupled THC processes have the potential to significantly alter the permeabilities of the fractured rock mass and to disperse and/or immobilize mineral constituents and released radionuclides. It is not likely that significant quantities of radionuclides will be released during the thermal pulse, due to the projected long lifetime of the engineered barriers (CRWMS M&O 2000ac, Figures 3-102 and 3-103).

Because the rock mass is fractured and heterogeneous, the temperature gradients generated by the thermal pulse in the near field have the potential to induce significant relative displacements of opposing fracture surfaces in the rock mass. Such movements, particularly shear displacements of rough fractures, have the potential to permanently alter fracture permeabilities in the affected regions by several orders of magnitude.

Based on the body of work on coupled processes on unsaturated-zone repositories (see, for example, Hardin and Chesnut 1997; Hardin 1998; Wilder 1993, 1996, and 1997), the relationships among the coupled processes and the relative strengths of the processes can be assessed. As summarized below, at Yucca Mountain several of the coupled processes dominate the others. The discussion is a road map of the processes to enable the reader to evaluate more detailed descriptions of individual processes in the larger context.

The NFE evolves in response to coupled processes in four categories, thermal (T), hydrological (H), chemical (C), and mechanical (M). The coupling of the processes is indicated by acronyms listing the processes involved; the sequence of letters in the acronym is not significant, and back-coupling is not indicated by listing letters more than once. In principle, thermal, hydrological, chemical, and mechanical processes in the NF are coupled through their process state-variables (such as temperature, liquid saturation, relative humidity, species concentrations, displacements, and corresponding process fluxes (such as heat flux, water and air fluxes, chemical-reaction rates). The couplings between these different processes, indicated in Figure 2-4, usually take place in both directions at different levels of strength and significance, e.g., the thermal effects impact the hydrological processes ( $T \rightarrow H$ ) and the back coupling hydrological effects impact the thermal processes ( $H \rightarrow T$ ). If the coupling between two processes is strong in one direction, while it is weak in the opposite direction, it is usually possible to neglect the weak coupling in the initial calculations and to evaluate its impact from the result of a calculation that is coupled only in one direction. Such approximations often significantly reduce the effort required to compute coupled problems.

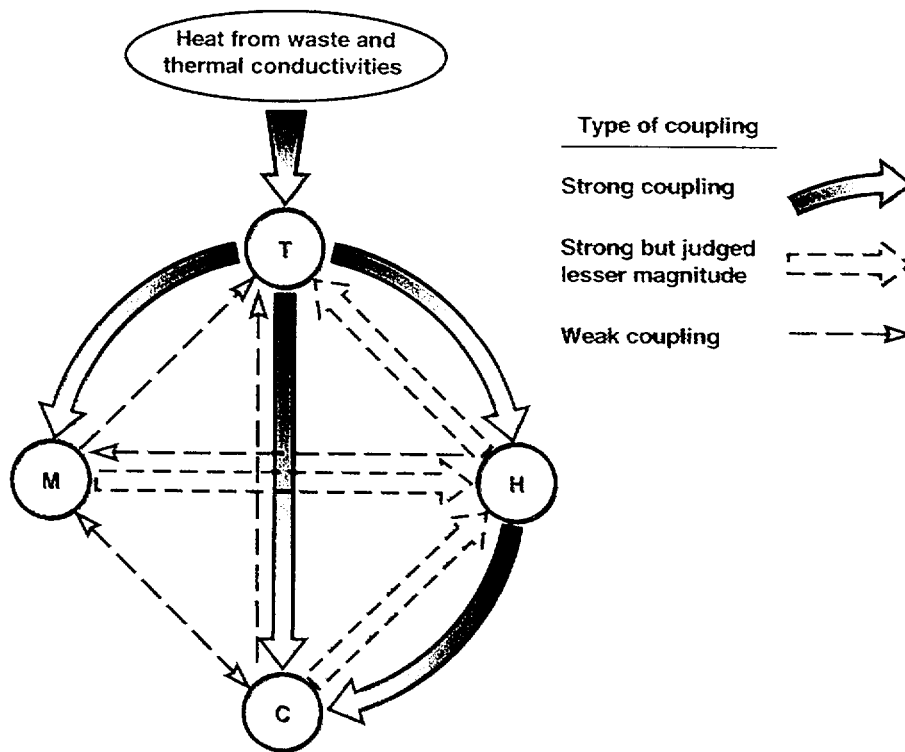


Figure 2-4. Coupling Between Thermal, Hydrological, Chemical, and Mechanical Processes

During the heating phase, TH processes in the NF are always strongly coupled in both directions:

- In the  $T \rightarrow H$  direction, the temperatures affect fluid densities and fluid saturations as a result of thermal expansion, and evaporation and condensation.
- In the  $H \rightarrow T$  direction, the fluid saturation, relative humidity and vapor and water movement affect the transport of sensible and latent heat. As noted in Section 3.2.1.1, heat pipes can prevent temperature rises above the boiling point, as has been demonstrated in field tests (Section 3.6.1.1).

For these reasons, fully coupled thermal-hydrological (TH) modeling of T and H processes is a mandatory requirement for NF modeling. The thermal effects on hydrology are the strongest, ranging from halting flux to enhancing it. The hydrological effects on thermal are significant, reducing NF temperatures and extending the near-boiling region for tens to ~100 meters, depending on the design. When  $H \rightarrow T$  coupling is strong, latent-heat transfer dominates sensible-heat transfer. Most NFE work in the past has focused on TH, including that described in Sections 2.2.1, 3.2.3, and 3.6.1.

In thermal-chemical (TC) coupled processes, the coupling is strong in one direction and weak in the other. Further, back-coupling is actually ternary, rather than binary:

- In the  $T \rightarrow C$  direction, chemical processes depend strongly on thermal processes through the temperature dependence of kinetic rates and phase changes. The solubility of  $\text{CO}_2$  in water is a function of temperature. At high temperature,  $\text{CO}_2$  degasses from

solution with pH shifting to higher values. This higher partial pressure gas migrates down temperature gradients to dissolve into cooler solutions, with pH shifting to lower values. These solutions cause more mineral dissolution to occur.

- In the C → T direction, the coupling is weak with chemical reactions having little impact on the NF energy balance of the system that is dominated by TH processes. There are also potential thermal effects in the far-field due to the endothermic alteration of zeolitic minerals (e.g., dehydration, conversion of clinoptilolite to analcime). These reactions are energy sinks and would probably result in “retardation” of higher temperatures beyond the zone being altered.
- There can be C → H → T coupling, which then can affect temperature through the H → T coupling described in the previous paragraph. However, chemically-driven changes in hydrological properties require significant reflux durations at near-boiling temperatures, and thus there would be a delay well beyond the peak of the temperature pulse before changes occur. This will limit the net C → T coupling from the ternary coupling.

In HC coupled processes, the coupling can be strong in both directions or strong only in one direction, depending on repository design and site characteristics.

- In the H → C direction, chemical processes depend strongly on hydrological processes through fluid flow rates that affect the availability of water, air and other chemical species that participate in the chemical reactions.
- In the C → H direction, there is a potential for permeability of pore and fracture flow pathways in the rock to be significantly altered through the precipitation and dissolution of solid phases, particularly when extended refluxing occurs. The significance of the chemically-driven hydrological property changes depends on repository design (drift and WP spacing, which impacts the duration and spatial extent of near-boiling conditions in the rock); the ambient hydrological properties, primarily fracture porosity; and the spatial localization of the boiling region. In Sections 3.3 and 3.4, calculations conclude that mineral precipitation will not significantly change fracture permeability. These calculations use the current design (which induces a limited duration and extent of near-boiling conditions compared to the VA design), a higher (~1 percent) fracture porosity, and a local boiling region at least 10 cm thick (the smallest zone size). While there are uncertainties, (e.g., including for computational simplicity the use of calcite precipitation rates decreased from those measured in the laboratory), the models reproduced the results of field tests and therefore are considered applicable to these calculations. Furthermore, sensitivity to permeability values is included in TSPA-SR to accommodate the uncertainty in C → H coupling.

Thus, in THC modeling, the T → H, H → T, T → C, and H → C couplings are strong. The C → H couplings can be strong or weak, depending on design and site characteristics. The C → T coupling is weak. In most calculations, the C → H has been treated as a weak coupling; and calculated separately.

Mechanical processes must be introduced in the context of ternary THM processes accounting for TH, TM, and HM coupled processes:

- In the  $T \rightarrow M$  direction, mechanical processes depend strongly on thermal processes through the impact of temperature on thermal expansion and thermally induced cracking of rock.
- In the  $M \rightarrow T$  direction, mechanical processes have little impact on the energy balance of the system that is dominated by TH processes, and this coupling may be neglected.
- In the  $H \rightarrow M$  direction, the impact of hydrological processes on mechanical processes in the unsaturated zone is small, because the pressure change in the gas phase, which determines the overall fluid-phase pressures, is quite small compared to thermal stress changes in the rock matrix.
- In the  $M \rightarrow H$  direction, coupling between the mechanical processes and the hydrological processes can be strong, because large thermal stresses developed in the near field can cause significant fracture displacements and changes in rock permeability in the near field. These permeability changes arise from both shear and normal displacements that are induced across pre-existing fractures, and from the creation of new micro-fracture systems that link into pre-existing fracture systems. While normal displacements can recover during the cooling phase, the impact of shear displacements and (less likely) micro-cracking on rock permeability is likely to be more permanent and to persist far into the future. Section 3.5 focuses on  $T \rightarrow M$  coupling and the consequent change in fracture hydrological properties (thus becoming  $T \rightarrow M \rightarrow H$ ). It should be noted that changes in the fracture hydrological properties are different during the early heating period and the later cool-down period. At early times (first few decades to a century after repository closure), feedback from hydrological property changes could affect peak temperatures. At later times, as the rock cools back to sub-boiling temperatures, there is little significance to the feedback to temperature, but there may be significant changes in seepage into the drifts. These potential changes in seepage are termed “thermal seepage” in this report because they are driven by the thermal pulse, even though they may not occur until later times when temperatures are well below boiling.

Thus, in THM modeling of NF processes,  $T \rightarrow H$ ,  $H \rightarrow T$ ,  $T \rightarrow M$ , and  $M \rightarrow H$  processes are strongly coupled while  $H \rightarrow M$ , and  $M \rightarrow T$  couplings are weak.

Finally, the impact of CM coupled processes must be considered to complete the full suite of coupled processes in the NF:

- In the  $C \rightarrow M$  direction, chemical processes can strongly affect mechanical processes through cementation or healing and dissolution processes in fractured rock that, given sufficient time, can significantly change rock deformability in the NF. Therefore, the  $C \rightarrow M$  coupling must also be considered to be potentially strong.

- In the  $M \rightarrow C$  direction, the direct energy transfer from mechanical processes to chemical processes is very small and this coupling can usually be neglected. The main coupling is if mechanical processes create more surface area for reactions.

To summarize the binary couplings contributing to full THMC coupling, of the twelve possible couplings:

- Seven are likely to be strong:  $T \rightarrow H$ ,  $H \rightarrow T$ ,  $T \rightarrow C$ ,  $H \rightarrow C$ ,  $T \rightarrow M$ ,  $M \rightarrow H$ ,  $C \rightarrow M$ .
- One can be weak or strong depending on repository design and site characteristics:  $C \rightarrow H$ .
- Four are likely to be weak:  $C \rightarrow T$ ,  $H \rightarrow M$ ,  $M \rightarrow T$ ,  $M \rightarrow C$ .

The strength of coupling and significance on performance depends on the time of coupling as well as the strength, as discussed above.

## 2.2 PREVIOUS NEAR-FIELD MODELING

A series of NFER have been published that summarize evolution of the NFE. These reports (Wilder 1993, 1996, and 1997) documented the results of model analyses of the NFE based on the repository design, parameter values, and understanding of the physical processes that existed at the time.

The NFERs were identified in the *Waste Package Plan* (Harrison-Giesler et al. 1991) as the formal means for transmitting and documenting information regarding the NFE and its evolution. The *Preliminary Near Field Environment Report* (Wilder 1993) included the environment that developed within the drifts and contacted the WPs and waste forms (WFs), all of the materials within the drifts, and the environment that developed within the rock mass and extended into the rock mass a distance that depended on the physical process being considered.

The *Near-Field and Altered Zone Environment Report* (Wilder 1997) describes the environment within the drifts NF, the evolving environment within the rock mass, and the AZ). Another, more recent, discussion and summary of the models and model development is contained in the *Near-Field Altered-Zone Models Report* (Hardin 1998).

Finally, the Total System Performance Assessment-Viability Assessment (TSPA-VA) Analysis Technical Basis Document, Chapter 3, Thermal-Hydrology (CRWMS M&O 1998b), provided a historical presentation of previous TSPAs (with respect to thermal-hydrology analyses), the abstraction and testing workshop leading into the viability assessment, the process model and abstracted base case for the TSPA-VA, and important TH sensitivity studies including, among others, the influence of rockfall on the thermal hydrologic in-drift environment and THM alteration of fractures below the repository horizon.

The previous modeling efforts will be discussed as TH, TC, and thermal-mechanical (TM) models in the following section.

### 2.2.1 Thermal-Hydrological Models of Near-Field Processes

Liquid water is the agent common to most, if not all, of the coupled NFE processes. Therefore, development of TH models is a necessary prerequisite for predicting the long-term coupled-system response to inputs representing repository-design parameters.

TH conceptual models are implemented in thermal-hydrological software codes, such as NUFT, VTOUGH and TOUGH2. These programs solve systems of partial differential equations representing the various flow and transport processes (e.g., saturated darcy flow, boiling and unsaturated flow, capillary imbibition, thermal diffusion and advection of heat) that are anticipated to be pertinent to the subsurface regime of Yucca Mountain. However, before the systems of equations can be solved to yield desired information about the state of the potential repository, a representation of the model must be input in the form of a defining list of physical, hydrodynamic and thermal properties that may exhibit dependence on a variety of other parameters, including location, time, and temperature. Depending on the degree of complexity, the list may involve constants, analytic functions of one or more variables (e.g.,  $x$ ,  $y$ ,  $z$ ,  $t$ ) or other discretely specified parameter distributions that contribute to completely defining the equations to be solved, along with the boundary and initial conditions that uniquely determine the solutions to the equations. Of course, the model is not complete without specifying the geometry, as embodied by the choice of coordinate system, computational-domain shape and symmetry. It should be noted that the software codes are capable of obtaining solutions to the differential equations (i.e., simulations) using a variety of numerical techniques. In the context of run-time, accuracy and numerical stability, the analyst implements a solution procedure for addressing a particular design or the input needs of performance assessment.

Past modeling efforts considered the NF to include what is now referred to as the EBS (see Section 1.2.1). Therefore, a discussion of past TH models will also discuss the EBS. During the thermal period (i.e., the period during which decay-heat strongly influences fluid flow), the potential sources of water seeping into emplacement drifts are heat-driven condensate flow and ambient percolation. During the post-thermal period (which primarily corresponds to the post-boiling period), ambient percolation is the dominant source of drift seepage. In both instances, the likelihood of water seeping into the drift increases with local ambient percolation flux. Besides seepage, another source of moisture flux in the drift is the condensation of water vapor at relatively cooler locations in the drift; this effect, which is called the cold-trap effect, is facilitated if there is a large disparity in local heat flux among the WPs and if the WPs are spaced far apart, so that heat is not effectively shared. The use of line-load WP spacing, in which the WPs are placed nearly end to end, and blending of spent nuclear fuel minimize local heat-flux variability as well as the corresponding tendency for the cold-trap mechanism to occur. Section 3.2.3.3 provides conclusions from a numerical study that contrasts designs with different degrees of thermal-hydrological coupling.

Within the emplacement drifts, the most important time-dependent NFE conditions are the relative humidity and temperature at the drip shield and WP surfaces, and the amount of liquid water (and its chemical composition) contacting the drip shields, WPs, and waste forms (CRWMS M&O 1998b, Volume 3, Section 3.4). These conditions depend primarily on design choices (e.g., the thermal-loading density, the choice of drift-liner materials, and the presence or absence of backfill) and secondarily on far-field boundary conditions (e.g., surface topography

and infiltration flux and the pre-emplacement state of the mountain). Thus, typical output from a particular TH model simulation is the evolution of liquid-water seepage flux, temperature, relative humidity (*RH*), and gas-phase air-mass fraction within the drifts as functions of time after repository closure. These are used directly as NFE performance measures in assessing total system performance. TH modeling also serves as the starting point for other process model calculations describing water chemistry, engineered-barrier performance, and radionuclide transport. These models compute distributions of temperature and flow velocity in the repository host rock, which are used with partially coupled models to evaluate whether more rigorous, fully coupled process models are needed.

A recent issue of the *Journal of Contaminant Hydrology* focused on Yucca Mountain. Two articles, (Haukwa et al. 1999, p. 217-255 and Wu et al. 1999, p. 185-215) are descriptions of thermal hydrology, with emphasis on the MS.

In this section, three TH conceptual models are described, some general TH results are presented, and detailed results are presented regarding application of these models for line and point spacing of waste packages, using the overall VA heat loading.

Even with current computing resources, modelers have found that it is impractical to explicitly model a complex network of fractures or conduct full 3-D simulations on the scale of realistic spatial variability in the fracture system. As a result, several approximate approaches to modeling the naturally complex fracture system of Yucca Mountain have been developed. The three TH models described in greater detail below vary by the means in which flow through fractures is represented.

The *Equivalent-Continuum Model* (ECM) assumes that the local matrix potential (water potential plus osmotic potential) is equal in the fractures and the adjacent matrix. Local thermodynamic equilibrium is assumed between the fractures and matrix. Composite functions are derived to describe the equivalent behavior of a single continuum and to define the relations between unsaturated hydraulic conductivity and liquid saturation and between matrix potential and liquid saturation (Klavetter and Peters 1986, for isothermal conditions, and Pruess et al. 1990 for non-isothermal conditions). The ECM does not treat fractures as discrete features; instead fracture-flow effects are averaged over the whole spatial domain. The ECM involves less computational effort than do other models described subsequently, because it uses a single continuum to represent the fractures and matrix. The assumption of local equilibrium between fractures and matrix is appropriate, if the liquid-phase flux in the fractures is sufficiently small (Buscheck et al. 1991, p. 313). Thus, the ECM is appropriate for modeling condensate drainage during periods of quasi-steady moisture movement in thermally driven models, but may be less well suited for modeling the early stages of repository heating, when the rate of thermally driven moisture reflux will be near its peak. The ECM assumptions are poorly suited for modeling the effects of transient boundary conditions (e.g., episodic infiltration events). This ECM approach has been applied in thermal-test analyses (see Section 3.6.1) with direct bearing on prediction of conditions in the near field and AZ:

- Pretest analysis of the DST (Buscheck et al. 1997d, p. 15)
- Posttest analyses of the Single Heater Test (SHT) (Buscheck et al. 1997c, Section 2.1)
- Posttest analyses of the Large Block Test (LBT) (Hardin 1998, Section 3.4.3)

The *Dual-Permeability Model* (DKM) treats the matrix and the fractures as two distinct porous continua, with transfer terms to represent the mass and heat flux between them. Because the DKM does not assume capillary-pressure equilibrium between fracture and matrix continua, it can handle much larger liquid-phase fluxes than can the ECM without producing conditions near 100 percent liquid saturation in the matrix. The DKM also allows thermodynamic disequilibrium between matrix blocks and the adjoining fractures, because of its capability to represent heat flow between these two continua. Because the DKM allows for gas-phase pressure disequilibrium between the matrix blocks and adjoining fractures, it can account for the way gas-phase pressure build-up in the matrix throttles (restricts) the rate of rock dryout. This throttling occurs early during the dryout period, when there is boiling in the rock matrix. It will persist if the matrix permeability is extremely small (e.g., matrix permeability is less than approximately 10 microdarcy) and the matrix blocks are large (e.g., greater than 3 m). Compared to the *Discrete Fracture Model* (DFM) described below, the DKM tends to overpredict gas-phase pressure build-up during the early stage of dryout in the rock matrix and, therefore, overpredicts the throttling of dryout during this period. For large matrix blocks, the DKM continues to overpredict throttling after the early dryout period (Hardin 1998, Section 3.3.3.2, p. 3-12).

The DKM is more computationally intensive than is the ECM, but less intensive than the DFM described below. Typical transfer terms for heat and mass transfer between the fracture and matrix continua do not represent the diffusive nature of matrix imbibition in the matrix block. In other words, the DKM does not treat fractures as spatially discrete features; rather, the effects of fracture flow are distributed throughout the spatial domain. Consequently, the DKM underpredicts the fracture-to-matrix liquid flux during the early stages of matrix imbibition and thus tends to overpredict the magnitude of condensate drainage (shedding) around emplacement drifts.

The DKM approach has been applied in DS TH models supporting TSPA-VA (DOE 1998, Volume 3, Section 3.2.1), with direct bearing on prediction of conditions in the NF/AZ. The DKM is applied to all the Line-averaged-heat-source Drift-scale Thermal-Hydrological (LDTH) model calculations used in the multi-scale TH modeling approach to predict NFE conditions for performance assessment (see Section 3.2.2.1). In this family of models, the fracture-to-matrix liquid flow is strongly influenced by the *Fracture Matrix Interaction* (FMX) parameter, which is specified for each hydrogeologic unit as a model input. This parameter varies between 0 and 1, and quantifies the fraction of the fracture surfaces that are wetted by the liquid phase. This fraction, together with a specified value for the fracture spacing, quantifies the interfacial flow area per unit volume of the rock matrix available for fracture-to-matrix liquid transfer. The FMX parameter for liquid-phase interaction accounts for channeling of flow as the liquid phase "fingers" through the fracture network. However, this factor probably under represents the wetted surface area of fractures that occurs during condensate drainage in TH models. Other approaches (Ho 1997), such as the *Active Fracture Model* (AFM) (Liu et al. 1998, pp. 2635 to 2636), account dynamically for changes in the influence of condensate drainage on the FMX. In such approaches, the parameter that is analogous to FMX increases with the magnitude of liquid flux in the fracture continuum. Because repository decay heat will generally produce greater liquid flux than that which occurs at ambient conditions, and because condensate flow may be more ubiquitous than ambient percolation in fractures, this dynamic approach results in a larger value of the interaction factor where there is development of condensate flow. As the repository

heat output declines, thermally driven reflux decreases asymptotically toward the ambient percolation levels, and the interaction factor decreases to its previous value. The DS TH calculations supporting TSPA-VA assumed a constant value for FMX rather than the dynamic FMX approach.

The DFM spatially discretizes the space occupied by the fractures and the matrix blocks, using finite-difference grid blocks (or elements). Because the location and morphology of individual fractures are not usually well known, their geometric characteristics are: (1) interpolated from field data, (2) randomly generated, or (3) represented using an idealized geometry. The third approach is commonly used (Buscheck et al. 1991, pp. 316 to 321; Nitao and Buscheck 1996, pp. 748 to 752; Kwicklis and Healy 1993, pp. 4091 to 4102; and Zimmerman and Bodvarsson 1996, pp. 433 to 438). The DFM is, by far, the most computationally intensive of the three approaches described here. Moreover, available data on the fracture networks may not justify using the DFM. The DFM more accurately represents fracture-to-matrix liquid flow and matrix-to-fracture gas flow, particularly at early time when the DKM tends to under-predict mass transfer between the fractures and matrix. The DFM has been used in modeling studies of episodic nonequilibrium percolation events (Buscheck et al. 1991, pp. 316 to 321) and analysis of the G-Tunnel heater test (Nitao and Buscheck 1996, pp. 748 to 752).

The selection of an approach (ECM, DKM, or DFM) for representing FMX must weigh the trade-off between computational complexity and physical accuracy. Relevant factors include the magnitude of liquid flux in fractures, the size of the domain being modeled, and the scale over which predicted results are desired. The ECM is adequate for some scoping calculations. The DFM is probably not practical for repository-scale and mountain-scale calculations, but it can be used to determine phenomenological parameters needed for the DKM. The DFM can also be useful in interpreting the results of laboratory-scale experiments. Complementary use of these three approaches is an effective way of incorporating some of the effects of nonequilibrium fracture-matrix behavior at any practical scale of analysis. Each TH NFE model in Sections 3.2.3, 3.3, 3.4, and 3.6 used the DKM flow model.

The TH models used in support of TSPA-VA are described in detail in the TSPA-VA (CRWMS M&O 1998b, Section 3.5). This section laid the technical foundation for the submodels and temperature correlations developed for the MSTHM as developed for and applied in the viability assessment TSPA and carried forward to the site recommendation TSPA. It also described the development of the mountain-scale TH models used to abstract the gas-phase flux and air mass fraction at the repository horizon before, during, and after repository heating.

Submodels of different scale, flow processes, and dimensionality were used to approximate the physical processes associated with repository thermal loading. Mountain-scale submodels developed for TSPA-VA were used to describe repository edge effects (large scale processes), while DS models were developed to characterize waste package variability (small scale processes) for a point loaded repository design (see Section 3.2.3.3 in this PMR or CRWMS M&O 1999b, Section 3.5.3). The thermal-hydrologic submodel included a DKM representation for heat and fluid flow to capture the effects of thermally enhanced fracture flow towards or away from the repository drifts (see Figure 2-3) during early heating. The TH submodel also included uncertainty in infiltration rate and hydrologic fracture flow properties in order to determine the influence of the ground surface boundary conditions and hydrologic flow

properties on the in-drift variables used by TSPA. Future (wetter) climate states were also applied to the TH models as specified by the UZ F&T PMR (CRWMS M&O 2000f).

The abstraction of the in-drift thermodynamic environment (e.g., waste package temperature and relative humidity) was based on the MSTHM results segregated into six repository subregions (CRWMS M&O 1998b, Figure 3-6). The abstraction TH results computed for each repository subregion were placed in bins (one set for the commercial waste another for the non-commercial waste) based on the time to reach a specified waste package relative humidity (85%) and the waste package temperature at times well after closure (5,000 years). Each bin may contain many waste packages that meet the specified criteria. Therefore, to reduce the amount of data to be analyzed by TSPA, a least-squares minimization is used to find the waste package closest to the mean relative humidity and temperature. The resulting abstraction (one time-history per bin with a maximum possible of 60 bins per repository subregion) is applied in the TSPA supporting models.

The abstracted time-histories of gas flux and air mass fraction were developed for the repository center and edge regions and applied in the incoming gas and water chemistry models in the TSPA total system model.

### 2.2.2 Past THC Modeling

THC modeling work prior to the VA were reported in the *Near-Field & Altered Zone Environment Report* (Wilder 1997, Volume I, Sections 4.5 and 5.4) and the *NF/AZ Models Report* (Hardin 1998, Chapter 5). This previous work focused on how water chemistry evolved within these zones over time on rock-water interactions that result in changed mineralogy, and on precipitates or salts left as the result of boiling and evaporation processes. This work was based on property set understanding, the conceptual designs and the hydrologic framework that existed at that time. All of these factors have since evolved and the specific results of those studies are not of direct value for the current design. However, they provided the framework for methodology development and model testing, as well as identified the issues that needed to be evaluated (e.g., hydrological property changes, mineral-cap formation, CO<sub>2</sub> exsolution).

As reported by Hardin (1998, Section 5.1.1, p. 2), "... The AZ-water-composition model [was] used to estimate the concentrations of major chemical species in water that interacts with the host rock at ambient and elevated temperature along flow paths upgradient from the NFE." One of the models used included dual-permeability (DK) TH processes, and considered evaporation and condensation so that the results are applicable to 2-phase systems where liquid-phase chemistry is of interest. However, the models could accommodate only a few chemical components (e.g., silica) and were limited with respect to the representation of complex processes, such as boiling. The chemical components included the major and minor ions present in J-13 water as well as the silicate minerals. The components included: Na, Si, Cl, S, Ca, F, Mg, Li, Al, P and CO<sub>2</sub> species. The gas phase composition was set to the ambient air composition with added water vapor (total pressure was allowed to vary).

Results of this previous work (Hardin 1998, pp. 5-81 to 5-83) indicated that, although evolution of recharge water compared to the J-13 composition depends on several rate-limited reactions, it is consistent with Yucca Mountain mineral and meteoric water interactions. They also

concluded that sufficient silica could be mobilized by repository TH processes to plug fractures (for the properties and design analyzed, initial porosity of  $3 \times 10^{-4}$  [Hardin 1998, Table 3-7] 30x less than used in Section 3.3). They concluded that minerals would accumulate where boiling occurs, predominantly at the bottom of the isothermal (heat-pipe) zone. Formation of a mineral cap above the emplacement drifts was predicted by those models for a broad range of conditions. This work did not include examination of the durability of the potential mineral cap from processes such as dissolution or seismic effects. While current models have reassessed this conclusion, the modeling work was valid for the conditions considered and helped to identify the need to evaluate this phenomena. Section 3.6.2 discusses the applicability of this work.

Other uncoupled reaction-transport simulations reported by Hardin (1998, pp. 5-70 to 5-73) (assuming saturated fractures and no matrix interactions) showed that dissolution of calcite will occur rapidly, particularly during a transient period of increased CO<sub>2</sub> fugacity, caused by evolution of CO<sub>2</sub> from the rock during the first few years of heating.

The THC modeling and abstraction, as applied to the viability assessment TSPA, are characterized in detail in the TSPA-VA (CRWMS M&O 1998c). The TSPA-VA NF geochemical environment is represented by time-dependent distributions of the gas and water compositions that interact with the waste package and waste form inside the potential repository emplacement drift. The parameters supplied to the total system model included the oxygen fugacity, the solution pH, the total dissolved carbonate, and the ionic strength of the water. These parameters were derived from a 13-component chemical system. The abstracted step change approximation for the time evolution of the four chemical parameters was based on the TSPA-VA thermal-hydrologic models. For each discrete time period, a batch calculation was performed with a geochemical model to determine the appropriate chemical composition of the groundwater during that time period based on the surrounding thermal-hydrologic conditions and the incoming composition of the groundwater reacting with iron oxides. The abstracted time periods were representative of repository center conditions.

Since the VA, THC modeling of the Drift Scale and Single Heater Tests has explored water-gas-rock reactions, including a variety of minerals (calcite, feldspars, clays, and zeolites, in addition to silica polymorphs), as well as gas-phase CO<sub>2</sub> equilibration and transport (Sonnenthal et al. 1998, pp. 57 to 70; Tsang et al. 1999, pp. 4-1 to 4-74). These studies have further quantified effects of CO<sub>2</sub> on water chemistry and on calcite dissolution and precipitation, as well as time- and space-dependent changes in mineralogy and water chemistry in a DK system. In particular, the models predict strong gravity drainage of condensate waters below drifts with greater calcite dissolution in these zones (Tsang et al. 1999, p. 4-46).

The significance of uncertainties raised by past TC work is addressed in Section 3.6.4.2.

### **2.2.3 Past THM Modeling**

Previous THM modeling efforts were focused on determining the impacts of TM on hydrologic and chemical aspects of the NFE. As was true for the TH and THC models, a discussion of the validity or usefulness of results from this previous modeling effort is contained in Section 3.6. However, some of the most useful results of the earlier work included insights into what needed

to be addressed by the models as well as assistance in the development and qualification process. The TM responses of most concern were:

- The closing, opening and sliding of fractures that might impact permeability and thus flow of water through fractures
- The impacts on chemistry as a result of formation of new surface area from fracturing
- Pressure dissolution, and precipitation of minerals in pressure-narrowed fractures
- Microfracturing that could affect drift stability, specifically the size of blocks that might fall, as well as to change the flow characteristics around the drifts
- Time-dependent (long-term, non-elastic “creep”) deformation behavior.

This previous work was largely reported in the *Near-Field and Altered-Zone Environment Report* (Wilder 1997) and the *Near-Field/Altered Zone Models Report* (Hardin 1998).

Previous modeling of mechanical impacts on hydrology focused on fracture impacts, because any changes in rock-mass permeability from TM effects can be attributed to the fractures. Changes to matrix permeability in response to stress and temperature are small (Hardin and Chesnut 1997). Moreover, the hydrologic behavior of a fractured rock mass is controlled by relatively few, well-connected fractures.

THM modeling studies were also considered for the viability assessment TSPA (CRWMS M&O 1998b, Section 3.6.8). The approach taken for this weakly coupled process model was to develop a one-dimensional, mountain-scale, dual permeability model to assess the impact of normal stress driven changes in joint aperture, abstracted from a 2-D mountain-scale TM model, on percolation flux in the fractures below the repository horizon. Shear stress changes were not considered in the analysis. Aperture changes in regions of thermal-mechanical tension and compression were translated directly into corresponding changes in the hydraulic fracture aperture. This in turn affected the flow characteristics in the mechanically altered regions in the NF host rock. The thermal-mechanical alterations in fracture aperture were considered in five discrete time segments from initial emplacement to 750 years after waste emplacement. Subsequently, fracture hydrologic properties in the TH model changed from the initial unaltered state as a function of the same discrete time segments developed in response to thermal-mechanical stresses. The thermal-hydrologic model simulation did not feed back temperature predictions to the TM model. That is, one-way coupling from TM to the TH model was assumed in this preliminary analysis. Fracture hydrologic properties in the TH model were altered at each discrete time increment with the zone of compression surrounding the potential repository horizon increasing with time, while the zone of tension above and below the horizon initially increased then decreased with time. The fracture hydrologic aperture was altered by a factor of two increase or decrease depending on the location of the zones of tension or compression, respectively. The fracture permeability, porosity, and van Genuchten alpha parameter were altered by change in fracture aperture. Parallel plate fractures were assumed in the analysis. It was found in the analysis that fracture liquid flow, matrix and fracture liquid saturation, and temperature were not drastically altered by normal stress changes to fracture aperture.

Laboratory studies (Bandis et al. 1983; Barton et al. 1985) have shown that greater hydrologic impact often results from shear displacement of fractures than from normal displacement. Permanent changes in hydrologic properties or flow paths can result from normal displacement, but they tend to be smaller than those caused by shear displacements. This has been observed in field studies (e.g., Wilder and Yow 1987).

A one-dimensional TH analysis was included in the TSPA-VA Technical Basis Document (CRWMS M&O 1998d, p. 3-152 to 3-157).

The results of thermal-mechanical simulations in the VA were coupled to TH simulations of the potential repository at Yucca Mountain. Past thermal-mechanical simulations (Mack et al. 1989) presented results that identified zones of altered rock where the fracture aperture either increased or decreased by a factor of two. These altered regions were used to update fracture properties at five discrete times (25, 50, 200, 250, and 500 years) during the TH simulation. The properties that were updated, as a result of the changes in fracture apertures, were fracture porosity, bulk fracture permeability, and fracture air-entry pressure (van Genuchten alpha parameter). Comparisons were made between altered and unaltered TH simulations during approximately 1,000 years of heating.

Results showed that the altered and unaltered simulations produced similar trends in fracture flow, liquid saturations, and temperatures. The fracture flow at and below the potential repository was increased by up to several orders of magnitude as a result of condensate drainage in both cases. However, in the altered case, the increased flow in the CHn persisted longer than in the unaltered case. It was postulated that the reduced apertures near the potential repository in the altered case allowed more water to be retained in the fractures because of higher capillary pressures. This subsequently produced larger fluxes through the fractures below the potential repository. The saturation profiles at 500 years of heating supported this hypothesis. In addition, the increased fracture flow was attenuated by 1,000 years of heating in both the altered and unaltered simulations. Finally, the temperature profiles at 500 years of heating revealed that natural convection was attenuated in the altered simulation because of reduced fracture apertures and, hence, fracture permeabilities near the potential repository. While the overall temperature distributions were similar between the altered and unaltered simulations, the temperatures in the altered simulation were slightly higher near the potential repository and more symmetric above and below the potential repository, indicating reduced convection in the compressed zones.

Other more direct formulations are presented in Hardin (1998, pp. 4-33 to 4-35) for permeability changes associated with shear-slip and normal deformation. For permeability changes associated with shear-slip, the resultant change is a function of a scaling exponent (relating in smooth or rough fractures) and a shear offset term resulting from thermal stresses. As previously described, shear alterations tend to impact the horizontal fracture sets. For permeability changes associated with normal deformation, the resultant change is a function of the stress change perpendicular to the fractures, fracture spacing, the initial fracture aperture, and the rock-mass modulus. Each of the models presented is driven by stress changes that result from an imposed temperature field.

Previous modeling efforts recognized that permeability changes in the repository host rock were important; however, no rigorous bases were available to analyze these effects. Models were

based on concepts such as the cubic law, Mohr-Coulomb slip criteria, idealized fracture stiffness, hypothetical scaling relations, and statistical assumptions.

Preliminary calculations have estimated the effect of shear deformation on fracture permeability (Blair and Berge 1997). Potential zones of slip were predicted for vertical and horizontal fractures. Slip on fractures due to induced shear stresses, were expected to be limited to a few small zones that are within about one drift diameter of the drift wall. Because the design has changed, the significance of this past work is more in development of the techniques than in predicted performance.

This work also supported model confidence building, and provided a basis for design and analysis of the in situ thermal tests (Section 3.6), as well as laboratory studies. The goal of the work was model confidence building. See Hardin (1998, Sections 4.3.4.4 and 4.4.2.2) for detailed description of these efforts.

Using a continuum approach, Blair and Berge (1997) calculated that significant TM effects on permeability within the DST may extend to a distance of several tens of meters from the drift. They concluded that enhanced permeability is likely in regions of increased thermal-stress gradients, so that a region of increased permeability may accompany the thermal pulse as it travels outward from the heat source. The work reported in Section 3.5, which uses a distinct element approach, is a significant advance in realism of the calculations.

Other laboratory work that has supported development of the THM models were reported by Martin et al. (1997) for laboratory experiments that investigated creep in Topopah Spring Tuff samples. The observed creep deformation was consistent with time-dependent crack growth. Blair and Berge (1995) have identified time-dependent, inelastic crack closure in response to stress that was oriented perpendicular to the cracks.

The effect of radiation on the THM behavior of the rock is uncertain. The radiation field is expected to affect only rock exposed on the surface of excavated drifts and to penetrate only a few centimeters into the rock. If spalling occurs, the rubble will bulk-up and form a radiation shield. Blair et al. (1996) tested over 40 samples of Topopah Spring Tuff, TSw2, and found that radiation may have caused degradation of fracture-filling and cementing minerals, which are thought to be composed primarily of carbonates. This could affect long-term deformation of rock at the wall of the emplacement drifts.

The significance of uncertainties raised by past TM work is addressed in Section 3.6.4.3.

## **2.3 THERMAL HYDROLOGY AND COUPLED PROCESSES WORKSHOP SUMMARY**

An M&O workshop on thermal hydrology and coupled processes (THCPs) for performance assessment (PA) was held on March 24 and 25, 1999 in Albuquerque, New Mexico. The topics covered at the workshop were thermal effects on flow, thermal effects on emplacement-drift seepage, THM processes, THC effects, and LADS. The discussions resulting from the LADS studies included a dissemination of the details associated with the EDA-II. The goal of the workshop was to develop work plans that would address the remaining issues for study that require further understanding to support the next Total System Performance Assessment for Site

Recommendation (TSPA-SR). The results of this workshop and its analyses established the direction and scope for this PMR, the UZ F&T PMR, and the EBS PMR.

The workshop was organized around issues for THCPs that had been raised in connection with the previous TSPA-VA and recently established criteria issued in the form of IRSRs by the NRC. Comments on the treatment of thermal-hydrology in TSPA-VA were received from the Performance Assessment Peer Review Panel, the NRC, the DOE through its Management and Technical Services contractor, and formal reviews of the TSPA-VA. In addition, some issues were identified internally with respect to TSPA-VA by the M&O. Criteria for acceptability of this component of TSPA in terms of a future LA have been issued by the NRC in the form of several IRSRs. In particular, the following IRRS documents were used to identify open issues for THCPs in TSPA:

- *Issue Resolution Status Report Key Technical Issue: Evolution of the Near-Field Environment*, Revision 2 (NRC 1999a)
- *Issue Resolution Status Report Key Technical Issue: Thermal Effects on Flow*, Revision 2 (NRC 1999b)
- *Issue Resolution Status Report Key Technical Issue: Total System Performance Assessment and Integration*, Revision 1 (NRC 1998)
- *Issue Resolution Status Report Key Technical Issue: Repository Design and Thermal-Mechanical Effects*, Revision 2 (NRC 1999c).

The key or most important issues, as identified from comments on TSPA-VA (DOE 1998, Volume 3) and the above NRC IRSRs, formed the bases for discussions at the workshop. An additional mechanism to ensure completeness in the coverage of THCP topics for TSPA is the features, events, and processes (FEPs) screening and scenario-development approach (see Section 2.5).

The issues presented at the workshop were discussed, modified, and agreed upon by the workshop participants. These issues are summarized below. Note that at the time of the workshops, the scope of the NFE had not been finalized in relation to other PMR topics, specifically the UZ F&T and EBS PMRs. Therefore, some of the issues discussed cover issues that are beyond the current scope of this PMR.

Seepage issues centered on how seepage may enter the emplacement drift before, during, and after the thermal perturbation. The TSPA parameters of interest include both seepage fraction and seepage-volume flow rate. Of particular concern, is how a pulse of water (possibly driven by repository decay heat) may penetrate the heat-transfer zone surrounding the emplacement drifts. A discussion of how this process may be facilitated by heterogeneity was also considered by the participants at the workshop. At that time, it was decided that future sessions of the workshops would consider DS heterogeneity in the coupled-process models used to estimate the impact of the thermal period on drift seepage. For TSPA-SR, thermally enhanced percolation flux in the NF host rock above the crown of the drift is to be abstracted from the multiscale TH model. The abstracted percolation flux provides a direct input into the TSPA seepage model. As

indicated in Section 3.2.2.1, the multiscale TH model being used for TSPA-SR applies homogeneous fracture properties in the NF host rock. The EBS PMR also describes the multiscale TH model and in-drift results.

For the issue of thermal effects on flow (TH processes), the participants decided that the impact of the overall heat pulse on mountain-scale (liquid-phase) flow fields below the repository horizon would be considered (now in the UZ F&T PMR, CRWMS M&O 2000f). (The focus was on below-drift locations, because for the EDA-II design, heat pipes above the drifts will be limited and shedding will increase flow below the drifts.) Previous TSPAs found that the thermal perturbation subsided after a few thousand years. However, these studies considered a higher areal mass loading (AML) than the repository design under consideration for site recommendation (CRWMS M&O 1999a, Table 6-3). For the critical time period of regulatory concern of 10,000 yr., the impact of the thermal perturbation would be considered using a reference repository design analogous to EDA II (CRWMS M&O 1999a, Table 6-3), base-case infiltration rates and climate states specified in the UZ F&T PMR (CRWMS M&O 2000f, Section 3.5), and appropriate conceptual flow models applied in a thermal-hydrological, mountain-scale model (CRWMS M&O 2000t).

The issue of THM processes centered on how the thermal pulse would affect the vertical and horizontal fracture permeabilities, both on the scale of the drift and of the mountain. All mechanical effects were ignored in TSPA-VA, which was based on a simple 1-D abstraction that showed that mechanical effects did not alter fracture flow significantly below the repository (Ho and Francis 1998). The single heater test, the LBT, and the DST, all provide valuable information on the possible movement of fractures induced by thermal stresses. These tests can be used to validate rock-joint constitutive models. It was decided that the potential influence of adding mechanical effects to thermal-hydrology would be abstracted from a thermal-mechanical calculation (CRWMS M&O 2000d) and introduced into the TSPA models, if the effects are found to be significant.

The issue of THC centered on how the thermal perturbation may drive chemical processes in the surrounding host rock and how this impacts seepage-water chemistry and gas-phase composition and flux at the emplacement-drift wall. Alterations of fracture hydrological properties above the emplacement drifts may also impact seepage fractions and seepage-volume flow rates. Discussions of THC processes included mineral-water reactions that alter host-rock properties, and result in different chemical components entering the emplacement drifts. Near-field host rock property alterations (e.g., by precipitation and dissolution reactions) provide the basis for how the in-drift physical and chemical environment evolves with time before, during, and after the thermal period.

Each of the process-level models (TH, THC, THM seepage) used to characterize the coupled processes were discussed at the workshop in the context of the thermal tests ongoing at the ESF and other field-test results. The DST, SHT, and the LBT, all allow the opportunity for conceptual flow-model analysis (ECM or DKM), boundary-condition testing, and assumption testing related to flow-property specifications, initial conditions, and other important TH process issues. Personnel from the thermal testing activities were present at the workshop in order to specify ways that PA may potentially include thermal-testing results in process-level models and abstractions.

## 2.4 SUMMARY OF OTHER VIEWS AND ALTERNATIVE CONCEPTUAL MODELS

The NFE involves complex coupling of thermal-hydrological-chemical-mechanical processes (THCM). Properly incorporating this complex coupling in fully-coupled models is very challenging and computationally demanding. Although progress is being made in developing more fully-coupled models, to date, most models applied to the NF have relied on various simplification approaches, including focusing on only one or two degrees of coupling (e.g., thermal-hydrological, or thermal-hydrological-chemical) with further simplifications as to how the coupling is reflected. For instance, if there is direct coupling between THC, a limited number of chemical species were commonly addressed, or simplifications of bounds on how the species are represented are incorporated into the models. Furthermore, the models commonly incorporate only forward coupling, such as considering the evolution of minerals under TH conditions, without coupling directly back into the TH analysis, specifically addressing permeability changes due to mineralogical changes. Therefore, iterative analyses are used to assess this interactive coupling. As a result, there are many different or alternative approaches that have been or could be applied to evaluations of the NFE. The basic tools available all rely on some combination of mass and energy conservation, as well as chemical interaction evaluations based on thermodynamic understanding of chemical species. However, the approaches to deal with the complexity of the coupling and the conceptualization of the processes can be quite different.

As long as there is heat associated with the design, the kinetics and coupling of the THCM processes are very much dependent on repository design, emplacement modes and operational sequences (loading), as well as ventilation. These engineering factors have been evolving. Furthermore, understanding of the properties of Yucca Mountain have also been evolving. Many of the past analyses of the NF that can be compared to those reported in this PMR have used different inputs and parameters. Therefore, making direct comparisons between conclusions from the various approaches is not very useful. What is useful is to understand the differences in approach or fundamental assumptions. Rather than trying to compare the specific results or even details of the various alternatives, this report will review the conclusions of reviews of the modeling processes that have been used to analyze the NFE. Other views will then be discussed in this context.

Although the processes are complexly coupled, for discussion purposes they will be grouped into essentially simply coupled processes related to thermal-hydrology, thermal-hydrology-chemistry, and thermal-mechanical processes. There is obvious coupling between these, but these single coupled processes facilitate discussion and reflect the simpler coupling that is often performed in iterative analyses.

Alternative TH, THC, and THM models are described in the following Sections (Sections 2.4.1 through 2.4.3). Section 2.4.4 summarizes the NFE-related issues developed by the TSPA Peer Review Panel. Section 2.4.5 summarizes the Expert Elicitation on NF/AZ Coupled Effects. Finally, Section 2.4.6 summarizes issues discussed in correspondence of the Nuclear Waste Technical Review Board and the NRC's Advisory Committee for Nuclear Waste (ACNW).

### 2.4.1 TH Alternative Models

The TH coupling of heat and mass transfer can be treated in a number of ways. For heat transfer, conduction models are the most straightforward, however; these fail to incorporate the coupling of heat transfer with moisture that can be dominant within the NFE. In regions where there is not active boiling or condensation, the conduction models can be used with confidence and are computationally less challenging. For the NFE, most of the approaches rely on TH models that include the impacts of latent and advective heat transfer. Different approaches to model the physical processes involving flow have included Equivalent Continuum, Discrete Fracture, and Dual Permeability (or porosity). For the NF, most of the analyses, including those reported in this PMR, have relied on DK (continuum) models with AFM to account for interactions between fractures and matrix.

Different or alternative views regarding the TH coupled model approach also relate to the properties and to the approaches of how to treat the interaction between fracture and matrix.

A peer review of the TSPA-VA (CRWMS M&O 1999c, p. 47) identified several concerns, if not alternative views. They noted that the use of van Genuchten "...model is not justifiable in the present context.", because it ignores a number of processes, including: unstable nature of gravity-driven infiltration; hysteresis during episodic flow, small scale (sub-grid) heterogeneities; effects of connectivity of fracture and matrix continua; and effect of abrupt changes in properties on transport fluxes. Further, they note that the fracture-matrix factor, while reasonable and justified to account for a variety of processes for which the physics are not directly incorporated in the models, is "...devoid of convincing physical meaning... This is not satisfactory and reflects a lack of understanding of the actual physics of the process and, more generally, the lack of progress in the scale-up of two-phase flow in the fractured system..."

The fracture-interaction factor reflects the observation that the contact area for interaction between water in fractures and the matrix is not the same as the fracture-surface contact area. There are both laboratory and field studies that support the understanding that flow in fractures does not occupy the entire fracture-system volume. Most of the studies, including laboratory studies, were under isothermal conditions, and many laboratory studies relied largely on artificial fracture studies (Nicholl et al. 1994; Liu et al. 1998). Currently, the model, called the AFM, uses a factor that varies as a function of saturation within the fracture. The AFM is intuitive, but is based essentially on inverse modeling to match saturation data from the field and not on a physical basis from laboratory studies, etc. (CRWMS M&O 2000f, Section 3.4.1.4.1).

These issues are mainly related to the UZ F&T and are discussed in that PMR, as well as in the EBS PMR, where the multi-scale abstraction is discussed. However, the issues relate to the NF in that these are the models and approaches that are used to determine the TH coupling within the NF, and two-phase flow is a dominant process within the NFE. Also, directly related to the NF is their comment that the model approaches ignore differences between wetting and drying cycles.

Some of the differences between views or approaches relate to the differences in design. During the TSPA-VA, the design did not include drip-shields. As a consequence, the peer-review panel (CRWMS M&O 1999c) comments included concerns about seepage being decoupled from the

TH. TH effects are considered for seepage within the UZ F&T PMR. Furthermore, a key assertion or basis of determinations of the impact of the NFE on performance is that the drip shield will perform its function throughout the period when the NFE is hot so that decoupling of processes regarding flow is justified. The impact of the NFE on flow is of concern only after the drip shields fail (CRWMS M&O 2000s). Therefore, the couplings that must be considered are those aspects of the NFE that cause permanent or long-lived changes to flow and transport (usually associated with coupling with chemistry or mechanics, not merely TH). Thus, one of the different approaches or views deals with whether the drip-shield lifetime projection is justified (the evaluations of drip-shield lifetime are discussed in the EBS and WPD PMRs).

The NRC use of MULTIFLO models found performance to be dominated by variation of UZ parameters (Hughson and Green 1999). This implies that, although not the only source of uncertainty, the understanding and accounting for the natural-system heterogeneity is of primary importance in evaluating repository performance. This natural-system heterogeneity cannot be designed away, and is not addressed directly in the NFE models. Sensitivity studies have been done, but these assume that there is not spatial or temporal coupling of the impacts of heterogeneity on other parts of the system. Some work, as discussed below in this section, indicates that this assumption may not be valid and that the THC responses can be influenced by adjacent regions with significantly different natural or engineered properties.

An additional alternative view deals with how well TH (as well as THC) processes are understood by the YMP. In a 1999 letter to DOE, the NWTRB expressed concern that elevated temperatures (particularly above the boiling point) increased uncertainty (Cohon 1999). They state, in part, "... thermal loading has a larger effect than any other single design attribute. ..."

"Unfortunately, the understanding of water mobilization and migration processes and effects during this initial high-temperature period is still far too limited to engender a reasonable degree of confidence. Some insight into thermal-hydrological response has been gained from in situ thermal tests. However, important results from the DST will not be available for several more years."

"In general, the cooler the repository, the lower the uncertainty about heat-driven water migration and the better the performance of waste package materials. Above this temperature, technical uncertainties tend to be significantly higher than those associated with below-boiling conditions."

While this view is primarily focused on TH, it can be applied more generally to THC where elevated temperatures lead to higher chemical reaction rates and, thus, lower kinetic barriers to reaching equilibrium for all kinetically inhibited reactions. The implications for uncertainties is better made in the broader context, i.e., in Section 2.4.2, TH/THC Alternative Models.

There are also differing views regarding the connectivity of the fracture system. As reported by Sagar et al. (1995, p. 4), there are questions regarding potential for pressure build-up that may suggest that "...fractures in a welded tuff are not well-connected and that gas pressures will in fact build up during the heating period...". No thermal tests have been conducted to date within the Tptpll, where the majority of the potential repository would be located.

Another area of differing views relates to the potential for heat-pipe formation. Green et al. (1991, pp. 164 to 165) reporting on laboratory experiments and minimal analyses of glass-bead experiments state "Based on these analyses and observations.... A heat-pipe process will occur only in the matrix block nearest the heat-generating source during the early stages after waste emplacement. Liquid water will only cross the fracture [to the next matrix block] when the moisture content of the matrix adjacent to the fracture is sufficiently high... to cause the fracture to saturate. Prior to this, the matrix block on the heated side of the fracture will desaturate thus denying the heat-pipe process the return flow of liquid water necessary to continue." Other questions regarding heat pipes were raised by Manteufel et al. (1993, p. 577) where they conclude that heat pipes will be negligible because of the low matrix permeability. The field test results address these issues, but the issue is fracture-matrix-block-geometry specific (vertically continuous matrix blocks would not be bound by these effects for horizontal fractures) and therefore the issue remains to be address by tests in the Tptll.

One of the principal means to validate the YMP NFE models is comparison with results of field tests, particularly the Drift-Scale Test. Hughson and Green (1999) used model analyses supported by the MULTIFLO code to evaluate the DST. They raised the concern (Hughson and Green 1999, p. 1-5) that inadvertent and unmeasured loss of moisture through the bulkhead, which would not be experienced under repository conditions, may compromise the utility of the test. They noted that although the DST was designed to address model hypotheses, that additional uncertainty caused by heat and water mass loss through the bulkhead

"...may render the DST an open system which can lead to increased modeling uncertainty. This modeling uncertainty can lead to increased uncertainty in performance assessments that are based on conceptual models evaluated and calibrated against the DST."

While the increased uncertainty caused by losses across the bulkhead cannot be eliminated, nevertheless the test results have been useful in building model confidence (see Section 3.6 and CRWMS M&O 2000a). Based on data collected since that time, it is judged that the test is still useful for model validation, although there are uncertainties introduced by this moisture loss.

In the discussion of coupling (Section 2.1), it was stated that TH processes are always strongly coupled in both directions. In an analysis by Manteufel et al. (1993, p. 581, Figure 2), the coupling is shown as primary in the T → H direction, but secondary in the H → T direction.

The significance of uncertainties revised by alternative TH views is addressed in Section 3.6.4.

#### **2.4.2 TH/THC Alternative Models**

Because of the complexity of coupling when considering THC, there are even greater differences in approaches or views regarding this coupling. This is reflected in the TSPA-VA peer review comment "Although the NFGE (near-field geochemical environment) models are logically constructed, there is little basis for accepting the results as indicative of repository behavior. The complexity of the models, the large uncertainties in parameter values, and the clearly coupled phenomena suggest that it is unlikely that the present NFGE model captures or usefully portrays the repository conditions in the near-field." (CRWMS M&O 1999c, p. 60).

As discussed in Sections 3.1.3 and 3.3, the analysis of THC processes for the DST used two approaches. One considered a relatively complete set of mineral assemblages and aqueous species needed to fully describe the NFE. The second included a less complex set of minerals and aqueous species. The analysis that included the less complex suite of minerals and aqueous species matched the CO<sub>2</sub> and water pH data from the DST. If the models properly incorporate all physical processes, appropriate properties, details of the test, and accurate thermodynamic and kinetic data are available, then the model with more complex mineral assemblages would be expected to more closely match the data, but it did not. Possible reasons for this result, as discussed in Section 3.1.3 and 3.3, are uncertainties in rate parameters and thermodynamic properties, and the short duration of the test.

As noted by Rosenberg et al. (1999, p. 7-8), limitations in THC modeling result, among other reasons, from limits in the geochemical data basis for high ionic strength solutions at elevated temperature. A modeler must presently choose a data file from several that are available. Each such file presently carries one of the following sets of limitations:

1. Includes essentially all requisite chemical species, covers the necessary temperature range, but requires use of a thermodynamic activity coefficient model that is only valid for dilute solutions.
2. Is valid for concentrated solutions, covers the necessary temperature range, but includes only some of the requisite chemical species.
3. Is valid for concentrated solutions, includes most of the requisite chemical species, but is, limited to a temperature of 25°C.
4. Includes essentially all requisite chemical species, covers the necessary temperature range, and can be used for concentrated solutions, but many of the activity coefficient model parameters are estimates not obtained from experimental measurement or a generally accepted estimation methodology.

The difficulty arises in that modeling of concentrated solutions requires a host of additional data (e.g., Pitzer interaction parameters) that is not required to treat dilute solutions. To model a complex system, the required quantity of such data can easily dwarf the required quantity of standard state thermodynamic data (e.g., equilibrium constants). Pitzer parameters are required for most pairs and triplets of chemical species in the modeled system.

In the THC model simulations for the DST and for predictions of THC processes accompanying waste package heating, completed dryout has occurred. Therefore, in these areas and in adjacent regions, the remaining liquids reached high ionic strengths. However, over much of the range of liquid saturation, and the regime of mineral dissolution and precipitation, the ionic strength of the modeled waters is quite low. The model results have shown that higher ionic strengths are reached only when liquid saturations are typically less than 1 percent and are, therefore, basically immobile (ignoring long-term changes in the local TH field) and less important to fundamental changes in seepage chemistry and permeability modification (Section 3.3). Water seeping into boreholes in the Drift Scale Test has been characterized by fairly low concentrations of aqueous species (CRWMS M&O 2000b, Section 6.2.7.3.1, Table 9).

The low saturation, high ionic strength regime is important for predictions of the final salts expected to be formed, especially within the EBS. If salts that formed in the NF during dryout have sufficiently different dissolution rates, their specific identities become more important once rewetting takes place during cooldown. In that case, the water compositions would most likely be dominated by dissolution of halides relative to sulfates, carbonates and silicates. Such behavior is not included in the current NF THC models.

Murphy and Pabalan (1994, p.3-38) note that there is an apparent discrepancy between dissolution-rate parameters determined in the laboratory and those deduced from field studies or natural-systems analyses. They point out the need to determine whether the kinetic models used should rely on near-equilibrium or far-from-equilibrium data, as some models do a better job of explaining one type of data than they do the other. They also point out the need to use consistent data sets.

Kinetic data (e.g., rate constants and activation energies) are currently available for many important rock-forming minerals. Generally, these are obtained from mono-mineralic laboratory experiments (e.g., in systems comprised of a sample of a single mineral along with distilled water or a simple pH buffer solution). In the case of minerals, for which little or no kinetic data are available, reasonable (e.g., order of magnitude) estimates for rate constants can often be inferred by comparison to known data for similar minerals. The larger problem in dealing with mineral-water kinetics is the dependence of rates on reactive surface areas (rates are proportional to reactive surface areas). No simple, direct methods exist for the measurement of the reactive surface area of a mineral in an actual rock. Uncertainties in reactive surface areas may span several orders of magnitude. Plug-flow reactor experiments, using crushed quartz and devitrified-crushed Topopah Spring Tuff (Johnson et al. 1998), have been useful for refinement of reactive surface areas and other kinetic constraints. However, under unsaturated boiling conditions, the character of water-rock reactions may be different from saturated systems, and there are, as yet, not completely analyzed experiments that can be used to further refine the reactive surface areas and other aspects of mineral precipitation under boiling conditions.

Reaction kinetics control the rate of approach to chemical equilibrium. The equilibrium state depends only on thermodynamic data. If a reaction approaches equilibrium rapidly on the time scale of interest, even relatively large errors in rate law parameters (including the reactive surface area) may not be significant to modeling the system. It may be proper to model such a reaction as approaching equilibrium instantaneously, thus, obviating the need for corresponding kinetic data. Reaction rates are accelerated by higher temperatures according to the Arrhenius activation energy principle. Thus, the consequences of uncertainties in kinetic data (including reactive surface areas) and even the need for such data tends to diminish at higher temperature.

One of the THC assumptions or inputs that is subject to alternate views is the relevant water chemistry used as input to TC and THC model simulations. Primarily, a water composition from the J-13 well in the same stratigraphic unit as the potential repository horizon has been used in TC simulations either directly or modified by evaporation or dilution. Compositions of several evolutions of J-13 water (concentrated, saturated, dilute, and acid-buffered) are shown in the Waste Package PMR (CRWMS 2000a, Table 3-2). Some previous coupled THC simulations for the DST (CRWMS M&O 2000b) and Single Heater Test (CRWMS M&O 1999d, Chapter 10) have used unsaturated zone pore water compositions because pore waters represent most of the

in-situ water, and geochemical arguments suggest that water flowing in fractures is likely to have largely equilibrated with pore waters in the PTn hydrogeologic unit. Simulations of THC processes described in this PMR (Section 3.3) and the supporting AMR (CRWMS M&O 2000b) used pore water from the Tptpmn unit in the potential repository horizon from rock in the vicinity of the DST. The differences in view as to which water composition is appropriate for calculations of THC in the NFE reflect differences in view of the hydrological system and what the composition would be of water flowing in fractures under ambient conditions. (This is problematic because of the inability to collect water from fractures for chemical analyses.) The chemistry of the water collected from the DST, which had most likely flowed through fractures, indicates that the water was not a simple mixture of the condensed water and the pore water. The water reacted with silicate minerals and calcite in the thermal setting of the test. CO<sub>2</sub> fugacity is also an important chemical uncertainty in the THC models, since the acidity of seepage water can be affected by it (CRWMS M&O 2000b).

As discussed in Section 3.3, model approaches have had to simplify the coupling in order to solve the problems. As noted by Hardin (1998, p. 8-12), "The different THC simulation approaches ...have shown that conflicting results arise when simulations that consider only aqueous processes are compared with simulations that include boiling processes but do not incorporate a full set of chemical components and reactions".

Another view, which on the surface may appear to be significantly different than that reported in this PMR, deals with the potential to plug fractures. Hardin (1998, Section 5, p. 82) concluded that "...sufficient silica would be mobilized by repository TH processes to cause significant local changes in fracture porosity." They postulated formation of a mineral cap above the emplacement drifts. Laboratory studies (Daily et al. 1987) have demonstrated fracture plugging. This is significantly different than conclusions reached in this PMR. These differences are potentially related to two fundamental changes in design and understanding that have taken place. The EDA-II design incorporates lower temperatures, so that the amount of water mobilized by the thermal pulse is reduced and, perhaps more fundamentally, the current estimate of fracture porosity is about 30x higher than used in earlier calculations. The current model also includes more components and physical processes than the earlier model.

A model proposed by Matyskiela (1997, pp. 1115 to 1118) suggests that silica precipitation in the rock matrix adjoining fractures will strongly reduce the permeability of the matrix, resulting in significantly decreased imbibition of percolating waters. The times for strong silica sealing of the matrix wall for a vitric tuff were five years for a solution having 350 ppm SiO<sub>2</sub> and 105 yr. for a solution having 125 ppm silica (SiO<sub>2</sub>). For a devitrified tuff, it was estimated that cristobalite dissolution followed by quartz precipitation would lead to a 1 mm-thick quartz fracture coating in about 30 yr. It is clear that several factors would immediately reduce the magnitude of the effects described by Matyskiela. First, the potential repository would be located in a devitrified tuff where the rates of reaction are orders of magnitude slower than for volcanic glasses. Second, the proposed model considered the system as fully saturated, maximizing the reactive surface area, the water available for reaction, and the diffusion coefficient. In an unsaturated system, only part of the fracture area would be contacted by water, so that the process would have to take place for much longer periods to actually affect a large part of the fracture surfaces. Third, it is considered by Matyskiela that the fracture water will have higher silica concentrations than matrix pore water, thus leading to a diffusion gradient into

the matrix. However, no clear reason exists for the fracture water to have a higher silica concentration, because it originated as pure condensate (zero SiO<sub>2</sub>) that has drained back toward the heat source, increasing its silica content through wall-rock reactions. Because the system is unsaturated, there is little driving force for convection, as in a single-phase hydrothermal system. A quantitative analysis of this problem was explored in Section 3.3 of this PMR and by Lichtner et al. (1999), who also questioned the interpretations and conclusions presented in the Matyskiela paper.

#### **2.4.3 THM Alternative Models**

The THM analyses have indicated that shear displacements can impact permeability, but that coupling to THC will not be strong since the additional surface area for reaction is not expected to be greatly increased. Reports on laboratory experiments of sheared rock (Mohanty et al. 1994, p. 258) have concluded that permeability changes due to shear displacements "...can be attributed primarily to the formation of fine materials." This would greatly increase the potential for coupling between TM and C.

Further, Mohanty et al. (1994, p. 4-1) reported on experiments with Apache Leap Tuff, noted "Forward and reverse normal stress showed a definite hysteresis in fracture permeability, with a similar trend being observed from mechanical aperture measurements." The THM calculations reported in this PMR have focused on shear displacements, because the normal displacements were assumed to be largely recoverable (elastic response) and resulting permeability changes of lesser magnitude than those associated with shear. However, the work of Mohanty et al. (1994) may indicate that normal stress displacements can not be ignored.

As noted, many of the alternate approaches or views deal with how to simplify coupling. The THM models used in the NFE PMR have included simplifications in coupling TH to M.

Other, more fully coupled THM approaches have also been developed. For example, work conducted in conjunction with the international Development of Coupled models and their validation against experiments in nuclear waste isolation program by countries developing repositories includes development of an analytical solution for coupled THM behavior by Rehbinder (1995) and a study of THM behavior of sparsely fractured rock by Nguyen and Selvadurai (1995). In addition, Jiao and Hudson (1995) have presented a fully-coupled model for engineered systems in rock. Unfortunately, the simpler TH algorithms included in these saturated-zone simulations are not adequate for analysis of THM behavior in a partially saturated, fractured-rock mass.

#### **2.4.4 TSPA Peer Review Panel**

The TSPA Peer Review Panel (the Panel) was formed to provide a formal, independent evaluation and critique of the TSPA-VA for the potential high-level waste repository at Yucca Mountain. The objectives of the Panel were to describe the technical strengths and weaknesses of the TSPA-VA, and to provide suggestions for improvement.

The Panel conducted a phased review over a two-year period to observe the development of the TSPA-VA and to review the completed TSPA-VA. During development of the TSPA-VA, the

Panel submitted three interim reports with recommendations and comments on the process models, model abstractions, and draft documentation for the TSPA-VA. The Final Report Total System Performance Assessment Peer Review Panel (CRWMS M&O 1999c) includes the major points from the three interim reports, updated as appropriate, as well as new findings that the panel developed during its review of the TSPA-VA. Key issues described in the Final Report that are pertinent to this PMR are compiled in Appendix B.

#### **2.4.5 Expert Elicitation**

The *Near-Field/Altered Zone Coupled Effects Expert Elicitation Project* (CRWMS M&O 1998a) was established to help quantify the large uncertainties associated with thermal, hydrologic, mechanical, and chemical processes. The expert elicitation panel was tasked to consider how these processes occur, both temporally and spatially, and over what range of values the hydrological properties (for example, fracture permeability) may be influenced.

The elicitation panel examined process models and experimental data on coupled processes from the single heater test. They considered THMC processes, potential changes to hydraulic interactions between fractures and the rock matrix, and effects of rockfall. Based on the results of the elicitation, the potential for thermally driven alteration of fracture properties (for example, permeability) fell within the range of the natural, spatial variability of the system. The net effect of combined THM and THC permeability changes would be to suppress convective heat transfer at the center of the repository block and increase lateral diversion of condensate on the downdip portion of the repository periphery. The panel concluded that the mechanical effects would tend to be reversible upon cooling, with the possible exception of horizontal changes in permeability caused by shear stress, but that chemical effects will be more permanent. The panel indicated that the FMX parameter used in the DK models might also be affected, because of chemical precipitation or dissolution. Although this effect may be permanent, the magnitude of such changes is uncertain.

Appendix B includes a list of the key issues pertinent to this PMR that were reviewed and discussed by the panel members. A full description of the expert elicitation is provided by the NF/AZ Coupled Effects Expert Elicitation Project (CRWMS M&O 1998a).

#### **2.4.6 Summary of Issues from Affected Organizations**

This PMR also addresses other key issues related to the NFE. These issues were identified by a review in the past two years of ACNW and Nuclear Waste Technical Review Board (NWTRB) meeting summaries and correspondence; Viability Assessment Volume 3, TSPA Peer Review Panel documentation; NRC comments on TSPA-VA: Expert Elicitation recommendations; licensing correspondence files for NRC; State and County correspondences; and issues noted by DOE's Management & Technical Support contractor. Appendix B provides a summary of key issues and describes how each issue is addressed in this PMR.

Furthermore, by letter to DOE (Cohon 2000) the NWTRB expressed "...The Board's understanding is that current performance assessment models may not adequately describe the interaction of heat, water flow, chemical reactions, and mechanical disturbances with rocks near heated emplacement drifts. If this is the case, then sensitivity analyses could fail to identify

coupled processes as principal factors. The Board recommends that DOE reexamine its evaluation of the importance of coupled processes in its identification of principal factor.”

## 2.5 FEATURES, EVENTS, AND PROCESSES

The initial set of FEPs has been created for scenario development in the YMP TSPA by combining lists of FEPs identified as relevant to the YMP. This FEPs list consists of 1,261 entries from the Nuclear Energy Agency working group, 292 FEPs from YMP literature and site studies, and 82 FEPs identified during YMP project-staff workshops. These FEPs are organized under 151 categories, based on NEA category headings, resulting in a total of 1,786 entries in the YMP *NFE FEPs* AMR (CRWMS M&O 2000e, Section 1.2). The FEPs have been identified by a variety of methods, including expert judgment, informal elicitation, event tree analysis, stakeholder review, and regulatory stipulation. All potentially relevant FEPs have been included, regardless of origin. This approach has led to considerable redundancy in the features, events, and processes (FEP) list, because the same FEPs are frequently identified by multiple sources, but it also ensures that a comprehensive review of narrowly defined FEPs will be performed.

Each FEP has been identified as either a primary or secondary FEP. Primary FEPs are those for which detailed screening arguments are developed. The classification and description of Primary FEPs strives to capture the essence of all the secondary FEPs that trace to the primary. Secondary FEPs are either FEPs that are completely redundant or that can be aggregated into a single Primary FEP. The resulting 310 primary FEPs have been assigned to associated PMRs. The assignments are based on the nature of the FEPs, so that the analysis and resolution for screening decisions reside with the subject-matter experts in the relevant disciplines. The resolution of other than system-level FEPs are documented in AMRs prepared by the responsible PMR groups. The assignment to the associated PMRs was made initially during a series of PA and PMR workshops. The initial assignment was then revised and now is consistent with the portion of the NF as covered in this PMR. There is overlapping, such that some FEPs are covered in more than one PMR. This section summarizes the screening decisions associated with the FEPs for the NFE PMR group. Details of the screening processes are documented in the *NFE FEPs* AMR (CRWMS M&O 2000e). Chapter 4 and Appendix D provide detailed mapping of NF related KTI subissues to this and other PMRs.

The scope of the FEPs screening is to identify treatment of primary FEPs affecting the NFE. The FEPs deemed potentially important to repository performance are evaluated, either as components for the TSPA or as separate analyses in the *NFE FEPs* AMR (CRWMS M&O 2000e). The scope for this activity involves two tasks, namely:

- Task 1: Identify which FEPs are considered explicitly in the TSPA (called included FEPs) and in which AMR report(s) these FEPs are addressed.
- Task 2: Identify FEPs not included in TSPA (called excluded FEPs) and provide justification for why these FEPs do not need to be a part of the TSPA model.

Of the original list of FEPs, 26 have been identified as primary in relation to the NFE. These FEPs are best dealt with at the system level; do not fall within other PMRs; or are directly

addressed by regulation, assumptions listed in the regulations, or in background information used in development of the regulations.

NFE FEPs that are either fully or partially included in the TSPA-SR, based on the screening, are the following:

- 1.1.02.00.00: *Excavation/construction* (Section 3.5 includes effects on seepage)
- 1.1.02.02.00: *Effects of pre-closure ventilation* (Sections 3.2, 3.5)
- 2.1.08.01.00: *Increased UZ water flux at repository* (Sections 2.2.1, 3.2.3, 3.3, 3.5)
- 2.1.08.02.00: *Enhanced influx* (UZ F&T PMR)
- 2.1.08.03.00: *Repository dry-out due to waste heat* (Sections 3.2, 3.3)
- 2.1.08.10.00: *Desaturation/dewatering of the repository* (Section 3.2)
- 2.1.08.11.00: *Resaturation of the repository* (Sections 3.2, 3.3)
- 2.1.09.01.00: *Properties of potential carrier plume in the waste and EBS* (EBS PMR)
- 2.1.09.12.00: *Rind (AZ) formation in waste, EBS, and adjacent rock* (Sections 3.2, 3.3)
- 2.1.11.01.00: *Heat output/temperature in waste and EBS* (Sections 3.2, 3.3, 3.4, 3.5)
- 2.1.11.02.00: *Non-uniform heat distribution/edge effects in repository* (Section 3.2)
- 2.2.07.10.00: *Condensation zone forms around drifts* (Sections 3.2, 3.3, 3.4)
- 2.2.07.11.00: *Return flow from condensation cap/resaturation of dry-out zone* (Sections 3.2, 3.3, 3.4)
- 2.2.08.03.00: *Geochemical interactions in geosphere (dissolution, precipitation, weathering and effects on radionuclide transport)* (Sections 3.3, 3.4)
- 2.2.08.04.00: *Redissolution of precipitates directs more corrosive fluids to container* (Section 3.3)
- 2.2.10.06.00: *Thermal-chemical alteration (solubility speciation, phase changes, precipitation/dissolution) THC input* (Section 3.3)
- 2.2.10.10.00: *Two-phase buoyant flow/heat pipes* (Sections 3.2, 3.3, 3.4)
- 2.2.10.12.00: *Geosphere dry-out due to waste heat* (Sections 3.2, 3.3, 3.4)
- 2.2.10.13.00: *Density driven groundwater flow (thermal)* (SZ PMR).

NFE FEPs that are not excluded or not fully included in the TSPA-SR, based on the screening, are the following:

- 1.1.02.00.00: *Excavation/construction*. Chemistry effects are excluded due to low consequence. The effects of chemistry due to coupled thermal-hydrologic-chemistry effects (which are included) are expected to be much larger than geochemical effects from boring or blasting.
- 1.2.02.01.00: *Fractures*. The effect of the alteration of fracture properties on transport are excluded due to low consequence, since transport times have been shown to be insensitive to fracture permeability.
- 2.1.08.01.00: *Increased UZ water flux at repository*. The effects of climate change resulting in increased water flux at the repository are included, but the section of the FEP relating to water rapidly cooling a waste package is excluded due to low consequence. The drip shield is expected to preclude water reaching the waste package during the thermal period.
- 2.1.09.12.00: *Rind (AZ) formation in waste, EBS, and adjacent rock*. The formation of a rind was included in the coupled THC model. These effects were found to be small and were not excluded, due to low consequence, in the TH models.
- 2.1.11.02.00: *Non-uniform heat distribution/edge effects in repository*. Both center and edge effects were included in the TH model. Thermal-mechanical effects on fractures around the drift were quantified based on a center location. TM effects on dose expected to be bounded by conservative implementation of seepage so are excluded from TH models base on low consequences (TBV).
- 2.2.01.01.00: *Excavation and construction related changes in the adjacent host rock*. Excavation related TM effects on dose expected to be bounded by conservative implementation of seepage, so are excluded from TH models base on low consequences (TBV).
- 2.2.01.02.00: *Thermal and other waste and EBS related changes in the adjacent host rock*. TM effects on dose expected to be bounded by conservative implementation of seepage, so are excluded from TH models base on low consequences (TBV).
- 2.2.01.03.00: *Changes in fluid saturations in the excavation disturbed zone*. Initial fluid saturations are expected to be lower than ambient values due to ventilation during the pre-closure period. The initial saturations in the TH models were the ambient values. This FEP was excluded due to low consequences. Implementation of initial saturations will result in higher-rate of earlier water flow onto waste packages than if lower initial saturations had been used as initial conditions.

- 2.2.06.01.00: *Changes in stress (due to thermal, seismic or tectonic effects) change porosity and permeability of rock.* TM effects on dose expected to be bounded by conservative implementation of seepage, so are excluded from TH models based on low consequences (TBV).
- 2.2.10.04.00: *Thermal-mechanical alteration of fractures near repository.* TM effects on dose expected to be bounded by conservative implementation of seepage, so are excluded from TH models based on low consequences (TBV).
- 2.2.10.05.00: *Thermal-mechanical alteration of rocks above and below the repository.* TM effects on dose expected to be bounded by conservative implementation of seepage, so are excluded from TH models based on low consequences (TBV).
- 2.2.10.06.00: *Thermal-chemical alteration (solubility speciation, phase changes, precipitation/dissolution).* Changes to hydrologic properties as a result of coupled THC processes were included in the THC model. The changes were found to be small and were excluded from the TH models due to low consequence.

The approach used for this analysis is a combination of qualitative and quantitative screening of FEPs. The analyses are based on the criteria provided by the NRC in the proposed 10 CFR Part 63 (64 FR 8640) and by the EPA in the proposed 40 CFR Part 197 (64 FR 46976) to determine whether or not each FEP should be included in the TSPA. The criteria were:

- Exclude on the basis of “Low Probability” if a FEP has less than one chance in 10,000 of occurring during 10,000 yr.
- Exclude on the basis of “Low Consequence” if omission of the FEP does not significantly change the expected annual dose.

For FEPs that are included in the TSPA, the TSPA Disposition includes a reference to the AMR that describes how the FEP has been incorporated into the process models that feed into the TSPA-SR abstraction.

For FEPs that are excluded from the TSPA based on NRC or EPA criteria, the screening argument includes a summary of the basis and results that indicate either low probability or low consequence. As appropriate, screening arguments cite work done outside this activity, such as in other AMRs. If needed, a more detailed discussion is provided in the Analysis and Discussion section of the *NFE FEPs AMR* (CRWMS M&O 2000e).

The FEPs screening analysis results for the 26 FEPs relevant to the NFE are summarized in Appendix C. The appendix, derived from the NFE FEPs AMR (CRWMS M&O 2000e, Table 3), shows the FEP number, FEP name and description, FEP screening decision (include/exclude) and basis for “Exclude” decision. The appendix also lists other PMRs that cover the FEP analysis, as appropriate.

INTENTIONALLY LEFT BLANK

### 3. PROCESS MODELS, ABSTRACTIONS AND CONFIDENCE BUILDING

This chapter describes the relationship between the process-level models, model abstractions, and supporting analyses that address the NFE processes. The processes and/or submodels included are explained in terms of the conceptual models that provide the bases for the process models. In addition to the AMRs supporting the NFE Process Model Report (NFE PMR), this section also includes summary results of the field thermal tests and natural analogs applicable to understanding coupled thermal-hydrological-mechanical-chemical (THMC) processes.

#### 3.1 INTRODUCTION

##### 3.1.1 Overview Description and Results of Models and Abstractions

The model components and analyses that support the NFE PMR include:

- The *Thermal Tests TH AMR* (CRWMS M&O 2000a) has a primary purpose that relates to building confidence in the models that describe the thermal-hydrological (TH) processes in the potential repository system. The AMR tests various property sets, proposed for use in design and TSPA, to characterize the potential repository geologic setting. The AMR compares measurements from field tests to calculated temperatures and saturations using these property sets. Note that the evaluation of the TH property sets inherently involves the evaluation of the coupled thermal-hydrological processes that are both numerically-simulated and field measured. The report is discussed in Section 3.1.2 and summarized in Section 3.6.
- The *THC Process AMR* (CRWMS M&O 2000b) discusses coupled THC processes. This AMR supports both this PMR and the UZ F&T PMR (and thus carries a second designation, U0110). The AMR focuses on the impact of coupled processes on fracture and rock hydrological property changes, and on mineral-water-gas reactions that drive changes to water and gas compositions within the NF that may enter potential drifts through fractures. The report is discussed in Section 3.1.3 and summarized in Section 3.3.
- The *Abstraction AMR* (CRWMS M&O 2000c) provides the technical basis for the TSPA abstraction of THC processes. It abstracts the results of the *THC Process AMR* for use in TSPA. It also compares the TH results for process-level and abstracted TH and THC models. The report is discussed in Section 3.1.4 and summarized in Sections 3.4 and 3.2.3.4.
- The *NFE FEPs AMR* (CRWMS M&O 2000e) identifies and examines the effects of features, processes, and events that are related to the NFE on repository performance and provides the technical basis of evaluation of those FEPs. The report is summarized in Section 2.5.
- The *THM Calculation* (CRWMS M&O 2000d) discusses the mechanical responses to the thermal pulse and the effects of the consequent fracture closure or opening on the hydrological properties of the rock mass. The report is summarized in Section 3.5.

The models and components that comprise the NFE model or analyses applied in TSPA-SR contain inherent uncertainties. Identification and propagation of parameter input and conceptual model uncertainty is required to correctly characterize the TSPA model. Input parameter and output variability are also contained in the models and components that make up the NFE models and analyses. Uncertainty and variability will be discussed in terms of each AMR used to support this PMR (see Table 3-1).

Table 3-1. Uncertainty in Major AMRs used in the Near-Field Environment PMR

Model/Analysis Component	Input Parameter Uncertainty and Variability	Conceptual Model Uncertainty	Output Uncertainty and Variability
Thermal Test AMR (CRWMS M&O 2000a; Section 3.6 in this PMR)	Spatial variability (DST only) in calibrated DS hydrologic parameters; input parameter uncertainty with the use of multiple hydrologic and thermal property sets; heat loss through bulkhead	DK model with and without interface-area reduction factor; dual permeability model-active fracture model (Liu et al. 1998) using fracture and matrix continuum instead of discrete fractures	Comparison of temperature variability at different locations in the tests (above boiling, below boiling at or near ends of drifts due to effects of bulkhead); the resulting uncertainty in temperature predictions (at different locations) based on multiple hydrologic and thermal property sets and two similar, but different, conceptual flow models
THC Process AMR (CRWMS M&O 2000b; Section 3.3 in this PMR)	Spatial variability in calibrated DS hydrologic parameters; temporal variability and uncertainty in temperature and precipitation (which is implemented in the model by three different climate states: present day, monsoonal, and glacial transition); duration of climate periods; uncertainty included in parameter calibration for different infiltration-flux cases; uncertainty in chemistry data (thermodynamic and kinetic data, chemistry of infiltrating water, different mineral assemblages); uncertainty in TptplI property sets	DK model-active fracture model (Liu et al. 1998); use of middle-nonlithophysal (Tptpmn) parameters instead of lower-lithophysal (TptplI) parameters	Temporal and spatial variability of water and gas composition, as well as uncertainty from different infiltration-flux cases (including climate) and different mineral assemblages
THC Abstraction AMR (CRWMS M&O 2000c; Sections 3.4 and 3.2.3.4 in this PMR)	Temporal and spatial variability of water and gas composition, as well as uncertainty from different infiltration-flux cases (including climate) and different mineral assemblages, which water chemistry is appropriate as input (pore water, perched water, J-13 etc.)	DK model-AFM (Liu et al. 1998); use of four discrete geochemical periods to represent water chemistries and gas-phase compositions	Simplified description of temporal variability of water and gas composition for a single location; characterization of the temporal and spatial uncertainty and variability of TH quantities from two different process-level models (THC and TH-only)

Table 3-1. Uncertainty in Major AMRs used in the Near-Field Environment PMR (Continued)

Model/Analysis Component	Input Parameter Uncertainty and Variability	Conceptual Model Uncertainty	Output Uncertainty and Variability
NFE FEP AMR (CRWMS M&O 2000e; Section 2.5 in this PMR)	Spatial and temporal variability in infiltration (including climate); spatial variability in calibrated parameters; uncertainty included in parameter calibration for different infiltration-flux cases; temporal and spatial variability of water and gas composition, as well as uncertainty from different infiltration-flux cases and different mineral assemblages; spatial and temporal variations in temperature and hydrologic conditions	Applicable conceptual model from process-level model that forms FEP basis	Characterization (both qualitative and quantitative) of heat-driven uncertainties and variabilities in TH processes in the NF host rock and how they may affect repository performance
THM Calculation (CRWMS M&O 2000d; Section 3.5 in this PMR)	Spatial variability in mechanical properties  Spatial variability in thermal-mechanical properties.  Spatial variability and uncertainty in joint properties.  Uncertainty in situ stress conditions.	Thermal Power input  Coulomb-Slip model for shear fracture behavior  Elastic model for rock matrix behavior  Linear relation between fracture deformation and fracture permeability change  Thermal model for infinite medium.  Idealized fracture distribution.	Temporal and spatial variability of stress  Temporal and spatial variability of displacement.  Temporal and spatial variability of permeability multiplier

### 3.1.2 Thermal Testing AMR

The *Thermal Testing AMR* (CRWMS M&O 2000a) compares experimentally measured quantities, such as host-rock temperature and liquid saturation, to simulation results from TH models specifically developed to estimate the TH processes that occur in the tested host rock as a result of controlled heat input. Temperature and liquid saturation measurements of varying duration and at different locations in the tests are compared to TH model simulation results. A number of comparisons are made for the host rock, both above and below the boiling point, in order to assess the ability of the TH models to reproduce the (simultaneous heat and fluid flow) processes that occur in regions of extreme changes in temperature or liquid saturation.

In order to assess the ability of any TH model to reproduce the processes initiated by heat addition, the model must be equipped with appropriate flow properties and conceptual flow models. The flow properties govern the rate at which heat or fluid flows through the system and the conceptual flow model predicts how the distribution of temperature and liquid saturation evolve in time. The DS hydrologic flow properties developed by the UZ Flow and Transport (UZ F&T) model (CRWMS M&O 2000f, Section 3.6.4.1) to reproduce ambient conditions in the

mountain are also applied in the TSPA-SR models and abstractions that include the influence of repository heating (CRWMS M&O 2000g, Section 3.1). Since this is the case, it must be ensured that hydrologic properties developed to reproduce the ambient conditions of the mountain can also (approximately) reproduce the transient flow processes that result in the event of a thermal perturbation. The same is also true for the conceptual flow model.

The DKM/AFM was developed to reproduce the ambient flow conditions of the mountain (CRWMS M&O 2000f, Section 3.4.1.4.1). This same conceptual flow model is also applied in the TSPA-SR models that include the thermal perturbation. An important question is whether hydrologic properties and conceptual flow models specifically developed for ambient flow conditions can be applied to models that include repository heating. The answer to this question only lies in direct comparison of experimentally measured quantities from the thermal tests to the results of the thermal test TH models that apply the same properties and conceptual flow models used in the TSPA-SR repository-heating models. Consequently, the TSPA-SR repository-heating models, although conducted at spatial and temporal scales not amenable to experimental verification, are at least based on hydrologic properties and conceptual flow models successfully tested against the more reasonably scaled (both in time and space) thermal tests that include the transient nature of thermally induced flow processes.

The comparison between experimentally measured data and TH model results, and the subsequent conclusions in the thermal AMR test indicate that application of the DS hydrologic property set, along with the flow model that uses the DKM and AFM, adequately reproduce the heat and fluid-flow processes initiated by a controlled thermal perturbation (CRWMS M&O 2000a, Sections 6.1, 6.2, and 7). Temperature comparisons between model and measured data at test locations, both above and below the boiling point, indicate that the hydrologic properties and DKM and AFM adequately represent the transient thermal response. Consequently, the DS hydrologic property set and DKM-AFM are deemed appropriate for use in TSPA-SR DS models used to represent the in-drift thermodynamic environment (e.g., temperature and relative humidity) and liquid-flow processes (e.g., rate of thermally enhanced fracture flow) in the host rock that influence seepage into the emplacement drift.

### **3.1.3 The THC Process AMR**

The *THC Process AMR* (CRWMS M&O 2000b) calculates water chemistry and gas-phase composition in the NF host rock. The water at the drift wall that may seep into the emplacement drift during and after repository heating provides the geochemical boundary condition for the TSPA-SR model. Determination of the aqueous species and gas-phase concentrations that result from mineral precipitation and dissolution processes initiated by repository heating and mineral-water reactions requires a fully-coupled computer code that includes both mass and energy transfer, as well as the reactive-transport processes of a number of different mineral assemblages.

Like the TH models described in the previous section, the DS THC model also requires appropriate hydrologic and thermal property inputs. Furthermore, it requires a working conceptual flow model that reasonably characterizes the processes initiated by a repository thermal perturbation. The THC model applies the DS hydrologic and thermal property set and the active-fracture conceptual flow model tested in the thermal test TH models. Since the model is used to estimate THC processes (e.g., evolution of water chemistry at the emplacement drift

wall) driven by repository decay heat, it must implement specifics related to repository design, such as emplacement-drift diameter, waste package and drip shield geometry, invert and backfill geometry, and waste package thermal-decay information (CRWMS M&O 2000b, Sections 4.1.1; 4.1.7; 5, assumption A.1; 6.1.5.1).

In addition to property, conceptual model, and repository-design inputs, the THC DS model requires parameters and conceptual models associated with reactive-transport processes. These include mineralogical data, initial water and gas chemistries, thermodynamic and kinetic data, transport parameters (e.g., diffusion of CO<sub>2</sub>), and kinetic-rate laws, including relationships for the reactive-surface areas (CRWMS M&O 2000b, Sections 4.1.2 through 4.1.6, and 6.1). The validity of the THC model and chemical-parameter inputs are based on measured results of the DST (CRWMS M&O 2000b, Section 6.2.7).

The DS THC process-level model provides time-histories (at different locations in the NF host rock adjacent to the emplacement drift wall) of CO<sub>2</sub>, pH, Ca<sup>2+</sup>, Na<sup>+</sup>, SiO<sub>2</sub>, Cl<sup>-</sup>, HCO<sub>3</sub><sup>-</sup>, SO<sub>4</sub><sup>2-</sup>, Mg<sup>2+</sup>, K<sup>+</sup>, AlO<sub>2</sub><sup>-</sup>, HFeO<sub>2</sub><sup>-</sup>, and F<sup>-</sup>. The results are based on analysis of complex mineral assemblages as well as a simplified mineral assemblage. The complex mineral assemblage represents a relatively full set of minerals and aqueous species needed to describe more fully the chemistry of the NFE. In addition to including the minerals and species from the less complex mineral assemblage, the model also includes a wide range of alumino-silicates, such as feldspars, clays, and zeolites. The reduced set of species and minerals is specified to capture many of the basic aspects of the Drift Scale Test measured water and gas chemistries. Its mineralogy includes calcite, silica phases, and gypsum. It is found that general consideration of the less complex geochemical system in the THC model adequately represents the measured chemical evolution of the Drift Scale Test (DST) (CRWMS M&O 2000b, Section 7). However, refinement of these results will be necessary in the future, given the need to more fully and accurately represent the observed mineralogy in the models, and to honor the measured dissolution rates of mineral phases.

In addition to the geochemical system-driven differences in water and gas-phase compositions, the differences in water and gas chemistry driven by infiltration rates are also incorporated in the THC DS model. Low, mean, and high infiltration-flux cases (including three climate states) in the DS THC model considered a 0.6 to 47 mm/yr. range in infiltration rates (CRWMS M&O 2000b, Table 12). Although not yet observed in the DST, rewetting periods in the model indicate an increase in CO<sub>2</sub> gas and aqueous carbonate concentrations in the drift wall host rock. Rewetting periods are largely influenced by infiltration rates and climate histories.

Abstraction of water chemistry and gas composition from the THC model, along with an analysis of TH-only and THC process-level model predictions of the important TH variables (e.g., host-rock temperature, fracture-liquid flux), is performed in the *THC Abstraction AMR* (CRWMS M&O 2000c).

### 3.1.4 The THC Abstraction AMR

The *THC Abstraction AMR* (CRWMS M&O 2000c) provides a simplified description of the time evolution of water and gas chemistry in the NF host rock. It also provides a detailed evaluation of process-level differences between the fully coupled THC and the TH-only models. The

evaluation is of the TH variables important for repository performance (e.g., liquid flux in host-rock fractures at the crown of the emplacement drift). The TH-only model used for comparison to the DS THC model is a 2-D submodel extracted directly from the draft multiscale TH model (CRWMS M&O 2000k, Section 6.3). Its infiltration boundary condition is altered to be consistent with the fully coupled DS THC model used in the evaluation analysis.

The water chemistry and gas-phase composition abstraction provides a simplified overview of the process-level THC model results. The abstracted evolution of water chemistry and gas-phase composition in the NF host rock (CRWMS M&O 2000c, Section 6.1) is taken from the projected chemistry of water in fractures at the crown of the emplacement drift from detailed model analyses of THC (CRWMS M&O 2000b). The abstraction from the DS THC process-level model occurs in discretely simplified time periods:

- Preclosure period (0 to 50 yr.)
- Boiling period (50 to 1,000 yr.)
- Transitional cool-down period (1,000 to 2,000 yr.)
- Extended cool-down period (2,000 to 100,000 yr.).

The detailed time-history results of the process-level THC model are simplified into a series of four discrete time periods as defined above. The abstraction provides a series of constant-value, geochemical periods that are used as in-drift geochemical TSPA boundary conditions. The four period, constant-value, THC abstraction includes five cations, six anions, pH, partial pressure of carbon dioxide, and the temperature during the abstraction boiling period used to re-equilibrate the condensate water with the carbon dioxide of the gas-phase adjacent to the emplacement drift. The impact of fracture dryout on water chemistry during the time period in which local host rock temperatures are at or above the boiling point of water, as characterized in the THC process-level model, is not used in the TSPA abstraction. Instead, the condensate water above the dryout zone is used as the water chemistry that may potentially enter the drift. Since the THC process model does not include fracture property heterogeneity, the condensate water above the dryout zone represents the water (chemistry) that could potentially seep through a heterogeneous fracture system (if included) thereby reaching the drift wall. Additionally, since the TSPA seepage model uses a value of percolation flux from a TH model, which is always greater than or equal to ambient percolation, a water chemistry calculation is required at all times. That is, seepage may occur (in the PA abstraction) even during the dryout period predicted by the 2-D process models that do not include repository edge cooling effects.

Abstraction results focus primarily on the mean infiltration flux case (CRWMS M&O 2000c, Table 3). Limited uncertainty included in the THC model results of water and gas-phase chemistry is accounted for with three infiltration flux cases (low, mean, and high) and two different mineral assemblages (e.g., quantification of uncertainty in the reactive surface area is not included in the process-level model). The THC abstraction includes only the mean infiltration flux case, using the primary aqueous constituents from the less complex geochemistry and the trace constituents from the more complex geochemical system. Use of only the mean infiltration flux THC results in the abstraction is justified by an order of magnitude analysis based on ratios of individual concentrations taken between the low and the mean and the high and the mean flux cases (CRWMS M&O 2000c, Section 6.1.2). The use of condensate water chemistry, rather than an evolving fracture-water chemistry, such as concentrated J-13 water,

during the “abstracted boiling period” is determined to be appropriate, as this is the water most likely to seep into the drift due to the enhanced saturation in this zone.

The *THC Abstraction AMR* also describes a detailed evaluation of process-level models that either include, or do not include, the fully coupled processes of thermal hydrology and reactive transport (CRWMS M&O 2000c, Sections 6.2–6.4). This evaluation is of the variables that characterize the TH performance of the repository and are important to TSPA in the overall total system description of the geologic system through time. Specifically, the evaluation is for potential differences in process-level model outcomes of host rock near the drift wall for: temperature, liquid saturation (both fracture and matrix), air mass fraction, fracture air flux, and fracture liquid flux. The results of this quantitative evaluation allows one to assess the relative importance of including a fully coupled reactive transport THC model when providing TSPA with the pertinent TH characteristics (defined above) used to determine performance of a geologic repository. A strict comparison of flux variables is not performed at the side and base of the drift-wall host rock due to differences in process-model boundary conditions applied at the drift-wall interface with the emplacement drift. Process-model evaluations are made at the crown of the drift where process-model conditions are the same. An analysis of this type is used to provide the necessary justification as to why a potential reduction in the numerical complexity of the problem (e.g., use of TH-only models instead of fully coupled THC models) does not negatively influence prediction of the overall TH performance of a potential geologic repository. Of course, if water chemical content and gas-phase composition are required, use of a fully coupled reactive transport code is necessary. However, if the TH variables used to characterize the NF host rock (percolation flux near the drift wall) or in-drift thermodynamic conditions (temperature and relative humidity) are required, the results of this analysis indicate that a TH-only model will not result in unacceptable error by not including reactive-transport processes (CRWMS M&O 2000c, Section 6.3).

In order to further quantify the impact THC processes may have on the TH variables used to predict repository performance, an evaluation of TH variables resulting from a fully coupled THC model that includes two different geochemical systems was also considered (CRWMS M&O 2000c, Section 6.2). This evaluation assessed whether the relative reaction rates of different mineral assemblages resulted in an appreciable alteration of hydrologic flow properties, which in turn translate to potential differences in predicted host-rock temperatures or liquid fluxes in fractures. It was found that the geochemical and reactive-transport alterations to the flow (and characteristic) properties (and how they alternatively occur for more or less complex geochemical systems) (CRWMS M&O 2000b, Section 7) are small, based on the 1 percent initial porosity and non-localized boiling front in the model. Given these assumptions, the hydrological changes are not enough to impact the fundamental properties of the geologic system (e.g., host-rock temperature adjacent to the emplacement-drift wall, and seepage) associated with repository heating processes. This holds true for the entire range of infiltration fluxes considered in the DS THC model analysis.

One final evaluation in the abstraction AMR concerns the lack of influence of repository edge proximity in the results of a periodic, 2-D, DS model (either TH-only or fully coupled THC models). This analysis compares drift-wall temperature and liquid saturation from the THC model to the multiscale TH model that includes repository edges. The influence of lateral heat loss to rock masses surrounding the loaded repository is quantified in the multiscale TH model.

This is done by implementing a sequence of models that approximate edge heat-loss effects, with a mountain-scale model that incorporates the surrounding unheated rock masses, coupled with a variety of different DS models that produce the in-drift TH environment and processes occurring in the NF host rock surrounding the emplacement drifts (CRWMS M&O 2000k, Section 6.1). The results of the analysis indicate that edge proximity results in far cooler temperatures and higher liquid saturations in the host rock directly adjacent to the drift wall (CRWMS M&O 2000c, Section 6.4). Recall that the water chemistry in the condensate zone, developed above a dryout zone computed by a process model that does not include repository edge effects, is used with the TSPA seepage model that expects non-zero values for the percolation flux (used as an input to the seepage model) even during the peak temperature thermal period.

### **3.1.5 Thermally Perturbed Percolation Flux in the Near-Field Host Rock**

The thermally perturbed percolation flux in the NF host rock is also considered in the THC abstraction covered in this PMR (Section 3.4), in the TH work summarized in Section 3.2.3, and in the thermal-test analyses (Section 3.6.1). Thermally “enhanced” liquid flux through fractures is a direct outcome of heat addition to the surrounding host rock. The process of enhanced fracture liquid flux is caused by increased host-rock temperatures with associated evaporation boiling of the fracture and matrix pore waters. Since the process-level models include a DK conceptual flow model, water vapor generated in the matrix is transported to the high permeability fractures (compared to the matrix) where it can flow away from the heat source primarily by pressure gradients or temperature-driven density gradients. When the vapor contacts a region of host rock at a lower temperature, the vapor in the fracture condenses on the fracture walls where it is either imbibed into the matrix or flows, driven by gravity, along the fractures.

For vapor that condenses above the repository drifts, this condensate water in the fractures can flow back into the heated zone (if fracture orientations are towards the heated zone) or away from it (when orientations are away from the heated zone). When vapor condenses below the drifts, or to the sides of the drifts, the condensate in fractures would drain away from the heated zone (with exception of nearly horizontal fractures, which might allow flow towards the drifts). See Figure 2-3.

For that part of the condensate that is imbibed, the water would move in response to gravity drainage and saturation-gradient diffusion (see Figure 2-3). For water imbibed above the drifts, both saturation-gradient diffusion and gravity drainage would be in the directions toward the drifts (heat zone). For water imbibed to the sides of the drifts, saturation-gradient diffusion would be towards the drifts, while gravity drainage would be downwards (essentially 90° from the saturation-gradient diffusion). The actual net movement would depend on the relative magnitudes of the two processes. It is estimated that saturation gradients will dominate. For condensate imbibed into the matrix below the drifts, saturation-gradient diffusion would be towards the drifts, while gravity drainage would be away from the drifts.

Superimposed on this flow is the effects of vaporization of water within the heated zone. Any water returned to the heated zone would, unless percolation fluxes exceed volumes that can be vaporized per unit time, be revaporized and moved outward from the heated zone. Because only

part of vaporized water returns to the heated zone, there would be a net removal of water (excluding water introduced by way of percolation flux).

Since this "heat-mobilized" water is in addition to the percolation water that is naturally present, the liquid flux is deemed enhanced. It is noted that the active-fracture parameters applied in the conceptual flow model (DKM) dictate the rate at which water in the fractures is conducted back into the matrix, and any water not calculated to be imbibed into the matrix is free to flow through the fracture.

Of interest in this PMR is how the spatially dependent percolation flux at a specified location in the NF host rock (above the drift) varies in time after waste emplacement and how this increases the volume of water within the fracture, or matrix if imbibed, interacting with minerals in the rock or fracture coatings. Increased volumes of water will change the rock-water ratio, which affects the chemical equilibrium state. Further, the chemistry of this mobilized water will potentially be different than the water in pores or fractures that had not been thermally mobilized.

Of interest to the UZ F&T and EBS PMRs is how this spatially and temporally-varying percolation flux drives the seepage-volume flow rate into the emplacement drifts, and the fraction of waste packages contacted by seeps, as discussed in the Abstraction of Drift Seepage (CRWMS M&O 2000l, Section 6.3.5).

The percolation flux above the crown of the drift is obtained from the multi-scale thermal-hydrologic model (described in Section 3.2.2.1) that includes different locations within the repository footprint (e.g., infiltration rate variability), three host rock units, and proximity to the repository edge, as described in the *Multiscale Thermohydrologic Model AMR* (CRWMS M&O 2000k, Section 6.6.13). The abstraction of the thermally-driven percolation flux into the TSPA model is described in CRWMS M&O (2000m, Sections 6.1 and 6.3.7). The abstraction by TSPA arranges waste package location-dependent results from the process-level model into infiltration-rate bin inputs for the TSPA models. The infiltration-rate bins defined by TSPA (CRWMS M&O 2000m, Sections 5.1, 6.2) are the following:

- 0 – 3 mm/yr
- 3 – 10 mm/yr
- 10 – 20 mm/yr
- 20 – 60 mm/yr
- > 60 mm/yr.

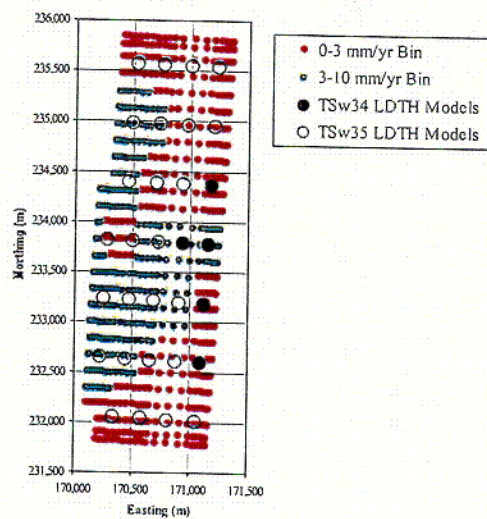
Each infiltration-rate bin provides percolation flux inputs for the TSPA seepage model. The waste package location-dependent information from the process model provides the in-drift (e.g., waste package temperature and relative humidity, etc.) and NF host rock (e.g., drift-wall temperature, percolation flux, etc.) data at 623 different locations within the repository footprint for three different infiltration-flux cases: low, mean, and high (CRWMS M&O 2000k, Section 6). Each of the 623 locations has associated with it a present-day, monsoonal, and glacial-transition climate state. The location-dependent data from the process model are arranged into an infiltration-rate bin (ranges defined above) by its glacial-transition climate. This is the climate state that is predicted to begin at 2,000 yr. after waste emplacement and persist for

times out to  $10^6$  yr., and is characterized by the highest mean and high infiltration rates of the climate scenarios considered.

The infiltration-rate bins defined by TSPA are distributed over the repository footprint, as shown (for the low, mean, and high infiltration-flux cases) in Figures 3-1 through 3-3. The figures also indicate the location of the LDTH models (CRWMS M&O 2000k, Section 6.3.1). Each infiltration-flux case contains 623 location-dependent data results from the process-level model. Each result represents a different location in the repository footprint. The spatial location (or repository coverage) of each infiltration bin in Figures 3-1 through 3-3 places the location-dependent data into a range of infiltration rates for abstraction by TSPA. The individual numbers of location-dependent results for all three infiltration-flux cases are presented in Table 3-2. The table also includes the total repository-area fraction represented by each infiltration bin associated with an infiltration flux case.

The (process model) data for percolation flux at selected distance above the crown of the drift are input into a TSPA model that characterizes the seepage-volume flow rate into the emplacement drift as a function of percolation flux. The selected height (5 m) is above the dryout zone at all times, for the location at which the THC abstraction was performed. Ongoing work may develop an abstraction in which percolation-flux sample height depends on other parameters.

623 Low Glacial Infiltration Bin Locations



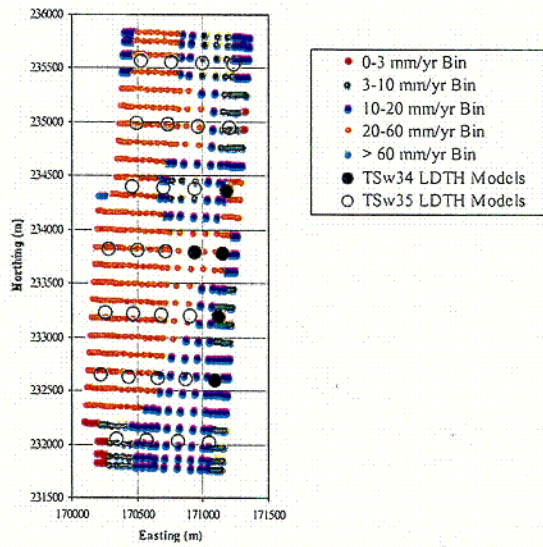
1400

Source: CRWMS M&O 2000m, Figure 18

Figure 3-1. The Location-Dependent Data in the Different Infiltration Bins for the Low Glacial Infiltration Map

L-3

623 Mean Glacial Infiltration Bin Locations

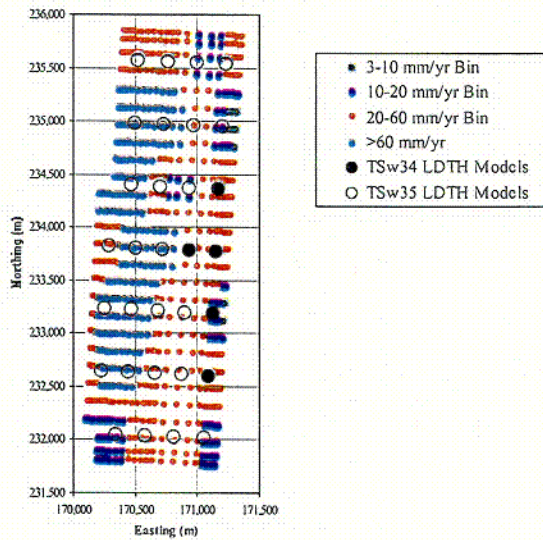


1-4.m

Source: CRWMS M&O 2000m, Figure 19

Figure 3-2. The Location-Dependent Data in the Different Infiltration Bins for the Mean Glacial Infiltration Map

623 High Glacial Infiltration Bin Locations



Source: CRWMS M&O 2000m, Figure 20

Figure 3-3. The Location-Dependent Data in the Different Infiltration Bins for the High Glacial Infiltration Map

C-4

Table 3-2. Distribution of Process-Level Model Results within Infiltration Bins

<b>Low Infiltration Case</b>	<b>Number of Location Dependent Entries in the Bin</b>	<b>Repository Area Fraction (%)</b>
0-3 mm/yr.	368	59.7
3-10 mm/yr.	255	40.3
10-20 mm/yr.	0	0
20-60 mm/yr.	0	0
> 60 mm/yr.	0	0
<b>Mean Infiltration Case</b>	<b>Number of Location Dependent Entries in the Bin</b>	<b>Repository Area Fraction (%)</b>
0-3 mm/yr.	21	1.6
3-10 mm/yr.	91	13.2
10-20 mm/yr.	174	32.1
20-60 mm/yr.	334	52.9
> 60 mm/yr.	3	0.3
<b>High Infiltration Case</b>	<b>Number of Location Dependent Entries in the Bin</b>	<b>Repository Area Fraction (%)</b>
0-3 mm/yr.	0	0
3-10 mm/yr.	14	1.2
10-20 mm/yr.	98	13.4
20-60 mm/yr.	318	54.8
> 60 mm/yr.	193	30.6

Source: CRWMS M&O 2000m, Table 5

## 3.2 THERMAL-HYDROLOGICAL PROCESSES AND MODELS

This section summarizes TH processes, TH models, and four case studies that use the models, including NF TH results for the SR design (EDA-II without backfill).

### 3.2.1 Thermal-Hydrological (TH) Processes Affecting TH Behavior

Under ambient conditions, liquid-phase flow in the repository host rock arises as a result of the infiltration of rainfall and snowmelt. Although most of the total fluid-storage capacity is contained in the matrix pores of this rock, the permeability in the matrix is very low. For the DS and MS base-case hydrological property sets (see CRWMS M&O 2000a; Section 4), the matrix permeability is as much as five and six orders of magnitude, respectively, less than that of the fractures in the repository host rock, and the percolation flux exceeds the unit gradient flow capacity of the matrix; consequently, fractures dominate liquid-phase flow. After the emplacement of radioactive waste, the thermally-driven transport of water vapor away from the heat source causes a redistribution of the pore fluids within a potentially large volume of rock. Depending on the thermal design of the repository, this volume can extend from the ground surface to some distance below the water table and over an area larger than the repository footprint. Water in the matrix pores evaporates, creating dryout zones around the emplacement drifts and condensation zones outside of the dryout zones. The generation of steam replaces air

within the boiling zone, reducing the gas-phase mass fraction of air to almost zero for a period of time.

The initial movement of water vapor is within the matrix pores. Once the decay-heat-driven water vapor has entered a fracture network, the direction of flow is generally away from the heat source; however, if the fracture permeability is high enough, buoyant gas-phase convection can cause water vapor movement to be predominantly upward in the vicinity of the emplacement drifts. Depending on the thermal design of the repository and the fracture permeability, vapor flow within fractures occurs over length scales of several meters to hundreds of meters.

Decay heat is transported away from the emplacement drifts (in the rock mass) by conductive and convective heat-transfer mechanisms. Thermal conduction is the dominant heat-transfer mechanism in the rock mass. Thermal radiation is the dominant heat-transfer mechanism within the open spaces inside the emplacement drifts; this applies particularly during the first several thousand years when temperatures in the drifts are relatively high. The transport of water vapor results in more efficient heat transport than does liquid-phase flow. Two important heat-transfer mechanisms involving the transport of water vapor and phase change (i.e., evaporation and condensation) are heat pipes and buoyant gas-phase convection. Heat pipes result from vapor transport away from the heat source, and gravity-driven and/or capillary-driven condensate flow back toward the heat source (i.e., refluxing). Buoyant gas-phase convection results from mass-density gradients driven by temperature gradients in the rock mass. Depending on the thermal design of the repository, this mechanism, which may occur at the DS and at MS, can increase the buildup of condensate above the repository. Buoyant gas-phase convection also contributes to heat transfer in the open spaces in the drifts.

The thermal-hydrological behavior of the repository can be divided into three sequential periods: drying, steady state, and rewetting. The concept of these three periods is applicable over dynamically changing spatial regimes in addition to temporal regimes. At a given time, certain locations in the repository footprint may have already progressed to the rewetting regime, while other locations remain in the drying regime. During the drying and steady-state periods, liquid-phase flux in the refluxing zone is greater than ambient local percolation flux.

In the host rock, local thermal-hydrological behavior is dominated by location (inside or outside the zone of boiling temperatures). Therefore, the spatial and temporal extent of the boiling zone is very important. Although thermal-hydrological processes such as evaporation occur at below-boiling temperatures, the most important processes (i.e., refluxing and dryout) require that temperatures are at the boiling point of water. Note that the boiling temperature can be higher than the nominal boiling temperature (96°C) at the repository horizon. The key aspects of the system are boiling-period duration and boiling-period temperatures (i.e., temperatures high enough to indicate superheated conditions or refluxing/heat-pipe conditions).

Two important quantities influence the thermal-hydrological conditions within the emplacement drift: temperatures at the drift wall and the temperature gradient between the waste package and the drift wall. The likelihood of water seeping into the drift is strongly affected by whether temperatures at the drift wall are above the boiling point. If the local heat flux at the drift wall is greater than the product of the local liquid-phase flux and the heat of evaporation, water cannot steadily seep into the drift. If the converse is true, then steady seepage into the drift is possible.

The temperature gradient between the waste package and drift wall strongly affects how much lower the relative humidity (*RH*) on the waste package is than at the drift wall.

Additional discussion of TH models is provided in the Multiscale TH & AMR (CRWMS M&O 2000k) and the UZ F&T PMR (CRWMS M&O 2000f).

### 3.2.1.1 The Thermal-Hydrological Near-Field State: General Observations

TH modeling is particularly critical to providing an overall indication of the TH state of the repository during the heating and cooling phases following repository closure. These phases can be combined broadly into the *thermally disturbed period*, followed by an indefinite period termed the *final state* during which temperatures are near-ambient (~30°C). The *thermally disturbed period* which includes the drying, steady-state, and rewetting periods described in Section 3.2.1, results from the emplacement of waste packages. During the *thermally disturbed period*, which is predicted to last several thousand years, the thermal power density in the repository is high resulting in perturbations to the original, ambient thermal-hydrological state. Ultimately, the thermal perturbation vanishes, owing to the decay of the radioactive waste and the removal of heat by transport processes; this results in a *final state* of the repository environment that is expected to resemble the original ambient regime. Fluid redistribution and other important features of the thermally disturbed system are illustrated schematically in Figure 3-4 at the drift scale and in Figure 3-5 at the MS.

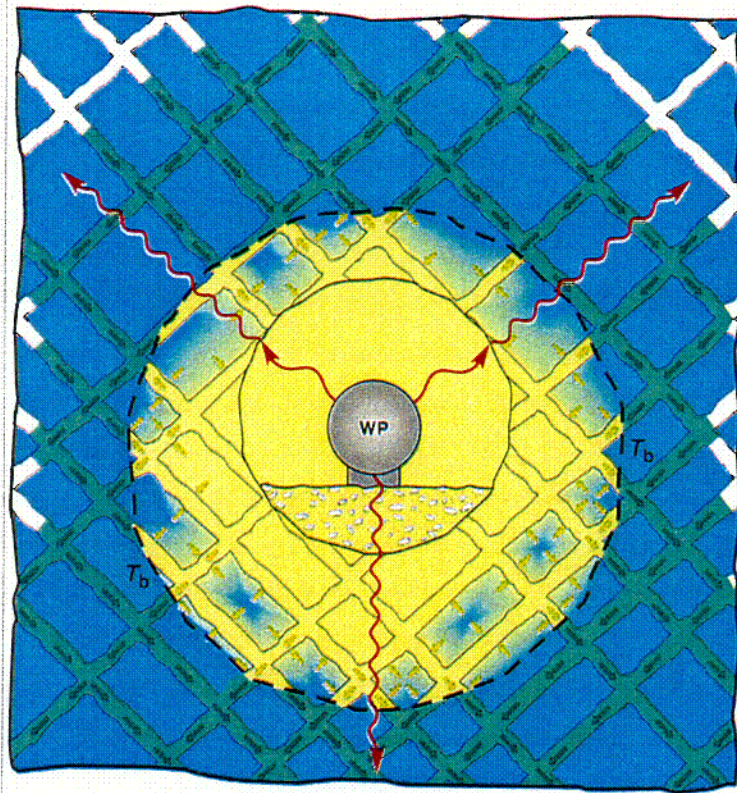
This thermally driven transport of water and water vapor away from the heat source (TH behavior) causes a redistribution of the pore fluids. Each of the following processes described below (may) occur as a result of repository heat addition and thermally driven transport of water and water vapor in the geologic setting at Yucca Mountain. Previous TH models, either for site characterization or TSPA, have shown each of these processes, to varying degrees, as potentially important when considering decay heating from a potential repository located in the unsaturated zone at Yucca Mountain. The extent and duration of each process is a highly complex function of geologic characterization (e.g., rock formation layering, hydrologic and thermal properties, etc.), infiltration rate and future climates, conceptual flow model, and repository design. As such, the evolution of understanding and associated importance of a particular TH process was accomplished only through analysis of a number of different designs (for instance the VA point-loaded design, see Section 3.2.3.3) throughout each iteration of TSPA. The overall importance of each TH process described below and depicted schematically varies with repository design. As an example, for the VA design, the development of a coalesced dryout zone between emplacement drifts implied an impediment to condensate drainage between drifts during the thermal period. The ability of project models to ascertain this potential behavior allows site characterization and TSPA personnel to guide the design criteria for future TSPAs. Indeed, the ability of the models to ascertain this behavior in the VA design allowed the project to alter the SR design to include wider emplacement drifts in which dryout zone coalescence does not occur.

- **Dryout zones** with liquid-phase saturation decreased from its initial value are created around the emplacement drifts. The relative humidity in dryout zones is also reduced, and, because the matrix potential is mathematically related to relative humidity via the Kelvin equation, the capillary suction potential will be much greater than ambient. The

vertical extent of the dryout zone increases with local decay-heat flux, distance from the repository edge, and decreasing percolation flux. For central locations away from the repository edge and percolation flux less than 5 mm/year, the vertical extent of dryout increases with repository depth below ground surface. This zone is yellow in Figure 3-4 and red in Figure 3-5.

- **Condensation zones** with liquid-phase saturation increase from initial values are created above and below the dryout zones. This zone is blue in Figures 3-4 and 3-5.
- **A region of reduced air mass fraction in the vapor phase is created.** The generation of steam replaces air within the boiling zone, reducing the vapor-phase mass fraction of air almost to zero. This reduction will occur as long as boiling liquid water is present, whether or not rock dryout occurs. Decay heat flows away from the drifts by conductive and advective (also called convective) heat-transfer processes. For heat convection, latent-heat transport (due to boiling and condensation) is much more important than sensible-heat transport; consequently, the flow of water vapor results in much greater heat transport than does liquid-phase flow. The following two bullets describe the two primary mechanisms for gas-phase, advective heat transfer.
- **Heat pipes** result when heat causes vaporization or boiling of water in matrix and fractures, with migration of the vapor away from the drifts into cooler regions where it condenses. The condensate then flows back towards the heat source due to gravity and/or capillary forces completing the heat pipe circuit. Because this mechanism requires either gravity-driven condensate flow in the fractures, or much slower saturation-gradient-driven matrix flow, heat pipes will primarily occur in zones with well-connected vertical fractures. Model results also indicate that the location of heat pipes is strongly affected by ambient percolation flux; high percolation flux (>10 mm/year) suppresses rock dryout and increases the tendency for heat pipes to form in the vicinity of drifts; low percolation flux (<5 mm/year) favors rock dryout and suppresses heat-pipe development near the drifts (Hardin 1998, pp. 3-7 and 3-8).
- **Buoyant gas-phase convection** results from mass-density gradients driven by temperature gradients in the rock mass. Based on model results this mechanism is significant if the rock-mass bulk permeability is more than about 1 to 10 darcy and the fractures are ubiquitous and well-connected over large distances. This mechanism, which may occur at both DS and MS, can increase the build-up of condensate above the repository. (Because the SR design provides for efficient drainage through the pillars, additional saturation above the drifts due to buoyant gas-phase convection is likely to be negligible). Heat flow in the rock causes a temperature build-up in the EBS and NF. The temperature build-up depends strongly on the thermal-loading conditions imposed by emplacement of WPs. The overall repository thermal-loading conditions are best quantified using the AML, expressed in metric tonnes of uranium per acre (MTU/acre). Details of the heat output from individual WPs strongly influence NF TH behavior, particularly the TH conditions immediately adjacent to and within emplacement drifts, including conditions on the WP surfaces. Gas-phase, advective heat-transfer mechanisms increase the overall efficiency of heat transfer away from the drift; consequently, these mechanisms decrease NF temperature buildup. If heat pipes extend

from the boiling front all the way back to the repository horizon, NF temperatures cannot increase much above the nominal boiling point ( $\sim 96^{\circ}\text{C}$ ). If buoyant gas-phase convection (e.g., mountain-scale) is significant, NF temperatures will be decreased, particularly at the edges of the repository. A key issue (or hypothesis) to be resolved through field-scale thermal testing and analysis is the following: Does conduction dominate heat flow or do heat pipes and buoyant gas-phase convection significantly influence heat flow around emplacement drifts and in the repository as a whole?

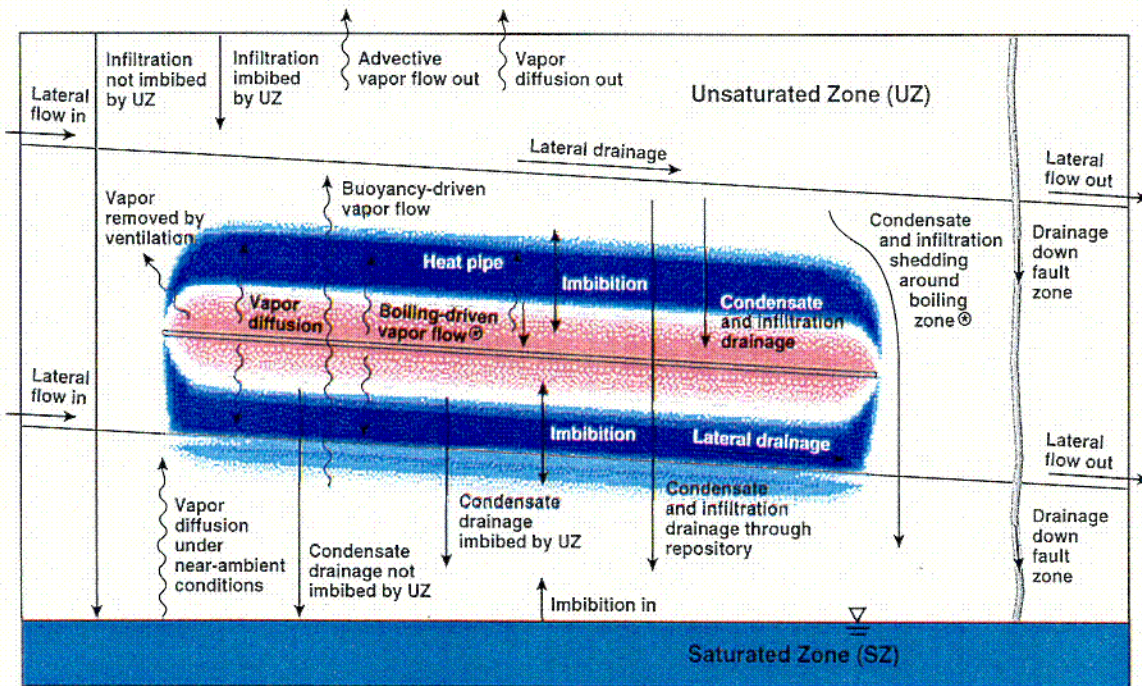


Source: Hardin 1998, Figure 3-2

NOTE: " $T_b$ " Refers to the Boiling Isotherm. Ventilation of the drifts during the preclosure period results in a significant amount of heat removal from the emplacement drift. Note that the majority of percolation and condensate drainage flux occurs in the fractures.

Figure 3-4. DS Schematic Showing Decay-Heat-Driven TH Flow and Transport Processes Fracture Flow is Shown with Solid Arrows, Water Vapor Flow with Dashed Arrows, and Heat Flow with Oscillatory Arrows

C-5



Source: Hardin 1998, Figure 3-3

Figure 3-5. Mountain-Scale Schematic Showing Decay-Heat-Driven TH Flow and Transport Processes that Influence Moisture Redistribution and the Moisture Balance in the UZ

The preceding discussion concerns long-term *transient* changes in the UZ associated with the redistribution of water by evaporation and condensation. Because of the long expected lifetime of the engineered barriers, it is likely that radionuclide release and transport will occur after the *thermally disturbed period*, that is, in the *final state* of the mountain following the thermal pulse. Compared to the initial ambient conditions, the permeability distribution changes in the *final state* because of the associated saturation changes and changes due to coupled processes. Were it not for the coupled processes, in principle, the mountain would return to something resembling its initial state, except for the effects of climate change, after decay of the thermal pulse and rewetting of the dried-out regions. However, the TH disturbance will also generate TC and thermal-mechanical (TM) alteration of hydrological and transport properties, particularly in the fractures, in both the unsaturated and saturated zones. Some changes, such as normal deformation fracture closure that results from TM effects, may be temporary. However, shear or slip displacement along fractures as well as non-elastic normal closure will have permanent impact on permeability distribution within the NF. TC effects, such as the filling of fractures may also be irreversible such that changes are or the process dominated by very slow reaction rates such that they are limited by kinetics so that recovery takes extremely long time. It is possible that these changes are sufficiently significant enough to require inclusion in long-term calculations of repository performance. These issues are discussed further in Sections 2.2.2, 2.2.4, 3.3, 3.4, and 3.5.

Recall that each of the processes defined above apply to varying degrees to the base case repository design for TSPA-SR. Comprehensive insight of each TH process described in this section (even those based on previous designs) was necessary in deciding which of these

C-6

processes needed to be emphasized or mitigated by a strategic choice of design parameters specified for SR. The next section provides some of the important details of previous TH analyses for the VA and LADS repository designs. The importance of understanding the processes initiated by each of the previous designs led to the specification of many of the features and criteria developed for the SR repository design (e.g., an 81 meter emplacement drift spacing to allow condensate drainage during the thermal period).

### 3.2.1.2 Key Factors Influencing Thermal-Hydrological Conditions in the NFE

Thermal-hydrological conditions in the NFE (as well as in the EBS) are influenced by a number of key factors:

- Repository-scale variability of percolation flux.
- Temporal variability of percolation flux (as influenced by climate change).
- Uncertainty in percolation flux (as addressed by the mean, high, and low infiltration-flux cases considered in TSPA).
- Repository-scale variability in and magnitude of hydrologic properties (e.g., those governing matrix imbibition diffusivity and capillary wicking in fractures).
- Edge-cooling effect (which increases with proximity to the edge of the repository).
- Dimensions and properties of the EBS components, such as the drip shield, engineered backfill and the invert.
- WP-to-WP variability in heat-generation rate.
- Repository-scale variability in overburden thickness.
- Repository-scale variability in thermal conductivity (with an emphasis on the host-rock units).

The influence of these factors is described in the MSTHM AMR (CRWMS M&O 2000k, Section 6.11). Sections 3.2.3.1 and 3.2.3.2 of this document discuss the influence of some of these factors on TH conditions in the NFE for the EDA-II design without and with backfill, respectively.

### 3.2.2 Thermal-Hydrological Models

The primary features that distinguish between various TH models involve: (1) dimensionality of the modeling domain, (2) dimensionality of the heat-source representation, and (3) representation of *Fracture Matrix Interaction* (FMX). With regards to modeling dimensionality, the two primary categories are drift scale and MS. DS TH models can be 1-D, 2-D, or 3-D. Mountain-scale TH models are typically 3-D; however, symmetry assumptions are frequently used that result in mountain-scale TH models being effectively 2-D (note that such models can be 3-D at the drift scale). With regards to heat-source representation, there are three primary categories:

(1) smeared-heat-source, over a horizontal plane, (2) line-averaged-heat-source, along the axis of the emplacement drift, and (3) discrete-heat-source, representing the actual dimensions of the WPs and WP spacing. The line-averaged heat source category may be applied to the cross section of the WP or to the entire cross section of the emplacement drift.

A summary of alternative conceptual models used to represent FMX is given in Sections 2.2.1 and 2.4.1. All of the calculations described in Section 3.2.3 of this report used the DKM, together with the AFM. The DKM conceptualizes the fractured rock as having two interacting materials, one representing the matrix and one representing the fractures. The interaction between the fractures and the matrix is explicitly calculated from the local temperature and pressure differences, thus allowing local disequilibrium between fracture and matrix to be represented. The AFM accounts for the contact area between the fracture and the matrix, as well as the frequency of fractures. In the AFM, fracture flow may only occur through some of the fractures. The flux through a fracture is greater when it has higher saturation and, therefore, focusing flow through a portion of the fractures (i.e., to active fractures) maximizes flux and results in higher flow velocities through the mountain.

NFE TH models used to date assume that the axial convection of heat (and moisture) by pre-closure ventilation can be approximated by reducing the magnitude of the pre-closure heat source. During post-closure, axial convection is expected to be less significant, and it is not included in the models. In-drift convection (in a plane perpendicular to the drift axis) is treated at low resolution by some NFE TH models; more sophisticated treatment may be necessary for EBS calculations of moisture movement in the drifts.

Ideally, a TH model of the repository would be fully 3-D at both mountain and drift scale. At MS, this model would represent the overall 3-D geometry of Yucca Mountain (including the topography of the ground surface and water table) and the engineered repository area, as well as the distribution of hydrostratigraphic units. At drift scale, this model would represent the 3-D geometry of the emplacement drifts, including details of the WPs, drip shields, and invert. This model would also represent the WP-to-WP variability of decay-heat generation and the areal and temporal distribution of infiltration flux throughout the repository area.

The need for a multi-scale approach stems from the fact that the performance measures depend on TH behavior within a few meters of the emplacement drifts, and also on thermal and TH behavior on a repository (or mountain) scale. A single numerical model cannot readily incorporate the required range of scales, for locations throughout the repository, without involving an infeasible number (millions) of grid blocks. Two alternative approaches to the multi-scale prediction problem are combining a series of various scale models (Section 3.2.2.1) and a model that embeds a 3-D DS model with a relatively fine mesh into a 3-D mountain-scale model with a coarse mesh. (Section 3.2.2.2)

### **3.2.2.1 Multi-scale Thermohydrologic Model**

Table 3-3 summarizes various TH models, as well as conduction (T) models. Several of these model types are process-level submodels for the MSTHM and others are abstracted models of the MSTHM.

Table 3-3. Summary of TH and T Model (or Submodel) Types, Including Those Used in the Multi-scale Thermal Hydrological Model

Model Type	Heat Source	Dimensionality	Process Type	In-Drift Thermal Radiation	Use in MSTHM
SMT	smearred	3-D mountain-scale	T	NA	Process-model input
SMTH	smearred	3-D mountain-scale	TH	NA	Process-model input <sup>1</sup>
LMTH	line-averaged	3-D mountain-scale	TH	yes	MSTHM result <sup>2</sup>
DMTH	discrete	3-D mountain-scale	TH	yes	MSTHM result <sup>2</sup>
SDT	smearred	1-D DS	T	NA	Process-model input
SDTH	smearred	1-D DS	TH	NA	Process-model input <sup>1</sup>
LDTH	line-averaged	2-D DS	TH	yes	Process-model input
DDT	discrete	3-D DS	T	yes	Process-model input
DDTH	discrete	3-D DS	TH	yes	Model-abstraction testing <sup>1</sup>

Source: Adapted from CRWMS M&O 2000k

<sup>1</sup> May be used in any potential future version of the multi-scale TH modeling approach

<sup>2</sup> Calculated with the MSTHM, see Figure 3-6)

All models have an upper boundary that corresponds to the ground surface. Temperature, gas-phase pressure, and relative humidity (or gas-phase air-mass fraction) are specified (as fixed values) at the upper boundary. Most of the TH models have a lower boundary that corresponds to the water table. The value of gas-phase pressure at the water table is established when the models are initialized at ambient conditions. The liquid-phase saturation at the water table is always 100%, while the temperature is a specified fixed value. The initialization model runs are continued until the temperature, liquid-phase saturation, gas-phase pressure, and gas-phase air-mass fraction distributions in the model attain steady-state.

The 3-D SMT model (Table 3-3) is a submodel used in the MSTHM calculations to determine the repository-scale variations in host-rock temperature resulting from the heat output from the entire inventory of 70,000 MTU of waste, including 63,000 MTU of CSNF and 7000 MTU of DHLW (vitrified high-level waste and DSNF WPs). The SMT model includes the influence of mountain-scale thermal-property distribution, the edge-cooling effect, which results from lateral heat loss at the repository edges, and the overburden-thickness distribution. (Overburden thickness is defined to be the depth of the repository horizon below the ground surface.) The SMT model domain extends from the ground surface to 1000 m below the present-day water table, and the lateral (adiabatic) boundaries are far enough away from the repository so that they do not affect repository temperatures. The temperature 1000 m below the water table is found by extrapolation, which is described in the Multiscale TH Model AMR (CRWMS M&O 2000k, Attachment XX). The extrapolation procedure assures the continuity of heat flux across the water-table boundary.

The Mutiscale TH AMR (CRWMS M&O 2000k) describes the model used to provide NF and EBS conditions in the TSPA-SR. That AMR is based on a number of historical publications, including Hardin (1998). In Hardin (1998, Sections 3.2.2 and 3.5.2), the physical understanding of the NF and in-drift conditions is summarized based on numerous calculations, and results are

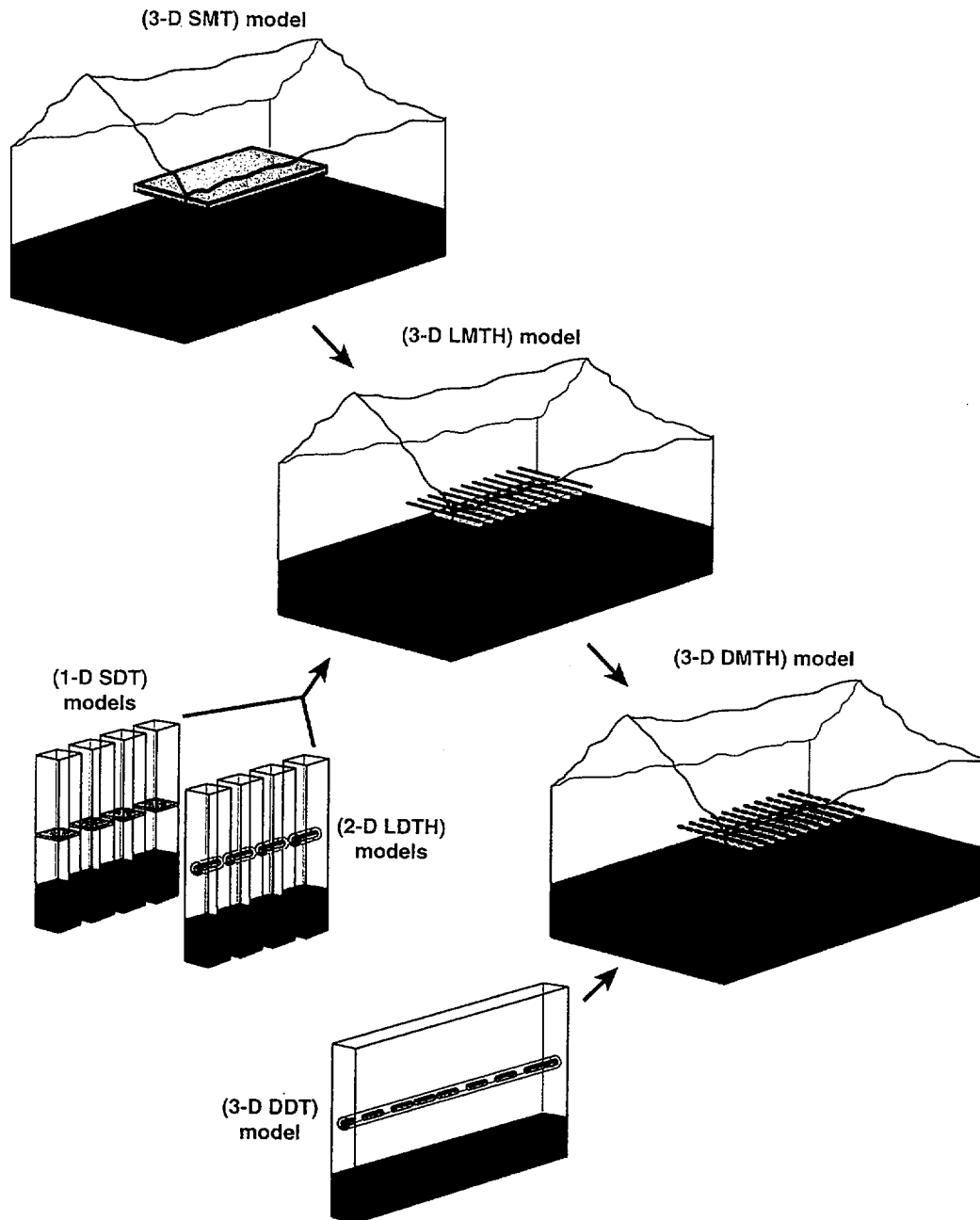
presented of a sensitivity study of waste package/drift spacing options and of hydrologic property sets. Section 3.2.3.3 is based on Hardin (1998).

The MSTHM calculates results that are similar to those expected from a full-scale, 3-D mountain- and repository-scale model with DS resolution (i.e., millions of grid blocks). Given the number of required implementations of the calculation procedure for TSPA-VA performance measures, the multi-scale approach was developed to efficiently incorporate as much detail as is computationally feasible (the current MSTHM captures all relevant processes except mountain-scale buoyant gas-phase convection). Submodels that comprise the current multiscale model (Figure 3-6) include:

- **Smearred-heat-source Mountain-scale Thermal conduction (SMT) models**, can either be 2-D or 3-D (SMT in Figure 3-6). Because these models smear out the overall heat generation from the potential repository over the repository area, they cannot distinguish between conditions within (or close to) the emplacement drifts from those in the center of the rock pillar separating the drifts. Early attempts to represent 3-D mountain-scale heat flow used a 2-D axisymmetric disk-shaped representation of the repository area (Buscheck and Nitao 1994, p. 7). These models represent the influence of the edge-cooling effect. The disk-shaped representation of the heat source has also been used in TH-model scoping calculations of large-scale *in situ* thermal tests (Buscheck et al. 1997c, Chapter 2).
- **Smearred-heat-source DS Thermal-conduction (SDT) models**, are typically 1-D (SDT in Figure 3-6). These models cannot distinguish between conditions within (or close to) the emplacement drifts from those in the center of the rock pillar separating the drifts; neither can they represent the influence of edge cooling effects.
- **Line-average-heat-source Drift scale Thermal-Hydrological (LDTH) models**, are typically 2-D or 3-D (LDTH in Figure 3-6). These models represent average conditions on the WPs (and other components in the drifts, such as drip shields). These models represent the 2-D distribution of conditions in the vertical plane orthogonal to the drift; therefore, they cannot distinguish between hotter and cooler WP locations; neither can they represent the influence of the edge-cooling effect. The "H" in the acronym indicates the submodel includes hydrological flow processes.
- **Discrete-heat-source, DS, Thermal-conduction (DDT) models**, are always 3-D (DDT in Figure 3-6). These models discretely represent the 3-D geometry of the emplacement drifts, as well as WP-to-WP variability of decay-heat generation; therefore, they can distinguish between hotter and cooler WP locations. However, these models cannot represent the influence of the edge-cooling effect. These models were introduced relatively recently to TSPA and repository design analyses (Wilder 1996, Section 1.10; Buscheck et al. 1997e, pp. 1030-1034) and have also been used to model the DST (Buscheck et al. 1997d, Chapter 2).

The Multi-scale Thermohydrologic Abstraction Code, MSTHAC (CRWMS M&O 2000k), is used to integrate the results from the SMT, SDT, and LDTH submodels to produce the MSTHM results, termed LMTH in Figure 3-6. (The LMTH is an intermediate output of the MSTHM). In

turn, the LMTH multi-scale results are combined with the DDT submodel results to produce the overall DMTH model results, the final output of MSTHM. (The software that combines the submodel results is termed MSTHAC, while the overall model is MSTHM.)



Source: Derived from CRWMS M&O 2000k, Figure 1-1

NOTE: The LMTH and DMTH models are combinations of results from feeder submodels.

Figure 3-6. The Submodels of the Multi-Scale Thermal Hydrologic Model

It is useful to think of the LDTH submodel as the "core" submodel. For the TSPA-SR, these 2-D DS TH submodels are run for 31 locations spaced evenly throughout the repository area for several AML values (nominal value and lower) to represent the influence of edge-cooling effects. The LDTH submodel includes the hydrological processes and parameters (e.g., surface infiltration rates, H properties) used to describe a location, given specific coordinates within the repository. The remaining three submodels, which are conduction only, are required to account for the influence of 3-D mountain-scale heat flow and 3-D DS heat flow on DS TH behavior. The coupling of 3-D mountain-scale heat flow to 2-D DS TH behavior is accomplished with the SMT and the SDT submodels. The SMT is 3-D and includes the influence of thermal-property variation in the mountain, lateral heat loss at the repository edges, and overburden-thickness variation with location, assuming a uniform, planar (i.e., smeared) heat source throughout the repository area. The SMT calculates temperatures at 623 locations within the repository footprint. The SDT submodel is a 1-D (vertical) submodel, run at the same 31 locations and for the same AMLs as the LDTH submodels. To obtain the "line-averaged" drift-wall temperature (which is roughly equivalent to an average WP location), the relationship between the drift-wall temperature in the LDTH submodel and the "smeared" repository-plane temperature in the SDT submodel are interpreted to the 623 SMT locations and used to modify the temperatures in the SMT submodel, thereby resulting in an MSTHM drift-wall temperature that approximates the effects of the most important TH processes at DS and the geometry effects of mountain-scale.

Because the SMT and SDT submodels both share the same smeared-heat-source approximation and thermal-conduction representation of heat flow, the relationship between the SDT submodel temperature and the LDTH submodel drift-wall temperature allows for the SMT submodel temperature to be "corrected" for both the influence of TH processes on temperature and for the influence of 2-D DS dimensionality (orthogonal to the axis of the drift). The SMT, SDT, and LDTH submodels all share a blended heat-generation history, which blends the heat-generation histories of the entire repository; hence, the heat-generation history is effectively that of an "average" WP. The DDT submodel is a 3-D DS submodel that includes individual WPs (with distinctive heat-generation histories) and accounts for thermal radiation in addition to thermal conduction between the WPs and drift surfaces. The drift-wall temperatures for an average WP, calculated with the combined use of the LDTH, SMT and SDT submodels, are then further modified to account for waste-package-specific deviations using the DDT submodel. This is accomplished by using the spatial variation of local temperatures at various "point" locations along the drift (such as on the drift wall, drip shield surface, and WP surface) and the corresponding "line-averaged" temperature in the DDT submodel.

The MSTHM has been used to develop time-varying estimates of key NFE performance measures for locations throughout the entire repository for the VA (DOE 1998, Volume 3, Section 3.2) and is being used in the TSPA-SR (see Section 3.2.3.1). Performance predictions vary significantly for different locations in the repository, because of differences in the local hydrostratigraphy and local percolation flux. The performance measures include drift-wall temperature, WP temperature, and drift-air RH (relative humidity) at the WP surface. Multi-scale methods use estimation procedures that are computationally fast enough to be conducted for many locations in the repository lay-out, and repeated for TSPA-VA sensitivity cases and alternative model exercises. This efficient method was also useful in conducting numerous TH-model calculations in support of the LADS (CRWMS M&O 1999a).

The measures in Table 3-4 were used by TSPA-VA (DOE 1998, Volume 3, Section 3.4.1.2) and TSPA-LADS (CRWMS M&O 1999a, Figure 5-11), and are currently being used by TSPA-SR to estimate WP corrosion rates, waste-form dissolution rates, and transport of radionuclides in the NFE. The use of conduction-only models will introduce small errors in the abstracted performance measures. The magnitude of these errors can be estimated by comparison of abstracted results with direct simulations. Where possible, conduction-only models are used to calculate temperature differences instead of absolute temperatures; this approach minimizes the abstraction errors. The TH performance measures (Table 3.A-b) were provided to TSPA-VA and TSPA-LADS for various combinations of repository location, heat production rates as determined by WP design and waste type (e.g., CSNF or defense high-level waste), WP spacing, sequencing of WP types in the emplacement drifts, and design options such as the line-load design or backfill. The TH performance measures were also provided for testing sensitivity of the TSPA-VA to variations in thermal and hydrological properties, distributions of infiltration flux, including the influence of climate change, conceptual models of FMX (e.g., comparing ECM with DKM results), and conceptual models of heat-flow conditions at the water table, (e.g., a fixed temperature vs. explicit representation of heat loss to the SZ). For the TSPA-SR, an expanded list of TH performance measures are being provided (Tables 3-5 and 3-6).

Table 3-4. List of NFE and EBS TH Parameters Calculated with the MSTHM for the TSPA-VA and for the TSPA-LADS

Location	<i>T</i>	<i>RH</i>	$X_{air,gas}$	$S_{liq}$	$q_{liq}$
Rock above drift wall	x	X	x	x	X
Rock at drift wall	X	X	x	x	x
Drift above WP		X			
WP surface	X	X			
Invert	x	X	X	X	

Measures calculated for TSPA-VA and TSPA-LADS are indicated by bold, uppercase X. Other measures also calculated by the approach are indicated by lowercase x. The measures are temperature (*T*), relative humidity (*RH*), gas-phase air-mass fraction ( $X_{air,gas}$ ), liquid phase saturation ( $S_{liq}$ ), and liquid-phase flux ( $q_{liq}$ ).

### 3.2.2.2 Unsaturated-Zone Mountain-Scale TH Model

The Mountain-Scale TH AMR (CRWMS M&O 2000t) documents the development of the MS Thermal-Hydrological (TH) model that evaluates the effects of heat on UZ flow and distribution of liquid and temperature over a period of 100,000 years. The issues addressed include the following: (1) extent of the 2-phase zone, (2) liquid and gas flux in near and far field, (3) moisture redistribution in the UZ, (4) temperature of drifts and pillars, (5) potential for flow and transport property change in the PTn and CHn, (6) TH effects on water table and perched water bodies, and (7) influence of climate and ventilation. While items (5) and (6) of the above are strictly far-field issues, all other items pertain to the NF environment.

Table 3-5. List of NFE and EBS TH Variables Calculated with the MSTHM at 623 Repository Subdomains for Backfill-Runs of the TSPA-SR

TH Variable	Drift-Scale Location
<b>NFE Parameters</b>	
Temperature	NFE rock (5 m above drift, and mid-pillar at repository horizon)
	Maximum lateral extent of boiling
	Upper drift wall (crown of the drift)
	Lower drift wall (below invert)
	Drift wall (perimeter average)
Relative Humidity	Drift-wall (perimeter average)
Liquid-phase matrix saturation	Drift wall (perimeter average)
Liquid-phase flux	NFE host rock (5 m, 3 m, and 0.2 m above crown of drift)
	Drift wall (crown, in matrix and in fractures)
Gas-phase (water vapor) flux	Drift wall (perimeter average)
Gas-phase (air) flux	Drift wall (perimeter average)
Evaporation rate	NFE rock
<b>EBS Parameters</b>	
Temperature	Drift wall (perimeter average)
	Backfill (crown)
	Drip shield (perimeter average and upper surface)
	WP (surface average)
	Invert (average)
Relative humidity	Drift-wall (perimeter average)
	Backfill (crown)
	Drip shield (perimeter average)
	Waste package
	Invert (average)
Liquid-phase matrix saturation	Drift wall (perimeter average)
	Drip shield (perimeter average)
	Invert (average)
Liquid-phase flux	Drip shield (crown, upper surface average, and lower side at the base)
	Invert (average)
Gas-phase air-mass fraction	Drip shield (perimeter average)
Gas-phase pressure	Drip shield (perimeter average)
Capillary pressure	Drip shield (perimeter average)
	Invert (average)
	Drift wall (crown, in matrix and in fractures)
Gas-phase (water vapor) flux	Drift wall (perimeter average)
Gas-phase (air) flux	Drift wall (perimeter average)
Evaporation rate	Backfill (crown)
	Drip shield (crown and perimeter total)
	Invert (total)

Table 3-6. List of NFE and EBS TH Variables Calculated with the MSTHM at 610 Repository Subdomains for No Backfill-Runs Rev 00 of the TSPA-SR

TH Variable	Drift-Scale Location
<b>NFE Parameters</b>	
Temperature	NFE rock (5 m above drift and along the entire repository horizon)
	Maximum lateral extent of boiling
	Upper drift wall (crown of the drift)
	Lower drift wall (below invert)
	Drift wall (perimeter average)
Relative Humidity	Drift-wall (perimeter average)
Liquid-phase matrix saturation	Drift wall (perimeter average)
Liquid-phase flux	NFE host rock (5 m and 3 m above crown of drift)
	Drift-wall (upper surface perimeter average in matrix & fractures)
Gas-phase (water vapor) flux	Drift wall (perimeter average)
Gas-phase (air) flux	Drift wall (perimeter average)
Evaporation rate	NFE rock
<b>EBS Parameters</b>	
Temperature	Drift wall (perimeter average)
	Backfill (crown)
	Drip shield (perimeter average and upper surface)
	WP (surface average)
	Invert (average)
Relative humidity	Drift-wall (perimeter average)
	Backfill (crown)
	Drip shield (perimeter average)
	Waste package
	Invert (average)
Liquid-phase matrix saturation	Drift wall (perimeter average)
	Drip shield (perimeter average)
	Invert (average)
Liquid-phase flux	Drip shield (crown, upper surface average, and lower side at the base)
	Invert (average)
Gas-phase air-mass fraction	Drip shield (perimeter average)
Gas-phase pressure	Drip shield (perimeter average)
Capillary pressure	Drip shield (perimeter average)
	Invert (average)
	Drift wall (crown, in matrix and in fractures)
Gas-phase (water vapor) flux	Drift wall (perimeter average)
Gas-phase (air) flux	Drift wall (perimeter average)
Evaporation rate	Backfill (crown)
	Drip shield (crown and perimeter total)
	Invert (total)

The mountain-scale TH model is developed based on the UZ model. It uses input parameters based on the Calibrated Properties AMR (CRWMS M&O 2000n), a spatially varying mean infiltration rate, with varying climates during the thermal-loading period. The simulations were performed using the average initial thermal load of 72.7 kW/acre, scale down by the natural decay curve over a total simulation period of 100,000 years. To account for ventilation, only 30% of this heat is used for the first 50 years of emplacement. The TH model uses the mathematical formulation employed in the TOUGH2 family of codes (Pruess 1987, pp. 2-11; 1991), the dual-continuum approach, and the van Genuchten capillary pressure and relative permeability relationships to describe the behavior of the UZ under thermal-loading conditions. This formulation is based on the traditional energy and mass conservation relationships.

The embedded 3-D mesh approach was used in the UZ F&T PMR (CRWMS M&O 2000f, Section 3.12) with detailed discussion of the numerical grids in the Numerical Grids and Mountain-Scale TH AMRs (CRWMS M&O 2000w and 2000t). In addition to the 3-D submodels, two 2-D cross section analyses were performed. Six cases, two 3-D without drifts, one 2-D without drifts, and three 2-D with drifts (UZ F&T PMR, Table 3.12-1) were performed. Another, somewhat similar approach was used to evaluate the DST (CRWMS M&O 2000a). In this approach, a series of 24 vertical 2-D sections, orthogonal to the drift, were calculated with extremely refined grids around the drift. These cross-sections were then extended and merged into the third dimension.

The MS TH modeling study uses both 2-D and 3-D submodels of the 3-D UZ flow model. This study shows that the available heat source and its distribution, as well as infiltration rates are the determining factors for boiling and re-wetting TH processes at the repository. With and without ventilation, two-phase heat-pipe conditions are developed in a region above the repository during 10-100 years after emplacement. Dry-out conditions are predicted near the drifts, in both the fracture and matrix continua with drift temperatures exceeding 100°C for hundreds of years. With ventilation, temperatures rise to boiling conditions only in the immediate area of the drifts. The temperature in the pillars rises to 80-85°C. At early times (less than 100 years), thermally induced liquid flux up to two orders of magnitude larger than the ambient percolation flux is predicted to move toward the drying area due to capillary pressure gradient. However, this liquid flux is vaporized by the repository heat and does not reach the drifts. The model predicts that vertical flow crossing the pillars between the drifts generally continues at a rate close to the ambient percolation flux for most of the thermal loading period. In some locations the flow may be enhanced by condensate drainage for a period of several hundred years. The MS TH model predicts a nearly 30 to 35°C temperature increase at the water table to an average of 65 to 70°. At the top of CHn stratigraphic unit, the predicted maximum temperature rises to 75-80°C for a period between 2,000 and 7,000 years. This temperature is not high enough to induce sorption property changes.

### **3.2.3 Thermal-Hydrological-Model Results**

Four case studies are described in this section. First, in Section 3.2.3.1, the detailed NFE TH results are presented for the current, no-backfill, SR design (using the MSTHM). Because these results are to be documented in an AMR ICN later than this PMR ICN, they are presented in detail here. Section 3.2.3.2 describes the MSTHM calculations of the initial SR design that included backfill. The final two subsections describe DS TH calculations that use the LDTH

model. Section 3.2.3.3 describes calculations used to support the philosophical shift in thermal design from mountain-scale dryout to maintenance of drainage in the pillars between the emplacement drifts. The LDTH submodels that were used in the MSTHM calculation were from the TSPA-VA. Section 3.2.3.4 describes a comparison of TH results from an LDTH submodel used in the TSPA-SR, a DS THC model, and a mountain-scale TH model.

### **3.2.3.1 Multi-scale Thermohydrologic Model Calculations for the Site-Recommendation Design with No Backfill**

The Multiscale TH AMR (CRWMS M&O 2000k), described in Section 3.2.2.1, has been used to calculate temperature, liquid-phase saturation, relative humidity, evaporation rate, capillary pressure, and liquid fluxes in the NF rock, and temperatures, humidity, and liquid-phase flux and gas-phase flux in the emplacement drifts (DTN: LL000509112312.003). In this PMR, selected values and graphical distributions of parameters are presented for the NFE host-rock results. All calculations shown in this section pertain to the mean infiltration-flux case.

#### **3.2.3.1.1 Temperature**

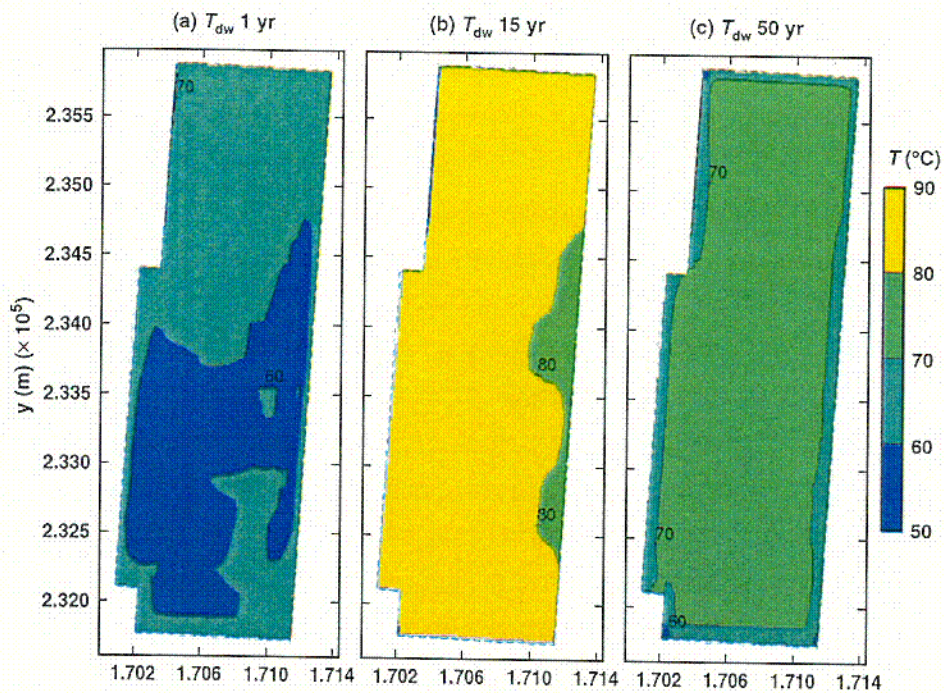
Figure 3-7 shows the spatial distributions (over the repository footprint) of perimeter-averaged drift-wall temperature. Preclosure drift-wall temperatures stay below the boiling point, while the WP temperature climbs above the boiling point as it peaks around 15 yr. Shortly after ventilation ceases, peak drift-wall temperatures occur. Peak drift-wall temperatures are generally less than 150°C. The edge-cooling effect is very evident thereafter, as temperatures around the repository edges are considerably less than at the repository center. Boiling at the drift wall ceases around 1,000 yr.

Figure 3-8 shows the spatial distributions of temperature in the host rock 5 m above the crown of the drift. This vertical location reaches the boiling point at about 100 year and remains slightly above the boiling point for less than 300 year.

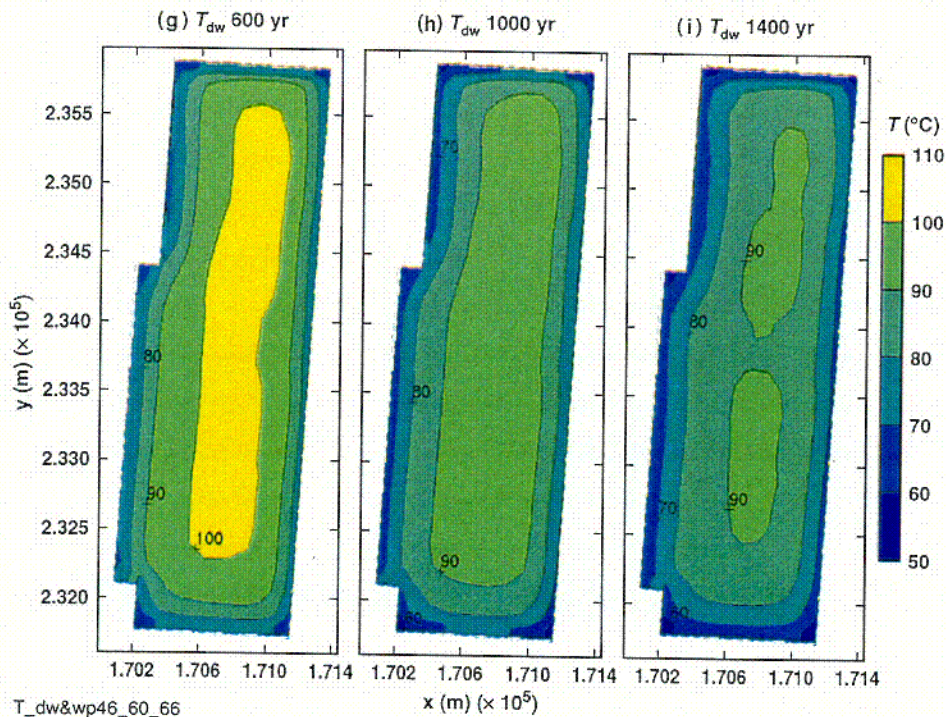
Figure 3-9 shows the spatial distribution of temperature 7.39 m laterally away from the springline of the drift. This location in the pillar is about 20% of the distance in toward the midline of the pillar. This depth into the pillar never quite reaches the boiling point at any location in the footprint, assuring that condensate and percolation flux can readily shed between emplacement drifts.

Figure 3-10 shows the temperature history at various locations in the NFE host-rock, as well as on the WP, for the geographical center of the repository and a location 27.5 m from the eastern edge of the repository footprint. The duration of boiling is considerably less at the edge (~100 year) than it is at the center of the repository. The temperature history 5 m above the crown of the drift is similar to that 7.39 m laterally away from the springline of the drift.

INTENTIONALLY LEFT BLANK



T\_dw&wp02\_06\_11

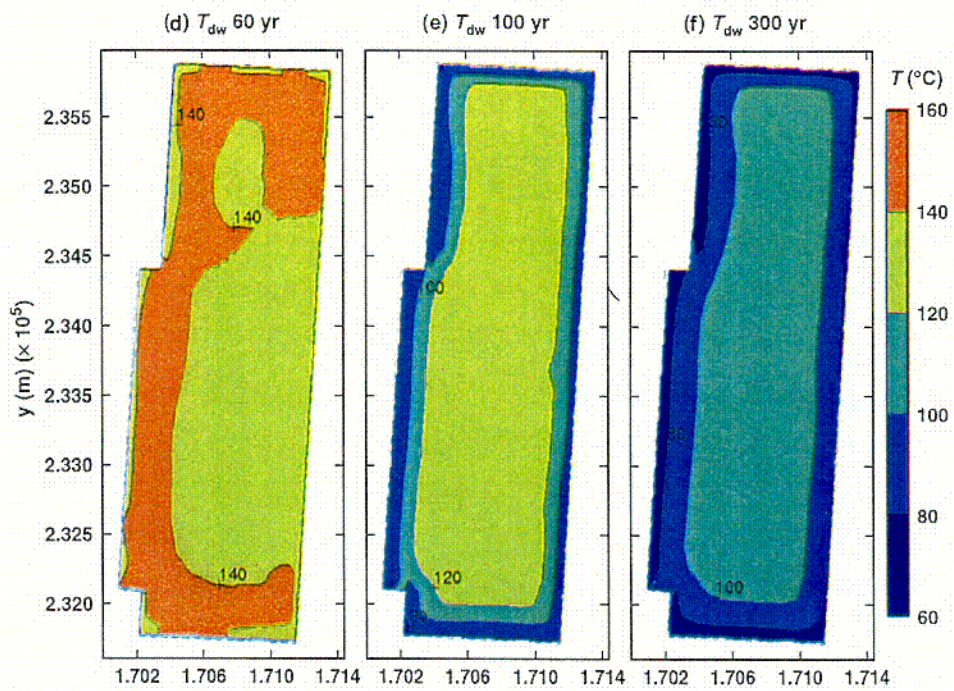


T\_dw&wp46\_60\_66

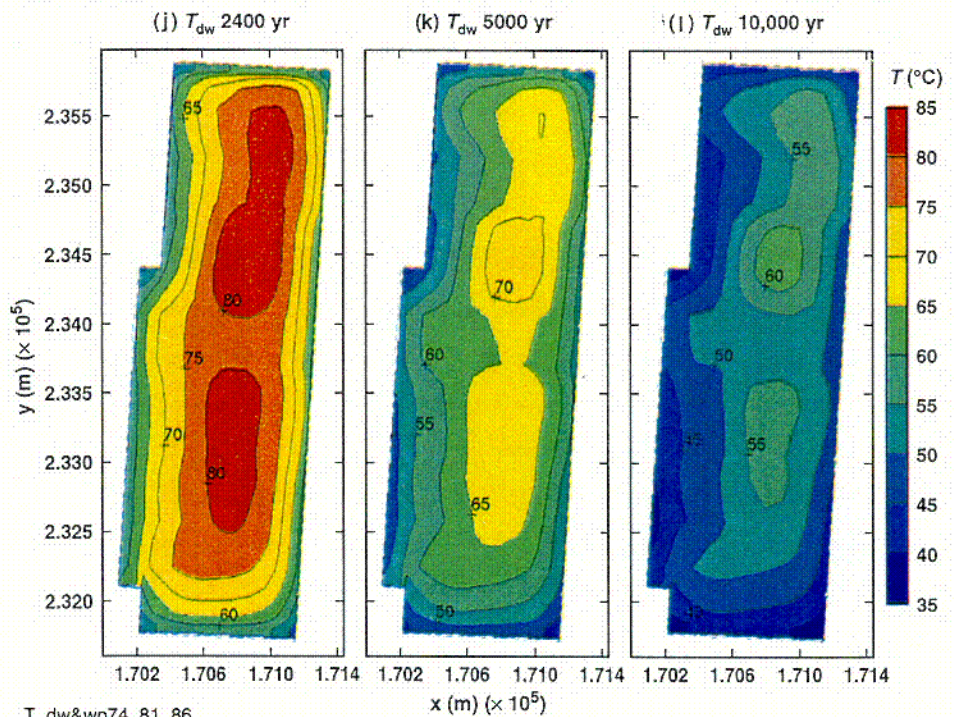
DTN: LL000509112312.003

Figure 3-7. Perimeter-Averaged Temperature on the Drift Wall for a 21-PWR WP for the Mean Infiltration-Flux Case for the Indicated Times (Page 1 of 2)

C-7



T\_dw&wp17\_21\_31

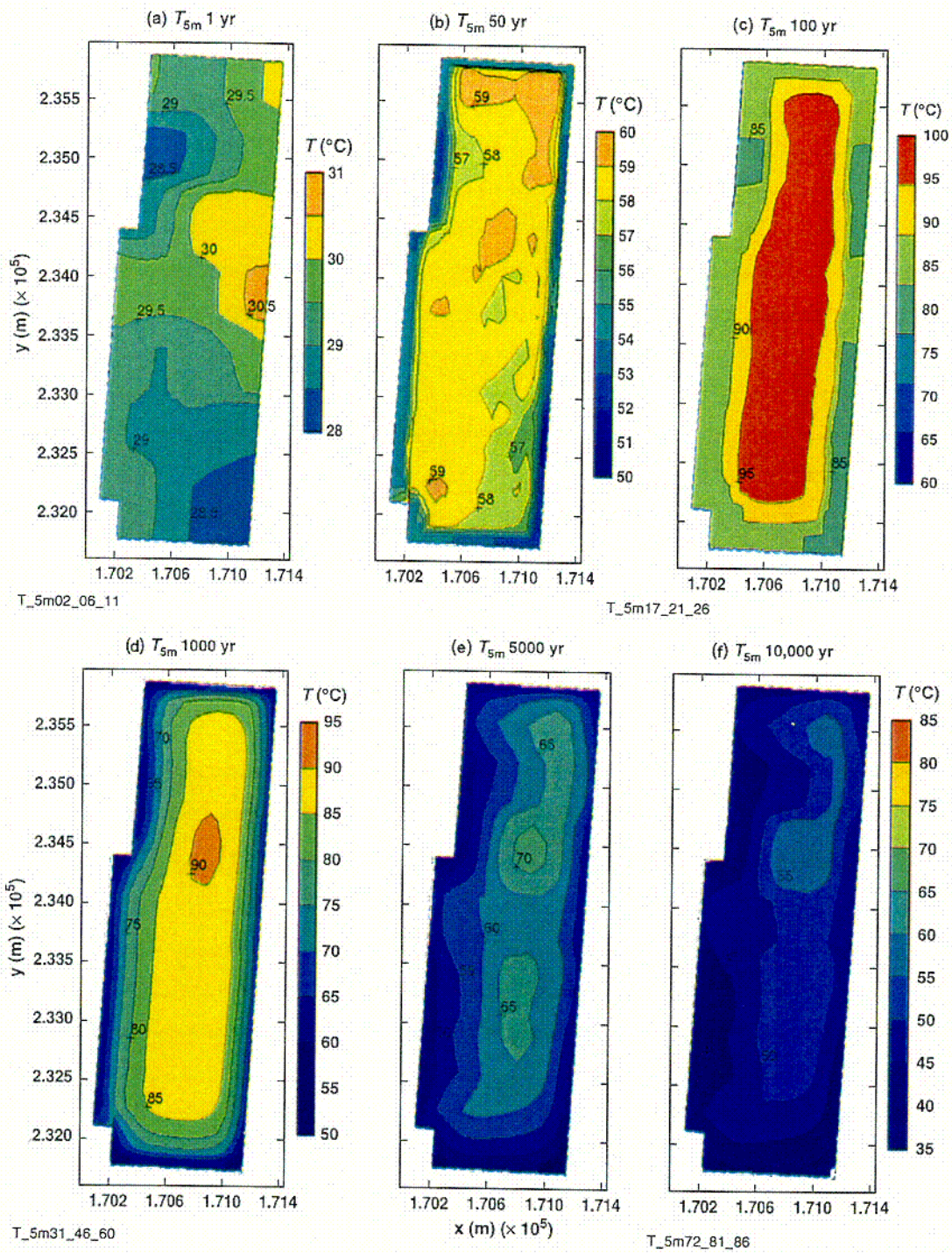


T\_dw&wp74\_81\_86

DTN: LL000509112312.003

Figure 3-7. Perimeter-Averaged Temperature on the Drift Wall for a 21-PWR WP for the Mean Infiltration-Flux Case for the Indicated Times (Page 2 of 2)

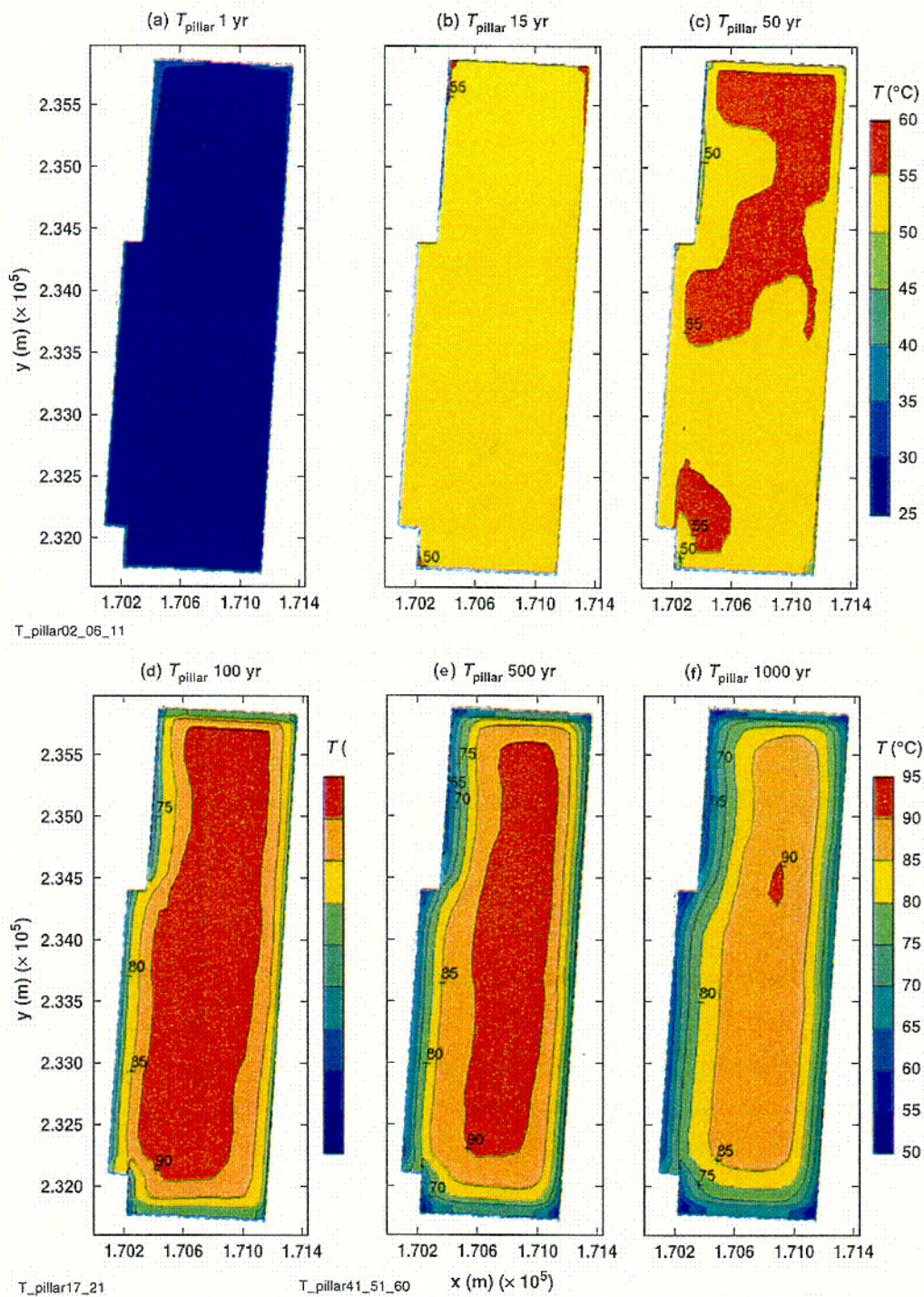
*0-8*



DTN: LL000509112312.003

Figure 3-8. Temperature 5 m above the Crown of the Drift in the Vicinity of a 21-PWR WP for the Mean Infiltration-Flux Case for the Indicated Times

2-9

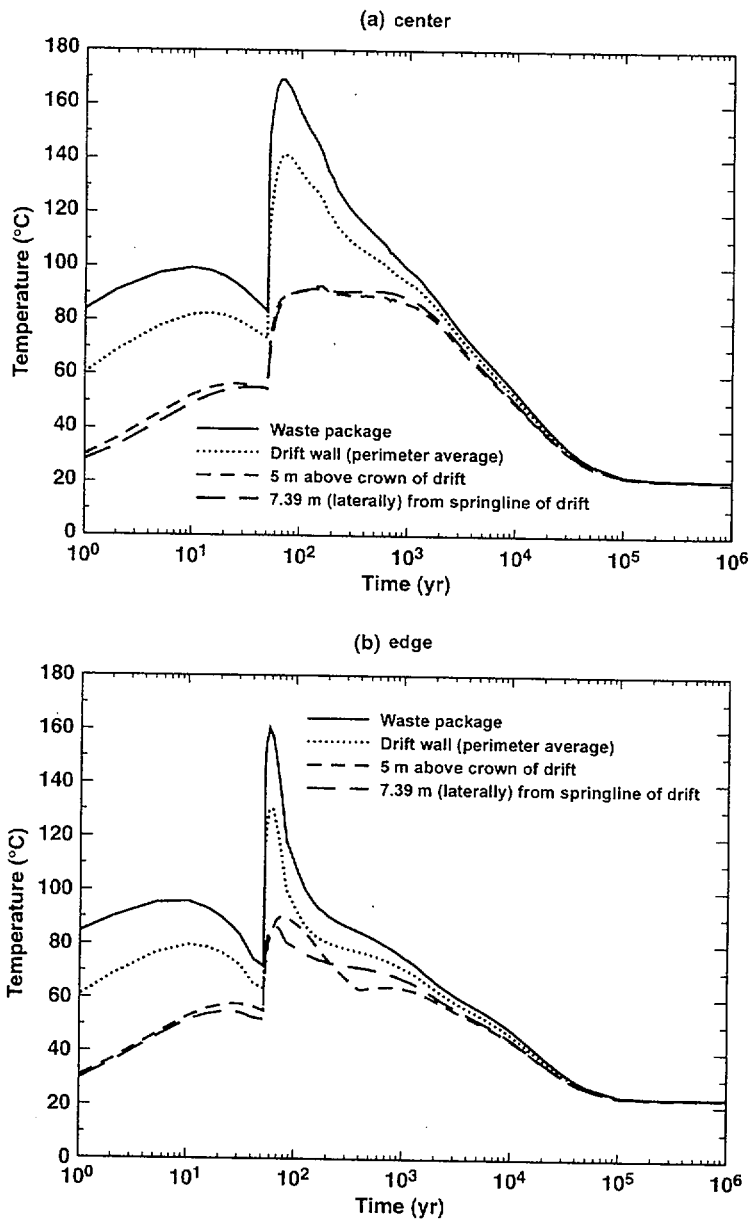


DTN: LL000509112312.003

NOTE: This location is about 20% of the distance in toward the midline of the pillar. This temperature is called  $T_{pillar}$ .

Figure 3-9. Temperature 7.39 m Laterally away from the Springline of the Drift in the Vicinity of a 21-PWR WP for the Mean Infiltration-Flux Case for the Indicated Times

L:10



Tall\_16\_16-24\_16

DTN: LL000509112312.003

NOTE: The temperatures occur in the vicinity of a 21-PWR WP for the mean infiltration-flux case for the indicated times.

Figure 3-10. Temperature History at the Indicated Locations at (a) the Geographical Center of the Repository and (b) a Location 27.5 m from the Eastern Edge of the Repository

Figure 3-11 shows the complementary cumulative distribution function (CCDF) for the peak temperature on WPs and on the drift wall, as well as showing the CCDF of the maximum lateral extent of the boiling point isotherm. The coolest WP location has a peak drift-wall temperature of about 115°C, while the hottest WP location has a peak of about 147°C. For the coolest WP location, the maximum lateral extent of boiling is about 6.5 m from the repository centerline, while for the hottest WP location, the maximum lateral extent of boiling is about 8.9 m. Therefore, between 78 to 84% of the repository horizon remains below the boiling point, which will assure that condensate and percolation flux can readily shed between emplacement drifts.

#### **3.2.3.1.2 Liquid-Phase Saturation and Relative Humidity**

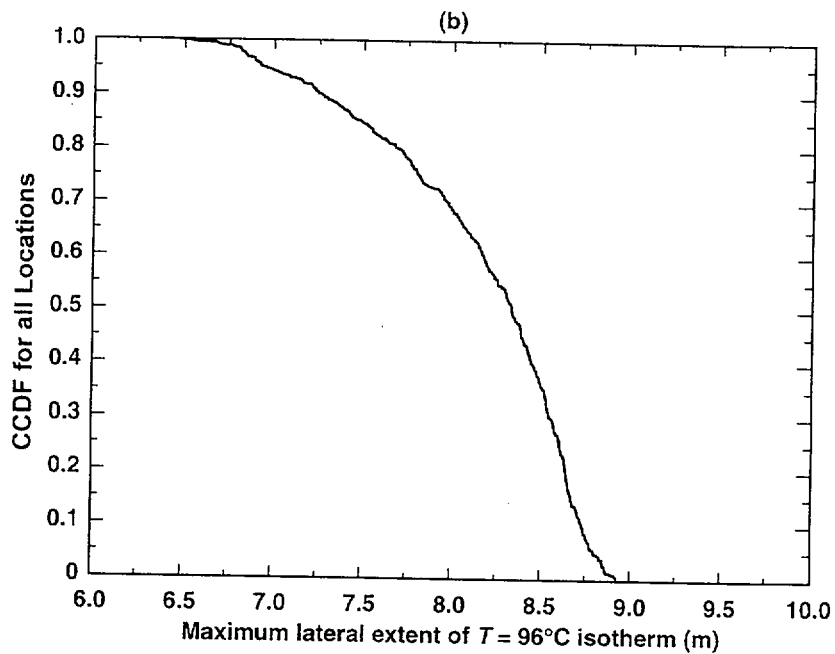
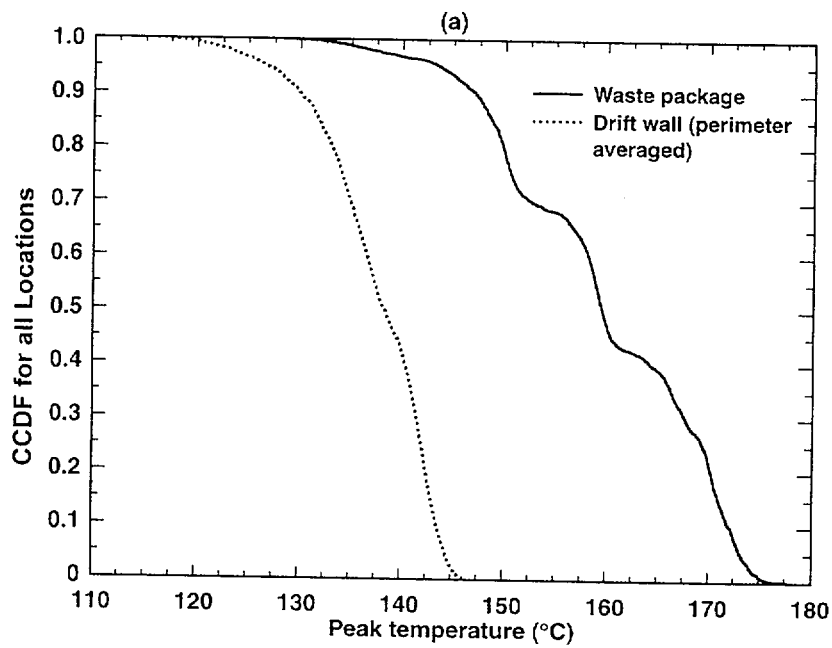
Figure 3-12 shows the spatial distribution of relative humidity in the host-rock at the drift wall. Figure 3-13 shows the perimeter-averaged drift-wall liquid-phase matrix saturation history and relative humidity history at the center and edge of the repository. Minimum liquid-phase saturations are about 0.2 at the repository center and slightly greater than 0.2 at the repository edge. Minimum values of drift-wall relative humidity are about 25% at the repository center and about 40% at the repository edge. The differences between the center and edge locations result from the edge-cooling effect. Significant reduction in drift-wall liquid-phase saturation (relative to ambient conditions) persists for up to about 2000 yr. Significant reduction in drift-wall *RH* (relative to humid ambient conditions) persists for up to about 2000 yr.

#### **3.2.3.1.3 Evaporation Rate**

Figure 3-14 shows the evaporation-rate history at the crown of the drift for the repository center and edge. Immediately after ventilation ceases there is a sharp spike in evaporation rate as boiling commences in the host-rock around the drift wall. After this spike, the evaporation rate is close to zero at the repository center; a secondary sharp spike in evaporation rate occurs at the end of the boiling period (about 1,000 year). This spike results from the boiling front collapsing back into the emplacement drift. At the repository edge, there is no second spike because the boiling front never progresses very far away from the drift wall. Some time after the end of the boiling period the evaporation rate declines to relatively small values.

#### **3.2.3.1.4 Capillary Pressure**

Figure 3-15 shows the capillary-pressure histories in the fractures and in the matrix at the repository center and edge. Under ambient conditions, capillary pressure in the fractures is an order of magnitude less than that in the matrix. During the preclosure period, changes in capillary pressure are small, primarily arising as a result of the temperature dependence of the surface tension of water. Shortly after ventilation ceases and boiling and dryout occur in the host rock around the drifts, the magnitude of capillary pressure in the matrix rises abruptly, attaining values about three to four orders of magnitude larger than ambient values. As the rock rewets to ambient liquid-phase saturation conditions, the capillary pressure declines to ambient values.

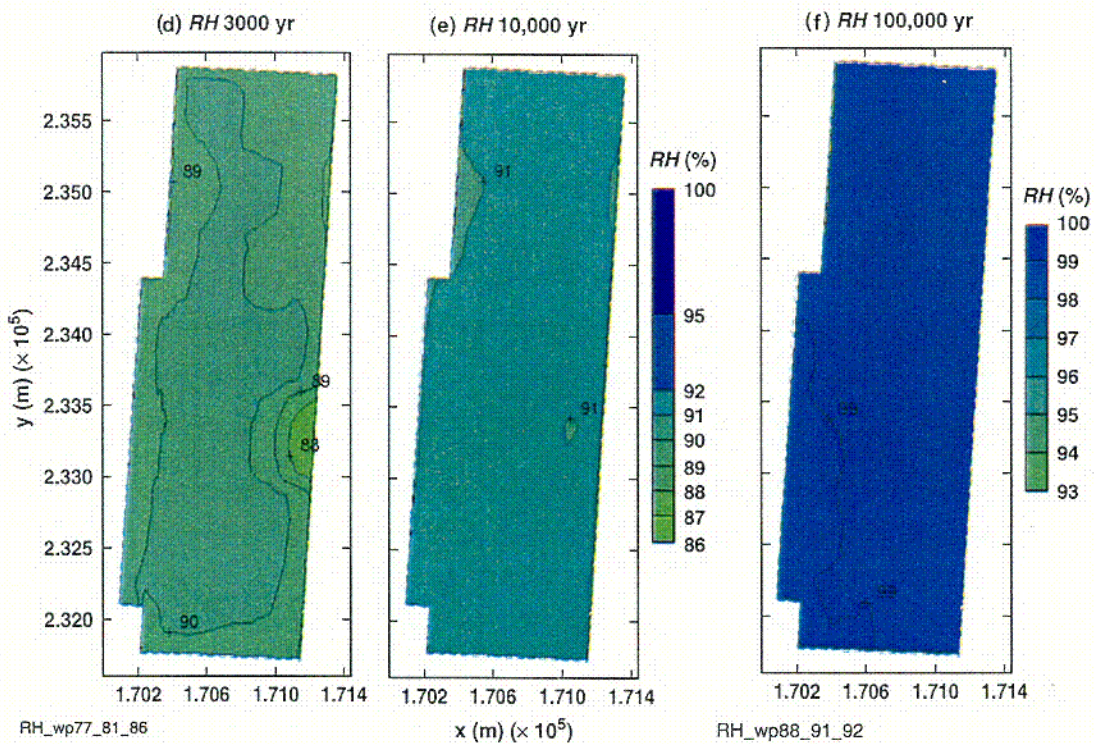
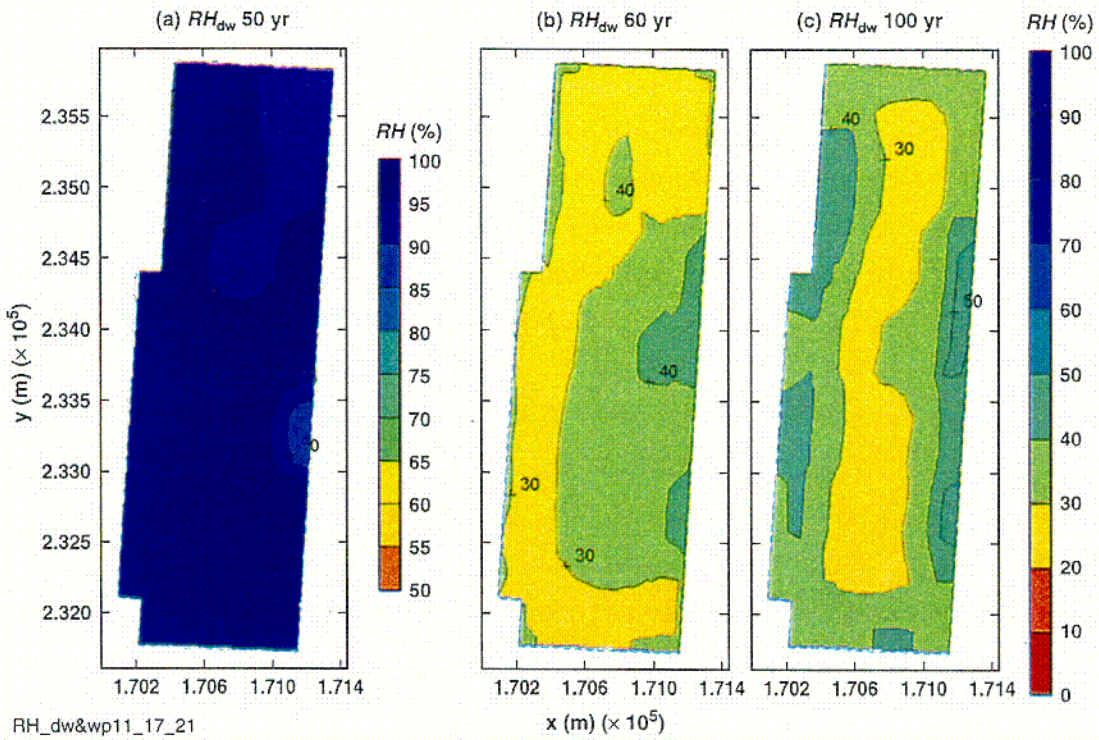


CCDF\_Tpeak\_T=96C

DTN: LL000509112312.003

NOTE: Uses the Mean Infiltration-Flux Case.

Figure 3-11. (a) The Complementary Cumulative Distribution Function (CCDF) for the Peak Temperature on Waste Packages and for the Peak Perimeter-Averaged Drift-Wall Temperature. (b) The CCDF of the Maximum Lateral Extent of the Boiling Point ( $T = 96^{\circ}\text{C}$ ).

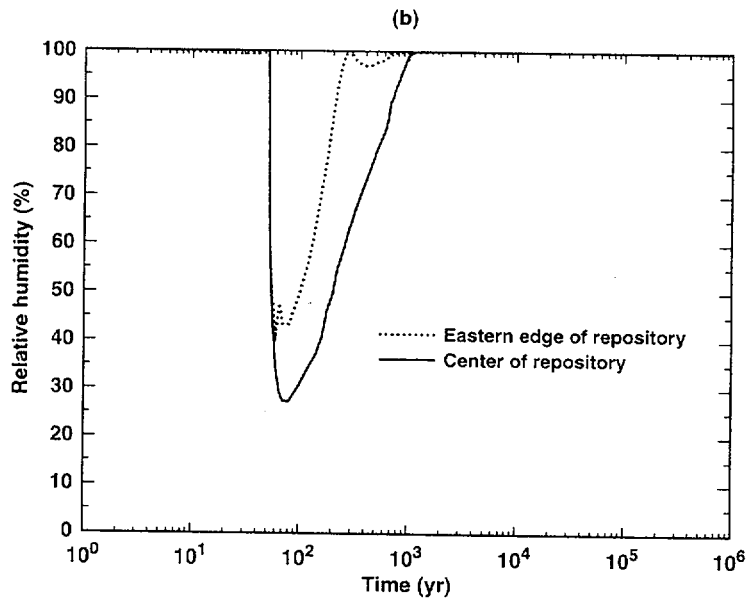
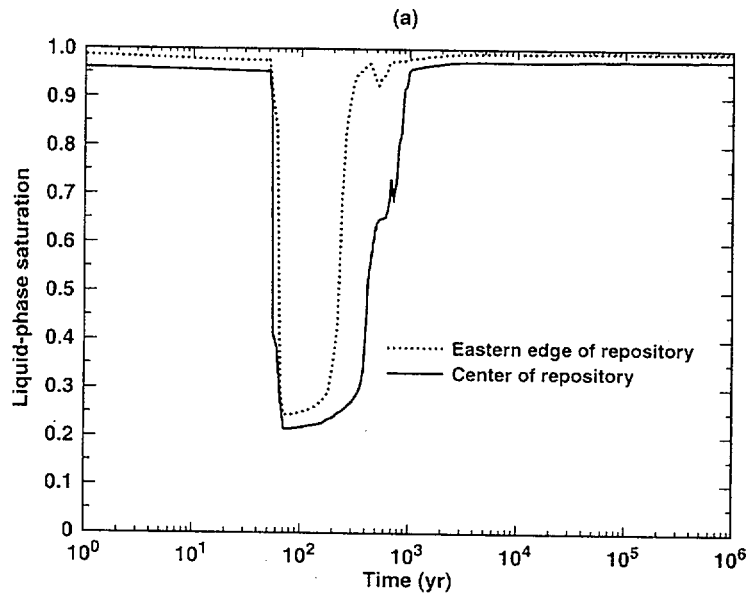


DTN: LL000509112312.003

NOTE: Contour labels and color bars indicate values.

Figure 3-12. Perimeter-Averaged Drift-Wall Relative Humidity for a 21-PWR WP for the Mean Infiltration-Flux Case for the Indicated Times

2-11

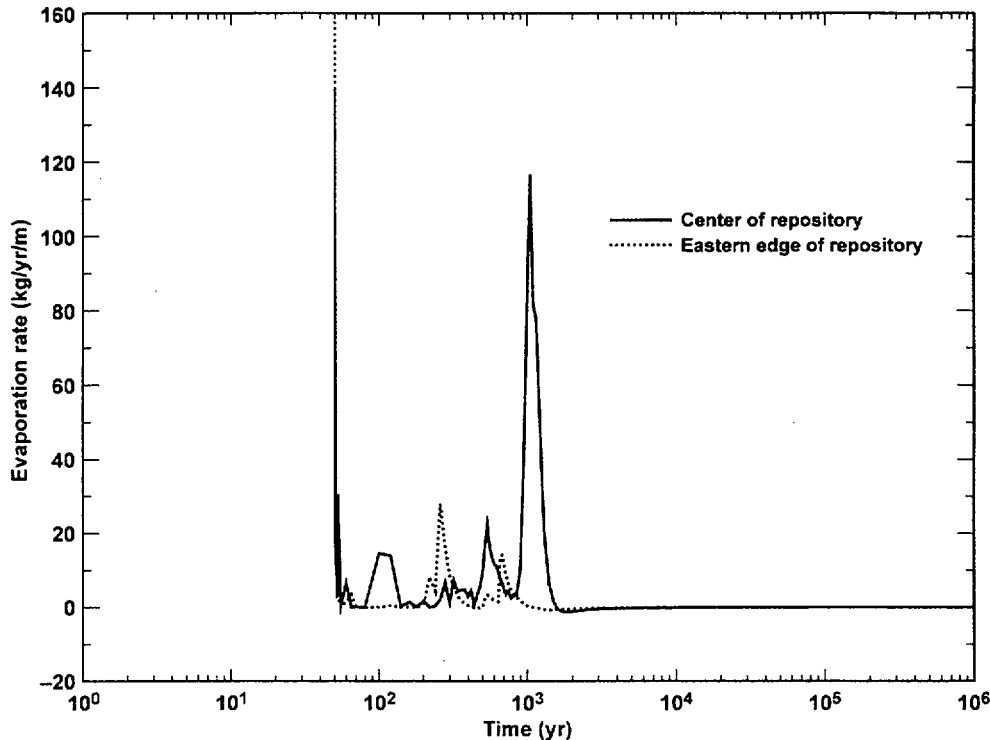


Sliq\_RH\_16\_16-24\_16

DTN: LL000509112312.003

NOTE: These conditions occur in the vicinity of a 21-PWR WP for the mean infiltration-flux case for the indicated times.

Figure 3-13. Perimeter-Averaged Drift-Wall Liquid-Phase Matrix Saturation History (a) and Relative Humidity History (b) at the Geographical Center of the Repository and a Location 27.5 m from the Eastern Edge of the Repository



Oevap\_16\_16-24\_16

DTN: LL000509112312.003

NOTE: These conditions occur in the vicinity of a 21-PWR WP for the mean infiltration-flux case for the indicated times.

Figure 3-14. Evaporation Rate History in the Host Rock at the Crown of the Drift at the Geographical Center of the Repository and a Location 27.5 m from the Eastern Edge of the Repository

### 3.2.3.1.5 Liquid-Phase Flux

Figure 3-16 shows the spatial distribution of liquid-phase flux 5 m and 3 m above the crown of the drift. Figure 3-17 shows the spatial distribution of liquid-phase flux at the drift wall. Figure 3-18 shows the liquid-phase-flux history at 5 m and 3 m above the crown of the drift, as well as at the drift wall for a repository center and edge location. The increase in liquid-phase flux (above ambient values) is called thermally-enhanced percolation.

At the repository center, the location 3 m above the crown of the drift experiences a very abrupt spike in liquid-phase flux just after ventilation ceases and boiling commences in the host rock around the drift. This primary spike is followed by a period of zero flux, which is then followed by a secondary spike (much smaller than the primary spike) that occurs shortly after boiling ceases. At the repository center, the location 5 m above the drift experiences a less abrupt spike in liquid-phase flux. Liquid-phase flux remains above ambient values until the end of the present-day climate (at 600 year); thereafter, the influence of thermally-enhanced percolation is swamped by the increased ambient percolation flux that results from the monsoonal and glacial climates.

At the repository edge, the duration of thermally-enhanced percolation flux (3 m and 5 m above the drift) is less than at the center of the repository. Percolation flux 3 m and 5 m above the drift returns to ambient values before the end of the present-day climate. At both center and edge locations, drift wall flux is low; the seepage model in the UZF&T PMR (CRWMS M&O 2000f) should be used for fluxes very near the drift wall.

### 3.2.3.2 Thermal-Hydrological Results for the EDA-II Design with Backfill

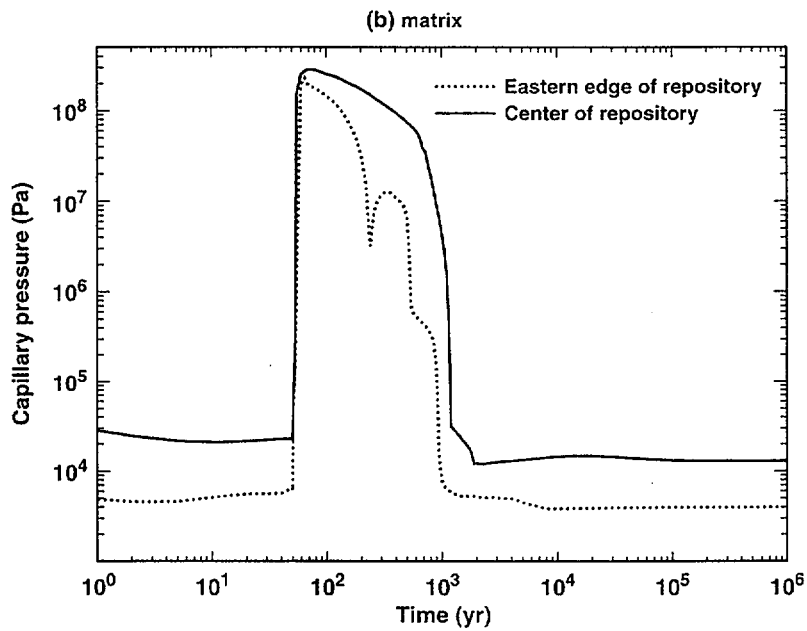
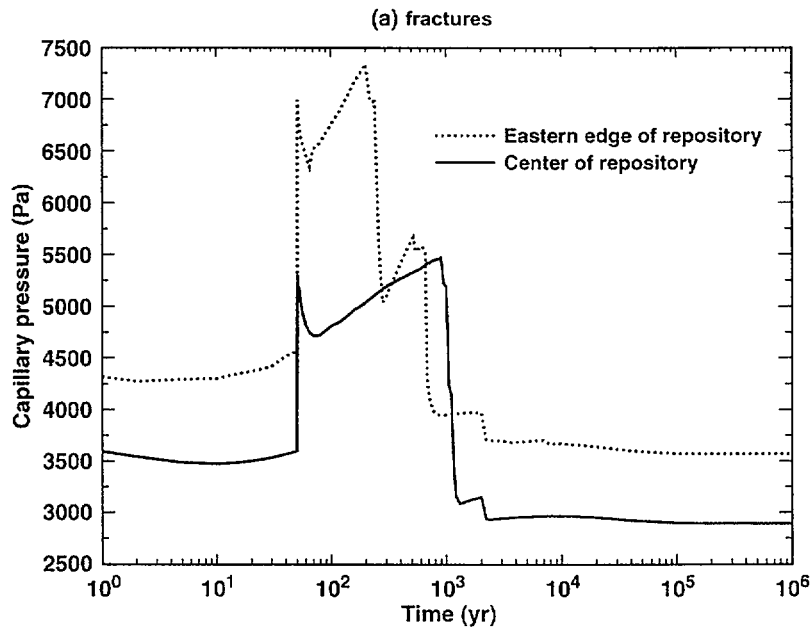
The Multiscale TH AMR (CRWMS M&O 2000k), described in Section 3.2.2.1, has been used to calculate temperatures, saturations, and liquid fluxes in the NF rock, and temperatures, humidities, and liquid fluxes in the emplacement drifts. In this PMR, selected values and graphical distributions of parameters are presented for the NF rock results.

Figure 3-19 shows the spatial distributions of peak drift-wall temperature (in time) across the repository footprint, for low, mean, and high infiltration-flux spatial distributions. The highest temperatures are for the low infiltration flux, since the water acts as a heat sink. The peaks (in time and space) are about 205, 195, and 190°C for the three infiltration-flux distributions. The temperatures are under the invert of the drifts. The 195°C peak temperature of the mean infiltration case is comparable to the peak ~150°C no-backfill drift wall temperature shown in Figure 3-7(d). The lower no-backfill temperature is averaged around the perimeter of the drift while the higher (backfill) design temperature is at the hottest location on the perimeter. The backfill design resulted in much higher downward heat flow (and temperature).

Figure 3-20 shows the liquid flux 5 m above the crown of the emplacement drifts as a function of time. A series of snapshots show the distribution across the footprint, for the mean infiltration flux scenario. The highest flux at this location is about 60 mm/yr, about 30 years after the repository is closed.

Figure 3-21 shows the liquid flux 0.2 m above the crown of the emplacement drifts as a function of time. A series of snapshots show the distribution across the footprint, for the mean infiltration flux scenario. The highest flux at this location is about 400 mm/yr, about 1 year after the repository is closed.

Figure 3-22 shows the liquid flux history at two locations in the footprint (near the center and near the eastern edge). At the drift scale, fluxes are shown at 5 and 0.2 m above the crown. At both locations, the near-drift-wall experiences a very high pulse of flux almost immediately after ventilation ceases and the repository is closed. As the NF rock dries out, the near-wall flux is negligible; this is followed by a gradual return to ambient flux levels (with step increases at the assumed times of climate change). For the center location, the zero-flux duration is about 300 years, and for the edge location, it is about 140 years. The center location also experiences a lesser-magnitude pre-closure flux peak at both the 0.2 and 5 m-depths into the rock, while the edge location does not.

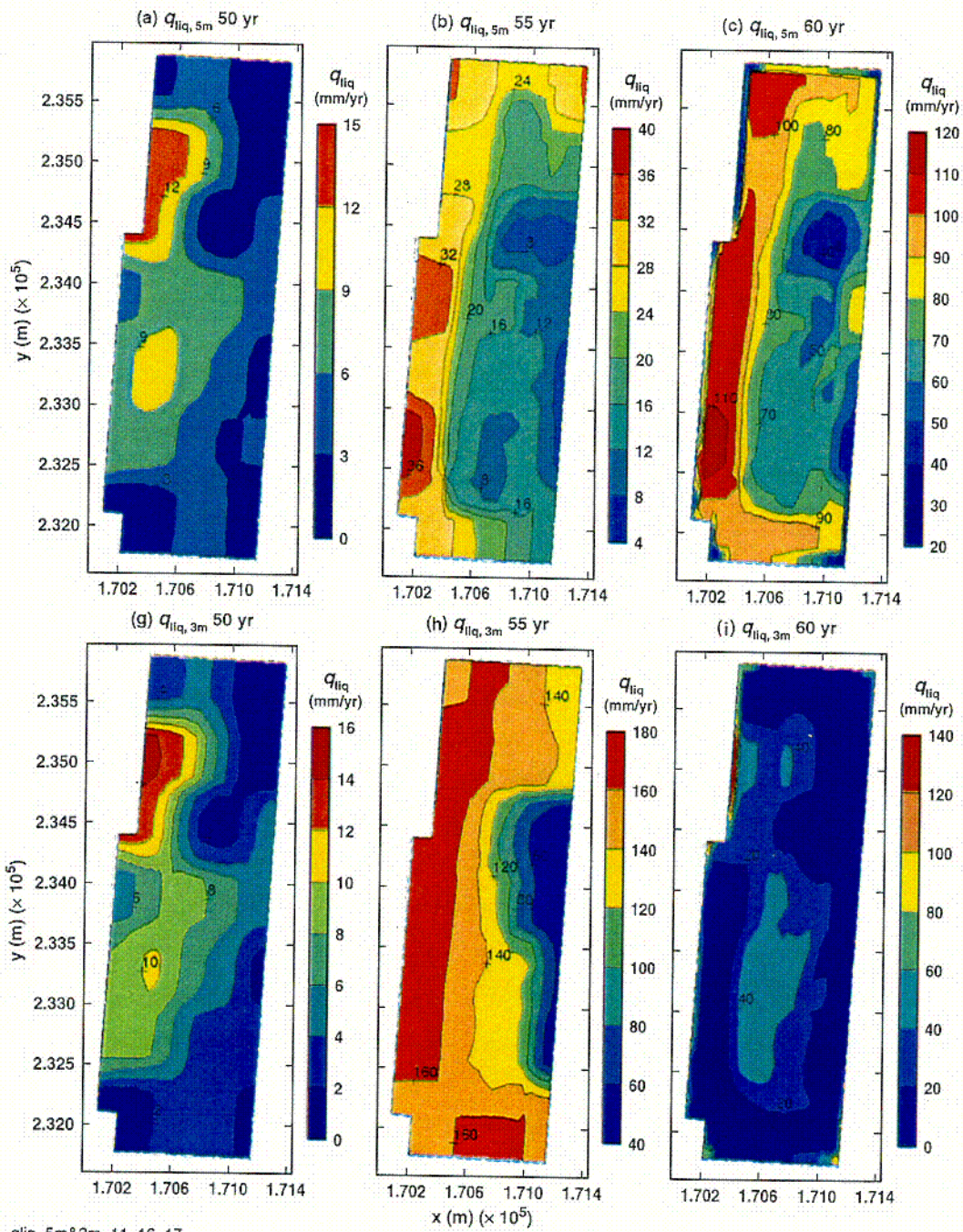


Pcap\_Fdw\_Mdw16\_16-24\_16

DTN: LL000509112312.003

NOTE: These conditions occur in the vicinity of a 21-PWR WP for the mean infiltration-flux case for the indicated times.

Figure 3-15. Capillary Pressure History in (a) the Fractures and in (b) the Matrix Averaged Around the Perimeter of the Drift Wall at the Geographical Center of the Repository and a Location 27.5 m from the Eastern Edge of the Repository



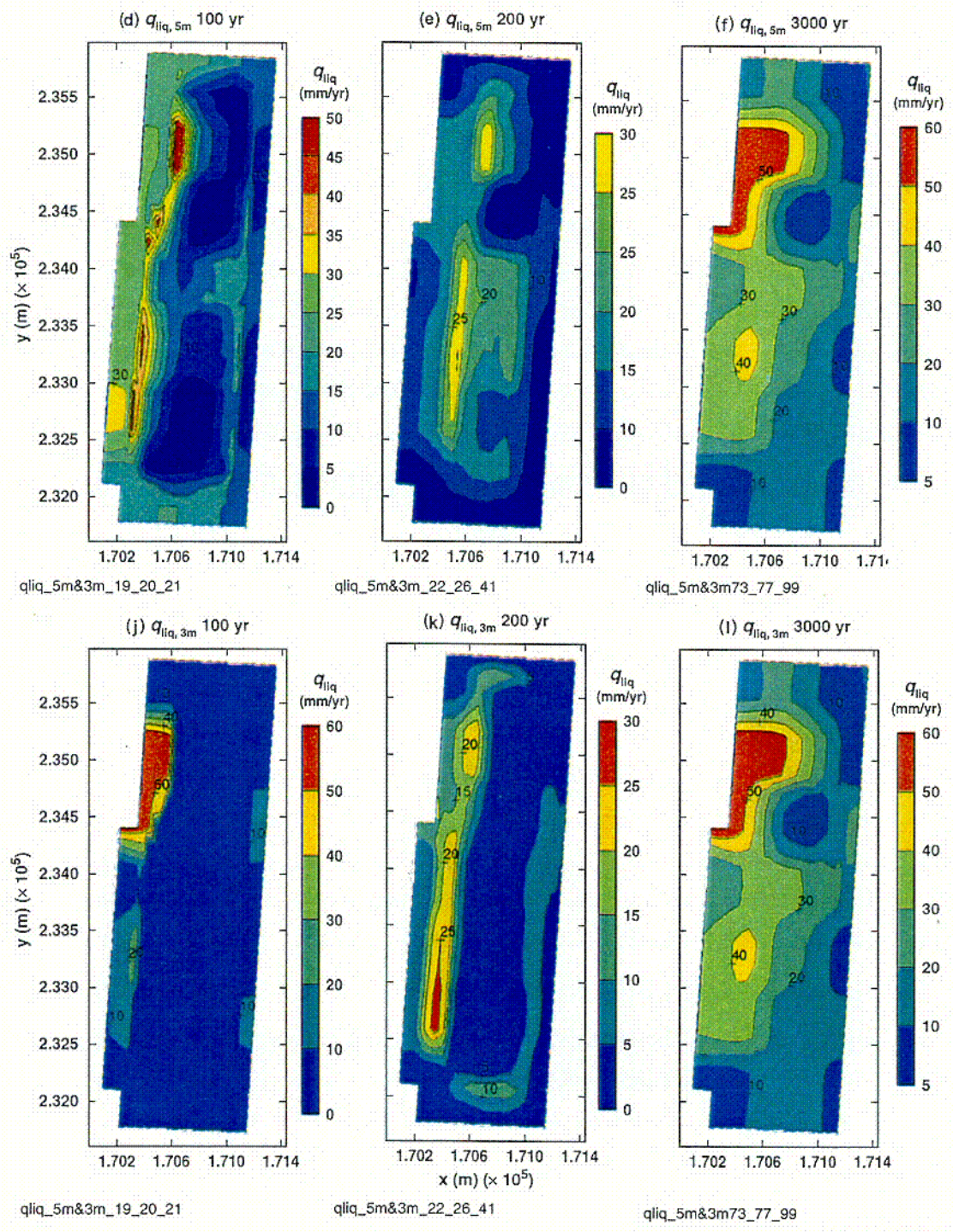
qliq\_5m&3m\_11\_16\_17

DTN: LL000509112312.003

NOTE: Contour labels and color bars indicate values.

Figure 3-16. Liquid-Phase Flux 5 m and 3 m above the Crown of the Drift and in the Vicinity of a 21-PWR WP for the Mean Infiltration-Flux Case for the Indicated Times (Page 1 of 2)

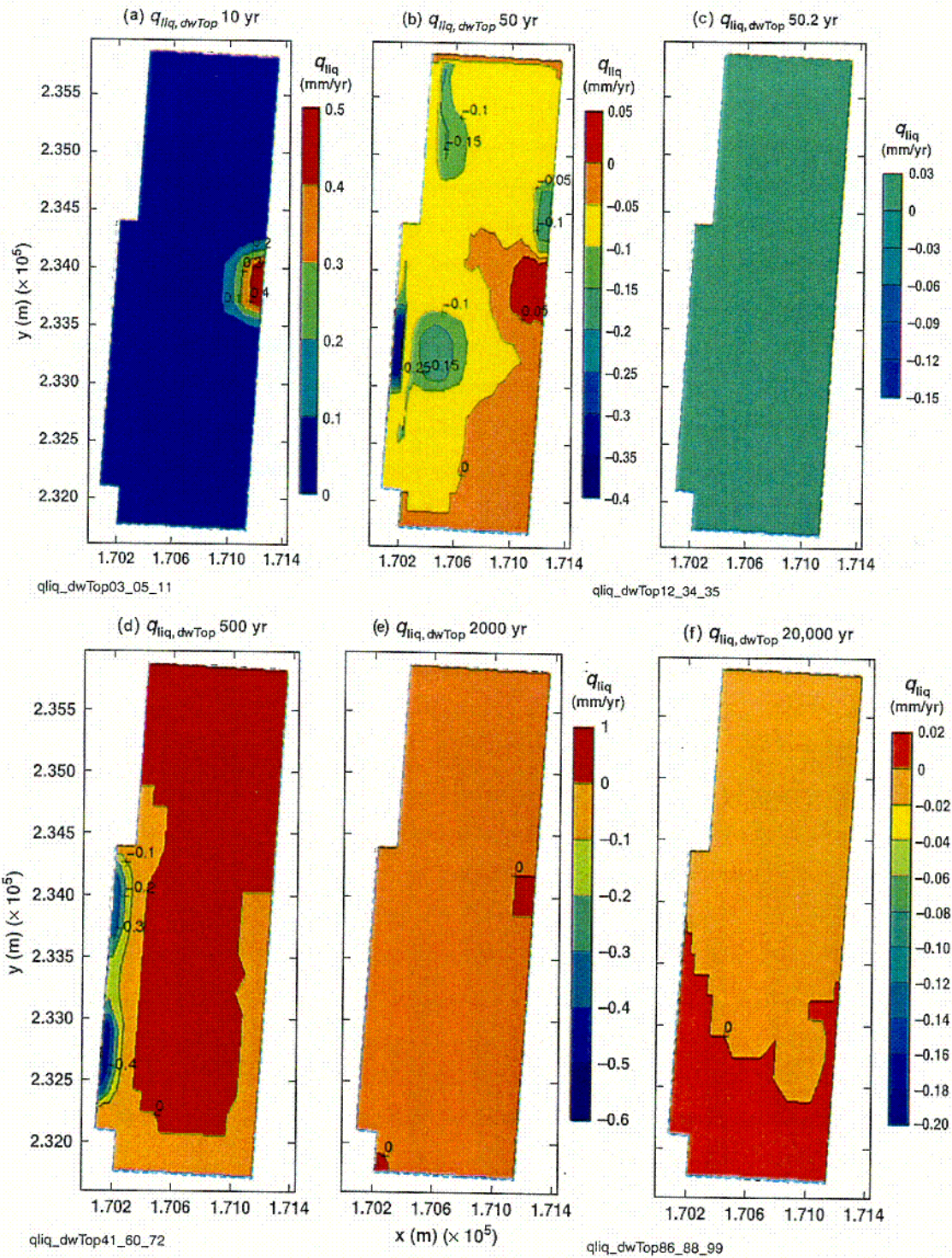
C-12



DTN: LL000509112312.003

Figure 3-16. Liquid-Phase Flux 5 m and 3 m above the Crown of the Drift and in the Vicinity of a 21-PWR WP for the Mean Infiltration-Flux Case for the Indicated Times (Page 2 of 2)

C-13

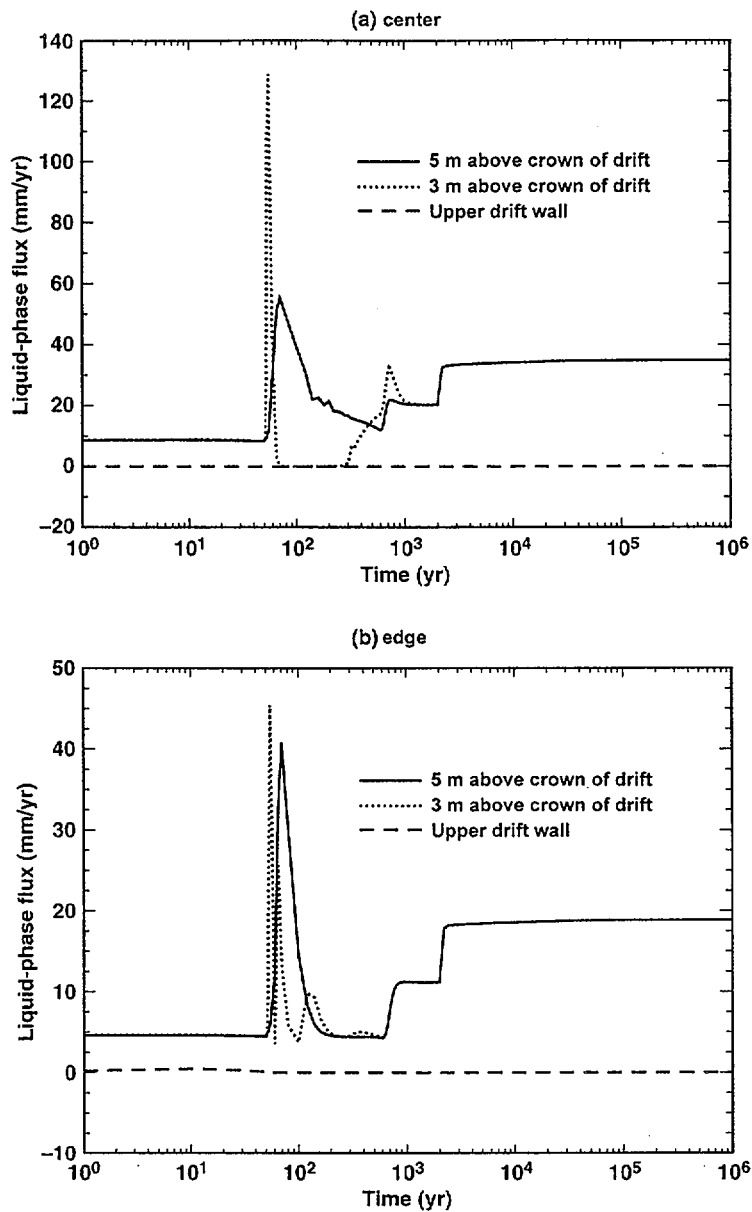


DTN: LL000509112312.003

NOTE: Contour labels and color bars indicate values.

Figure 3-17. Liquid-Phase Flux at the Upper Drift Wall in the Vicinity of a 21-PWR WP for the Mean Infiltration-Flux Case for the Indicated Times

C-14

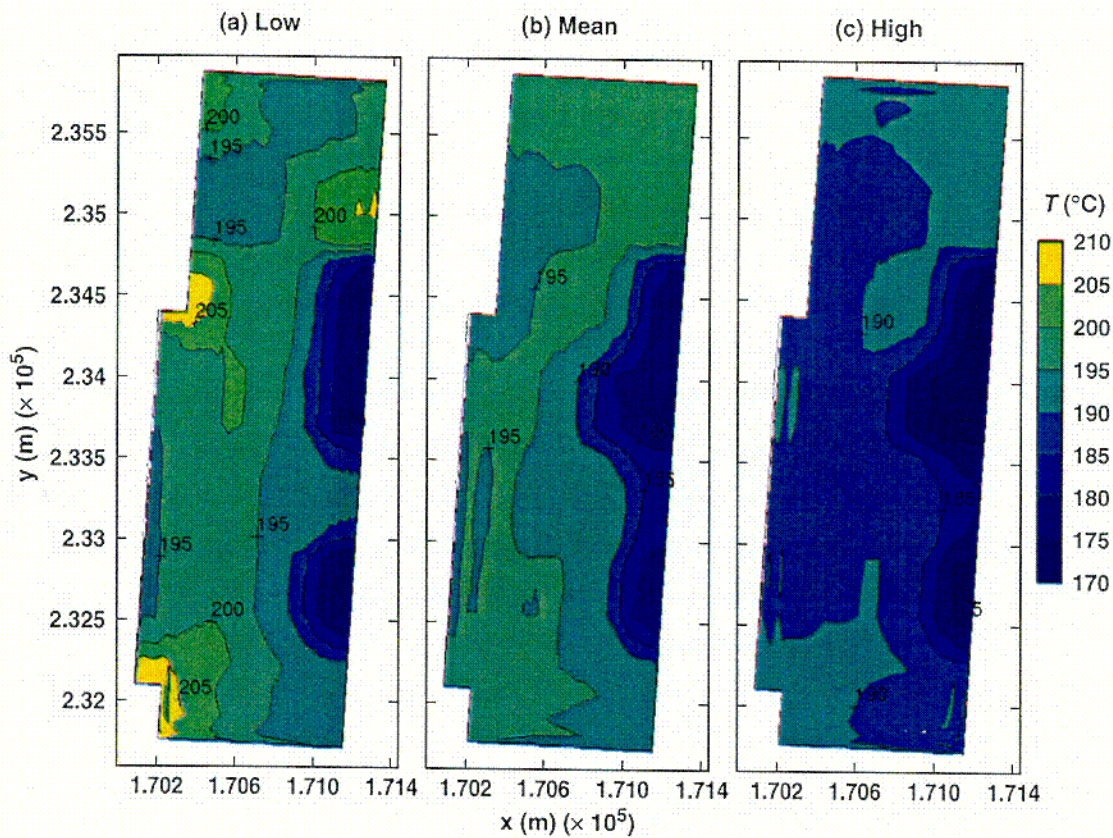


qliq\_16\_16-24\_16

DTN: LL000509112312.003

NOTE: These conditions occur in the vicinity of a 21-PWR WP for the mean infiltration-flux case for the indicated times.

Figure 3-18. Liquid-Phase Flux History at the Indicated Locations above the Drift at (a) the Geographical Center of the Repository and (b) a Location 27.5 m from the Edge of the Repository



TB\_AMR\_lmu\_T\_dw\_lower\_max

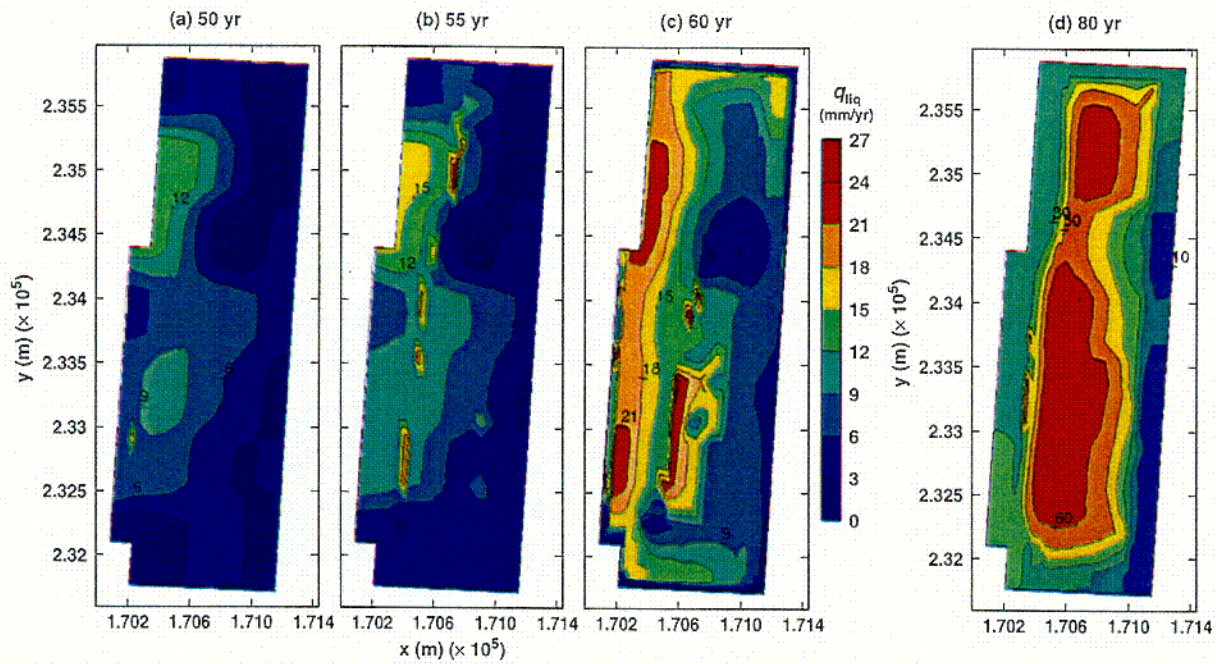
Source: CRWMS M&O 2000k, Figure 6-15

NOTE: Contour labels and color bars indicate values.

Figure 3-19. Peak Temperature on the Lower Drift Wall (Below the Invert) for the Low, Mean, and High Infiltration-Flux Cases

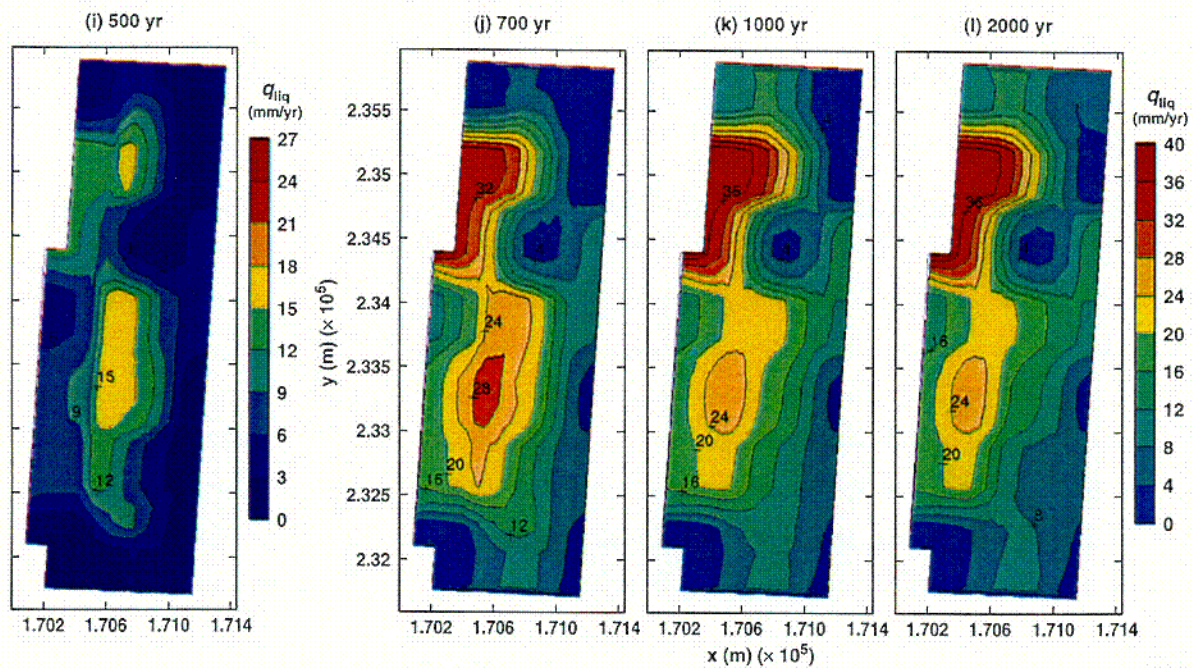
C-15

INTENTIONALLY LEFT BLANK



TB\_AMR\_mean\_qliq\_5m\_pwr2\_11-17

TB\_AMR\_mean\_qliq\_5m\_pwr2\_20-23

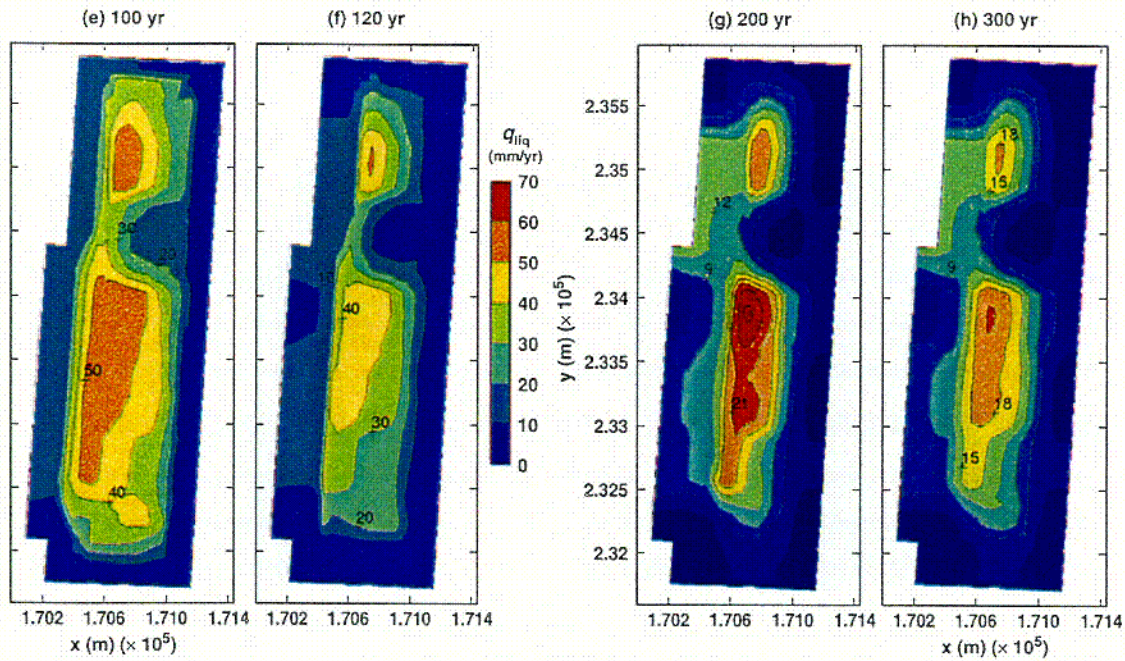


TB\_AMR\_mean\_qliq\_5m\_pwr2\_144-254

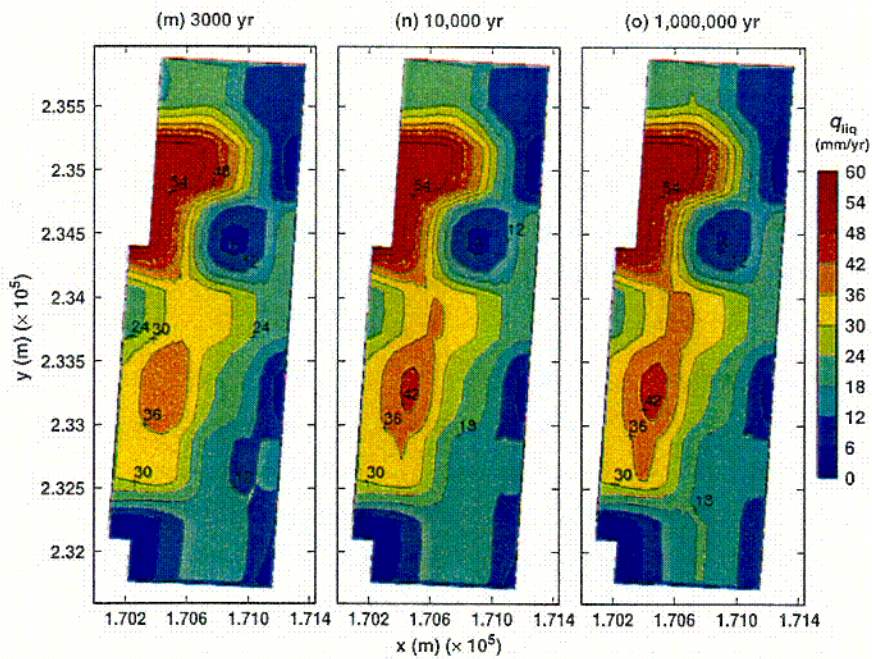
Source: CRWMS M&O 2000k, Figure 6-26

NOTE: Contour labels and color bars indicate values.

Figure 3-20. Liquid-Phase Flux 5 m above the Crown of the Drift for the Mean Infiltration Flux Case for the Indicated Times (Page 1 of 2)



TB\_AMR\_mean\_qliq\_5m\_pwr2\_31-104



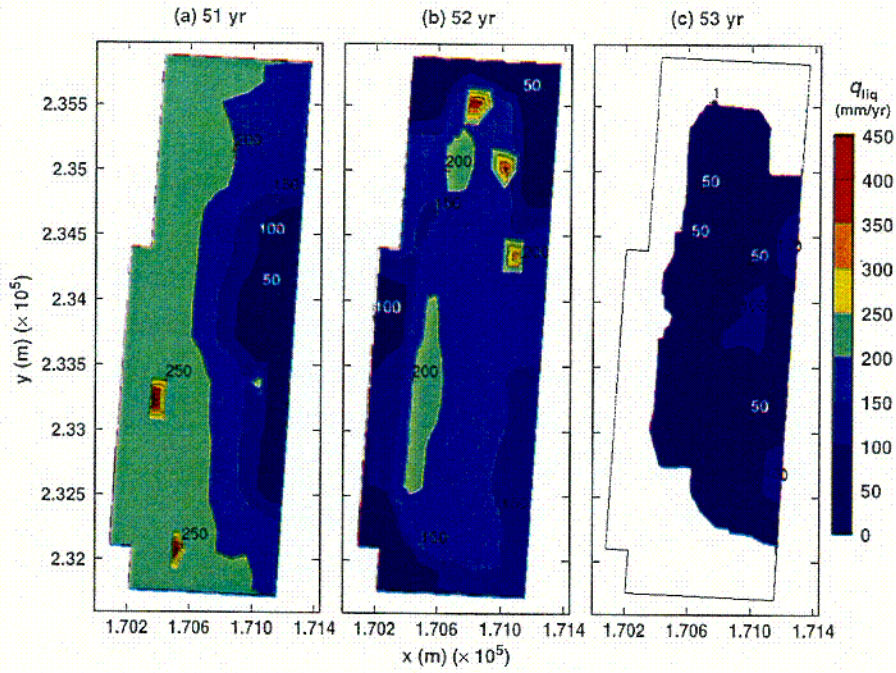
TB\_AMR\_mean\_qliq\_5m\_pwr2\_283-352

Source: CRWMS M&O 2000k, Figure 6-26

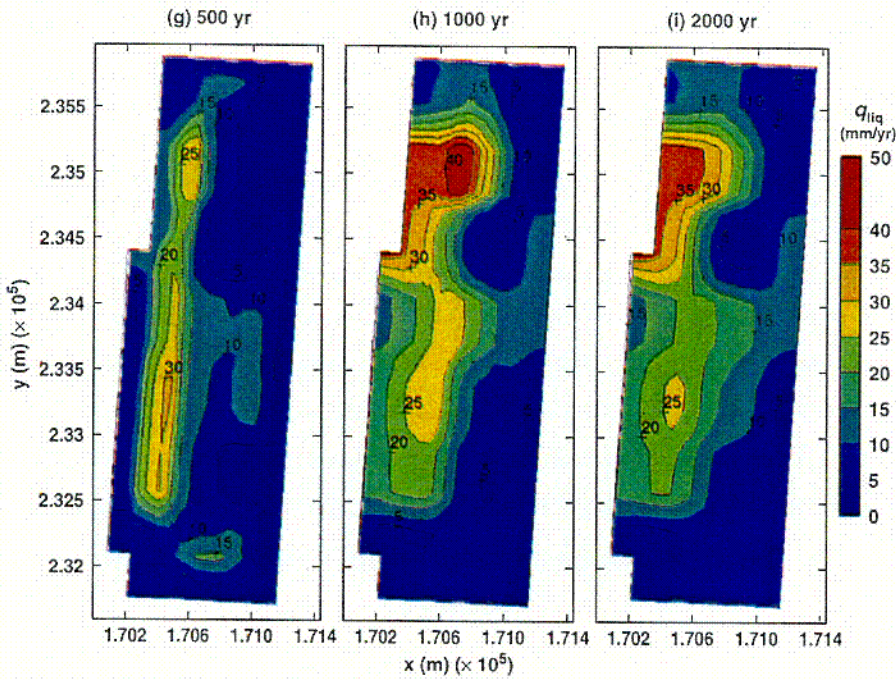
NOTE: Contour labels and color bars indicate values.

Figure 3-20. Liquid-Phase Flux 5 m above the Crown of the Drift for the Mean Infiltration-Flux Case for the Indicated Times (Page 2 of 2)

C-17



TB\_AMR\_mean\_qliq\_dw\_pwr2\_13-15

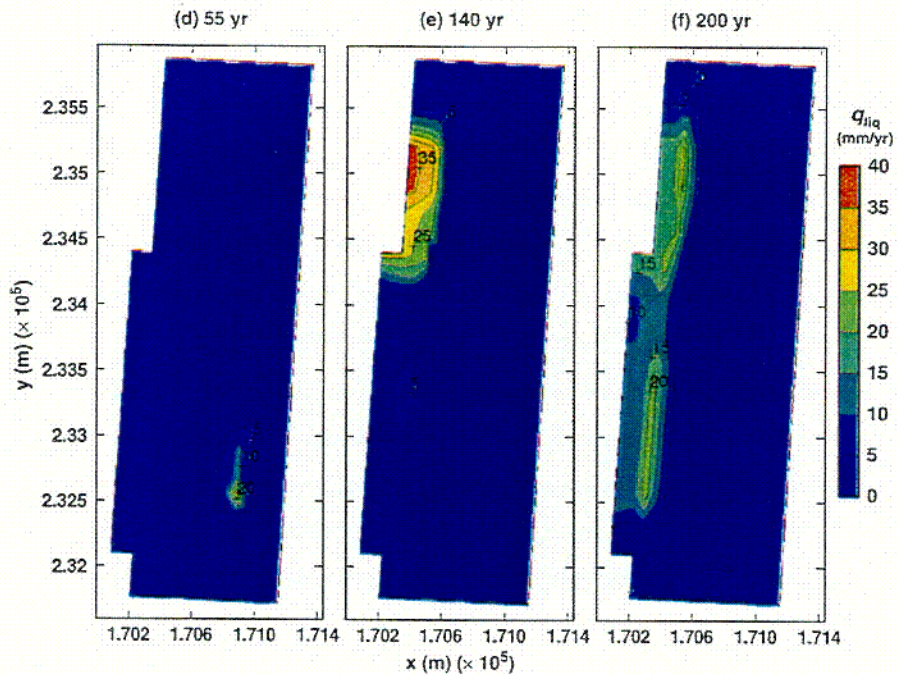


TB\_AMR\_mean\_qliq\_dw\_pwr2\_104-254

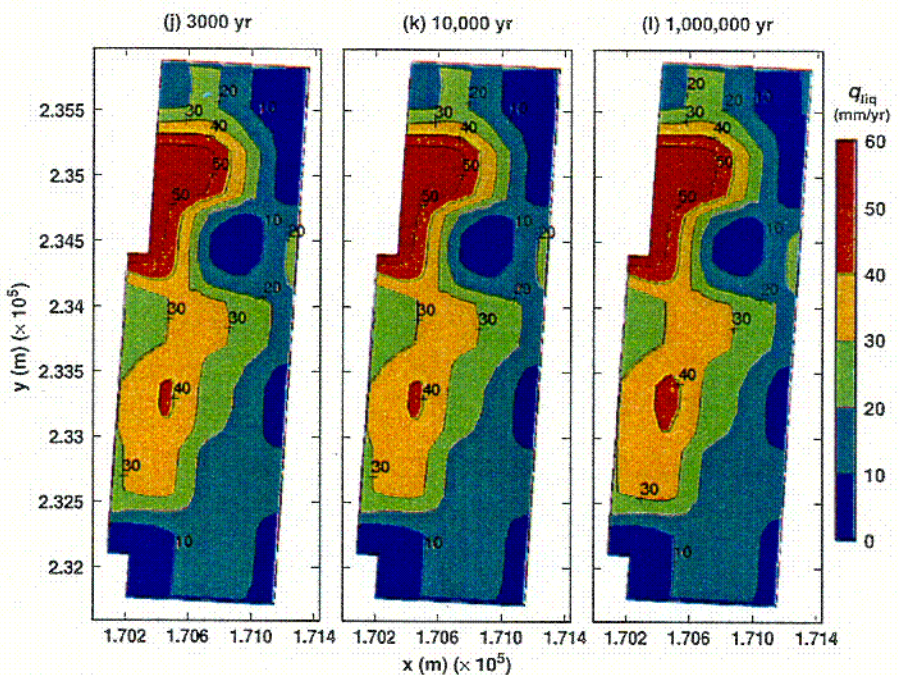
Source: CRWMS M&O 2000k, Figure 6-27

Figure 3-21. Liquid-Phase Flux 0.2 m above the Crown of the Drift for the Mean Infiltration-Flux Case for the Indicated Times (Page 1 of 2)

C-18



TB\_AMR\_mean\_qliq\_dw\_pwr2\_16-31

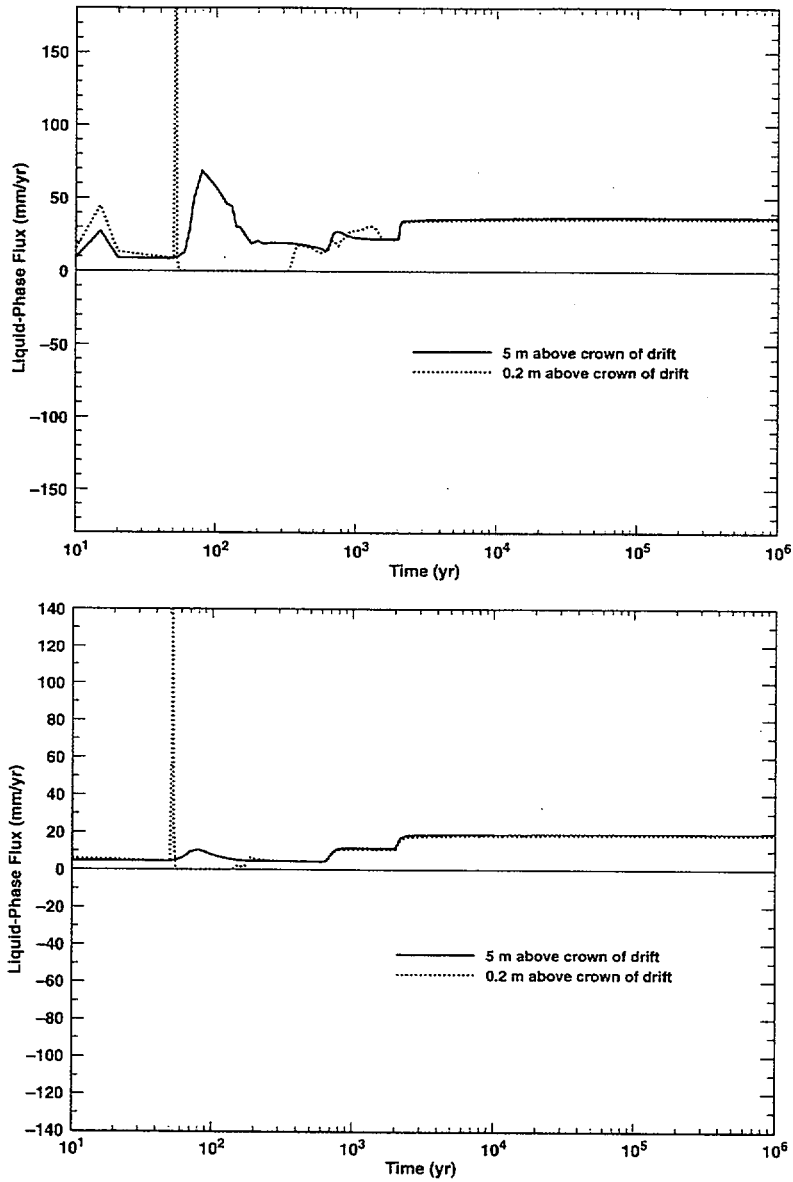


TB\_AMR\_mean\_qliq\_dw\_pwr2\_283-352

Source: CRWMS M&O 2000k, Figure 6-27

Figure 3-21. Liquid-Phase Flux 0.2 m above the Crown of the Drift for the Mean Infiltration-Flux Case for the Indicated Times (page 2 of 2)

C-19



Source: CRWMS M&O 2000k, Figure 6-41

Figure 3-22. Liquid-Phase Flux History at Indicated Drift-Scale Locations for the Mean Infiltration Flux Case at (top) the Geographic Center of the Repository, and (bottom) a Location 27.5 m from the Eastern Edge of the Repository

### 3.2.3.3 LDTH Calculations of Point and Line Loads

This section reports the results of applying the LDTH submodel described in Section 3.2.2.1 as a tool to evaluate design options. This work was done as a sensitivity case for TSPA-VA, and led to more sophisticated calculation in support of LADS. As discussed in the LADS report (CRWMS M&O 1999a, Section 7.2), a design with excellent performance, such as the VA design, could be improved by reducing uncertainties in the effects of coupled processes on repository performance. The LDTH submodel was used to evaluate temperatures, saturations, and liquid fluxes that were used as surrogates for uncertainty evaluation. This section describes the results of trading drift spacing against waste package spacing, with constant inventory and repository area (i.e., AML). Other trade-off studies described in the LADS report included ventilation rate and duration, and different AMLs. The conclusion of LADS was that EDA-II (see the Introduction to Chapter 2) met the uncertainty reduction goal by using a combination of these thermal-management techniques.

Two-dimensional cross sectional TH models were used to calculate DS spatial distributions of temperature, liquid-phase saturation, relative humidity, liquid-phase flux, and air mass fraction, as functions of time. Two designs were compared: point-loading with 28 m drift spacing (and with spaces between WPs about the same as the length of the WPs), and line loading with 56.6 m drift spacing (and with only a small gap between WP ends). These results led to adoption of the EDA-II design, which uses line-loading with 81 m drift spacing (AML reduced from 85 to 60 MTU/acre compared to VA) and preclosure ventilation.

#### 3.2.3.3.1 Model Inputs and Assumptions

The surface location of the model was at the crest of Yucca Mountain, halfway between the northern and southern boundaries of the repository footprint and one-third of the way from the western to the eastern boundary. The nominal infiltration flux is 16.0 mm/year at this location (Flint et al. 1996). Mountain-scale lateral heat and mass flow are neglected in the model; the error introduced is thought to be small for locations near the center of the repository, but it is probably significant for the edges of the repository.

The hydrostratigraphy used in the models is that reported within the UZ F&T PMR (CRWMS M&O 2000f). As noted in that PMR, the tuffs comprising Yucca Mountain are identified by lithostratigraphic name and by major and detailed hydrogeologic unit nomenclature. Table 3-7 provides this nomenclature. The UZ Model Layer nomenclature and the properties of those layers were used in the TH models that will be reported in this PMR.

The following *boundary conditions* were used. The water table was considered to be a constant-property boundary with specified fixed temperature, liquid saturation, and gas pressure. The surface of the mountain was considered to be a constant-property boundary with specified fixed temperature and gas pressure. Because the imposed infiltration is the net of water influx and water vapor outflux, the relative humidity at the surface of the mountain was assumed to be 100 percent; eliminating the need to explicitly calculate vapor flux near the surface. The temperature values at the water table and ground-surface boundaries were taken from the site-scale UZ flow model (Bodvarsson et al. 1997). At the water table, liquid-phase saturation is

Table 3-7. Major Hydrogeological Unit, Lithostratigraphic Unit, Detailed Hydrogeological Unit, and UZ Model Layer Nomenclatures (adapted from CRWMS M&O 2000w, Table 10)

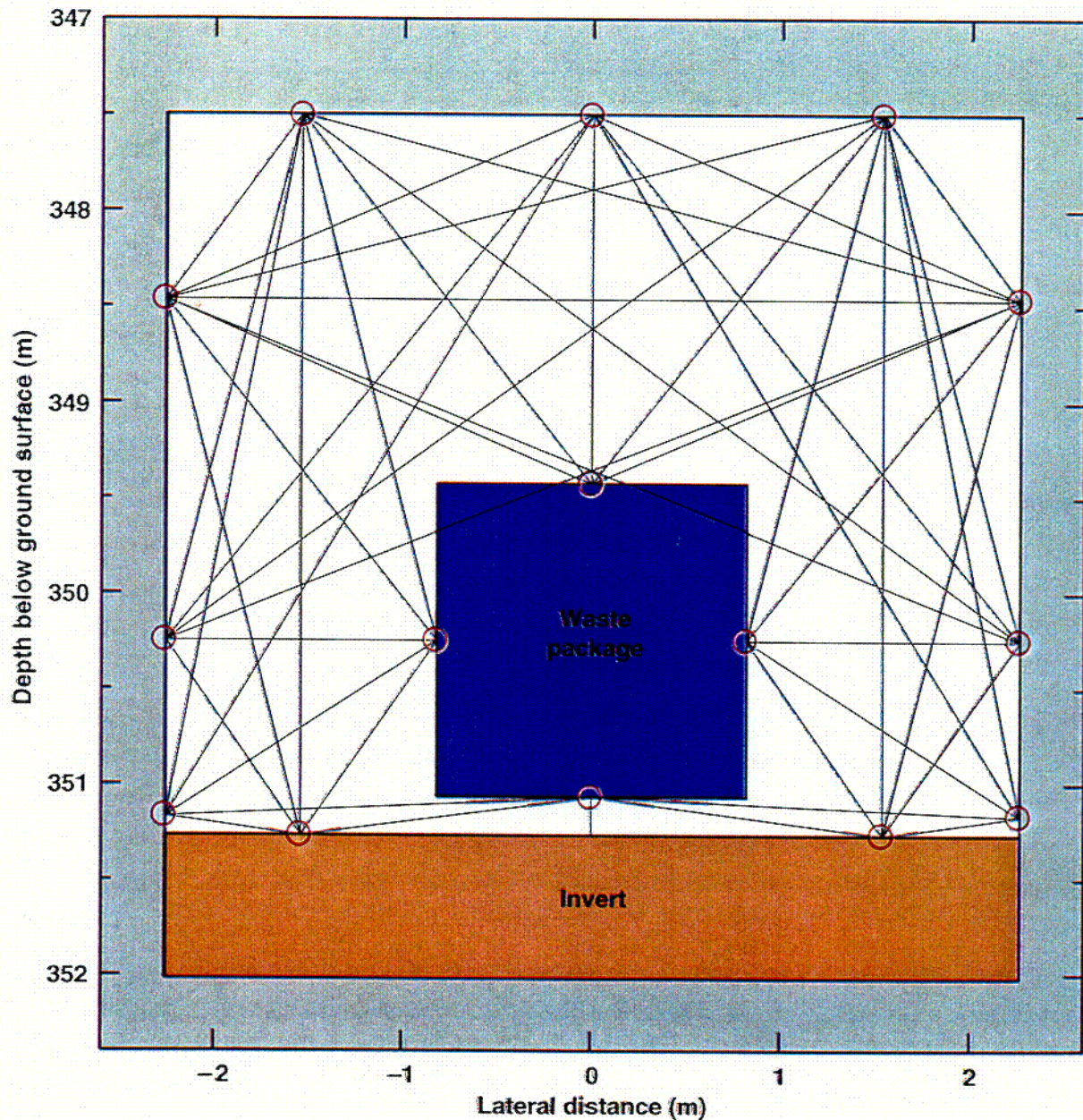
Major Hydrogeological Unit	Lithostratigraphic Unit		Detailed Hydrogeological Unit	UZ Model Layer	
Tiva Canyon welded (TCw)	Tiva Canyon Tuff	Tpcr	CCR, CUC	tcw11	
		Tpcp	CUL, CW	tcw12	
		Tpcpv3	CMW	tcw13	
		Tpcpv2			
Paintbrush nonwelded (PTn)	Bedded tuff	Tpcpv1	CNW	ptn21	
		Tpbt4	BT4	ptn22	
	Yucca Mountain Tuff	Tpy	TPY	ptn23	
	Bedded tuff	Tpbt3	BT3	ptn24	
	Pah Canyon Tuff	Tpp	TPP	ptn25	
	Bedded tuff	Tpbt2	BT2	ptn26	
					Tptrv3
Topopah Spring Tuff	Tptrv2				
Topopah Spring welded (TSw)		Tptrv1	TC	tsw31	
		Tptrn	TR	tsw32	
		Tptrl	TUL	tsw33	
		Tptpul			
		Tptpmn	TMN	tsw34	
		Tptpll		TLL	tsw35
				TM2 (upper 2/3)	tsw36
			TM1 (lower 1/3)	tsw37	
		Tptpv3	PV3	tsw38	
		Tptpv2	PV2	tsw39	
Tptpv1	BT1 or BT1 a (altered)				
Calico Hills nonwelded (CHn)	Bedded tuff	Tpbt1	BT1 or BT1 a (altered)	ch1 (vit, zeo)	
	Calico Hills Formation	Tac	CHV (vitric) or CHZ (zeolitic)	ch2 (vit, zeo)	
				chi (vit, zeo)	
				ch4 (vit, zeo)	
				ch5 (vit, zeo)	

Table 3-7. Major Hydrogeological Unit, Lithostratigraphic Unit, Detailed Hydrogeological Unit, and UZ Model Layer Nomenclatures (adapted from CRWMS M&O 2000w, Table 10) (Continued)

Major Hydrogeological Unit	Lithostratigraphic Unit		Detailed Hydrogeological Unit	UZ Model Layer
Calico Hills nonwelded (CHn) (Cont'd)	Bedded tuff	Tacbt	BT	ch6
	Prow Pass Tuff	Tcpuv	PP4 (zeolitic)	pp4
		Tcpuc	PP3 (devitrified)	pp3
		Tcpmd	PP2 (devitrified)	pp2
		Tcplc		
		Tcplv	PP1 (zeolitic)	PP'
	Bedded tuff	Tcpbt		
Crater Flat undifferentiated (CFu)	Bullfrog Tuff	Tcbuv		
		Tcbuc	BF3 (welded)	bf3
		Tcbmd		
		Tcblc		
		Tcblv	BF2 (nonwelded)	bf2
	Bedded tuff	Tcbbt		
	Tram Tuff	Tctuv		
		Tctuc	Not Available ,	tr3
		Tctmd		
		Tctlc		
	Tctlv & below	Not Available	tr2	

100 percent; eliminating the need to explicitly calculate vapor flux near the surface. The temperature values at the water table and ground-surface boundaries were taken from the site-scale UZ flow model (Bodvarsson et al. 1997). At the water table, liquid-phase saturation is 100 percent. The value of gas pressure at the ground surface was taken from the site-scale UZ flow model. The value of gas pressure at the water table is consistent with the value of gas pressure at the ground surface and the pressure profile of a static gas column from the ground surface to the water table.

Figure 3-23 is a vertical cross section, showing radiation connections, of the simplified (square) emplacement drift, orthogonal to the drift axis. By using periodic boundaries, the vertical plane through the centerline of the drift becomes a plane of symmetry (although care must be taken in the radiation connections across the plane) and, consequently, provides an adiabatic, no-flow boundary. The centerline of the pillar between drifts provides the other adiabatic, no-flow boundary in the  $x$  direction. The (later) LADS and SR calculations included round drifts with larger drift spacing.



Source: Hardin 1998, Figure 3-14

NOTE: This diagram is a segment of the model domain; the full domain extends between mid-pillar locations and from the ground surface to the water table.

Figure 3-23. Vertical Cross Section of the Emplacement Drift in the DDT and LDTH Model Showing the Thermal Radiation Connections Among the Surfaces in the Drift that are used in Thermal Simulations

For the calculations shown here, the WP diameter was 1.67 m, and the emplacement drift diameter was 5.1 m. For earlier DS-model calculations for TSPA-VA, the WP diameter was assumed to be 1.85 m (Hardin 1998, Section 3.5.1.2). The invert, which is at the bottom of the

drift, was assumed to occupy 16.6 percent of the drift cross section. As was demonstrated previously (Wilder 1996, Section 1.10.4), a circular WP in a circular drift can be accurately represented by a square WP in a square drift, provided that the respective circular and square cross sectional areas are equal. In the model, the WP dimensions are 1.445 m square, and the drift measures 4.52 m square. The invert was assumed to be filled with concrete, consisting of fractured and jointed matrix blocks. Heat flux from the WP sources is averaged over the length of the drifts and coupled to the drift surfaces primarily by radiant heat transfer. Thermal radiation is also accounted for between different locations on the drift surface. An efficient heat-transfer mechanism distributes the heat flux uniformly to the perimeter surfaces of the emplacement drift. The drift-wall and drift-floor surfaces are assumed to be black-bodies (emissivity = 1), and the WPs have an emissivity of 0.8. This allows the use of a constant heat-flux boundary condition at the drift perimeter.

The *initial conditions* were set as follows: the value of gas pressure at the water table is established when the models are initialized at ambient conditions. The initialization model runs are continued until the temperature, liquid-phase saturation, gas pressure, and air-mass fraction distributions in the model attain steady-state distributions.

The *grid* for the numerical calculations was established as follows: the DKM approximation is used in the LDTH submodel to represent fracture-matrix coupling. Because different properties are assigned to fracture elements and matrix elements, two grid blocks must be assigned to each spatial location, (i.e., twice as many as would be required to give the same spatial resolution with the ECM). Sixteen grid blocks are used in the *x* direction for the point-load design, and 18 are used for the line-load design. In the vertical direction, 80 grid-block layers are used to represent the hydrostratigraphy; thus, the point-load design requires 1,280 grid blocks, whereas the line-load design requires 1,440 grid blocks.

*Thermal and hydrological properties* were established based on the base-case property set, using information from thermal testing and site-scale measurements.

### 3.2.3.3.2 TH Model Results for Line and Point Loading

Figure 3-24 (a through l) shows contour plots around two drifts for temperature and liquid saturation in the *x-z* plane for *point loading* at *t* = 50, 100, 500, 1,000, 2,000, and 5,000 years, respectively. A single drift is shown in Figure 3-25 (a through l) for the *line-load*. The figure is representative of a line-loaded repository with a drift spacing of 56.6 meters as opposed to 81 meters, which is the drift spacing utilized as the base case in TSPA-SR.

For the line-load design (characterized by close waste package spacing and wide emplacement drift spacing), there is no significant dryout (<50 percent saturation) at the mid-pillar and the 100°C isotherm never coalesces between the drifts (Figure 3-25). However, for a *point loading* (Figure 3-24) design (characterized by waste package spacing on the order of emplacement drift spacing), the entire pillar (at 500 years) boils and pillar saturations are less than 60 percent (about 15 m below the repository horizon). The heat-flux density, which is greater by a factor of two along the *line-load* drifts, as compared to the *point-load* drifts, results in much higher temperature rise (and a much steeper temperature gradient) in the vicinity of the drifts than for *point-loading*. The line-loaded design is incorporated in the TSPA-SR model. The *line-loaded*

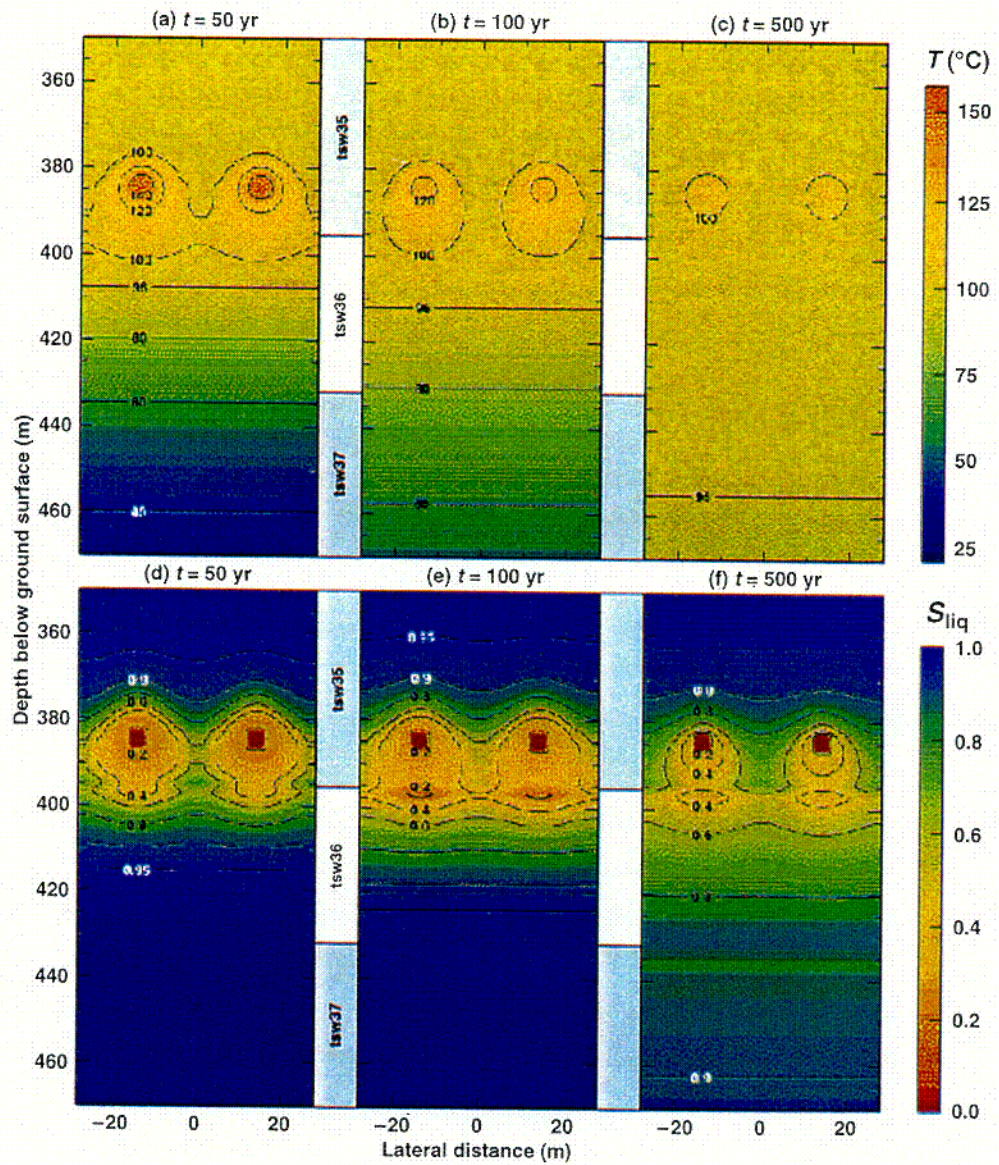
drift contains very closely spaced waste packages (separation distance of 0.1 meters) which tends to concentrate the heat along the axis of the loaded drift. In the vicinity of the waste packages, closely spaced neighboring waste packages share heat with each other and along the drift wall causing locally higher temperatures within the loaded portion of the drifts. The thermal gradient along the axis of the drift is uniform due to a nearly uniform heat sharing between waste packages. The temperature gradient radially away from the waste package is much larger for the line-loaded design due to the local concentration of heat near closely spaced waste packages. The *point-loaded* drift contains a much wider waste package spacing. For this design, heat sharing between waste packages is far less prevalent and hence the axial thermal gradient is very non-uniform as one transitions along the drift when including waste package heat output variability. Since the heat output surrounding neighboring waste package is not as concentrated (e.g., not shared), local temperatures are much lower. Subsequently, the radial temperature gradient away from the waste packages is not as large as that developed in the line-loaded design.

The key point from comparison of *line* and *point loads* at the common ambient fluxes and properties in this section is that the *line load* had the potential to dryout NF rock, while maintaining pillar drainage. In contrast, the *point load* had less NF dryout and a period of pillar blockage.

These differences are subtle in Figures 3-24 and 3-25, but are more pronounced in the more widely spread drifts considered in LADS. The following more detailed observations were made about the TH behavior modeled in these and related calculations:

- **Liquid flux is much greater than percolation flux for early time** ( $t=100-500$  years), then gradually declines to the magnitude of percolation flux.
- **Liquid flux is insensitive to percolation flux for early time** (less than 200 years). At 100 years, liquid flux is nearly the same for all of the percolation flux cases considered. Therefore, when liquid flux is greatest (i.e., early time), it does not depend on the magnitude of percolation flux. For later time (greater than 200 years), the magnitude of liquid flux increases with percolation flux.
- **Liquid flux above the drifts is the same for the *point-* and *line-load* designs.** The magnitude of liquid flux depends only on the total heat flux available to mobilize water and not on how efficiently condensate sheds around the drifts. The more efficient condensate shedding for the *line-load* design results in less return flow of condensate to the drift from the previous refluxing cycle. The heat not required to repeatedly boil the condensate shed off to the sides is, in effect, "excess" heat that is available to mobilize additional water vapor from the rock matrix. Thus, the total return flow of condensate toward the drift comprises water from the previous refluxing cycle, plus water vapor that has just been mobilized from the rock matrix and condensed in the fractures. The only difference near the drifts between the *point-* and *line-load* designs is that a larger fraction (compared with the *point load*) of the heat for the *line load* is available for rock dryout, which allows the upper dryout front to advance more rapidly for the *line load* than for the *point load*.

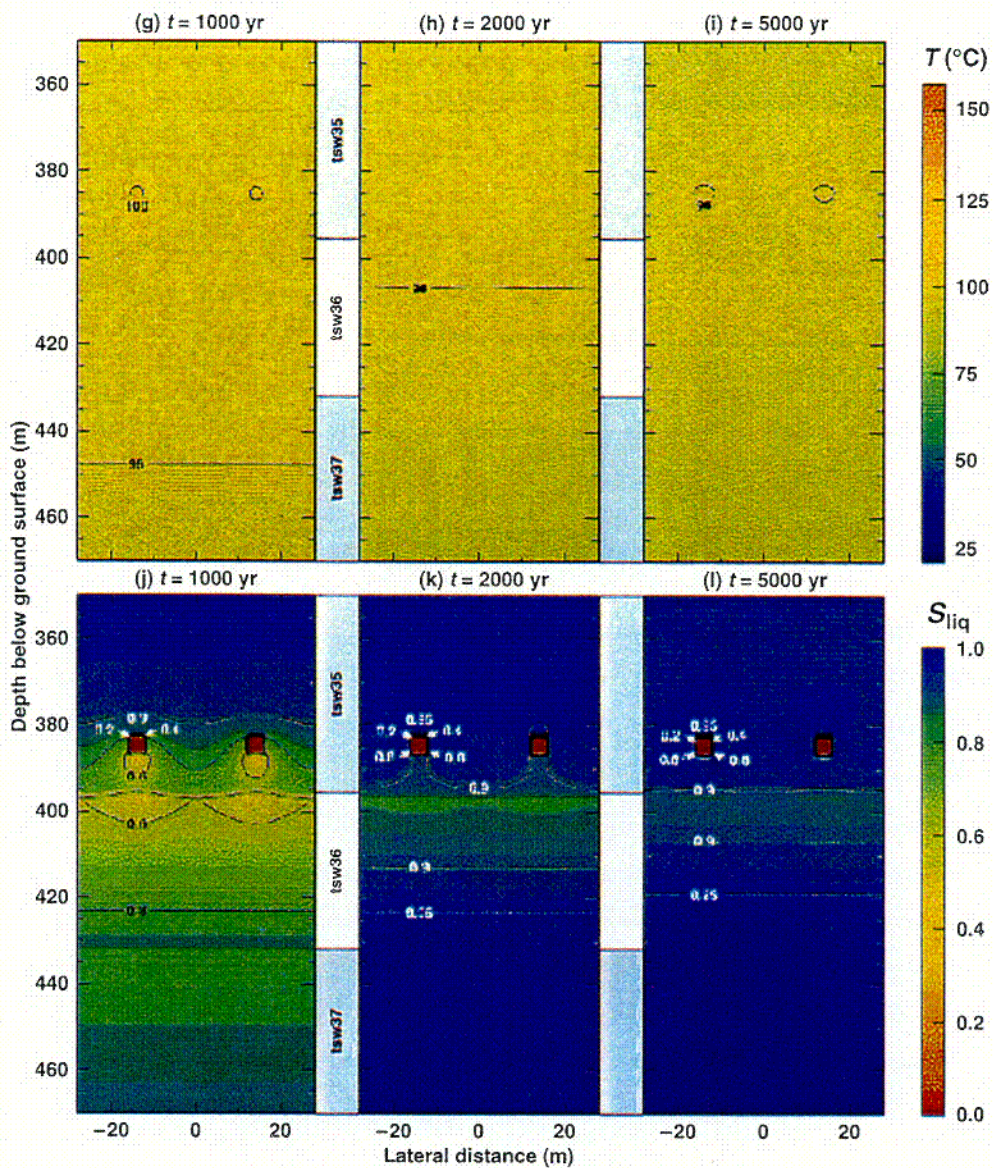
INTENTIONALLY LEFT BLANK



Source: Hardin 1998, Figure 3-17

NOTE: Contour labels and color bars indicate values.

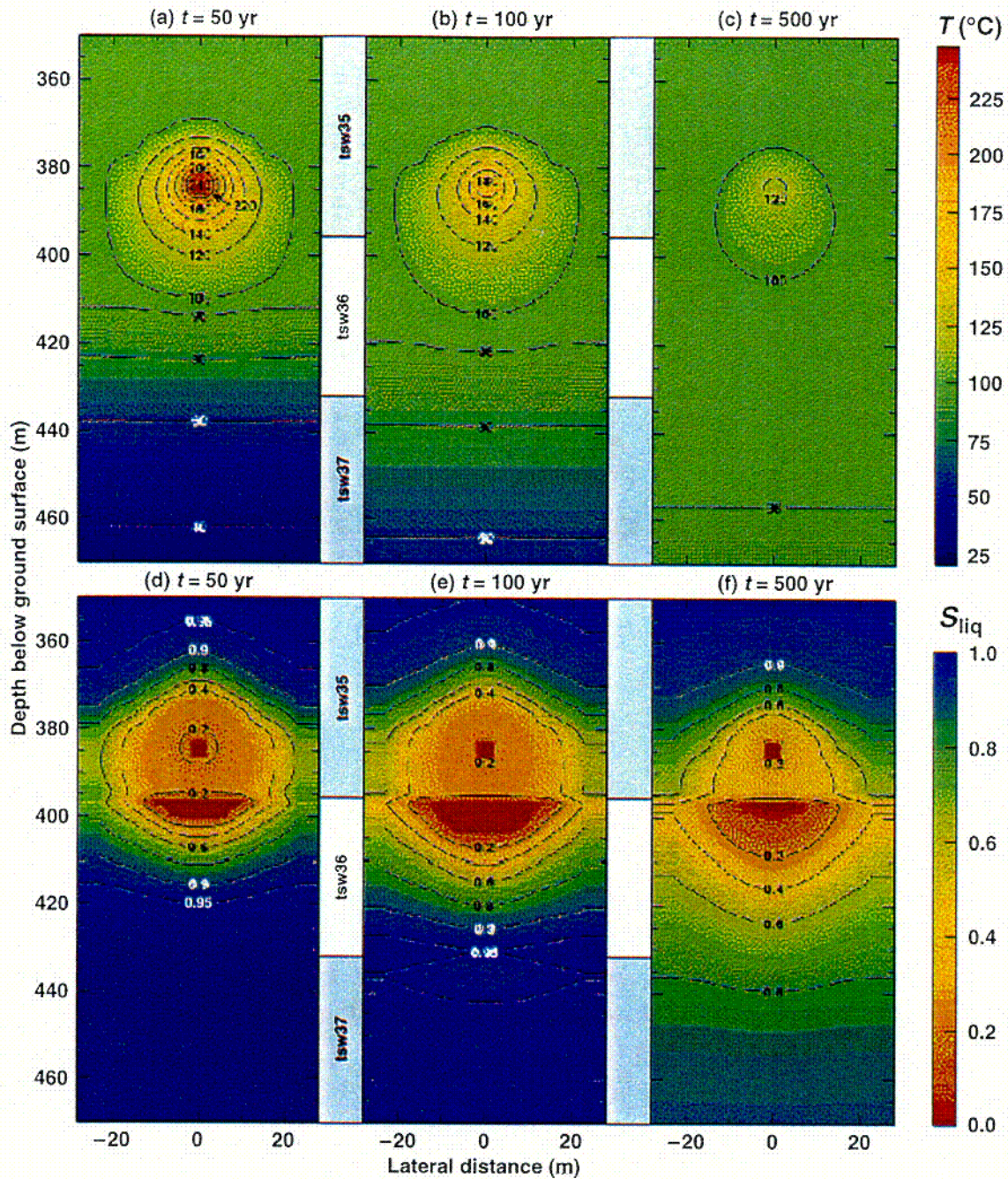
Figure 3-24. Temperature and Liquid-Phase Saturation Distributions for *Point Loading* of 28 m-Spaced Drifts (Page 1 of 2)



Source: Hardin 1998, Figure 3-17

NOTE: Contour labels and color bars indicate values.

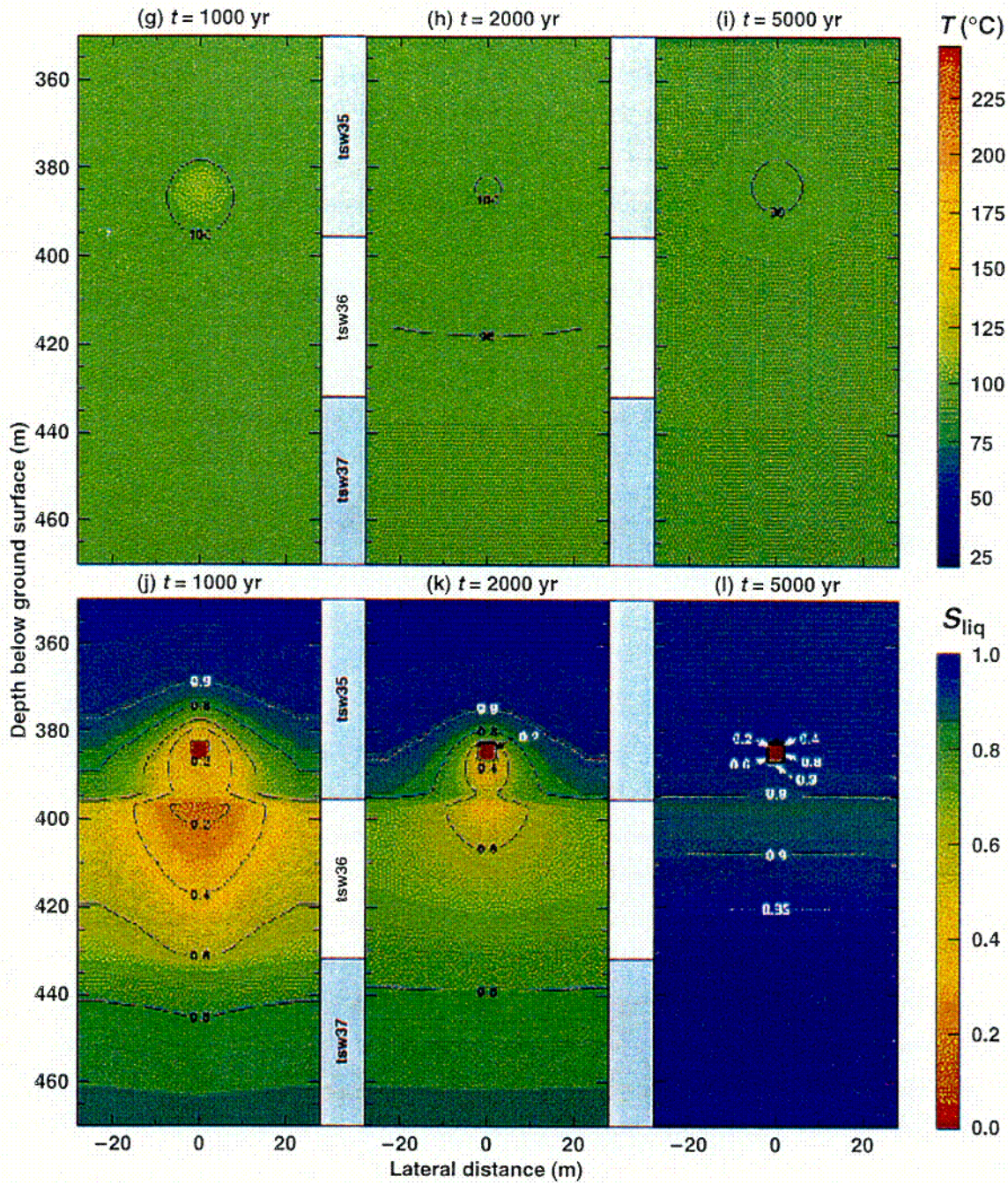
Figure 3-24. Temperature and Liquid-Phase Saturation Distributions for *Point Loading* of 28 m-Spaced Drifts (Page 2 of 2)



Source: Hardin 1998, Figure 3-19

NOTE: Contour labels and color bars indicate values.

Figure 3-25. Temperature and Liquid-Phase Saturation Distributions for *Line Loading* of 56.6 m-Spaced Drifts (Page 1 of 2)



Source: Hardin 1998, Figure 3-19

NOTE: Contour labels and color bars indicate values.

Figure 3-25. Temperature and Liquid-Phase Saturation Distributions for *Line Loading* of 56.6 m-Spaced Drifts (Page 2 of 2)

- **The vertical length of the heat-pipe zone is less for the *line load* than it is for the point load at early time.** For low percolation flux, the heat-pipe-zone length is also less for the line-load design at later times. The smaller heat-pipe-zone length for the line-load design arises from the more efficient condensate drainage between the line-load drifts, which results in less condensate build-up above the line-load drifts.
- The vertical length of the heat-pipe zone increases with repository depth below the ground surface.
- The tendency **for dryout zone coalescence decreases with increasing *percolation flux*** and is less for the line-load design than it is for the point-load design.

It is stressed that the results illustrated in this section are not directly applicable to the TSPA-SR repository design and how it may evolve in time after the emplacement of heat generating wastes in the unsaturated zone at Yucca Mountain. However, the results and knowledge gained from TH analysis of previous repository designs provides a strong technical basis for project decisions made to mitigate and/or emphasize certain processes in the base case TSPA-SR design. Specifically, the knowledge gained from previous analyses allowed the specification of certain design criteria (for TSPA-SR) that would eliminate the processes associated with coalescence of dryout zones between emplacement drifts, thus limiting the ability of the system to allow thermally enhanced condensate drainage to occur between drifts. Based on this knowledge, the drift spacing is increased from the 28 meter spacing specified for the point-loaded VA repository design to an 81 meter spacing for the SR design. An increased drift spacing for TSPA-SR also serves to greatly lower the total thermal load (kW/acre at closure) of the repository when combined with a preclosure ventilation period. This reduces the host rock temperatures thereby decreasing or eliminating many of the TH processes discussed in this section. Specific TH results for the SR repository design (without backfill) are shown in detail in Section 3.2.3.1 in this PMR as well as in the Multiscale TH AMR (CRWMS M&O 2000k) and the In-Drift Environment AMR (CRWMS M&O 2000m, Section 6). Confidence in the TH NFE models is further discussed in Section 3.6.4.1.

#### 3.2.3.4 Comparison of Results from TH and THC Models

In this section, the TH output variables used to describe the performance of a geologic repository with decay heating are compared using the 2-D DS THC model, a 2-D DS model extracted from the multiscale TH model, and the full MSTHM results that include repository edge effects. The resulting process model comparisons are for a repository design that includes 50 years of ventilation at 70 percent heat-removal efficiency, with backfill and drip-shield emplacement at repository closure. The specific analyses summarized in this section of the PMR are necessary to determine which process-level models of varying degrees of complexity can be used to address various process issues associated with repository heating. Quantities used by TSPA that are altered by repository heat-addition include the in-drift temperature and relative humidity, drift-wall temperature, drift-wall liquid saturation, percolation flux in the NF host rock, and water and gas composition at the drift wall. This section focuses primarily on the coupled processes of reactive transport and thermal hydrology, and how these interact in the NF host rock. Arguments are made that some of the quantities of interest to TSPA do not need to be computed with a model that includes fully-coupled reactive transport with thermal hydrology. That is, a thermal-

hydrology model uncoupled from reactive transport is sufficient. This simplification allows one to neglect the additional mass-transport equations for individual species, as well as the chemical thermodynamics and kinetics associated with precipitation or dissolution reactions.

Although also initiated by repository heating, mechanical processes occurring in the NF host rock are not included simultaneously with the processes described in this section. They are decoupled from the processes of chemistry and hydrology and described separately in Section 3.5 of this PMR.

In the cases where water and gas compositions are required in the NF drift-wall host rock, fully-coupled reactive-transport models, including thermal hydrology, are required. Although uncertainties exist in how the reactive-transport model describes mineral-water chemical reactions in its process description (refer to Section 3.3.4), the chemical content of the water and gas can be obtained within the framework of the assumptions applied in the THC process model. The anion, cation, pH, and partial pressure of CO<sub>2</sub> concentrations abstracted from the THC process model are fixed by reactive-transport assumptions and inputs, such as mineral reaction rate constants, activation energies, mineral reactive-surface areas, and mineral contents and compositions. Other assumptions and inputs associated with flow include infiltration flux and climate-state variability, along with the conceptual flow model used to describe heat and fluid flow. Of particular importance is how fluid-flow properties (such as fracture permeability) are altered in response to mineral-water chemical reactions. The THC process model assumes parallel-plane fractures of uniform aperture, relating changes in fracture porosity (which can increase when minerals dissolve or decrease when minerals precipitate) to subsequent changes in fracture permeability and capillary pressure. Consequently, the abstracted water chemistry and gas composition used by TSPA and summarized in Section 3.4 are applicable in the time periods shown and only for these assumptions that form the basis of the process model. Furthermore, the abstraction for TSPA, shown in Table 3-11 in Section 3.4 is valid only for the mean infiltration flux case (with climate change), but would require only a factor of 2 to 10 change in concentrations to account for the full range of infiltration-flux cases considered by other TSPA models (refer to Section 3.4.2.2).

In the cases where in-drift thermodynamic environment or NF percolation flux are concerned, it is argued in this section that recourse to a fully-coupled reactive-transport code with thermal hydrology is not necessary. TSPA can obtain the desired quantities (waste package temperature, drift-wall temperature, host-rock percolation flux, etc.) for abstraction purposes from a process model that includes thermal hydrology only. A thermal-hydrology model computes the flow of fluid and heat without physical alteration to fluid-flow properties by dissolution or precipitation mineral-water reactions. Since the TH-only model neglects chemical alteration to the flow properties, an evaluation (of the differences between THC and TH-only models) in both state and flow variables is presented in the *THC Abstraction AMR* (CRWMS M&O 2000c, Section 6.3) and summarized in this section. Primary focus of the PMR discussion is on how differences may occur in flow variables between models, since the changes in flow properties by dissolution or precipitation are neglected in the TH-only models.

The result of the process-model evaluations described in Sections 3.2.3.4.1 and 3.2.3.4.2 indicate that the flow and state variables in the NF host rock are nearly identical for two different geochemical systems and are not appreciably different for models that may or may not include

reactive transport (Section 3.2.3.4.2). The no-consequence conclusion of this process-model evaluation is primarily a result of the fracture porosities applied in the THC process model (1 percent) (CRWMS M&O 2000a, Table 5). For such initially large fracture porosities, the relative change in the fracture volume as a result of precipitation or dissolution is quite small. This results in little or no change in the fracture liquid or gas flows. For small initial porosity (as applied in TSPA-VA), reactive transport processes result in much larger changes in the flow variables, when compared to TH-only calculations, due to larger relative changes in fracture volume.

In addition to providing an abstraction for water chemistry and gas-phase composition in the NF host rock, the *THC Abstraction AMR* (CRWMS M&O 2000c) also serves to illustrate the potential differences in the thermal-hydrologic response of a potential repository obtained from process models that either do or do not include reactive-transport processes coupled with the thermal-hydrologic processes that occur in response to repository heat-addition. An initial comparison is made with the DS THC model that includes fully-coupled reactive-transport processes for two mineral sets: complex and reduced. This evaluation compares drift-wall host rock temperature, liquid saturation, air mass fraction, gas flux in fractures, and liquid flux in fractures (CRWMS M&O 2000c, Section 6.2). The purpose of the TH variable comparison from the same process model that incorporates two different geochemical systems is to highlight that the resultant differences in the NF rock mineralogy only weakly influences the overall TH response of the geologic system. Another evaluation in the *THC Abstraction AMR* compares process-level models that incorporate the same boundary conditions and repository specifications, but may not include all of the fully-coupled processes in the rock that occur in response to heat-addition.

A comparison of process-level models (TH-only vs. THC) is considered in the *THC Abstraction AMR* (CRWMS M&O 2000c, Section 6.3). Since the DS THC model described above has been developed independently of the TH-only model used to determine the in-drift thermodynamic environment (CRWMS M&O 2000k), a 2-D DS, TH-only model taken directly from the Multiscale TH AMR (CRWMS M&O 2000k, Section 6.3) is compared to the TH results of the 2-D DS THC model developed in the *THC Process AMR* (CRWMS M&O 2000b). This comparative analysis is used to determine whether (and how) reactive-transport processes occurring in the host rock as a result of repository heat-addition alter the fundamental TH properties of the geologic system (e.g., temperature, liquid flux in fractures, etc.). An evaluation of this type allows an assessment of the appropriateness of an abstraction of TH variables that describe the performance of a geologic repository from a process-level model that does not include the fully-coupled reactive-transport processes. (This is the approach used in the TSPA abstraction of the TH variables used to describe repository performance, since reactive-transport processes do not appreciably alter fracture flows.)

A final comparison is made in the abstraction AMR (CRWMS M&O 2000c, Section 6.4). The DS THC model thermal-hydrologic results are compared to the multiscale TH model (CRWMS M&O 2000k, Section 6.1) results at the emplacement drift-wall. This evaluation provides an assessment of the extent of repository edge effects (and how this may affect the THC abstraction) on the TH variables obtained from DS models that incorporate no-flow lateral boundary conditions (e.g., do not include edge effects). Both the 2-D DS TH-only and THC

models compared in Section 6.3 of the *THC Abstraction AMR* apply the no-flow boundary assumption on the lateral boundary conditions.

#### 3.2.3.4.1 TH Model

The major TH model-set supporting this PMR is the MSTHM. One component TH submodel is a 2-D column model similar to the THC models described in Section 3.3. That is, essentially 2-D radial heat flow into the host rock with no flow boundaries at the pillar half-spacing. Another submodel in the MSTHM calculates the 3-D heat flow from a smeared heat source that is in the shape of the repository footprint. A third MSTHM submodel calculates the 3-D heat flow in a column that includes a set of discrete waste packages with a distribution of thermal powers that is consistent with the overall repository-wide distribution, based on the variability of the waste stream and the blending of hot and cold waste within individual waste packages. Two- and three-dimensional columns are calculated in a number of locations, edge and central, to capture the variability of geological conditions.

The results of the MSTHM submodels are combined to capture the time- and space-dependent temperature and saturation distributions, including effects of the repository footprint edges, the distribution of geologic properties and ambient percolation flux, geometric effects at the drift scale, and the effects of variability in heat output of individual waste packages.

The MSTHM submodels are implemented using the NUFT heat and mass transfer code (CRWMS M&O 2000k). As in the THC model described in Section 3.3, the 2-D DS submodels used in the MSTHM are also based on an active-fracture, DK conceptual flow model for matrix and fracture continua.

The MSTHM submodels that calculate the space- and time-dependent temperatures, saturations, and percolation fluxes are used in the TSPA models. The TH models also calculate the space- and time-dependent temperatures and relative humidities within the emplacement drifts, as described in the EBS PMR (CRWMS M&O 2000g, Section 3.1.4). These results are key inputs to performance of the engineered barriers (drip shields and waste packages), described in the WPD PMR (CRWMS M&O 2000o) and the mobilization of radionuclides from breached waste packages, described in the WFD PMR (CRWMS M&O 2000ab).

It is noted that this ensemble of TH models can be used to approximate the effects of waste package-edge proximity, variability in host rock in which heat is placed, variability in infiltration rate and climate-state, and variability in heat output for different waste package-types. The mineral-water reactions or ambient rock-stress alteration that proceed in the fractures or matrix in response to repository heat-addition are not included in these models. Therefore, flow-property (and hence flow-rate) alterations by precipitation or dissolution reactions or tension and compression processes are not included in this modeling ensemble. Although an increase in model complexity occurs as a result of including, for instance, lateral heat losses due to surrounding unheated rock masses, the processes initiated by heat, other than thermal hydrologic processes, are not included. Since this is the case, an evaluation of neglecting these heat-induced processes in the TH models used by TSPA for abstraction is necessary. A comparison of TH-only to THC processes is considered in the following sections.

### 3.2.3.4.2 THC Model

The THC models supporting this PMR are described in more detail in Section 3.3.

In the results described below, the THC model is implemented at a location in the northeast part of the potential repository footprint, in which the repository horizon is located in the middle non-lithophysal geologic sub-unit (referred to as the Tptpmn or tsw34 sub-unit); this permits use of thermal and hydrologic properties as well as measured water chemistry and gas compositions obtained from the DST.

The THC models account for 2-D heat and mass transfer within the drifts and in the surrounding rock, using separate continua in the rock to represent the connected network of fractures and the rock matrix in which the fractures reside. Movement of mass (liquid water, water vapor, and air) between the fractures and matrix is calculated using a submodel, termed an "active-fracture" DKM. This flow model specifies a means for fracture flow through the system. The THC models available for TSPA abstraction only include mineralogical-water reaction processes occurring in the host-rock matrix and fracture pore space; the chemical evolution of the emplacement drift is not included. Subsequently, the evolution of gas in the emplacement drift due to chemical (e.g., interaction of heat with backfill materials) or radiolitic processes is not included in the THC process model.

The THC models include chemical reactions in selected geochemical systems. Two systems are considered in the results described below. A *Less Complex* system includes  $\text{H}_2\text{O}$ ,  $\text{H}^+$ ,  $\text{Ca}^{2+}$ ,  $\text{Na}^+$ ,  $\text{SiO}_2$ ,  $\text{Cl}^-$ ,  $\text{HCO}_3^-$ , and  $\text{SO}_4^{2-}$  as main component species and all other aqueous species that can be derived from these components, together with  $\text{CO}_2$  gas and Calcite, Tridymite,  $\alpha$ -Cristobalite, Quartz, Amorphous Silica, Glass, and Gypsum.

A *complex* system includes  $\text{H}_2\text{O}$ ,  $\text{H}^+$ ,  $\text{Na}^+$ ,  $\text{K}^+$ ,  $\text{Ca}^{2+}$ ,  $\text{Mg}^{2+}$ ,  $\text{SiO}_2$ ,  $\text{AlO}_2^-$ ,  $\text{HFeO}_2$ ,  $\text{Cl}^-$ ,  $\text{HCO}_3^-$ ,  $\text{SO}_4^{2-}$ , and  $\text{F}^-$  as main component species and all other aqueous species that can be derived from these components, together with  $\text{CO}_2$  gas and Calcite, Tridymite,  $\alpha$ -Cristobalite, Quartz, Amorphous Silica, Glass, Gypsum, Hematite, Fluorite, Goethite, Albite, Microcline, Anorthite, Ca-Smectite, Mg-Smectite, K-Smectite, Illite, Kaolinite, Sepiolite, Stellerite, Heulandite, Mordenite, and Clinoptilolite.

This section compares the THC DS model (using the *complex* set of cations and anions listed above) to the Multiscale TH AMR (CRWMS M&O 2000k, Section 6.6). The multiscale model considers repository edge-cooling effects and WP thermal output variability, in addition to the thermal-hydrological processes considered by both models. The comparison focuses on the drift-wall temperatures and liquid saturations. For computational efficiency, the periodic lateral boundary conditions of DS models, such as the THC model, simulate a location at the center of an infinite repository. The limitations of this assumption are most pronounced near the repository edges, but can also influence temperatures at the repository center after enough time has passed. The results of this comparative analysis will provide TSPA with the basis to perform temperature-dependent alterations to the THC abstraction, so that edge effect cooling may be accounted for in the abstraction of aqueous species concentrations and gas phase compositions.

### 3.2.3.4.3 The Influence of the THC Chemical Constituents on TH Parameters

The TH output variables (gas flux, liquid flux, temperature, liquid saturation, and air mass fraction) are compared in this section, based on two implementations of the THC model, using the less detailed and more-detailed sets of chemical constituents (see Section 3.3.2.4). In particular, this comparative analysis evaluates how different geochemistry (e.g., including different mineral assemblages) may alter the TH variables associated with repository heating. The analysis uses the mean infiltration rate with climate change (as described in CRWMS M&O 2000b, Table 12) and compares conditions at the drift crown.

The analysis (CRWMS M&O 2000c, Section 6.2) shows that the two geochemical systems result in nearly identical TH parameters at the drift crown. In each case, the calculations involving more minerals produced the same temperature, liquid flux, gas flux, air mass fraction, and liquid saturation as the calculations involving fewer minerals. Furthermore, this trend is true for the other drift-wall locations (side and base), as well as the other infiltration-flux cases (high and low). Therefore, the geochemical and reactive transport alterations to the flow (and characteristic) properties, as described in the *THC Process AMR* (CRWMS M&O 2000b, Section 6.1.6, Equations 16-19), are not enough to impact the fundamental properties of the repository system associated with heating processes (e.g., host-rock temperature adjacent to the emplacement-drift wall). This also holds true for the low and high infiltration cases considered in the *THC Process AMR* (CRWMS M&O 2000b, Table 12).

The results in this section are based on a fracture porosity of about 1 percent. The results indicate that dissolution and precipitation would be inadequate to significantly alter fracture-flow capability. For a significantly smaller fracture porosity, the calculated amount of mineral precipitation could be enough to reduce fracture flow in the NF region above the drift. In addition, the limitations of continuum modeling do not permit the calculation to address concentration of precipitation in localized regions, which could potentially reduce fracture flow significantly, even when the overall porosity reduction is not large; these types of localized effects are well known in chemical engineering and biological systems. Ongoing work may address the localized effects. As indicated previously, chemical interaction of gas constituents contained within the emplacement drift and how they may interact with the NF host rock are not included in the reactive-transport processes occurring in the NF host rock.

### 3.2.3.4.4 Comparison of TH Parameters from the 2-D THC and 2-D TH-Only Models

Both the THC and TH-only DS models use the same conceptual flow models (DKM/AFM). The TH DS model, as described in a line-averaged-heat-source, DS, Thermal-Hydrological (LDTH) submodel selected from the Multiscale TH AMR (CRWMS M&O 2000k, Section 6.3), is compared directly to the THC DS model. For consistent boundary conditions, the selected LDTH model location, l3c1, is near the stratigraphic location of the THC model (i.e., near the northeast section of the repository, located near borehole SD-9). See Figures 3-1 through 3-3 for LDTH column locations. Both models use periodic boundary conditions laterally (e.g., symmetry boundary along the drift centerline and a no-heat or mass-flow boundary at the pillar midpoint). Both also use similar (calculated) initial matrix saturations and identical infiltration-rate boundary conditions and climate-state changes. In the *THC Abstraction AMR* (CRWMS M&O 2000c), the l3c1 infiltration-rate boundary condition is altered from the

Multiscale TH CRWMS M&O (2000k) to be consistent with the THC model. Finally, the time-dependent heat-source thermal outputs are also identical. The DS models that apply a mean infiltration flux-case with climate changes at 600 and 2,000 years are used in this comparison.

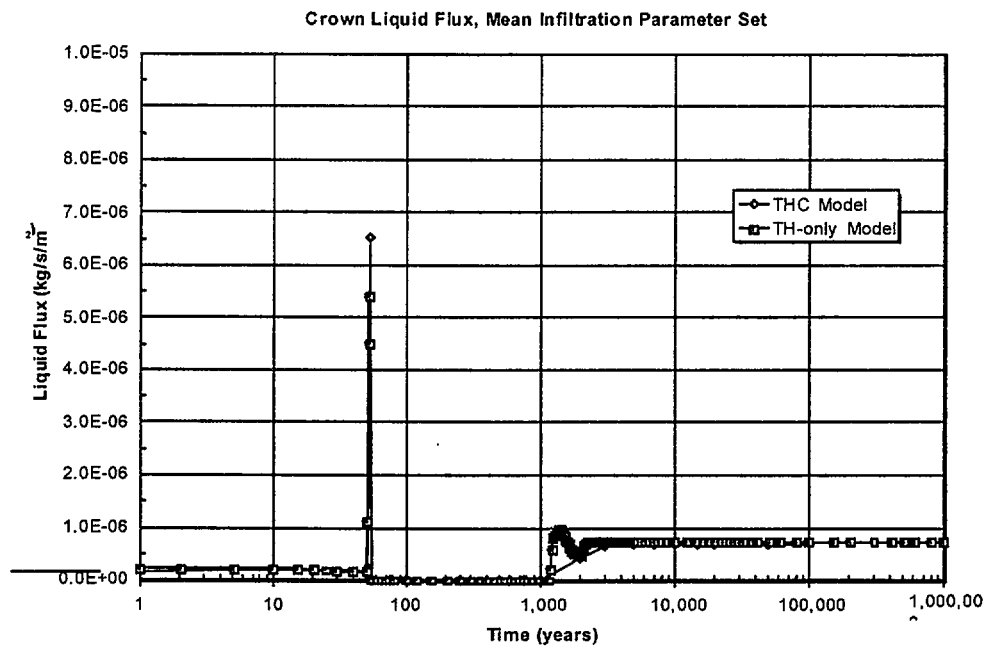
At both the crown and side of the drift wall, preclosure temperatures agree for the two models, within a degree or two. Between closure and 2,000 years, the THC model calculates higher temperatures than the TH model, up to 8°C. Because the THC temperatures are higher, the reaction kinetics will increase so that the THC analyses represent bound conditions. After 2,000 years, until about 20,000 years, the THC model temperatures are up to 6°C lower than the TH model. The results of THC analyses for this period of time cannot be assumed to represent the bound case, since the temperatures (and thus kinetics) are lower. After 20,000 years, the two models produce identical temperatures, within a fraction of a degree (CRWMS M&O 2000c, Figures 8-9). The differences during the above boiling period are primarily due to the difference in the amount of water in the host rock-matrix at these locations near the drift wall. This is primarily driven by differences in implementation of the capillary-pressure curves in the models.

In both models, at the crown of the emplacement drift, all of the water is driven out of the fractures during the above boiling period. However, both before and after boiling, the TH model calculates a few percent higher fracture saturation than the THC model (CRWMS M&O 2000c, Figure 11). This difference (which is calculated prior to the addition of heat, during the establishment of equilibrium initial conditions) is most likely due to subtle differences in how the AFM is implemented in the two models. Of particular importance is how the capillary pressure curve is treated at low fracture saturations (linearization or capillary pressure cut-off).

Both models result in similar air compositions near the drift wall (CRWMS M&O 2000c, Figures 12 and 13). The gas flux in the fractures at the crown of the drift is similar between the two models during the preclosure period. During the above boiling and transition periods, the TH-only model predicts higher gas (air) fluxes than the THC model (CRWMS M&O 2000c, Figure 14). The difference in gas flux between models at this (crown) location during the boiling period is about two orders of magnitude lower in the fully coupled model. This difference is attributed largely to the extensive boiling zone developed in the THC model, but not present in the corresponding TH-only model. During the boiling period in the THC model, a large amount of water is driven out of the matrix (vaporized), thereby decreasing the air mass fraction at this location during this time period. Subsequently, the air mass fraction from the THC model during boiling is somewhat lower than that from the TH-only model. As a consequence, the air flow near the crown of the drift during the boiling period in the THC model is primarily attributed to diffusion which occurs at a much lower rate than advection. After boiling, the models are in agreement to within about an order magnitude or less out to about  $1 \times 10^5$  yr. The late time response is generally more important to TSPA since chemical environments associated with later times are more pertinent to EBS corrosion. Figure 3-26 (CRWMS M&O 2000c, Figure 15) shows the magnitude of the fracture liquid flux at the crown of the drift. Although the trends of the two models are similar, the liquid flux in the TH-only model is slightly greater at this location except for the early time spike shown in the figure. The differences in liquid flux at the side and at the base of the emplacement drift are largely driven by the no-flow boundary drift wall assumption made in the THC model (CRWMS M&O 2000b, Section 5, assumption C.1). This results in flow being diverted around the drift wall. The TH model allows water to cross the drift wall interface at locations in the emplacement drift where the backfill material contacts the

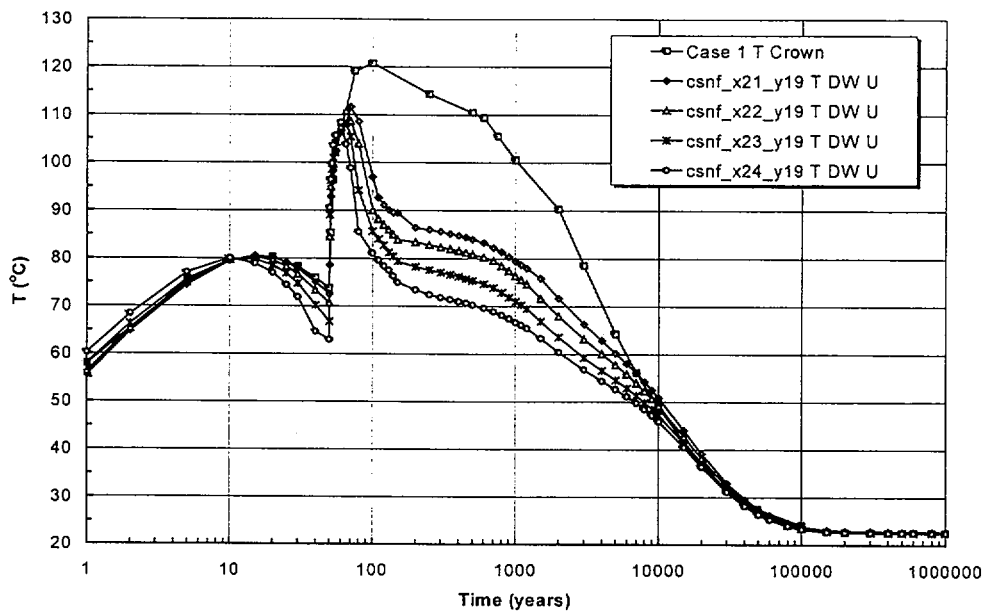
drift wall. Consequently, at the drift base in the TH model, the percolation fluxes in the fractures will be larger, because water from the backfill drift-wall interface is not diverted around the drift opening (CRWMS M&O 2000c, Figure 16).

The spike in the fracture-liquid flux shown in Figure 3-26 coincides with the time of repository closure (50 years). At the time of closure, repository ventilation ceases (all remaining waste package heat output is now available for host-rock heating), and backfill and drip shields are emplaced in the drifts. Enhanced liquid flow back to the crown of the drift occurs when water evaporated during the preclosure period condenses in the fractures (recall that 30 percent of the waste package heat was available for input into the surrounding host rock) immediately at the time of backfill emplacement. After about 20 years of ventilation, the heat removal rate by ventilation exceeds the waste form heat rate, and drift temperature decreases. At closure, ventilation ceases and backfill is added. During the time immediately following backfill (only for the first year after backfill), the drift-wall crown temperature drops slightly due to an increased resistance (represented by the low thermal-conductivity backfill) to heat flow between the waste package and the drift wall. When the backfill has been heated, drift wall temperatures begin to increase due to the lack of heat removal by ventilation. The drift wall rapidly increases in temperature (Figure 3-27) and the liquid flux is driven to zero (a few years after backfill).



Source: CRWMS M&O 2000c, Figure 15

Figure 3-26. Host-Rock Fracture Liquid Flux at the Emplacement-Drift Crown



Source: CRWMS M&O 2000c, Figure 17

NOTE: The multi-scale model used mean infiltration rate with climate change. The four "csnf" curves are the multi-scale model results at four locations in the repository footprint. The "Case 1" curve is from the THC model.

Figure 3-27. Comparison of Drift Crown Temperatures Using the THC Model Multiscale TH Model

The small differences (<10%) in process-model predictions of fracture flux (both liquid water and air) at the crown of the drift are potentially attributed to reactive-transport processes occurring in the THC model and/or potential differences in model implementation of capillary pressure characteristic curves, which may alter the driving force for the fluxes. In regions of precipitation around the emplacement drift at the crown, potential permeability reductions caused by mineral precipitation in the fractures of the THC model could result in the reduced gas and liquid fluxes, when compared to the TH-only model (in which permeability remains unchanged after pore water boiling). If the conventional cubic law (Raven and Gale 1985) is used, a 1 percent reduction in fracture aperture will cause a 3 percent reduction in fracture permeability. Relative permeability to water is a function of saturation. Fracture volume (aperture) changes, if water volumes remain constant, may result in increased fracture saturation. Thus, a 3% reduction in permeability may result in fluid flux reductions between zero and 3%.

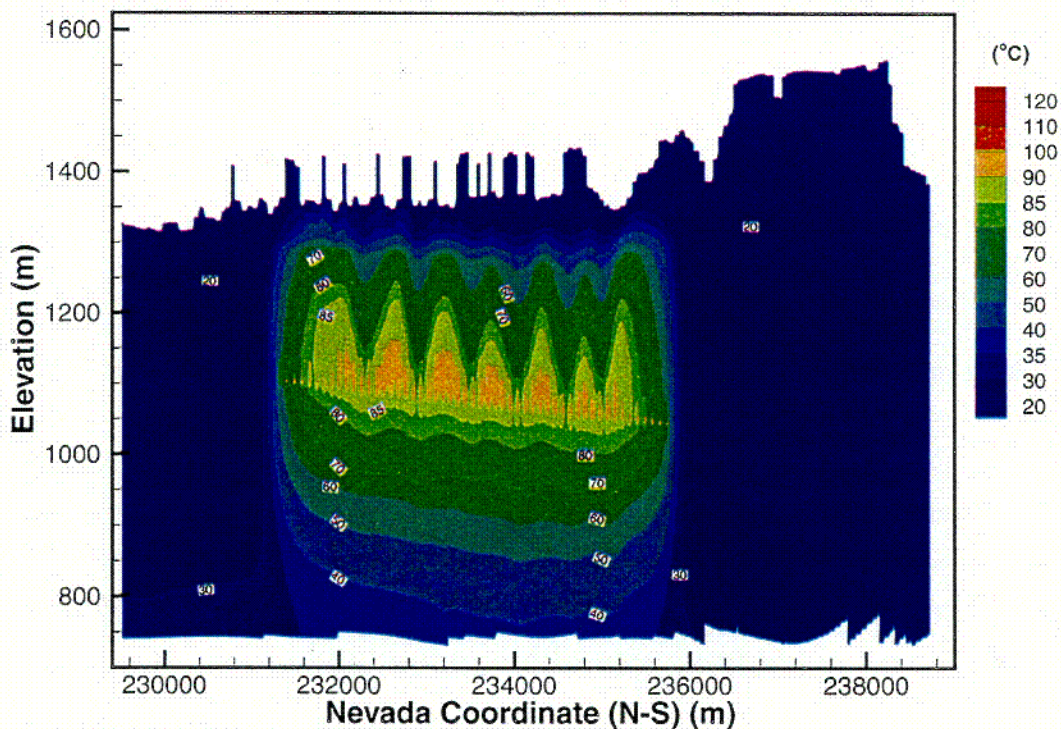
From Figure 3-26, the late-time ratio (10,000 years) of percolation flux from the THC model to the TH-only model is 0.94. This difference is of similar magnitude to the cubic law estimation of flux (permeability) changes due to aperture decreases. Subsequently, the reactive-transport processes and/or potential differences in characteristic curve implementation between models in the fracture medium causes a very slight reduction in the liquid-phase flux in the fractures.

Therefore, as indicated previously when comparing state variables (e.g., temperature), either model is appropriate when predicting the TH flow variables used to determine the performance of the potential repository.

Indeed, when the quantities of interest are the thermodynamic variables within the emplacement drift or the NF host rock percolation flux (e.g., temperature and relative humidity in the engineering barrier system components and percolation flux at the crown of the drift), the TH-only model is preferred since its computational complexity is far less than that of a fully coupled reactive transport model. However, if an assessment of the water chemistry and gas-phase composition is required, a fully coupled reactive transport model is needed.

### 3.2.3.4.5 Comparison of Temperatures from the Multi-Scale TH Models with a 2-D Mountain-Scale Model

The 2-D Mountain-Scale TH model described in Section 3.2.2.2 was used to calculate temperature along a north-south section through the repository. A typical result is shown in Figure 3-28 (CRWMS M&O 2000f, Figure 3.12-5b). The rock temperatures at 1,000 years are similar to the drift wall and pillar temperatures shown in Figures 3-7 and 3-8. The two models are complementary. The 2-D model captures mountain-scale convection spanning ~10 drifts (in the N-S direction only) not currently modeled in the MSTHM and is well suited to calculate pillar temperature where gradients are not as steep as at the drift wall. Its coarse zoning near the drifts results in an underprediction of drift wall temperature at the peak of the thermal pulse (earlier than shown in Figure 3-33). Conversely, in addition to more accurate peak drift wall temperatures, the MSTHM addresses a number of factors not included in the 2-D mountain-scale model, such as E-W edge and property effects and axial heat source variation.



Source: CRWMS M&O 2000f, Figure 3.12-5(b)

Figure 3-28. Temperature Distribution Calculated at 1,000 Years in a 2-D Mountain-Scale TH Model

C-25

### 3.2.3.4.6 Repository Edge Behavior

The *THC Process AMR* does not include repository edge effects (e.g., lateral heat loss to unheated rock mass) since it implements periodic boundary conditions in its model formulation. This DS modeling assumption is generally more representative of the repository center where a particular emplacement drift is flanked on either side by additional heated drifts. An edge location is surrounded by unheated rock masses without drifts. Since it is postulated that edge heat loss due to the absence of neighboring heated drifts affects both the temperature and liquid saturation evolution at the boundaries of the potential repository, a comparison is made between process models that include varying complexity associated with repository edge heat losses. As discussed in Section 3.2.3.4.1, the multiscale TH model includes edge-heat loss in its formulation. Therefore, an assessment can be made as to the duration and influence of not including the edge effect in the 2-D model. The comparison of models is made at a location in the repository footprint in which the geologic stratigraphy and infiltration rate are nearly identical (e.g., infiltration rates are identical). Temperature and liquid saturation at the crown of the emplacement drift are compared.

The edge-cooling effect results in dramatically lower temperatures in the multiscale TH model at the drift wall (CRWMS M&O 2000c, Figures 17-18). The drift-wall crown temperatures at this near-edge location are 30-40°C lower in the multiscale TH model, from about 200 to 800 yr. Each of the potential repository footprint locations shown in Figure 3-27 indicates a variety of location-dependent results of an average drift wall temperature from the multiscale TH model near the THC model domain. Four different locations are specified from the multiscale TH model domain for comparison to the THC model. For example, location CSNF\_x21\_y19 T DW U represents a location-dependent result (stratigraphically) near the THC model domain for the upper drift wall adjacent to an average CSNF waste package. The peak temperature, which occurs between closure and 100 years, is about 10°C lower in the multiscale model, due to the repository edge-effect at this location.

Corresponding differences in liquid saturation occur as well (CRWMS M&O 2000c, Figure 19). In the multiscale TH model, liquid saturation at the crown of the drift resaturates much more quickly (within a few centuries) than does the DS THC model (within a few millennia). This is primarily due to a lower maximum temperature and about 900 fewer years of temperatures above boiling at this location.

The temperature comparison between a model that includes edge effects (multiscale TH model) to a model that does not (the THC model) illustrates how lateral heat loss influences the drift wall thermal conditions over time. Since the THC model was based on a borehole at a location near the edge of the potential repository (but the model applies periodic no-flow lateral boundary conditions, i.e., representative of the center repository), an assessment of the potential temperature and moisture conditions at the drift wall is made with this edge proximity comparison to determine if the duration of boiling obtained from the THC model may be overestimating the time at which the drift wall is dry. The result is that although the extent and duration of the boiling zone predicted by the THC model may be in direct response to a modeling assumption (e.g., periodic boundary conditions), the TSPA abstraction estimates the water chemistry at the drift wall during this boiling period by using the water chemistry obtained (from the DS THC model) in the condensate zone that develops above the boiling region. This

approach minimizes the impact of the boundary conditions and ensures that an appropriate water chemistry is used. This compositional boundary condition is then applied during the abstracted boiling period in conjunction with other models to determine the in-drift geochemical environment at all potential repository locations.

The abstraction of the condensate water composition applied at the drift wall during the boiling period is considered appropriate for the water that may potentially enter a heterogeneous fracture network and flow by gravity from the condensate zone to the drift wall (the location of the THC abstraction). This effective water composition at the emplacement drift wall during the boiling period is then coupled with the TSPA seepage model used to determine the volume flow rate of water into the drift in order to determine the quantity and chemistry of the water entering the emplacement drifts. This method is applied at all locations within the repository, center or edge, and is considered reasonable since the combination of different models (e.g., seepage model, THC model, and multiscale TH model) used to determine the physical and chemical environment within the drifts accounts for each of the different processes separately.

Since the TSPA seepage model utilizes the percolation flux from a location in the multiscale TH model which is always greater than or equal to the ambient fracture percolation flux, a water composition (adjacent to the drift wall) is required from the THC model that tends to predict the development of an extended dryout zone, since the process of edge cooling is not included in its model development. In order to provide the necessary water chemistry at the emplacement drift wall, the condensate composition above the dryout zone predicted by the THC process model is used as the composition of water that could potentially flow from the condensate zone to the drift wall. The TSPA models for the in-drift geochemical environment utilize location dependent temperatures and relative humidities from the multiscale TH model, as well as the seepage volume flow rate obtained as a function of the percolation flux computed from the multiscale TH model. As a consequence, the condensate water chemistry from the *THC Process AMR*, coupled with the appropriate location-dependent in-drift thermodynamic environment from the multiscale TH model provides for an approximate location-dependent (e.g., center and edge) geochemical result obtained from the abstracted in-drift chemical environment models.

#### **3.2.3.4.7 Conclusions of the TH Model Comparison**

As indicated by this process-model evaluation (Sections 3.2.3.4.3 and 3.2.3.4.4) of reactive-transport impact on TH performance of a potential geologic repository, either model is appropriate when predicting the TH state (temperature, liquid saturation) or flow variables (percolation flux) required by TSPA. Permeability reduction is approximately 3 percent, as described by parallel-plate (uniform-aperture) theory (CRWMS M&O 2000b, Equation 17). Figure 3-26 indicates a difference in liquid flux between models that can be explained by this as well as by potential difference in the driving forces in the models. As shown in the figures, the fracture liquid flow rates at the crown of the drift are nearly the same regardless of the model-type (THC or TH-only). It should be kept in mind that the results of this evaluation are a function of the initial fracture porosity used in the reactive-transport model. If the fracture porosity were to decrease, the chemically altered fracture permeability would be very different from the initial fracture permeability.

Since the differences (in state and flow variables) between models used to describe the performance of a potential geologic repository are small, TSPA can accept TH variables (i.e., drift-wall temperature, percolation flux in the NF host rock, etc.) that describe the performance of a potential geologic repository from models of either type (THC or TH-only). Indeed, when the quantities of interest are thermodynamic variables within the emplacement drift or the NF host-rock percolation flux (e.g., temperature and relative humidity in the EBS components and percolation flux at the crown of the drift), the TH-only model is preferred since its computational complexity is far less than that of a fully-coupled reactive-transport model, and accounts for 3-D and edge effects. However, when an abstraction of the water chemistry and gas-phase composition is required, a fully-coupled transport-model is necessary and can be used to produce chemical boundary conditions for the TSPA model. It can do so since it has been shown not to produce inconsistent thermal-hydrologic results when compared to a TH-only model.

### **3.3 DRIFT-SCALE THERMAL-HYDROLOGICAL-CHEMICAL PROCESSES AND MODELS**

The purpose of this section is to describe: (1) the conceptual model and input data for coupled thermal, hydrological and chemical (THC) processes; (2) the DST THC Model; and (3) the THC Process Model (termed the "THC Seepage Model" in the UZ F&T PMR). Abstractions done by Performance Assessment on the results of the THC Process Model are discussed in Sections 3.4 and 3.2.3.4. The conceptual model for THC processes provides a comprehensive basis for modeling the pertinent mineral-water-gas reactions in the host rock under thermal-loading conditions, as they influence the water and gas chemistry that may enter drifts over 100,000 yr. The purpose of the DST THC Model is to validate the conceptual model and input data by comparison of measured gas and water chemistry from the DST to the results of simulations. The purpose of the THC Process Model is to evaluate the effects of THC processes in the rock around emplacement drifts on the possible seepage-water chemistry, gas-phase composition, and the potential effects of THC processes on UZ flow and transport. This model was used to evaluate the effects of mineral dissolution and precipitation; the effects of CO<sub>2</sub> exsolution and transport in the region surrounding the drift; the potential for forming zones of calcite, silica or other minerals; the resulting changes to porosity and permeability; and the potential effects on seepage. The THC Process Model and validation of the data and processes, using the DST data, are addressed in the *THC Process AMR* (CRWMS M&O 2000b).

#### **3.3.1 Thermal-Hydrological-Chemical Conceptual Model**

The THC conceptual model underlies the numerical simulations of THC processes in the DST THC Model and in the THC Process Model. The conceptual model must be able to describe processes involving liquid and vapor flow, heat transport, and thermal effects resulting from boiling and condensation, transport of aqueous and gaseous species, mineralogical characteristics and changes, and aqueous and gaseous chemistry. A conceptual model of reaction-transport processes in the fractured welded tuffs of the potential repository host rock must also account for the different rates of transport in very permeable fractures, compared to the much less permeable rock matrix (see for example, Steefel and Lichtner 1998, pp. 186-187).

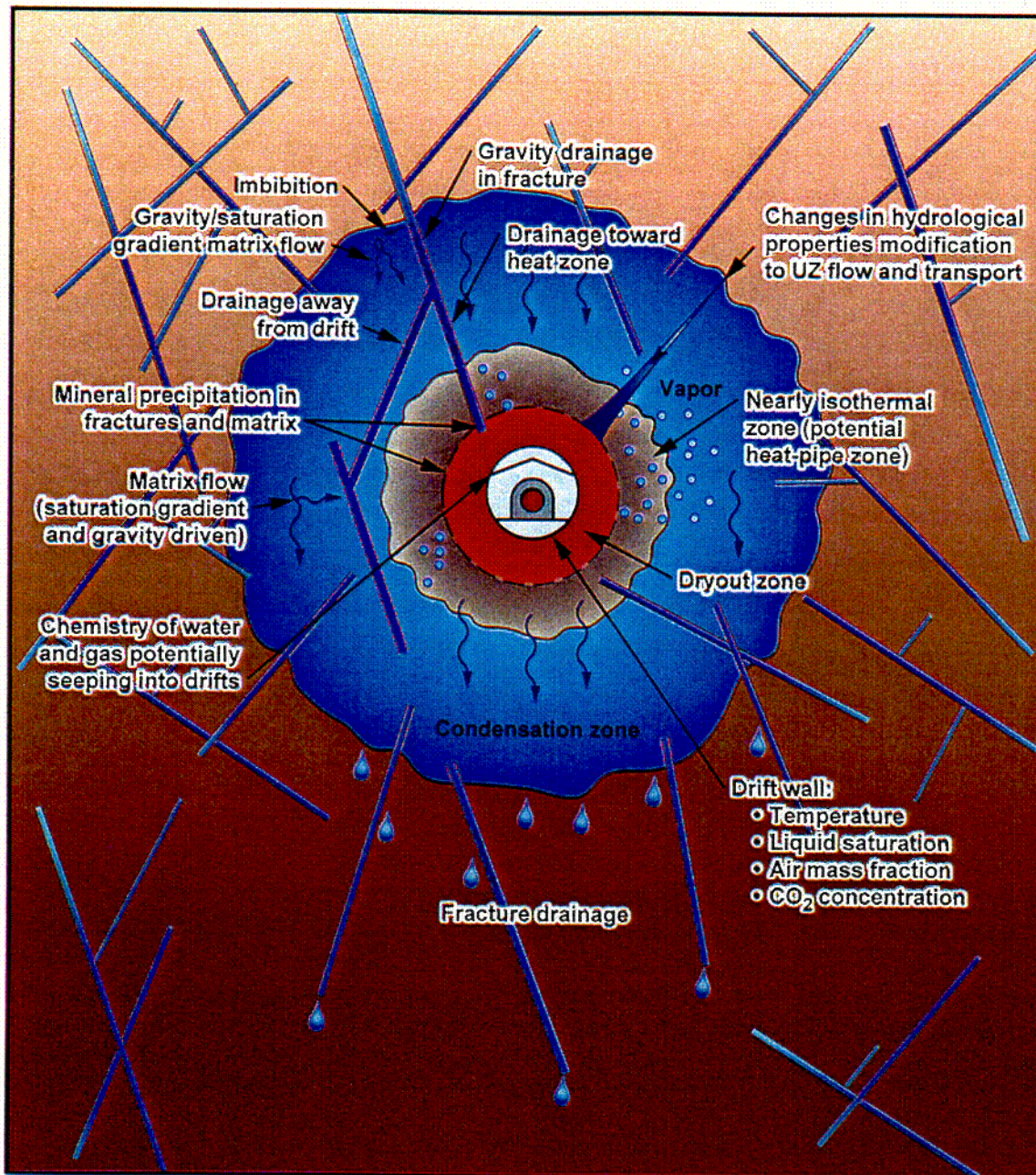
In addition to the unsaturated hydrological properties required to simulate THC processes in the UZ, the data necessary for evaluation of THC processes include the initial and boundary water

and gas chemistry, the initial mineralogy, mineral-volume fractions, reactive-surface areas, equilibrium thermodynamic data for minerals, aqueous and gaseous species, kinetic data for mineral-water reactions, and diffusion coefficients for aqueous and gaseous species. The following sections describe the conceptual model for TH, geochemical, and coupled THC processes in the fractured tuffs.

### 3.3.1.1 TH Processes

TH processes in the fractured, welded tuffs at Yucca Mountain have been examined theoretically and experimentally since the early 1980s (Pruess et al. 1984; Pruess et al. 1990, pp. 1235 to 1248; Buscheck and Nitao 1993; pp. 418 to 448, Pruess 1997; Tsang and Birkholzer 1999; pp. 385 to 425, Kneafsey and Pruess 1998, pp. 3349 to 3367). A conceptual model showing the important TH processes occurring around a drift, as derived through these studies and through observations of the Single Heater Test and the DST (CRWMS M&O 2000a), is shown in Figure 3-29. The design shown here includes backfill; however, this conceptual model is not dependent on the presence of backfill. To summarize the processes depicted in the figure, heat conduction from the drift wall into the rock matrix results in vaporization and boiling, with vapor migration out of matrix blocks into fractures. The vapor moves away from the drift through the permeable fracture network by bouyancy, by the increased vapor pressure caused by heating and boiling, and through local convection. In cooler regions, the vapor condensés on fracture walls, where it drains through the fracture network either down toward the heat source from above or away from the drift into the zone underlying the heat source. Slow imbibition of water from fractures into the matrix, particularly with some disequilibrium in matrix and fracture capillary pressures due to limited interaction area and to fracture coatings, gradually leads to increases in liquid saturation in the rock matrix. Under conditions of continuous heat loading, a dryout zone may develop closest to the heat source, separated from the condensation zone by a nearly isothermal zone maintained at about the boiling temperature. Where this nearly isothermal zone is characterized by a continuous process of boiling, vapor transport, condensation, and migration of water back to the heat source (either by capillary forces or gravity drainage), this zone may be termed a heat pipe (Pruess et al. 1990, pp. 1235-1248).

The design shown in Figures 2-1 and 2-2 includes backfill; however, this conceptual model is not dependent on the presence of backfill. A design change was made in January 2000 that removed backfill from the reference design. Qualitatively, this change does not affect the THC processes occurring in the rock around the drifts; however, the absence of backfill will result in a slightly different temperature distribution at the drift-wall and different times of maximum drift-wall temperature, maximum dryout and rewetting (compare Sections 3.2.3.1 and 3.2.3.2 for these changes). These different rates of heating may affect the time variation of water and gas chemistry around the drifts.



Other issues:

- Climate changes
- Mineral assemblage
- Water and gas initial compositions

Figure 3-29. Schematic Diagram of THC Processes Around a Potentially Heated Drift

### 3.3.1.2 Effects of TH Processes (Boiling, Condensation, and Drainage) on Water and Gas Chemistry and Mineral Evolution

The chemical evolution of waters, gases, and minerals is closely coupled to the TH processes discussed in the Section 3.3.1.1. The distribution of condensate in the fracture system determines where mineral dissolution and precipitation can occur in the fractures, and where there can be direct interaction (via diffusion) between matrix pore waters and fracture waters. Figure 3-30 shows schematically the relationships between TH and geochemical processes in the zones of boiling, condensation, and drainage in the rock mass outside of the drift and above the heat source.

One important aspect of the system is exsolution of CO<sub>2</sub> from the liquid phase as temperature increases. The exsolution and transport of CO<sub>2</sub> away from the boiling zone results in a local increase in pH and a decrease in pH in the condensation zone into which the vapor enriched in CO<sub>2</sub> is transported. This has been documented in data collected from the DST and discussed in the *THC Process AMR*. The extent to which the pH is shifted depends strongly on the rates of mineral-water reactions, which can buffer the change in pH. Because the diffusivities of gaseous species are several orders of magnitude greater than of aqueous species, and because the advective transport of gases can be more rapid than that of liquids, the region where CO<sub>2</sub> degassing affects water and gas chemistry could be much larger than the region affected by transport of aqueous species.

Effects of TH processes on water chemistry are varied and depend on the behavior of the dissolved species and its relation to mineral-water reactions. Conservative species (i.e., those that are unreactive and nonvolatile), such as chloride (Cl<sup>-</sup>), become concentrated in waters undergoing vaporization or boiling, but are absent from the vapor condensing in the fractures. Therefore, the concentration in the draining condensate waters is determined by mixing with fracture pore waters and interaction with matrix pore waters via diffusion. Concentrations of aqueous species, such as Ca<sup>+2</sup>, are also affected by calcite dissolution or precipitation as well as reactions involving Ca-bearing zeolites, clays, and plagioclase feldspar.

Zonation in the distribution of mineral species may occur as a result of varied temperature effects on mineral solubility. The inverse relation between temperature and calcite solubility (compared to the silica phases, which are much more soluble at higher temperatures) may cause zonation in the distribution of these phases in the condensation and boiling zones (Figure 3-30). Precipitation of amorphous silica or another silica phase is likely to be confined to a narrower zone where evaporative concentration from boiling exceeds its solubility. Hence, calcite may precipitate in fractures over a broader zone of elevated temperature and where CO<sub>2</sub> has degassed. Alteration of feldspars to clays and zeolites is likely to be most rapid in the boiling zone, because of their increased solubility (as well as dissolution and precipitation rates) at higher temperatures (Lasaga 1998, p. 66). In drainage zones, there may also be zonation in mineral alteration within the rock matrix adjacent to the fracture similar to that observed as a function of distance along the transport path (Steefel and Lichtner 1998, pp. 186-199). At Yucca Mountain, there is no evidence for such zonation from the thermal tests, but it is implied from model results presented in the *THC Process AMR* (CRWMS M&O 2000b). The importance of mineral zonation patterns is that the spatial distribution of mineral alteration will influence the hydrological property changes that may occur.

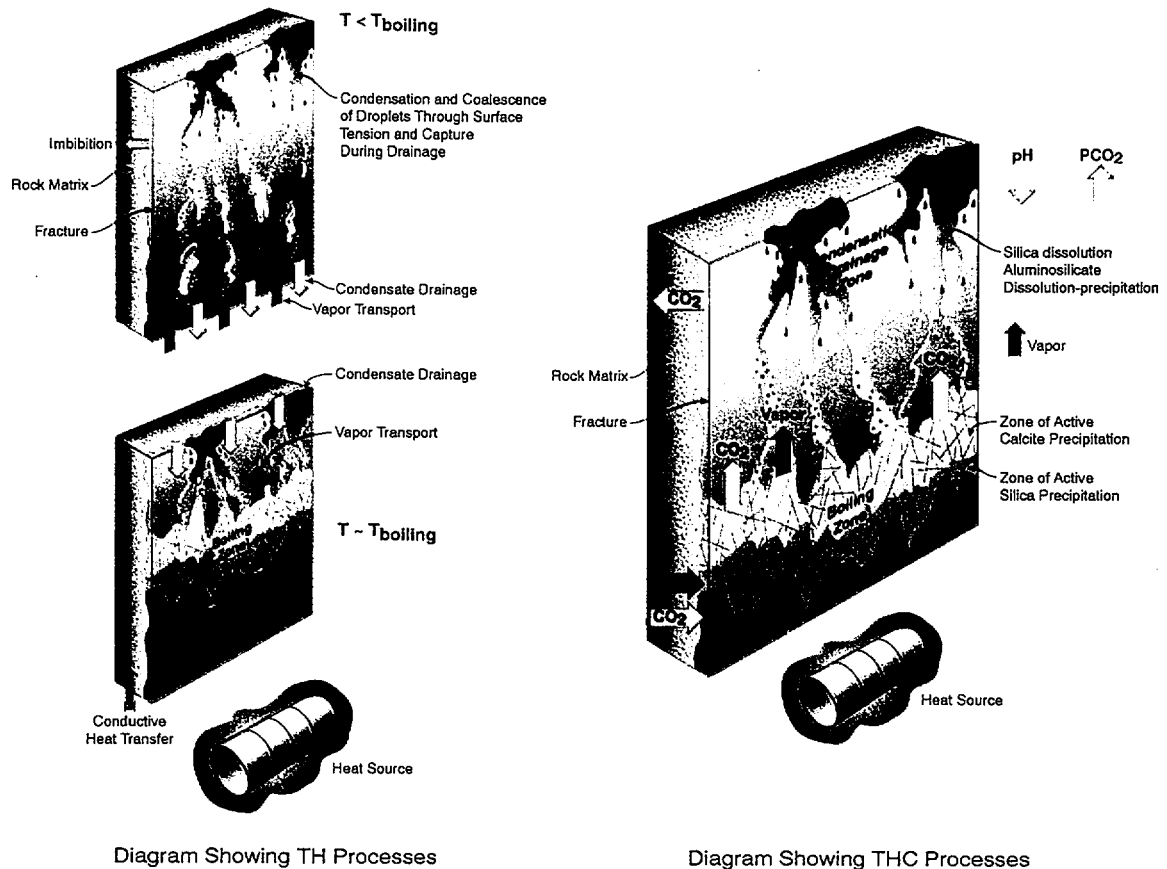


Figure 3-30. Schematic Diagram Showing Relation Between TH Processes and THC Processes

### 3.3.1.3 Effects of Infiltration and Climate Changes on THC Processes

Early in the thermal history of the potential repository, much of the chemistry of the unsaturated zone (UZ) around drifts will be constrained by the chemistry of ambient fracture and matrix pore water, which may change in concentration as a result of boiling, by dilution with condensate water, or by mineral-water-gas reactions. Once the peak thermal period has subsided, percolating water mixes with any condensate water above the repository and eventually rewets the dryout zone. The composition of the percolating waters (before mixing) will likely be dominated by flow in fractures, which would be of meteoric-water composition modified by reaction with fracture minerals. The degree of modification from meteoric composition depends on the velocity of flow, or more precisely the residence time of water in the fractures. While it has been assumed in this report that infiltrating water may be similar to that presently found at and above the repository as matrix pore water, no samples of percolating water have been obtained. The fraction of the percolation flux through the matrix is expected to be minor in comparison to the fraction through the fractures, and residence time in pores would allow interaction between rock and water to approach equilibrium. This would imply that the infiltrating water may be similar to that presently found above the potential repository as matrix pore water or more likely would reflect more dilute water. Implications are that analyses assuming pore-water composition should bound the precipitation of minerals, but may underestimate dissolution. Changes in percolation flux also affect the extent of mineral

deposition and dissolution, because of changes in the flux of dissolved species to the region around drifts. For example, the greater the flux of Ca, the more calcite would be precipitated, at a given concentration. Higher percolation fluxes could increase the dissolution rates of minerals that are undersaturated in the fluid, because it can increase the degree to which the mineral is undersaturated.

#### **3.3.1.4 Hydrologic Property Changes in Fractures and Matrix**

Mineral precipitation and dissolution in fractures and matrix have the potential for modifying the porosity, permeability, and unsaturated hydrologic properties of the system. Because the molar volumes of minerals created by hydrolysis reactions (i.e., anhydrous phases, such as feldspars, reacting with aqueous fluids to form hydrous minerals, such as zeolites or clays) are often larger than the molar volumes of the primary reactant minerals, dissolution-precipitation reactions can often lead to porosity reductions. The extent of mineral-water reactions is controlled by the surface areas of the mineral phases in contact with the aqueous fluid, and the distribution of minerals in the fractures is heterogeneous. Therefore, changes in porosity and permeability caused by these processes may also be heterogeneously distributed. Other factors that may lead to heterogeneity in property changes are the distribution of liquid saturation in fractures, the proportion of fractures having actively flowing water, and the rates of evaporative concentration due to boiling, which may change the dominant mechanisms of crystal growth and nucleation.

As summarized in the preceding section, the conceptual model for THC processes incorporates a wide range of coupled physical and chemical processes. The following section deals with implementation of this conceptual framework into a quantitative numerical model.

#### **3.3.2 Modeling Approach, Assumptions, Inputs and Outputs**

The flow of information between various models and data sources, the DST THC Model and THC Process Model is presented in Figure 3-31. The DST THC Model takes its inputs from the DST TH Model (grid and power output) (CRWMS M&O 2000a), the Calibrated Properties Model (CPM)(CRWMS M&O 2000n), and numerous sources of geochemical data as discussed in the *THC Process AMR* (CRWMS M&O 2000b). Geochemical data include mineral abundances and compositions, and water and gas chemistry. The THC Process Model obtains its inputs from the CPM, geochemical data, the repository design, and the UZ Flow Model (CRWMS M&O 2000q). One key input is the fracture porosity of 1 percent in the Tptptm unit (CRWMS M&O 2000f, Section 3.6.3.2). Repository Design provides the drift geometry and drift spacing, and the thermal and hydrological properties of EBS components (such as the drip shields, waste packages, and invert) (CRWMS M&O 2000g). The UZ Flow and Transport Model (CRWMS M&O 2000f) provides the hydrogeologic layer boundaries and pressure and temperature boundary conditions. Results of sensitivity studies on mineral assemblages and conceptual model validation in the DST are used to guide development and analysis of the THC Process Model. Although direct numerical output from the DST THC Model is not used in the THC Process Model, understanding gained from simulations of the DST and comparison to measured data allow for a more focused approach in the THC Process Model calculations and analysis. Output data from the THC Process Model are water chemistries in fractures at the drift crown, side, and base (which are linked to seepage volumes in the UZ F&T PMR). The fracture-water chemistries are abstracted for use in TSPA and discussed further in Section 3.4.

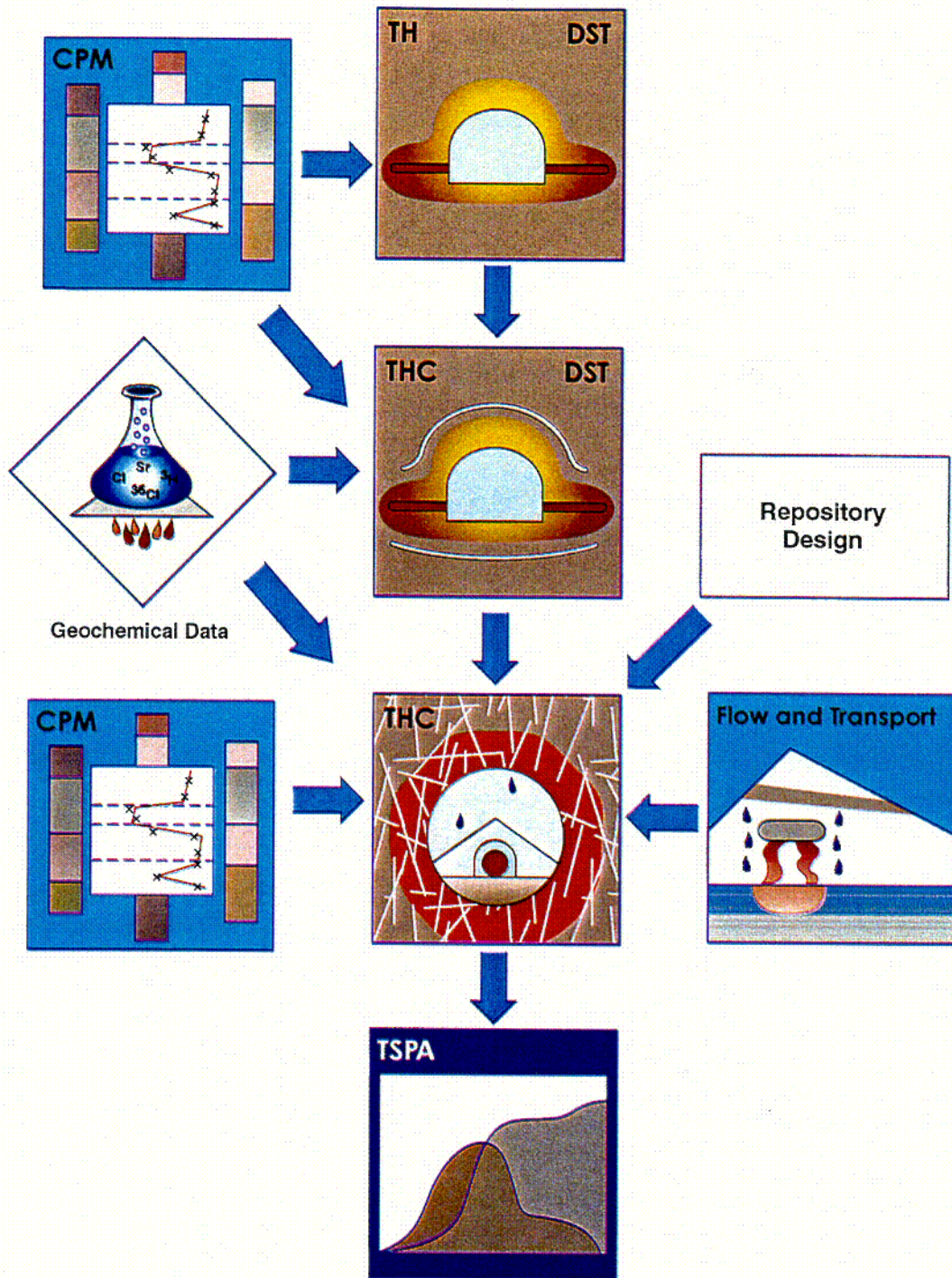


Figure 3-31. Model Diagram Relating Inputs and Outputs for the THC Process Model (labeled THC) and THC Drift Scale Test Model (labeled THC DST)

The following sections describe in more detail implementation of the conceptual model as a mathematical description of THC processes in the fractured tuffs. Data that form the basis of the DST THC and THC Process Model are also discussed.

### 3.3.2.1 Dual-Permeability Model for Reaction-Transport Processes

To treat separate yet interacting processes in fractures and matrix, the DKM (described in Section 2.2.1) was adopted for all aspects of the system (flow, transport, and reaction). Transport rates greater than the rate of chemical equilibration via diffusion necessarily lead to disequilibrium in water chemistry between fractures and matrix. This can lead to differences in dissolution and precipitation rates, and therefore the rate of change in porosity and permeability between the two media. Because the system is unsaturated and undergoes boiling, the transport of gaseous species is an important consideration. The model must also capture the differences between initial mineralogy in fractures and matrix and their evolution. In the dual-permeability method, each gridblock is separated into a matrix and fracture continuum, each of which is characterized by its own pressure, temperature, liquid saturation, water and gas chemistry, and mineralogy.

The fracture continuum is considered as separate from, but interacting with, the matrix continuum in terms of the flow of heat, water, and vapor through advection and conduction. Aqueous and gaseous species are transported via advection and molecular diffusion between fractures and matrix. It is assumed that the DK approach, with appropriate material and fracture properties and an appropriate discretization of time and space, is a sufficiently accurate approximation of the real world for the spatial scales of interest. The DK approach for modeling hydrologic processes in fractured porous media is also discussed in other sections of this PMR. This approach is validated by comparison of measured geochemical data to results of simulations presented in the *THC Process AMR* (CRWMS M&O 2000b), and is discussed in Section 3.6.4.2. The key observation that supports the DK approach is the strong disequilibrium between waters that have collected in hydrology boreholes in the DST and the matrix pore waters. The extent of the disequilibrium is captured by the model quite closely as judged by the pH and concentrations of other components.

### 3.3.2.2 Active Fracture Model for Reaction-Transport Processes

The AFM (Liu et al. 1998; CRWMS M&O 2000d, Section 6.4.5) has been used in many of the modeling studies described in this report. Because a major intent of the method is to modify the fracture-matrix area for the liquid phase as a function of liquid saturation, for consistency the AFM should also be used for calculation of the surface area of minerals on fracture walls in contact with the liquid phase. The reference saturation for the active-fracture concept is the residual liquid saturation, below which flow is considered to be absent. However, mineral-water reactions are expected to occur at all saturations above zero. Therefore, a modification of the AFM was implemented for mineral-water reactions, such that the reference saturation is taken as some arbitrarily small value ( $1 \times 10^{-4}$ ), consistent with that implemented for mineral-water reactions and transport near conditions of complete dryout. This value is an approximate cut-off at which evaporative concentration increases the ionic strength of the residual pore water to values outside the range of the validity of thermodynamic relationships for dilute systems.

### 3.3.2.3 Equilibrium and Kinetic Models for Mineral-Water-Gas Reactions

Mineral-water reactions are considered to take place under kinetic or equilibrium conditions. The methods used to express the kinetic and equilibrium reactions are described in the *THC*

*Process AMR* (CRWMS M&O 2000b) and are similar to those described in Reed (1982) and Steefel and Lasaga (1994). Because the dissolution rates of many mineral-water reactions are quite slow, most phases were treated using pseudo-first-order reaction kinetics (CRWMS M&O 2000b, Table 4). Data for kinetic mineral-water reactions were derived from published experimental data. This assumption is likely reasonable (considering the uncertainties in the reactive surface areas) for most reactive transport calculations, except during the final stages of boiling where nucleation kinetics may be more important. Gas species, such as CO<sub>2</sub>, were treated as ideal mixtures of gases in equilibrium with the aqueous solution. The validity of these methods to the problem are only known for particular cases; therefore, comparison of model results to data collected from thermal tests has been done.

### 3.3.2.4 Initial and Infiltrating Water and Gas Chemistry and Mineralogy

The initial water chemistry for the DST THC Model and the THC Process Model was an average of measurements made of pore waters from Alcove 5, near the DST (CRWMS M&O 2000b, Section 6.1.2). This alcove is in the TSw hydrogeologic unit and represents in situ water in the NFE location under ambient conditions. The chemistry of this average water composition is given in Table 3-8.

Table 3-8. TSw Pore Water Composition and CO<sub>2</sub> Partial Pressure

Parameter	Units	Concentration
pH (at 25°C)	pH Units	8.32
Na	mg/L	61.3
SiO <sub>2</sub> (aq)	mg/L	70.5
Ca	mg/L	101
K	mg/L	8.0
Mg	mg/L	17
Al	mg/L	9.92x10 <sup>-7</sup> (1)
Fe	mg/L	6.46x10 <sup>-8</sup> (2)
HCO <sub>3</sub> (3)	mg/L	200
Cl	mg/L	117
SO <sub>4</sub>	mg/L	116
F	mg/L	0.86
CO <sub>2</sub> (gas) (4)	Pa	85.2

Source: CRWMS M&O 2000b, Table 3

- NOTE: (1) Calculated by equilibration with Ca-smectite at 25°C.  
 (2) Calculated by equilibration with hematite at 25°C.  
 (3) Total aqueous carbonate as HCO<sub>3</sub><sup>-</sup>, calculated from charge balance.  
 (4) Calculated at equilibrium with the solution at 25°C.

The infiltrating water chemistry could be chosen from either the pore water chemistry in the UZ at or above the potential repository horizon or from a more dilute composition found in the perched water or saturated zone (e.g., J-13 water). The perched waters are much more dilute (e.g., lower Cl) than UZ pore waters (CRWMS M&O 2000r, Tables 6 and 8), and isotopic compositions (<sup>36</sup>Cl/Cl, <sup>18</sup>O/<sup>16</sup>O, D/H, <sup>14</sup>C) and Cl concentrations also suggest the presence of a large proportion of late Pleistocene to early Holocene water (Levy et al. 1997, p. 906; Sonnenthal

and Bodvarsson 1999, pp. 107 to 108; CRWMS M&O 2000r, Table 9). It was assumed that the infiltrating water and the water in the fractures have the same chemical composition as the matrix pore water. The water chemistry is uncertain as indicated in Section 2.4.2. The sample chosen was collected in the TSw hydrogeologic unit at Alcove 5 near the DST, and its chemistry is listed in Table 3-8. Analyses of PTn pore waters (and some at the top of the TSw) and many Cl analyses of TSw pore waters are consistent with this interpretation (Sonnenthal and Bodvarsson 1999, pp. 140 to 141; CRWMS 2000r, Table 6).

The minerals, aqueous and gaseous species, shown in Table 3-9 (denoted as *more complex* or *complex*), include the major phases found in fractures and the matrix in the TSw and others that are likely to occur under thermally perturbed conditions, based on their occurrence in deeper zeolitized units. Two sets of geochemical species were chosen, so the sensitivity to the mineral assemblage could be evaluated, and additional information could be obtained for PA abstractions. The other set of species (denoted as “*Less Complex Mineral Assemblage*”), represents a smaller set of species and minerals (calcite, gypsum, silica phases) that captures many basic aspects of the DST water and gas chemical evolution, such as the pH and gas-phase CO<sub>2</sub> concentrations, but neglects Al, Fe, K, Mg, and F-bearing aqueous species and minerals. Simulations of the DST and the THC Process Model considered both geochemical cases.

### **3.3.2.5 Relations for Mineral Reactive Surface Areas**

Reactive surface areas of minerals on fracture walls were calculated from the fracture-matrix interface area-volume ratio, the fracture porosity, and the derived mineral-volume fractions (CRWMS M&O 2000b, Section 6.1.5.1). The fracture-matrix interface areas and fracture porosities for each unit were taken from the DS calibrated properties set (CRWMS M&O 2000q, Section 6.2). These areas were based on the fracture densities, fracture porosities, and mean fracture diameter. The wall of the fracture is treated as a surface covered by mineral grains having the form of uniform hemispheres.

Mineral surface areas in the rock matrix were calculated using the geometric area of a cubic array of truncated spheres that make-up the framework of the rock (CRWMS M&O 2000b, Section 6.1.5.2). Clay minerals are considered as coatings of plate-like grains. The grains forming the framework of the rock matrix are considered to be the primary high-temperature phases of the tuff (i.e., quartz, cristobalite, tridymite, and feldspars). The abundance of secondary phases (i.e., those that formed as alteration products or low-temperature coatings on the primary assemblage), such as clay minerals, is used to reduce the free surface area of the framework grains.

### **3.3.2.6 Relations for Hydrological Property Changes**

Changes in porosity, permeability, and capillary pressure as a result of mineral precipitation and dissolution are treated in the *THC Process AMR* (Sections 6.1.6.2 – 6.1.6.3). Porosity changes in matrix and fractures are directly linked to the volume changes resulting from mineral precipitation and dissolution. Fracture permeability changes are approximated using the porosity change and an assumption of plane, parallel fractures of uniform aperture (Steeffel and Lasaga 1994, p. 556). This simplification of the fracture geometry is used because it is not possible to predict the actual form and distribution of mineral precipitates at a very small scale.

This is because of the complexities of the fracture geometry and the complex nature of mineral nucleation and growth under changing physical and chemical conditions. Thus, the permeability changes are approximate and apply to average conditions. However, these analyses reflect the trends, or overall magnitude of changes, that could be expected. Matrix permeability changes are calculated from changes in porosity, using ratios of permeabilities calculated from the Carmen-Kozeny relation (Bear 1988) and ignoring changes in grain size, tortuosity, and specific surface area. The Carmen-Kozeny equation has been used for many years to approximate the relation between permeability and porosity for packed spheres. In addition to changes in porosity, and changes in intrinsic saturated permeability as predicted by the Carmen-Kozeny relation, the retention characteristics of the fractures may also be altered. Jury et al. (1991, pp. 88-93) developed models for retention in soils as a series of capillary tubes. This model can be generalized to a series of parallel plates with varying size apertures. As rock deformations due to shear dilatancy occur, the fracture system will exhibit increased tendency to drainage or reduced tendency to retention that reduces fracture permeability.

Because of the exceedingly small initial matrix permeabilities of the welded Topopah Spring Tuff, simplification in the matrix relations is immaterial. If mineral precipitation caused very substantial changes in permeability, or the permeability of the fracture system was already very low, then it would be necessary to treat the relations between permeability changes and porosity changes more rigorously. If significant volumes of mineral precipitation were predicted, then back-coupling would need to be included in the analyses. Changing permeability and porosity also induces changes in the unsaturated flow properties of the rock. Therefore, the capillary pressure is modified using the Leverett scaling relation (Slider 1976, p. 280). Through Leverett scaling, the capillary pressure then shifts to higher values as the permeability decreases, thus leading to greater suction.

### **3.3.2.7 Basis for Numerical Code TOUGHREACT V2.2**

The geochemical module incorporated in TOUGHREACT V2.2 (STN: 10154-2.2-00) simultaneously solves a set of chemical mass-action, kinetic-rate expressions for mineral dissolution and precipitation, and mass-balance equations. Implementation of multiphase flow and heat transport for DK media is equivalent to TOUGH2 V1.4 (STN: 10007-1.4-01), which was used for other UZ flow calculations and TH calculations (CRWMS M&O 2000q) and for TH calculations of the DST (CRWMS M&O 2000a). TOUGHREACT V2.2 provides the extent of reaction and mass transfer between a set of given aqueous species, minerals, and gases at each gridblock of the flow model (Xu and Pruess 1998; Xu et al. 1998). Equations for heat, liquid and gas flow, aqueous and gaseous species transport, chemical reactions, and permeability and porosity changes are solved sequentially (Steefel and Lasaga 1994, p. 550). It is assumed that the physical properties of the gas phase are unaffected by changes in the partial pressure of CO<sub>2</sub> resulting from heating, calcite reactions, and gas-phase transport. This assumption is justified by the results of the DST THC Model and the THC Process Model runs, which show that the volume fraction of CO<sub>2</sub> is generally less than 5 percent and always less than 10 percent (CRWMS M&O 2000b).

Table 3-9. Model Mineral Assemblage, Aqueous and Gaseous Species

Species	Minerals
<b>Aqueous:</b>	
H <sub>2</sub> O	Calcite
H <sup>+</sup>	Tridymite
Na <sup>+</sup>	α-Cristobalite
K <sup>+</sup>	Quartz
Ca <sup>+2</sup>	Amorphous Silica
Mg <sup>+2</sup>	Hematite
SiO <sub>2</sub>	Fluorite
AlO <sub>2</sub> <sup>-</sup>	Gypsum
HFeO <sub>2</sub>	Goethite
HCO <sub>3</sub> <sup>-</sup>	Albite
Cl <sup>-</sup>	Microcline
SO <sub>4</sub> <sup>-2</sup>	Anorthite
F <sup>-</sup>	Ca-Smectite
	Mg-Smectite
<b>Gas:</b>	Na-Smectite
CO <sub>2</sub>	K-Smectite
	Illite
	Kaolinite
	Sepiolite
	Stellerite
	Heulandite
	Mordenite
	Clinoptilolite
	Volcanic Glass

Source: *Complex Geochemical System*;  
CRWMS M&O 2000b, Table 7

### 3.3.3 THC Process Model

The NFE may impact seepage if hydrologic properties change within the NFE. The assessment of TH effects on seepage is reported within the UZ F&T PMR (CRWMS M&O 2000f, Section 3.10.5) and the results are fed to the EBS PMR directly from the UZ F&T PMR and associated AMRs. The impacts on seepage are reported here in order to put the NFE results into context, and to identify the two-way coupling that exists between percolation flux and the NFE.

This section describes the THC Process Model and the results of predictions of water and gas chemistry that may seep into drifts over the next 100,000 yr. This model also considers any changes in the hydrological properties as a result of mineral precipitation and dissolution. The overall abstraction results as used by TSPA are summarized in Table 3-10.

### 3.3.3.1 THC Process-Model Description

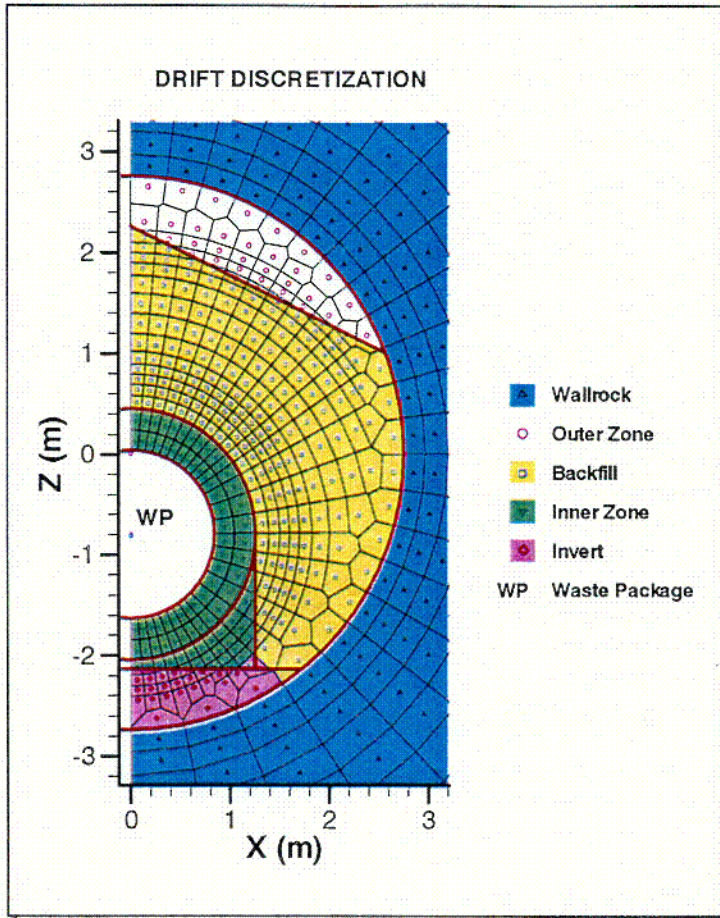
A THC Process Model incorporates elements of the EDA II (Wilkins and Heath 1999, Enclosure 2) to represent waste package heating over time, changes in heat load due to ventilation, the effective heat transfer within the drift, the addition of backfill after 50 yr, and THC processes (CRWMS M&O 2000b). This 2-D model incorporated the initial layering in hydrologic and thermal properties and mineralogy from the surface to the Calico Hills Formation zeolitic unit, along with different initial mineralogy and reactive surface areas in fractures and matrix (Figure 3-32). A number of cases were evaluated for different calibrated property sets, climate-change scenarios, and geochemical systems. The climate scenarios were constructed from average values of the present-day infiltration, monsoon and glacial-transition climates, along with the upper and lower bounds. These averages were calculated from about 30 TH chimney models in the potential repository footprint. Predictions were presented of the water and gas chemistry that may enter the drifts for a period of 100,000 yr, including a pre-closure period of 50 yr with 70 percent heat removal by ventilation.

### 3.3.3.2 TH Effects

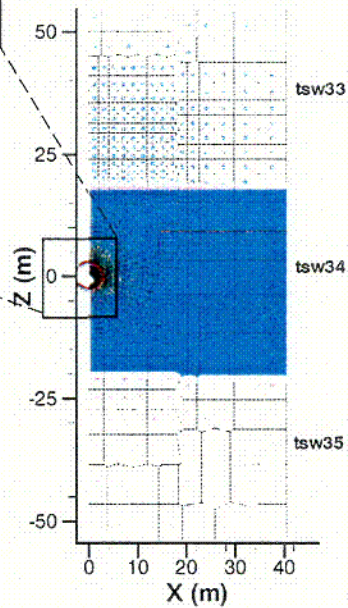
TH effects on liquid saturation and flow around drifts were investigated in the *THC Process AMR* (CRWMS M&O 2000b). The TH effects on liquid saturation and temperature around drifts are a function of the infiltration rate and initial liquid saturations calculated from steady-state simulations, using specific calibrated property sets (CWRMS M&O 2000n). Liquid saturations and temperature are shown around the drifts at 600 yr, which is approximately the time of maximum dryout extent for the three climate cases investigated (Figure 3-33). These climate cases considered three time periods (0-600, 600-2,000, and 2,000-100,000 yr) and different infiltration rates for each period (6/6/3, 6/16/25, and 15/26/47 mm/yr) for a lower, mean and upper bound, respectively (CRWMS M&O 2000b). The dryout zone is asymmetric around the drift as a result of the position of the waste package and backfill, and the effect of infiltration above the drift. The smaller dryout zone in the lowest infiltration case compared to the mean infiltration case is apparently the result of differing property sets rather than differences in the infiltration rate. Higher liquid saturations in the pillar region are a result of water diverting around the drift.

### 3.3.3.3 Gas-Phase CO<sub>2</sub> Evolution

The CO<sub>2</sub> evolution in the gas phase is a controlling factor for the pH and mineral-water reactions. Time profiles for gas-phase CO<sub>2</sub> concentrations at three locations around the drift are shown in Figure 3-34 for the *Less Complex* (calcite-silica-gypsum) geochemical system. Carbon dioxide concentrations in fractures drop significantly during dryout and increase again during rewetting. The increase in CO<sub>2</sub> concentrations in the gas phase during rewetting is likely a result of heating of these waters as they approach the drift wall, as suggested by the high-infiltration case showing the largest CO<sub>2</sub> concentration after rewetting (near 12,000 ppmV). Another component of this increased CO<sub>2</sub> concentration is the dissolution of calcite previously precipitated during heating and boiling of condensate and matrix pore water. The highest concentrations are similar to those observed during the DST, although rewetting has not taken place in the DST because it is still in the heating phase.



THC SEEPAGE MODEL MESH  
(top at +221m, bottom at -335m)

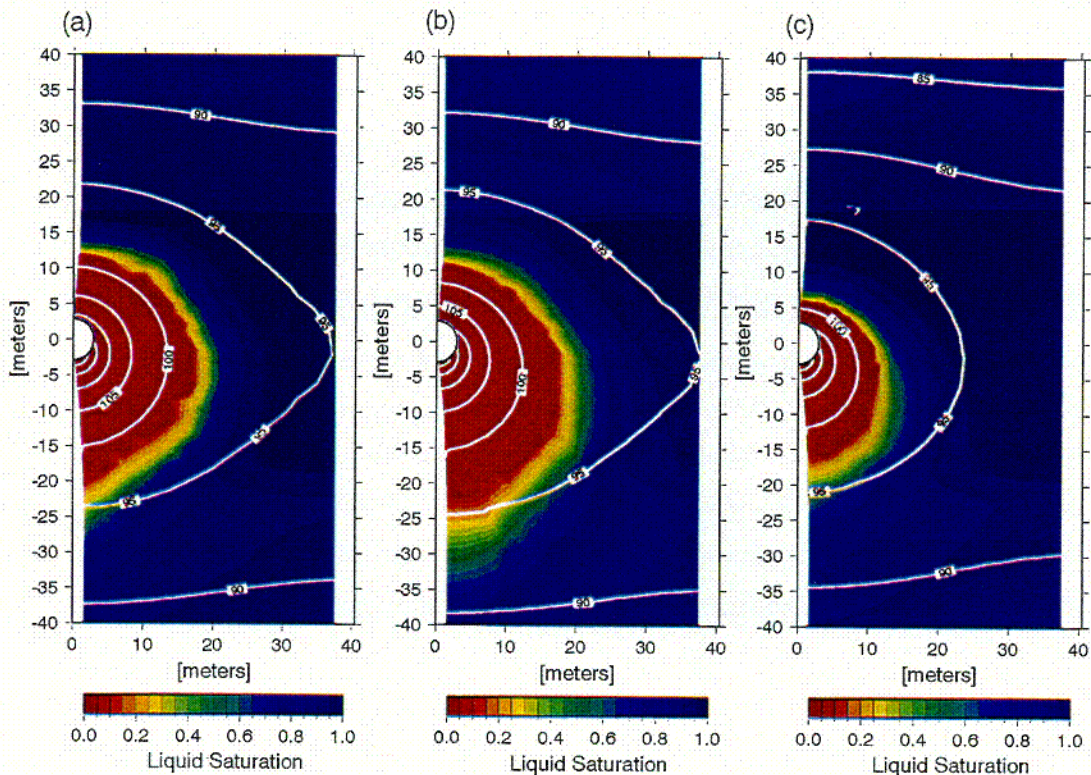


Source: Adapted from CRWMS M&O 2000b, Figures 18 and 19

NOTE: Topopah Spring Tuff Upper Lithophysal (tsw33), Middle Non-Lithophysal (tsw34), and Lower Lithophysal (tsw35) Units, and Blow-up Showing Discretization of In-Drift Design Components.

Figure 3-32. THC Process Model Mesh Showing Hydrogeologic Units in Proximity of the Drift

C-28



Source: CRWMS M&O 2000b, Figure 26

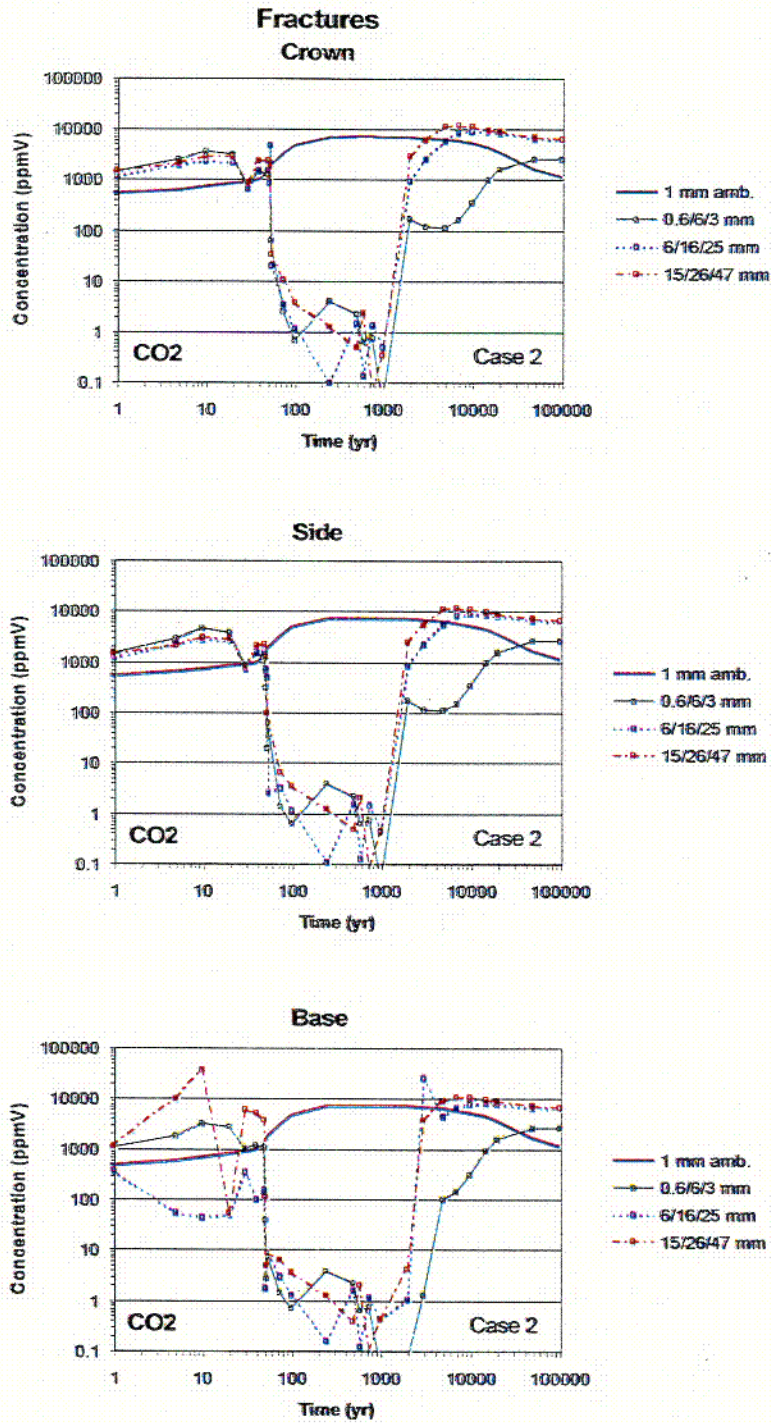
NOTE: (a) Low, (b) Mean, and (c) High (*less complex system*). Temperature ( $^{\circ}\text{C}$ ) line contours are overlaid on the saturation color contours.

Figure 3-33. Contour Plot of Modeled Liquid Saturations in the Matrix at 600 Yr (Near Maximum Dryout) for Three Climate-Change Scenarios

### 3.3.3.4 Water-Chemistry Evolution

Chloride is a useful indicator of the extent of boiling or dilution, and interaction of condensate waters in fractures that are low in Cl with matrix pore waters having much higher chloride concentrations. Chloride concentrations are plotted in Figure 3-35 as a function of time at three locations around the drift. The gap in concentrations between about 75 and 1,000 yr. reflects the dryout period when no aqueous phase is present at the drift wall. Upon rewetting, chloride concentrations drop relatively quickly below 400 mg/L toward ambient values near 110 mg/L. There is no evidence of water with high concentrations of chloride at liquid saturations above residual saturation during the reflux period (after about 1,000 yr). Therefore, waters that are most likely to seep into drifts will not be significantly more concentrated in chloride than the ambient pore water.

1-29

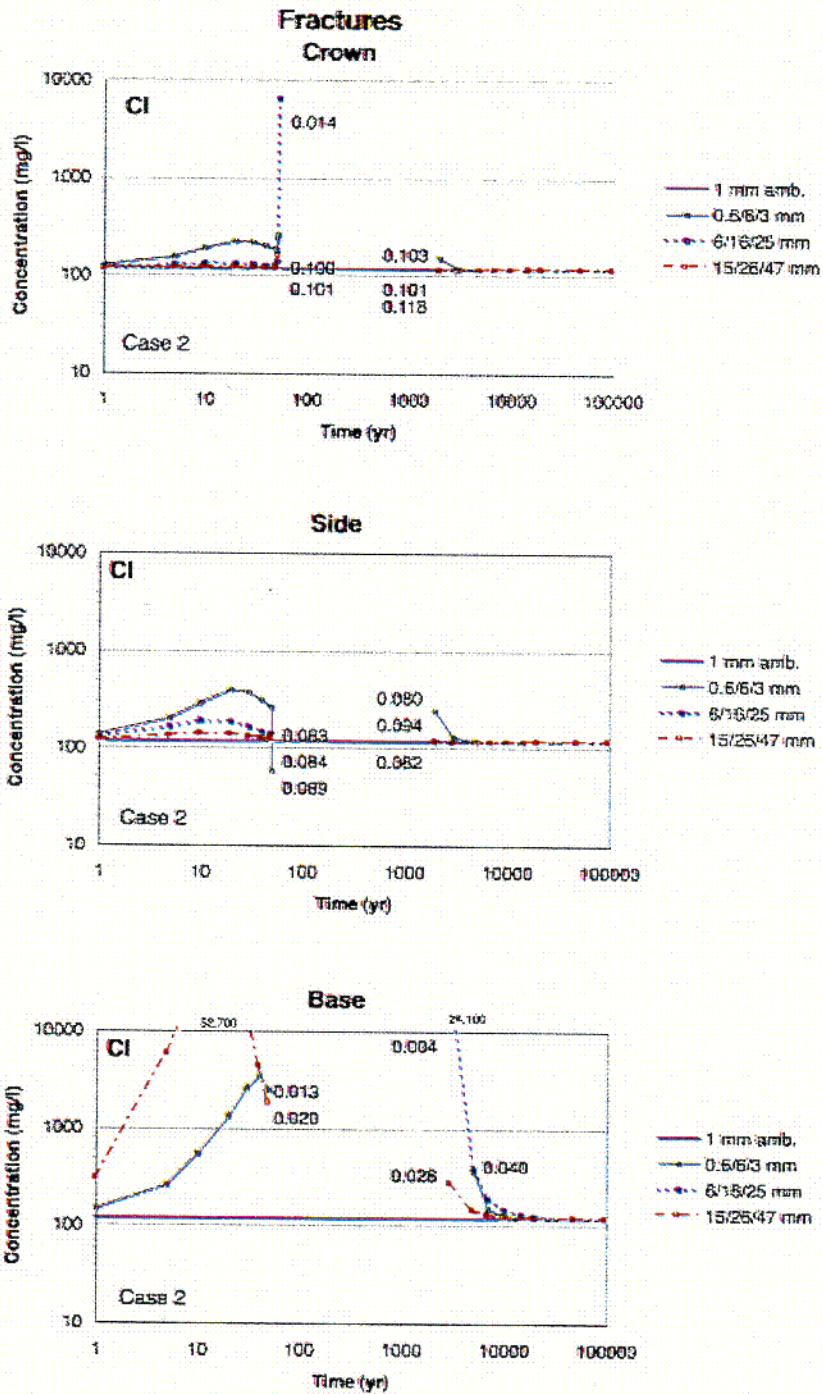


Source: CRWMS M&O 2000b, derived from Figure 29

NOTE: The "base" location water chemistry does not consider effluent from the drift.

Figure 3-34. Time Profiles of Modeled CO<sub>2</sub> Concentrations in the Gas Phase in Fractures at Three Drift Wall Locations for Different Climate-Change Scenarios (*Less Complex Calcite-Silica-Gypsum System*)

L-30



Source: CRWMS M&O 2000b, Figure 39

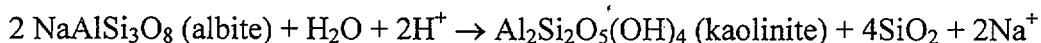
NOTE: Numbers inside plot refer to liquid saturation at point shown, either just prior to complete dryout or at time of rewetting. Numbers outside plot refer to concentrations that are off-scale.

Figure 3-35. Time Profiles of Modeled Total Aqueous Chloride Concentrations in Fracture Water at Three Drift-Wall Locations for Different Climate-Change Scenarios (*Complex Mineral Assemblage*)

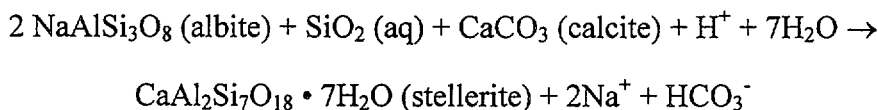
C31

Predicted pH and total aqueous carbonate concentrations (as  $\text{HCO}_3^-$ ) in fracture pore water are shown in Figures 3-36 and 3-37 for the calcite-silica-gypsum system. The calculated pH is generally higher for the *Complex* system results (approximate range 8.5 to 9.8; shown in the *THC Process AMR* [Figure 30]) than for the *Less Complex* system (approximate range 7 to 8.5). The composition of waters reaching the drift wall during rewetting were roughly neutral in pH (7.2 to 8.3) for the *Less Complex* system, and approximately 8.6 to 9.0 for the full geochemical system. Total aqueous carbonate concentrations are higher in the *Complex* system at the drift crown (maximum, after rewetting, near 10,000 mg/L for the low infiltration case) than in the calcite-silica-gypsum system (near ambient values of 200 mg/L after rewetting).

The pH-carbonate- $\text{CO}_2$  data show different trends when aluminosilicates in the mineral assemblage are considered. The aluminosilicate reactions are sensitive to competing effects of infiltration rate and gas-phase  $\text{CO}_2$  diffusion relative to calcite dissolution and precipitation, feldspar dissolution, and calcium-zeolite precipitation. The dissolution of feldspars to form zeolites and clays directly affects the pH. For example, the dissolution of albite (Na-feldspar) to form kaolinite (clay) results in an increase in pH, as follows:



Feldspar dissolution also indirectly causes an increase in pH when Ca-rich zeolites precipitate, depleting calcium from solution and destabilizing calcite, as in the following reaction:

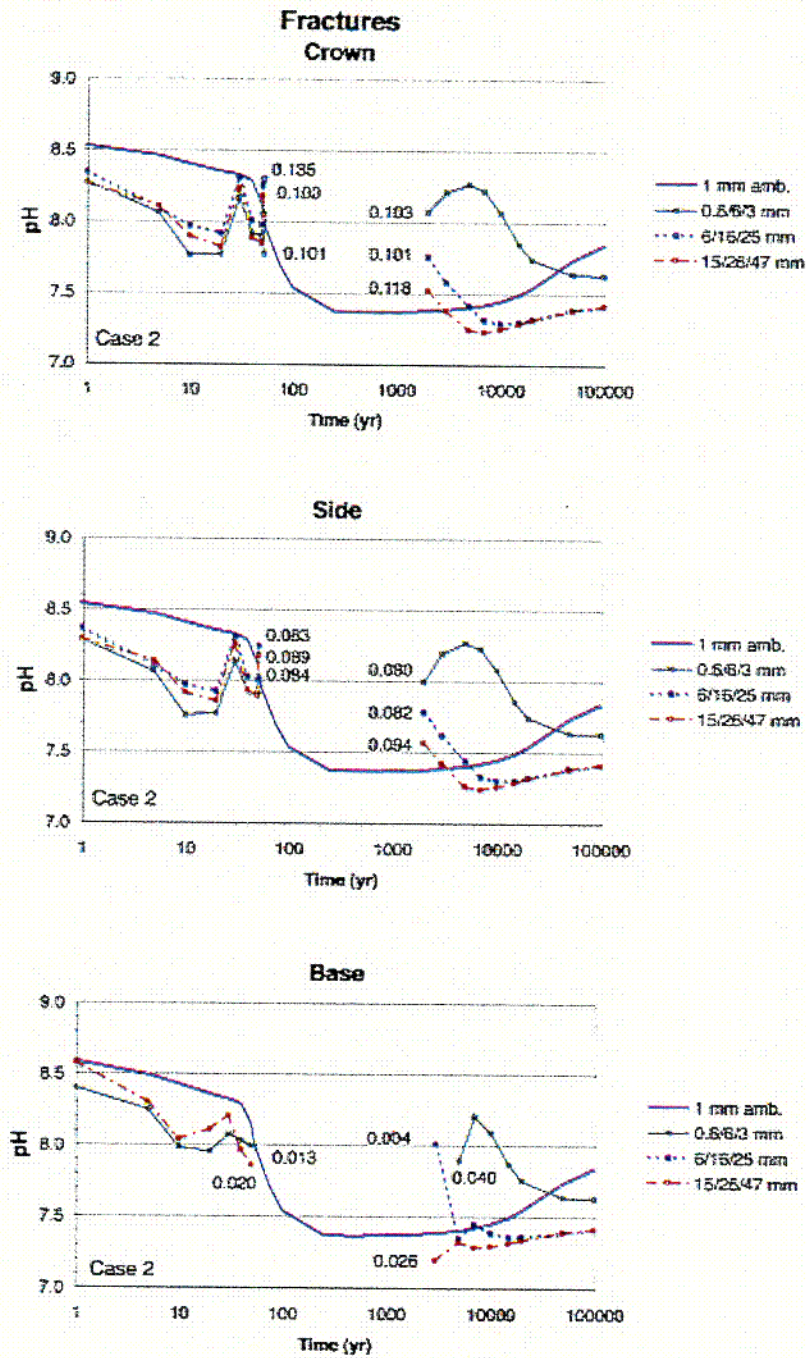


As a result, simulations that consider aluminosilicate reactions generally yield higher pH and total aqueous carbonate concentrations and generally lower  $\text{CO}_2$  partial pressures than simulations with the *Less Complex* calcite-silica-gypsum system. Simulations of the DST show that results from the *Less Complex* system matches the observed pH, bicarbonate, and calcium more closely than the *Complex* system. However, over longer and more stable periods of reflux and boiling, the system may trend toward the chemistry of the *Complex* system.

### 3.3.3.5 Porosity and Permeability Changes and Assessment of Precipitation “Cap” Formation

The calculated change in fracture porosity in the vicinity of the drift, at a simulation of 10,000 yr., is shown in Figure 3-38 for the three climate scenarios and the *Less Complex* system. The maximum porosity reduction (negative in the plots) occurs for the high-infiltration case and is predominantly above the drift, adjacent to the tsw33 and tsw34 hydrogeologic unit contact. In all cases, the porosity change is relatively small (less than ~1 percent of the initial porosity) and mostly to smaller values. The porosity decrease results primarily from calcite precipitation (as in the DST simulations). In the full geochemical system, the fracture porosity change is similarly small, but is dominated by zeolite reactions. Because the fracture porosity changes are small and permeability changes are negligible, TH processes were not determined by this analysis to be significantly affected by mineral precipitation or dissolution. The analysis assumed that the porosity changes are uniformly distributed along the fracture surfaces. The models cannot assess

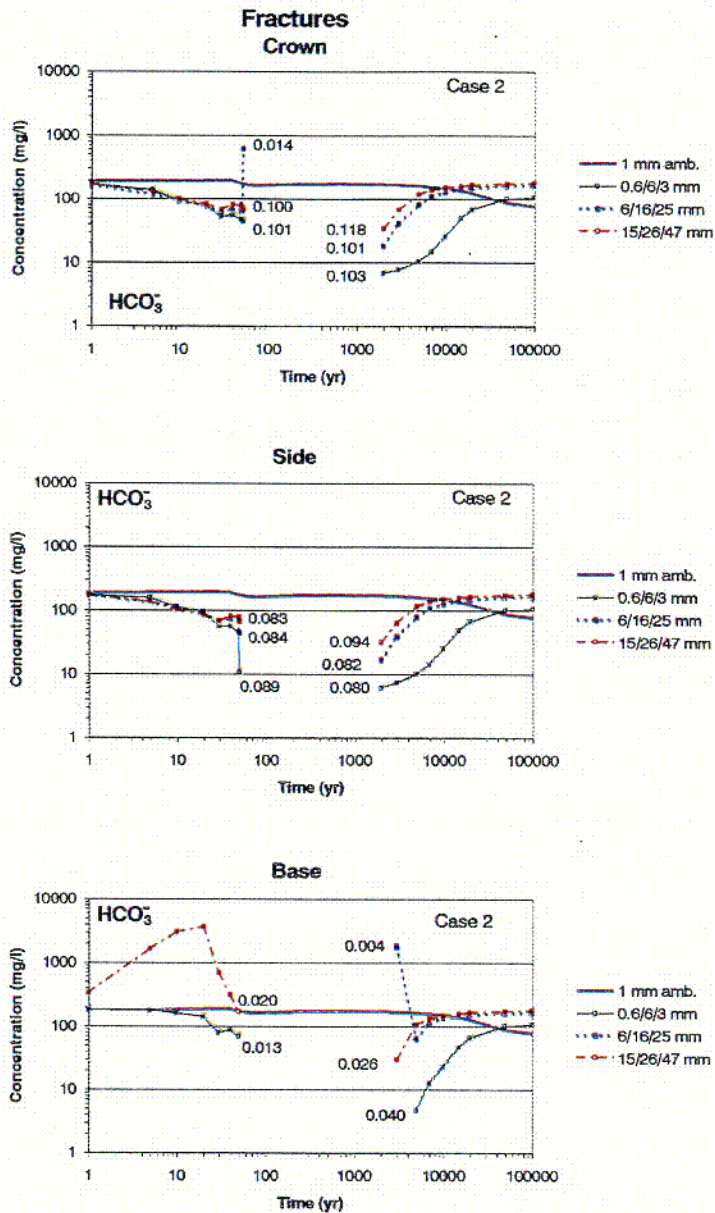
fine structure changes (e.g., those that reflect variation in asperities). If mineral deposition is localized in smaller openings, they may have greater impact on permeability; this possibility is still being evaluated.



Source: CRWMS M&O 2000b, Figure 31

NOTE: Numbers inside plot refer to liquid saturation at point shown, either just prior to complete dryout or at time of rewetting.

Figure 3-36. Time Profiles of the Modeled pH of Fracture Water at Drift-Wall Locations for Different Climate-Change Scenarios (*Less Complex System*)



Source: CRWMS M&O 2000b, Figure 33

NOTE: Numbers inside plot refer to liquid saturation at point shown, either just prior to complete dryout or at time of rewetting.

Figure 3-37. Time Profiles of Modeled Total Aqueous Carbonate Concentrations (as  $\text{HCO}_3^-$ ) in Fracture Water at Drift-Wall Locations for Different Climate-Change Scenarios (Less Complex System)

### 3.3.3.6 Zeolite and Water Table Impacts

An assessment was made of the potential impact on zeolite dehydration and water table chemical changes by considering the estimates of temperatures within those zones. However, THC coupled process model analyses were not performed to determine these potential impacts.

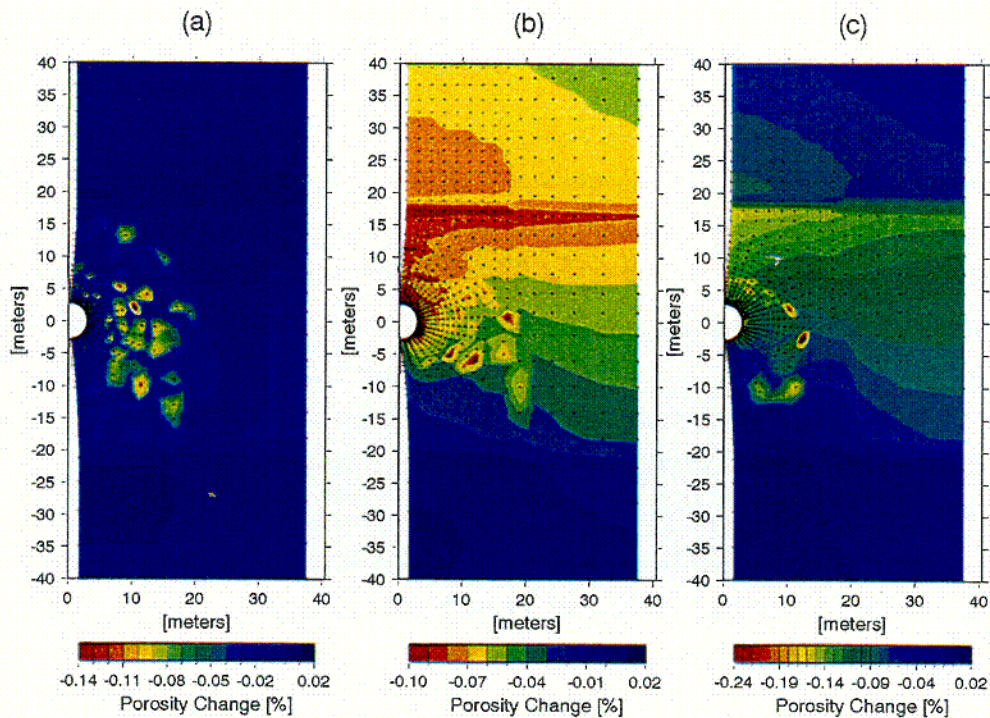
The UZ F&T PMR (CRWMS M&O 2000f) reports that for the EDA-II design, the models estimate a maximum temperature of 70-75°C at the top of the Calico Hills nonwelded unit (CHn), between 2,000 and 7,000 yr. This temperature range suggests minimal potential for temperature-induced mineralogical changes to occur within the zeolites of the nonwelded CHn hydrogeological unit (CRWMS M&O 2000f, pp. 280-281 and p. 287). Because the temperatures at the water table are of similar range, similar conclusions were drawn for the impact on rock units that include the saturated zone.

### 3.3.4 Uncertainties and Limitations

Many uncertainties exist in the thermodynamic and kinetic parameters used to describe mineral precipitation and dissolution. Limitations also arise under specific geochemical and/or physical conditions. For example, as the concentrations of dissolved solutes increase during boiling of pore water, the activity coefficients of the dissolved species may deviate significantly from one, and the ionic strength at which the models yield reasonable results is exceeded. Rapid boiling can also lead to mineral supersaturation outside the range of the pseudo-first-order kinetic models employed, which are generally reasonable under near-equilibrium conditions. Mineral precipitation may then be controlled by nucleation kinetics and other surface-energy-related phenomena. These uncertainties and limitations are generally difficult to quantify, because the models also introduce simplifications in the process of using these data, and the physical regimes under which the model breaks down may not be important for the overall dynamics of the system. Geochemical reactions are a strong function of temperature and the presence of water, which are better constrained than the rates of reaction and may control the spatial distribution, even if the exact quantities of the phases at a given time are uncertain.

Relations between permeability changes and porosity changes are also highly uncertain. These uncertainties are difficult to quantify, because they depend on the detailed geometry of the pore space and throats; however, some methods have succeeded in quantifying this effect in diagenetically altered rocks (Ehrlich et al. 1991). Although these methods were developed for porous media and not in fractures, there may be some similarities because of the aperture variations in fractures. However, quantification of the effect of porosity reductions in fractures on the fracture permeability may be more uncertain.

The model is also limited to the middle nonlithophysal unit of the Topopah Spring Tuff. Lithophysal units may exhibit different TH behavior that would change the interaction of fracture and matrix waters. Differences in the mineralogy of fractures and lithophysae could change the chemistry of the system somewhat, although the bulk-rock chemistry is very similar for all of the welded TSw units. The effective reactive surface area is more important than mineral abundances. More important than small differences in mineral abundances is the effective reactive surface area, which could be larger in lithophysal units because of the (a) greater abundance of vapor-phase minerals and (b) because of the interaction of waters flowing between fractures and lithophysae.



Source: CRWMS M&O 2000b, Figure 42

NOTE: (a) Low, (b) Mean, and (c) High. The red areas indicate the maximum decrease in porosity as a result of mineral precipitation.

Figure 3-38. Contour Plot of Calculated Total Fracture Porosity Change at 10,000 Yr for Three Climate-Change Scenarios (*Less Complex*)

These uncertainties do not, in general, limit the applicability of the models, because of the ability to calibrate effective reaction rates to fit the results of laboratory and in situ experiments (i.e., thermal tests). Some of the uncertainties inherent in the thermodynamic and kinetic data have been addressed by consideration of a simplified and a more complex mineral assemblage. Validation of the model by comparison to geochemical data from the DST provides the best degree of confidence building, and these comparisons have shown that the model is reasonable. Differences in the model results between the two geochemical systems, showing that the pH and CO<sub>2</sub> concentration in the gas phase for the simpler system compares more favorably to data from the DST shows the model provides important bounds on reaction rates. The good agreement in pH reflects the role of calcite dissolution in moderating pH, which would be much lower (4 to 5) given the elevated gas-phase CO<sub>2</sub> concentrations in the condensate regions. Results from the more complete system yield a higher pH than in the measured waters from the DST, which is due to a greater calculated reaction rate for feldspars. Therefore, porosity reductions as a result of feldspars altering to clays and zeolites likely take place at rates less than that given by the model, giving an important upper bound. Over the longer time period of the potential repository, the system may tend toward the behavior of the complex system, in comparison to the thermal tests, where time of the interaction of condensate waters with minerals is short-lived and only the minerals with the largest reaction rates affect the chemistry significantly.

134

### 3.3.5 Summary and Conclusions

The conceptual model for THC processes provides a comprehensive basis for modeling the pertinent mineral-water-gas reactions in the host rock, under thermal-loading conditions, as they influence the water and gas chemistry that may enter drifts over 100,000 yr. Data are incorporated from the DS calibrated property sets, the UZ Flow and Transport Model, geochemical data (fracture and matrix mineralogy, aqueous geochemistry, and gas chemistry), thermodynamic data (minerals, gases, and aqueous species), data for mineral-water reaction kinetics, and transport data. Simulations of THC processes included coupling between heat, water, and vapor flow, aqueous and gaseous species transport, kinetic and equilibrium mineral-water reactions, and feedback of mineral precipitation and dissolution on porosity, permeability, and capillary pressure (hydrologic properties) for a DK (fracture-matrix) system. The effect of these coupled THC processes on the time evolution of flow fields in the UZ around drifts has been investigated for different climate-change scenarios, calibrated property sets, and initial mineralogy. Validation of the model was done by comparison of measured gas and water chemistry from the DST to the results of simulations using the DST THC Model. In particular, simulation results were compared to measured gas-phase CO<sub>2</sub> concentrations and the chemistry of waters collected from hydrology boreholes during the test.

Comparisons of water chemistry (pH) and CO<sub>2</sub> concentrations in the gas phase from the DST indicate that a *Less Complex* set of aqueous species and minerals (calcite, silica phases, gypsum), but including gaseous CO<sub>2</sub>, can describe the general evolution of DST water quite closely. Including a wide range of aluminosilicates, such as feldspars, clays and zeolites yields information on additional species (i.e., Al, Fe, F), but their inclusion causes shifts in the water and gas chemistry that are more rapid than observed. These effects may be more important over longer time periods, leading to similar but less rapid changes (i.e., a slightly closer approach to equilibrium). However, over the time scale of the DST, the effective reaction rates and/or thermodynamic properties of these phases will clearly require some refinement. Section 3.6.4.2 summarizes the use of field and laboratory data to validate THC models.

The THC Process Model incorporates elements of the EDA II design to represent waste package heating over time, changes in heat load due to ventilation, effective heat transfer within the drift, addition of backfill after 50 yr, and THC processes in the unsaturated zone. A number of cases were evaluated for different calibrated property sets, climate-change scenarios, and geochemical systems. The THC Seepage simulations indicate that there may be an increase in the CO<sub>2</sub> gas and aqueous carbonate concentrations around the drift during rewetting. The extent of the dryout zone and the time of rewetting were different for each climate history and calibrated property set, although the general character was unchanged. As in the DST THC simulations, notable differences in the pH and CO<sub>2</sub> concentrations appeared in the two geochemical systems. The composition of waters reaching the drift wall during rewetting were roughly neutral in pH (7-8.5) for the *Less Complex* geochemical system (without aluminosilicates) and approximately 8.6-9.0 for the *Complex* geochemical system. The predicted pH and HCO<sub>3</sub><sup>-</sup> concentrations in the *Less Complex* geochemical system simulations are supported by data from the DST. However, the long-term evolution could trend in the direction of the *Complex* system chemistry, if the slow reaction rates of the aluminosilicates limit the changes in water chemistry that can be observed over the short heating time of the DST. Because the models are based on no-flow boundaries on the drift walls, no exchange of gas between the in-drift environment and the rock around the drift

is considered within these analyses. The impact of this back-coupling to the THC models cannot be assessed, because the in-drift gas composition would be affected by ventilation, gas transport along drifts, and reactions with engineered materials within the drift.

Even with the apparently overestimated reaction rates for the full mineral assemblage, the changes in porosity and permeability around drifts over 100,000 years were small (less than 1 percent of the total fracture porosity), and, therefore, effects on flow and transport are considered negligible. Estimates of potential for plugging of fractures are very sensitive to the fracture porosity that is assumed. Estimates of potential plugging as reported in the 1998 time frame (Hardin 1998) were based on fracture porosities in the tsw33, 34, and 35 layers of  $1.05 \times 10^{-4}$ ,  $1.24 \times 10^{-4}$ , and  $3.29 \times 10^{-4}$  respectively, as shown on Table 3-10. The current estimates of potential plugging, which indicate plugging will be insignificant, are based on revised estimates of fracture porosities from gas tracer tests. The current estimates are approximately 100 times greater than earlier estimates, as is shown on Table 3-10. Estimates of plugging have been consistent, when the porosity is considered, as discussed in Section 3.2.3.4 and Figure 3-100 in Section 3.6.2.2. Further, it should be noted that application of property values from the Tptmn to the entire repository footprint (as recommended in Section 5.4) introduces uncertainty that cannot be qualified without testing in the Tptll.

Table 3-10. Comparison of Fracture Porosities Used in Analyses of Potential Fracture Plugging

UZ Model Layer	1998 Reported Fracture Porosity (Hardin, 1998) from RIB (MO9901RIB00044.000)	Current estimates of Fracture Porosity (DTN: #LB997141233129.001)
tsw 33	$1.05 \times 10^{-4}$	$6.6 \times 10^{-3}$
tsw 34	$1.24 \times 10^{-4}$	$1 \times 10^{-2}$
tsw 35	$3.29 \times 10^{-4}$	$1.1 \times 10^{-2}$

The results of this section were abstracted for use in TSPA-SR, as discussed in Section 3.4. The thermal tests that are much of the basis of the NFE THC model are discussed in more detail in Section 3.6.1. Pertinent natural analogs are discussed in Section 3.6.2.2. Finally, the status of validation of the THC model is addressed in Section 3.6.4.2.

### 3.4 THC MODEL ABSTRACTION

The *THC Abstraction AMR* (CRWMS M&O 2000c) describes a THC abstraction, for the TSPA model, of the NF host rock water chemistry and gas-phase composition. It also provides an abstracted process-model analysis of potentially important differences in the thermal hydrologic (TH) variables used to describe the performance of a geologic repository obtained from models that include fully coupled reactive transport with thermal hydrology and those that include thermal hydrology alone. Specifically, the motivation of the process-level model comparison between fully coupled thermal-hydrologic-chemical (THC) and thermal-hydrologic-only (TH-only) is to provide the necessary justification as to why the in-drift thermodynamic environment and the NF host rock percolation flux, the essential TH variables used to describe the performance of a geologic repository, can be obtained using a TH-only model and applied directly into a TSPA abstraction without recourse to a fully coupled reactive-transport model. Section 3.2.3.4 further addresses this issue.

### 3.4.1 Inputs to the Abstraction

Abstraction, as used in the context of the analysis described in the *THC Abstraction AMR* (CRWMS M&O 2000c), refers to an extraction of essential data or information from the process-level model. The abstraction analysis reproduces and bounds the results of the underlying detailed process-level model.

The DS THC process model developed in the *THC Process AMR* (CRWMS M&O 2000b) and discussed in Section 3.3 serves as the primary input used in the THC abstraction analysis. The THC model results are used to define the major (i.e., order-of-magnitude) changes to water and gas compositions resulting from thermally-driven coupled reactive transport in the geosphere. Specifically, the process model provides the basis for an abstraction of a time evolution of the aqueous water chemistry and gas-phase composition as obtained from an analysis that includes both a *Complex* mineral assemblage as well as a *Less Complex* mineral assemblage. In addition to including the minerals and species from the *Less Complex* mineral assemblage, the *Complex* set also includes a wide range of alumino-silicates, such as feldspars, clays, and zeolites. The *Less Complex* mineral set includes only calcite, silica phases, and gypsum. The *Less Complex* mineral assemblage applied in the THC process model is used to describe the general evolution of the DST. Since the *Less Complex* mineral assemblage represents the measured results of the DST more accurately than the complex set of minerals; it provides the data input for abstraction of primary chemical species in the host-rock fracture water. The *Complex* mineral assemblage is used solely to abstract time-evolution data for the trace constituents that are not included in the *Less Complex* THC simulations. Although representing a more comprehensive set of components, the complex mineral assemblage results have additional uncertainty, because of: (1) larger uncertainty in the kinetic behavior of the additional phases, and (2) lack of additional mineralogic species that could affect some of the changes to major elements related to the carbonate subsystem (CRWMS M&O 2000b). The time-dependent abstraction THC data are used in the in-drift geochemical models developed for total system performance assessments (TSPA).

One purpose of the THC modeling is to determine whether the values of the parameters in the *Less Complex* set change significantly when the additional cations and anions are included in the calculation. Another objective is to determine whether the chemical reactions have a significant effect on the hydrological parameters of the NF rock, such that seepage into the emplacement drifts could be affected. This section of the PMR summarizes how the THC results (described in Section 3.3) are abstracted for use in the TSPA models.

The THC models are implemented in the TOUGHREACT software package, which is one of the TOUGH family of heat and mass-transfer codes. As described in the UZ F&T PMR (CRWMS M&O 2000f, Section 1.3.2), the TOUGH family of codes is also used to calculate the hydrological property distribution in the mountain (using inverse modeling), the percolation flux distribution, and seepage into emplacement drifts.

### 3.4.2 Abstraction of THC Results

The results of the abstraction of water and gas composition for TSPA are given in Table 3-11. They provide boundary condition inputs for other in-drift geochemical models used by the TSPA

model. The results in Table 3-11 shown below are abstracted from the process THC model described in Section 3.3. Consequently, they are constrained by the process-model assumptions and inputs. If, for example, the initial pore water composition used as input to the DS THC model, is only representative of the Topopah Spring Tuff middle nonlithophysal geologic unit (Tptpmn) and not the other host units, the abstraction may not be fully representative at repository locations other than the Tptpmn (initial pore waters used in the model are based on samples taken from the DST alcove, which is excavated in the Tptpmn). Under equilibrium conditions, the pore waters would reflect the interaction with the local mineral assemblage at that temperature and gas composition, which would create distinct waters within each rock unit. However, the mineral assemblages and their abundance within the potential repository units differ insignificantly and temperatures vary only minimally. This should not be construed to suggest that the pore water chemistry in the other units is fundamentally different than that of the Tptpmn, this was merely given as an example of the need to be aware of underlying assumptions or input when evaluating results of abstraction models. If the water chemistry is in equilibrium with the rock, given that the basic mineralogy is similar, then the water chemistry should be similar in all of the units. However, it cannot be ruled out that the chemistry might differ, the chemistry is not in total equilibrium. The point, as noted above, is that input uncertainties need to be recognized when considering the results of the abstractions. In this same vein, the abstraction results are valid only for the infiltration flux cases with climate change considered in the THC model (infiltration flux cases for low, mean, and high).

#### 3.4.2.1 Mean Infiltration Flux Case

The THC abstraction of the mean infiltration flux (with climate change at 600 and 2,000 yr.) case is given in Table 3-11 (CRWMS M&O 2000c, Section 6.1.1).

Table 3-11 represents the abstraction of water and gas compositions for the THC boundary conditions adjacent to the drift wall. Each of the time periods has a defined composition of gas and water that represents those constituents that can enter into the drift during those times, based on the process-level THC models for the thermally perturbed geosphere. Four periods, preclosure, boiling, transitional cool-down, and extended cool-down are defined for use in TSPA-SR calculations. This provides roughly constant chemical conditions for the purposes of calculating in-drift processes for those representative time periods. The abstraction method reduces the coupling between the NFE and EBS models, allowing a larger degree of parallel work in developing the TSPA for the Site Recommendation.

Note the abstracted temperatures listed in Table 3-11 are provided for reference only. Only the temperature in Boiling Period 2 will be used to calculate reequilibration of condensate with the CO<sub>2</sub> gas composition.

The abstraction includes both the *Complex* and *Less Complex* geochemical systems considered in the THC process model described in Section 3.3.2.4. For the constituents included in both chemical systems, (common constituents), major differences (factor of 10 or one log unit or more) are limited to Ca<sup>2+</sup>, Na<sup>+</sup>, and HCO<sub>3</sub><sup>-</sup>. The other constituents contained in both geochemical systems, while not the same, are also not different by more than an order-of-magnitude. The primary goal of the TSPA abstraction is to capture order-of-magnitude changes in species concentrations. Therefore, the smaller differences between common constituents

would not be represented in the abstraction. In order to maintain consistency with the geochemical system that is most representative of the DST results, the constituents from the *Less Complex* system were chosen for abstraction. In the case of aqueous calcium, sodium, and carbonate, the primary differences result from the additional uncertainties associated with the kinetic representation of the *Complex* geochemical system (CRWMS M&O 2000c, Section 6.1.1). As in the case of the other common constituents, the abstraction for these three components also stems from the *Less Complex* system.

The THC water chemistry and gas-phase composition abstraction represents the fracture waters impinging at the crown and sides of the potential emplacement drifts. The abstraction uses the detailed time-history results of the process-level THC model and discretizes them into four distinct geochemical periods for which compositional boundary conditions are provided for the potential in-drift geochemical environment for TSPA models. The abstraction compositional boundary conditions include constituents represented by five cations, six anions, and pH. In addition, this abstraction includes the partial pressure of carbon dioxide in the gas phase, in fractures adjacent to the potential drifts (and, during the abstraction boiling period, the equilibration temperature used for that gas with the condensate water composition). These boundary conditions to the potential drifts allow incorporation of time-varying, thermally perturbed water and gas compositions in the assessment of chemical interactions of the in-drift environment.

Use of the abstracted THC process model results for the *Less Complex* mineralogy is based on the fact that it reproduces more accurately (than the *Complex* mineral set) the observed changes to water and gas compositions in the DST (see Section 3.3.3 of this report, and CRWMS M&O 2000b, Sections 6.1.7 and 6.2.7). This corresponds to using the mineralogic phase constraints represented in the *Less Complex* system to set the major-element composition of the water and gas.

The first abstraction period defined goes from 0 to 50 year and represents the entire preclosure period. This is followed by the defined boiling period 2, during which the fractures are calculated to have zero saturation. The water that may enter the drift through these fractures would be that moving rapidly down from the condensate zone. This boiling period is followed by a transitional cooldown period from 1,000 to 2,000 years during which temperature is still high, but below boiling. Finally an extended cool-down period 4 is defined from 2,000 to 100,000 years, over which temperatures return to ambient and water compositions change gradually.

Table 3-11. THC Abstraction for the Mean Infiltration Rate Case with Climate Change

	Preclosure	Boiling	Transitional Cool-Down	Extended Cool-Down
	Period 1	Period 2	Period 3	Period 4
Parameter	Abstracted Values	Abstracted Values	Abstracted Values	Abstracted Values
Time	0 - 50 yr.	50 - 1000 yr.	1000 - 2000 yr.	2000 - 100,000 yr.
<b>Constituents Considered in Less Complex Chemical System (calcite-silica-gypsum)</b>				
Temperature, °C	80	96	90	50
log CO <sub>2</sub> , vfrac	-2.8	-6.5	-3.0	-2.0

Table 3-11. THC Abstraction for the Mean Infiltration Rate Case with Climate Change (Continued)

	Preclosure	Boiling	Transitional Cool-Down	Extended Cool-Down
	Period 1	Period 2	Period 3	Period 4
<b>Constituents Considered in Less Complex Chemical System (calcite-silica-gypsum) (Continued)</b>				
pH	8.2	8.1	7.8	7.3
Ca <sup>2+</sup> , molal	1.7E-03	6.4E-04	1.0E-03	1.8E-03
Na <sup>+</sup> , molal	3.0E-03	1.4E-03	2.6E-03	2.6E-03
SiO <sub>2</sub> , molal	1.5E-03	1.5E-03	2.1E-03	1.2E-03
Cl <sup>-</sup> , molal	3.7E-03	1.8E-03	3.2E-03	3.3E-03
HCO <sub>3</sub> <sup>-</sup> , molal	1.3E-03	1.9E-04	3.0E-04	2.1E-03
SO <sub>4</sub> <sup>2-</sup> , molal	1.3E-03	6.6E-04	1.2E-03	1.2E-03
<b>Additional Constituents Considered in the Complex (Full) Chemical System</b>				
Mg <sup>2+</sup> , molal	4.0E-06	3.2E-07	1.6E-06	7.8E-06
K <sup>+</sup> , molal	5.5E-05	8.5E-05	3.1E-04	1.0E-04
AlO <sub>2</sub> <sup>-</sup> , molal	1.0E-10	2.7E-07	6.8E-08	2.0E-09
HFeO <sub>2</sub> <sup>-</sup> , molal	1.1E-10	7.9E-10	4.1E-10	2.4E-11
F <sup>-</sup> , molal	5.0E-05	2.5E-05	4.5E-05	4.5E-05

Source: CRWMS M&O 2000c, Table 3

During the second abstraction period, the boiling period, fracture saturation around the drifts is calculated to be zero in the THC process model results. The chemical composition of the condensate water calculated to be in the zone of highest saturation above the fracture dryout is used to represent the water that may flow rapidly through fractures during the boiling period. The composition of such water is given in Table 3-11 with the value of the partial pressure of CO<sub>2</sub> in the gas surrounding the drift wall during that dryout time. The flux of such water would be at a minimum during this period, so the CO<sub>2</sub> concentration at the drift wall can be used to represent the concentration at equilibrium with this water. This value is given in Table 3-11. Gas composition and associated boiling temperature should be used to equilibrate with the abstracted condensate water composition shown for this period in Table 3-11. This represents the abstracted water may flow rapidly down fractures into the dryout zone from the overlying condensate zone.

The following should be noted for the abstraction shown in Table 3-11:

- The first 50 years represents the repository preclosure period with 70 percent heat removal via ventilation. However, because the Performance Assessment only starts at closure, these values are not used and are only provided for completeness of the time span. It is emphasized that the values probably would not be representative of preclosure conditions, because the potential chemical effects of ventilation are not included in the process model.
- The values for abstraction period 3 correspond to the process-level model results at 2,000 years after initial waste emplacement. This is because, as soon as the drift-wall rock resaturates, the CO<sub>2</sub> very rapidly approaches about 1x10<sup>-3</sup> bars and the pH and water composition are taken consistently with this gas chemistry. A rapid transition

occurs in the water and gas compositions from 1,000 to 2,000 yr. In this time span, the drift-wall temperature drops from above boiling to below boiling. Therefore, the THC process-level model results at 2,000 years first represent water and gas compositions at temperatures below boiling (since the preclosure period). This partial pressure of carbon dioxide and corresponding water compositions at the drift wall represent conditions just as the host-rock temperature drops below the boiling point of water at that location (e.g., at 2,000 years).

- The 10,000-yr process-level model results are used for the abstraction values in the last period as a reasonable approximation of the water composition average for that whole period. This is due to the fact that the water composition does not change appreciably from 10,000 to 100,000 yr. For example,  $\text{HCO}_3^-$  and  $\text{Ca}^{2+}$  increase by less than a factor of 1.5 from 10,000 to 100,000 yr. These particular ions represent the largest change of all considered. All other concentrations vary even less from 10,000 to 100,000 years (CRWMS M&O 2000b, Figures 33 and 35). For instance,  $\text{Na}^+$ ,  $\text{Cl}^-$ , and  $\text{F}^-$  show no change during this time period (CRWMS M&O 2000b, Figures 37, 39, and 40). The  $\text{CO}_2$  concentration and pH also change, but very slightly during this period (CRWMS M&O 2000b, Figures 29 and 31). Other trace constituents accounted for in the abstraction are also nearly constant during this time period.

The additional constituents taken from the results of the *Complex* chemical system are, in general, trace constituents compared to those taken from the *Less Complex* chemical system. Even though combination of these results may lead to discrepancies of the trace constituents that could be large in a relative sense, their contributions to the absolute uncertainties of the major constituents will remain small. Only potassium approaches the concentrations of the constituents taken from the less detailed chemical system, and even it is one to two orders of magnitude lower in concentration than the major cation species  $\text{Ca}^{+2}$  and  $\text{Na}^+$  included in the *Less Complex* system results.

#### 3.4.2.2 Low and High Infiltration-Flux Cases

This section discusses and quantifies the THC conceptual uncertainty in these results due to the variability in infiltration that stems from uncertainty in the infiltration rate at Yucca Mountain. This aspect of uncertainty is based on comparison of the mean infiltration case results (used for the abstracted values given above) with those from both the low-and the high-infiltration flux cases representing the uncertainty in infiltration rate at Yucca Mountain. However, this provides an assessment of only part of the uncertainty within these results. Other aspects that contribute to uncertainty are related to the process model and include conceptual uncertainties about the initial water composition, specific mineral abundances and distributions, the effective surface areas of minerals and other kinetic parameter values for the phases (CRWMS M&O 2000b). In addition to these uncertainties in the chemical aspects of the model, all those for the hydrologic model of the system also apply. Because these parts of the system are highly non-linear, rigorous uncertainty quantification for all these aspects is not straightforward. That is why the validation activities for the process model (CRWMS M&O 2000b, Section 6.2.7) are a primary method for assessing the level of applicability of the results.

Abstraction of uncertainty in the abstracted fracture-water compositions shown in Table 3-11 is based on the mean infiltration flux, low infiltration flux, and the high infiltration flux cases and uncertainty in the condensate-water compositions for these infiltration-flux cases (*THC Abstraction AMR*, Section 6.1.2).

An estimate of uncertainty in the THC abstraction indicates that for most constituents the values calculated for the high- and low-infiltration cases are within about a factor of two of the mean-infiltration flux case used in the abstraction. The exceptions to this correspond primarily to those constituents evaluated for the period where the fractures are dry (saturation of zero). In almost all cases, this represents the inclusion of artifact water compositions that occur because the process-level THC calculation cut-off the solution chemistry either at the point the solution reaches a maximum of 2 molal ionic strength or the saturation reaches a minimum of 0.0001 (CRWMS M&O 2000b, Section 6.3.5.2). Also, the three infiltration-flux cases (low, mean, and high) considered in the process model result in the different temperature histories for each mineral set. Variability in the temperature history leads to different rewetting times, potentially causing different water and gas compositions in the fractures when they resaturate. A dry fracture condition (CRWMS M&O 2000b, Figure 24) results in gaps in representation of reasonable, calculated fracture-water composition during that time (CRWMS M&O 2000b, Figures 31, 33, 35, 37, and 39), even though the gas composition calculation is continuous through this time (CRWMS M&O 2000b, Figure 29). In all cases, values that are different by more than an order of magnitude only occur for dissolved constituents during these situations. Even during those times, the water-chemistry values are different by more than one order of magnitude, but not by more than two orders of magnitude. As indicated, there is little meaning to the water composition as the fractures begin to dry (during the above-boiling period in the process-level model) because the water composition is "fixed" once fracture saturations are too low or ionic strength too high in the model.

The differences in the rewetting process for the fractures is most pronounced for the CO<sub>2</sub> gas compositions in the low climate history results compared to those for the mean climate history. The CO<sub>2</sub> values from the low infiltration rate case are only about 2 to 5 percent of those for the mean climate, until about 10,000 years. This variation in gas composition is reflected in an increase of about 10 percent in the solution pH. This result appears to be driven primarily by the lower flux of water moving through the system for the low climate-history case. The liquid flux is both a major source of CO<sub>2</sub> mass moving back to the drifts and a mechanism for heat removal. Both of these processes are enhanced for the higher infiltration-rate cases compared to the case for the low fluxes.

For comparison of calculated condensate water-compositions (for period 2 in the abstraction) for the various infiltration histories, the only species for which results differ by more than an order of magnitude are the Mg and Al constituents, which for the low infiltration case are about 8 percent and 6 percent, respectively, of their mean infiltration-rate case values. This represents only a small difference, because in all other cases the values are generally within a factor of two.

Given the observations from these comparisons, the abstracted water and gas compositions provided in Table 3-11 would only require about a factor of between two and ten to account for the variation in results from the other infiltration-flux cases. Using a factor of two to represent the standard deviation of such a distribution should encompass 95 percent of the variations that

are meaningful, whereas using a value of 10 would conservatively encompass all of the meaningful variations within the uncertainty bands.

As this variability is expected to be relatively small compared to that expected for changes driven by the in-drift evaporative processes accounting for higher concentration fluids and salt formation, it should not be necessary to explicitly incorporate this variability into a stochastic representation of the system until the larger variability of different conceptual processes is incorporated into this approach.

### **3.5 THERMAL-HYDROLOGIC-MECHANICAL CALCULATIONS**

This section briefly describes the TM behavior of rock in the NFE and the coupling of this behavior with hydrologic processes. In particular, the influence of TM effects on fracture permeability is discussed.

The stress field in the rock mass surrounding emplacement drifts in a potential repository at Yucca Mountain will be altered by excavation of drifts and by the heating and cooling cycle associated with emplacement of radioactive waste. The directions and magnitudes of the principal stresses will change significantly due to thermal loading, and then will return to near-ambient values during cool-down. Compressive stress will build up rapidly in the host rock, especially after the end of the ventilation period. The stress field will gradually decay as the temperature in the rock decreases.

The proposed repository host rock is a fractured, densely welded, ash-flow tuff. These fractures are expected to deform as stress conditions evolve. Two types of fracture deformation will contribute to THM coupling: normal displacement perpendicular to the fracture plane, and shear displacement parallel to a fracture plane.

Rock-mass permeability is an important TH property for assessment of repository performance. Because the rock has low matrix permeability, the rock-mass permeability is mainly associated with fractures, and fracture permeability is highly dependent on fracture deformation.

In this section, the relationship of fracture deformation to fracture permeability is discussed, and a TM model for the rock mass surrounding an emplacement drift incorporates discrete fractures. Fracture deformation during various phases of the heating-cooling cycle is used to predict changes in rock-mass permeability. These changes can be coupled back to TH or THC models.

In this section, a methodology for estimating TM effects on permeability is presented, using a distinct-element model that can capture the mechanical behavior of discrete fractures. Estimated permeability changes for selected times after waste emplacement, based on the EDA-II design (CRWMS M&O 1999a, Table 6-3; Wilkins and Heath 1999), are calculated using this method. In the distinct-element method, the rock mass is composed of an assembly of deformable blocks that are interfaced by discontinuities. In a distinct-element code (Itasca 1998), fractures in the rock mass are entered individually, and both normal and shear deformation are predicted for the individual fractures. The example calculation discussed in this section uses fracture spacing appropriate for the middle non-lithophysal region of the repository.

The effects of TM processes on fracture hydrologic properties are not directly incorporated in abstraction for TSPA-SR. Consequently, the effects of TM processes are screened out of TSPA based on low consequence ("to be verified" status by future calculations). A range of uncertainty in fracture hydrologic properties is included in the TSPA seepage model that may potentially account for processes not directly included in TSPA (CRWMS M&O 2000l, Section 6.2.3). However, this range is not based on explicit information associated with TM effects on fracture properties.

### 3.5.1 Approach to Coupling TM to TH Behavior

Coupling of TM and TH behavior is principally through the temperature and permeability fields. At present, several sophisticated algorithms for predicting TH behavior in partially saturated fractured rock are available. Moreover, these sophisticated simulators, such as NUFT, are needed to capture the TH behavior, which controls the temperature field over long periods of time. However, these algorithms are also computationally complex and intensive, and have not been directly implemented into a fully coupled THM code. Accordingly, for this report, temperature distributions generated by TH simulators are approximated using the simpler (conduction-only, with a simplified heat source) thermal models currently incorporated into available TM simulators. The thermal-stress distributions associated with the approximated thermal field are analyzed using a conceptual model for fracture-permeability change in response to deformation. The changes in permeability are then fed back to the TH models for refinement of the TH simulations.

### 3.5.2 Distinct-Element Calculation of TM Effect on Permeability – EDA-II Design

A calculation to provide an estimate of bounds for TM effects on fracture permeability has been conducted and is documented in the *THM Calculation* (CRWMS M&O 2000d). One purpose of this estimate of bounds was to provide essential input to performance assessment analysis of the potential repository system. The method used in this calculation was to simulate the TM behavior of a region of fractured rock that surrounds a section of a long horizontal emplacement drift in the Topopah Spring Tuff at Yucca Mountain.

The rock mass surrounding an emplacement drift is simulated in three dimensions as a rectangular prism 50 m wide by 60 m high by 30 m thick, defined as shown in Figure 3-39. A cylindrical drift 5.5 m in diameter is excavated through the region in the x direction and brought to stress equilibrium. This drift is horizontal, and oriented perpendicular to the narrow dimension of the region. The prism is intersected by three sets of fractures: one vertical set oriented parallel to the drift, one vertical set oriented perpendicular to the drift, and one horizontal fracture set. It should be noted that the drift orientation is consistent with that of the EDA-II design (CRWMS M&O 1999a, Table 6-3; Wilkins and Heath 1999), but the fracture orientations are based on field observations (Albin et al. 1997). Two fracture densities are used for each set of fractures, a low fracture density (0.1/m) for regions more than 15 m from the drift, and a higher fracture density (0.5/m) for regions within 15 m of the drift. This nested fracture density distribution was to facilitate computation of individual fracture movement. That is, the available computational resources limited the number of fractures that could be included. These fracture densities are lower than those observed in situ, and lower than those used in thermal-hydrologic modeling (CRWMS M&O 2000a), but are appropriate, as not all fractures are

mechanically and hydrologically active in the field. Only active fractures are considered here, and work by Barton et al. (1997) presents convincing evidence that fractures that conduct fluids are fractures that are critically stressed in shear. Joint and rock-mass properties used in this calculation (CRWMS M&O 2000d) were taken from field and laboratory studies of rock and fracture behavior, such as those by Barton et al. 1985, and Olsson and Brown 1994. Stresses equivalent to the in situ stresses are imposed on the sides and top of the prism. The base of the prism is fixed in the vertical direction, but allowed to move in the horizontal directions. The model boundary conditions are intended to approximate in situ conditions and are similar to those used in previous thermomechanical modeling (Berge et al. 1998) and are based on field stress measurements. Fracture-deformation values estimated at a series of times are then used to compute permeability change in a cross section perpendicular to the emplacement drift. These values for permeability change at each time were then contoured.

### 3.5.2.1 Thermal Field

The commercial 3DEC (Itasca 1998) distinct-element code was used for the simulations. This model utilizes a weakly coupled approach to thermal mechanical analysis. The thermal field imposed by the emplacement of nuclear waste containers is simulated within the 3DEC code using a conduction-only thermal model that calculates temperatures in an infinite medium. The thermal model allows adiabatic and isothermal boundary conditions to be applied in the thermal formulation. This thermal model is used to compute temperatures at all gridpoints in the mechanical model of the problem being studied. The temperature change (from initial temperature) for each zone is used to calculate a stress change in each zone. This stress state is treated as an initial condition for the mechanical calculation, and the standard 3DEC mechanical calculation is used to reach equilibrium.

The calculation is intended to evaluate rock behavior for a section of an emplacement drift within a potential nuclear waste repository. To do this, a block of rock is defined that includes a section of an emplacement drift. Within this block, a line heat source is used within the emplacement drift to simulate emplaced waste containers. To assure constant heat load along the section of simulated emplacement drift, the heat source extends approximately 30 m beyond the boundaries of the simulated block in both directions, as shown in Figure 3-40. The calculation is designed to simulate the EDA-II design; thus identical heat sources are placed at 81 m to the north and south of the tunnel heater array in the surrounding rock continuum, as shown in Figure 3-40.

The thermal simulator incorporated into 3DEC is an isotropic uniform, conduction only model, and thus the estimated temperatures are expected to be elevated near the drift wall compared to those predicted using more sophisticated TH models that include cooling due to convection and latent heat (heat-pipes). Temperature distributions at several times after emplacement are given in the *THM Calculation* (CRWMS M&O 2000d). Overall, at locations more than a few meters away from the drift, the temperatures match those predicted using TH models well enough for use in this bounding calculation. Because the THM calculation is a bounding calculation, elevated temperatures near the drift wall are not an issue.

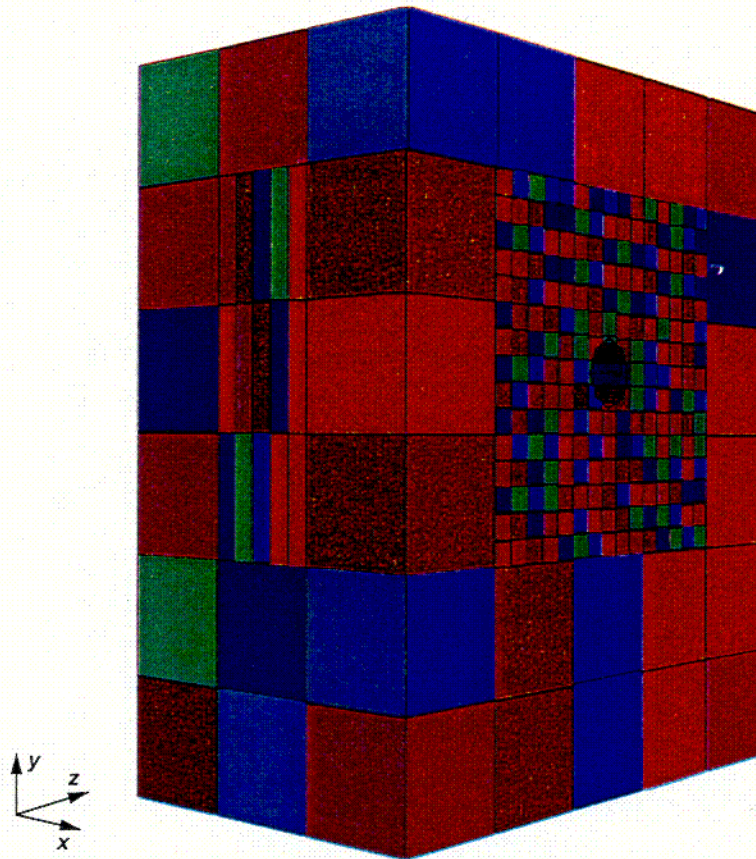
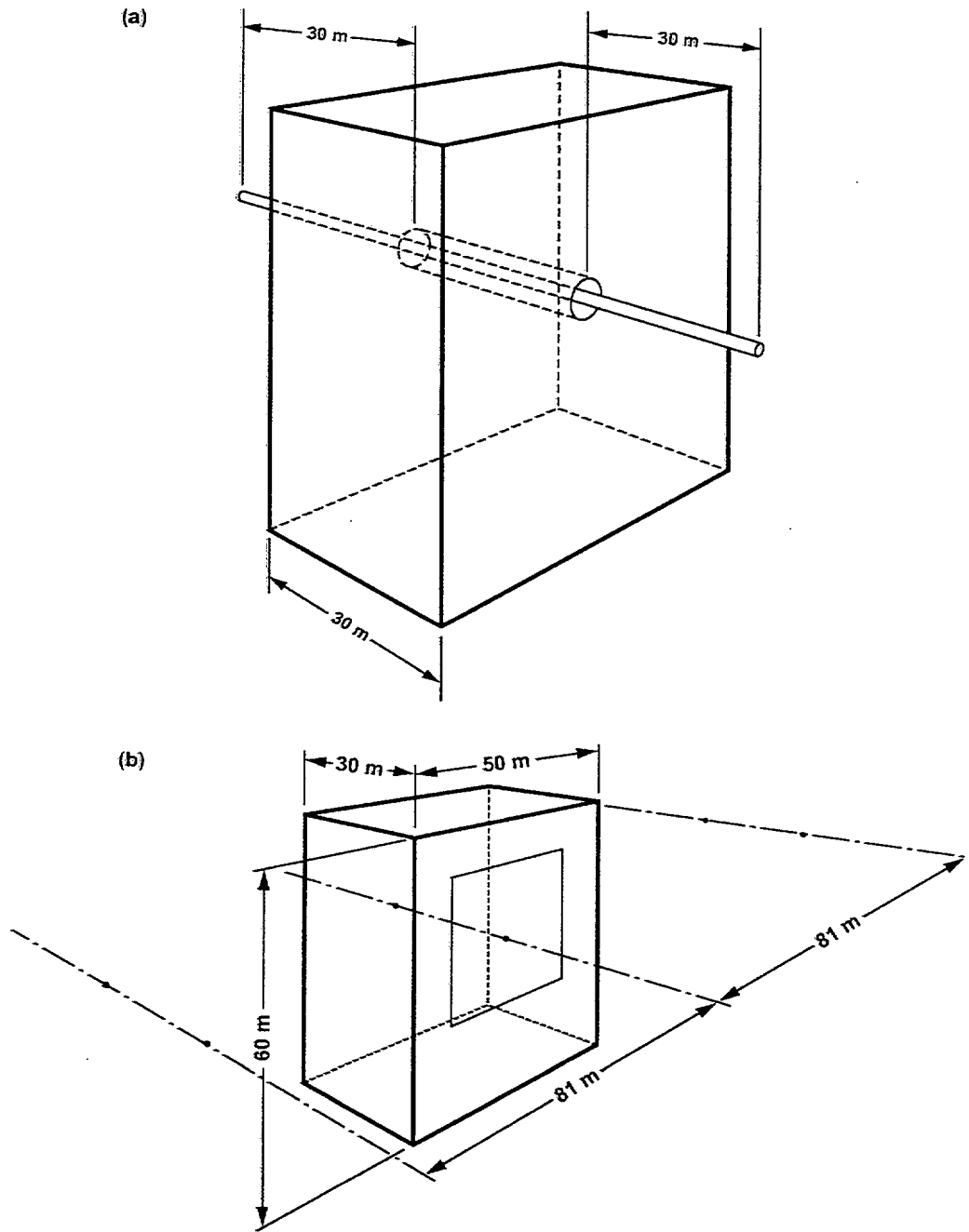


Figure 3-39. Simulated Rock Mass for TM Coupled Effects Showing Three Sets of Fractures and Two Fracture Densities for Each Set

The thermal load of the model (see Figure 3-41) is based on the EDA-II design, in which ventilation is used to remove heat from the emplacement drift for the first 50 years after emplacement. The EDA-II design shows a “spike” in the pillar temperature starting at 50 years, when ventilation ceases, followed by slower cooling.

A simple step function was used for the thermal power input (Figure 3-41). Power was supplied at a constant level of 460 watts for 50 years to simulate the ventilation phase, then raised to 615 watts and held constant for another 100 years, then reduced to zero. This heating schedule produced temperatures similar to the maximum pillar temperature, but over a longer time, followed by a more rapid cooldown than TH calculations (Sections 3.2.3 and 3.3) with a more realistic source. Since the objective of the THM calculation is to calculate bounds for stresses and displacements, the faster cool down is appropriate as faster cooling produces higher stress gradients in the region around the drift than does cooling at a slower rate. These higher stress gradients in turn produce larger deformations in the NF rock. Moreover, the fast cool-down is more compatible with the assumption of a constant value of joint cohesion over the time span of the calculation. This is because fracture properties are thought to be time dependent *Drift Degradation Analysis* (CRWMS M&O 2000ac).

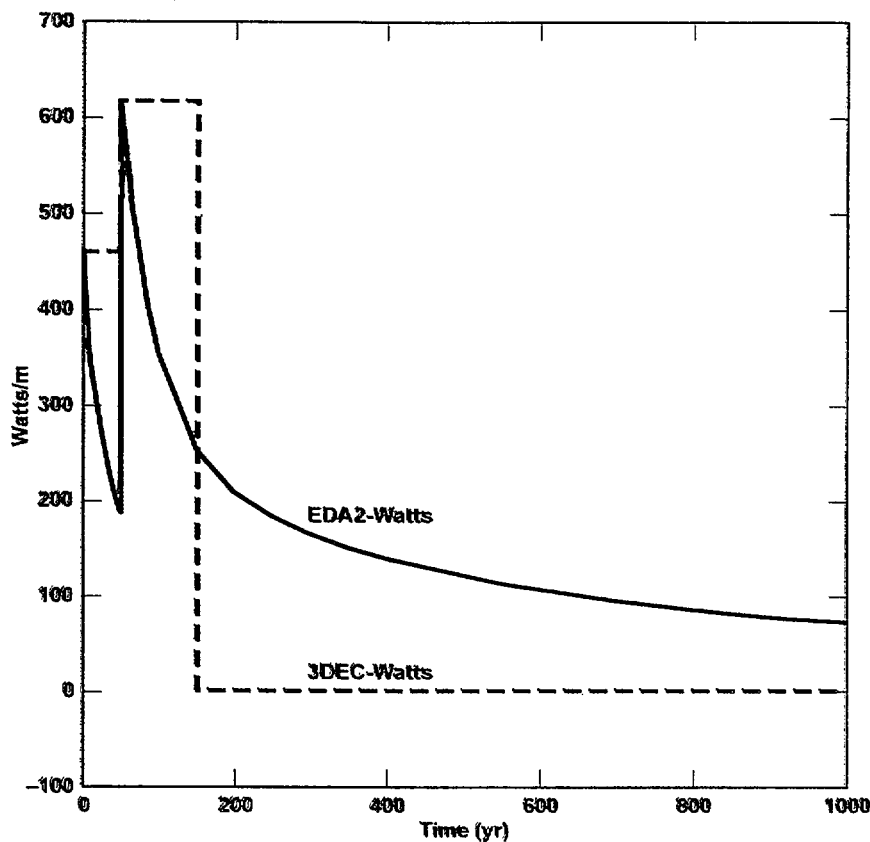
L335



Source: CRWMS M&O 2000d, Figure 3

- NOTE:
- a. The heater array extends approximately 30 m beyond the boundaries of the mechanical model in both the + and - directions.
  - b. Identical heat sources (dashed lines) are placed at 81 m to the north and south of the tunnel heater arrays.

Figure 3-40. Schematic of Heater Layout for Simulation



Source: CRWMS M&O 2000d, Figure 4

Figure 3-41. Thermal Power History for Simulation

### 3.5.2.2 Fracture Deformation

After non-heating equilibration to account for excavation effects, the numerical model was used to estimate stress and deformation values in the block at a series of times after emplacement. Both normal and shear deformation were predicted for multiple locations on each fracture face.

Normal displacement is associated with changes in normal stress. Fractures stiffen readily as they close in response to normal compression, which limits the relative magnitude of the permeability change that can be produced. Several investigators have shown that increasing compressive stress across the apparent fracture faces causes a reduction in fracture aperture, and, to a first approximation, flow in a fracture is widely accepted to be related to the cube of the fracture aperture (Raven and Gale 1985, pp. 251-261). Heating the rock generally increases stress and thereby reduces the fracture aperture in proportion to fracture normal stiffness. If the average normal stress is maintained well below the intact rock strength, and if creep is not significant, fractures generally return to their previous aperture when unloaded (i.e., normal displacement is reversible). Fractures open in response to decreasing normal stress and eventually open at zero load. If fracture surfaces remain well aligned, and if shear displacement does not occur, fracture opening is also reversible. Fracture closing is expected during the

heating phase in response to thermal expansion of the rock mass. Fracture opening is expected during cooldown.

The TM response of fractures may also include shear displacement along the face of the fracture. Moreover, field studies during the last few years (Barton et al. 1997) have shown convincing evidence that fractures that are critically stressed in shear, are likely to conduct fluids. In addition, experimental studies on laboratory samples have shown that fracture shear displacement can significantly increase fracture permeability and that the magnitude of change in permeability may be large. This is because even small shear displacements cause fractures to dilate, which mobilizes the surface roughness and decreases the spatial correlation or "matedness" of fracture surfaces. This opens up void space in the fracture and can greatly increase permeability with only a small change in normal aperture (Barton et al. 1985).

The tendency for slip in response to shear stress is controlled by the frictional properties and geometry of the fracture surfaces, the hydraulic conditions within the fracture, the deformation history of the fracture, and the normal stress on the fracture. Frictional and geometrical properties are represented for all fractures in the host rock at Yucca Mountain by average property values that are similar to those used for analysis of drift degradation (CRWMS M&O 2000ac). Fractures in the host rock may be wet, but there will be no significant positive pressure head in the unsaturated zone.

In the calculation of THM effects on permeability, the estimated joint-deformation values for a series of selected times are used to compute permeability change in a cross section perpendicular to the emplacement drift.

### 3.5.2.3 Calculation of Permeability Change

The distinct-element method was selected for this study because it allows discrete fractures to be simulated. Moreover, it is the only method that provides direct simulation of normal and shear displacement and other behavior on discrete fractures. When a distinct-element model is used for simulations, both normal- and shear-fracture deformations are computed directly. In this case, one approach for computing a change in fracture permeability is to define  $k_0$  as the initial fracture permeability and  $k_t$  as the fracture permeability at time,  $t$ , due to TM effects. If  $df$  is defined as the magnitude of fracture displacement in mm (shear or normal), then a permeability multiplier,  $\bar{k}$ , can be computed as the dimensionless ratio

$$\bar{k} = k_t/k_0 = 1 + (10/\text{mm}) \cdot df \text{ (mm)}$$

Using this expression, shear deformation always produces an increase in permeability, while normal deformation will increase permeability if the fracture opens ( $df > 0$ ) and will decrease permeability if the fracture closes ( $df < 0$ ). This approach was used in the *THM Calculation* (CRWMS M&O 2000d). The calculated joint deformations were used to compute permeability changes in a cross section perpendicular to the emplacement drift. Maximum shear and normal deformation values were computed along an array of lines parallel to the drift, then projected onto a plane perpendicular to the drift. The displacements were then used to estimate permeability changes with the proportionality relationship given in the above equation. Moreover, while the model is generally symmetric about the mid-length of the heated region, the

permeability estimates are not expected to show well developed symmetry around this plane. This is because these estimates are based on 3-D displacement estimates that are projected onto a 2-D plane, and because of small asymmetries in the 3DEC grid.

The parameter  $\bar{k}$  provides a straightforward linear approximation of permeability change as a function of deformation. This was made for several reasons. First, the relationship between shear slip and permeability change is poorly known. Second, use of the linear relation between permeability change and shear slip is consistent with the results of laboratory studies by Olsson and Brown (1993), who observed shear-induced fracture dilatancy and increased permeability with rotary shear slip, and by Esaki et al. (1999) who observed permeability increases of 1.2 to 1.6 orders of magnitude for the first 5 mm of lateral shear slip. Assuming a linear relationship between slip and permeability, the results of Esaki et al. (1999) yield a permeability increase of between factors of 3 to 8 per mm of slip. Because this is a bounding analysis, a factor of 10 permeability change per mm slip was used in the simulations. The combined effect of normal and shear deformation has not been considered, and will be addressed in future studies of coupled THM behavior.

The same linear relationship for both normal and shear deformations was used for the bounding calculations. This approach is also consistent with numerical modeling work (CRWMS M&O 2000a), which found that increasing fracture permeability by two orders of magnitude, to simulate the opening of vertical fractures, was required to provide realistic predictions of temperatures in the LBT. Fracture opening displacements in the LBT were on the order of a few millimeters (Wilder et al. 1997).

Finally, because it is assumed that all permeability change is due to deformation on fractures, it is the spatial distribution of fracture deformation that is of fundamental interest and this is independent of the relationship used to estimate the magnitude of changes.

#### 3.5.2.4 Results of Distinct-Element Calculation

Results are presented as 2-D images of permeability multipliers,  $\bar{k}$ , calculated from predicted values of normal and shear displacement of fractures. Stress gradients in the rock mass are directly related to temperature gradients due to thermal expansion of the rock. Given the thermal-loading regime presented in Figure 3-41, one time of interest is 55 years after emplacement, as this is five years after the end of ventilation, when thermal gradients in the rock are high. The greatest values for displacement at this time were computed for the plane perpendicular to the drift and were approximately 0.3 mm for normal (opening) displacements and 0.9 mm for shear displacements.

Figure 3-42 shows an estimate of permeability change due to normal deformation of fractures at this time. The plot indicates the largest change in permeability at 55 yr after emplacement occurs within one drift-diameter of the drift wall. These include a decrease in permeability (multiplier values <1) in the ribs of the drift, and regions of increased permeability (multiplier values >1) above and below the drift. This is consistent with closing of vertical fractures in the drift rib as the rock tries to expand horizontally, and opening of vertical fractures above and below the drift. It is important to note that as described above, stress boundary conditions were used on the top and sides of the block in this simulation, and this influences the TM response.

These boundary conditions were used in the bounding calculation as they allow more movement than fixed boundaries. Moreover, despite this boundary condition, the magnitude of the predicted increase is relatively small (less than 2) and that a multiplier near one is estimated for much of the rock mass. This figure also shows that a slight increase in permeability is expected for horizontal fractures at distances greater than two drift-diameters. This is attributed to vertical thermal expansion of the rock in the near-drift region. Again, note that the predicted increase in permeability is small ( $<1.5x$ ).

Figure 3-43 is the 55-yr estimate of permeability change due to shear displacement. Shear displacement values at this time were a maximum of 0.9 mm in the plane perpendicular to the drift and 0.24 mm in the plane parallel to the drift. Figure 3-43 shows that after 55 years of heating, shear displacement may be expected to increase permeability as much as 3-6.5 $\times$  in the region within one drift-diameter. Results in the *THM Calculation* (CRWMS M&O 2000d) show that this permeability enhancement was caused by the initial heating (0 year) and the additional heat at 50-55 years did not substantially change the permeability.

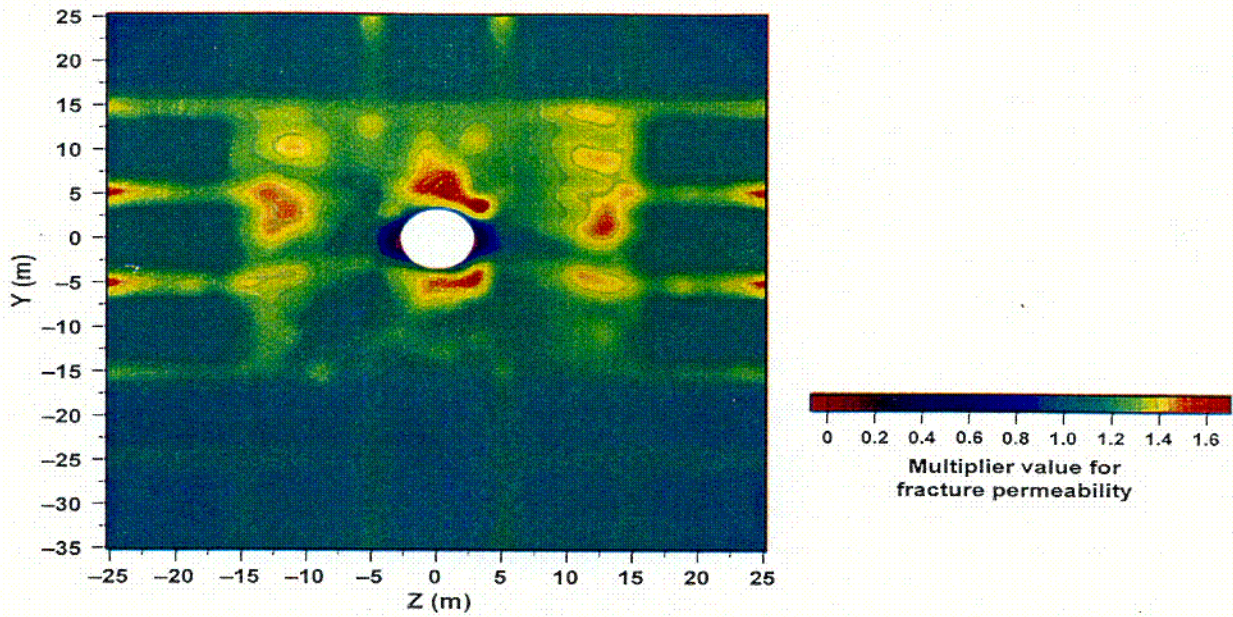
Potential changes in fracture permeability are also important for evaluating repository performance at cooldown. Using the thermal regime shown in Figure 3-41, cooldown occurs at a time of 1,000 yr. Normal displacements were computed for the cooldown phase and maximum values were about 0.15 mm for planes both parallel and perpendicular to the drift. Estimated changes in permeability for normal deformation of the fractures at cooldown are shown in Figure 3-44. These results indicate that during cooldown, vertical fractures above the drift may open, increasing the permeability by a factor of two.

The largest shear deformations (1.2 mm) were computed for both planes parallel and perpendicular to the drift at 1,000 yr. Figure 3-45 shows permeability multiplier values due to shear displacement at 1,000 yr. This figure shows that shear deformation on vertical fractures during cool down produces the maximum amount of permeability change, an order of magnitude above and below the drift, and increases in permeability by a factor of 5 may occur on vertical fractures at distances beyond two drift-diameters from the drift wall.

### 3.5.3 Summary of Thermal-mechanical Models

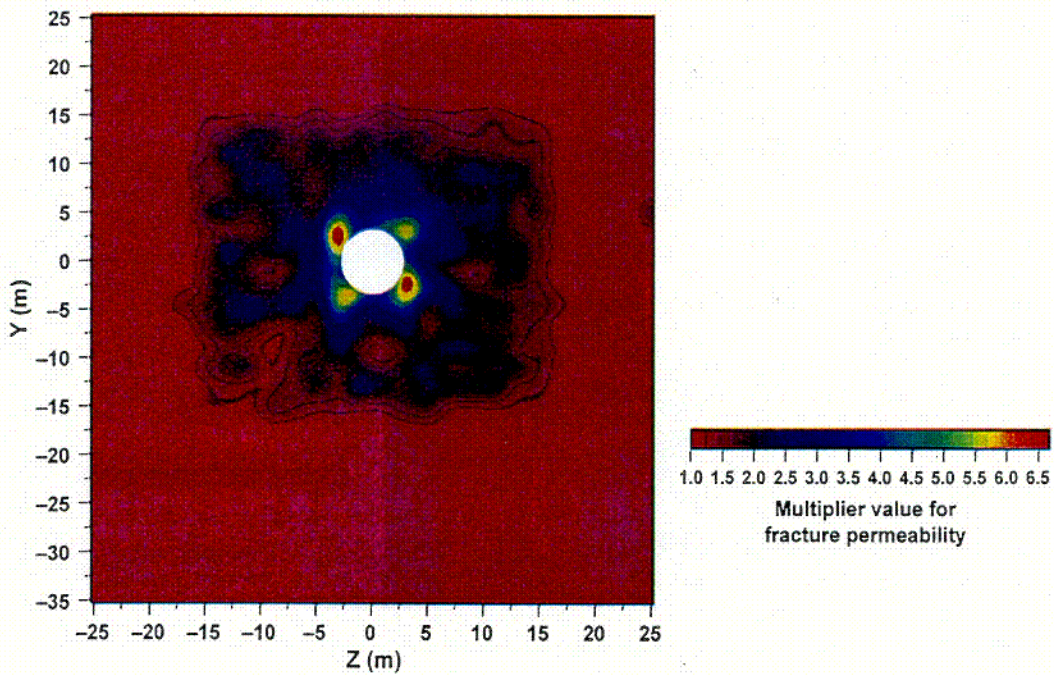
Results of this calculation indicate that the major TM effect on fracture permeability occurs during cooldown for both shear and normal deformation.

These results indicate that shear deformation of fractures during cooldown of a potential geologic repository may cause permeability of the fractures in a region within two drift-diameters of a drift wall to increase in permeability by as much as an order of magnitude. Specifically, shear deformation on vertical fractures during cooldown produces the maximum amount of permeability change, and increases in permeability on the order by a factor of 5 may occur on vertical fractures at distances beyond two drift-diameters from the drift wall.



Source: CRWMS M&O 2000d, Figure 6(c)

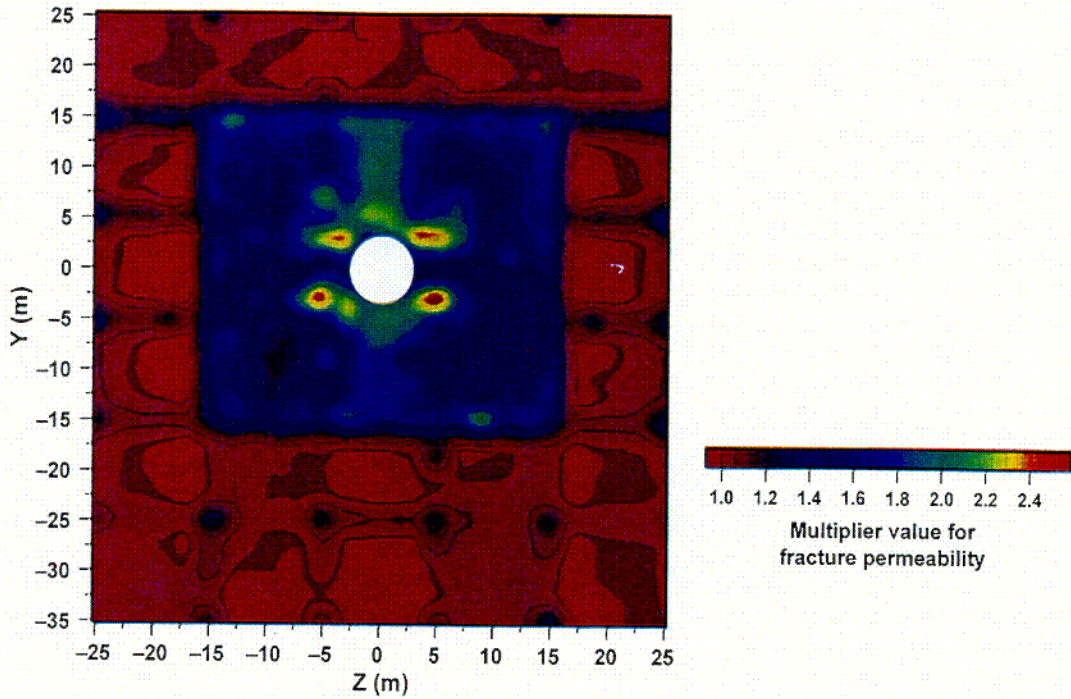
Figure 3-42. 55-year Estimate of Permeability Change Due to Normal Displacement



Source: CRWMS M&O 2000d, Figure 6(c)

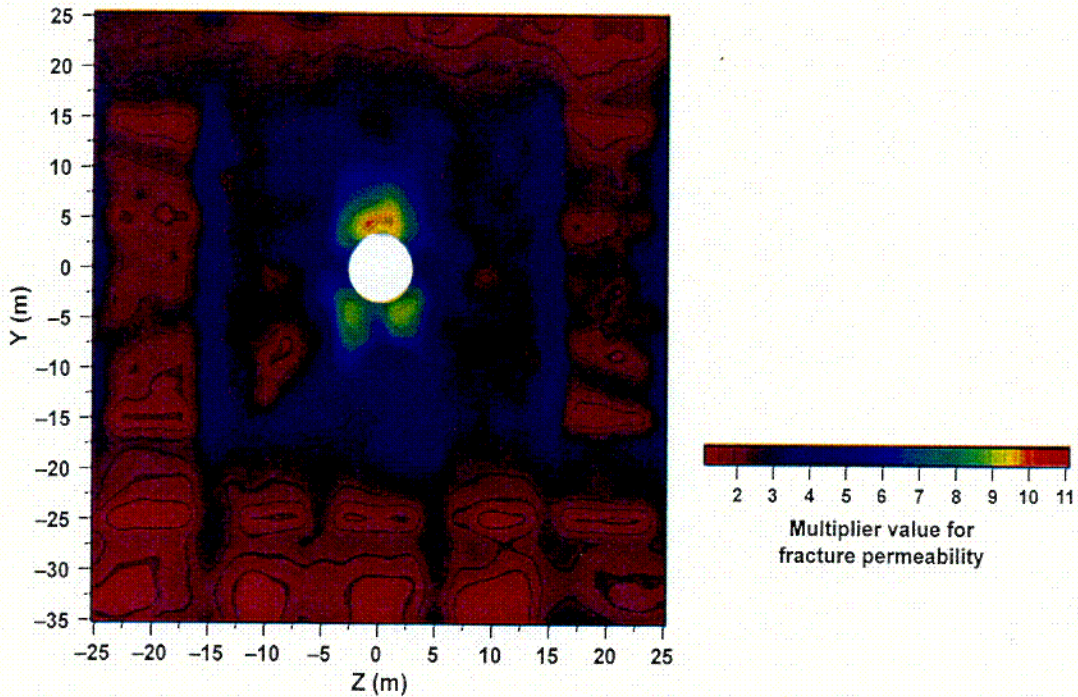
Figure 3-43. Permeability Multiplier Values Due to Shear Displacement at 55 Years

c-36



Source: CRWMS M&O 2000d, Figure 5(g)

Figure 3-44. Permeability Multiplier Values Due to Normal Displacement at 1,000 Years



Source: CRWMS M&O 2000d, Figure 6(g)

Figure 3-45. Permeability Multiplier Values Due to Shear Displacement at 1,000 Years

Results indicate that normal deformation of fractures may cause permeability to increase as well, but to a lesser extent than shear deformation. Closing of fractures during heating may cause permeability to decrease significantly within one drift-diameter of the drift wall. During cooldown, vertical fractures above the drift may open, increasing the permeability by a factor of two. It is important to note that the actual fracture permeability or "hydraulic aperture" is a function of displacements both parallel and perpendicular to the fracture wall. A quantitative description of how both types of fracture deformation affect flow in fractures has not yet been developed. Such a relationship might include a cubic term for normal deformation combined with an exponential term for shear deformation.

It is important to note that as this is a bounding estimate, primarily concerned with fracture deformation, stress boundary conditions were chosen for the vertical sides of the model. This in effect provides a lower limit on normal stress across vertical fractures, thus making it easier for them to open and/or slip. Use of a roller boundary condition on the vertical sides to prevent lateral displacement at the mid-pillar would provide an upper limit on normal stress across vertical fractures with increasing temperature. That is, stress would build as the rock tries to expand in the lateral direction as temperature rises. Use of the roller boundary would provide an alternative distribution of permeability change. It is also important to note that Figures 3-29 to 3-32 represent projections of 3 dimensional predictions projected onto a 2 dimensional plane. Thus, the symmetry normally associated with two dimensional calculations is not in evidence.

Recall that the effects of TM processes on fracture hydrologic properties are not directly incorporated in abstractions for TSPA-SR. Consequently, the effects of TM processes driven by repository heating are screened out of TSPA based on low consequence ("to be verified" status by future calculations).

### **3.6 VALIDATION OF NFE MODELS FOR USE ON YUCCA MOUNTAIN**

When discussing validation of models for use on Yucca Mountain, it is important to have a clear understanding of what is meant by a model, and the distinction between model and software validation. One definition of a model is "A tentative description of a system or theory that accounts for all of its known properties". AP-3.10Q defines models similarly, "A representation of a process, system, or phenomenon, along with any hypothesis required to describe the process or system or explain the phenomenon, often mathematically." In the strict sense of the word reflected by these definitions, much of the processes and software descriptions that are imbedded within various software codes are models. However, a general distinction can be made between models, which describe the system, including physical conceptualizations and all of the system's processes and interactions with other systems, and the software or codes used to perform the mathematical or numerical manipulations needed to quantify this description. For purposes of this PMR, validation of models as discussed in this section refers to models that describe the system and its response, while software codes are considered to be the tools used to analyze the models. It is recognized that codes have embedded within the software a numerical description of submodels, however the submodels included within the coding of the software are "validated" as part of the code validation, as discussed in Appendix A for example. There is no distinction in building confidence, because confidence in the model also must address the submodels within the codes.

There are many different types of models, some conceptualizations of big systems, others are models of specific processes. The models to be validated can be grouped into a hierarchy of models often depicted as a pyramid with detailed mechanistic models at the base, with abstracted models in the middle, and overall models (TSPA) at the top (Figure 3-45).

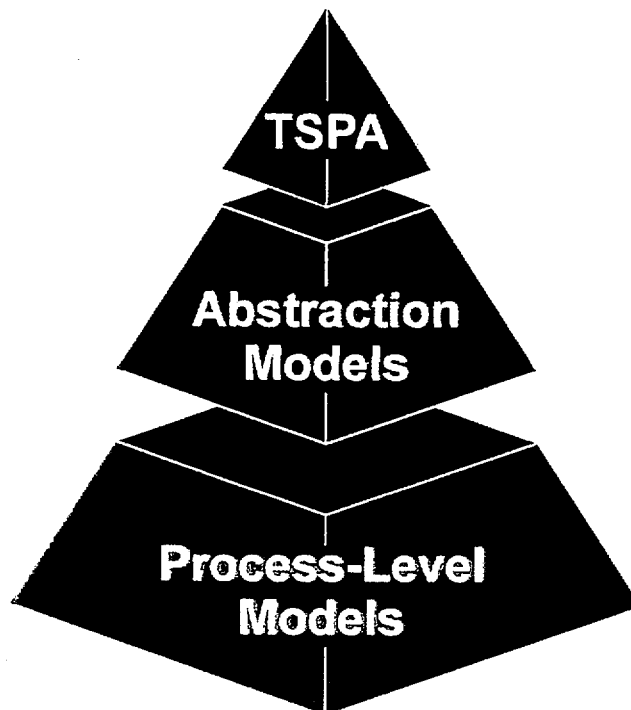


Figure 3-46. Hierarchy of Models

This PMR discusses the detailed or mechanistic models and their abstractions. As noted in Section 1.4.2, there are three overall models that describe the NFE. These are the TH, THC, and THM models. For each of these models there are detailed or mechanistic models (e.g., the *THC Process AMR*) and abstracted models (e.g., the *THC Abstraction AMR*). Associated with the models are the inputs of properties from site characterization, as well as conceptual understanding of processes (e.g. fracture flow). All of these interactions must be considered in model validation efforts. The confidence building or validation efforts are based on testing the detailed models and therefore building confidence in the abstraction models that are based on the detailed models. This is necessary because the measurements against which models can be tested are usually of processes and results at the detailed level, not the abstracted level. The testing also provided a means of determining which property sets from the site characterization are appropriate for the various models. The relationship between the models in the hierarchy and the property and site characteristics inputs are shown on Figure 3-47. As noted, the models shown as process-level models are the ones that can be directly tested against field and laboratory tests. Table 3-12 lists the models of consideration for the NFE. The table indicates the general conditions and ranges over which model validation applies.

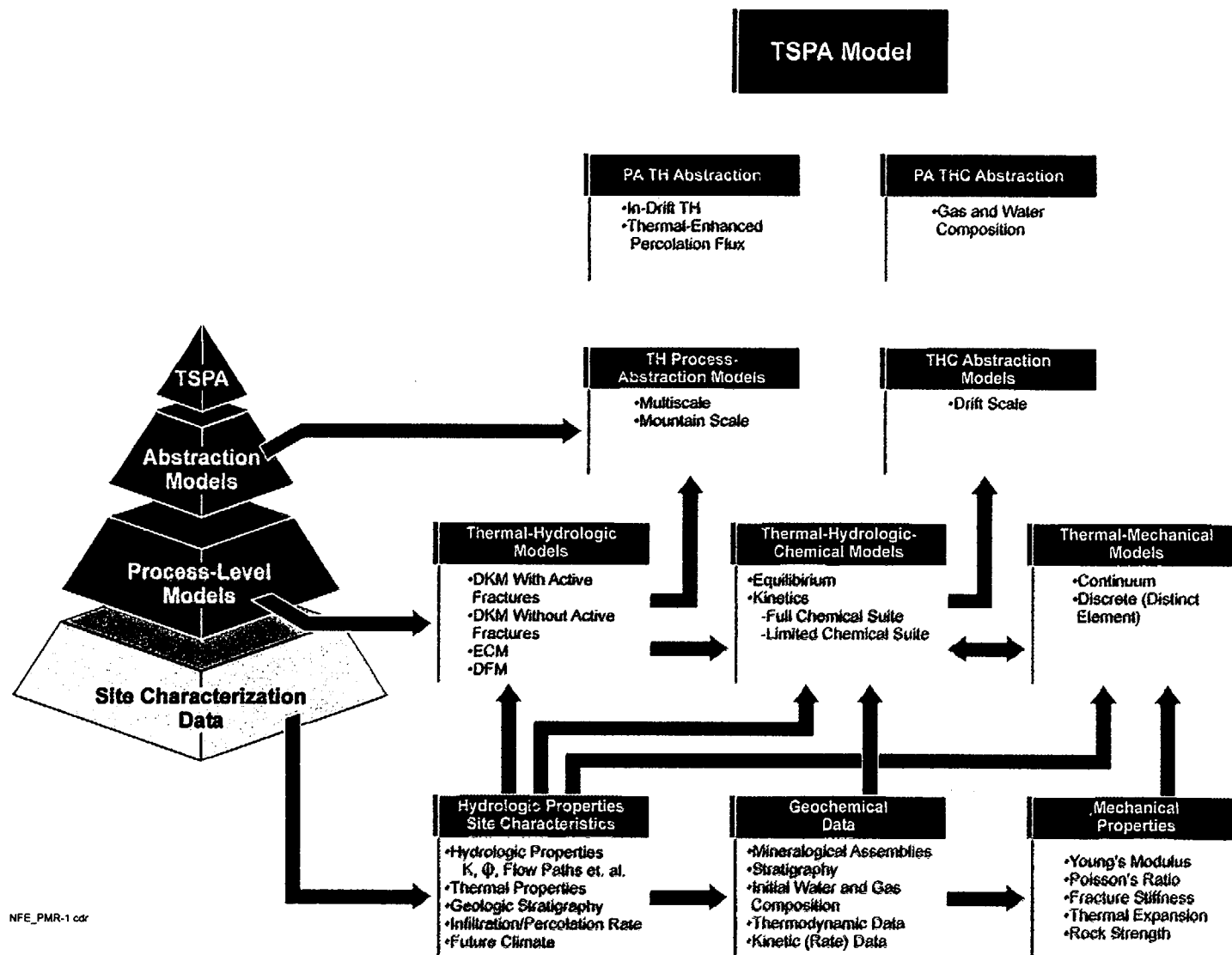


Figure 3-47. Hierarchy of NF Models and Relationship to Data Inputs and to TSPA

Table 3-12. List of NFE Models, by Hierarchy, Showing Details Pertinent to Validation

	Processes/ Equations	Boundary Conditions	Dimensionality	Range of Material Properties	Numerical Codes Used	Validation
<b>Repository Models</b>						
<b>TH</b>						
• Multi-Scale TH Model (MSTH)						
-SMT, thermal conduction	<ul style="list-style-type: none"> <li>Thermal Conduction</li> <li>Large Scale Repository Heat Source</li> </ul>	Constant T at ground surface & Constant T below UZ-SZ interface to 1,000 m	Mountain-scale 3-D	Thermal conductivity	NUFT	DST, Geo-thermal Analogs
-Line-average-heat-source, MS, TH	<ul style="list-style-type: none"> <li>Fluid flow</li> <li>Thermal Conduction</li> <li>Radiation</li> <li>Convection</li> </ul>	Constant T, $S_{liq}$ , $P_{gas}$ , & $X_{air,gas}$ at ground surface, constant UZ-SZ interface	Mountain-scale 3-D	DS property set; low, mean, & high infiltration	NUFT,	Conceptual result from the combination of the SMT, SDT, and LDTH submodels
-Smeared-heat-source, drift scale, thermal conduction (SDT)	<ul style="list-style-type: none"> <li>Thermal Conduction</li> <li>Smear Heat Source</li> </ul>	Constant T at ground surface & WT	Drift-scale (DS), 1-D	Thermal conductivity	NUFT	DST (wing heaters)
-Line-average-heat-source, drift scale TH (LDTH)	<ul style="list-style-type: none"> <li>Fluid flow</li> <li>Thermal Conduction</li> <li>Radiation</li> <li>Convection</li> <li>Average Discrete Heat Source</li> <li>DKM Active Fracture Option</li> </ul>	Constant T, $S_{liq}$ , $P_{gas}$ , & $X_{air,gas}$ at ground surface & WT	Drift-scale, 2-D	DS, calibrate hydrologic and thermal properties, low, mean and high infiltration	NUFT	DST (floor heaters)
-Discrete-heat-source, MS TH	<ul style="list-style-type: none"> <li>Fluid flow</li> <li>Conduction</li> <li>Convection</li> </ul>	Constant $S_{liq}$ , $P_{gas}$ , & $X_{air,gas}$ at ground surface & WT; Constant T at ground surface & 1 Km below WT	Mountain-scale 3-D	DS, calibrate hydrologic and thermal properties, low, mean and high infiltration	NUFT, MSTHAC	DST, Conceptual result from the combination of the SMT, SDT, LDTH, and DDT submodels
-Discrete-heat-source, drift-scale, thermal-conduction (DDT)	<ul style="list-style-type: none"> <li>Conduction</li> <li>Radiation</li> </ul>	Constant T at ground surface & WT	Drift-scale, 3-D	Thermal conductivity	NUFT	DST (drift heaters)

Table 3-12. List of NFE Models, by Hierarchy, Showing Details Pertinent to Validation (Continued)

	Processes/ Equations	Boundary Conditions	Dimensionality	Range of Material Properties	Numerical Codes Used	Validation
<ul style="list-style-type: none"> <li>MS TH Models</li> </ul>	<ul style="list-style-type: none"> <li>Fluid flow</li> <li>Thermal Conduction</li> <li>Convection</li> <li>Large Scale Repository Heat Source</li> </ul>	Constant T, constant gas pressure, constant $S_{liq}$ 1,000 m below UZ-SZ interface, surface: RH, infiltration, T	MS-2-D & multi 2-D extrapolated to 3-D	Calibrated Hydrologic Properties, Thermal Properties	TOUGH2	Geo-thermal Analogs  DST
-DKM with Active Fracture	<ul style="list-style-type: none"> <li>Separate Fracture and Matrix Continua</li> <li>Measure of Fracture Activity (hydraulically active fractures given by <math>\gamma</math>)</li> <li>Capillary Pressure for Active Fractures (fn of <math>\gamma</math>)</li> <li>Liquid Relative Permeability for Active Fractures (fn of <math>\gamma</math>)</li> <li>Fracture and Matrix Interface Reduction Factor for Active Fractures (fn of <math>\gamma</math>)</li> </ul>	(same as above)	Valid for any dimension	Calibrated Parameter for the Activity of connected fractures ( $\gamma$ )	NUFT, TOUGH2	DST, SHT, LBT
-DKM without Active Fracture	<ul style="list-style-type: none"> <li>Separate Fracture and Matrix Continua</li> <li>Fracture and Matrix Interface Reduction Factor as a Constant Value</li> </ul>	(same as above)	Valid for any Dimension	Calibrated Constant Value Reduction Term	NUFT, TOUGH2	SHT
-ECM	<ul style="list-style-type: none"> <li>Composite Continuum</li> <li>Assumed Capillary Pressure Equilibrium between Fractures and Matrix</li> </ul>	(same as above)	Valid for Any Dimension	Thermal properties, hydrological properties, bulk permeability, moisture retention curves of porous media	NUFT, TOUGH2	SHT, G-Tunnel

Table 3-12. List of NFE Models, by Hierarchy, Showing Details Pertinent to Validation (Continued)

	Processes/ Equations	Boundary Conditions	Dimensionality	Range of Material Properties	Numerical Codes Used	Validation
-DFM	<ul style="list-style-type: none"> <li>Discrete fracture</li> <li>Thermal conduction</li> <li>Thermal convection</li> <li>Fluid flow in fractures</li> </ul>		Valid for any dimension	Thermal conductivity Hydrological properties of fractures	NUFT	G-Tunnel
<b>THC</b>						
Drift Scale Process Model	Equilibrium and kinetics	Constant T, $S_{liq}$ , $P_{gas}$ , & $X_{air,gas}$ at ground surface & WT, pore water chemistry as initial condition	Drift-scale, 2-D	Limited and extended chemical species list	TOUGH-REACT	DST
<b>THM</b>						
-Distinct element (allows for displacement along fractures)	Stress and displacement of rock mass and fractures, thermal conduction	Two cases: Fixed zero-displacement boundaries; constant applied stress at boundaries	Drift scale, repository scale, or MS; 2-D and 3-D	Use same hydrologic and thermal properties as in NUFT modeling	3DEC	DST, LBT, SHT
-Continuum (without fracture displacement)	Stress and displacement of rock mass as porous medium, thermal conduction	Two cases: Fixed zero-displacement boundaries; constant applied stress at boundaries	Drift scale, repository scale, or MS; 2-D and 3-D	Use same hydrologic and thermal properties as in NUFT modeling	FLAC	DST, LBT, SHT
<b>TH FIELD TEST MODELS</b>						
DST TH Model using DKM with AFM	<ul style="list-style-type: none"> <li>Conduction and TH heat transfer</li> <li>Interaction btw fractures and matrix</li> <li>Line averaged heat source</li> </ul>	Surface conditions determine subsurface S&T Boundary @ <100m horizontal, vertical at tsw34 contact conditioned to 1D initialization	Multiple 2-D, extrapolated to 3-D.	DS and MS property sets, $0 < S < 95\%$	TOUGH2	DST: Compare to Measured Temperatures at various locations around the DST heat sources

Table 3-12. List of NFE Models, by Hierarchy, Showing Details Pertinent to Validation (Continued)

	Processes/ Equations	Boundary Conditions	Dimensionality	Range of Material Properties	Numerical Codes Used	Validation
DST TH Model using DKM with AFM	<ul style="list-style-type: none"> <li>• Conduction and TH heat transfer</li> <li>• Interaction btw fractures and matrix</li> <li>• Line averaged heat source</li> <li>•</li> </ul>	Measured saturations and temperatures at DST used to determine surface and WT conditions. Boundaries horizontal: 250 - 300 m. Upper-mtn surface Lower-WT (constant T, p)	2-D, 3-D	DS and MS property sets, $0 < S < 92\%$	NUFT	DST: Compare to Measured Temperatures at various locations around the DST heat sources
LBT TH Model using DKM with AFM	<ul style="list-style-type: none"> <li>• Conduction and TH heat transfer</li> <li>• Interaction btw fractures and matrix</li> <li>• Line averaged heat source</li> </ul>	3x3x5 m heat flux horizontal boundaries, constant T top	3-D	DS and MS property sets	NUFT	LBT: Compare to Measured Temperatures at various locations around the DST heat sources
Single Heater Test TH Model using DKM with AFM	<ul style="list-style-type: none"> <li>• Thermal Conduction</li> <li>• Thermal Convection</li> <li>• Thermal Diffusion</li> <li>• Liquid Flow in Fractures and Matrix (advection)</li> <li>• Gas Flow in Fractures and Matrix (advection and diffusion)</li> <li>• Fluid and Energy Transfer Between Fracture and matrix</li> <li>• Interface Area Reduction by Fracture Saturation of Active Fracture Network</li> </ul>	(this is not for the LBT) heat flux horizontal boundaries, constant T top	3-D	DS Property Sets	TOUGH 2	SHT: Compare to Measured Temperatures at various locations around the single heater test heat source

Table 3-12. List of NFE Models, by Hierarchy, Showing Details Pertinent to Validation (Continued)

	Processes/ Equations	Boundary Conditions	Dimensionality	Range of Material Properties	Numerical Codes Used	Validation
Single Heater Test TH Model using DKM without AFM	<ul style="list-style-type: none"> <li>• Thermal Conduction</li> <li>• Thermal Convection</li> <li>• Thermal Diffusion</li> <li>• Liquid Flow in Fractures and Matrix (advection)</li> <li>• Gas Flow in Fractures and Matrix (advection and diffusion)</li> <li>• Fluid and Energy Transfer Between Fracture and matrix</li> <li>• Interface Area Reduction by Fracture Saturation of Active Fracture Network</li> </ul>	Discrete Heat Input onstant Property Boundaries (T, P, SI), Insulation BC that allowed for heat flow according to the insulation thermal properties but did not allow for vapor flow, no-flow boundary to both heat and mass transfer	3-D	TSPA-VA Base Case Property Set Median Kb Property Set Measured Local to the SHT	TOUGH2	SHT: Compare to Measured Temperatures at - various locations around the single heater test heat source
Single Heater Test TH Model using DKM without AFM	(same as above)	Boundaries horizontal: 52.5 - 62.6 m, adiabatic, imperm. Upper-mtn surface and WT: fixed T, P, S.liquid, RH	3-D	$K_f$ $9.84 \times 10^{-10} \text{ m}^2$ $K_m$ $4.07 \times 10^{-18} \text{ m}^2$ Therm cond 1.67 W/m-K dry, 2.1 W/m- K wet	NUFT	SHT
Single Heater Test TH Model using ECM without AFM	Thermal conduction Thermal diffusion Thermal convection Fluid flow in porous media	Boundaries horizontal: 52.5-62.6 m, adiabatic, imperp. Upper-mtn surface and WT: fixed T, P, S.liquid, RH	3-D	$K_b$ $1.22 \times 10^{-13} \text{ m}^2$ , $K_f$ $9.84 \times 10^{-10} \text{ m}^2$ $K_m$ $4.07 \times 10^{-18} \text{ m}^2$ Therm cond 1.67 W/m-K dry, 2.1 W/m- K wet	NUFT	SHT

Table 3-12. List of NFE Models, by Hierarchy, Showing Details Pertinent to Validation (Continued)

	Processes/ Equations	Boundary Conditions	Dimensionality	Range of Material Properties	Numerical Codes Used	Validation
ECM	Equivalent Continuum	Constant T, S.liquid outside heated zone	2-D	Grouse Canyon tuff measured properties	predecessor code to NUFT	G-Tunnel
DFM	Discrete Fracture	Constant T, S.liquid outside heated zone	2-D	Grouse Canyon tuff measured properties	predecessor code to NUFT	G-Tunnel

There are essentially four TH process models. They are based on model approaches, and as shown on Figure 3-47 include the Dual Permeability Model (DKM) with and without inclusion of the AFM, the equivalent-continuum model (ECM), and the DFM. The DKM models treat the matrix and fractures as separate continua. The models provide for equilibrium between the two continua and the AFM allows adjustment to the amount of interaction between the continua. The ECM model treats the matrix and fractures as a single continuum with properties that reflect the bulk average (thus the name Equivalent Continuum). The DFM accounts for disequilibrium between the fractures and matrix. As such, it treats the fractures discretely and must, therefore, either address fractures as single fractures or as repeatable sets. In theory each fracture could be handled separately. However, this is not practical computationally nor based on limits from site characterization regarding individual fracture properties. Each of these models have been evaluated in field testing. However, the DKM with AFM is the model which has been more completely tested and therefore will be the focus of the validation discussion here.

A number of simulations were conducted in support of the NFE PMR. The *Thermal Test AMR* included four thermal-hydrological models (one each for the LBT and SHT and two for the DST). The *THC Process AMR* also included a thermal-hydrological submodel as an integral part of the THC analysis. Finally, the MSTHM shared by the EBS PMR and the NFE PMR included a TH submodel. Each of these six models used a similar base case set of TH properties, although the sets have slightly different designators. For the purpose of determining the sensitivity of thermal and hydrological response of the field tests to selected thermal and hydrological properties, some of these models were run with modified TH property sets. Table 3-13 summarizes the property sets used in each model.

Two abstracted TH analyses (multi-scale and MS) as reported in this PMR are based on the DKM with AFM TH process model using the NUFT (LLNL 1999) and TOUGH2 (LBNL 2000) codes respectively. The first, discussed in Sections 3.2 and 3.6.4.1, is the multi-scale abstraction that uses the NUFT code as the analytical tool, and is reported in the *THC Abstraction AMR*. The second, discussed in Sections 3.3 and 3.6.4.2, was the TH part of the THC analysis, which relied on the TOUGH2 code for the numerical analyses or solutions, as reported in the *THC Process AMR*. These analyses were conducted under QA procedure AP-3.10Q.

The THC process model (CRWMS M&O 2000b) includes both kinetics and thermodynamic submodels. The model utilizes the TOUGHREACT (LBNL 1999) code. Two model options were included, a complete mineral and chemical assemblage model and a model with a more limited suite of chemical and mineral assemblages. The validation status of these models is discussed in Section 3.6.4.2. The abstraction of the THC process model is discussed in detail in the Abstraction of Drift-Scale Coupled Processes (DSCP) AMR (CRWMS M&O 2000c).

There are two basic THM models. The first is one that models the processes as being an inelastic continuum that uses various constitutive relationships (e.g. ubiquitous joint or compliant joint) to describe the deformation of blocks and joints. FLAC (Itasca 1996), is one code implementing the continuum model that has been used in reports. The other model is the Discrete Joint Model or Distinct Element Model which uses deformable (elastic or plastic) blocks and various constitutive relationships for the behavior. This model utilizes distinct block elements (thus the name) which allows displacements along fractures. The model validation

efforts discussed in this report were for the 3-D distinct element model with the 3DEC code. There are no THM abstraction models at this time.

Table 3-13. Thermal-Hydrological Property Sets Used in TH Models in the NFE PMR

Base Case (CRWMS M&O 2000f, TH Property Set from UZ Flow and Transport Model)					
Thermal Test AMR (CRWMS M&O 2000a)				THC Process AMR (CRWMS M&O 2000b): Inputs from the CPM (CRWMS 2000n)	Multiscale TH Model AMR (CRWMS M&O 2000k): DS
SHT (TOUGH2): DS	DST (TOUGH2): DS/AFM-UZ99	DST (NUFT): DS	LBT (NUFT): DS		
Sensitivity Cases (CRWMS M&O 2000a)					
TSPA-VA: TH Property set from Total System Performance Assessment - Viability Assessment Case	DKM-TT99: Dual Permeability (matrix and fracture) property set from the thermal test region	MS Property Set: only the bulk fracture permeability differs from base case	MS Property Set: only the bulk fracture permeability differs from base case		
Single Heater Test Median Bulk Permeability (Median $k_b$ ): Based on Air-k measurements from SHT		MS Local Thermal Conductivity: Different thermal conductivity from MS property set	MS Local Thermal Conductivity: Different thermal conductivity from MS property set		
		Conduction Only: Hydrologic properties not included	Conduction Only: Hydrologic properties not included		
			MS Higher Fracture Permeability): Higher bulk fracture permeability by two orders of magnitude		

Source: Modified from CRWMS M&O 2000a, Table 3.

Validation of the process models was performed by comparison of model results with field and laboratory tests, as specified in AP-3.10Q, Section 5.3b. The results of the field tests are discussed in the *Thermal Test*, also prepared under controls of AP-3.10Q. This section discusses the results of comparisons of the models with those field-test results. There is repetition in that each model will be compared to essentially the same set of results from the field tests.

Validation of models (perhaps more appropriately described as confidence building) is provided by first building an understanding of the processes to be modeled through a combination of laboratory and field experiments, as well as considerations of basic principles, and then by testing these models.

The assessment of the performance of a high-level nuclear waste geological repository requires prediction of the performance of waste package materials, and the flow and transport characteristics of radionuclides from the emplacement drifts to the accessible environment. Those predictions require information regarding the THCM conditions within the emplacement drift and the region between the drifts and the accessible environment, as functions of time and space. Model analyses are needed in order to predict the THCM conditions in a repository for its entire life span. Test data are needed to enhance confidence of those model analyses.

A series of tests have been designed and conducted in order to build confidence in the models and the parameters used as inputs to those models. These tests were designed to address geometric-scale issues, as well as issues of rates of NF processes and representative geologic units. Table 3-14 summarizes the scale and purposes of the tests.

The testing program thus included core-sized laboratory tests to determine property values, and to determine physical processes for laboratory samples that were mostly focused on processes in matrix or single fracture and typically of relatively short duration. Advantages of the laboratory tests include the ability to control laboratory conditions.

The second scale of tests were block or bench-scale test on blocks of about 1 m x 1 m x 0.5 m size. These tests allowed the response to be tested on both single and multiple fractures, as well as larger matrix sized. These tests provided for longer duration, with stresses applied to the faces of the block, with somewhat diminished boundary controls.

The third scale test was conducted on a large-block (3 m x 3 m x 4.5 m) excavated on an outcrop at Fran Ridge (see Figure 3-48). This LBT was of sufficient size to include at least 100 fractures and allowed processes of THMC to be tested, including interconnections of fracture systems. The boundaries did not include stress, nor active controls on heat losses. They did include insulation and monitoring of heat loss from the sides of the block and temperature control of the top. This test was of sufficient size to provide for longer duration testing with heat-flux rates somewhat comparable to possible repository rates. Due to its surface location, the test was not intended to simulate the actual responses expected in YM. Rather, it was to identify coupled processes, and test conceptual models of those processes in a representative rock mass.

The fourth scale of tests was in situ, small and large-scale tests performed underground in one of the lesser host rock units. These tests (SHT and DST) allowed testing of physical processes and models under in situ conditions and included sufficient size to test multiple fractures and interconnections. The SHT involved a smaller rock region than the DST, and included only a single heater. Thus, the temporal and spatial scale was not sufficient to allow all coupled processes to be tested at scales representative of a potential repository. However, the duration of the SHT allowed sufficient volume of rock to be elevated in temperature to consider THC effects, and the test successfully captured mobilized water in instrument boreholes. The test also

measured in situ rock thermal and mechanical properties for the first time in the repository setting.

The DST is a large-scale (1,500 m<sup>2</sup>) and long-duration (four years heating, four years cooling) test in which the heating rate, size of the test and duration allow THC coupling to be tested at appropriate scales.

The size of the DST provides for an assessment to be made of heterogeneity effects on THC responses. Three measurement arrays perpendicular to the DST axis, in addition to longitudinal measurements, provide for this assessment.

Table 3-14. Test Strategy

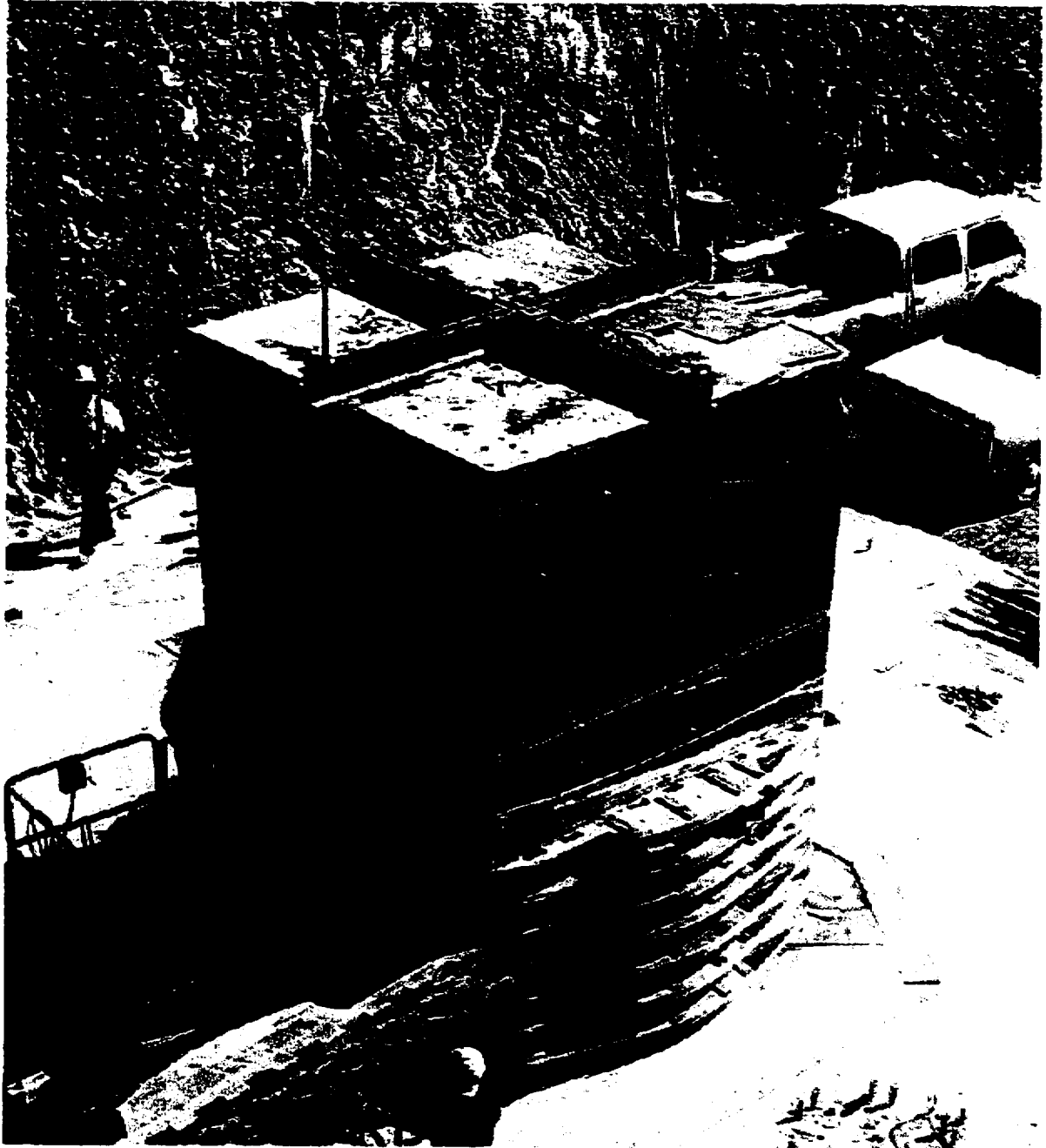
Scale	Description	Purpose
Core	Core up to 1 ft. Hrs. to days (some long-term)	Property Measurements Matrix Processes Single-Fracture Processes Limited Model Testing
Bench	1 ft. to 1 m blocks	Multiple Fracture Processes Fracture Interconnectivity Phenomena
Outcrop	3 to 5 m block, ~ 2 yr.	Coupled Processes
Small in situ Heater	Up to ~ 100 m <sup>2</sup> , ~ 1 yr.	Site characterization In Situ Hydrothermal/Geochemical/Geomechanical Responses
Large in situ Heater	Up to 1,500 m <sup>2</sup> , ~ 8 yr.	Scaling Effects, Natural Heterogeneity Impacts
Internal Drifts	Repository-Scale Monitoring 50 – 200 yr.	Performance Confirmation
	Analogs 10,000 years Large-Scale	Long-Term Coupled Effects

Modified From: NWTRB 1992 Denver

As depicted in Table 3-14, Repository-Scale monitoring is the ultimate test of performance against which models must be judged. These tests will be based on monitoring the response to actual emplaced waste, where the scale issues will be addressed directly. However, the duration of the response monitored, even at repository scale, will be very short, perhaps 50-200 yr, in comparison to the period of active evolution of the NFE (1,000 to 10,000-yr).

Therefore, even repository monitoring can provide testing or confidence in only part of the temporal regime covered by the models.

Testing of the models ability to accurately predict performance over these large time frames can only be provided by comparisons with geologic analog sites, where the duration of THCM processes are appropriate for repository time-scales.



Source: CRWMS M&O 2000a, Figure 10.

Figure 3-48. Photograph of Large Block Test Site

Natural analogs provide opportunities for testing models and building understanding of thermally coupled processes by assessing data from fossil hydrothermal systems, by observing ongoing processes in geothermal fields, and by using data from geothermal systems to test and build confidence in numerical modeling codes, and in thermodynamic and kinetic databases.

- 1) The challenge is first to find analogs that are sufficiently representative of the repository processes and characteristics that conclusions are not misleading. Murphy and Pabalan (1994, pp. 4-28) point out as an example of this challenge that the variations in temperature for the repository environment are relatively short duration compared "...to metamorphic or major hydrothermal systems, but..." long duration compared to most volcanic or hyababyssal systems.
- 2) Second, the challenge is to find analogs for which the geologic history, (environmental conditions with time) and processes are well understood.

If analogs meeting these criteria are found, they can provide confidence building in the long-term prediction capability of the models.

Because the actual coupled processes are no longer active, except for the analogs such as hydrothermal or geothermal fields, the analyses are based on interpretations of the minerals present and fracture systems present, which are essentially the permanent or long-lived effects of the coupled processes. This section focuses on the field-scale tests and natural-analog analyses that are used to build confidence in the models. The laboratory tests used to develop the models and provide property values for use in the models are covered in the individual model AMRs, and in past reports (e.g., Hardin and Chestnut 1997; Hardin 1998).

The field validation tests are described below in Section 3.6.1 in order of scale, following the general philosophy depicted in Table 3-14. The natural-analog studies are then discussed in Section 3.6.2. Section 3.6.3 discusses several laboratory scale tests. Finally, Section 3.6.4 summarizes the validation status of the TH, THC, and THM models.

### **3.6.1 Model Confidence Building through Field Thermal Testing**

The ESF thermal tests and the LBT will be used to help specify appropriate conceptual flow models, thermal perturbations to hydrological flow properties, coupled-process data specifications, and assessments of implementation of ambient-flow hydrologic properties in thermally driven models. Thermal-hydrological simulation of the field thermal tests were conducted using both MS and Multi-Scale models, utilizing the DS property set and/or the mountain-scale property set, from the UZ F&T Model for comparative analyses with the measured data from the tests.

Three field thermal tests are being, or have been, conducted to provide data for enhancing the confidence of the model analyses. Those tests are the LBT at Fran Ridge, the Single Heater Test (SHT) and the DST. Both SHT and DST are conducted at Alcove 5 of the ESF. A detailed description of the LBT can be found in LBT Status Report (Wilder et al. 1997, Section 2 and 4). A detailed description of the SHT can be found in *Single Heater Test Status Report* (CRWMS M&O 1997a, Section 3). Finally, the detail description of the DST can be found in *Drift Scale*

*Test Design and Forecast Results* (CRWMS M&O 1997b, Section 3). A brief description of these tests will be provided here to facilitate discussion of the test results.

The primary purposes of these field thermal tests are to provide data regarding the coupled TMHC processes, so that they can be used to build confidence in the TH model, the THC model, and the THM model, which will be used to predict the performance of a repository (CRWMS M&O 1997a, p. 1-1; CRWMS M&O 1997b, p. 1-1; and Wilder et al. 1997, pp. 3-4). It was understood that the test regions of these tests are relatively small compared with the size of the potential repository, and that the major part of the potential repository will not reside in the rock unit in which these tests were conducted. Therefore, the primary purpose of these tests was not for testing the properties of the host-rock unit of much of the potential repository, but rather to gain understanding of the processes that may occur in a repository. Then the processes can be modeled with the appropriate property sets determined for the potential repository.

A primary objective of these tests was to determine whether the conceptual and mathematical models properly account for the important physical processes and phenomena, and to gain understanding of the processes that may occur in a repository. The tests were designed to accomplish this objective by identifying the hypotheses and postulations of how the NF system would respond to emplacement of waste, specifically from the heat generated by the waste, and then designing the tests to monitor the responses hypothesized.

Beyond testing hypotheses, the tests also provide data by which it can be determined whether any important physical processes were overlooked in the conceptual and mathematical models or improperly emphasized. Once assurance is gained that the models properly incorporate the important physical processes, then confidence in their ability to predict repository performance is increased. Once model confidence is established and properties are obtained, the appropriateness of the PA calculations can be established through use of measured and inversely-modeled property sets for specific locations in the potential repository. Thus, the second objective of the field tests is to provide a means to test the inversely-modeled property sets for use in the repository performance models.

The host rock for all three field thermal tests: the LBT, the Single Heater Test and the Drift Scale Test is the middle nonlithophysal unit of the Topopah Spring welded tuff unit (TSw). However, the repository emplacement area will be located in three units of the Topopah Spring welded tuff. These are described, in downward sequence, as the middle nonlithophysal (Ttpmn), the lower lithophysal (Ttpll), and the lower nonlithophysal (Ttpln) units. In both the VA design and the EDA-II design, a majority (approximately 70%) of the emplacement area will be in the lower lithophysal unit. The characteristics of the three TSw layers differ primarily because of the nature and abundance of lithophysae and the nature and frequency of fracturing. Though the physical and chemical coupled processes are universal and independent of the geological units, the different fracture and lithophysal properties of the lower lithophysal unit may give rise to thermal-hydrological (TH) behavior that differs from that observed in the LBT, SHT, and DST. In order to have confidence in our ability to predict the TH response of the potential repository to heating, a thermal test in the lower lithophysal unit is being designed.

The ESF Main Drift is largely in the Ttpmn with only the upper part of the Ttpll exposed near the South Ramp. Consequently, the database on the Ttpmn, compared to that of Ttpll and

Tptpln, is extensive, having been derived both from surface-based drilling and observations, mapping, and testing in the ESF. The recent excavation of the Enhanced Characterization of the Repository Block (the Cross Drift) has provided access to all three Topopah Spring units. Mapping along the Cross Drift shows that in the nonlithophysal units, the density of fractures up to several meters in length is high, whereas in the lithophysal unit, there are few fractures that are longer than one meter, though density of fractures less than one meter appears similar to that of the middle nonlithophysal unit. Further, lithophysal cavities of size ranging from 15 cm to 100 cm abound in the lower lithophysal unit. While the mapping of the Cross Drift is complete, hydrological tests to characterize the Tptpl are still in their initial phase. The tests in progress include monitoring downward water movement from injection boreholes in Alcove 8 in the Cross Drift to the ESF cross-over point in Niche 3; the investigation of seepage threshold in Niche 5; and systematic characterization of seepage characteristics in boreholes at 30-m intervals.

The Cross Drift Thermal Test (CDTT) is currently being designed to begin construction in the Tptpl at the start of FY2001. The main objectives of CDTT is to investigate the premise that heat-mobilized pore water will shed/drain between emplacement drifts to below the repository horizon, and to test the premise that liquid water can penetrate through zones/regions at or above boiling temperature. The design uses five (5-meter-long) heaters installed in parallel boreholes and is patterned to test the pillar drainage concept for the EDA-II design. Numerical modeling for the design of CDTT makes use of the currently available Tptpl properties based on surface based boreholes. Data from hydrological testing of the Tptpl in the Cross Drift will be incorporated in the predictive modeling of the CDTT as they become available.

The field-thermal test data included in this PMR have been referenced in the following two AMRs: *THC Process AMR* (CRWMS M&O 2000b) and *Thermal Test AMR* (CRWMS M&O 2000a). This PMR summarizes the field-thermal test data and the THMC processes that those data represent.

### **3.6.1.1 Large-Block Test**

The primary purpose of the LBT was to investigate the coupled TMHC processes in a controlled one-dimensional heating condition so that the test results can be readily compared with model calculations. Comparison of the test results with model calculations will enhance the confidence of the model. The description of the LBT can be found in Large-Block Test Status Report (Wilder et al. 1997). A free-standing 3 x 3 x 4.5 m square column of Topopah Spring Tuff was isolated at the outcrop at Fran Ridge, Nevada. The rock-type of the block was the same as the middle non-lithophysal unit of the Topopah Spring tuff in the potential repository horizon in Yucca Mountain. Preconstruction characterization and pre-test scoping model calculations indicated that the fracture characteristics, bulk permeability, the initial moisture content, and the size of the block are suitable for testing the coupled TMHC processes. During the construction, small blocks of the rock adjacent to the large block were collected for tests in the laboratory. The mineralogical composition of the small blocks, especially the secondary minerals in the fractures, will serve as a baseline of mineralogy. The mineralogical baseline can be used to investigate the chemical processes due to heating. Fractures in the block were mapped on the five exposed surfaces and in boreholes. Five heaters were installed in the block to form a horizontal heater plane at about 2.743 m from the top. Instruments were installed in boreholes to

measure temperature, gas pressure, relative humidity, moisture content (using neutron logging), and deformations. In addition, instruments installed on the block-surface include electrodes for electrical-resistance tomography, fracture gauges, and resistance-temperature devices (RTD) to monitor the near-surface temperature gradients. Labeled native microbes were introduced into the heater holes and two vertical holes in the block so that their survivability and migration could be studied. Four observation holes were constructed near the bottom of the block to conduct qualitative observations of fracture flows and microbial migrations. Coupons of candidate waste package materials were placed at designated locations within the block. The four vertical sides of the block were coated with a moisture-barrier layer, then covered with three layers of insulation: (from inside outward, Ultratemp boards, fiberglass, and reflexic). Water vapor was allowed to leave the block through the top. A heat-exchange unit was installed on the top to control the top temperature. Wilder et al. (1997, Section 4.0) plotted the location of the boreholes in the LBT (Figure 3-49).

The heaters were energized to full power (450 W each) on February 28, 1997 (CRWMS M&O 2000a, Section 6.1.4). The temperature on the top was allowed to rise until it reached 60°C, then the heat-exchange unit was turned on to maintain the 60° temperature at the top of the block. When the temperature near the heater horizon reached 140°C, the heater-power was adjusted to keep the temperature between 135 and 140°C. The heating phase of the LBT was terminated on March 10, 1998, and monitoring of the LBT was terminated on September 30, 1998 (CRWMS M&O 2000a, Section 6.1.4). Cores have been collected after the test. Analyses of the post-test cores for assessing the effects of heating on the mechanical, hydrological, and mineralogical characteristics of the rock are still on-going.

A small part of the LBT results has been included in the *Thermal Test AMR* for comparing with model predictions (CRWMS M&O 2000a, Sections 6.2.4, 6.4.4, and 6.5.4). The bulk of the LBT results are presented here to facilitate discussions of the TMHC processes.

#### **3.6.1.1.1 Temperature Distribution in the Block**

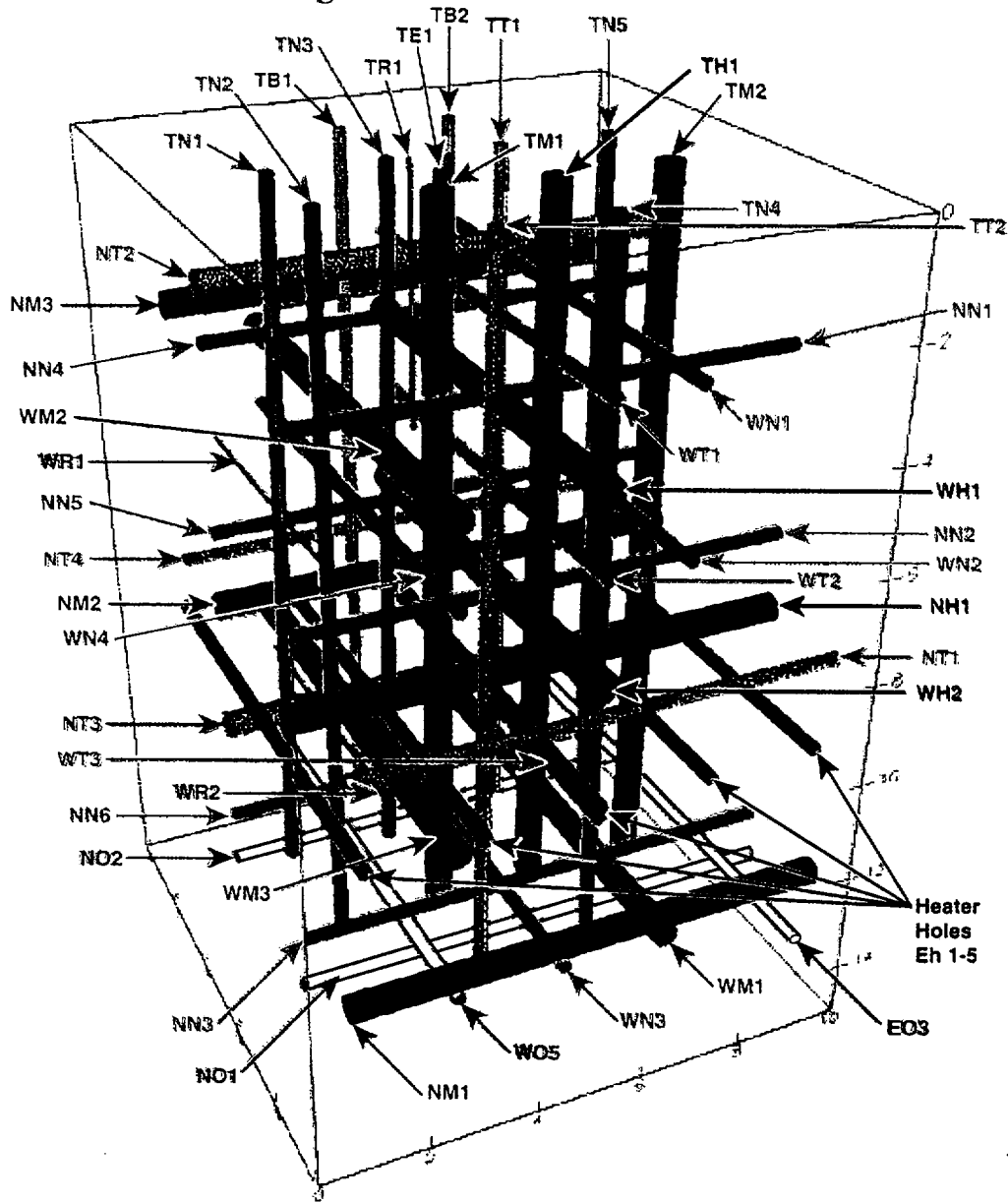
The temperature in the block was measured along two vertical holes (TT1 and TT2) and seven horizontal holes (NT1 through 4 and WT1 through 3). In each hole, the temperature was measured every 20 cm. Only a small part of the measured temperature data will be shown in this report to facilitate discussions. The sensors in the two vertical boreholes, located nearest to the heater horizon, were designated TT1-14 and TT2-14, for the TT1 and TT2 boreholes, respectively. Figures 3-50 and 3-51 show the highest temperature, measured along the two vertical holes, TT1 and TT2 respectively, as a function of time for the entire test history. The downward spikes at 552 hour, 1,036 hour, 3,802 hour in both figures were due to short periods of power outages. Those short power outages did not have significant impact on heating of the block. The heaters were turned off on March 10, 1998 (8,999.5 hour). The temperature at TT1-14 was about 15°C greater than that at TT2-14. This was probably due to two causes: (1) TT2 was closer to the edge of the block than TT1, and therefore influenced more by heat loss from the block, and (2) due to the difference in total depth of the two vertical holes, TT2-14 is 8.2 cm below the heater horizon, whereas TT1-14 is 2.1 cm below. The temperature drop at TT1-14 at 2,525 hour and the subsequent temperature fluctuations at both TT1-14 and TT2-14 (8 cm below heater plane) were probably caused by thermal-hydrological events, which will be discussed later.

Figures 3-52 and 3-53 show examples of temperature variations along the horizontal RTD holes NT3 and WT3. The data gap in the curves for 9/10/97 and 10/24/97 was due to malfunction of RTD#6 in WT3. Sensor number RTD#14 was located at about 12.8 cm from the collar in each of the horizontal holes. This is one of the reasons why the temperature at RTD#14 was lower than the others in the same hole, as shown in those figures. RTD#1 in each one of the horizontal holes was located at about 30.5 cm from the opposite block surface. The temperatures in WT3 show greater heat loss at the block surfaces than that in NT3. It is generally true that the temperature variation in an east-west horizontal hole was greater than that in a north-south hole. Nevertheless, temperatures in the horizontal holes show that the block was heated fairly one-dimensionally.

### 3.6.1.1.2 Boiling of Pore Water

Temperature measured just below the heater plane by sensor RTD-TT1-14 is shown in Figure 3-50. The relatively flat region at a temperature of about 97°C in TT1-14 between 922 and 1,127 hours (Figure 3-50) was probably caused by the balance of energy from the heaters and the energy required to evaporate pore water in proximity to RTD TT1-14. In TT2-14 (8 cm below the heater plane Figure 3-51), the relatively flat temperature occurred between 1,907 and 2,647 hours, at a temperature of about 98°C. If the flat temperature-time curve was indeed caused by evaporation, the longer duration of the flat temperature region at TT2-14 may be caused by either a greater amount of pore water to be evaporated or a slightly slower heating rate at TT2-14 than at TT1-14. Hole #TT2 is closer to the edge of the block than #TT1; therefore, greater heat loss in the block-sides may have caused the slower heating rate at the RTDs in TT-2. The temperature at which the flat temperature-time curve occurs relates to the boiling point of water. The measured temperatures from the RTDs at those two locations were accurate to within 0.1°C. These results indicate that the boiling point of the pore water at TT1-14 was greater than that at TT2-14 by about 1°C (97°C vs. 98°C). The difference in the boiling point of water may be due to several factors, including differences in the transmittal of barometric pressure, the suction potential of the pores, the difference in ionic concentration in the pore water, or possibly different fracture spacing. Based on the Steam Table (Keenan et al. 1969), the boiling point of pure water at the elevation of the LBT is 96.6° C. The boiling point of the water in the block, inferred by the measured temperature, was slightly greater than that of pure water. This is probably due to the suction potential in the pores, and the ionic concentration in the water.

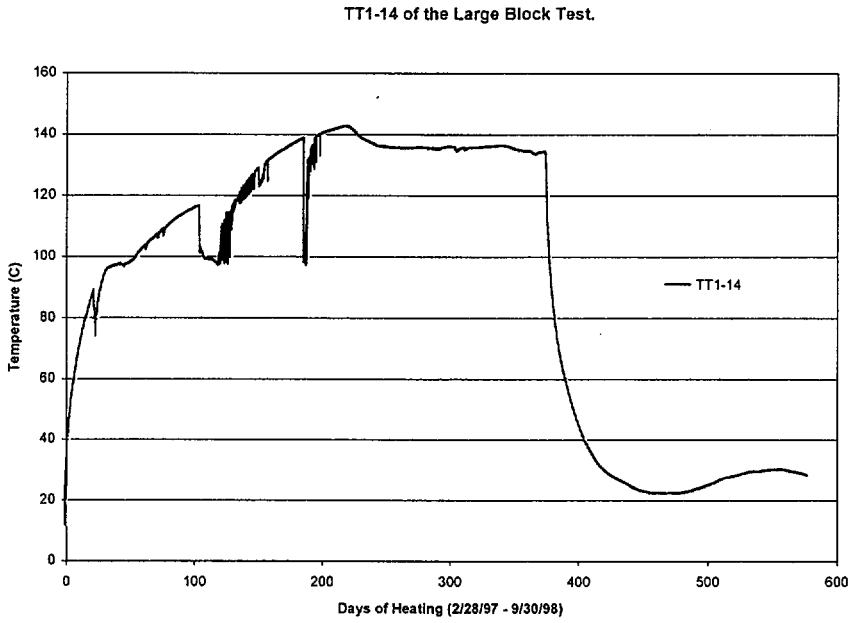
### Large Block Test Instrument Holes



Source: Wilder et al. 1997

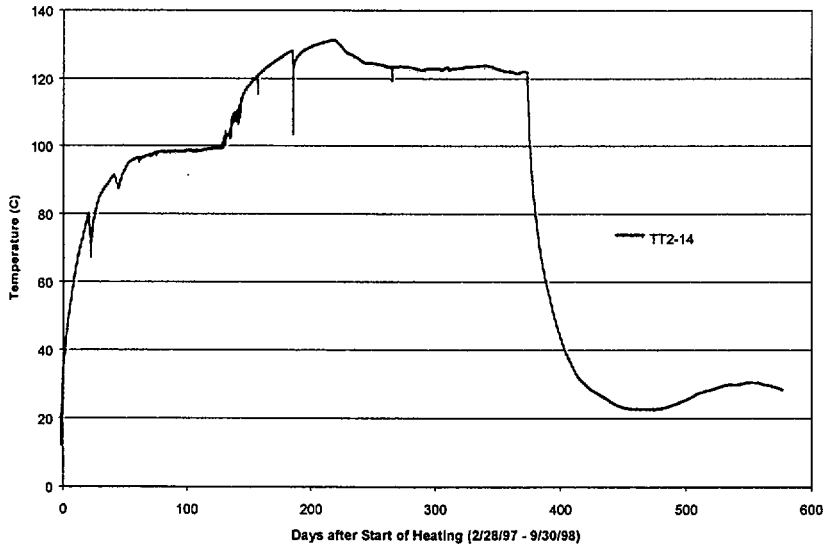
NOTE: The first letter for each hole refers to the collar location (top, west, etc.). The second letter refers to the hole function: Temperature, Neutron logging, Hydrology, Observation, Mechanical, REKA (thermal properties), Biology, and electrical-resistance tomography (ERT) (saturation). Heater holes are EH. The holes are also color coded.

Figure 3-49. LBT Instrument Holes



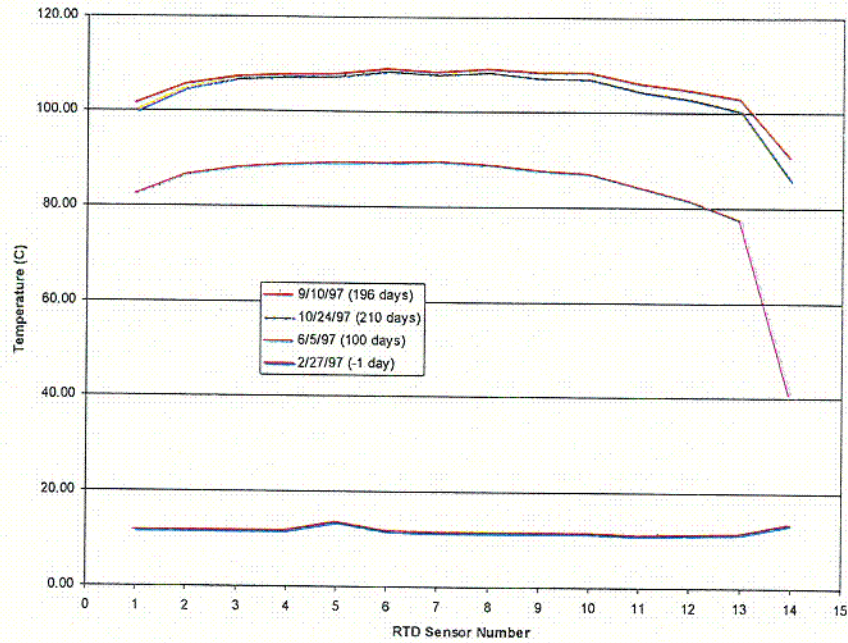
Source: Modified from CRWMS M&O 2000a, Figure 67

Figure 3-50. Temperature Measured in Borehole TT1-14 of the LBT as a Function of Elapsed Time



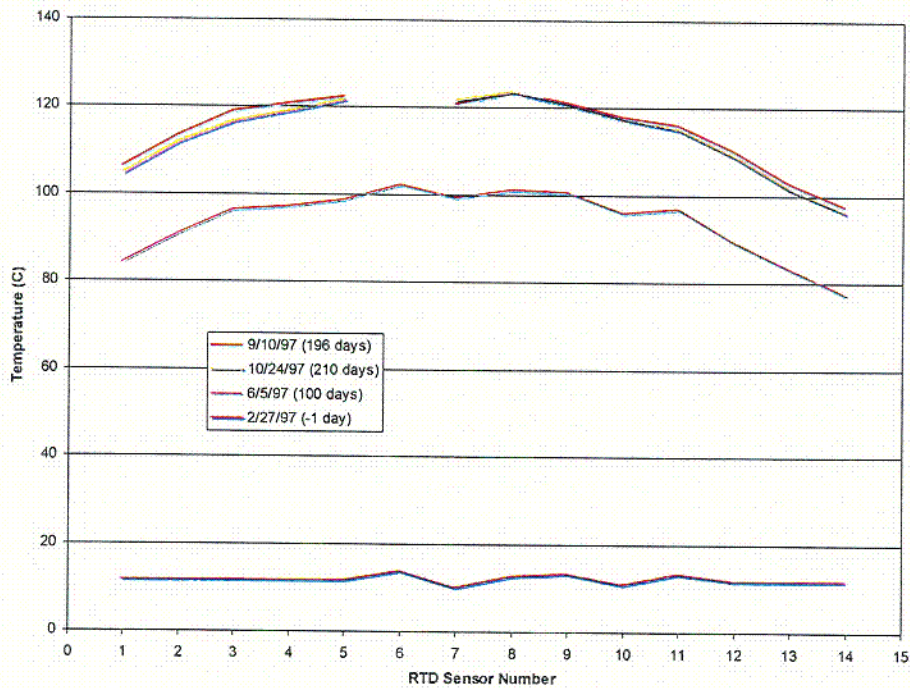
DTN: LL970803004244.036

Figure 3-51. Temperature Measured in Borehole TT2-14 of the LBT as a Function of Elapsed Time



DTN: LL970803004244.036

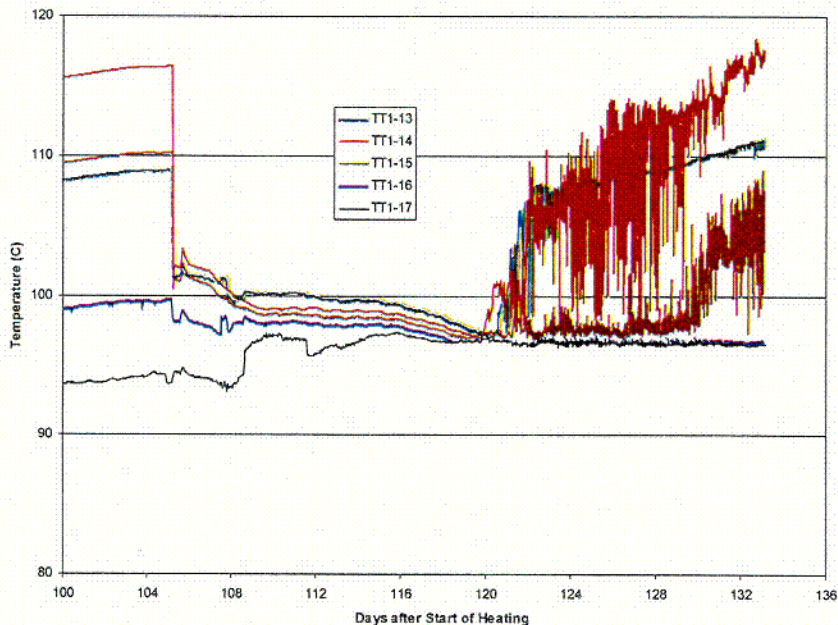
Figure 3-52. Snapshots of the Temperature in NT3 of the LBT at the Location of each RTD Sensor in the Borehole



DTN: LL9708030041244.036

Figure 3-53. Snapshots of the Temperature in WT3 of the LBT at the Location of each RTD Sensor in the Borehole

C-38



DTN: LL970803004244.036

Figure 3-54. Temperatures at Several RTDs in TT1 Show Fluctuations Due to a Thermal-Hydrological Event on June 13, 1997

### 3.6.1.1.3 Thermal-Hydrological Processes

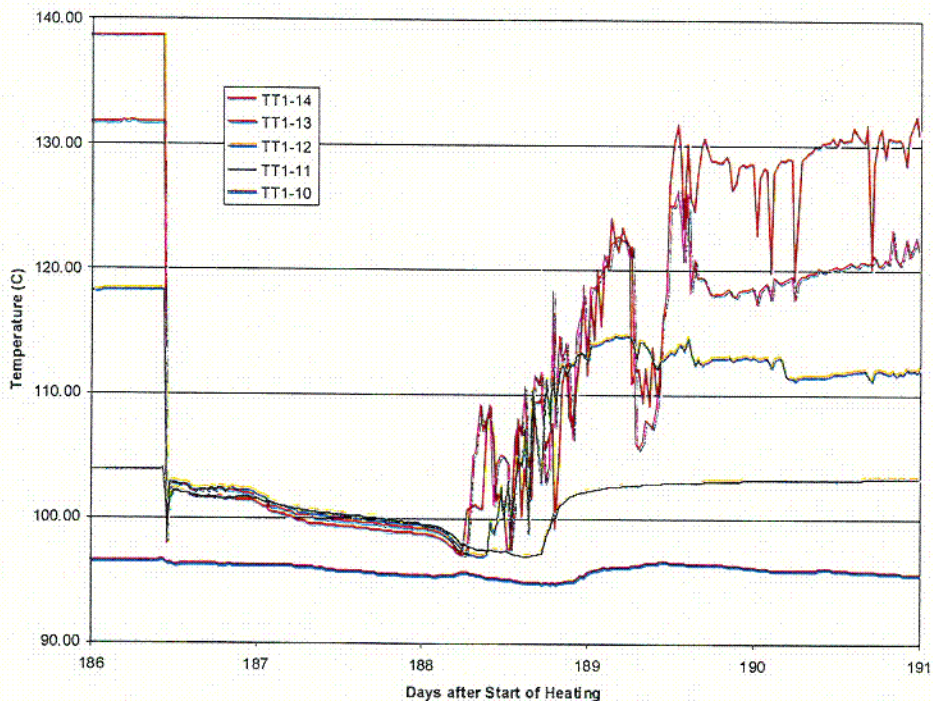
The sudden drops of temperature at TT1-14 at 105 days (6/13/97) and 186 days (9/2/97), as shown in Figure 3-50, and at TT2-14 at 186 days, as shown in Figure 3-51, and the subsequent temperature fluctuations, were probably caused by thermal-hydrological processes. Some examples of the temperature data affected by the thermal-hydrological events on 6/13/97 and 9/2/97 are shown in Figures 3-54 and 3-55, respectively. Figure 3-54 shows the temperatures measured at TT1-13 (18 cm above the heater plane) to TT1-17 (62 cm below the heater plane) between the 100 and 133 days. During the event, all of the temperatures converged to around the boiling temperature of the pore water, then the temperatures rose and the fluctuation started. At the onset of the event at 105 days, the above-boiling location experienced a rapid temperature drop to the boiling point. Nearly below-boiling locations increased temperature to the boiling point (TT1-17), indicative of heat transferred to this zone, possibly by hot water or vapor. Examining the temperature measured at other locations in TT1 indicates phenomena similar to those shown in this figure. The influence of this event reached to TT1-8 (118 cm above the heater plane). It appears that the temperature changes were related to hydrological processes, and the temperature fluctuations were caused by condensate refluxing. However, the causes of this thermal-hydrological event are not clear. The thermal-hydrological event and the subsequent temperature fluctuations may have been caused by rain water that infiltrated into the block, or the releasing of overheated water within the block. It was reported that a weather

6-39

station about 5 km southeast of Fran Ridge registered rain on 6/13/97, but there was no direct measurement of precipitation at Fran Ridge during that time.

Although the initiating event may have been rapid, temperatures persisted at near-boiling for about 16 days indicating persistence of water that moved to these locations. Then, initially-hot locations returned to their initial temperatures over a four week period, with a large amount of temperature fluctuation during the recovery, possibly due to rapid movement of the last residual water from place to place.

Figure 3-55 shows the temperatures measured at TT1-10 (78 cm above the heater plane) to TT1-14 (2 cm below the heater plane) from 186 to 192 days. Similar to the earlier event shown in Figure 3-54, the temperatures converged to the boiling point of water, held steady for some time, and then returned to pre-event temperatures over a period of time, with fluctuating temperatures during the recovery period. For this event, the durations of the hot temperature and recovery periods were only a few days each.



DTN: LL970803004244.036

Figure 3-55. Temperatures at Several RTDs in TT1 Show the Fluctuations Due to a Thermal-Hydrological Event on September 2, 1997.

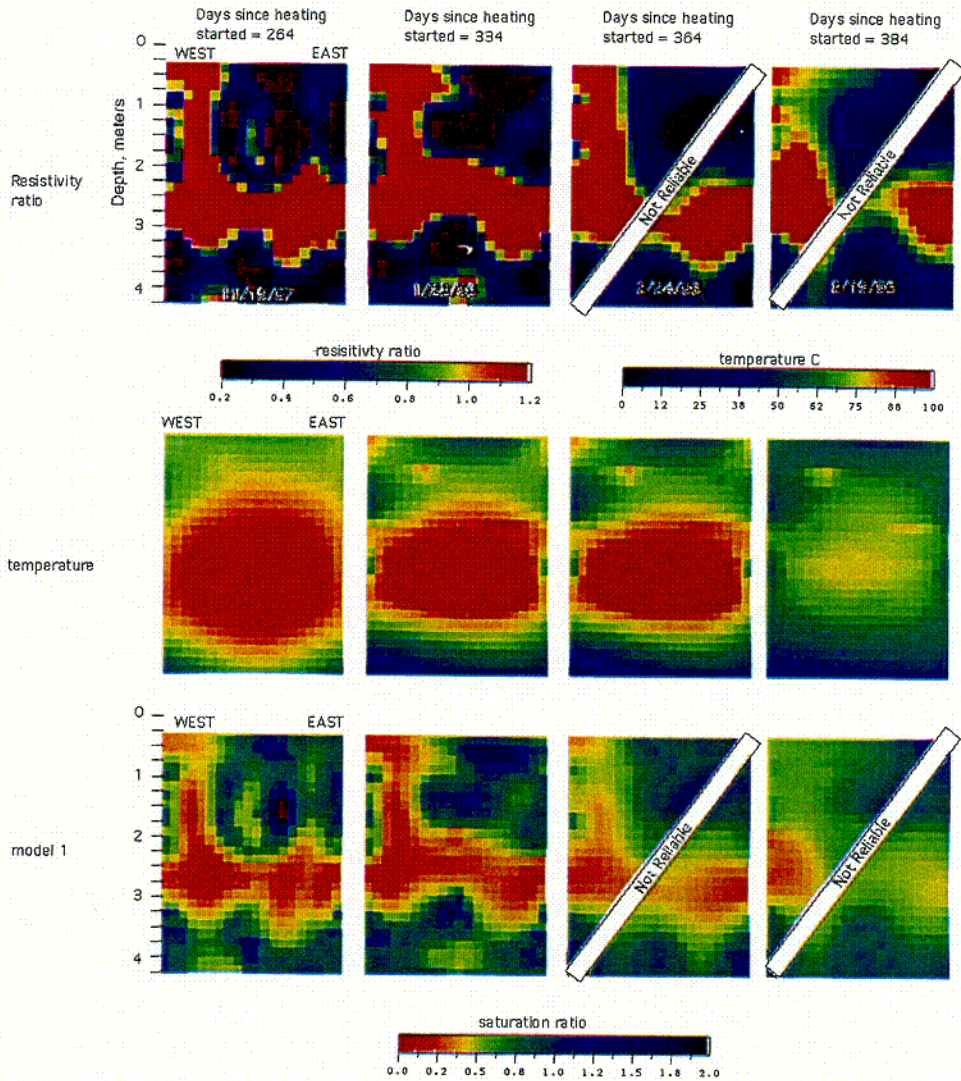
Examining the temperature measured at other locations for the September 2, 1997 event indicates that the temperatures decreased rapidly and simultaneously, and then converged to the boiling point of water. The influence of this event reached to the TT1-11 sensor location 58 cm above the heater plane. One of the causes of this event was clearly related to rain. It rained hard at Fran Ridge the night before this event. The fact that all of the measured temperatures along TT1

show a decrease in temperature at the onset of this event is also indicative of the influence of rain water on this event, and again, the temperature fluctuations were probably caused by condensate refluxing. The external rainwater may have influenced this event in two ways: (1) it triggered this event, and (2) it supplied enough water to sustain a condensate refluxing for about 2 days. The time period in which the temperatures stayed at the boiling point of water was about 2 weeks for the June 13, 1997 event, but only about 2 days for the September 2, 1997 event. This difference was probably due to more available heat in the block to evaporate the water more quickly, because more insulation was added to the block surfaces at about 125 days. It is also possible that the matrix of the block during the September 2, 1997 event had been dried out more than that during the June 13, 1997 event or that less water was involved in the event. The vertical extent of the disturbance was also less for the second event.

#### **3.6.1.1.4 Moisture Distribution**

Moisture distribution in the block was measured by two methods: ERT and neutron logging. The electrode configuration is shown in Figure 5 of Wilder et al. (1997). Figure 3-56 shows some examples of the ERT images in the East-West vertical plane of the LBT. The East-West vertical plane passes the middle of the block. The four columns of images represent ERT measurements on four dates. The three rows of images represent resistivity ratio, temperature, and saturation ratio, respectively. The resistivity is a function of both temperature and saturation. When the temperature field is independently measured, the resistivity ratio and temperature can be used to deduce the spatial distribution of saturation (the third row). In Figure 3-56, the resistivity ratio and the saturation ratio are with respect to the baseline data obtained before heating was started, on February 28, 1997. The heaters were turned off on March 10, 1998. The ramp-down of heater power was started on October 6, 1997, in order to keep a constant temperature in the block. So, the first three columns of the images in Figure 3-56 show the ERT obtained during the final stage of the heating period, when the block temperature was almost constant. The saturation-ratio images on November 19, 1997 and January 23, 1998 (the third row in Figure 3-56) show a dryout region at the heater horizon (centered at about 2.74 m from the top), and extended vertically near the west side of the block. The vertical dry zone may be related to one of the high-angle major fractures near the west side of the block (Wilder et al. 1997, Figure 2-10). There were no other major features in the saturation distribution, except one localized small region in each image, which shows increased moisture content. The saturation-ratio image on February 24, 1998 and March 19, 1998 seems to indicate that the dryness in the previous dryout zones was decreasing. However, there was no significant change in the moisture content in other locations. Field measurements indicate that due to the dryness on the block surface, the quality of the signals in the later ERTs was not as good as the earlier ones. Therefore, the apparent rewetting in the dryout zones may not be very reliable.

Neutron logging was conducted in five vertical holes and ten horizontal holes (six from the North side and four from the West side), as described in Wilder et al. (1997, Figures 4-1, 4-2, and 4-5). The data from one of the vertical neutron holes are presented below as an example of the variation of moisture distribution in the LBT due to the heating.



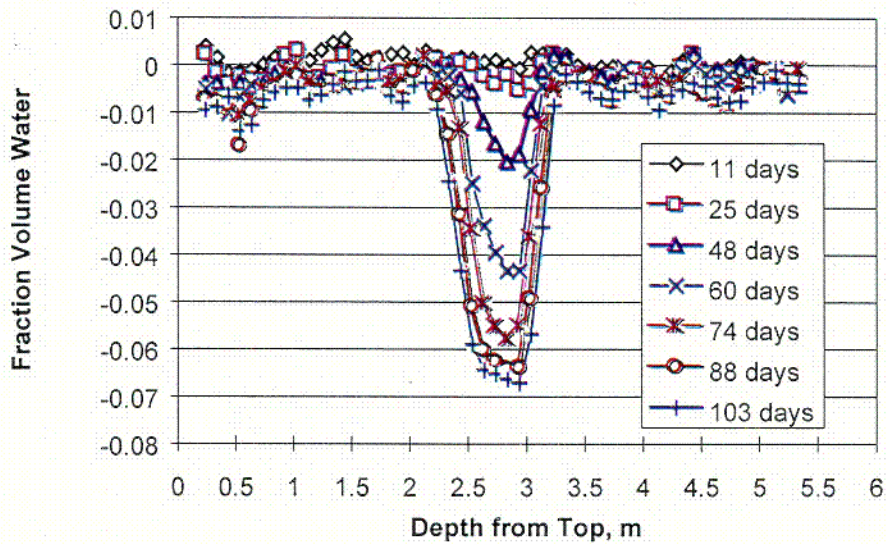
DTN: LL980913304244.072

Figure 3-56. Temperature and the Electrical-Resistance Tomograph of an East-West Cross Section of the LBT

Figures 3-57 and 3-58 show the difference of volume-fraction water content as measured along neutron hole TN3 on various days of heating. TN3 was the vertical neutron hole located closest to the middle of the block (Wilder et al. 1997, Figure 4-1). The zero volume-fraction water in these two figures means no difference from the pre-heat baseline data. These two figures clearly show development of a dry-out zone. The neutron data from other vertical neutron holes were similar to those shown here. The drying seemed to start in an area slightly below the heater horizon, which is about 2.74 m from the top. The maximum drying region then gradually extended below the heater horizon in most of the holes. In TN5, the maximum drying area extended above the heater horizon. In TN1 the maximum drying region extended both below and above the heater horizon. These variations may be caused by the heterogeneity in the block, however, they are relatively minor compared to the intensity and extension of the drying zone.

All of the neutron data along the vertical holes show that the width of the drying zone and extent of drying virtually did not change between the 334th and 361st days of heating. The absolute-volume-fraction moisture content in the driest region was about 0.85 to 1 percent.

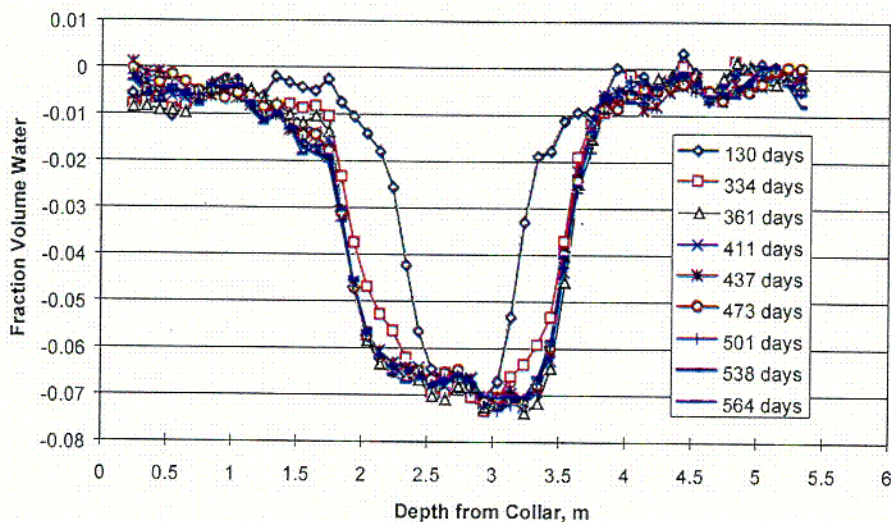
In summary, both ERT and neutron logging show that the heating created a significant dry out zone in the block. The width of this dryout zone ranged from 1.5 to 1.7 m. The ERT shows a localized vertical dryout region extending to the upper part of the block. This is not shown by the neutron data, probably due to the lack of a vertical neutron hole in that part of the block. Within the dryout zone, the drying could only reduce the moisture content to about 1 percent volume-fraction.



DTN: LL980919304244.075

Figure 3-57. Difference Volume-Fraction Water in TN3 of the LBT as a Function of Depth, up to 103 Days of Heating

C-47



DTN: LL980919304244.075

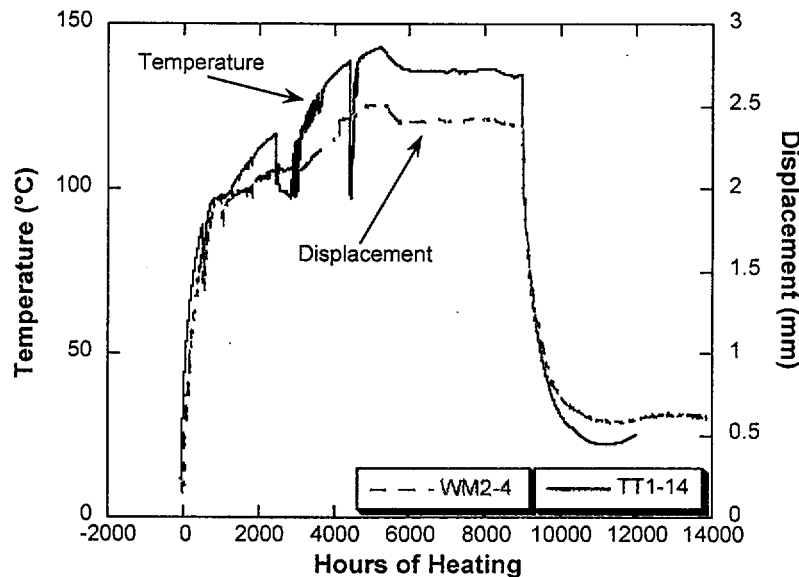
Figure 3-58. Difference Volume-Fraction Water in TN3 as a Function of Depth, from 103 to 565 Days of Heating

The labeled (double-drug resistant) native microbes were found in observation holes, about 1.5 m below the heater holes, during the heating phase of the LBT. This is an indication that microbes may have survived the heat, and liquid water flow below the heaters was able to facilitate the migration of the microbes. It is emphasized that this observation serves as an indication only because the microbial investigation was scoping in nature, and therefore, was non-Q.

### 3.6.1.1.5 Deformations in the Block

Deformations within the block were measured by multiple-point borehole extensometers (MPBXs), for bulk displacements within the block, and fracture gauges, for deformations across fractures on the block surfaces (Wilder et al. 1997, p. 19). Overall block deformations near the heater plane was closely correlated with temperature as shown in Figure 3-59. The MPBX measurements showed that the block experienced expansion in the upper half during the heating phase of the test. The surface fracture-gauge measurements showed that during the June 13, 1997 thermal hydrological event (Wilder et al. 1997, and Section 3.6.1.1.3 of this PMR) the horizontal fracture near the top of the block (at about 30 to 60 cm below the top) experienced opening of about 0.094 to 0.11 mm at the northern and eastern sides, and a 0.058 mm shear displacement on the western side. Those deformations may have changed the hydrological properties of the block.

c-43



DTN: LL970803104244.037

Source: CRWMS M&O 2000a, Figure 67

NOTE: Temperature sensor TT1-14 was located approximately in the center of the block, near the heater plane. Anomalies in the temperature at 2250 and 4400 hours were associated with weather disturbances and may indicate refluxing in the fractures. MPBX anchor WM2-4 monitored horizontal deformation approximately 3 m above the base of the block.

Figure 3-59. Thermal and Deformation History for the Large Block Test

### 3.6.1.1.6 Microbial Studies

The transport of bacteria in the LBT was also studied (Lin et al. 1998a). Two bacterial species, *Bacillus subtilis* and *Arthrobacter oxydans*, were isolated from the Yucca Mountain tuff. Natural mutants that can grow under the simultaneous presence of the two antibiotics, streptomycin and rifampicin, were selected from these species by laboratory procedures. The double-drug-resistant bacteria, which could be thus distinguished from the indigenous species, were injected into the five heater boreholes of the large block hours before heating was initiated. The temperature, as measured 5 cm above one of the heater boreholes, rose slowly and steadily over a matter of months to a maximum of 142°C. Samples were collected from the boreholes that were approximately 5 ft below the injection points. Double-drug-resistant bacteria were found in the collection boreholes nine months after injection. Surprisingly, they also appeared in the heater boreholes where the temperature had been ~ 140°C throughout much of the test. These bacteria appear to be the species that were injected. The number of double-drug-resistant bacteria that were identified in the collection boreholes increased with time. An apparent homogeneous distribution among the observation boreholes and heater boreholes suggests that a random

motion could be the pattern that the bacteria migrated in the block. These observations indicated the possibility of rapid bacterial transport in a thermally perturbed geologic setting.

#### **3.6.1.1.7 Post-Test Thermal-Mechanical Analysis**

Post-test characterization activities for the LBT consisted primarily of drilling/coring to provide boreholes and samples for post-test characterization of the block, and laboratory testing and analysis of core samples collected by the drilling/coring activity. A post-test analysis of rock mechanical properties was conducted in order to determine if elevated temperatures and high thermal gradients may have induced grain boundary scale microcracks in the tuff. This effect was expected to be the most pronounced near the borehole heaters where conditions were most extreme. Thermal micro cracking would contribute to the mechanical degradation of the rock, leading to a loss of compressive strength and a reduction in elastic modulus. A loss of mechanical strength in the rock surrounding nuclear waste canisters would have adverse consequences for repository performance. The purpose of this work was to ascertain if measurable mechanical degradation resulted around at least one of the heater boreholes during the LBT. Two suites of twelve samples were collected. One suite, consisting of cores from one of the heater boreholes, was never exposed to elevated temperatures. The other suite, taken from overcore of the same borehole, experienced the highest temperatures and thermal gradients attained during the LBT.

Results showed that no statistically significant differences in dry density, ultrasonic velocity, compressive strength or Young's modulus between the thermally-cycled overcore and non-thermally cycled heater core suites. The dry densities, ultrasonic velocities, uniaxial compressive strengths, and elastic moduli obtained for these specimens are also similar to those obtained for Topopah Spring tuff in other laboratory studies. No evidence was found that the tuff specimens were damaged in the LBT.

#### **3.6.1.1.8 Model Analysis of the Large Block Test Results**

The DKM with Active Fracture using the NUFT code was used to analyze the temperature and neutron data from the LBT (CRWMS M&O 2000a, Section 6.1.4). Both the DS property set and the mountain-scale property set were used in the analyses. The purpose of the model analyses was to identify a property set that would give a better prediction of the measured data. As mentioned before, the LBT was for understanding processes, not for testing properties. It was concluded from the comparison that both the DS property set and the mountain-scale property set provided generally good predictions of the measured temperature. Figure 3-60 (CRWMS M&O 2000a, Figure 65) shows one example of the comparison. The DS property set had a better statistical fit than the mountain-scale property set, as shown in Figure 3-61 (CRWMS M&O 2000a, Figure 66). Both property sets were able to capture the major characteristics of the measured temperature variations with time and space. Figure 3-62 (CRWMS M&O 2000a, Figure 67) shows one example of the comparison using the drift-scale property set. This means that the DKM model was able to simulate the processes that affected the measured temperatures. The model, using the DS property set, was able to capture the shape of the volume-fraction water versus depth curves measured by neutron logging quite well. But neither property set could predict the extent of drying, nor the increase of water content outside the drying zone, as illustrated by Figures 3-63 and 3-64 (CRWMS M&O 2000a, Figures 68 and 101). Again, from

the simulation of processes point of view, the DKM/AFM did well on the moisture distribution in the LBT. As expected, the model could not simulate the two thermal-hydrological events as discussed in Section 3.6.1.1.3 which were likely caused by localized events (in one or more fractures).

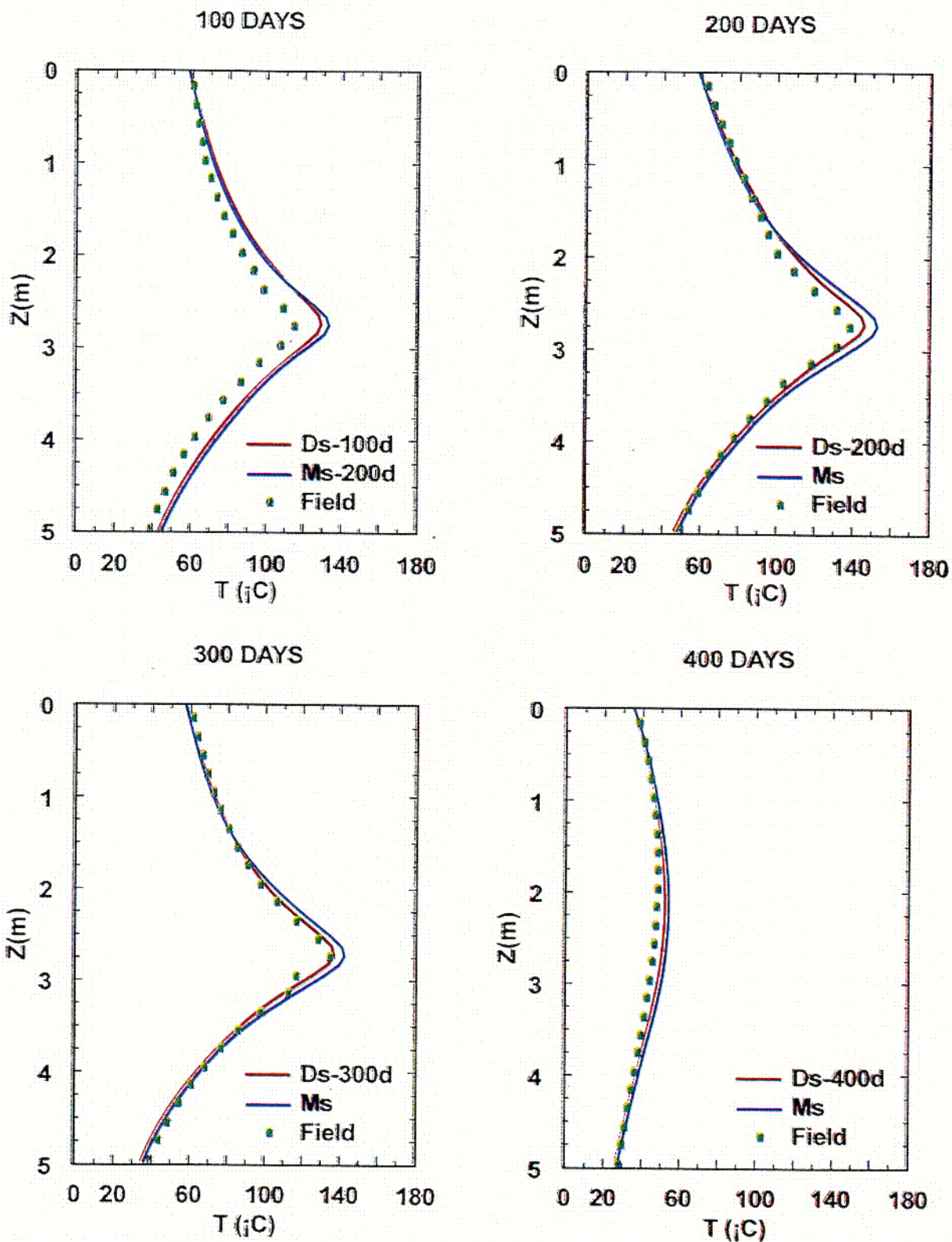
#### **3.6.1.1.9 The LBT Summary**

The LBT performed as designed. The heating of the block was close to the designed one-dimensional heating. A uniform dryout zone was created at the heater horizon. The moisture distributions above and below the dryout zone varied, probably due to the heterogeneity of the block. Refluxing of condensates, due to boiling at the heater horizon, were illustrated by the temperature fluctuations. The water, which was involved in at least one of two observed thermal hydrological events was supplied by rain. Monitoring and labeled microbes placed at the heater horizon indicate that the microbes may have survived the heat, and that liquid water flow below the heaters was able to facilitate the migration of the microbes. The microbes were found in the observation holes, about 1.5 m below the heater holes, during the heating phase of the LBT. There was some indication of coupling between block deformation and thermal-hydrological processes. The DKM/AFM calculated the processes that governed the general temperature and moisture distributions. Analyses of the posttest cores are still on-going. The results from the post test analyses are expected to provide insight to chemical processes in the LBT. At that time, some assessments of the coupled THCM processes can be performed.

#### **3.6.1.2 Single Heater Test**

This section includes experimentally determined data from the SHT (CRWMS M&O 1999d). This section will describe the SHT and explain how the data derived from the test have been used to help specify appropriate conceptual flow models, thermal perturbations to hydrologic-flow properties, coupled-process data specifications, and assessments of implementation of ambient-flow hydrologic properties in thermally driven models.

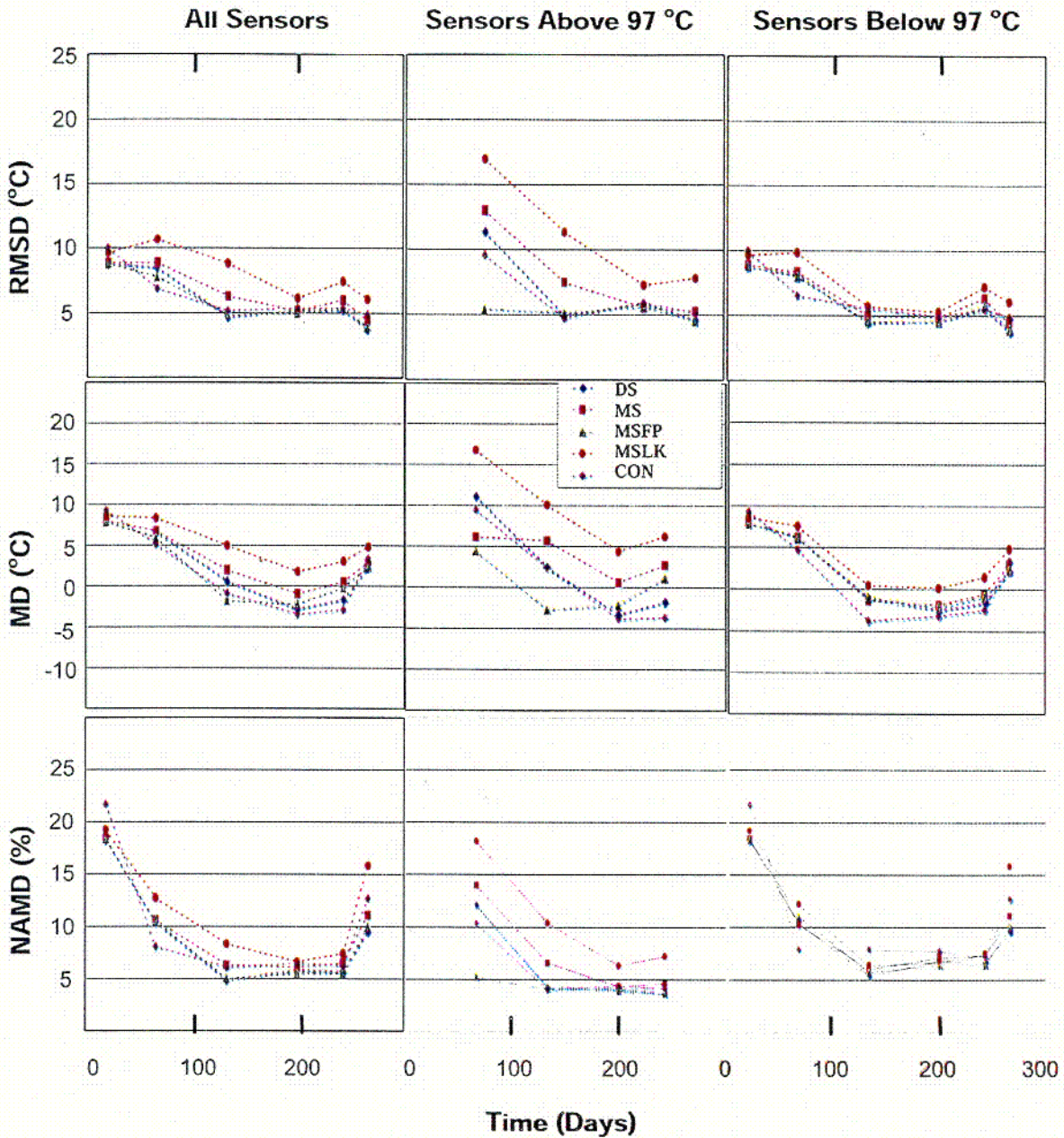
The primary purpose of the SHT was to investigate the thermal-mechanical responses of the rock mass caused by heating from a single heater in a borehole. The objectives of the SHT was to provide data and information on the rock-mass thermal and TM properties, preliminary information on coupled thermal-hydrological -chemical-mechanical (THCM) response, and preliminary information on ground support and rock interaction at elevated temperatures (CRWMS M&O 1996, p. 2-1). The test design and the borehole layout were focused on providing data for the TM responses. Boreholes for monitoring water saturation and other coupled THCM related responses were located so that interference with the TM measurements was avoided.



Source: CRWMS M&O 2000a, Figure 65

NOTE: The y-axis,  $Z$ (m), is the distance below the top of the block.

Figure 3-60. Simulated Temperature Profile Along Borehole TT1 in the LBT Computed Using the DS and MS Rock Property Data Set, Compared to Measured Data

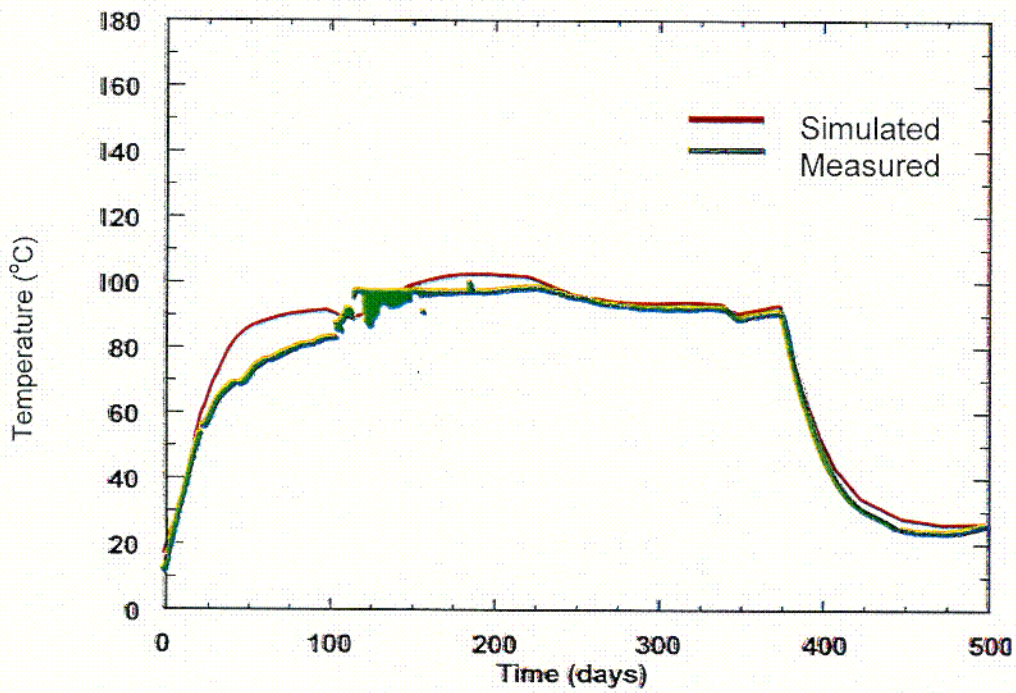
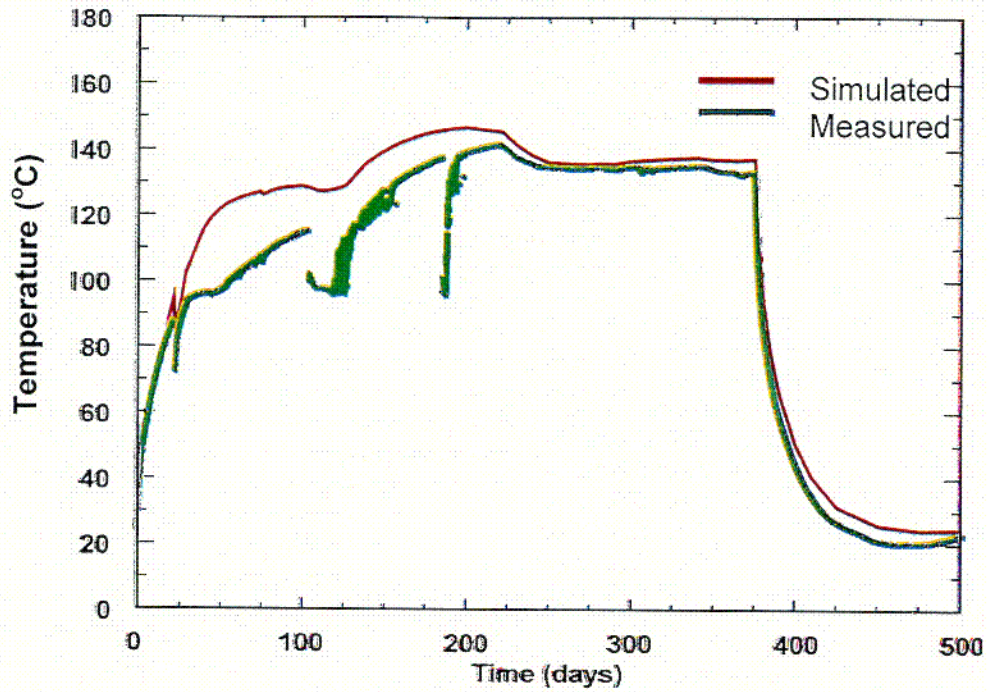


Source: CRWMS M&O 2000a, Figure 66

- NOTES:
1. The property sets tested were the Drift Scale (DS) set used in TSPA-SR calculations, a MS set with higher fracture permeability, a second MS set with still higher fracture permeability, a third MS set with a narrower range of thermal conductivity dependence on saturation, and a conduction-only (CON) set that does not track mass transfer.
  2. The three statistical measures (averaged over all sensors within a given range) are the root mean square difference (RMSD) which indicates the scatter in the data, the mean difference (MD) which indicates trends (bias) between measured and calculated temperatures, and normalized absolute mean difference (NAMD), which indicates scatter in the data normalized to the total amount of heating.
  3. The three columns are averaged over all temperature sensors, all above-boiling sensors (at each plotted time), and all below-boiling sensors, respectively.

Figure 3-61. Statistical Measures for LBT Thermal Analyses

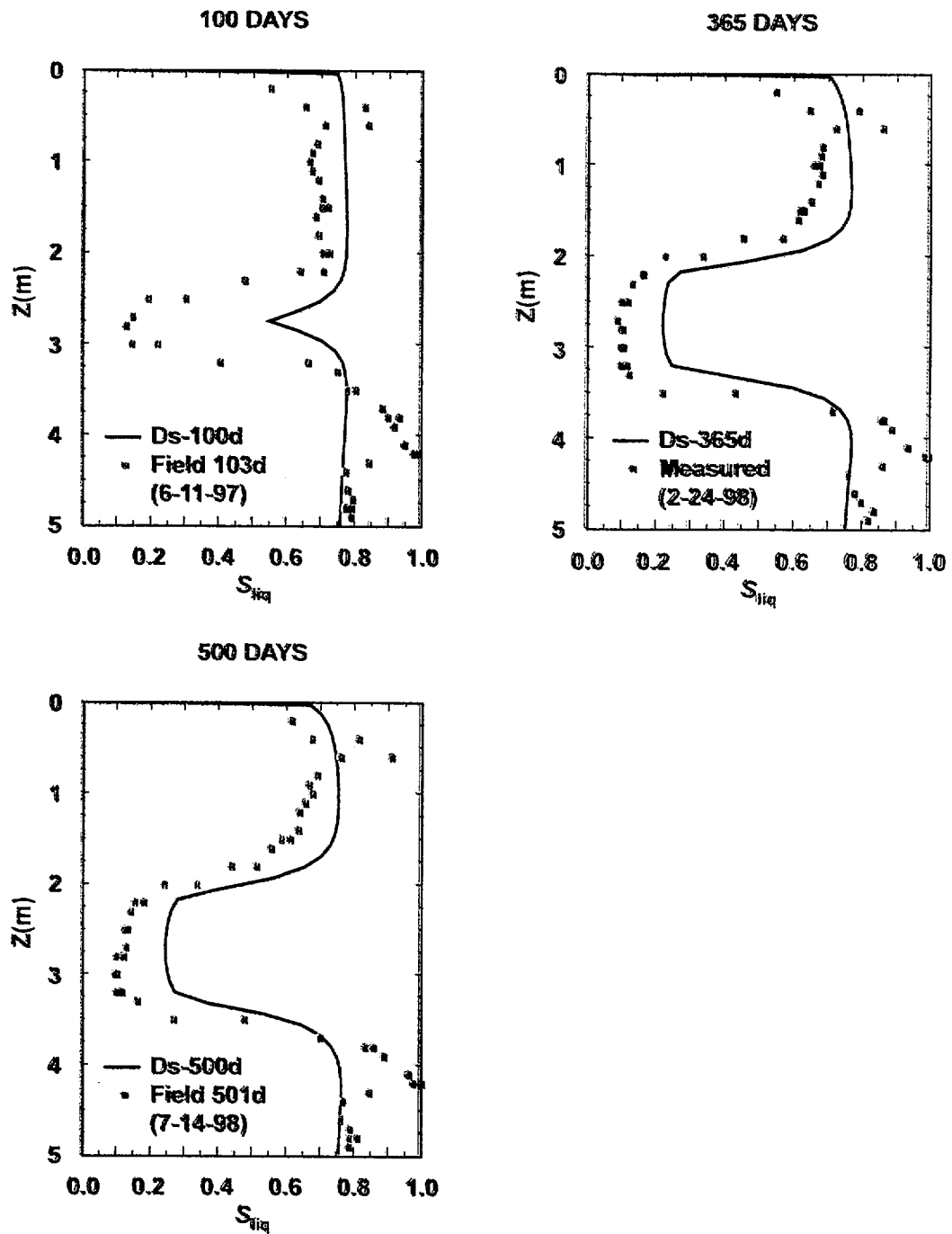
C-45



Source: CRWMS M&O 2000a, Figure 67

Figure 3-62. Simulated Versus Measured Temperature Histories for Sensors TT1-14 (Top) and TT1-19 (Bottom) in Borehole TT1 of the LBT. The DS Property Set was Used in the Simulation

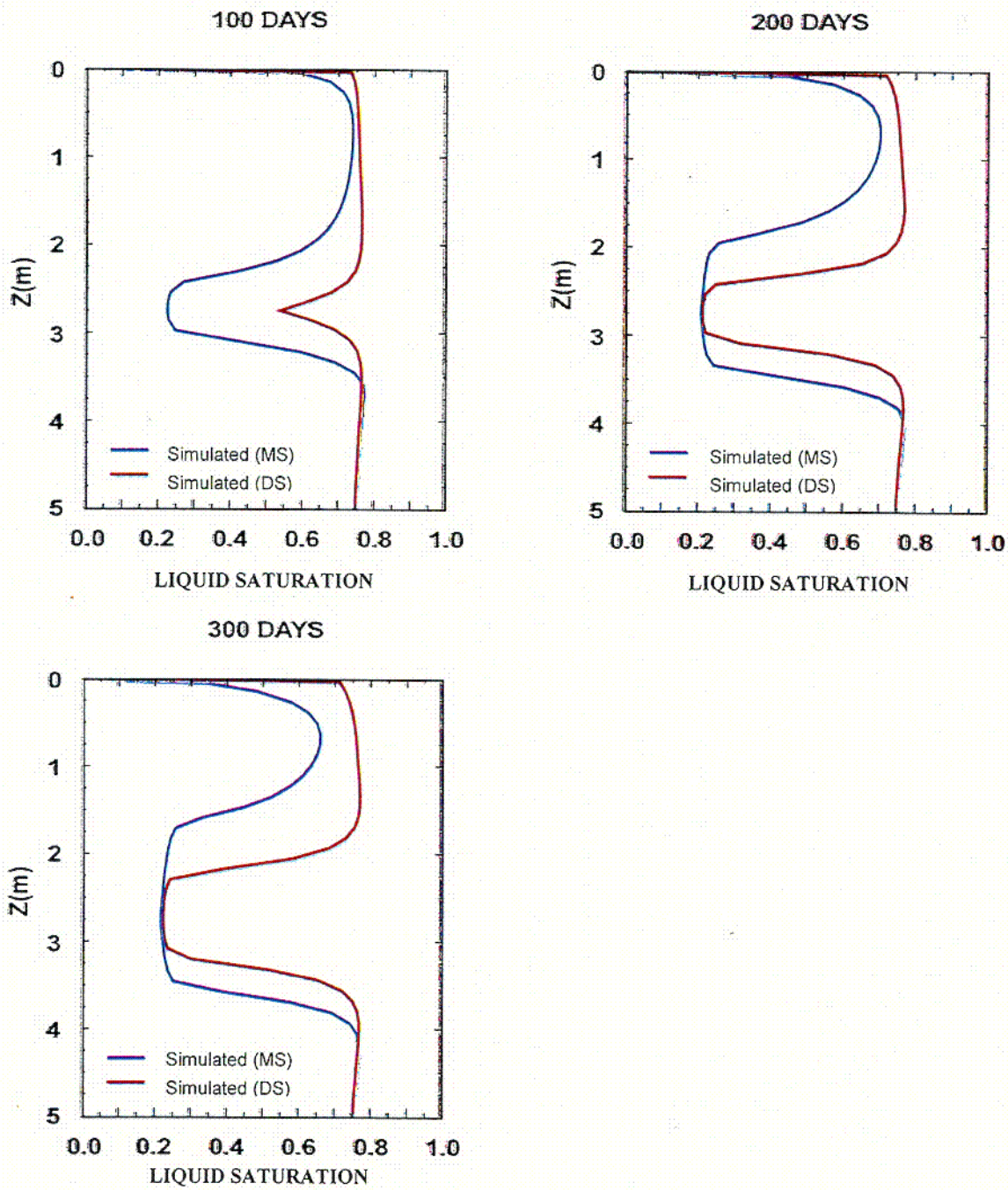
c-46



Source: CRWMS M&O 2000a, Figure 68

NOTE: The y-axis,  $Z(m)$ , is the distance below the top of the block.

Figure 3-63. Liquid-Saturation Profile Along Borehole TN3 for the LBT. The DS Property Set was Used in the Simulation



Source: CRWMS M&O 2000a, Figure 101

NOTE: The y-axis, is the distance below the top of the block.

Figure 3-64. Comparison of Liquid Saturation Along Borehole TN3 in the LBT for the DS and MS Rock Property Data Sets

c-47

The borehole layout of the SHT is shown in Figure 3-65 and Table 3-15 (CRWMS M&O 1999d, Figure 3-2 and Table 3-1). In the SHT, the temperature was measured by thermocouples in seven thermocouple holes (TMA-TC-1 to -7) and by resistance thermal devices in four neutron holes (TMA-NEU-1, TMA-NEU-3, TMA-HYD-1, and TMA-HYD-2); the rock-mass displacements were measured in four MPBX bores (TMA-MPBX-1 to -4) and two optical MPBX holes (TMA-OMPBX-1 to -2); ERT was conducted in four ERT holes (TMA-ERT-1 to -4); hydrological measurements and sampling were conducted in TMA-NEU-2 and TMA-NEU-4. The SHT was also used to test the methodology of using chemical sensors in the Science and Engineering Associates Membrane In-situ Sampling Technology (SEAMIST) system for in situ chemical monitoring. The SEAMIST system was installed in TMA-CHE-1 and TMA-CHE-2.

The following instruments and boreholes were used to measure data for the TM responses, mechanical properties of the rock mass, and ground support and rock interaction: thermocouples, MPBXs, borehole jack, rock bolt with load cell, and tape extensometers. Neutron logging, ERT, relative humidity and gas-phase pressure (in packer holes), and chemical sensors (in SEAMIST holes) were used to measure data for the coupled thermal-hydrological-chemical (THC) responses. Candidate waste package material coupons were also placed in the packer holes. The test block in the SHT was bounded by the observation Drift, Thermo-mechanical Alcove, and Thermo-mechanical Alcove Extension in Alcove 5 of the ESF (CRWMS M&O 1997a, Figure 3-1). The test block was heated by a 4-kW heater from August 26, 1996 till May 28, 1997. The block was cooled naturally after the heater was turned off on May 28, 1997.

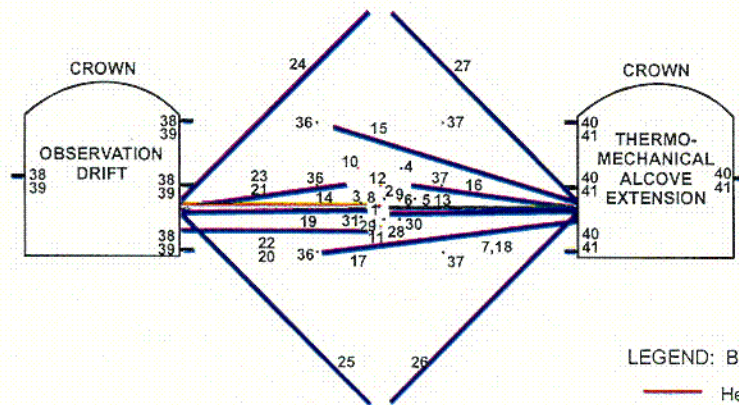
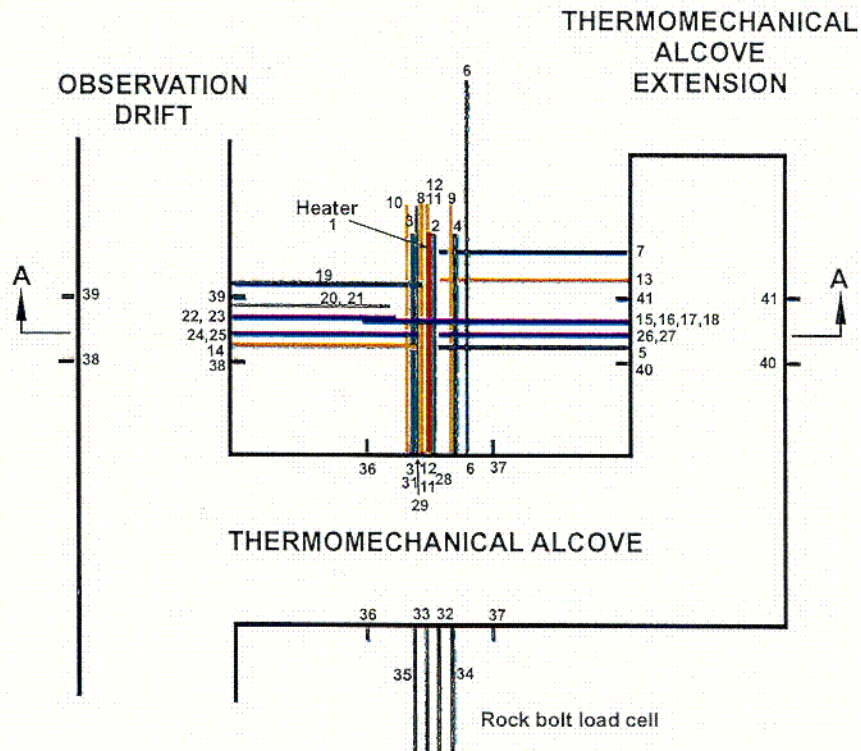
#### **3.6.1.2.1 The Single Heater Test Results**

A listing of data obtained from the Single Heater Test can be found in the SHT Final Report (CRWMS M&O 1999d, Section 2.3).

The chemical sensors in the SEAMIST system did not work as expected. Only the discussion of test results that are related to the NFE and AZ are summarized below. Detailed discussion of the test results can be found in the SHT Final Report (CRWMS M&O 1999d).

MPBX measurements in the SHT were made in directions both parallel and perpendicular to the heater. During the test, MPBX instruments oriented parallel to the heaters registered mostly expansion of the rock mass. The MPBX perpendicular to the heater registered compression movement at the beginning of heating, followed by expansion after about 40 to 50 days of heating. Figure 3-66 (CRWMS M&O 1999d, Figure 9-5) presents data for MPBX-2 which measured deformation parallel to the heater at a distance of 0.69 m from the heater. Gaps in the data are due to power outages that occurred during the SHT. The data show general extension between all pairs of anchors during the heating period, with exception of anchors 4 and 5, which show compression near the end of heating phase. These measurements are consistent in form with predicted values (using the FLAC computer code) for this location shown in Figure 3-67 (CRWMS M&O 1999d, Figure 9-6). Comparison of these two figures shows that the measured displacement values are consistently lower than the observed displacements. Cooldown data show a few minor jumps that may be associated with stick-slip behavior on a fracture. The data

indicate that the rock has a lower coefficient of thermal expansion, and lower stiffness than measured for lab samples.



- LEGEND: Boreholes
- Heater
  - Thermal
  - Mechanical
  - Hydrological
  - Chemical

REFERENCE ONLY  
(NOT TO SCALE)

Source: Adapted from Figure 3-2 of CRWMS M&O 1999d

Figure 3-65. Borehole Layout for the Single Heater Test

C-48

Table 3-15. Borehole Numbers, Types, and Locations for the Single Heater Test

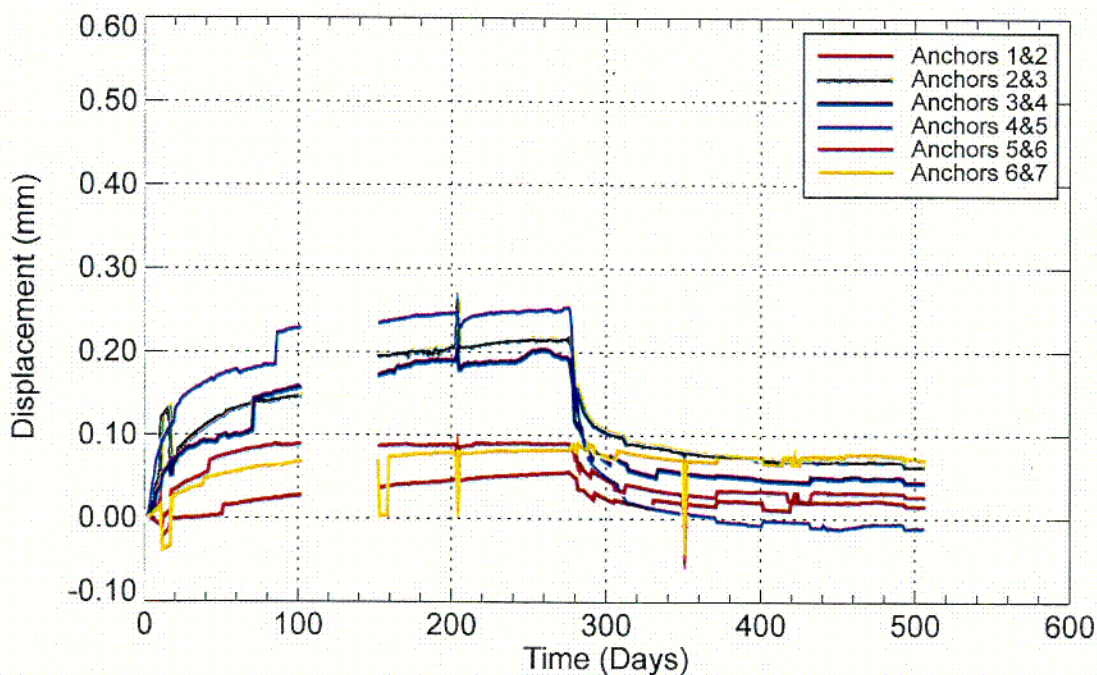
Borehole Number	Borehole Identification	Primary Purpose	Collar Coordinates			Bottom Coordinates			Orientation Degree	Length meters
			x	y	z	x	y	z		
1	ESF-TMA-H-1	Heater	0.01	0.04	-0.03	0.00	6.97	-0.01	0.5	7.00
2	ESF-TMA-MPBX-1	MPBX - Rock Mass Displacement	0.18	0.08	0.27	0.14	6.99	0.28	0.5	7.00
3	ESF-TMA-MPBX-2	MPBX - Rock Mass Displacement	-0.62	0.23	0.21	-0.62	7.25	0.25	0.5	7.00
4	ESF-TMA-MPBX-3	MPBX - Rock Mass Displacement	0.75	0.10	1.24	0.78	7.00	1.29	0.5	7.00
5	ESF-TMA-MPBX-4	MPBX - Rock Mass Displacement	6.43	3.50	-0.11	0.40	3.50	-0.21	0.5	6.20
6	ESF-TMA-OMPBX-1	Optical MPBX	1.19	-0.05	0.28	1.21	11.99	0.13	-0.5	12.00
7	ESF-TMA-OMPBX-2	Optical MPBX	6.20	6.49	-0.17	0.30	6.45	-0.27	-0.5	6.20
8	ESF-TMA-TC-1	Thermocouple	-0.18	0.15	0.28	-0.27	7.85	0.34	0.0	8.00
9	ESF-TMA-TC-2	Thermocouple	0.63	0.06	0.21	0.62	8.15	0.26	0.0	8.00
10	ESF-TMA-TC-3	Thermocouple	-0.75	0.23	1.26	-0.71	8.05	1.31	0.0	8.00
11	ESF-TMA-TC-4	Thermocouple	-0.02	0.03	-0.69	-0.09	5.49	-0.77	0.0	8.00
12	ESF-TMA-TC-5	Thermocouple	0.00	0.16	0.65	-0.04	6.84	0.68	0.0	8.00
13	ESF-TMA-TC-6	Thermocouple	6.26	5.49	-0.01	1.87	5.46	-0.04	0.0	6.20
14	ESF-TMA-TC-7	Thermocouple	-6.59	3.46	-0.01	-0.34	3.43	-0.02	0.0	6.20
15	ESF-TMA-NEU-1	Neutron Probe & Temp	6.10	4.29	0.33	-1.60	4.28	2.74	17.0	8.50
16	ESF-TMA-NEU-2	Hydrology	6.19	4.30	0.04	1.14	4.32	0.71	7.5	5.50
17	ESF-TMA-NEU-3	Neutron Probe & Temp	6.16	4.30	-0.45	-1.78	4.31	-1.47	-7.0	8.50
18	ESF-TMA-NEU-4	Hydrology	6.17	4.29	-0.22	1.51	4.28	-0.28	-0.5	5.00
19	ESF-TMA-BJ-1	Borehole Jack	-6.55	5.52	-0.14	-0.34	5.51	-0.07	0.5	6.20
20	ESF-TMA-CHE-1	Chemistry - SEAMIST	-6.64	4.91	-0.66	-1.51	4.93	-0.77	-0.5	5.00
21	ESF-TMA-CHE-2	Chemistry - SEAMIST	-6.59	5.01	-0.01	-1.06	5.10	0.63	7.5	5.50
22	ESF-TMA-HYD-1	Neutron Probe & Temp	-6.60	4.43	-0.66	-1.56	4.39	-0.74	-0.5	5.00
23	ESF-TMA-HYD-2	Neutron Probe & Temp	-6.57	4.43	0.00	-1.31	4.42	0.65	7.5	5.50
24	ESF-TMA-ERT-1	Electrical Resistivity Tomography	-6.56	3.89	0.12	-0.41	3.82	6.28	45.0	8.70
25	ESF-TMA-ERT-2	Electrical Resistivity Tomography	-6.57	3.91	-0.13	-0.29	4.07	-6.22	-45.0	8.70
26	ESF-TMA-ERT-3	Electrical Resistivity Tomography	6.25	3.89	-0.36	1.15	3.85	-5.71	-45.0	8.70
27	ESF-TMA-ERT-4	Electrical Resistivity Tomography	6.25	3.90	0.36	0.38	3.97	6.29	45.0	8.70
28	ESF-TMA-RB-1	Rock Bolt w/ Load Cell	0.14	0.05	-0.38	0.26	4.21	-0.38	0.0	4.00

Table 3-15. Borehole Numbers, Types, and Locations for the Single Heater Test (Continued)

Borehole Number	Borehole Identification	Primary Purpose	Collar Coordinates			Bottom Coordinates			Orientation Degree	Length meters
			x	y	z	x	y	z		
29	ESF-TMA-RB-2	Rock Bolt w/ Load Cell	-0.23	0.00	-0.35	-0.18	4.22	-0.42	0.0	4.00
30	ESF-TMA-RB-3	Rock Bolt w/ Load Cell	0.59	0.10	-0.31	0.60	4.03	-0.35	0.0	4.00
31	ESF-TMA-RB-4	Rock Bolt w/ Load Cell	-0.68	0.13	-0.29	-0.59	4.18	-0.23	0.0	4.00
32	ESF-TMA-RB-5	Rock Bolt w/ Load Cell	0.14	-5.37	-0.39	0.06	-9.47	-0.41	0.0	4.00
33	ESF-TMA-RB-6	Rock Bolt w/ Load Cell	-0.20	-5.45	-0.42	-0.21	-9.45	-0.42	0.0	4.00
34	ESF-TMA-RB-7	Rock Bolt w/ Load Cell	0.59	-5.49	-0.30	0.64	-9.60	-0.36	0.0	4.00
35	ESF-TMA-RB-8	Rock Bolt w/ Load Cell	-0.64	-5.38	-0.31	-0.73	-9.43	-0.45	0.0	4.00

Source: Table 3-1 of CRWMS M&O 1999d

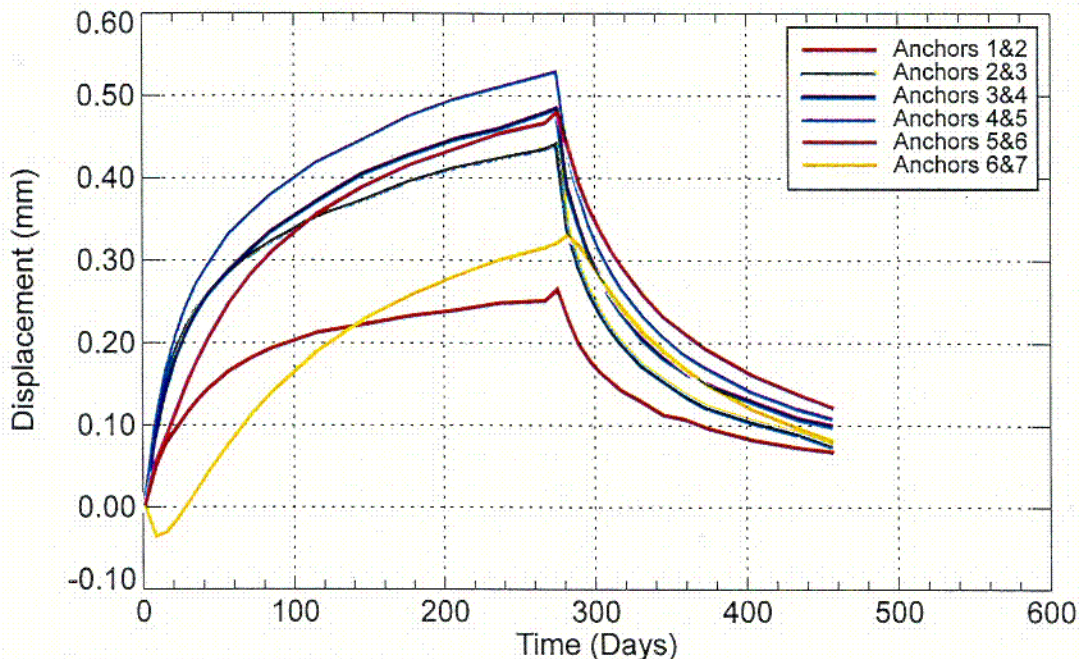
NOTE: Borehole Coordinates are Referenced to a 0,0,0 Coordinate Located at the Center of the Collar for the Heater Borehole.



NOTE: No data collected from about day 100 to about day 150 due to a blown fuse in the signal conditioner for the LVDTs.

Figure 3-66. Displacement History for ESF-TMA-MPBX-2 (Corrected for Rod Thermal Expansion; Extension Positive)

c-49

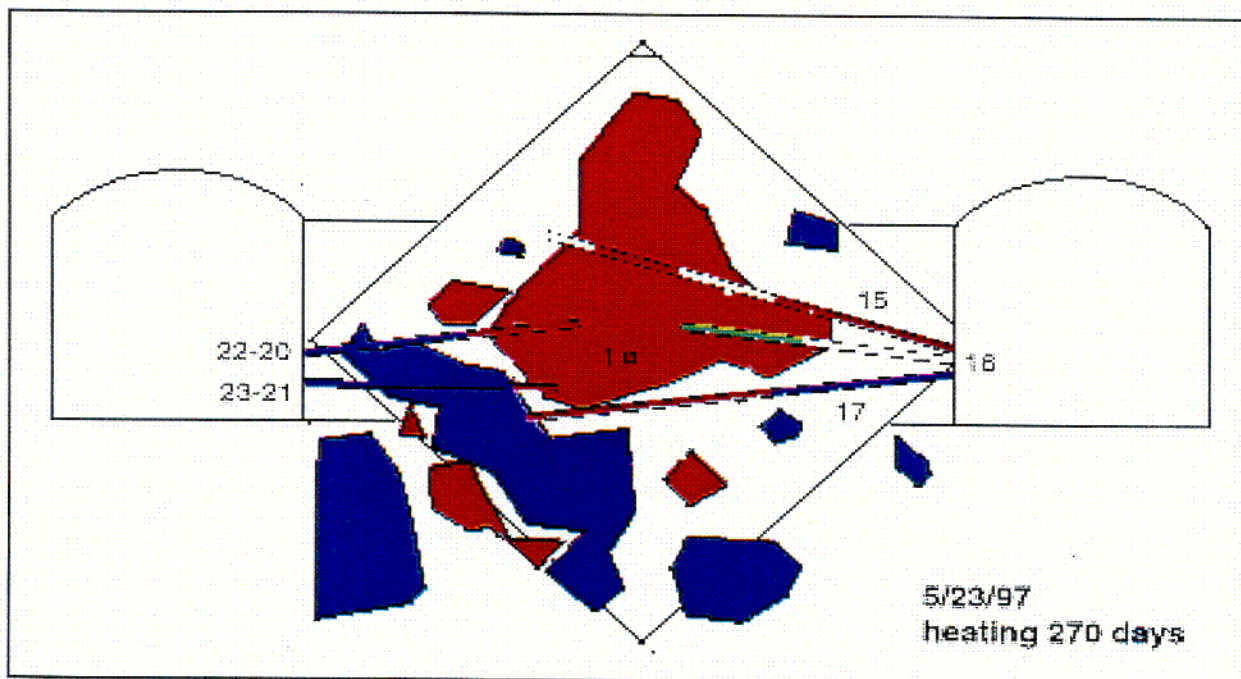


Source: CRWMS M&O 1999d, Figure 9-6

Figure 3-67. Pretest Predicted MPBX-2 Anchor-to-Ancor Displacement History Relative to the Borehole Collar

Figure 3-68 shows that both ERT and neutron logging measured significant drying in a region that was at least four times larger than the region where the temperature was greater than the boiling point of water (CRWMS M&O 1999d, Figures 8-45 and 8-65). The temperature in the neutron holes, where significant drying had occurred, was below 90°C (CRWMS M&O 1999d, Figures 7-18 and 8-65). The ERT also showed some increase in moisture content in regions below the heater hole. About 17 liters of water was collected from zone 4 in Hole 16 (TMA-NEU-2), one of the two packer holes. Hole 16 was drilled from the Thermal-mechanical Alcove Extension toward the heater hole with a upward inclined angle of about 7.5°. The end of this hole was about 1 m above and 1.14 m to the side of the heater hole. Zone 4 was the last zone in Hole 16, counted from the collar. Therefore, this zone, which was about 2 m in length, was at a radial distance of at least 1.5 m from the heater (CRWMS M&O 1999d, Figure 7-36). At the end of the heating phase of the SHT, the boiling-point isotherm reached a radial distance of about 1 m from the heater. When water was collected from Hole 16, the water-producing zone was beyond the boiling region, therefore in the condensation region. This zone was about 2 m from the heater hole (CRWMS M&O 1999d, Figure 3-2). The chemical composition of the water indicated that the water was more diluted than J-13 water and pore water of the Topopah Spring Tuff, except for the concentration of calcium. The calcium composition in the Borehole 16 water was about the same as in the J-13 water. Also, the pH value in the Hole 16 water ranged from 6.2 to 6.9, which was lower than the 7.4 for the J-13 water (CRWMS M&O 1999d, Table 4-1). One of the interpretations of the chemical characteristics of the Hole 16 water is that the pore water in the rock mass near the heater hole was evaporated, condensed in the outer and cooler region, then flowed along fractures into Hole 16. On its way to Hole 16, the condensed water interacted with minerals on the fracture surfaces to pick up calcium, and

generate greater CO<sub>2</sub> partial pressure, which lowered the pH in the water (CRWMS M&O 1999d, Section 4.1.7). Air-permeability measurement by cross-hole injection between Hole 16 and 18 (TMA-NEU-2 and -4) indicated reduced permeability during heating. For example, the permeability near zone 4 in Hole 16 decreased from  $1.10 \times 10^{-14} \text{ m}^2$  (preheat) to  $2.58 \times 10^{-15} \text{ m}^2$  (on 2/4/97) (CRWMS M&O 1999d, Table 8-3). After cooling, the air permeability in these holes increased by factors, ranging from 0.2 to 3.5 orders of magnitude of the pre-heat values (CRWMS M&O 1999d, Table 8-5). Increases in water saturation and/or reduced fracture aperture may have caused this reduction in air permeability during heating. The displacement measurements in the SHT, using MPBX, did not generate information suitable for inferring coupling between the TM responses and TH responses.



Note: Sampling interval for water samples is



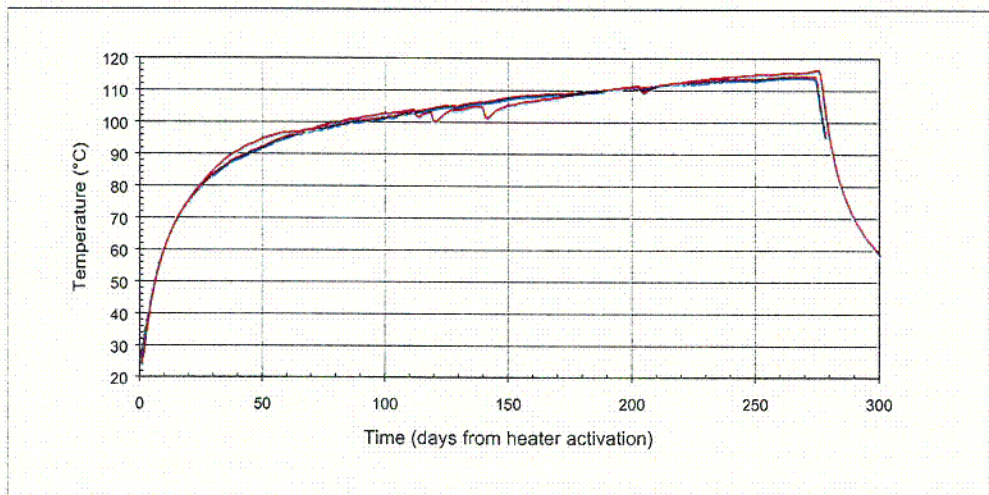
Source: CRWMS M&O199d, Figure 12.1, BAB0000000-01717-5700-00005, Rev 00

Figure 3-68. Synthesis of ERT and Neutron Logging Measurements of the Single Heater Test

### 3.6.1.2.2 Model Analysis of the Single Heater Test Results

Part of the SHT results (Single Heater Test Final Report, CRWMS M&O 1999d) were compared to model results in the *Thermal Test AMR*. The model used constant temperature, pressure and saturation boundaries at three locations far from the heater and insulation boundaries to simulate the insulated but occupied access drifts. Since the experiment was symmetric around a vertical plane through the heater, only half of the heated rock was modeled. The DKM model, using

TOUGH2 with dual permeability active fracture modeling and the DS property set, was used. TSPA-VA and Median  $k_b$  property sets were used for analyses, along with the DS property set (CRWMS M&O 2000a, Section 6.3.1). The Median  $k_b$  property set is a "local" hydrologic property set representative of the measurements taken at the actual single heater test location. The temperature data measured in three of the thermocouple boreholes (TMA-TC-1A, TMA-TC-4A, and TMA-TC-5A) and the temperature as a function of the radial distance from the heater were compared (CRWMS M&O 2000a, p. 40). The *Thermal Test AMR* conclusion was that the simulated temperature in the SHT matched the trend of the measured temperature data (CRWMS M&O 2000a, p. 73). As shown in Figures 3-69, 3-70, and 3-71 (Figures 15, 16, and 17 of the *Thermal Test AMR*), the temperature matches indicate that the active-fracture, DK model adequately represents the thermal-hydrological processes of the SHT. In some locations, the median  $k_b$  property set (CRWMS M&O 2000a, Table 4) represents the SHT temperatures better than the other two property sets as shown in Figures 3-72 and 3-73 (CRWMS M&O 2000a, Figures 77 and 79). The Thermal Test AMR used statistical measures to assess agreement between simulated and measured temperatures (CRWMS M&O 2000a, Section 6.2.1.2). Root-mean-square difference (RMSD), MD, and normalized absolute mean difference (NAMD) were the statistical measures used in the AMR. The statistical assessment of the property sets for the SHT temperatures are shown in Figure 3-74 (CRWMS M&O 2000a, Figure 18).

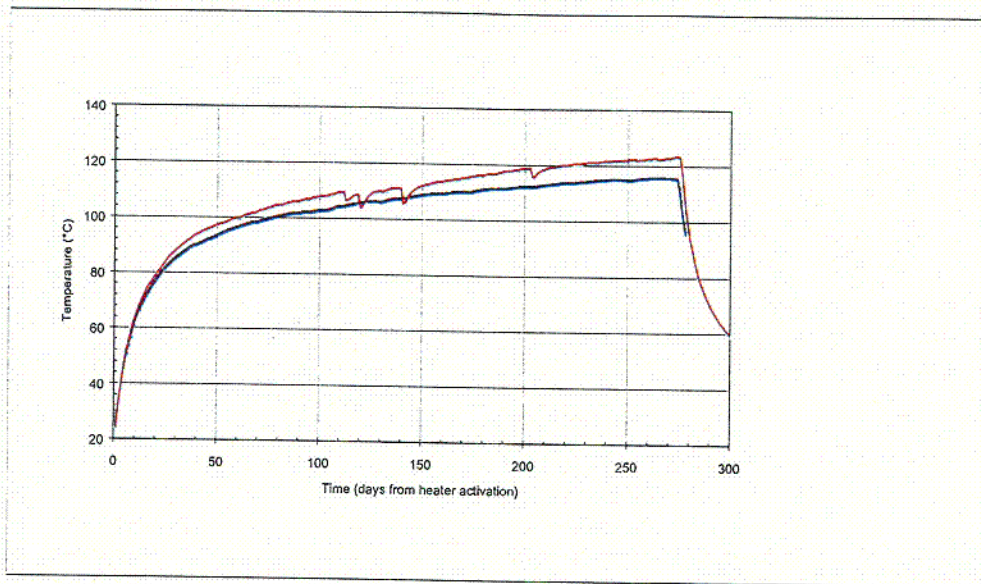


Source: CRWMS M&O 2000a, Figure 15

Legend = Red is measured data, black is simulated data.

Figure 3-69. Comparison of the DKM/TOUGH2 Simulation Using the Drift-Scale Property Set and the SHT Measured Temperatures at Thermocouple Location TMA-TC-4A-6 (73 cm below the heater center)

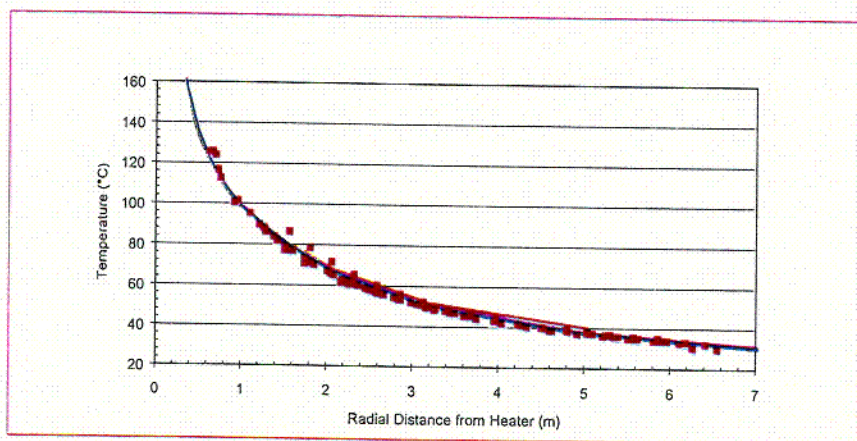
C-52



Source: CRWMS M&O 2000a, Figure 16

Legend: Red is measured data, black is simulated data.

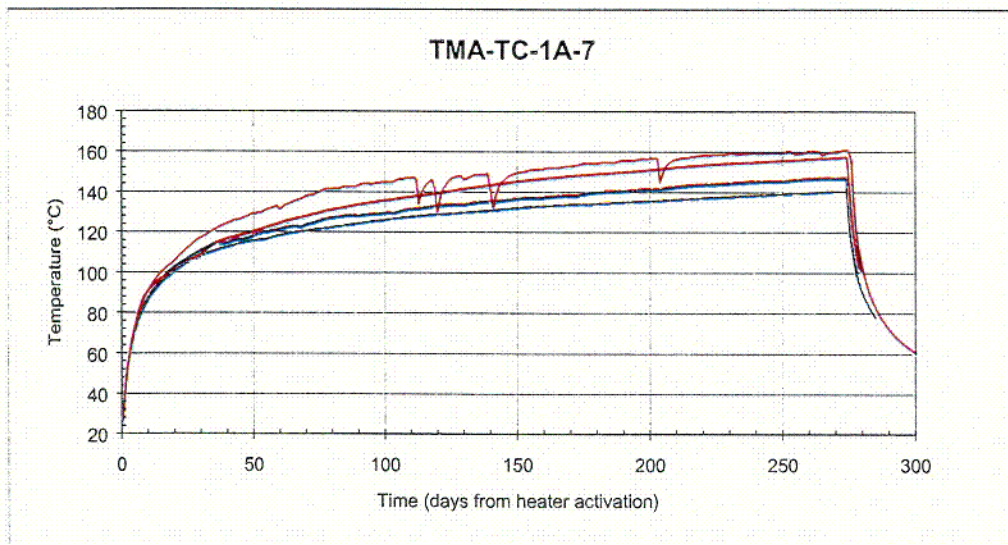
Figure 3-70. Comparison of the DKM/TOUGH2 Simulation Using the Drift-Scale Property Set and the SHT Measured Temperatures at Thermocouple Location TMA-TC-5A-7 (66 cm above the Heater Center)



Source: CRWMS M&O 2000a, Figure 17

Legend: Red line is lateral direction simulated data, green line is upward direction simulated data, blue line is downward direction simulated data, and red squares are measured data.

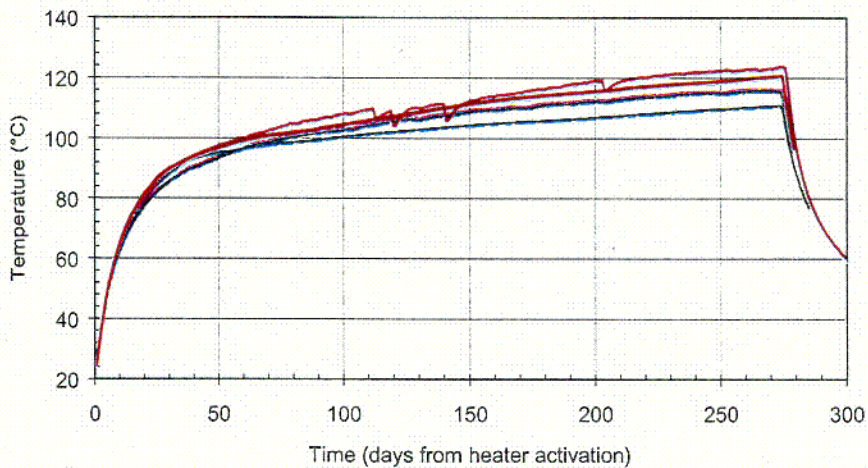
Figure 3-71. Comparison of the DKM/TOUGH2 Simulation Using the Drift-Scale Property Set and the SHT Temperatures Measured Radially Around Heater Mid-Length



Source: CRWMS M&O 2000a, Figure 77

Legend: Blue is simulated data with DS property set, green is simulated data with TSPA-VA property sets, brown is simulated data with median bulk permeability, red is measured data.

Figure 3-72. Comparison of Three SHT DKM/TOUGH2 Simulations (Property Sets: DS, Median  $k_b$ , and TSPA-VA) and Measured SHT Temperatures at Thermocouple Location TMA-TC-1A-7

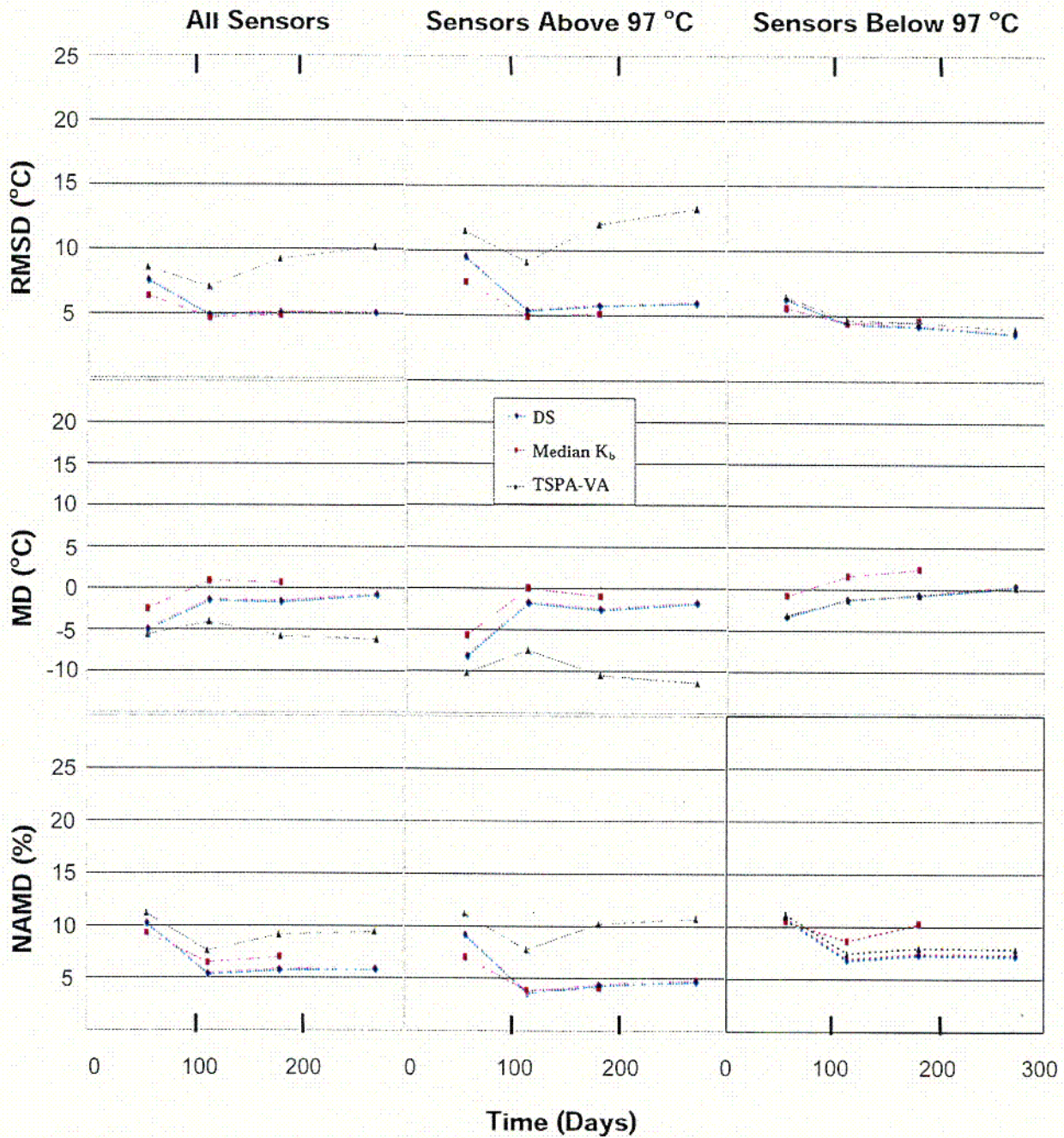


Source: CRWMS M&O 2000a, Figure 79

Legend: Blue is simulated data with DS property set, green is simulated data with TSPA-VA property sets, brown is simulated data with median bulk permeability, red is measured data.

Figure 3-73. Comparison of Three SHT DKM/TOUGH2 Simulations (Property Sets: DS, Median  $k_b$ , and TSPA-VA) and Measured SHT Temperatures at Thermocouple Location TMA-TC-5A-7

C.54



Source: CRWMS M&O 2000a, Figure 18

- NOTES:
1. The property sets tested were the Drift Scale (DS) set used in TSPA-SR calculations, the TSPA-VA set with higher fracture permeability but lower fracture porosity, and the Median  $K_b$  set with lower fracture permeability and porosity and a narrower range of thermal conductivity dependence on saturation.
  2. See Note 2 of Figure 3-56 for descriptions of the statistical measures.
  3. See Note 3 of Figure 3-56 for sensor group descriptions.

Figure 3-74. Statistical Measures for SHT Thermal Analyses

C-55

### 3.6.1.2.3 SHT Summary

The TM displacement measurements in the SHT generated good information of the effect of heating on bulk deformation of the rock mass. The SHT generated interesting information about the coupled THC in a heated rock mass, even though it was not designed particularly for that purpose. The test confirmed the process that heat drives water away in vapor form. The water vapor appears to have condensed when it reached cooler regions. Further, it appears that the condensed water may have traveled through fractures. Rock-water interaction between the condensed water and mineral coating on fracture surfaces can occur within a relatively short period of time, in the order of months. The *Thermal Test AMR* conclusion was that the simulated temperature in the SHT, from the DKM active-fracture modeling using TOUGH2 and the DS property set, matches the trend of the measured temperature data well. The drift scale property set and the median  $k_b$  property set matched the measured temperature values better than the median TSPA-VA set (CRWMS M&O 2000a, Section 6.3.1).

Important coupled processes observed from the SHT include:

- Dryout of rock occurred in regions below the boiling-point temperature. The region of drying exceeded that of the region where temperatures were greater than the boiling-point temperature by more than four times
- Moisture increased below the heater (presumably due to condensation)
- Chemical composition of water sampled was consistent with the concept of evaporation, condensation, and flow along fractures
- Low pH in the sampled water is probably caused by excess CO<sub>2</sub> generation from rock-water interaction during flow along fractures
- Air permeability measurements noted reduced permeability during heating in regions outside of the dryout zone, and increased permeability after the rock had cooled.

These changes in permeability are possibly the result of mobilization, during the thermal period, of water from the dryout zone with condensation of that water in the fractures outside of the dryout zone. This increased saturation in fractures would reduce the relative permeability of air within the fractures. After cooling, as the increased fracture saturation in the condensate zone dissipated, the relative permeability to air would increase.

Another possible reason for the changes in air permeability are changes in fracture aperture that resulted from the mechanical responses to the increased temperatures. As the rock expanded during the thermal pulse, the fracture apertures would decrease, thus decreasing the permeability. After cooling, the rock deformations would decrease so that the apertures would return to preheating conditions, with an accompanying increase in permeability.

- The conceptual and mathematical model simulates temperatures consistent with measured temperatures.
- The *Thermal Test AMR* was focused on TH responses and therefore did not report mineralogical change in the SHT due to the heating. Posttest cores and over-cores were obtained from the SHT block. Detail descriptions of the mineralogical analysis of the post-test cores and over-cores can be found in Single Heater Test Final Report (CRWMS M&O 1999d). The analysis of the post-test cores for the mineralogical change is summarized below.

Calcite, gypsum, and opal-A were identified as the principal alteration products of the SHT. These minerals were observed on pretest borehole surfaces and in natural fractures adjacent to the boreholes (from post-test over-cores). The distribution and textural attributes of the mineral deposits in a borehole within the condensation zone may be most compatible with mineral precipitation during the post-test cooldown period. The amounts of secondary minerals available from post-test overcores (producing annular samples) were minimally adequate to identify the mineralogical test products. Given the combined limitations of time constraints on posttest analysis and availability of suitable core, a 3-D distribution of mineral deposition could not be established. Such a database could test whether attributes of mineralogy or mineral textures correlate with the geometry of the dryout, condensation, and reflux zones.

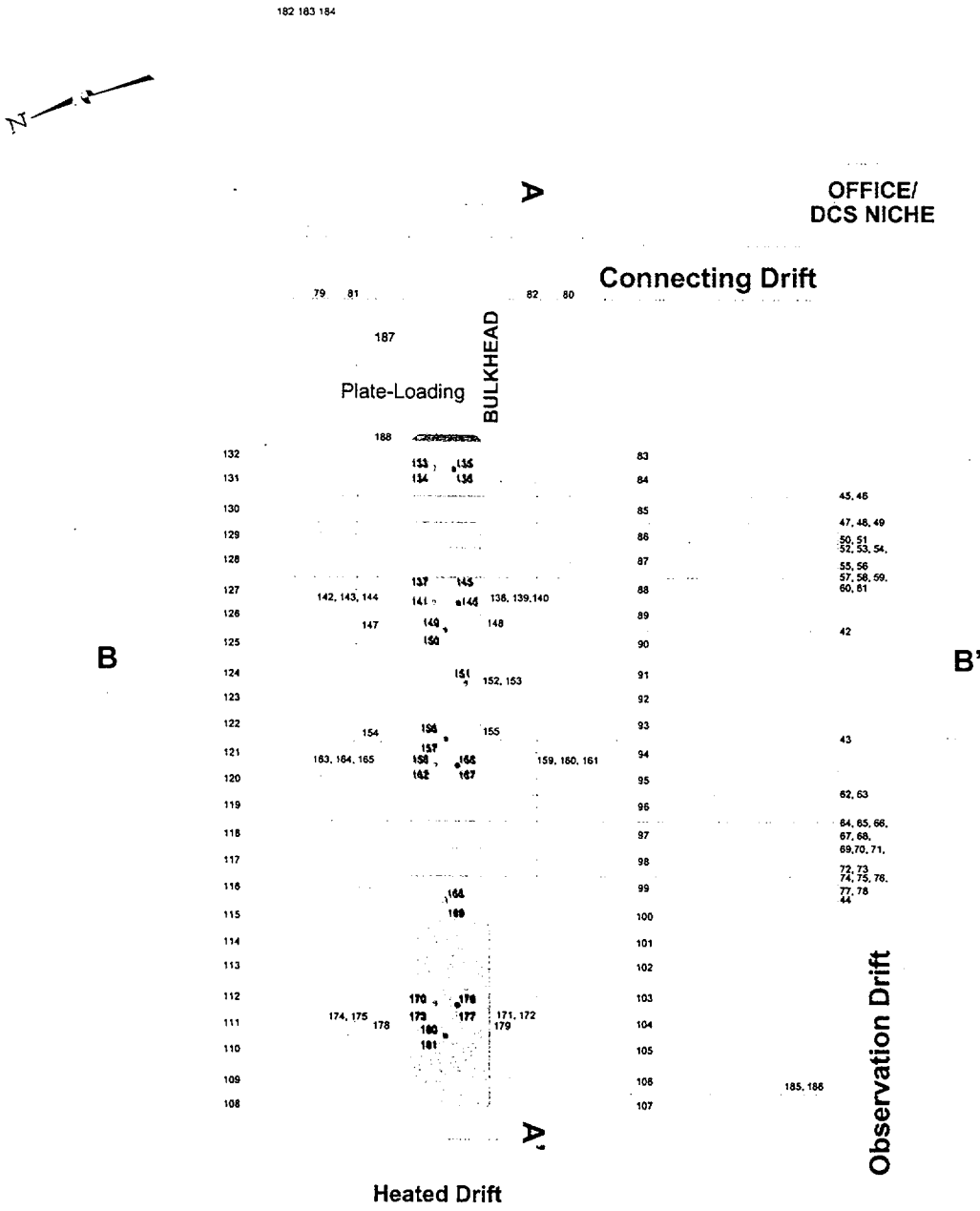
There are indications that the mineralogical products of the SHT may reflect an influence of materials introduced during drilling operations. Introduced materials such as gypsum could alter the sulfate budget of the water and rock system. The magnitude of this influence is probably small, but additional documentation would be required to increase confidence in this assessment. Existing geochemical models of the test do not account for introduced materials that may participate as reactants or catalysts. (CRWMS M&O 1999d, Section 6.4.10).

### 3.6.1.3 Drift Scale Test

The DST was designed to collect data on coupled THCM processes in an in situ DS setting, and to test conceptual and mathematical model understanding, specifically the hypotheses of the processes. Although the DST was designed to test processes and process models at the repository horizon, it also considered the conceptual repository design at the time of the DST planning. This goal of understanding heat-driven coupled processes is not directly linked to a specific repository design and does not require replication of potential repository conditions, geometries, and heating rates, nor is such replication practical in limited-duration field test. The fundamental nature of the DST is to test conceptual process models in the system and the ability to model quantitatively the system's response to those processes. Once confidence is developed in the coupled-process models, they can be applied to a range of repository designs. Therefore, although the test was focused on a VA design rather than the EDII design, the testing of physical processes is judged to be applicable. The detailed description of the objectives and design of the DST can be found in DST Design and Forecast Results (CRWMS M&O 1997b, Sections 2 and 3). A brief summary of the DST will be given here to facilitate discussion of the test results. The drift configuration of the DST consists of an Access/Observation Drift (AOD),

Connecting Drift (CD), and Heater Drift (HD). The AOD connects with the main ESF Tunnel at about 2.88 km from the North portal of the main Tunnel. The HD is about 47.5 m in length, starting from a thermal bulkhead that is located near its intersection with the CD. The heat source in the DST includes nine canister heaters lined up on the floor of the HD, and 25 wing heaters on each side of the HD. Each of the nine canister heaters is about 4.7 m in length and 1.7 m in diameter. Each of the 50 wing heaters is about 10 m in length. Each of the wing-heaters is placed in a horizontal wing-heater hole, which is 11.5 m in length, and was drilled into the sidewall of the HD at about 0.25 m below the springline. The total power of the nine canister heaters and the wing heaters are about 68 kW and 143 kW, respectively. Each wing heater consists of two sections of heating elements. The outer (further away from the HD) heating element has a rated power output of about 1.719 kW; the inner section has a power of about 1.145 kW.

The borehole layouts for the DST are shown in Figures 3-75, 3-76, and 3-77. Temperature is measured in RTD holes that are arranged radially from the HD (CRWMS M&O 1997b, Figure 3-3 and Table 3-1, Holes 133, 134, 137-144, 158-165, 168, 169, and 170-175). In addition, temperature is also measured in two longitudinal neutron-RTD holes (CRWMS M&O 1997b, Figure 3-1, Hole 79 and 80) that are parallel to the HD, at about 3.5 m above the midpoint of the wing-heater plane. The ERT is conducted in vertical planes parallel to the HD, and in two vertical planes perpendicular to the HD from the AOD, at 4.57 and 24.69 m from the bulkhead. Neutron logging is conducted in two sets of holes from the AOD. Each set of neutron holes (five holes) forms a fan-shape vertical plane perpendicular to the HD, with three holes that extend above the HD, and two holes that extend under the HD. The two neutron-hole sets are located at 6.4 and 26.52 m from the bulkhead. Gas-sampling ports and water-absorbing pads are installed in the SEAMIST system in two sets of Chemistry holes, which were drilled from the AOD. Similar to the neutron holes, each set of the Chemistry holes forms a fan-shaped vertical plane perpendicular to the HD, with three holes extending above the HD, and two holes extending under the HD. The two Chemistry hole sets are at 8.23 and 28.35 m from the bulkhead. Four packers with gas-injection and sampling capabilities were installed in two sets of Hydrology holes, which were drilled from the AOD. The arrangement of the Hydrology holes is the same as the SEAMIST holes. The two sets of Hydrology holes are located at 10.06 and 30.18 m from the bulkhead. In addition, two more hydrology holes were drilled from the AOD at 44.8 m from the bulkhead, with one extending above the HD, and one extending below the HD. The displacement in the rock mass is measured by MPBX in the MPBX holes. Those are Hole #42, 43, 44, 81, 82, 147, 148, 149, 150, 154, 155, 156, 157, 178, 179, 180, 181, 187, and 188, as shown in the DST Design and Forecast Results (CRWMS M&O 1997b, Table 3-1 and Figure 3-1). In situ thermal conductivity and thermal diffusivity are measured in the three REKA holes (Hole #151, 152, and 153) at 17.37 m from the bulkhead. All of the instrumentation holes, except the MPBX holes, were sealed by cement grout, packers, or SEAMIST. The effect of the thermal-hydrologically open MPBX holes on the coupled THCM processes to be tested in the DST will have to be assessed. The heaters in the DST were energized on December 3, 1997. The test is now in the third year of its four-year heating phase, then the heaters will be turned off to start a natural cooling phase, which is planned to last for another four years.

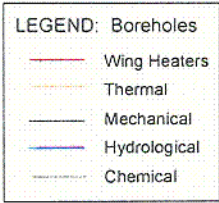
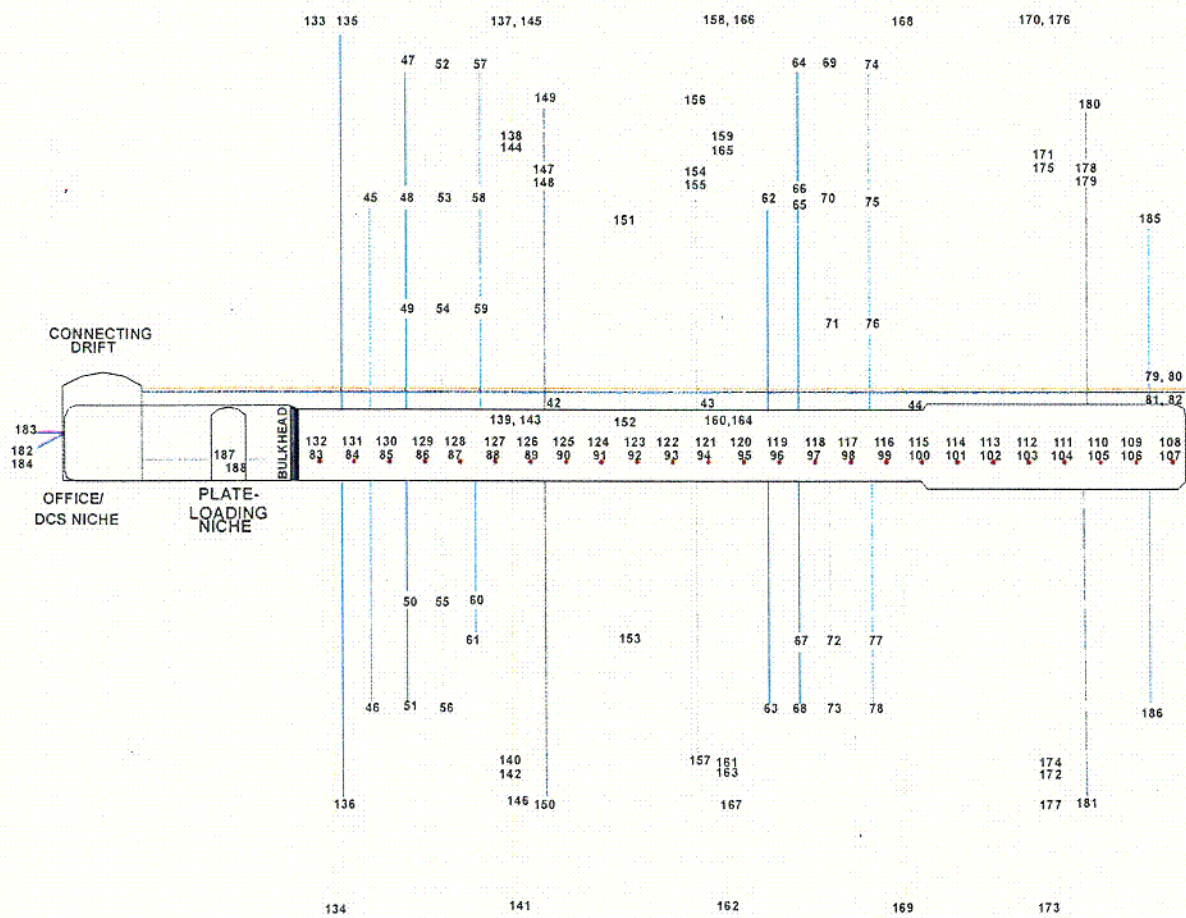


**LEGEND: Boreholes**  
 Wing Heaters  
 Thermal  
 Mechanical  
 Hydrological  
 Chemical

**LEGEND: Ground Support System**  
 Rockbolts and welded wire used  
 throughout heated drift for safety and  
 stability purposes only  
 Cast-in-place concrete

Source: CRWMS M&O 2000a, Figure 4

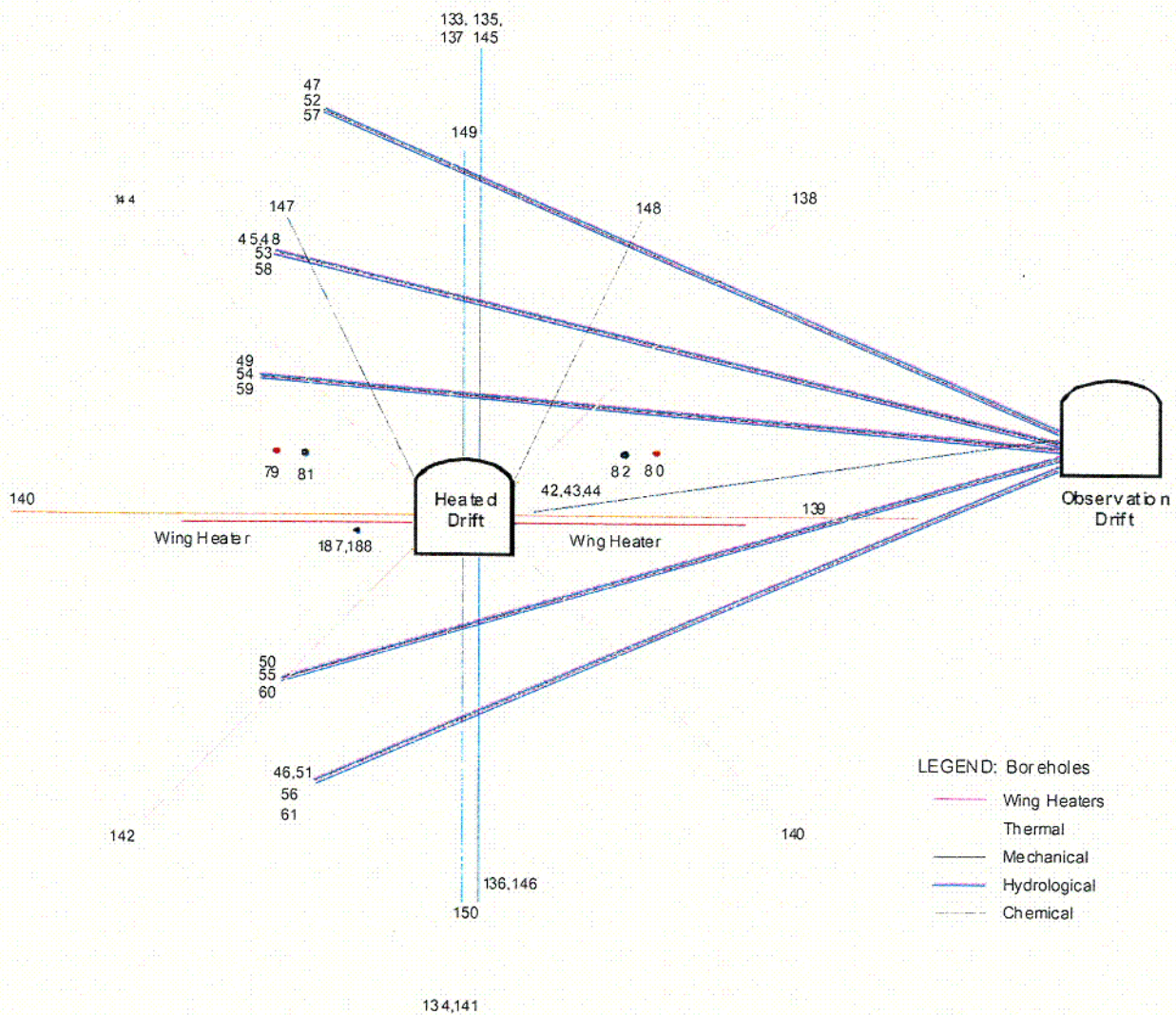
Figure 3-75. Plan View of the DST



Source: CRWMS M&O 2000a, Figure 5

Figure 3-76. Cross Section (A-A') Parallel to the Heated Drift in the DST

C-56



Source: CRWMS M&O 2000a, Figure 6

Figure 3-77. Cross Section (B-B') Orthogonal to the Heated Drift in the DST

### 3.6.1.3.1 The Drift Scale Test Results

Because the test is ongoing, any discussion of the THCM processes inferred from the test results is preliminary. The temperature and the moisture distribution data of the DST were analyzed and included in the *Thermal Test AMR* (CRWMS M&O 2000a). The water chemistry and gas chemistry data of the DST were analyzed and included in the *THC Process AMR* (CRWMS M&O 2000b). The analyses of the DST data conducted for the *Thermal Test AMR* focus on comparison of the measured temperature and moisture distribution simulated by DKM with

C-57.

AFMs using TOUGH2 and NUFT codes with the objective of identifying a property set that yields the best temperature and saturation predictions.

The *Thermal Test AMR* analyses are summarized in Section 3.6.4.1. In addition to property-set evaluations, and discussions of the DST temperature profile and evaluation reported in the *Thermal Test AMR*, this report examines the processes that can be inferred from the DST results. Those processes are boiling of pore water, movement of moisture, effect of the bulkhead on measured results, and drying of rock mass.

Inspection of the temperature data can provide several insights into the TH processes. When conduction dominates or is the only heat-transfer mechanism, heat flow is a function of temperature gradients and thermal conductivity of the medium. Therefore, at any point within the DST, the response should show increases in temperature with time, with the slope of the increase decreasing with time. However, there are three TH-related processes that can impact that general response. The first is conduction, which is sensitive to the 25 to 40 percent, is a difference between wet- and dry-rock thermal conductivity (CRWMS M&O 2000a, Tables 4 and 5). The thermal conductivity decreases once rock has become dry. The second condition is the heat capacity of the rock mass changes with its moisture content. Decreasing moisture content of the rock mass will decrease its heat capacity. The total effect of these two is that, as the rock within the region of a sensor dries out, the slope of the temperature-time curve may increase. The third effect is that vaporization or boiling of water requires energy. This will result in temperatures approaching the boiling point of water and remaining at that temperature until the water has been removed from that region of rock mass. On a plot of temperature as a function of time, this will cause a flattening of the slope of the temperature curve at the boiling point temperature.

Whether there is a flattening of the curve or merely an inflection point, it is a function of how long water remains in proximity of the sensor. The amount of inflection also depends on whether water remains in the rock until the boiling point is reached, or if the evaporation rate increases sufficiently that the rock mass becomes dry prior to reaching the boiling point of water. The evaporation rate depends, among other factors, on the suction potential and the permeability of the rock mass near the temperature sensor. If water remains in the system until the temperature reaches boiling, there would be a flattening of the temperature curve, with the curve remaining at the boiling point until the water was removed. If much of the water were removed prior to the temperature reaching boiling, there would be a very short period of time at which the temperature would remain at the boiling point. Depending on how short this period was, the result could be an inflection at the boiling point, but not a flattening that extended for any length of time. If the water had been entirely removed from the system prior to the region reaching the boiling point, the temperature response would not change as the temperatures reached and then passed the boiling point temperature.

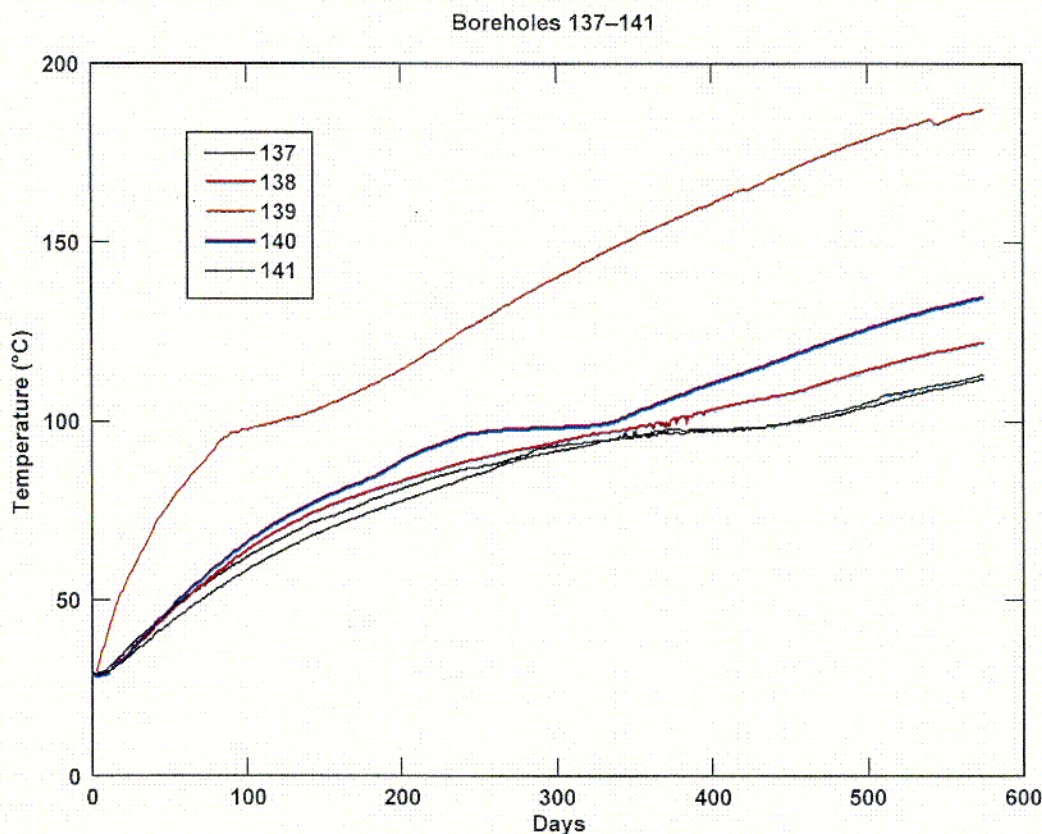
With these principles in mind, data from the DST can be inspected to determine whether a distinction can be made regarding the physical processes that occurred. Two arrays of sensors are considered. These are "fan" arrays of boreholes 23 m from the bulkhead and 12 m from the bulkhead. As shown on Figures 3-75, 3-76, and 3-77, an array of 8 boreholes were installed at each of these locations to monitor responses in those locations. For simplicity, the comparisons were made for half of each array, assuming that the results will be symmetrical. The boreholes

considered for the array 23-m from the bulkhead consist of holes 158 to 162. These boreholes were drilled from the HD with borehole 158 drilled vertically upward, borehole 159 drilled 45° upward, borehole 160 drilled horizontally toward the AOD, borehole 161 drilled 45° downward, and borehole 162 drilled vertically downward, thus forming a fan of boreholes oriented at 45°s from each other, with a common apex. The array considered at 12 m was a similar fan array consisting of boreholes 137 (vertical upward), 138 (45° upward), 139 (horizontal), 140 (45° downward) and 141 (vertical downward).

All of the figures of temperature in this section are based on the temperature data in the TDMS, as listed in the *Thermal Test AMR* (CRWMS M&O 2000a, Table 8). Figures 3-78 and 3-79 show the temperatures measured at a depth of about 2 m from the collar in the five Holes #137 to 141 and 158 to 162, respectively, as a function of time (days) since heating commenced. The purpose of presenting those figures is to show boiling of the pore water as measured from different orientations with respect to the HD. Boiling of pore water and reflux or influx water at the temperature sensors are illustrated as a flat temperature-time curve, at about the boiling point of water, about 96°C in the DST. Different profiles would indicate different interactions with water, non-uniform porosity and saturation or thermal conductivity, or the effects of different temperature gradients. Consider first, the monitored temperatures from the array at 23 m from the bulkhead where end effects should be minimal. All of the holes show either flattening or inflection of temperature with time at the boiling point temperature (Figure 3-79). The least amount of flattening was exhibited in borehole 159, which is oriented 45° upward. The most well defined flattening (boiling) occurred in borehole 160, which was horizontal. This flattening lasted for about 35 days. If the data are accurate for borehole 158 (temperature plot is less uniform around 450-500 days), this vertical borehole exhibited the longest duration of impact of boiling or flattening. The array at 12 m indicates a similar response, but the horizontal borehole (hole 139) shows less well-defined flattening, and the 45° upward borehole shows no flattening, not even an inflection. Because flattening indicates the presence and boiling of water, and not all boreholes exhibited the same response, there are either physical processes that are not uniform in all of the boreholes or the rock is not uniform in properties and/or saturation. Because the pattern of differences is similar for the two fan arrays, it appears that more than property differences must be considered.

By inspecting the plots, hypotheses can be made as to why the boreholes responded differently. It should be noted that the fracture system is dominated by vertical fractures. For the region of rock sampled by the vertical upward boreholes, water that was vaporized would likely move up the fractures as vapor, then condense and return along the same fracture back to the area of the sensor. This is essentially a gravity driven heat-pipe as discussed in Section 3.2.1. This would explain the nearly 70 to 120 day cycle of boiling of water in vertical boreholes 137 and 158, respectively. It is unlikely that there was sufficient water in the pores of the rock to maintain boiling effects for nearly 100 days and, if so, there should have been a similar volume of water to cause similar boiling effects in the 45°-upward boreholes. For other than purely vertical boreholes, the moisture migration is potentially more complex. Water vapor will migrate either in response to pressure or density (buoyancy). Further, the water that is vaporized will be water within the matrix (the fractures are essentially drained, except during episodic percolation events). Within the matrix, vaporization will cause pressure gradients. The overall direction of vapor migration within matrix blocks in response to this pressure would be radially

outward from the heat source. Buoyancy will cause vertically upward migration. It is unlikely that two-phase flow would impede vapor flow, unless the pores are nearly saturated. A differential between the dried portion of the matrix and the saturated portion can not be eliminated, but is not expected to be a dominant process. The largest impact on the migration direction for vapor is the presence (or lack) of fractures. If the matrix blocks are not too large, and the fracture permeabilities are greater than about 10 millidarcies, pressure buildup in the matrix will not be large enough to throttle evaporation.



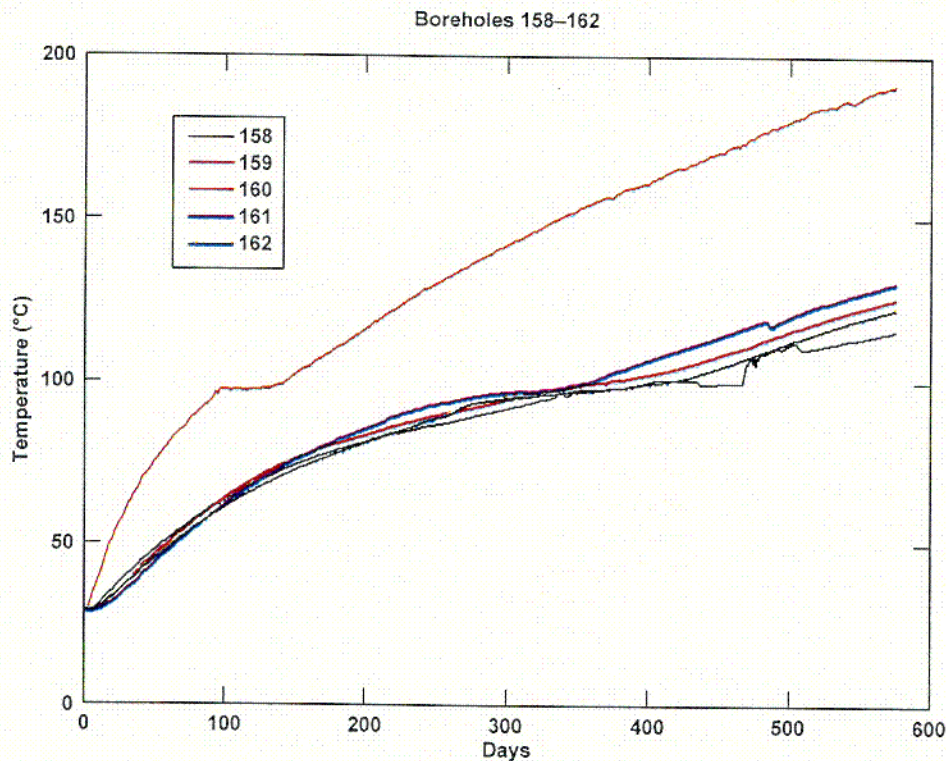
DTN: MO9807DSTSET01.000, MO9810DSTSET02.000, and MO9906DSTSET03.000.

Figure 3-78. Temperature at a Depth of 2 m from Collar of Holes #137 To 141 as a Function of Elapsed Time

Given these complexities, it can nevertheless be generalized that pressure gradients dominate the movement of vapor in the matrix and thus water vapor will tend to be driven radially away from the heat source. Therefore, water vaporized around the sensor of the 45°-upward fracture would be driven (essentially) radially outward through the matrix and upward from the point it entered into the fractures. As water condensed, it would tend to drain vertically downward. Thus, the behavior of the vertical and 45°-upward sensors could be expected to be potentially different and the data does indicate this. Furthermore, the horizontal boreholes, particularly borehole 160, showed well-defined impact of boiling that lasted for approximately 35 days. However, these boreholes are close to the wing heaters. Water vaporized in this region would tend to be driven perpendicular to the heaters through matrix and then vertically in fractures. Thus, it is likely that

the horizontal boreholes are exhibiting effects of reflux. The difference in boiling between Holes 139 and 160 may be caused by localized heterogeneous hydrological properties and/or by the effect of the bulkhead.

A similar conclusion regarding boiling can be drawn for the 45°-downward inclined holes. For these regions, the water removed as vapor would tend to migrate through the matrix, radially away from the heat source, if vapor was driven by pressure. Within fractures, buoyancy dominated, the vapor would tend to migrate vertically. Thus, either the fracture system is sufficient to allow buoyancy to dominate so that reflux can occur or the vapor would be driven by pressure radially away from the sensor, where boiling was occurring, and then condensate would drain vertically and not return to the sensor area. If reflux dominates, the responses would be similar to those observed in the vertical borehole. If pressure redistribution dominates, the condensate contribution to maintaining temperatures at the boiling point would be reduced or eliminated. However, it is likely that sensors would be subjected to a combination of refluxing of water from the sensor location as well as influx of water condensate driven from rock regions above the sensor. This might explain the flattening, noted particularly in borehole 140 where it occurred for approximately 60 days. Because these sensors are located below the wing heaters, it is possible that water from above was migrating and causing boiling effects similar to those seen by the horizontal-hole sensors. The difference between the 45° down and the horizontal regions may also be influenced by the plane heat source of the DST created by the wing heaters.



DTN: MO9807DSTSET01.000, MO9810DSTSET02.000, MO9906DSTSET03.000

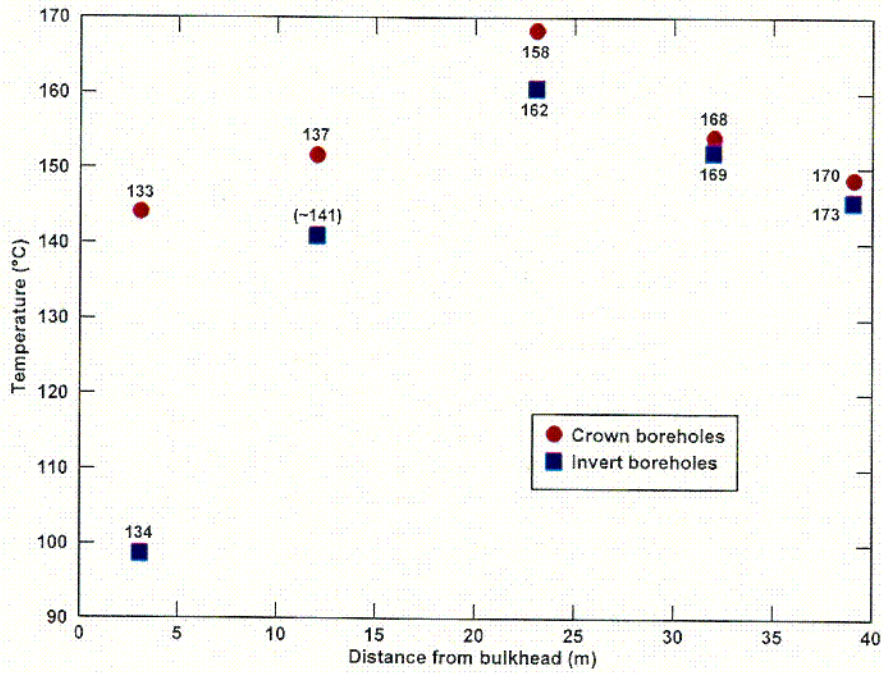
Figure 3-79. Temperature at a Depth of 2 m from Collar of Holes #158 to 162 of the DST as a Function of Elapsed Time

C:59

The vertical downward boreholes are more problematic. Water vaporized would tend to move downward through the matrix and fractures, in response to pressure gradients. Vapor movement in the fractures would be expected to be upward by buoyancy. However, any vapor that moved upward would move into hotter regions, and therefore would not condense. Thus, refluxing by gravity drainage would not be anticipated. Saturation-gradient liquid return through the matrix, described in Section 3.2.1 as saturation-gradient matrix-flow (the classic heat-pipe mechanism) would be the only reflux mechanism. Water influx from rock above would be the only other likely source for water returning to the sensor region. If the saturation gradient were the water-return mechanism, any vapor lost through upward migration (either pressure within matrix or buoyant in fractures) would cause a continual diminishing of volume of water available for return. However, the vertical downward holes exhibit a similar response to the vertical upward oriented boreholes, at least for the 137, 141, and 162 boreholes. If the vertical-upward responses were the result of reflux, a similar response with flattening to be exhibited by the vertically downward boreholes, where the water vapor that was displaced below the sensor and condensed would drain in the same vertical downward direction away from the sensor. As noted, it is possible to have heat-pipe effects in which water is returned within the matrix itself by way of saturation gradients, in the classic heat-pipe effect. However, if this were the case and matrix reflux was the major contributor to the boiling effects observed, all of the boreholes should have shown similar behavior, unless the hydrologic properties of the matrix was not uniform among those boreholes. Another possibility is that water was continuously supplied to the sensor in Hole 141 and 162, either from below via a larger-scale convection cell or from drainage from regions above.

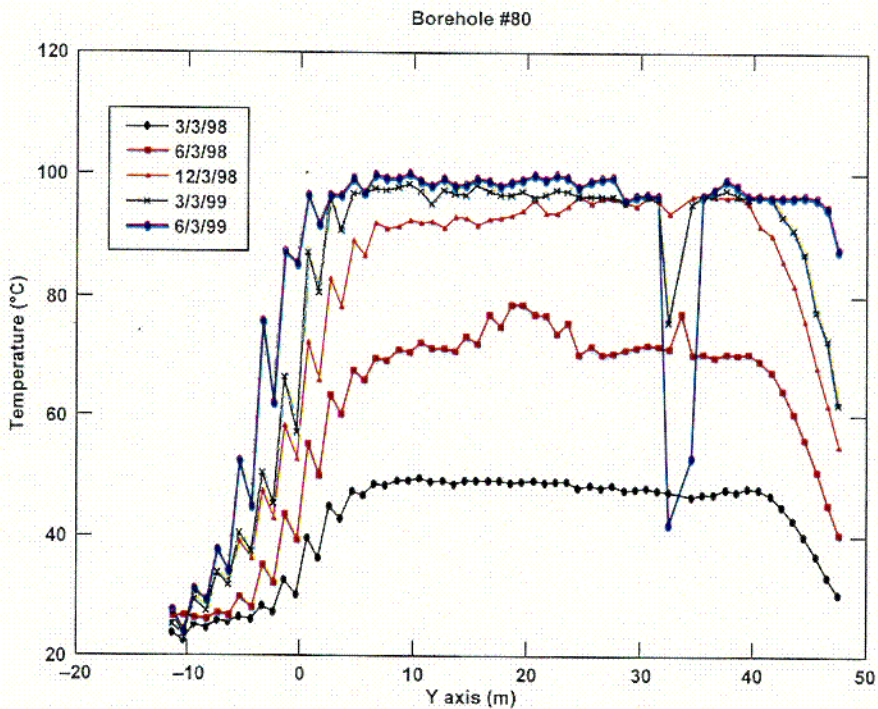
Figure 3-80 shows the temperature measured at about 0.4 m from the collar of 10 vertical holes drilled from the HD, as a function of distance from the bulkhead. Five of those holes (#133, 137, 158, 168, and 170) were in the crown of the HD; the other five (#134, 141, 162, 169, and 173) were in the invert of the HD. There was no temperature sensor at depth shallower than 1.5 m from collar in Hole 141. The temperature value for Hole #141 was projected using the thermal gradient established by other measurements between the depth of 0.4 m and 1.5 m from collar. Figure 3-80 shows the thermal effect of the bulkhead. The temperature measured in the crown of the HD showed no effect of the bulkhead in that the temperature gradient from borehole 158 was approximately 1.3°C/m towards either end of the drift. However, the effect of the bulkhead seems to be significant for temperatures in the invert. The gradient toward the end of the drift is similar to that in the crown. However, the gradient towards the bulkhead was nearly double (2.3°C/m) that measured in the crown and towards the far-end invert.

Figure 3-81 shows temperature snapshots along Hole #80, which was parallel to the axis of the HD at about 3.5 m above the midpoint of the wing-heater plane. The bulkhead is at 0 m in the horizontal axis of the plot. Similar to the water-content data shown in Figure 3-82, the measured temperatures in the rock above the heaters showed no effect of the bulkhead. The temperature in Hole 80 showed some episodic fluctuations, at a depth range of 16 to 24 m, and a trend of decreasing temperature at a depth range of 32 to 36 m. The borehole video in this hole showed an extended fracture zone between 33.9 and 34.8 m depth. The temperature fluctuations may be related to vapor or gas movement in fractures.



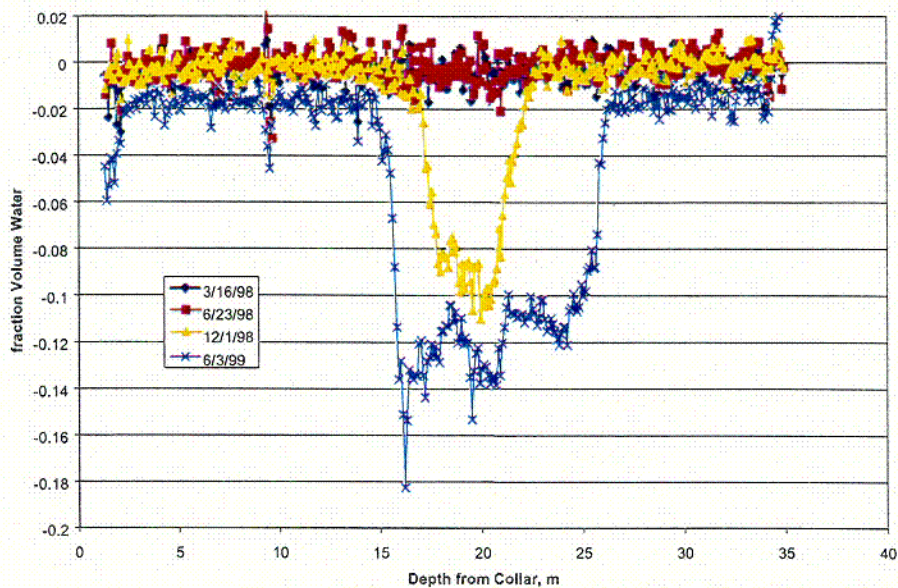
DTN: MO9807DSTSET01.000, MO9810DSTSET02.000, MO9906DSTSET03.000

Figure 3-80. Temperature at About 0.4 m from the HD Wall in All Vertical Temperature Holes of the DST, as a Function of Distance from the Bulkhead



Source: Adapted from CRWMS M&O 2000a, Figure 50

Figure 3-81. Temperature Snapshots along Hole #80 of the DST, as a Function of Distance from the Bulkhead



DTN: LL990708904243.033

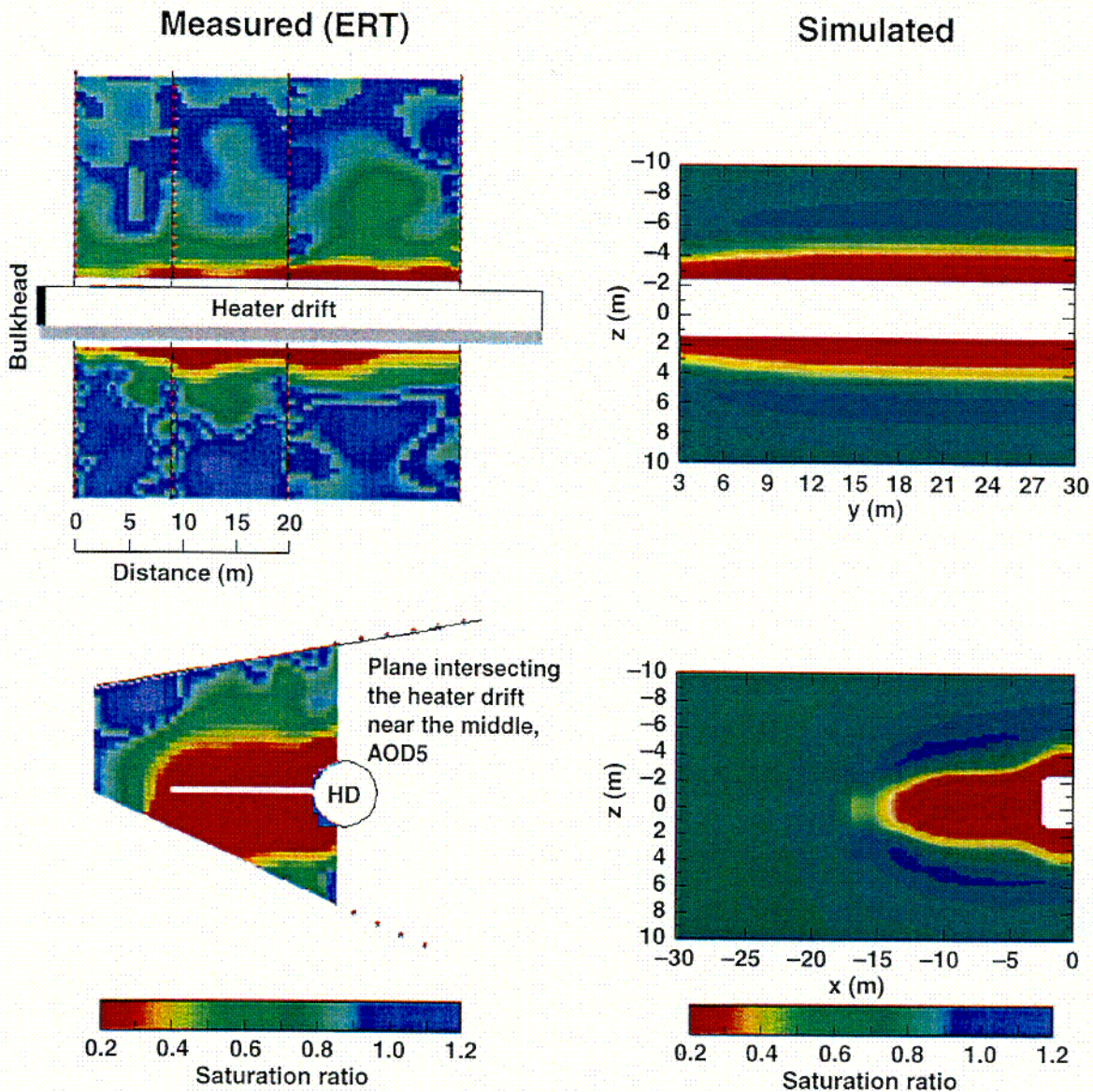
Figure 3-82. Difference Volume-Fraction Water in Hole #50 of the DST, as a Function of Depth from Collar

The drying of the rock mass in the DST, as monitored by ground-penetrating radar (GPR), ERT, and neutron logging, is discussed in the *Thermal Test AMR* (CRWMS M&O 2000a, Figures 6-35, 6-50 to 6-56). There are five figures in the *Thermal Test AMR* showing moisture distribution in the DST measured by GPR and ERT (CRWMS M&O 2000a, Figures 33, 53 to 56). Those figures show that moisture distribution varied with time and location, with respect to the HD and the Wing Heaters. It is difficult to draw conclusions regarding the vertical symmetry of the drying and wetting regions with respect to the heat source. For example, Figure 3-83 (CRWMS M&O 2000a, Figure 56) shows a more extended dry region below the wing heater. But Figure 3-84 (CRWMS M&O 2000a, Figure 33) seems to show a wetter region at a distance greater than 3 m below the inner wing heater than at the same distance above.

Some plots of neutron data are included to illustrate the local drying process, and spatial variability of the drying. Figures 3-82 and 3-85 show four snapshots of the volume water fraction difference, as measured by neutron logging in Boreholes 50 and 67, respectively. Boreholes 50 and 67 are in about the same configuration in the DST, refined below the heated drift and wing heaters from the observation drift, except that Borehole 50 is much closer to the bulkhead than Borehole 67 (6.4 m and 26.5 m, respectively) (CRWMS M&O 1997b, Figures 3-2 and 3-3). Drying started in Borehole 67 several months before that in Borehole 50. This may be related to the thermal evolution of the DST, influenced by the bulkhead. The drying region in Hole 67 was still expanding at the end of 18 months of heating, but the drying in this hole seemed to have reached maximum, which represented a decreased water content equal to about 0.16 percent of the volume of the rock mass. Figure 3-86 shows that drying in Borehole 68, which was at the same location as Borehole 67, but declined 6° more, started even later. Figure 3-86 illustrates that in regions further away from the heaters, the drying had been more uniform along hole 68. Figure 3-87 shows the drying along Borehole 80, which was parallel to the HD at about 3.5 m above the mid point of the wing-heater plane. The drying in this hole was

C-61

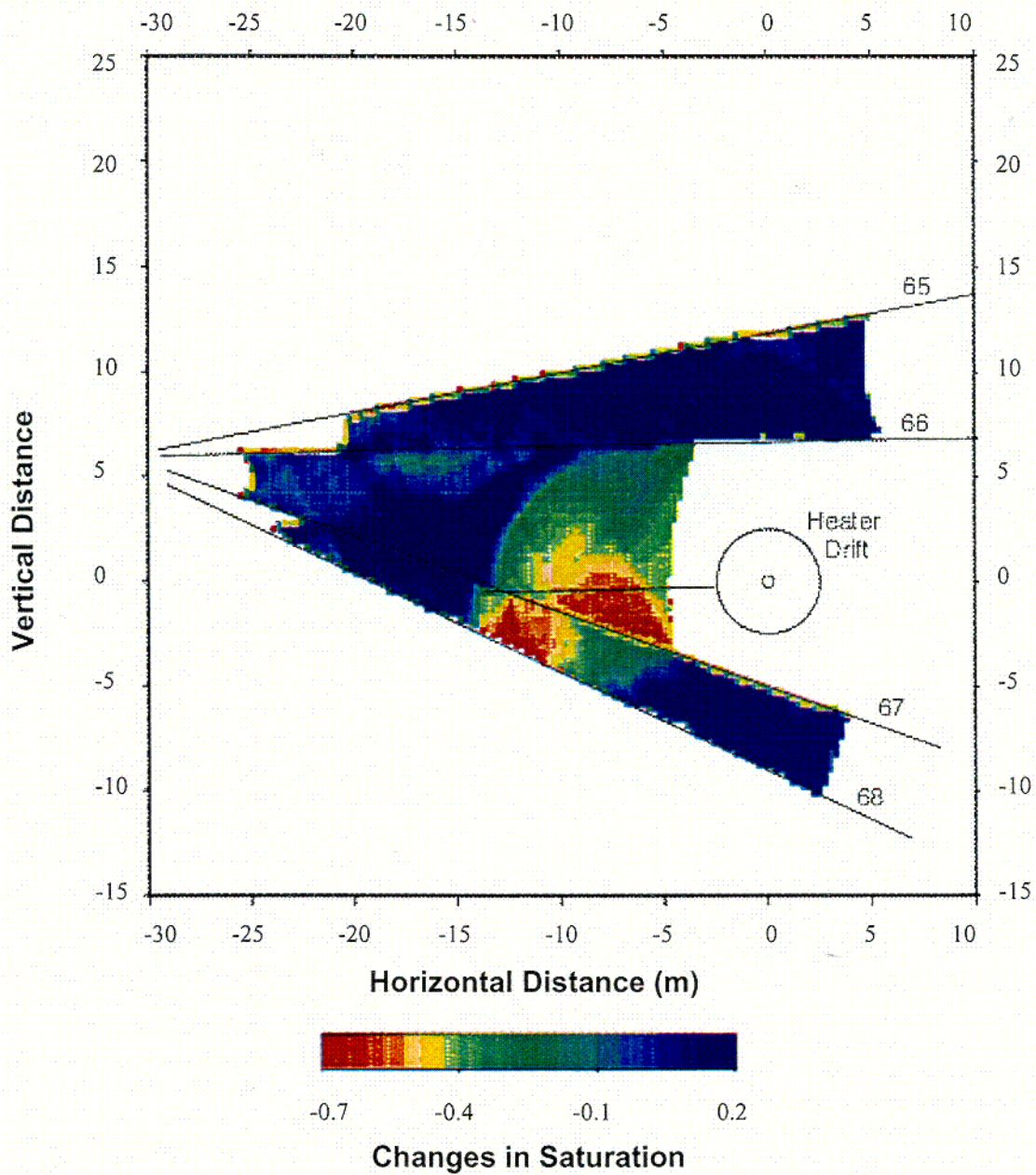
accompanied by localized increase of moisture content. It is possible that this might be related to heat-pipe effects. The high water content region between 40 and 50 m from the collar was associated with the temperature fluctuation shown in Figure 3-81.



Source: CRWMS M&O 2000a, Figure 56

NOTE: Measured ERT-derived water saturation ratio (at 558 days) for the longitudinal cross-section through the HD axis (top) and transverse cross-section OD#5 (Boreholes 62, 63) (bottom).

Figure 3-83. Comparison of Distributions of Measured and Simulated (NUFT) Water Saturation at 547 Days for the DST, Using the DS Property Set



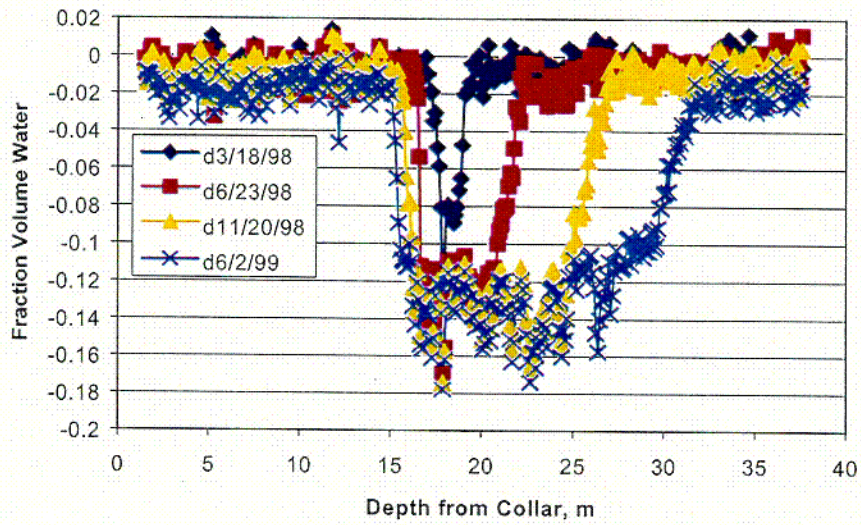
Source: CRWMS M&O 2000a, Figure 33

NOTE: The observation drift is just to the left of the figure, where the borehole lines would converge.

Figure 3-84. Tomogram Showing Saturation Change from Pre-Heat Ambient Values Derived from a Cross-Hole Radar Survey Taken in January of 1999 (~13 months of heating) in the Plane of DST Boreholes 64-68

*6-63*

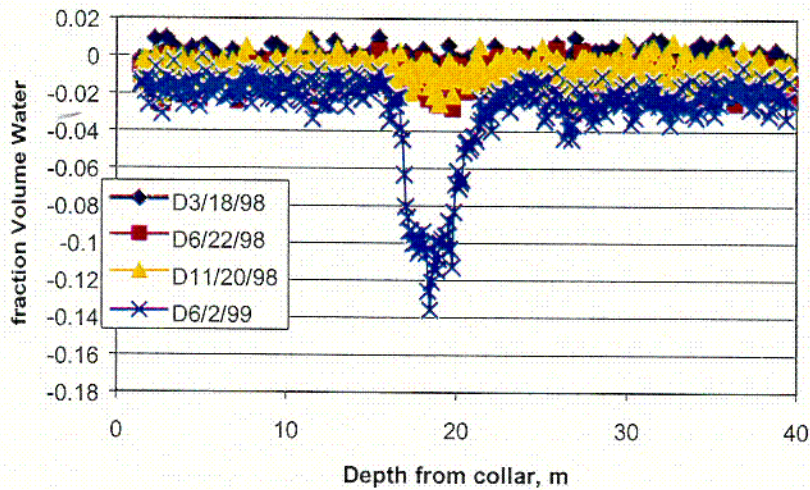
Difference fraction volume water, with respect to the 2/98 measurements, in Hole #67 of the DST as a function of depth.



DTN: LL990708904243.033

Figure 3-85. Difference Volume-Fraction Water in Hole #67 of the DST, as a Function of Depth from Collar

Difference fraction volume water, with respect to the 2/98 measurements, in Hole #68 of the DST as a function of depth.



DTN: LL990708904243.033

Figure 3-86. Difference Volume-Fraction Water in Hole #68 of the DST, as a Function of Depth from Collar

*C-64*

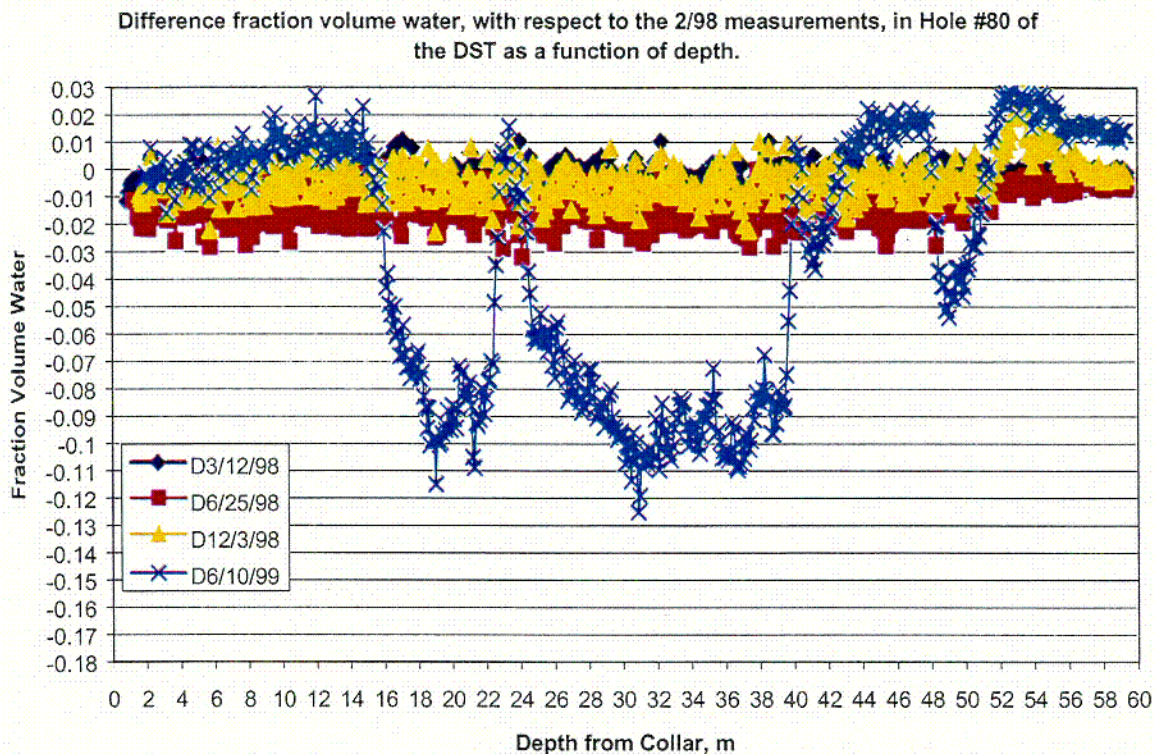


Figure 3-87. Difference Volume-Fraction Water in Hole #80 of the DST, as a Function of Depth from Collar

The measured CO<sub>2</sub> concentration in the DST after 12 months and 15 months of heating showed high values above and below the heaters, and the CO<sub>2</sub> concentrations after 15 months of heating were greater than that after 12 months of heating (CRWMS M&O 2000b, Figure 8). Four water samples were collected from hydrological Holes 60 and 186 between December 11, 1998 and January 26, 1999. The chemical composition of those water samples, along with that of the pore water of Topopah Spring Tuff, are shown in the *THC Process AMR* (CRWMS M&O 2000b, Table 9). The waters that were collected from the hydrological holes are generally more dilute (lower Cl<sup>-</sup> and SO<sub>4</sub><sup>2-</sup>) and have lower pH than the initial pore water. The aqueous silica concentrations are similar to or much higher than in the pore water, indicating that the collected waters were not simply a mix of the pore water and pure condensate water. The water from a hotter interval (60-3) had a greater pH and SiO<sub>2</sub> concentration than from a cooler interval (186-3). This trend is consistent with the evolution of pure condensate water. The concentration of HCO<sub>3</sub><sup>-</sup> is lower in 60-3 relative to 186-3. This is also expected because of the greater temperature in 60-3 (CRWMS M&O 2000b, p. 65).

### 3.6.1.3.2 Model Analyses of the DST Results

In the *Thermal Test AMR* (CRWMS M&O 2000a), the measured temperature and moisture content data of the DST were compared with the simulated data from the TOUGH2 and NUFT models, using the following property sets: the DS property set, mountain-scale property set, and DKM-TT99 property set. Statistical measures, such as root-mean-square-error, mean-error, and normalized-absolute-mean-error, were used to compare the fitness of the property sets to the

measured temperature data. Sensitivity analyses were conducted to assess the effect of certain parameters on the predicted temperature and moisture content.

The *Thermal Test AMR* (CRWMS M&O 2000a) results indicated that the temperatures predicted by the DKM model with TOUGH2 simulations were in good agreement with the measured ones. There are three figures in the *Thermal Test AMR* showing the measured DST temperature profiles and those simulated by the DKM/AFM using TOUGH2, and the Drift Scale property set. Figure 3-88 (CRWMS M&O 2000a, Figure 21) illustrates one example of the comparison. There are a few minor differences between the measured and the simulated temperatures. The simulation under-predicted the temperature in the two horizontal holes (Hole 139 and 143). This is probably caused by smearing of the data from the wing heater source in the simulation. The simulation over-predicted the temperature near the heater-drift wall. This may imply that the model did not adequately represent heat losses in the test block. Another difference between the measured and simulated temperatures is the temperature signature of the boiling processes (heat-pipe effect). Figure 3-89 (CRWMS M&O 2000a, Figure 83) shows one example of the TOUGH2 simulation, using property set DKM-TT99. This property set seems to represent the heat-pipe effect better than the DS/AFM-UZ99 property set (CRWMS M&O 2000a, Section 6.3.2.2). The statistical comparison between the measured temperature and that simulated temperatures using TOUGH2 is in good agreement, as shown in Figure 3-90 (CRWMS M&O 2000a, Figure 25). For the NAMD of the sensors below 97°C, the DKM-TT99 property set seems to be better than that of the DS/AFM-UZ99 property set.

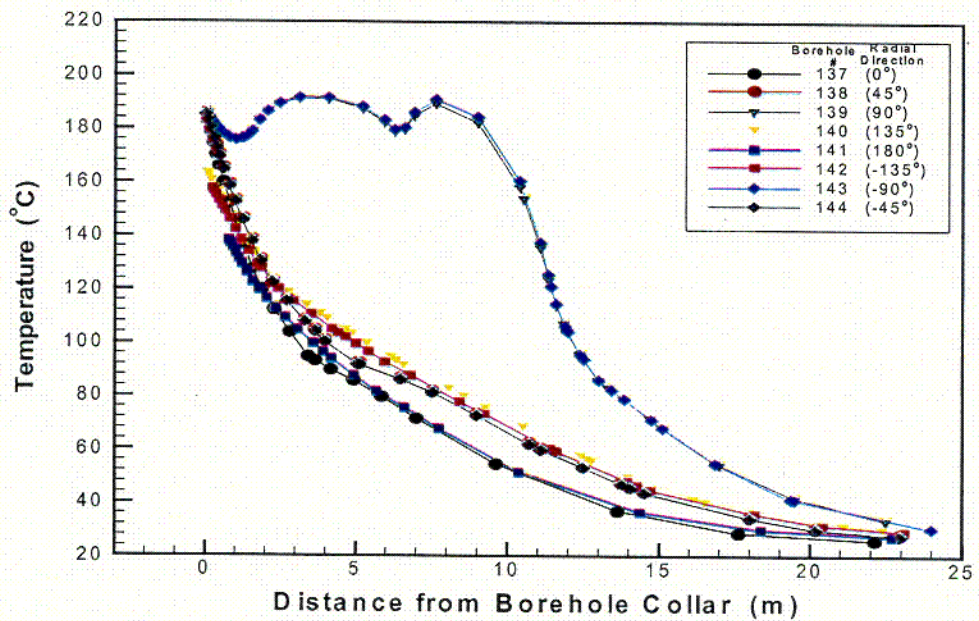
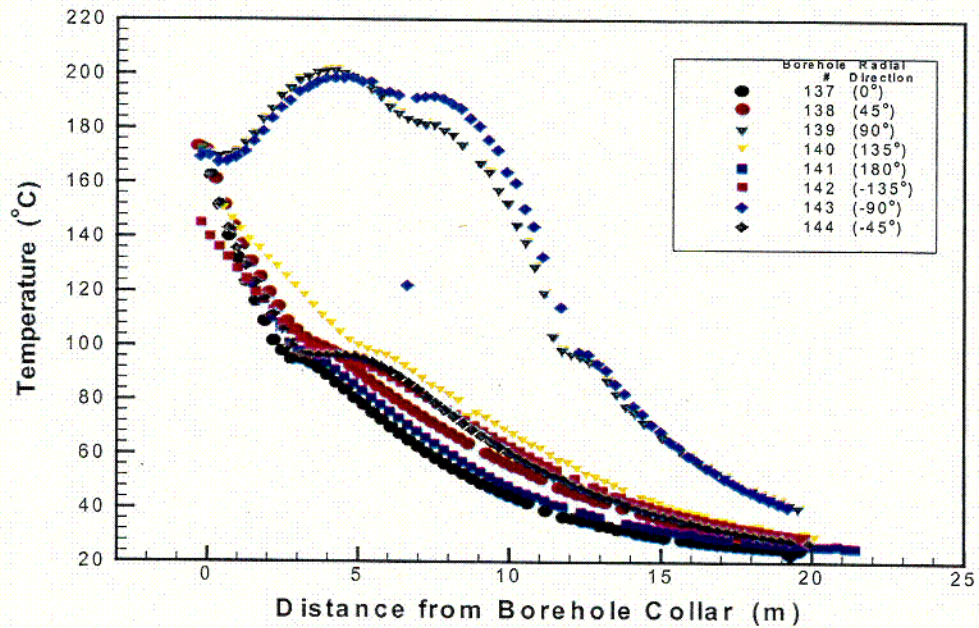
The DKM/AZ TOUGH2 simulation using the drift-scale property set (DS/AFM-UZ99) was also used in the *Thermal Test AMR* to compare the measured to simulated temperature evolution in the DST. (CRWMS M&O 2000a, Figures 22-24). Figure 3-91 (CRWMS M&O 2000a, Figure 22) is presented as an example of the comparison of this temperature evolution. Generally, the predictions agree with the measured ones reasonably well. However, the model seems to have under-predicted the temperature, except during the time when the measured temperatures showed boiling. The model results did not show the boiling signature.

The DST temperatures simulated by the DKM model using NUFT and the DS property set, were reported in the *Thermal Test AMR* (CRWMS M&O 2000a, Figures 35 to 56). Figure 3-92 (CRWMS M&O 2000a, Figure 43) shows good comparison of the measured and simulated temperatures as a function of distance from the centerline of the HD in vertically-upward hole 137. The temperatures in horizontal-hole 160 simulated by NUFT also compare well with the measured results, as shown in Figure 3-93 (CRWMS M&O 2000a, Figure 46). Similar to the DKM TOUGH2 simulation (Figure 3-91), the DKM NUFT simulation also did not capture the boiling signature. A statistical evaluation indicates that NUFT simulations are apparently not as good as the TOUGH2 simulations, as shown in Figure 3-94 (CRWMS M&O 2000a, Figure 51). Possible causes for the differences in performance of the DKM model using NUFT and TOUGH2 may include the difference in the drift shape and model domain size. NUFT used a rectangular drift shape and model domain that extended from 267 m below the HD to 321 m above the HD (i.e. from the ground surface to the water table). TOUGH2 used a circular drift shape and a model domain that extended 100 m above the HD and 150 m below the HD.

They may also result from the difference in how the boundary conditions and property sets were used in the models. The TOUGH2 simulations used the boundary conditions to determine

saturation for use in the model whereas the NUFT simulations used the measured saturations to determine the boundary conditions.

The DKM/TOUGH2 simulations showed that the calculated temperatures of the fractures are practically the same as in the nearby matrix, implying that, for all practical purposes, the matrix and fracture are in thermal equilibrium (CRWMS M&O 2000a, Section 6.2.2.1). The DKM/TOUGH2 simulations also showed that the temperature distribution was not very sensitive to the thermal conductivity values over the range considered. The thermal conductivity values in the DS property set and the DKM-TT99 property set were both within an acceptable range, based on comparison of measured data and calculated temperatures (CRWMS M&O 2000a, Section 6.3.2.2). For the hydrological processes, the comparison between the measured and calculated water saturation was more qualitative. Qualitatively, the moisture distribution calculated by the DKM model (using NUFT) agreed with that measured by ERT, especially after one year of heating (CRWMS M&O 2000a, Figures 53 to 56). One example of the comparison is shown in Figure 3-83 (CRWMS M&O 2000a, Figure 56). The TOUGH2 calculation of water saturation in the matrix was in general agreement with the neutron data of the DST in the region below the heaters, as shown in Figures 3-95 and 3-96 (CRWMS M&O 2000a, Figures 34 and 59). The simulated distribution of saturation also qualitatively agrees well with the GPR results, as shown in Figures 3-95 (CRWMS M&O 2000a, Figure 33). In the region above the wing heaters, the predicted saturation in the matrix was greater than that measured by neutron logging (CRWMS M&O 2000a, Figures 34 and 61). The DKM/TOUGH2 model results showed that the DKM-TT99 property set seemed to have better predicted measured air-permeability, based on saturation changes in the fractures. However, both property sets used the DKM/TOUGH2 model simulation are considered to have predicted results that were within acceptable limits of the measured data from the DST (CRWMS M&O 2000a, Section 6.2.2.3). It should be noted that the model analyses using TOUGH2 assumed that the measured air-permeability changes were solely due to changes in water saturation in fractures. Fracture permeability is very sensitive to changes in the fracture aperture. The fracture aperture in a heated rock mass can be changed due to thermal expansion and slips along fractures. Coupling of TM calculation results to TH simulations is ongoing.

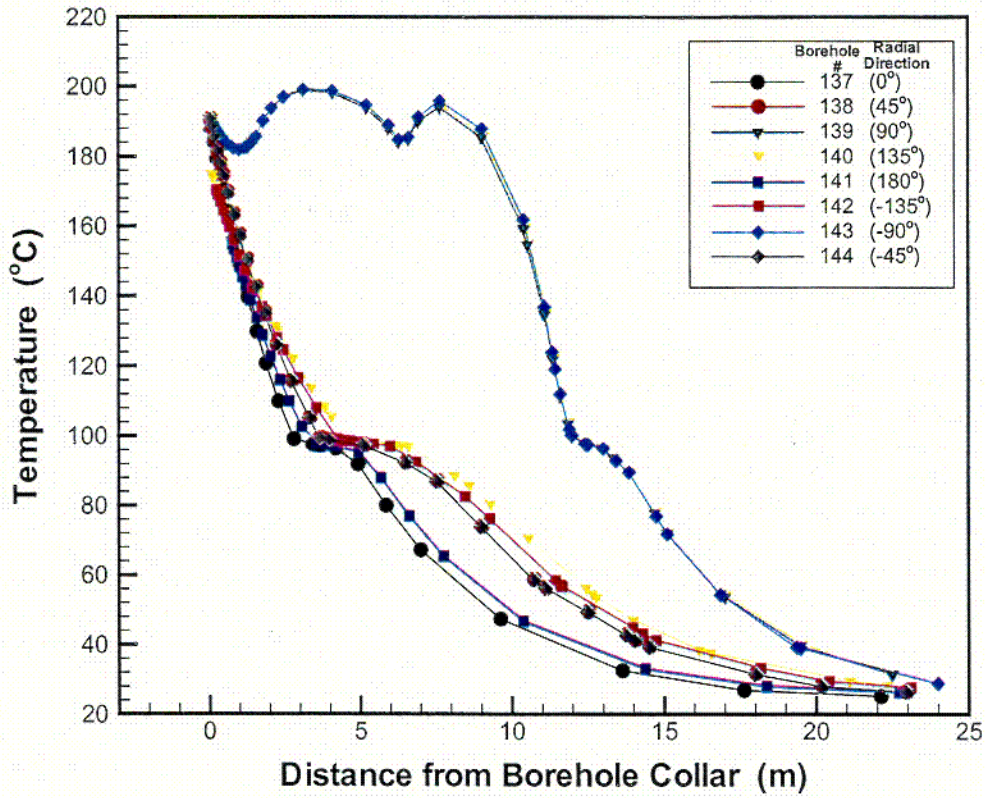


Source: CRWMS M&O 2000a, Figure 21

NOTE: The DS/AFM-UZ99 properties were used in the simulation.

Figure 3-88. Measured (top) and DKM/TOUGH2 Simulated (bottom) DST Temperatures, as a Function of Distance of Sensor Locations from Borehole Collars in RTD Boreholes 137-144, after 18 Months of Heating

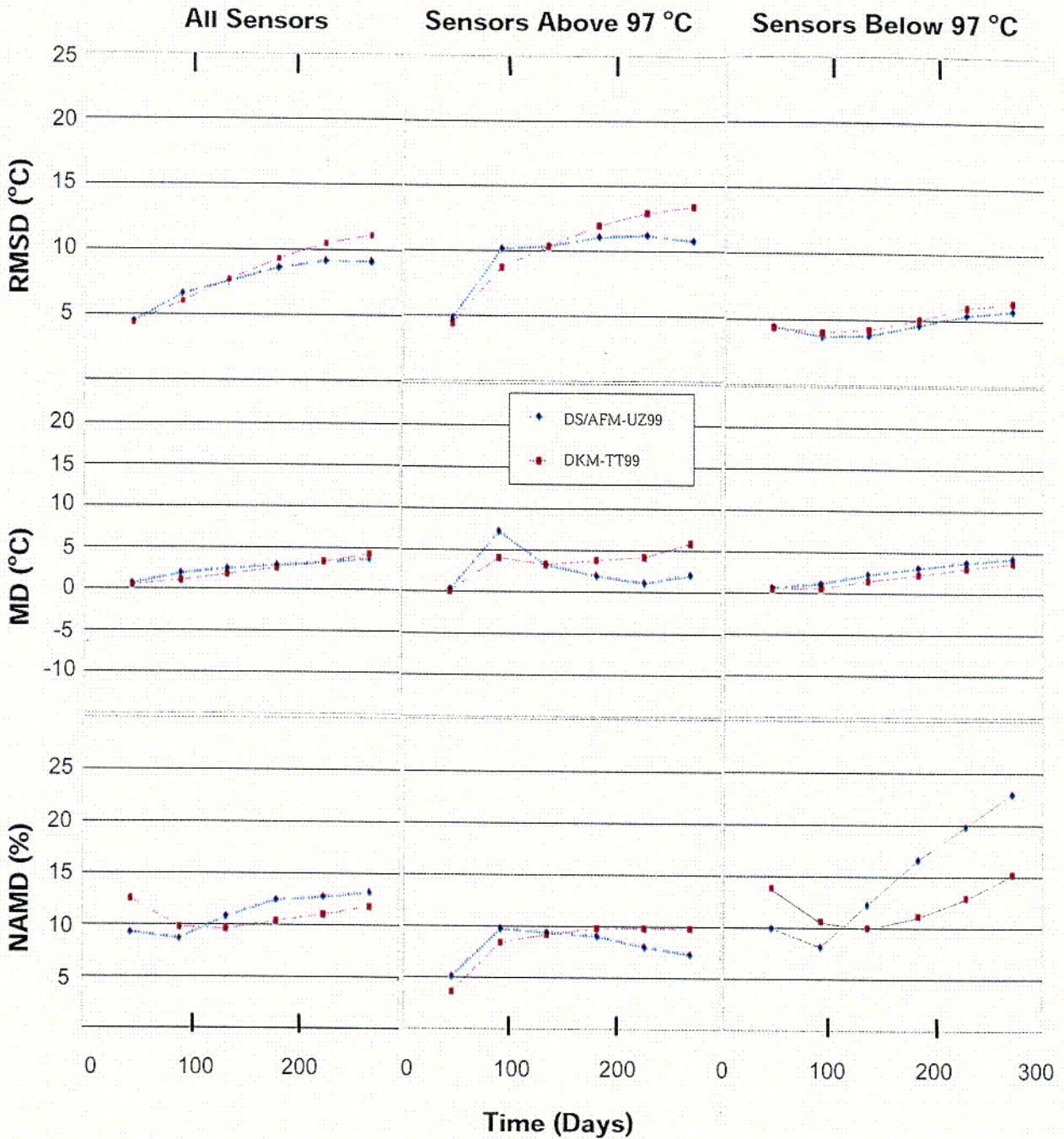
*C-666*



Source: CRWMS M&O 2000a, Figure 83

Figure 3-89. DKM/TOUGH2 Simulated Temperatures along RTD Boreholes 137-144 after 18 Months of DST Heating

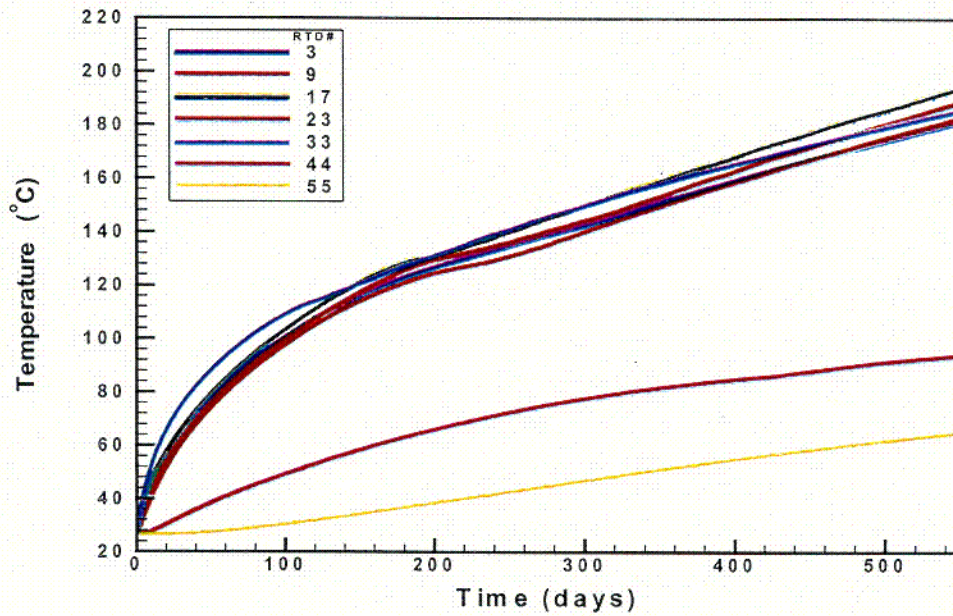
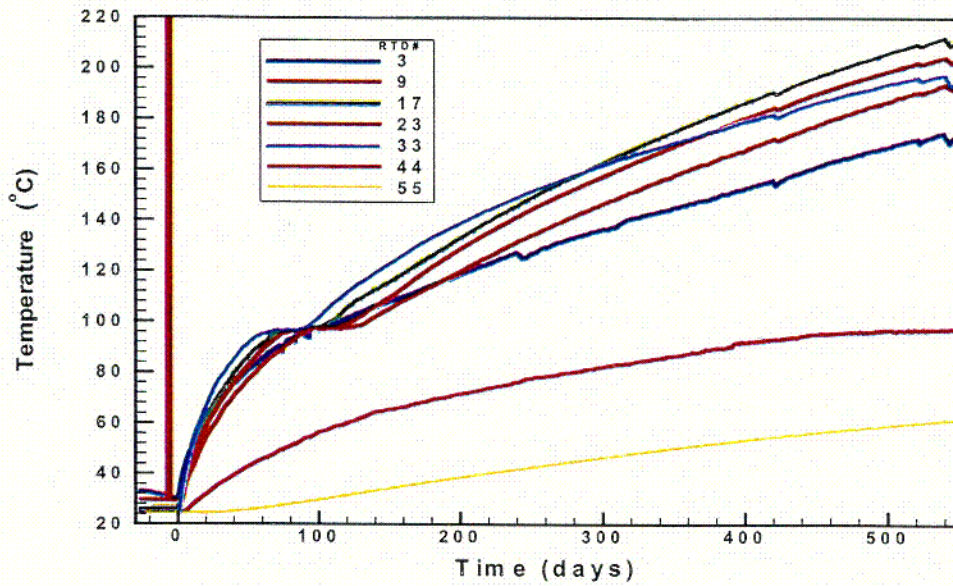
C-67



Source: CRWMS M&O 2000a, Figure 25

- NOTES: 1. The property sets tested were the Drift Scale (DS/AFM-UZ99) set used in TSPA-SR calculations and the DKM-TT99 set which has higher fracture permeability, lower fracture porosity, and a narrower range of thermal conductivity dependence on saturation.
2. See Note 2 of Figure 3-61 for descriptions of the statistical measures.
3. See Note 3 of Figure 3-61 for sensor group descriptions

Figure 3-90. Statistical Measures for DST DKM/TOUGH2 Thermal Analyses

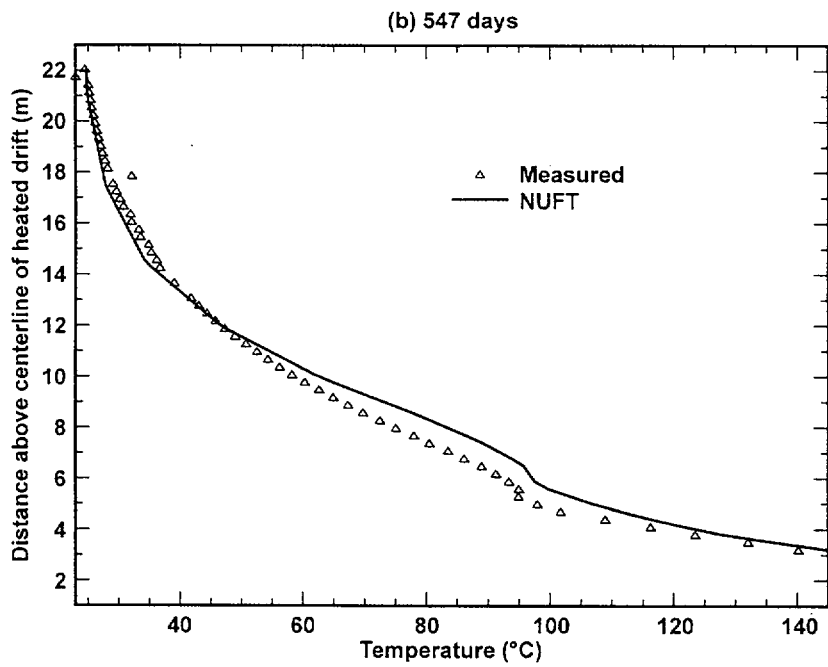
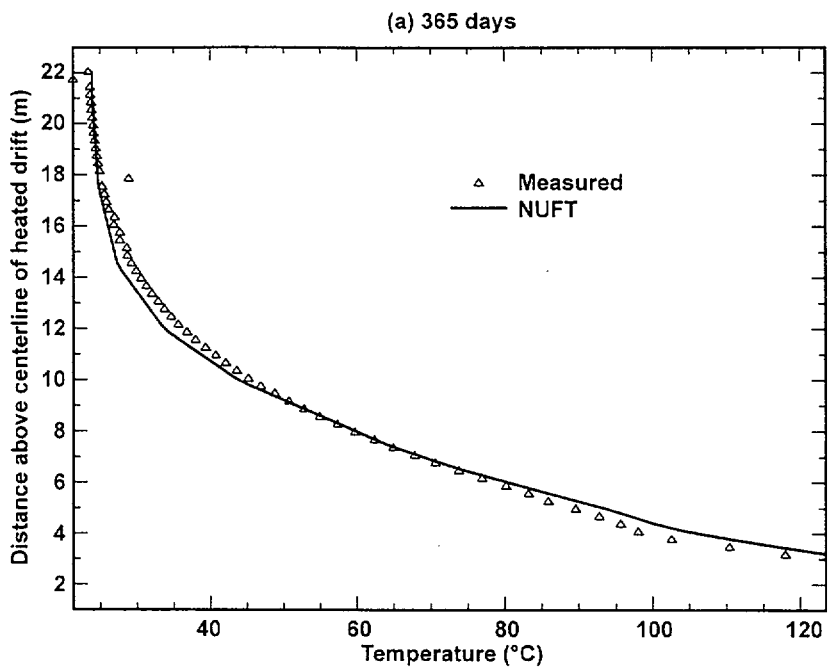


Source: CRWMS M&O 2000a, Figure 22

NOTE: The DS/AFM-UZ99 properties were used in the simulation.

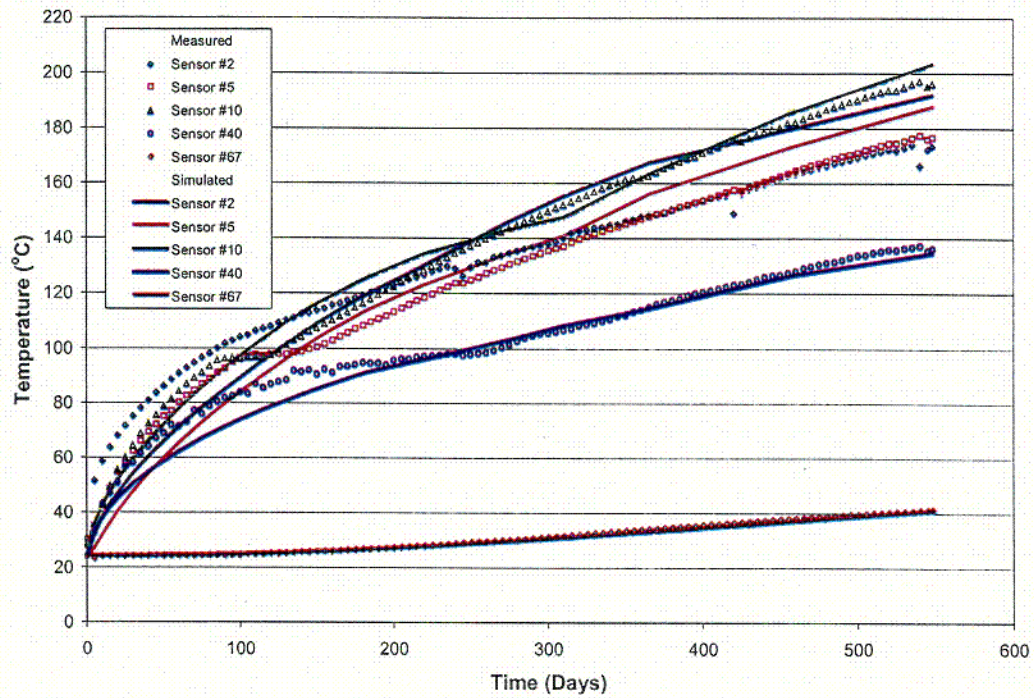
Figure 3-91. Measured (top) and DKM/TOUGH2 Simulated (bottom) DST Temperatures, as a Function of Time at Selected Sensor Locations in Borehole 160 (Horizontal, near the Wing Heaters)

C-69



Source: Adapted from CRWMS M&O 2000a, Figure 43

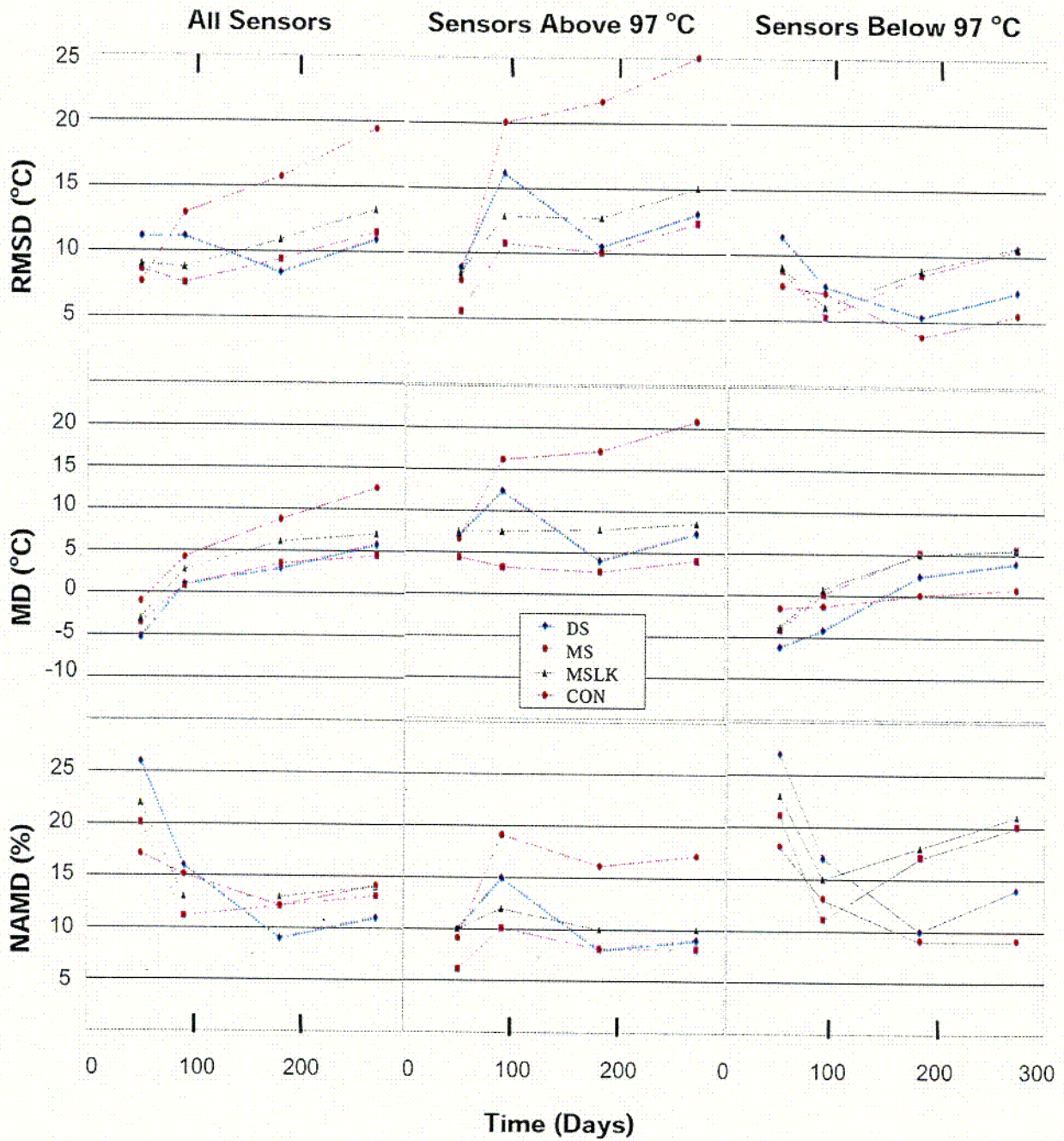
Figure 3-92. Comparison of DKM/NUFT Simulated and Measured Temperatures from the DST, Along Borehole 137 (Vertical-Upward) at (a) 12 Months and (b) 18 Months



Source: CRWMS M&O 2000a, Figure 46

Figure 3-93. Comparison of DKM/NUFT Simulated and Measured Temperature Histories for Sensors No. 2, 5, 10, 40, and 67 Over 18 Months of Heating in Borehole 160 (Horizontal, near the Wing Heaters) for the DST, Using the DS Property Set

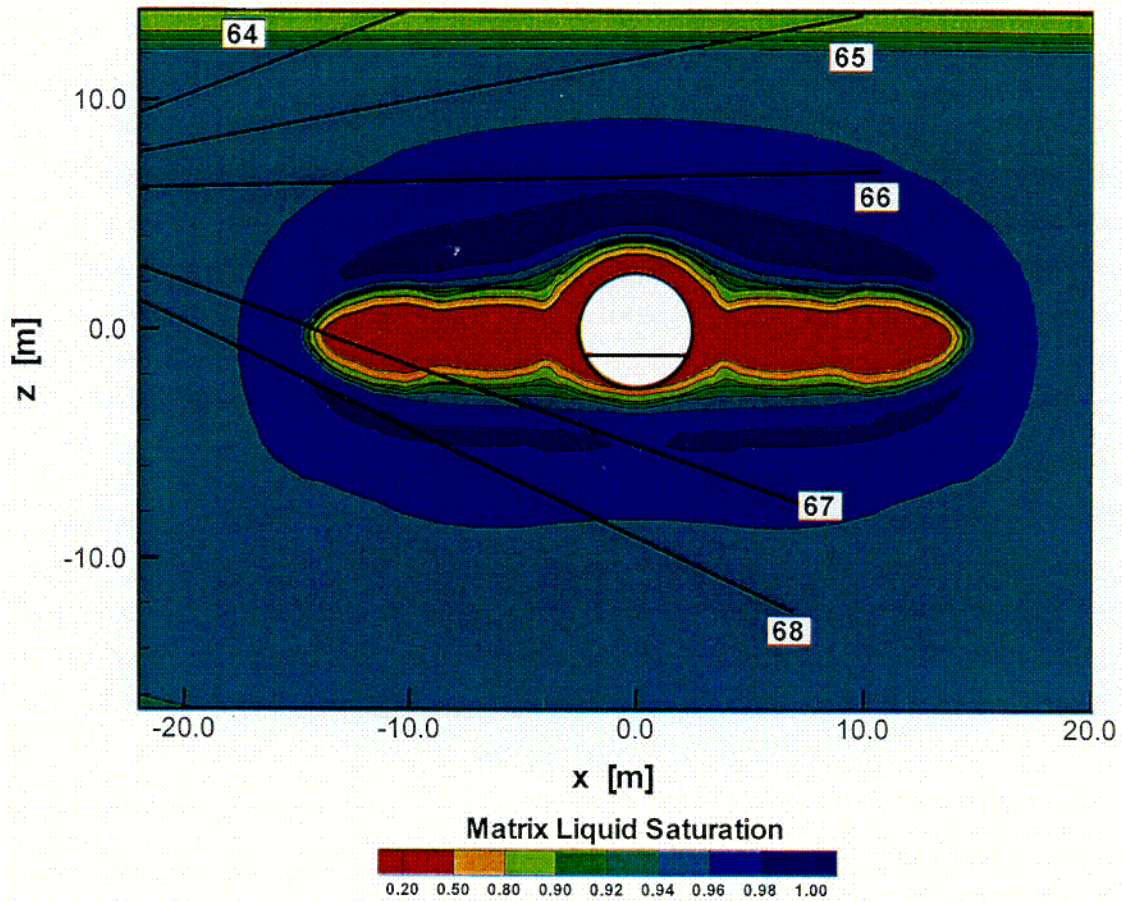
C-10



Source: CRWMS M&O 2000a, Figure 51

- NOTES: 1. The property sets tested were the Drift Scale (DS) set used in TSPA-SR calculations, MS set with higher fracture permeability, a second Mountain Scale (MSLK) set with a narrower range of thermal conductivity dependence on saturation, and a conduction-only (CON) set that does not track mass transfer.
2. See Note 2 of Figure 3-61 for descriptions of the statistical measures.
3. See Note 3 of Figure 3-61 for sensor group descriptions

Figure 3-94. Statistical Measures for DST DKM/NUFT Thermal Analyses

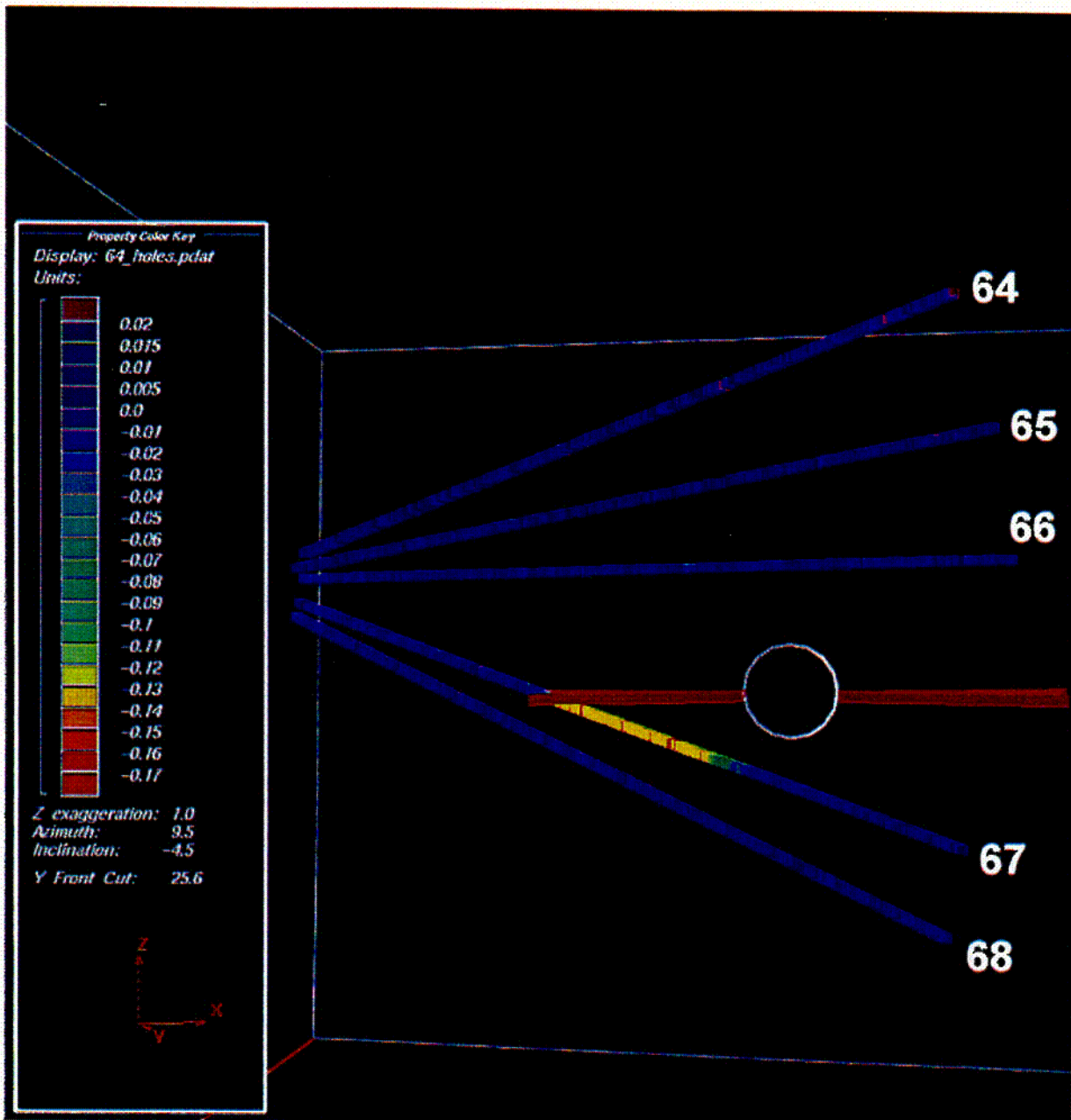


Source: CRWMS M&O 2000a, Figure 34

NOTE: The x- and y-axes are the horizontal and vertical distances from the drift centerline. The hydrology boreholes converge at the observation drift, just beyond the upper left edge of the figure.

Figure 3-95. TOUGH2 Simulated Matrix Liquid Saturation in the Plane of DST Boreholes 64-68 After 12 Months of Heating, Using the DS/AFM-UZ99 Properties

C-72



Source: CRWMS M&O 2000a, Figure 59

Figure 3-96. Fraction-Volume of Water Content in DST Boreholes as Measured by Neutron Logging Boreholes 64 to 68 for Nominal Heating Duration of 12 Months

In the *THC Process AMR* (CRWMS M&O 2000b) THC model calculations using TOUGHREACT were conducted to analyze evolution of the measured gas phase CO<sub>2</sub> and the chemistry of the water. Two sets of chemical components and mineral assemblages were used in the simulations: *Complex* and *Less Complex*. The *Complex* geochemical system was a “full” set, including the major solid phases (minerals and glass) encountered in the geologic unit at Yucca Mountain. The *Less Complex* geochemical system was a subset that excluded aluminum-

silicate minerals (CRWMS M&O 2000b, Section 6.1.7). Model calculations of the *Less Complex* set predicted the locations of high CO<sub>2</sub> concentration and the range of the CO<sub>2</sub> concentration reasonably well. The *Less Complex* set model calculations also predicted the evolution of CO<sub>2</sub> concentration, in the first 9 to 12 months of heating, quite well. However, in the later months of heating the model predictions were not as good, except for measurements in the third packed-off region of Borehole 74 (Interval 74-3), which is bounded by the nodes, as shown in Figure 3-97 (CRWMS M&O 2000b, Figure 10). The apparent lower CO<sub>2</sub> concentration at 20 months of heating, as shown in Figure 3-97(b), may be due to a 6-day power outage that occurred about 1 month before the measurement. The greater than predicted CO<sub>2</sub> concentration in Borehole Intervals 76-3 and 78-3 may be due to drying of the gas phase when the gas sample was collected (CRWMS M&O 2000b, Section 6.2.7.2). The *More Complex* set model predicted similar locations for the CO<sub>2</sub> concentration as the *Less Complex* set. However, for the *More Complex* set, model-predicted CO<sub>2</sub> concentration values were much less than those of the *Less Complex* set model.

The chemical compositions of four water samples, collected from hydrology Boreholes 60 and 186 on December 11, 1998 and January 26, 1999 (CRWMS M&O 2000b, Section 6.2.7.3.1), are shown in Table 3-16. The water samples collected during the test were obtained from zones that were hotter than the temperatures given for the samples, because water temperatures were measured after collection and they had cooled substantially. Both intervals are located in the zone below the wing heaters. Borehole Interval 186-3 is lower and probably cooler than Borehole 60-3. Borehole 60 is located approximately in the same location as Borehole 77, and borehole 186 corresponds to about the position of Borehole 78.

Waters that were collected from the hydrology boreholes at elevated temperatures are generally more dilute (lower Cl and SO<sub>4</sub>) and lower in pH than the initial pore water. Aqueous silica concentrations are similar to or much higher than in the pore water, indicating that these waters are not simple mixtures of pore water and pure condensate water. Some clear trends in water chemistry of the condensate waters in both intervals over time are increases in pH and SiO<sub>2</sub> (aq) concentration, and a drop in Ca. A similar trend for pH and SiO<sub>2</sub> (aq) exists between the boreholes, where the hotter interval (60-3) has a higher pH and SiO<sub>2</sub> (aq) concentration than the 186-3 interval at each time. The concentration of HCO<sub>3</sub> is also lower in 60-3 relative to 186-3 as expected from the higher temperature of 60-3. Other relationships are less obvious.

The modeled pH of condensate waters in fractures (Figure 3-98) compares favorably with those collected from the hydrology boreholes (Table 3-16). As in the measured data collected at two times before the borehole intervals dried out, the model results show the effect of increasing pH with time and with increasing temperature in areas greater than 60°C. Therefore, in a given zone, the pH in the fractures first starts to drop because of steam condensation; then once the temperatures increase, so that the rate of evaporation and mineral-water reactions (and loss of CO<sub>2</sub>) are greater than the rate of addition of water (and CO<sub>2</sub>) via condensation, then the pH rises.

Some of the processes that could explain the water chemistry of samples collected in the hydrology boreholes include: mixing of pure condensate water with fracture pore waters, equilibration of condensate waters with matrix pore waters via molecular diffusion, reaction of condensate waters with fracture-lining minerals, and mineral precipitation due to reaction, boiling, temperature changes, or pH changes. The higher silica concentration in the waters

collected in January compared to those collected in December, relative to chloride and the initial pore water silica concentration, is consistent with dissolution of a silicate phase, rather than increased concentration by boiling. However, concentrations of K, Mg, and Na are higher than what would be expected by dilution of original pore water (as evidenced by the low chloride concentrations). Therefore, the silicate phases that dissolved must have been some combination of cristobalite, opal, feldspar, clays or zeolites, rather than just a single silicate-phase. The drop in Ca over time is consistent with calcite precipitation, which would be expected as the condensate waters were heated further and underwent CO<sub>2</sub> degassing, resulting in an increase in pH.

Table 3-16 Measured Concentrations in TSw Pore Water from Alcove 5 and Chemistry of Water Taken from Hydrology Boreholes

Parameter	Units	Pore Water(1)	60-3(2) (12/11/98)	60-3(2) (1/26/99)	186-3(2) (12/11/98)	186-3(2) (1/26/99)
Temperature	C	25	26.5-49.6	51.7	34.3-34.8	Unknown
pH		8.32	6.92	7.4	6.83	7.2
Na	mg/l	61.3	20.3	19.1	17	25.9
SiO <sub>2</sub> (aq)	mg/l	70.5	115.5	139	58.2	105.5
Ca	mg/l	101	13.9	5.9	20.2	2.92
K	mg/l	8.0	7.8	4.1	3.9	5.9
Mg	mg/l	17	3	1.2	5.7	6.3
Al	mg/l	9.92x10 <sup>-7</sup> (3)	n.d. (< 0.06)	n.d. (< 0.06)	n.d. (< 0.06)	n.d. (< 0.06)
HCO <sub>3</sub> <sup>3</sup> (3)	mg/l	200	n.a.	41	n.a.	116
Cl	mg/l	117	20	10	19	23.3
SO <sub>4</sub>	mg/l	116	30.8	13.5	26.2	21

DTN: LL990702804244.100.

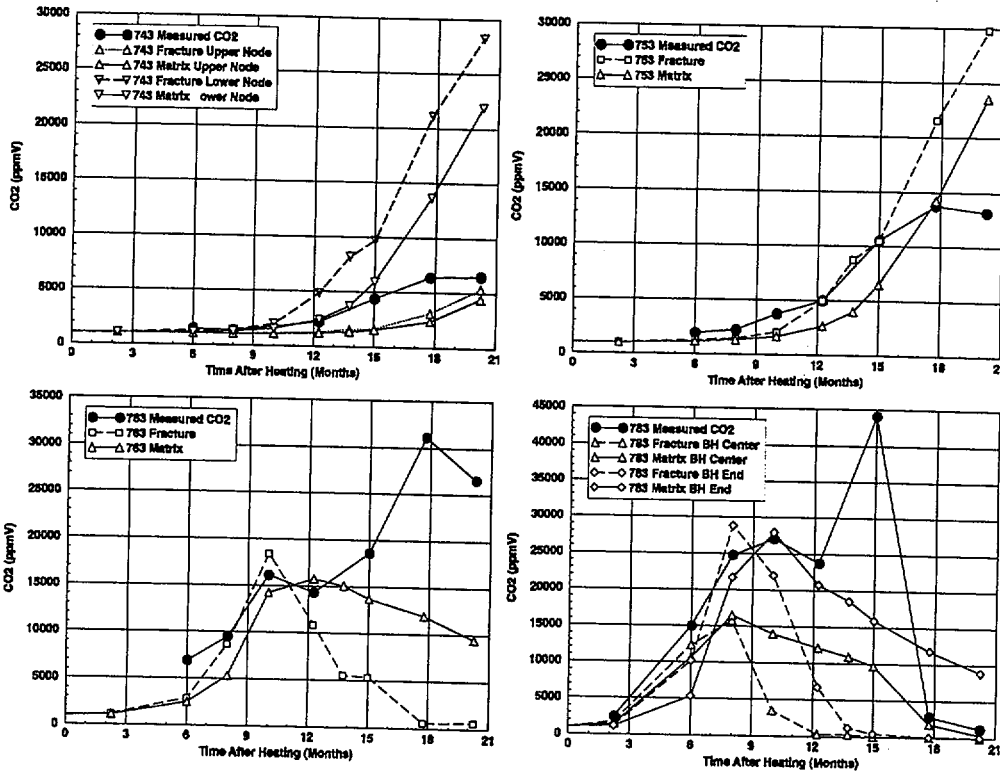
NOTES: (1) Average of porewater analyses ESF-HD-PERM-1 (30.1'-30.5') and ESF-HD-PERM-2 (34.8'-35.1'). DTN: LL990702804244.100.

(2) Calculated by assuming equilibration with Ca-smectite at 25°C.

(3) Total aqueous carbonate as HCO<sub>3</sub><sup>3</sup>, calculated from charge balance.

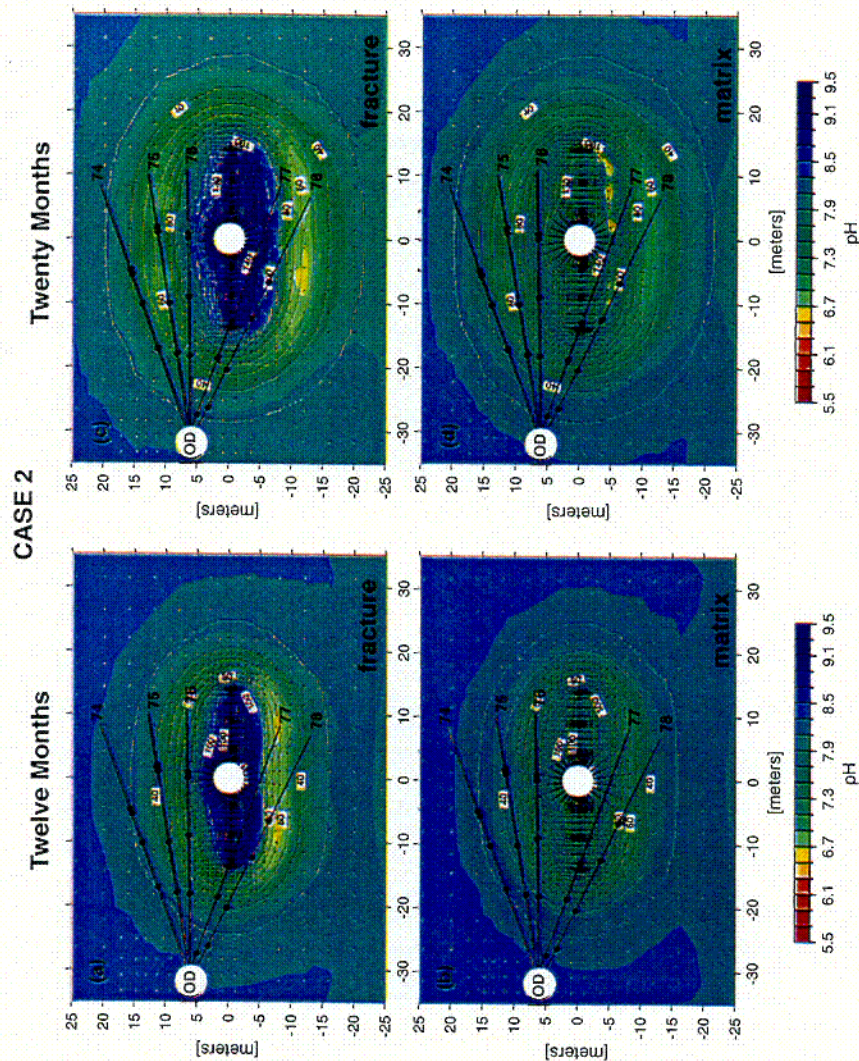
n.a.=not analyzed, n.d.=not detected

The model results also predicted precipitation of calcite in the fractures above and to the margins of the heaters, with some dissolution of calcite below the wing heaters. In the matrix, the models predicted a uniform region of calcite precipitation in the dryout zone. However, the change of either fracture or matrix porosity due to the precipitation and dissolution of calcite was no more than 0.1 percent, and the effect on the changes in permeability and capillarity was negligible (CRWMS M&O 2000b, Section 6.2.7.5). It should be noted that the change in fracture permeability is not just the result of porosity change due to mineral precipitation and dissolution. Laboratory studies of fracture healing indicate that smoothing of the fracture asperities by dissolution and precipitation can effectively change the permeability (Daily et al. 1987, p. 7861). Most fractures in an underground rock mass are under compressive stresses. Decreases in fracture roughness allow fractures to close under compressive stresses, and fracture permeability may be significantly reduced. Therefore the mechanical effects should be considered in assessing the THCM processes.



Source: CRWMS M&O 2000b, Figure 10

Figure 3-97. Comparison of Modeled CO<sub>2</sub> Concentrations (*Less Complex*) in Fractures and Matrix Over Time to Measured Concentrations in Boreholes (a) Borehole Interval 74-3 at Nodes Above and Below (upper left); (b) Borehole Interval 75-3 (upper right); (c) Borehole Interval 76-3 (lower left); and (d) Borehole Interval 78-3 at Nodes Near Center and End (lower right).



DTN: LB991200DSTTHC.002

Source: CRWMS M&O 2000b, Figure 13

NOTE: Results are for the *Less Complex* Geochemical System.

Figure 3-98. Distribution of pH and Temperature at 12 Months (Fracture – 13a, Matrix – 13b) and at 20 Months (Fracture – 13c, Matrix – 13d)

### 3.6.1.3.3 Summary of the DST

After 18 months of heating, the DST had heated the rock mass such that boiling of pore water, drying of pore water, changing of the CO<sub>2</sub> concentration, and changing of the chemistry of the water had occurred. Along with boiling of the pore water, heat-pipe effects may have occurred in regions above the heaters. Both the TOUGH2 and NUFT models predicted the temperature, and saturation reasonably well. The *Thermal Test AMR TH* model analyses showed that temperature distribution in a repository is not very sensitive to the values of thermal conductivity used in the models. This indicates that very high confidence is justified when using the thermal

conductivity of the rock mass to predict average temperature distributions. The comparison of measured and simulated temperature distributions in those model analyses was focused on the statistics of the mean temperatures. Detailed analysis of spatial and temporal temperature variations provided insight into the processes of moisture movements and variations, including possible convection at a scale greater than the size of the drift. Investigation of more localized phenomena of boiling and drying, in specific fractures, for example, is on-going. The THC model using TOUGHREACT code provided reasonably good predictions of the variation of CO<sub>2</sub> concentration due to heating, boiling, drying, thought to be associated with local heterogeneity in the rock and fracture systems. This is because the models are designed to simulate large scale behavior, and are not expected to predict localized behavior. The bulkhead seemed to have some effects on temperature distribution, variation of CO<sub>2</sub> concentration in the HD, and, possibly the spatial variations of drying. The test is ongoing and is in the third year of a four-year heating phase that will be followed by a four-year cooling phase. Understanding of the THCM processes is expected to improve as the test progresses and more data are available.

### **3.6.2 Confidence Building through Use of Natural Analogs**

As noted in the Section 3.6 introductory material, validation of models is accomplished by testing at various scales. Natural analogs provide the opportunity to test the models at very large spatial scales and at temporal scales consistent with the long duration of the coupled processes that would be present in a repository. This section on use of natural analogs will discuss the confidence building in the models that results from, or might result from, the study of natural analogs. The confidence building efforts have proceeded roughly in progression with scale, that is the smaller scale tests of shorter duration are more mature or complete than the larger scale tests, which were based upon the previous work at smaller scales. Of all of the scales of testing, the natural analogs studies are the least mature, and therefore much of the discussion will identify the processes that can be addressed by specific analogs, and to some extent the observations are discussed. For this and other reasons, that will be discussed, natural analog studies are most useful in providing qualitative data against which the model processes can be judged rather than the quantitative data typical from other testing. As an example, Table 3-7 lists coupled process components within TSPA under the column called Yucca Mountain Issues. The analog processes that can be observed at geothermal sites, along with the sites identified that exhibit those processes, are listed on the table. Because the geothermal analogs address components of the TSPA, these analogs provide validation of TSPA models more directly than the smaller scale tests that more effectively provide validation of the detailed process models, as was discussed in Section 3.6 introductory material. This section also discusses analogs of the TH and THC process models and the confidence obtained from those studies.

Table 3-17. Application of Geothermal Field Information as Analogs to Coupled Processes Anticipated at a Potential Yucca Mountain Repository (CRWMS M&O 2000p, Table 6-13)

Yucca Mountain Issue	Geothermal Analog	Potential Sites	Possible Approach
Multiphase Flow (liquid, vapor, gas)	Multiphase Flow (liquid, vapor, gas)	All	Numerical Modeling, Conduct and Review Geothermal Post Audits
Hydrologic Properties	Hydrologic Properties	Kamojang (Indonesia), Tianjin (China), Wairakei (New Zealand), Oguni (Japan), Sumikawa (Japan)	Numerical Modeling
Preferential Flow	Preferential Flow	Wairakei (New Zealand), The Geysers (CA), Dixie Valley (NV), East Mesa (CA), Cerro Prieto (Mexico)	Numerical Stochastic Modeling, Evaluate Geothermal Tracer Study Results
Fracture Network Permeability	Fracture Network Permeability	All Modeled Fractured Sites, e.g. Cerro Prieto (Mexico), Krafla (Iceland), Matsukawa (Japan), Sumikawa (Japan), Olkaria (Kenya), Krafla (Iceland), Wairakei (New Zealand), Geysers (CA), Kamojang (Indonesia), Larderello (Italy)	Reservoir Model Calibrations Used
FMX	FMX	Yellowstone (WY), Long Valley (CA), Olkaria (Kenya), Fenton Hill (NM), Dixie Valley (NV)	Field and Laboratory Experiments, Evaluate Geothermal Tracer Study Results
Heat Pipes, Boiling and Condensation	Heat Pipes, Boiling and Condensation	The Geysers (CA), Kamojang (Indonesia), Matsukawa (Japan), Larderello (Italy)	Numerical Modeling to Extend Measurements
Mineral Precipitation and Dissolution	Mineral Precipitation and Dissolution	Larderello (Italy), Dixie Valley (NV), Wairakei (New Zealand), Broadlands (New Zealand), Long Valley (CA), Yellowstone (WY)	Laboratory Experiments, Analog Site Investigation, Numerical Modeling
Self-Sealing	Caprocks	The Geysers (CA), Kamojang (Indonesia), Matsukawa (Japan), Larderello (Italy), Cerro Prieto (Mexico), Reykjanes (Iceland)	Core Sample Evaluation, Water Chemistry Evaluation, Numerical Modeling
Mineral Alteration	Mineral Alteration	Wairakei (New Zealand), Broadlands (New Zealand), Dixie Valley (NV), Yellowstone (WY)	Core Sample Evaluation, Numerical Modeling
Thermo-Hydro-Mechanical Effects	Subsidence, Flow Changes	Wairakei (New Zealand), Bulalo (Philippines), Krafla (Iceland)	Numerical Modeling

Table 3-18. Similarity of Analog Sites to Yucca Mountain

	Similar Water Chemistry	Similar Geology	Similar Alteration Mineralogy
Larderello (Italy)		✓	possibly
Yellowstone (WY)	✓	✓	✓
Fenton Hill (NM)		✓	
Dixie Valley (NV)			✓
Wairakei (New Zealand)	✓	✓	✓
Broadlands (New Zealand)	✓	✓	✓
Long Valley (CA)	✓	✓	possibly

The ideal analog would be similar in all respects to a potential repository at YM. It is not practical to find an analog that simultaneously matches spatial, temporal, mineralogical, heat flux, stress conditions and hydrological characteristics of a potential repository. Therefore, a series of analogs were identified that can provide information on TH and THC processes. In addition, a number of geothermal analogs have been investigated as potential sites against which models could be tested (see Tables 3-17 and 3-18). Although all analog sites essentially exist because of THC processes, the analogs have been divided into those that provide evidence for testing TH coupling and those that provide evidence for THC coupling. Three analog sites are discussed as TH analogs: The Eldora Stock in Colorado, the Alamosa River Stock in Colorado, and Grants Ridge in New Mexico. Four sites are discussed as analogs for THC processes. These are: Yucca Mountain, Banco Bonito obsidian flow in New Mexico, Grants Ridge in New Mexico, and Paiute Ridge in Nevada (Nevada Test Site). No analog sites have been identified for THM.

### 3.6.2.1 Thermohydrological Analogs

In early studies, elemental migration across the 2-m-wide contact zone around the Eldora Stock in Colorado was investigated as an analog to elemental transfer in a crystalline repository during heating by waste canisters (Brookins 1986; Wollenberg and Flexser 1986). Oxygen-isotope data showed a distinct contrast between the 60 Ma quartz monzonite stock and the Precambrian metamorphic country rock, which Wollenberg and Flexser (1986) interpreted to indicate a lack of convective hydrothermal cooling. No systematic uranium enrichment or depletion that could be related to distance from the contact was detected (Wollenberg and Flexser 1986), but data were insufficient to ascertain whether uranium mineralization occurred before or after emplacement of the stock.

In contrast to the Eldora stock, intrusion of the Alamosa River, Colorado stock, a monzonite body that intruded tuffaceous and andesitic volcanic rocks about 30 million years (Ma) ago (Brookins 1984), appears to have established a large-scale convecting hydrothermal system (Brookins 1986). Alteration of the tuffs is observable to 60 m from the contact, with the occurrence of calcite intergrown with the rock matrix, chlorite and sericite, quartz overgrowths, and epidote (Wollenberg and Flexser 1986). The contact itself contains a dense intergrowth of epidote, sphene, and fine hematite-filled fractures. Uranium occurs in sphene, but is otherwise absent from the contact (Wollenberg and Flexser 1986). Concentration gradients of Cs, Th, and

Co in the tuff increase toward the contact, but other trace elements show no indication of migration between the stock and the tuff (Wollenberg and Flexser 1986).

The influence of a shallow basaltic intrusion into pyroclastic deposits at Grants Ridge, New Mexico, was studied by WoldeGabriel et al. (1999). At this location, a 2.6-Ma basalt plug intruded into 3.3-Ma nonwelded, pumice-rich, compositionally homogeneous, rhyolitic tuff and volcanoclastic sediments. A 10-m wide aureole characterized by color variation, contact welding, brecciation, partial melting, and stopping developed around the 150-m wide basalt plug. Despite the high-temperature basaltic intrusion, there was no evidence in the country rock of pervasive hydrothermal circulation and alteration that could have been caused by extensive fluid-driven convective heat transfer.

### 3.6.2.2 THC Analogs

A good analogy for understanding future repository behavior is the fossil hydrothermal system at Yucca Mountain itself (Bish and Aronson 1993). Detailed mineralogical examination of Yucca Mountain tuffs showed that most zeolitic alteration occurred about 13 to 11.6 Ma, at about the same time as tuff emplacement. After formation of the major zeolitic horizons, deep-seated hydrothermal activity persisted until about 10 Ma. This activity was limited to temperatures of 90 to 100°C, the zeolite stability limit; at prolonged exposure to temperatures greater than 90°C, the sorptive zeolites clinoptilolite and mordenite are altered to analcime plus quartz and/or calcite.

Conceptual models for mineral evolution at Yucca Mountain (Carey et al. 1997) suggest that the most likely mineralogical reactions caused by repository heating would include dissolution of volcanic glass and precipitation of clinoptilolite, clay and opal-CT; dissolution and precipitation of silica polymorphs (cristobalite, opal-CT, tridymite, and quartz); alteration of feldspars to clays; and, finally, reactions involving calcite and zeolites. Figure 3-99 illustrates paleotemperatures that were inferred from mineralogical data in several drillholes at Yucca Mountain. Measured present-day temperature profiles are shown for comparison.

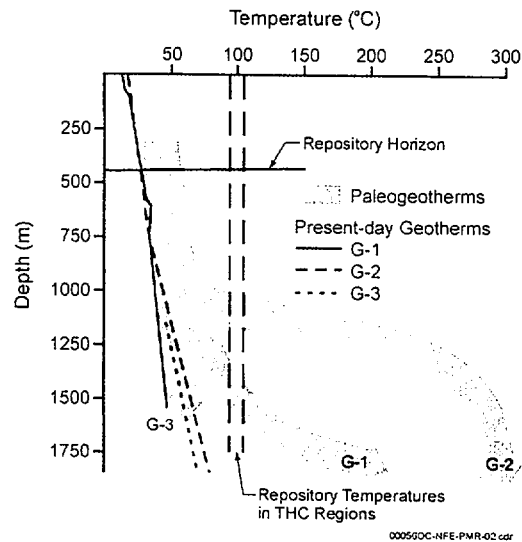
As can be noted, the temperatures projected to be typical of the NFE for 1000s of years are those represented by the G-2 core at about 1,100 m-depth and G-1 core at about 1,600 m-depth. There are no depth dependencies determined for the mineralogy, and therefore the repository horizon shown on the figure is not of direct relevance to the analog comparisons. However, it provides insight into the thermal gradients that are projected to exist, in comparison with existing gradients. The paleothermal gradient most comparable with projected repository thermal gradients are those of G-1 at approximately 1,500 m-depths. It can be seen from the figure that present-day temperatures in drillhole G-3, which is within the repository block, compare closely to inferred paleotemperatures. In contrast, increasingly higher paleotemperatures are inferred for drillholes G-1 and G-2, which are closer to the center of the Timber Mountain caldera source of eruption (G-2 being the farthest north). Figure 3-99 shows mineral and glass abundance and clay mineralogy from GU-3/G-3 drill core that were used to infer the paleotemperatures. Similar mineral abundance diagrams for G-1 and G-2 drill core indicate northward progression of an increasing abundance of clays and zeolites, along with decreased abundance of glass. This is in keeping with the reactions stated above.

Thermodynamic modeling results indicate that the stability of various zeolites is a function of silica activity, temperature, aqueous sodium concentration, and the mineralogy of silica polymorphs. Increasing temperature or sodium concentration causes the alteration of zeolites to other phases. Kinetic effects are, however, important in assessing the significance of thermodynamic and natural analog study conclusions. Kinetic data suggest that saturated conditions are necessary for notable progress in these reactions, as discussed by Carey et al. (1997). Therefore, under ambient conditions the reactions are likely to proceed more slowly in the Yucca Mountain unsaturated zone (excluding perched-water zones) than below the water table. Similarly, the persistence of opal-CT below the water table indicates that silica reaction kinetics at Yucca Mountain are slower than laboratory studies would suggest (Carey et al. 1997). However, if prolonged boiling occurred in saturated tuffs, significant progress in all these reactions could occur. The thermal design of the repository would limit the occurrence of temperatures above 100°C to the Topopah Spring welded unit, and to the region immediately surrounding the drifts. The current EDA-II design scenario includes sufficient drift spacing to allow temperatures between drifts to remain below boiling (CRWMS M&O 1999a).

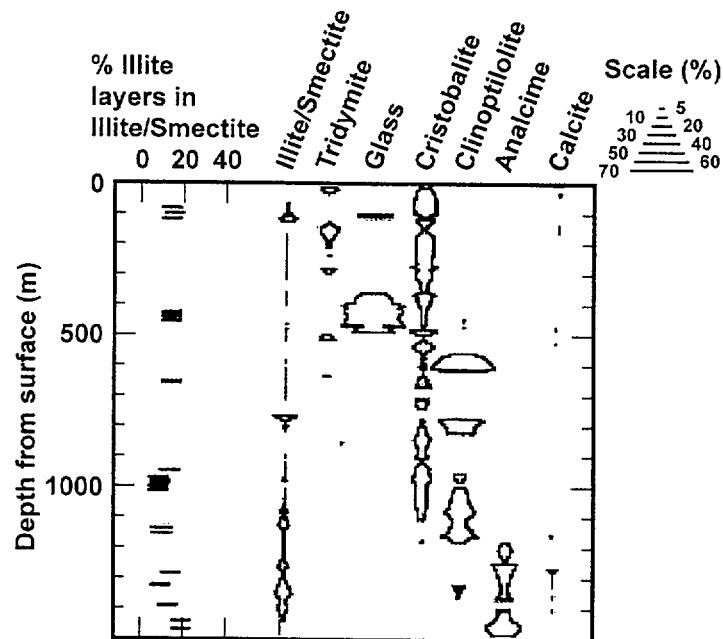
The contact between the Banco Bonito obsidian flow and underlying Battleship Rock Tuff in a steep-walled canyon on the southwest rim of the Valles Caldera, New Mexico, provides an analog for THC in an unsaturated environment. This site has been the focus of a number of analog studies (Krumhansl and Stockman 1988; Stockman et al. 1994). The Banco Bonito flow filled a steep-walled canyon cut in the Battleship Rock Tuff about 400 ka (thousands of years ago). Present hydrologic conditions are unsaturated. The obsidian, initially at temperatures of 850°C, heated the porous tuff in the canyon walls to 150-350°C for decades, and, according to models, vaporized much of the pore water and caused refluxing of water. Contact effects include a reddish "baked" zone extending tens of feet into the tuffs. Krumhansl and Stockman (1988) found that Cs and Rb showed little variation with distance from the contact, whereas Th, Ta, Hf, Co and rare-earth elements showed slight concentration trends; however, it is possible that these trends may have predated the obsidian flow. Stockman et al. (1994) observed no evidence of trends in trace element migration at the contact; however, water and Cl are depleted near the contact, whereas F is slightly enriched toward the contact. No evidence of hydrothermal alteration was noted, suggesting that the area was unsaturated at the time of contact.

The Valles analog site presents several interesting features. First, the Battleship Rock Tuff is very homogeneous in major and trace-element composition, such that it would be possible to detect distinct elemental differences caused by heating at the contact. Second, there is no hydrothermal overprint that could blur the effect caused by deposition of the obsidian flow. Based on a detailed mineralogical, chemical, and isotopic study, Stockman et al. (1994) concluded that, overall, the effects of heating in this unsaturated environment appeared to have been slight and were limited to the tuff nearest the contact. Some evidence existed for devitrification and migration of volatile elements in the tuff within 10 m of the contact, but variations in major and trace-element chemistry were small and difficult to distinguish from the natural variability of these elements in the rock. Apart from devitrification, the principal mineralogic change in tuff near the contact was the development of feldspar-silica linings on voids in the pumiceous tuff matrix; no significant development of zeolites was found. It was not possible to map paleoisotherms from the heating event, but Stockman et al. (1994) developed a model to predict the temperatures in the obsidian and tuff as a function of time. The model

predicts the movement of a boiling front several tens of meters into the tuff over several hundred years and is relatively insensitive to assumed saturation.



(b)



Source: Modified from CRWMS M&O 1998a, pp. F6.1-75, 76

NOTE: (a) Illustrates paleotemperatures inferred from mineralogical data in drill holes USW G-3, G-2, and G-1 along with present-day temperature profiles. (b) Compares mineral and glass abundance in drill-core USW GU-3/G-3 determined by x-ray powder diffraction.

Figure 3-99. Yucca Mountain Mineralogy, an analog for potential Mineral Alteration

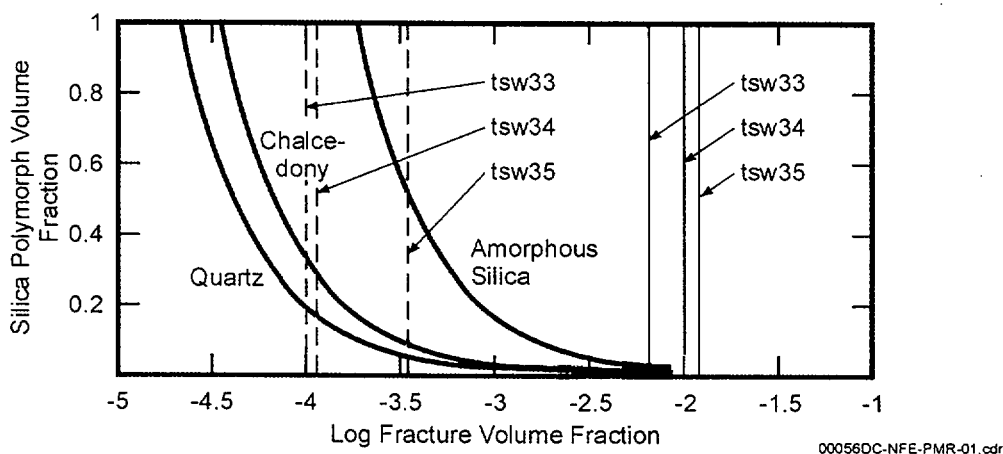
The Grants Ridge site, discussed previously as a TH Analog (Section 3.6.2.1), provides additional information regarding THC processes. WoldeGabriel et al. (1999) found that the proportion of volcanic glass, volatile species, Fe, and some trace-element and rare-earth element contents in the host rocks were somewhat depleted at the contact of the intrusion. In contrast, the degree of devitrification and potassium content were higher along the contact. The authors postulated that vapor-phase expulsion of elemental species could have been responsible for the minor depletion of elements during devitrification of the silicic glass at near-solidus temperature related to the basaltic intrusion.

The WoldeGabriel et al. (1999) study performed finite-difference numerical modeling to model the Grants Ridge intrusion as a dry, conduction-dominated system and compared its results with those of an analytical solution, and with the heat-and mass-transfer code FEHM (Zyvoloski et al. 1992, 1997). Modeling results, which agreed well with geochemical and mineralogical data, indicated that contact welding of the host rocks apparently occurred at temperatures  $> 700^{\circ}\text{C}$  under a density-driven lateral load of approximately 1 MPa, corresponding to the observed depth below the former ground surface of  $\sim 100$  m. Other physical changes in the host rock, represented by partial devitrification and color changes, apparently occurred at temperatures of  $500$  to  $600^{\circ}\text{C}$ , which probably persisted for up to 55 yr. after emplacement of the basaltic plug (WoldeGabriel et al. 1999). Because devitrification is generally enhanced by the presence of aqueous fluids, the abundance of volcanic glass within a short distance ( $\sim 10$  m) from the plug is consistent with the authors' inference that the plug intruded into an unsaturated environment. Although no apparent hydrothermal alteration was recognized in the contact zone, this field study and others like it provide an upper temperature bound natural analog to evaluate the effects of heat from decay of radioactive waste. Results of these types of studies are also important for performance assessment of basaltic-magma intrusions into or close to a potential repository environment. Field and laboratory data from the analog study can also be used to build confidence and to calibrate models of such processes within similar physical and chemical environments.

The Paiute Ridge area of the Nevada Test Site analog provides insights regarding alteration of glass and potential to plug pores. Late Miocene basaltic magma intruded a sequence of 22 to 11 Ma tuffs in a single magmatic pulse (Lichtner et al. 1999). The intrusions formed as dikes, sills, and lopoliths. The original depth of the intrusions was on the order of 150 to 250 m (Crowe et al. 1983). A contact aureole  $\sim 3$  m-wide surrounds the intrusions. Matyskiela (1997) studied alteration surrounding one intrusion, the 50 m-wide Papoose Lake sill, in proposing the Paiute Ridge intrusive complex as a natural analog for THC processes at Yucca Mountain. Matyskiela's (1997) analysis was based on a pure heat-conduction model. Matyskiela's (1997) model results indicated maximum temperatures in the tuff host rock of  $550^{\circ}\text{C}$  and cooling times ranging from 10 to 400 yr. Matyskiela's (1997) major finding was alteration of glass shards to cristobalite and clinoptilolite within 60 m of the intrusion. He interpreted the alteration as hydrothermal in origin, resulting from emplacement of the intrusion (although he never conclusively demonstrated that the alteration post-dated the intrusion). Most significant was Matyskiela's (1997) observation of complete filling of pore spaces with silica at fracture-matrix interfaces, thus creating open conduits for infiltrating fluid flow along fractures.

Matyskiela (1997) estimated enhanced fracture flow to be as much as five-times ambient conditions. This appears to be the opposite behavior to formation of a silica cap, as predicted by

recent simulations conducted for Yucca Mountain (Hardin 1998, pp. 5.57 to 5.58) in which fractures would become filled with quartz or chalcedony, thus inhibiting further flow. It is also not consistent with calculations reported in this PMR that show very minor changes in permeability due to THC processes. This analog provides insight into the extent to which a fracture can be filled by the silica contained in matrix pore water. Figure 3-100 shows that, for a given matrix porosity, the degree of sealing of the fracture depends on the fracture volume fraction and the particular silica polymorph that precipitates (Lichtner et al. 1999). This analysis is predicated upon the assumption that, as pore fluid in the matrix is brought into equilibrium with respect to a particular silica polymorph (e.g., amorphous silica) at boiling conditions, the matrix fluid boils and escapes into the surrounding fracture network. As the fluid vaporizes, its released silica content precipitates in fractures. Lichtner et al.'s (1999) two-phase numerical simulation results suggest that at distances of tens of meters from the larger of the Paiute Ridge intrusions that they studied (width  $\geq 39$  m), prolonged boiling conditions were established for times on the order of several thousands of years. The analysis shown in Figure 3-100 represents a limiting case and is dependent on all pore water flashing to steam in the fracture. Amorphous silica, with its higher solubility, gives the largest fracture filling, followed by chalcedony and quartz. For complete sealing of the fracture, a very small fracture-volume fraction is necessary. Moderate filling could represent fracture coatings that armor the fracture.



Source: Derived from Lichtner et al. 1999, Figure 10

NOTE: A volume fraction of one represents complete filling of the fracture, assuming that the fracture was initially open. Dashed vertical lines use fracture volumes from Hardin (1998). Solid vertical lines use fracture volumes from CRWMS M&O 2000a, Table 5.

Figure 3-100. Volume of Silica Polymorphs Precipitated in Fracture as a Function of Volume Fraction for a 10 Percent Matrix Porosity

The dashed vertical lines shown on the figure reflect values of fracture porosity used in the calculations reported in Hardin (1998, Table 3-7). As indicated for those porosities, if the fluid equilibrium was with amorphous silica, the fracture porosity would be completely filled for the tsw33 and 34 hydrostratigraphic units, and 50 percent filled in the tsw35 unit. For fluid interactions with quartz and chalcedony, the fracture filling would be approximately 20 and 30 percent respectively. In contrast, the current estimates of fracture porosity (CRWMS

M&O 2000a, Table 5) are plotted as solid lines. Note that fractures with these porosities would not fill and that even fluid interactions with amorphous silica would produce virtually no reduction in porosity.

### **3.6.3 Summary of Laboratory Tests**

The laboratory tests that may play significant roles in the understanding of the THCM processes are those dealing with TH and THC processes. Some of those laboratory test results may have already been incorporated in the complex TH and THC models, such as the NUFT DKM model and TOUGH2 DKM model.

#### **3.6.3.1 Hydrological Properties**

First, variations associated with temperature changes have been found to be much less than variations between samples in matrix permeability of the Topopah Spring welded tuff (Lin and Daily 1988; Hardin and Chesnut 1997, Section 2.10). Second, no enhancement in vapor diffusion was observed in Topopah Spring tuff core samples (Wildenschild, et al. 1998). Finally, the wetting/drying hysteresis typically observed in saturation vs. water potential functions at ambient temperature was reversed at 90°C and was virtually nonexistent at 78°C (Lin and Roberts 1996).

#### **3.6.3.2 Chemical and Transport Properties**

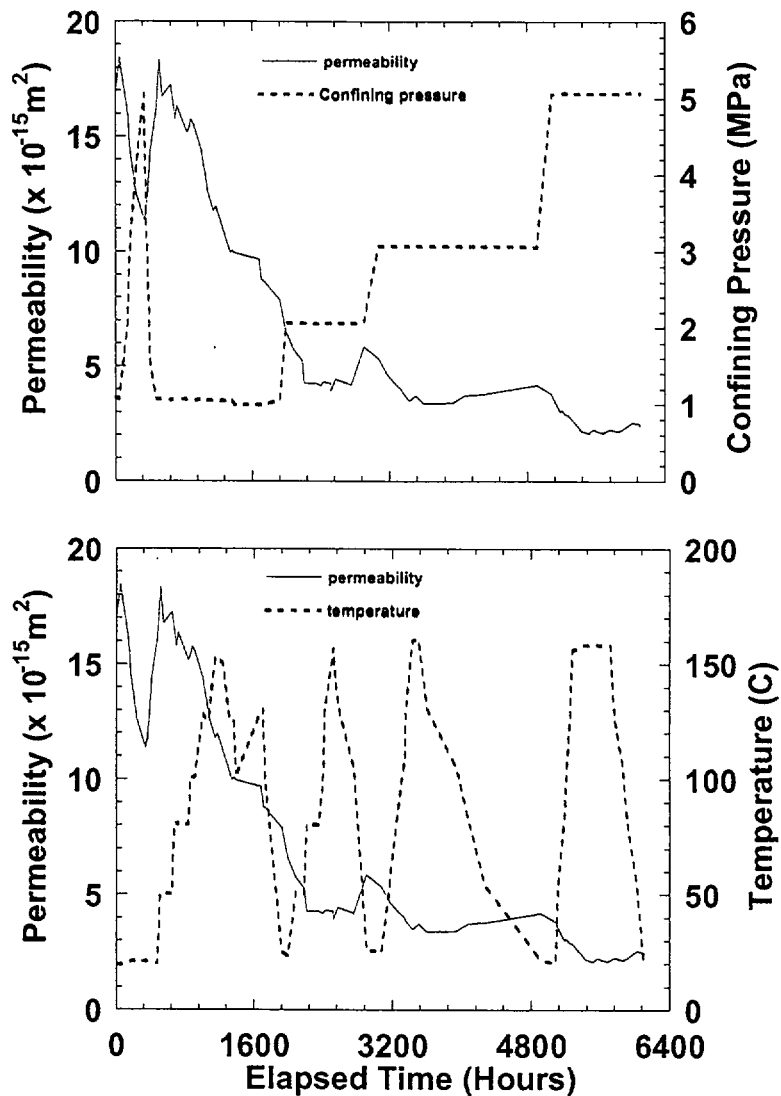
First, investigation of spiked J-13 water at temperatures as great as 100°C indicated that Pu solubility decreased, but U, Np, and Am solubility remained the same or increased (Nitsche 1991). Carbonate complexes appeared to be important to the solubility of U, Np, and Am at elevated temperature (Wruck and Palmer 1997). Second, changes in the composition of water in contact with the tuff were moderate at temperatures as great as 150°C, with slight alteration of the tuff over a few months. At higher temperatures, similar alteration products were produced, but reaction rates increased significantly. Accelerated experiments on crushed tuff at temperatures greater than 150°C produced more extensive alteration, including metastable phases (Hardin and Chesnut 1997, Section 2.10). Finally, zeolites could have a significant effect on the heat and water balance where they are abundant because zeolite dehydration requires more energy than evaporation of water on a molar basis (Bish 1995; Bish et al. 1996; Carey and Bish 1996). Zeolite hydration is apparently reversible (at dehydration temperatures as great as 215°C for clinoptilolite), so complementary effects are expected during repository cool-down (Hardin and Chesnut 1997, Section 2.10).

#### **3.6.3.3 Laboratory-Scale TH Processes**

Fracture healing experiments have shown (Figure 3-101) that flowing hot water or steam will significantly reduce fracture permeability, and the effect is strongest at temperatures greater than 90°C (Lin and Daily 1989; Lin et al. 1995). Observations reported in the literature can be explained by three mechanisms:

1. Dissolution of fracture asperities by flowing water and consequent aperture reduction under the influence of confining stress,

2. Dissolution/precipitation reactions that clog porosity by redistributing silica or by creating alteration products with greater molar volume, and
3. Heating the rock matrix, which causes flow of matrix pore water toward fractures where the pressure is lower and evaporation or boiling occurs, clogging fractures or matrix porosity.

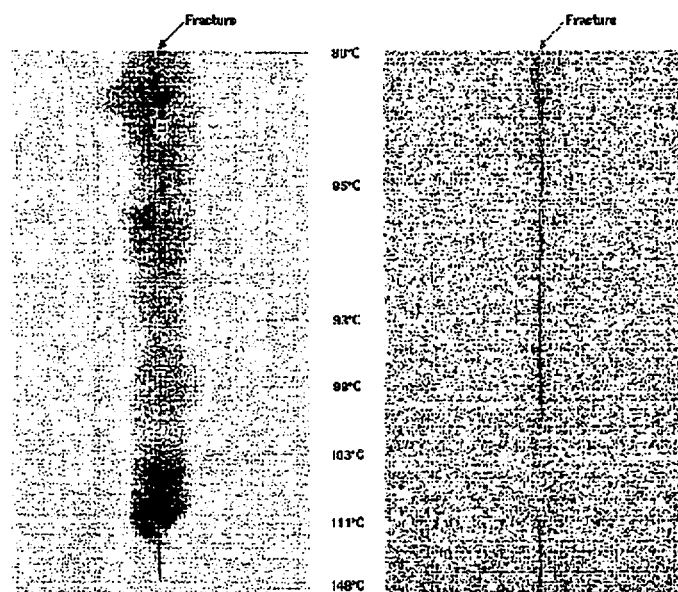


Source: Lin et al. 1995

NOTE: Temperature and confining pressure variation during the test series are plotted for comparison.

Figure 3-101. Permeability of a Single Fracture in a Core Sample of Topopah Spring Welded Tuff, Which Varied as a Function of Time and Exposure to Flowing Water

Fracture flow and matrix imbibition laboratory studies (Roberts and Lin 1997; Lin et al. 1998b) have physically demonstrated the relationship between fracture-matrix coupling in welded tuff (Figure 3-102). Results indicate that under some conditions it is difficult for water to penetrate the boiling region, but that water can penetrate this region under certain circumstances, for example, sufficient hydraulic head and sufficient flow rate. Fracture flow stopped or slowed significantly when a region of porosity higher than the surrounding matrix was encountered. Rapid evaporation events were frequently observed, and pressure pulses from those events were observed in glass fracture models and in a hanging column of water at an appreciable distance compared to the physical size of the events.

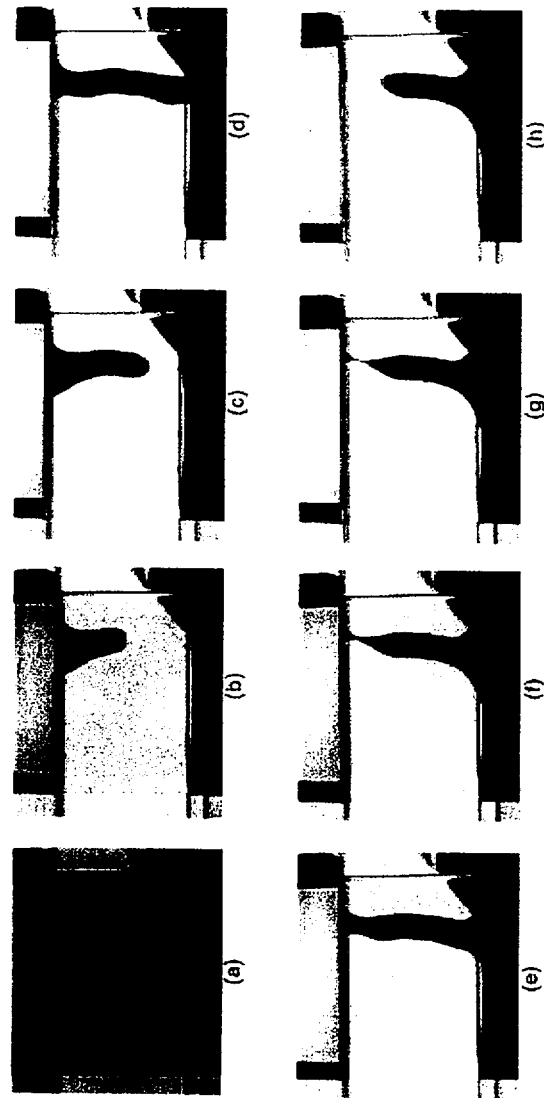


Source: Lin et al. 1998b, Figure 5 and 6

NOTE: Thermal gradient is indicated between the figures, ranging from 80°C at the top to 148°C at the bottom. The difference between these two experiments was the height of the water column, 0.26 (left) and 0.46 (right) m respectively. The difference in head was large enough to force flow through the boiling region in the right image.

Figure 3-102. Difference X-Ray Radiography Images of 7.2 (Left) and 0.67 (Right) Hours after Flow was Initiated

Flow channelization visualization experiments (Geller et al., 1996) showed that fracture flow in response to constant boundary conditions can be unsteady and associated with intermittent rivulets that “snap off” and reform periodically (Figure 3-103). These ambient-temperature experiments demonstrated that parallel plate fractures and epoxy casts of natural fractures can produce unsteady, episodic fracture flow in response to constant upstream boundary conditions. Similar flow can be expected in the fractures of a heat-pipe zone. These data have important qualitative/conceptual implications for FMX, especially in areas of the fracture traversed by the unsteady flow and where the contact time available for matrix imbibition or chemical reactions is limited.



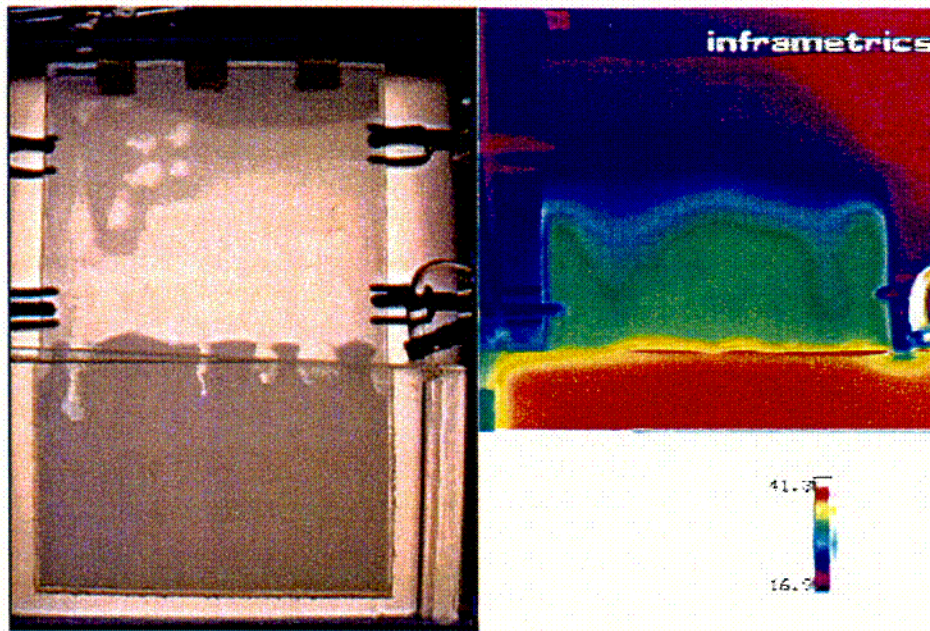
Source: Geller et al. 1996, Figure 19

NOTE: Fracture Aperture Varies in Zones, and the Middle Zone has the Largest Aperture. The right side of each snapshot is the bottom of the flow cell, and that bottom edge is inclined 30 degrees from the horizontal with the right end higher. Snapshots (a) through (h) are a time sequence. The snapshots have been cropped to show only a small part of the upper and lower zones.

Figure 3-103. Physical Model of Water Flow in an Unsaturated Fracture Consisting of Parallel Plates of Acrylic Plastic

Physical models of heat pipes have been studied in fracture thermal-hydrology visualizations (Kneafsey and Pruess 1997; 1998). Conditions were examined (e.g., fracture saturation, temperature difference, and fracture dimensions) that support heat-pipe development. Heat pipes were observed in parallel plate fractures containing obstacles, heat sources, and vents, and using fluids with low boiling points. Film flow as well as meniscal flow were observed to produce

heat pipes (Figure 3-104). Unsteady rivulet-flow behavior, analogous to episodic fracture flow at ambient temperature, was observed (Geller et al. 1996). Rapid evaporation events occurred when “islands” of fluid became superheated and suddenly boiled, constituting another mechanism for unsteady flow with the potential to rapidly disperse solute. A few of these observations were repeated with a half-cast model incorporating welded tuff as one fracture wall. With this kind of mechanism, there is the potential for large-scale episodic reflux flow into emplacement drifts. The thermal-hydrological event on June 13, 1997 in the LBT (Section 3.6.1.1.3) could be related to this kind of mechanism.



Source: Adapted from Kneafsey and Pruess 1998, Figure 5

NOTE: Experiment 9:  $T_{\text{bath}} = 42.4^{\circ}\text{C}$ .

Figure 3-104. Pentane Visualization (Left) and Temperature Distribution (Right) Showing a Heat Pipe

L-75

### **3.6.4 Summary of Model Validation and Confidence Building**

The following three sections discuss the validation status of TH, THC, and THM process models, respectively. Each section is based on available site specific data (Section 3.6.1), process models (Sections 3.2, 3.3, and 3.5), historical work (Section 2.2) and alternative views (Section 2.4). Sections 3.6.4.1 through 3.6.4.3 discuss in some detail the model validation status of individual models. See Chapter 5 for a higher level summary discussion of NFE model validity.

#### **3.6.4.1 Validation of TH Models**

This section discusses the validation or confidence building efforts related to the TH models. The confidence building consists of both checking that the codes used to do the mathematical manipulations can be relied on (usually referred to as code validation), and on assessing that the overall models (including conceptual models, embedded physics, assumptions, boundary conditions used, property sets and codes selected) applications are appropriate for the analyses of Yucca Mountain conditions and performance. The validation of the codes is discussed in Appendix A. The latter assessment (appropriateness of overall modes) as discussed here was provided by comparisons of model results with field and laboratory studies.

The following applications or studies that demonstrate appropriateness of TH models are examined for YMP calculations:

- The AMR that presents comparisons of the DST and LBT field data with fully 3-D model calculations, using two different DKM material-property sets
- Comparison of field results with TH calculations of the G-Tunnel test
- Comparison of field results with TH calculations of the SHT
- Simulation of vadose-zone tritium transport at the Lawrence Livermore National Laboratory Site
- Code-testing for QA qualification
- Early verification and benchmark testing of the code

##### **3.6.4.1.1 TH Model Confidence Building based on non-Yucca Mountain Cases**

This section examines the performance track record of model studies using the NUFT and TOUGH2 codes (Nitao 1993, Pruess 1991) and documents the rigorous testing and wide range of applications work that build confidence in both the codes and in ability to model TH responses applying these codes in the modeling of multiple problems or cases. Confidence in the ability to model these processes using the NUFT and TOUGH2 codes to simulate thermohydrologic processes in porous and fractured media has increased significantly since initial testing of the codes and modeling of YM. As noted, Appendix A will include discussion of qualification of the codes themselves.

An international cooperative project was established for theoretical and experimental studies of coupled thermal, hydrologic, and mechanical processes in hard (crystalline) rock. This project is called DECOVALEX and is described by Jing et al. (1995). In this work, different mathematical models and computer codes were used to study problems of interest to geologic disposal of nuclear waste. In particular, eleven codes were evaluated; these included both 2-D and 3-D finite-element codes in which the rock was modeled as a porous-fracture medium and a 2-D discrete-element code in which the rock was modeled as discrete deformable block assemblages. Much of the work done for DECOVALEX is documented in a special issue of the *International Journal of Rock Mechanics* (Stephansson 1995).

As part of the DECOVALEX program, two intercode benchmark comparisons were performed. The benchmark test BMT1 considered a large-scale (kilometer-scale) mass of rock as described by Millard et al. (1995). The benchmark problem BMT2 involved a system of nine blocks of intact, hard rock separated by two pairs of soft fractures, as described by Chan et al. (1995). For each of these exercises, both finite-element and distinct-element methods were used. Chan et al. (1995) found that, for the BMT2 test, heat convection significantly affects the distribution of temperature, thermal stresses, and displacements, and that the predominant coupled effect is fracture closure caused by thermal expansion of the rock-blocks. Results for DECOVALEX also indicate that, for tests BMT1 and BMT2, the different modeling techniques produced very similar results. This indicates that use of the continuum codes is adequate for study of host-rock behavior for a Yucca Mountain repository.

Another study used a physical model to simulate waste emplacement for evaluating a nuclear waste disposal concept in Japan. The large-scale laboratory test involved heating and flow testing, and was simulated with a software code that includes vapor-flow processes (Borgesson and Hernelind 1995). The test was performed using a partially saturated buffer material surrounding a simulated waste package in a hollow cylinder of rock. The calculations resulted in a prediction of void ratio, temperature, water saturation, pore pressure, and effective stress. The calculations were coupled THM; the hydrologic and thermal results compared well with the experiment, but the prediction of mechanical response did not. The 3-D finite-element model THAMES underestimated the experimental measurements of temperature in the buffer material (Ahola et al. 1994a and 1994b).

For another field-scale experiment, FLAC 2-D (Itasca Consulting Group Inc., 1996) was used to model heat and water flow through a 50 m x 50 m block of fractured granite (Israelsson 1995). Stress-induced permeability changes were limited to one order of magnitude, and fractures were assumed to be randomly oriented, thus allowing use of the continuum approach in FLAC.

#### **3.6.4.1.2 Large Block Test**

The results of DKM with active fracture model using NUFT were compared with temperature and liquid-phase saturation fields measured in the block. Temperature histories at selected sensor locations and temperature profiles along selected boreholes were graphically compared with model results. Liquid-phase saturation profiles, measured along boreholes by neutron probe, were also compared with corresponding field profiles. Graphical comparisons were done for liquid-phase saturation.

A statistical goodness-of-fit analysis was performed to compare model and field temperatures at all sensor locations in the block. Three statistical measures of goodness-of-fit were used, the root-mean-squared difference (RMSD), MD, and normalized-absolute-mean-error between measured and simulated temperatures.

Two different rock property data sets were used in the calculations: the DS data set and the MS data set. Hydraulic and thermal properties of the tsw34 unit of these property sets were used in model calculations, because the hydrogeologic unit of the LBT area is equivalent to the tsw34 model unit (Tptpmn) of the site-scale UZ flow model. The main difference between the DS and MS properties for the tsw34 unit is a higher fracture permeability of  $1.70 \times 10^{-11} \text{ m}^2$  for the MS versus  $2.76 \times 10^{-13} \text{ m}^2$  for the DS.

Results of this comparative analysis using the DS and MS data sets contribute to the validation of the NUFT code and underlying models to simulate the thermal hydrological process in a repository. Specifically:

- Model results using both rock-property data sets, DS and MS, show very good agreement with field temperatures
- Model results obtained using the DS data set show slightly better agreement with the field temperatures than simulation results obtained using the MS data set
- Both data sets slightly over-predict temperatures, particularly in and adjacent to the heater horizon, but the degree of over-prediction is less for the DS data
- The RMSD for the DS data set, computed at six times from 30 days to 400 days, varied from 3.7°C to 8.7°C
- The RMSD for the MS data set, computed at six times from 30 days to 400 days, varied from 4.3°C to 8.8°C
- The MD for both the DS and MS is generally positive, confirming the slight overprediction of temperature observed in the graphical comparisons
- The dryout zone modeled using the DS data is in good agreement with the dry out zones measured by neutron probe; the model dryout develops slower, but later catches-up with the field zone
- The dryout zone modeled using the MS data property set is significantly larger than the zones modeled using the DS property set and zones measured by neutron probe

The LBT was conducted in the tsw34 unit of the Topopah Spring tuff that outcropped at Fran Ridge. The rock properties of the test block were neither expected, nor required, to be identical to those of the potential repository horizon at Yucca Mountain. The purpose of the LBT was not to test property sets, but to test the capability of models in representing the coupled THCM processes. However, testing the capability of models to analyze THCM processes for the potential repository requires a property set that is at least representative of the properties at

Yucca Mountain in order to conduct appropriate model validation. If the property set that provided the best (or at least a good) match between the simulated and measured results from the LBT is also the one that provides an appropriate match for other field tests, then the LBT model validation procedure will not only build confidence in the models themselves, but also add confidence in use of that property set to evaluate the performance of the overall potential repository.

The focus of the LBT was on TH model capability testing, with some THM and THC testing, but these latter were not the main focus of the test. The DK TH models, using both DS and MS property sets and using the NUFT code to make the numerical analyses, were able to predict the temperatures in the LBT well. This enhances confidence that the DKM/AFM TH model has the ability to properly represent the heat transfer mechanisms in a potential repository, and therefore has the ability to properly predict temperatures in the near field.

The DK TH model, using the DS property set in NUFT code, predicted the moisture distributions in the LBT well. The DK TH model did not match the moisture distributions as well when using the MS property set. This does not necessarily imply that the use of MS property sets is inappropriate for use in calculations of the potential repository responses. It indicates that the moisture distributions are somewhat sensitive to the property sets, and using properties that represent averages of many units do not match the data as well as when using the properties that are specific to the unit of the test. In some respects this enhances the confidence in the models ability to discriminate between the property sets. It also enhances confidence that property measurements of specific units can be appropriately utilized, but indicates the need to use care in selecting the most appropriate property set. Because the tsw34 unit is not representative of the major portion of the potential repository, the DS property set should not be automatically selected as representative of the potential repository.

The matching of moisture distributions enhances confidence that the TH model has the ability to properly represent water flow, evaporation, and condensation in a potential repository. The fact that the DS property set did well in this test case enhances confidence that it is appropriate for use in predicting moisture distributions in the near field of a potential repository within the tsw34 unit. It also enhances confidence that once properties are determined for the units representing the remainder of the potential repository, the models will be appropriate for use in predicting moisture distributions within these units.

#### **3.6.4.1.3 Single Heater Test**

The SHT was one phase of the field-scale thermal-testing program of the Yucca Mountain Site Characterization Project. The SHT Final Report (CRWMS M&O 1999d) describes the test in more detail. The primary purpose of the SHT was to study the TM behavior of the densely welded, non-lithophysal Topopah Spring Tuff at the ESF. The SHT was also used as a shake-down for testing thermal-hydrologic-chemical-mechanical processes in situ, testing that will be conducted in the Drift Scale Test.

In the SHT, a line-heat source 5 m-long was placed in a pillar and used to heat the pillar for approximately nine months. The thermal field was relatively cylindrical about the line-heat source. The heater was turned-off after nine months of heating, and the rock mass was

monitored during the cool-down for another nine months, until May 28, 1997, when the test was terminated.

Thermal neutron-logging was used to monitor moisture content in four boreholes during the SHT. Neutron-logging data and analysis presented here indicated drying of the rock mass during the heating phase of the test. Neutron-logging results were in good agreement with ERT results. The degree of drying seemed in good correlation with temperatures in the rock. ERT and neutron-logging data indicated drying in regions of rock that reached 60°C and more.

The TH behavior during the heating and cooling stages of the SHT was analyzed with the DKM AFM using the NUFT code. Two different conceptual models for FMX were considered: the ECM, which assumes equilibrium between the fracture and matrix continua, and the DKM that accounts for disequilibrium processes between the fracture and matrix continua. All of the models in this study included the influence of vapor and heat flow along the heater borehole.

The DKM model predicted temperatures that were in excellent agreement with the observed temperatures throughout the heating stage of the SHT. The ECM model agreement was not as good: it predicted lower temperatures, but a more extensive dry-out region, than did the DKM model. Both the ECM and DKM models predicted a pronounced cold-trap effect in the heater borehole. Vapor and latent heat flowed from the heated interval of the heater borehole to the cool end of the heater borehole adjacent to its collar, where the vapor condensed, resulting in focused condensate drainage and a local increase in liquid saturation in the matrix. The cold-trap effect efficiently transferred heat along the heater borehole toward the TM alcove. The cold-trap effect is a potentially important mechanism influencing TH behavior in emplacement drifts.

For the SHT, the comparison of the predicted and the measured moisture distributions was not discussed in the *Thermal Test AMR* (CRWMS M&O 2000a). The following summary of the predicted and measured moisture distributions is extracted from SHT Final Report (CRWMS M&O 1999d). Due to the nature of the measured moisture distribution data, only qualitative comparisons between the simulated results and the measured data are possible.

- The simulation of the moisture distribution in the SHT using the TOUGH2 DKM qualitatively agreed well with the data from GPR and air-permeability measurements. The model predicted that, at the end of the heating, drying had extended to a radial distance of about 1.2 m from the heater. In cooler regions, the vapor condensation at the fracture walls resulted in an increase of liquid saturation in both fractures and the matrix. At 3 months of heating, strong downward drainage flux in the fractures was observed below the heater. The rock matrix was drier above the heater than below. GPR data showed, at 5 months of heating, a drier region close to the heater and a wetter region about 1 m away from the heater. The GPR data at 7 and 9 months showed a further drying near the heater, but no significant changes in the regions beyond the 1-m radius. After 3 months of heating, the measured air permeability in the predicted condensate regions decreased by factors of 2 to 4, compared to the preheat values. This decrease in the air permeability was likely due to increased water saturation in the fractures (CRWMS M&O 1999d, Section 8.7.3.1). The TOUGH2 ECM model was also used for sensitivity analyses of the SHT. It was concluded that DKM is better suited to

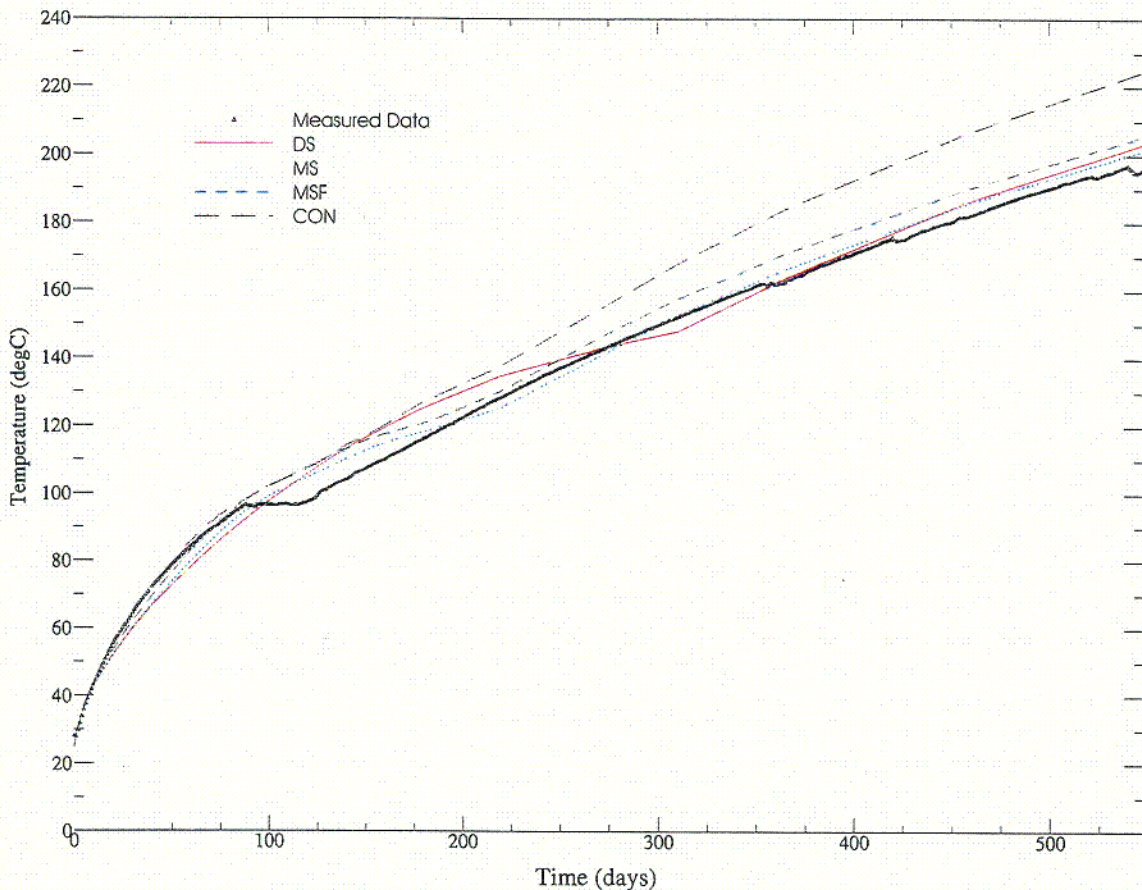
realistically represent thermal-hydrological processes in the SHT than ECM (CRWMS M&O 1999d, Section 8.7.3.3.2).

- The simulated moisture distribution in the SHT using the NUFT DKM model was in good qualitative agreement with the neutron logging data. The radial extent of the dry-out zone predicted by the NUFT ECM model was less than that measured by neutron logging. The NUFT DKM model calculated a condensate-shedding zone that was to the sides and below the dry-out zone, which was qualitatively consistent with the liquid-phase saturation changes measured by the ERT. The ECM model calculated a pronounced condensation zone that was vertically symmetrical about the heater axis; this was inconsistent with the liquid-phase saturation changes measured by ERT. The SHT was not sensitive to the magnitude of percolation flux (CRWMS M&O 1999d, Section 8.8.7).

#### 3.6.4.1.4 Drift Scale Test

The results of DKM Active Fracture model with NUFT calculations were compared with temperature fields measured in the DST. Temperature histories at selected sensor locations, and temperature profiles along selected boreholes were graphically compared with model results. Figure 3-105 shows a graphical comparison for a typical thermal sensor. A statistical goodness-of-fit analysis was performed to compare model and field temperatures at all sensor locations in the field. Three statistical measures of goodness-of-fit were used, the RMSD, MD, and normalized-absolute-mean-difference (NAMD) between measured and simulated temperatures.

Two different rock-property data sets were used in the calculations: the DS data set and the MS data set. Hydraulic and thermal properties of all hydrogeologic units along a stratigraphic profile through the DST test area were used in the model calculations. However, the HD and wing heaters are located in the tsw34 unit; therefore, tsw34 and its immediate neighbors tsw33 (above) and tsw35 (below) were expected to have greatest influence on rock temperature and liquid saturation.



Source: CRWMS M&O 2000a, Figure 96

Figure 3-105. Comparison of DKM Simulated (NUFT) and Measured Temperature Histories for Sensor #10 in Borehole 160 (Horizontal, Near the Wing) for All Property Sets in the DST

Graphical comparisons of model-temperature profiles and temperature histories with field data show very good agreement, except at locations adjacent to the heat sources. Some over prediction of temperature, up to about 16 percent, was observed adjacent to the HD and in the wing-heater areas. In general, the comparison between the simulated and measured temperatures is poor for all sensors located very close to the heated drift at small times (less than 100 days). This is at least partially the result of the computational grid spacing being too coarse to resolve the large temperature gradients generated near the heat sources at early times. At later times, in excess of 1 year, the results improve significantly as the temperature profiles smooth in space.

Agreement between model and field temperatures was better in the sub-boiling zones than in above-boiling zones. Better agreement in the sub-boiling zones indicates that heat flow is dominated by conduction and that the value used for wet thermal conductivity ( $0.92 \text{ W/m}\cdot\text{C}$ ) is reasonable.

The RMSD, MD, and NAMD between the simulated and measured temperatures were selected as measures of the goodness-of-fit of the simulated values to the field values. These results, like the graphical comparisons discussed earlier, show good agreement between model and field temperatures. For the Drift-Scale data set, the RMSD above  $97^\circ\text{C}$  is generally two to three times

C-76

higher than the RMSD below 97°C (12–16°C compared to 6–7°C) and at times greater than 182 days, it does not vary significantly with time. Also, for the Drift-Scale data set, the MD shows that temperature is generally over-predicted by the model at large times for temperatures both above and below 97°C. As with the LBT, model results using the DS data set are in slightly better agreement with field temperatures than results obtained with the MS data set.

#### 3.6.4.1.5 G-Tunnel

Nitao and Buscheck (1996) used the ECM TH model with NUFT to analyze the thermo-hydrologic flow in variably saturated, fractured, welded tuff for the Prototype Engineered Barrier System Field Tests (PEBSFT) in G-Tunnel at Yucca Mountain. Post test analyses were also conducted using the DFM TH model with NUFT. The PEBSFT (Ramirez 1991) were conducted to evaluate the applicability of measurement techniques, numerical models, and procedures developed for large-scale field tests at Yucca Mountain. The primary objective of the tests was to provide the basis for determining whether tests planned for Yucca Mountain had the potential to be successful. The PEBSFT was conducted prior to the current QA program and as such can not be used directly. However, the results can be used to corroborate experimental results from the ESF tests.

The tests were performed in a section of the tunnel referred to as the G-tunnel Underground Facility. The Small-Diameter Heater Alcove and the Rock-Mechanics Incline bounded the test block. A 30.5 cm (12 in.) horizontal heater-emplacement borehole was drilled to a depth of 10.7 m. A 3 m long heater element was placed inside the borehole with its midpoint positioned at 8.5 m from the collar. The heater power-level was maintained at about 3.2 kW for 128 days. The power was then ramped down to zero over a 67 day period. Rock temperature, moisture content, and other hydrothermal variables were monitored in twelve instrumentation boreholes. All instrumentation boreholes were grouted after drilling. The highest borehole-wall temperature measured was 242°C.

The test was modeled using the ECM and the DFM approaches. For the ECM, local thermodynamic equilibrium is assumed between the matrix and fractures within a representative elementary volume. The ECM is actually a single-continuum model with composite characteristic curves derived as a function of bulk-averaged liquid saturation in the matrix and fractures. For the DFM, the matrix and fractures are separated into distinct spatially discretized domains, which can represent disequilibrium between the matrix and fractures.

Good agreement was observed between model and field temperatures for histories at the lower borehole wall, and at points 0.55 m below and 2.4 m above the heater axis. The best agreement was apparently obtained for 280 and 524  $\mu\text{m}$  fractures. The 1,048- $\mu\text{m}$  case shows some over-prediction of field temperatures, possibly because buoyant gas-phase convection was over-predicted.

The rock matrix dry-out volume, measured by neutron probe, was reasonably well predicted by both the DFM and ECM models. The neutron measurements also showed preferential drying along the fractures, which was observed in the results of both models.

### 3.6.4.1.6 TH Model Validation Conclusions

The heating and cooling stages of the SHT were modeled by ECM and DKM TH models with the NUFT code, using the December 1997 TSPA-VA base-case hydrologic parameter set, which was modified to include the field measurements of bulk permeability in the SHT area. Two different conceptual models for FMX were considered: the ECM, which assumes equilibrium between the fracture and matrix continua, and the DKM that accounts for disequilibrium processes between the fracture and matrix continua. For the DKM-model calculations, two different approaches for representing the FMX were considered: a fixed-FMX approach and a dynamic-FMX approach. For the ECM-model calculations, two different western boundaries were considered: one that placed the western boundary at the eastern wall of the TM alcove and one that placed the western boundary 33 m to the west of the western wall of the TM boundary. Unlike earlier TH models of the SHT, all of the models in this study included the influence of vapor and heat flow along the heater borehole. This modeling study resulted in the following observations and conclusions:

- The DKM model predicts temperatures that are in outstanding agreement with the observed temperatures throughout the heating stage of the SHT.
- The DKM predicts higher temperatures in the superheated, dry-out zone than does the ECM model, primarily because the DKM model predicts a substantial gas-phase pressure increase in the matrix blocks, whereas the ECM model assumes gas-pressure equilibrium between the matrix and adjoining fractures. The gas pressure increase predicted by the DKM model causes the saturated temperature (which is the boiling temperature at the local pressure) to increase well above the nominal boiling point (96°C).
- The ECM model predicts temperatures that are in good agreement with the observed temperatures in the sub-boiling region of the SHT during the heating stage. In the superheated, dryout zone, the ECM model predicts temperatures that are lower than the observed temperatures during the heating stage.
- For the DKM model, the predicted radial extent of the dryout zone is in good, qualitative agreement with the neutron-probe measurements of liquid-phase saturation change. For the ECM model, the radial extent of the dryout zone is less than that predicted by the DKM model (and is somewhat less than that indicated by the neutron-probe measurements).
- The DKM model predicts a condensate-shedding zone that is to the sides and below the dry-out zone, which is qualitatively consistent with the measurements of liquid-phase saturation change made with ERT.
- The ECM model predicts a pronounced condensation zone that is vertically symmetrical about the heater axis; this is inconsistent with the measurements of liquid-phase saturation change made with ERT.

- The SHT cannot distinguish between alternative conceptual models of the FMX factor. Both approaches result in the same outstanding agreement with observed temperatures, and both approaches predict the same distribution of liquid saturation in the matrix continua.
- The models with an extended western boundary predict temperatures that are in better agreement with the observed temperatures than are those predicted by the model with the western boundary located at the eastern wall of the TM alcove.
- All of the models underrepresented heat loss to the TM alcove, resulting in predicted temperatures being greater than observed temperatures in the vicinity of the TM alcove; this over-prediction increases as the distance to the TM alcove decreases. The cause for this over-prediction is the manner in which heat flow in the TM alcove is treated. Had thermal radiation from the warmer to cooler wall surfaces in the TM alcove been accounted for in the SHT models, the cooling rate on the eastern TM alcove wall would have been much greater, resulting in lower predicted temperatures in the vicinity of the TM alcove.

#### 3.6.4.2 Validation of THC Models

The current understanding of the effect of coupled THC processes on the Near Field is based on various experiments from small-scale to field-scale (see Table 3-14), modeling of water-rock reactions (Hardin, 1998; Johnson et al. 1998), coupled modeling of water-gas-rock reactions (Lichtner and Seth 1996, pp. 133 to 142; Hardin, 1998; Sonnenthal et al. 1998; Tsang et al. 1999; CRWMS M&O 2000b), and observations of zeolitization due to higher-temperature alteration that took place early in the history of the tuffs (see Section 3.6.2).

Although a few water samples were collected from the Single-Heater Test, that were mildly acidic to near neutral in pH and moderately dilute, data on gas chemistry were lacking and the test was too short for significant alteration to have taken place. Most of the quantitative data on coupled THC processes in the Near Field have come from the ongoing Drift-Scale Test, which has yielded water samples in several hydrology boreholes above and below the heaters. Gas samples have been collected in numerous borehole intervals around the test and approximately quarterly since heating was initiated in December 1997. In general, water compositions have been similar to, but not as dilute, as those collected from the Single Heater Test, with pH values in the Drift Scale Test ranging approximately from just above 6 to nearly 8. The gas chemistry exhibits large regions of increased CO<sub>2</sub> concentrations that have been attributed to exsolution, gas transport, and calcite dissolution. Significant shifts in stable carbon, oxygen and hydrogen isotopic ratios (CRWMS M&O 2000b) have been attributed to isotopic fractionation accompanying boiling, vapor transport, and condensation.

Lab and field experiments have provided insight and data pertaining to the effects of THC processes on the chemistry of water and gases, but for the most part there is only indirect evidence for mineral dissolution and precipitation. Increased silica concentrations relative to chloride (a generally conservative species) have indicated significant reaction of silicates as shown in Table 3-16 (CRWMS M&O 2000b, Table 9). The modeling presented in Section 3.3 has indicated only minor changes in porosity as a result of mineral precipitation and dissolution.

Such small changes in hydrologic properties are consistent with a return to higher air permeability after boiling zones dried-out in the DST (CRWMS M&O 2000a). The first two years of the test were generally in a heating-up phase, and during the following two years a more stable boiling zone should persist and be more conducive to localized mineral precipitation.

Modeling of coupled THC processes (CRWMS M&O 2000b, Section 3.2) has indicated that calcite and silica polymorphs are the dominant dissolving and precipitating mineral phases, with feldspars, clays, and zeolites modifying the water composition, and pH to a lesser extent. The model results that were based on a relatively complete geochemical system produced shifts in pH to somewhat higher values than those observed in the Drift Scale Test, indicating that the model most likely overestimated the effective reaction rates for these phases. Thus, if the DST water chemistry is representative of the long-term water compositions accompanying the thermal period of the potential repository, then the modeling results may be viewed as an upper limit to the effect of these phases on system behavior. Modeling of the water and gas composition in fractures in the Near Field was shown to also depend on the infiltration rate.

Data from the field tests and associated modeling suggest the following general characterization of the NF THC processes:

- Exsolution of CO<sub>2</sub> by heating and boiling of predominantly matrix pore water will result in an expanding zone of elevated CO<sub>2</sub> concentrations (1 to 2 orders of magnitude above atmospheric levels)
- Accompanying the zone of increased CO<sub>2</sub> will be an area of higher fracture-liquid saturation due to condensation, and pH values of water less than the ambient porewater (~ pH 8.3, but generally not lower than about 6)
- Strong drainage of lower pH condensate water in fractures will result in calcite dissolution
- Enhanced precipitation of calcite, amorphous silica, and possibly zeolites will be localized above and to the sides of the drifts
- Overall changes in fracture porosity and permeability will be minor, although some fractures could be more tightly sealed than others
- Waters that reach the drift during the early stage of rewetting will not be strongly elevated in salts, because of rapid dissolution and strong dilution, but may have increased carbonate and silica concentrations.

#### 3.6.4.2.1 Summary of THC Model Validation Using Tests

The DS THC Model has been extensively validated by comparison of gas and water geochemical data collected during the DST, as discussed in Section 3.6.1.3 and described in detail in the *THC Process AMR* (CRWMS M&O 2000b). These comparisons include gas-phase CO<sub>2</sub> concentrations as a function of time and space, the pH of waters collected in boreholes, and general observations on changes in concentrations of Cl and other aqueous species. The model

can thus be considered valid for its intended use, which is to interpret data for the SRCR. For LA, DST cooling data will be available to more extensively validate the model.

The DST is the second underground thermal test being performed in the ESF at Yucca Mountain, Nevada. The purpose of the test is to evaluate the coupled thermal, hydrological, chemical and mechanical processes that take place in unsaturated fractured tuff over a range of temperatures from approximately 25°C to 200°C. The heaters were activated in December 1997 and are planned to run for four years followed by a four year cooling period.

The thermal tests provide the only field-scale experiments that have produced seepage under thermally perturbed conditions. Numerous samples of water have been collected from several borehole intervals during the DST, and previously a few samples were collected in the Single Heater Test (CRWMS M&O 2000a).

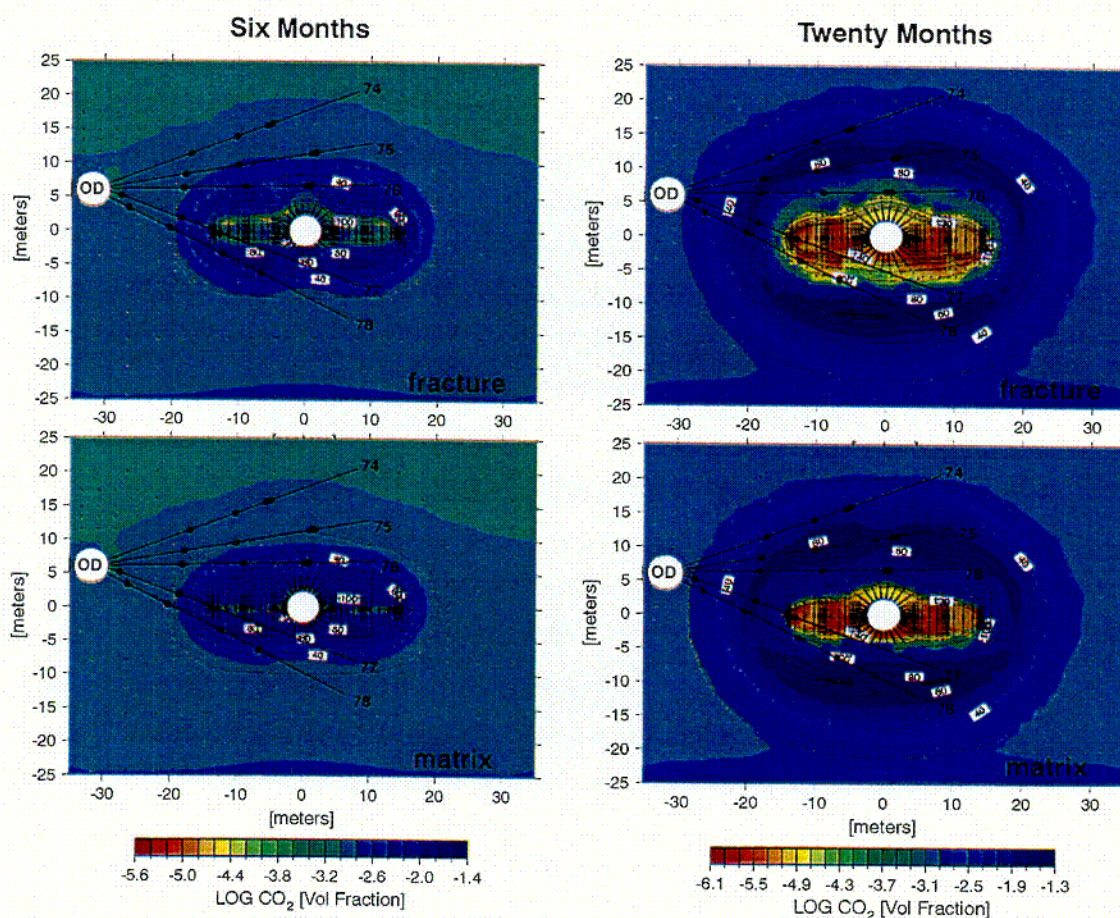
Simulation of DST THC processes provides an important validation test for the THC conceptual models and input data used in the THC Seepage Model for a much longer time-scale. Geochemical input parameters have not been calibrated to measured data collected during the DST and therefore the DST THC Model simulations are an independent test of the conceptual model and input data used also in the THC Seepage Model. Detailed analysis of THC processes in the DST and validation tests are presented in the *THC Process AMR* (CRWMS M&O 2000b). This validation process involves examination of areas of modeled fracture drainage compared to locations where water was collected during the test, the comparison of CO<sub>2</sub> concentrations collected from sampled gases, and comparison of the chemistry of waters collected from boreholes over time. These validation exercises are continuing as more data is collected from the DST and the models are improved to represent the physical and chemical processes more accurately. The following section compares modelling results to measured CO<sub>2</sub> concentrations collected from boreholes. Brief descriptions of the evolution of water chemistry and mineralogy follow.

#### 3.6.4.2.1.1 Gas-Phase CO<sub>2</sub> Evolution

In the first test, CO<sub>2</sub> concentrations measured in gas samples taken from boreholes during the DST are compared to simulation results using the DST THC Model. It is very important to properly simulate evolving gas-phase CO<sub>2</sub> concentrations, because they strongly control the pH of condensate waters, are sensitive to temperature, and CO<sub>2</sub> transport is sensitive to the fracture hydrologic properties. CO<sub>2</sub> also affects HCO<sub>3</sub><sup>-</sup> concentrations in fracture waters, which are important for the in-drift geochemical environment. Modeled distributions of CO<sub>2</sub> concentrations and temperature in fractures and matrix are shown after 6 and 20 months of heating (which are also times for which CO<sub>2</sub> measurements are available) in Figure 3-106 for the calcite-silica-gypsum geochemical system (*Less Complex*). At both times, and in both fractures and matrix, a halo of increased CO<sub>2</sub> concentrations appears centered approximately at the 60°C isotherm. Over the 14-month period, between 6 months and 20 months, the halo increases considerably in extent and magnitude. Areas close to the HD that have dried-out and are at above-boiling temperatures show a decline to much lower CO<sub>2</sub> concentrations.

To evaluate how the model predicts the time-evolution of CO<sub>2</sub> concentrations in the gas phase, measured CO<sub>2</sub> concentrations from intervals that were repeatedly sampled from February 1998

to August 1999 (20 months) are compared to model results for the same times. Figure 3-106 shows the time-evolution of CO<sub>2</sub> concentrations in borehole intervals 74-3, 75-3, 76-3, and 78-3 (see Figure 3-106 for locations of borehole intervals). In borehole interval 74-3, there were only grid nodes above (cooler side) and below (hotter side) the interval, and therefore results from both nodes are plotted to see if they bracket the measured compositions. In borehole interval 78-3, two locations (center and end) were chosen, because of the strong thermal gradient across this region. The comparison shows that the simulations generally follow the trends in measured CO<sub>2</sub> concentrations. Two exceptions are when a known heater power-loss occurred (around 19 months; see slope change in 74-3 and 75-3 at 20 months) or when the samples were at boiling temperatures and were nearly all water vapor (instead of air), and had much of the water condensed-out during sampling (76-3 and 78-3, largest peaks). In the latter case, the modeling results should diverge from the measured data, because they reflect the CO<sub>2</sub> concentration in the full water vapor-air mixture. This effect is discussed in the *THC Process AMR* (CRWMS M&O 2000b, Section 6.2.7.2).



NOTE: Temperature Contours are Superimposed. "OD" refers to the Observation Drift (adapted from CRWMS M&O 2000b, Figures 5 and 6). Contour labels and color bars indicate values.

Figure 3-106. Simulated CO<sub>2</sub> Volume-Fractions in Fractures and Matrix, After 6 and 20 Months of Heating, During the Drift-Scale Test (*Less Complex case*)

C-77

#### **3.6.4.2.1.2 Water Chemistry Evolution**

The modeled chemistry of waters in fractures is shifted from an initial pH of about 8.3 to 6.5, and is captured as changes in time and space. The lowest modeled pH values are in the region of highest gas-phase CO<sub>2</sub> concentrations. The shift in pH in the modeled fracture water is similar to that observed in the water collected from hydrology boreholes at the same times and in the expected regions during the DST (CRWMS M&O 2000b), which were also areas of high gas-phase CO<sub>2</sub> concentrations. Chloride concentrations in waters collected from hydrology boreholes are considerably more dilute (a factor of 5 to 10) than the matrix pore water, which was also predicted by the modeling. The good agreement between simulation and measurement for pH and chloride indicates that the degree of communication between fractures and matrix in the simulation is appropriate. Stronger communication in the simulation would predict higher pH and higher chloride than measured in the samples. Other species, such as Ca and Si, show similar trends in the modeled fracture-water compositions compared to measured water compositions. These trends indicate increasing silicate mineral dissolution and calcite precipitation, as condensate waters undergo heating (CRWMS M&O 2000b, p. 72). Additional information on water chemistry can be found in the *THC Process AMR* (CRWMS M&O 2000b).

#### **3.6.4.2.1.3 Mineralogical Changes**

In the model simulations, calcite is the major phase forming in the zone above the heaters, although the abundances are exceedingly small. Secondly, amorphous silica also precipitates, but is much less abundant compared to calcite. No direct observation of the precipitation or dissolution of calcite has been found, because the DST is ongoing; however, trends such as decreasing Ca in water found in boreholes with increasing temperature, pH and silica concentrations are strongly suggestive of calcite precipitation as shown in Table 3-16 (CRWMS M&O 2000b, Table 9). Fracture porosity changes in the DST simulations are very small after 20 months of simulation (on the order of 0.01 percent) and follow closely the area of calcite precipitation (CRWMS M&O 2000b, Figure 17). Such small changes likely have no measurable effect on the hydrologic properties of the rock. More data are being collected from the DST, including <sup>14</sup>C concentrations in gas-phase CO<sub>2</sub> and hydrogen, carbon, oxygen, strontium, and uranium isotopic measurements that will allow for more careful testing of the DST THC Model.

#### **3.6.4.2.2 Corroborative Evidence**

Data collected from the DST over the next several years will include water and gas chemistry, and eventually samples of rocks around boreholes. These data will be invaluable in testing of the models developed to predict long-term repository performance. No other data can be used to directly corroborate the model, because of the uniqueness of the system. However, studies from natural analogs have been useful in analyzing aspects of the Yucca Mountain THC performance, as discussed in Sections 3.6.2 and 3.6.4.4.

#### **3.6.4.3 Validation of TM and THM Models**

The TM and THM behavior of rock in the near field has been simulated using two fundamentally different techniques (e.g. the continuum and distinct-element techniques). The continuum technique simulates a rock mass as a continuous body with properties that may vary from place

to place, while the distinct-element technique simulates the rock masses a collection of independent blocks separated by individual fractures. For problems involving coupled behavior in partially saturated, fractured rock, these two types of simulators are generally weakly coupled to the TH models, via temperature and permeability parameters. This is because the thermal and fluid-flow capabilities in TM models are generally much less sophisticated than for the TH models, and because simulation of TM response in a rock mass requires a much different grid than is generally used for TH response. This is especially true in the case of the discrete-element model in which blocks of rock move independently. The coupling between TH and TM is generally done by first computing a temperature field using the TH model and passing this temperature field to the TM model. The TM model predicts a deformation or change in stress, which causes a change in permeability, which is passed back to the TH model.

The T results of TH portions of the THM models are compared with results from TH models discussed in Section 3.2.4, the validation of which is discussed in Section 3.6.4.1. No separate model validation or confidence building exercise was performed for the TH portions of the THM models. The temperature fields are what are coupled to the mechanical models.

The TM model validation or confidence building is provided mainly by comparisons with field tests. Confidence building of the TM models in a non-YM specific context was provided by an assessment of various model approaches made as part of the international cooperative DECOVALEX project. As noted by Ahola et al. (1994a and 1994b), there is "...good agreement among the predicted temperatures and displacements, and lesser agreement among the predicted stresses and fluid fields". However, as they point out, validation requires comparison to actual field data.

The YMP approach is consistent with the above observation in that one of the primary means of model validation for the TM models has been comparison of measured and computed displacements for the field-scale thermal tests, including the LBT, the SHT and the DST. Additionally, a large number of laboratory tests have been conducted on samples ranging from a few mm to 0.5 m in scale. The laboratory tests have provided essential data on rock properties and insight into the coupled THM behavior of the rock under well-controlled conditions.

The field-scale thermal tests provide deformation data mainly via displacement measurements using MPBX instrumentation. These instruments are installed in boreholes and provide measurement of displacement along the axis of the borehole. Thus, they are essentially a line or point measurement and, when used in an array, can provide deformation data for a test block. These data can then be used to compute rock-mass thermal expansion, and can sometimes indicate movement on fractures. MPBX instrumentation has also been used in conjunction with plate-loading apparatus to provide information on the deformation modulus at a scale containing numerous fractures. Comparison of deformation from different tests and from different sections of a field test can provide an assessment of how the heterogeneity of the rock mass affects TM properties. These field tests have also provided data on the temperature dependence of mechanical properties.

Stress measurements can also be used in TM model validations. A few Goodman Jack stress measurements were made in association with the SHT. However, these measurements did not

provide useful information on the stress field in the rock during this test and were not further considered.

Laboratory tests on cores and small-block samples have provided data on mechanical properties of rock and rock fractures. In particular, a few tests on fractures have been conducted, including fracture properties such as friction angle, fracture stiffness, and fracture cohesion on samples on a scale up to 0.5 m. It is important to note that some of these properties are difficult or impossible to measure in the field. A few tests designed to characterize fracture flow at elevated temperature and stress conditions have also been conducted, and results of these can be used to gain confidence in model simulations.

#### **3.6.4.3.1 TM analysis of the Large Block Test**

The LBT was conducted on a rectangular block of near-surface fractured rock exposed (via excavation) at Fran Ridge. Deformation of the block at a scale of 1 mm and above was monitored using MPBX instrumentation. Overall block deformations near the heater plane was closely correlated with temperature as discussed in Section 3.6.1.1. A series of pretest simulations of the TM behavior of the LBT were performed using a continuum model. Comparison of the observed and simulated profiles indicates that the predicted deformation below the heater plane has the same direction as the observed deformation, but the magnitude of displacement is over predicted (Blair and Wood, 1998). This may indicate that the value of thermal expansion used in the model was too large, and more recent field measurements confirm this. Above the heater plane the predicted and observed profiles diverge dramatically. The predicted profile shows a decrease in horizontal deformation with height that can be associated with the vertical thermal gradient imposed on the block. However, the observed horizontal deformation continues to increase with height and is independent of the thermal profile above the heater plane. Moreover, MPBX data from boreholes in the upper portion of the block show that most of the deformation occurs in discrete vertically oriented zones (Wilder, et al. 1997). This is attributed to opening of vertical fractures in this upper region. This result indicates that the LBT is more suitable for simulation using the distinct element technique. Efforts are ongoing in the use of a distinct element model to simulate the LBT. This model is based on the drift scale distinct element model discussed in Section 3.5.

#### **3.6.4.3.2 TM Analysis of the Single Heater Test**

The SHT is described in Section 3.6.1.2. MPBX instrumentation was installed both parallel and perpendicular to the heater in this test. During the test MPBX instruments oriented parallel to the heater registered mostly expansion of the rock mass, while the MPBX oriented perpendicular to the heater registered compression movement at the beginning of the heating, followed by expansion after about 40 to 50 days of heating. The SHT was simulated with a continuum TM model. Comparison of the MPBX data along the heater with and model simulations shows good correspondence during the test, although the measured displacements tend to be smaller than the pretest model predictions by about 20 percent during the heating cycle. However, several aspects of the SHT deformation data were not adequately simulated by the model. These primarily included localized offsets of anchors that were of opposite sense to the continuum predictions.

Results indicate that the coefficient of thermal expansion measured in the field is about 50% lower than values measured on core samples in the laboratory. The general trends—from the initial compression, followed by general extension, and ending with the sharp extension after the heater is deenergized—are consistent between both laboratory data and model predictions.

#### **3.6.4.3.3 TM Analysis of Drift Scale Test.**

The DST is described in Section 3.6.1.3. MPBX data, for two locations above the center of the heated drift, have been most extensively analyzed. These correspond to locations approximately 4 m into the rock above the crown of the drift. Comparison of observed and simulated deformations show good agreement for both sets of comparisons in terms of trend and magnitude. Further analysis of the DST deformation is underway using both continuum and distinct element techniques.

A plate loading test was also conducted in conjunction with the DST. This test applied horizontal load to opposite sides of a niche in the DST Alcove in order to determine the deformation modulus of the rock mass. Results showed that the heated side had a Young's modulus of approximately 40 GPa, while the cool side had a modulus of approximately 12 MPa. This result was unexpected, but may be due to the proximity of the cool side. Additional plate loading tests are planned for this location, and further analysis of this result is underway.

#### **3.6.4.3.4 Coupled Analysis**

Much of the work on hydromechanical behavior of fractures has focussed on normal deformation of fractures and the cubic law. Recent work by Barton et al (1997) provides convincing evidence that shear deformation of fractures plays an important role in their hydromechanical behavior.

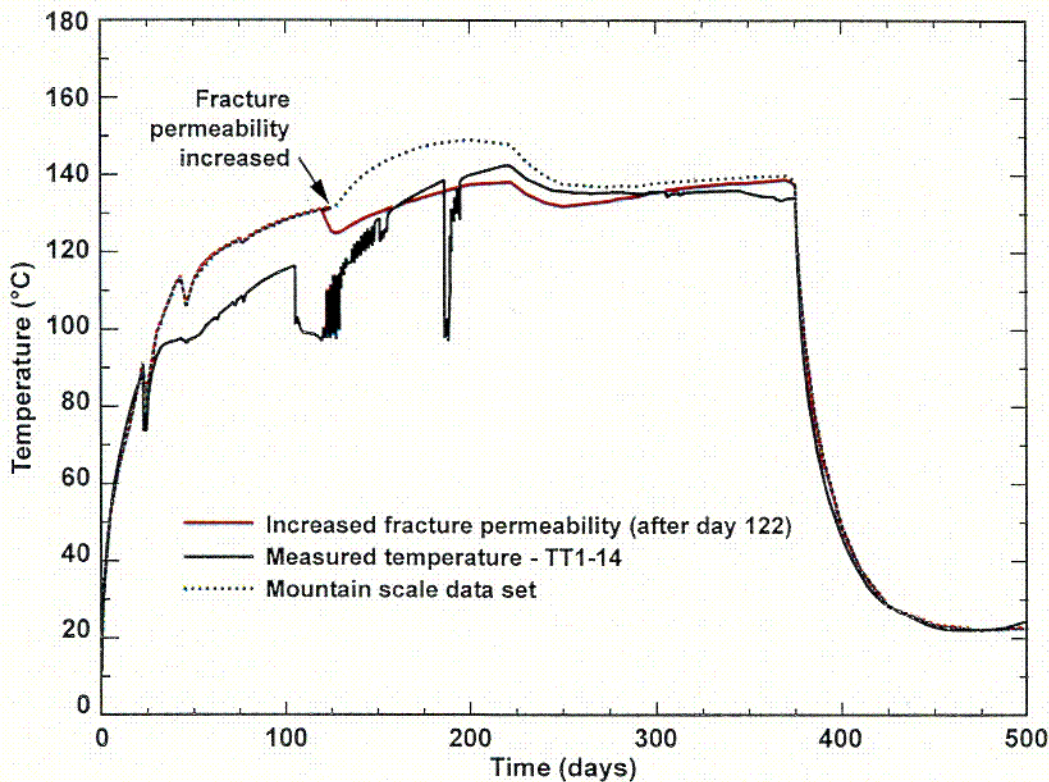
Initial efforts to integrate shear deformation into THM analysis for YMP used the approach presented by Berge et al. 1998 in which a continuum model was used to predict zones where shear deformation could be expected on fractures of a given orientation. This approach was used to simulate the SHT and the DST and was applied to emplacement drift geometry in the Near-field Altered-Zone Models Report (Hardin 1998).

This analysis was difficult to verify, given the data available from the field tests. For instance, the analysis of the DST indicates zones of increased permeability in areas where no instrumentation had been placed.

These initial analyses were in 2-D for cross sections perpendicular to heat sources. Berge et al (1998) did a 3-D calculation using this approach for an emplacement drift analysis and found that the 3-D problem slip was predicted in some locations in the direction parallel to the drift. This technique has a serious limitation in that it only calculates where slip might occur, but does not indicate the amount of slip, nor does it provide for stress relaxation after slip, nor for dilation and other aspects of shear deformation. Subsequently, analysis using the distinct element method has been initiated as discussed in Section 3.5.

Section 3.6.4.3.1 discussed the observed deformation of the LBT. These results have been used to inform a thermal-hydrological simulation of the LBT. In this calculation, a Dual Permeability Model (DKM) was used to simulate the temperature history of the LBT. One set of simulations

utilized the YMP MS data set. Figure 3-107 shows that for this calculation, calculated and observed temperatures agree very well during the first 25 days of heating, but the model overpredicts temperatures during the period from 25 to 225 days (dotted line in Figure 3-107). A second model calculation was made that attempted to incorporate the opening of fractures. For this calculation, the fracture permeability used in the model was increased at Day 125 to simulate fracture opening. The solid line in Figure 3-107 shows the results. These results indicate that increasing the fracture permeability reduce the predicted temperature to values much closer to those observed in the test.



DTN: LL00031430242.094

Source: CRWMS M&O 2000a, Figure 67

Figure 3-107. Comparison of Two Simulations with Temperatures Measured During the Large Block Test. Increasing Fracture Permeability at 122 Days Causes Temperatures to Drop to Values Closer to Those Observed.

It appears that the opening of fractures and associated increase in fracture permeability caused an increase in the amount of heat and vapor transported out of the portion of the block above the heaters, thus lowering the temperature. This provides an example of how thermal mechanical effects may influence thermal hydrologic behavior in a fractured rock mass. More refined calculations are underway.

#### **3.6.4.3.5 Summary of TM and THM Validation**

Validation of TM models is in the preliminary stage. The main avenue of validation of TM calculations to date has been through comparison of calculated deformation to line displacement measurements, and reasonable agreement has been found between continuum calculations and selected observations of deformation for the underground tests. However, more robust data describing field deformation is needed to improve confidence in the THM simulations. Moreover, observations made at the LBT indicate that a distinct-element approach is needed to accurately simulate the test. Deformation data for the SHT and DST also show behaviors that are not readily simulated using continuum models. These behaviors include localized extensions or contractions detected by a particular MPBX anchor that are not detected by adjacent anchors.

Validation of THM simulations using either the continuum or discrete element models is also in initial stages. THM continuum calculations have been done for the SHT (CRWMS M&O 1999d) and DST (Blair et al, 1997) as discussed above.

These studies indicate that pursuit of an alternative modeling approach is warranted for simulation of the TM and THM behavior of rock in the Near Field Environment. This alternative is the drift scale distinct element model as described in Section 3.5. This model provides for the inclusion of discrete fractures, and can predict localized fracture deformation in both normal and shear modes. Application of this model to the field scale thermal tests is ongoing.

#### **3.6.4.4 Summary of Validation from Analog Studies**

Two analogs, Eldora and Grants Ridge, show different hydrothermal convection. Eldora indicates there was a significant large scale (at least 60m) convecting hydrothermal system, whereas at Grants Ridge there was no evidence of pervasive hydrothermal convection. The Eldora stock developed under saturated conditions that are not representative of YM. Therefore, the Grants Ridge analog results, which indicates no pervasive hydrothermal convection, would be expected to be the better analog for NFE.

The analogs for THC processes also vary. The Yucca Mountain self analog suggests potential for hydrothermal development of mineral suites dominated by analcime and illite/smectite and minor calcite and clinoptilolite (based on trends shown on Figure 3-99(b) that show other minerals dropping out with depth-temperature).

The Banco Bonito, Valles and Grants Ridge show minimal (10 m) hydrothermal alteration, which is interpreted to be due to unsaturated conditions at the time of contact. This is consistent with THC model results.

Finally, analysis of the Paiute Ridge indicate that THC analyses of fracture plugging (mineral cap), have been consistent with this analog study.

## **4. RELATIONSHIP TO NRC ISSUE RESOLUTION STATUS REPORTS**

The NRC has indicated it plans to structure its review of issues that are subjects of Process Model Reports (PMRs) around the NRC's KTIs and Issue Resolution Status Reports (IRSRs). This chapter of the PMR describes how the acceptance criteria in the IRSRs relevant to the NFE PMR have been addressed.

### **4.1 SUMMARY OF THE KEY TECHNICAL ISSUES**

As part of the review of site characterization activities, the NRC has undertaken an ongoing review of information on Yucca Mountain site characterization activities to allow early identification and resolution of potential licensing issues. The principal means of achieving this goal is through informal, prelicensing consultation with the DOE. This approach attempts to reduce the number of, and to better define, issues that may be in dispute during the NRC licensing review, by obtaining input and striving for consensus from the technical community, interested parties, and other groups on such issues.

The NRC has focused prelicensing issue resolution on those topics most critical to postclosure performance of the potential geologic repository. These topics are KTIs. Each KTI is subdivided into a number of subissues. The KTIs are:

- Activities Related to Development of the Environmental Protection Agency (EPA) Standard
- Container Lifetime and Source Term
- ENFE
- Igneous Activity
- Radionuclide Transport
- Repository Design and Thermal Mechanical Effects
- Structural Deformation and Seismicity
- Thermal Effects on Flow (TEF)
- Total System Performance Assessment and Integration (TSPAI)
- Unsaturated Zone (UZ) and Saturated Zone (SZ) Flow Under Isothermal Conditions.

Identifying KTIs, integrating their subissues into a risk informed approach, and evaluating their significance for postclosure performance help ensure that NRC's attention is focused on technical uncertainties that will have the greatest affect on the assessment of repository safety.

Early feedback among all parties is essential to define what is known, what is not known, and where additional information is likely to make a significant difference in understanding future

repository safety. The IRSRs are the primary mechanism that the NRC staff uses to provide feedback to the DOE on the status of the KTI subissues. IRSRs focus on NRC acceptance criteria for issue resolution and the status of issue resolution, including aspects of agreement or disagreement. IRSRs also communicate comments or questions from the NRC staff. Open meetings and technical exchanges between NRC and DOE, provide additional opportunities to discuss issue resolution, identify areas of agreement and disagreement, and develop plans to resolve any disagreements.

Additional issues include those identified by the Performance Assessment Peer Review Panel, the ACNW, the Total System Performance System Assessment - Viability Assessment (TSPA-VA), the Near-Field Expert Elicitation, and others, as described in Section 2.4 of this document. Generally these concerns are closely related to the KTI subissue acceptance criteria.

#### 4.2 RELATIONSHIP OF THE NEAR-FIELD ENVIRONMENT PMR TO THE KTIs

The following sections describe the KTIs and the subissues relevant to the NFE PMR. Table 4-1 lists the KTIs that contain subissues relevant to the NFE PMR. The relevant subissues are shown in italics. Appendix D lists the acceptance criteria relevant to the NFE PMR and provides a description of the PMR approach. In many cases, a given PMR may only partially address acceptance criteria. For acceptance criteria relevant to the NFE PMR that are addressed in more than one PMR, cross-references to other PMRs are provided. For all ENFE IRSR acceptance criteria, pointers to this and other PMRs that contain details relevant to ENFE IRSR acceptance criteria are provided in Table 4-2.

Table 4-1. Issue Resolution Status Report/Key Technical Issues Related to the NFE PMR

Issue Resolution Status Report/Key Technical Issues	Subissues*
ENFE	<i>Effects of Coupled THC Processes on Seepage and Flow</i> <i>Effects of Coupled THC Processes on the Waste Package Chemical Environment</i> Effects of Coupled THC Processes on the Chemical Environment for Radionuclide Release <i>Effects of Coupled THC Processes on Radionuclide Transport Through Engineered and Natural Barriers</i> Coupled THC Processes Affecting Potential Nuclear Criticality in the Near-Field (Addressed in Topical Report)
Thermal Effects on Flow (TEF)	<i>Is the U.S. Department of Energy TH testing program, including performance confirmation testing, sufficient to evaluate the potential for thermal reflux to occur in the near field?</i> <i>Is the U.S. Department of Energy TH modeling approach sufficient to predict the nature and bounds of thermal effects on flow in the near field?</i> Does the U.S. Department of Energy Total System Performance Assessment (TSPA) adequately account for thermal effects on flow?

Table 4-1. Issue Resolution Status Report/Key Technical Issues Related to the NFE PMR (Continued)

Issue Resolution Status Report/Key Technical Issues	Subissues*
Repository Design and Thermal-Mechanical Effects	Implementation of an Effective Design Control Process Within The Overall Quality Assurance Program Design of the Geologic Repository Operations Area for the effects of seismic events and direct fault disruption <i>Thermal-Mechanical Effects on underground facility design and performance</i> Design and long-term contribution of repository seals in meeting postclosure performance objectives
Total System Performance Assessment and Integration (TSPAI)	<i>System description and demonstration of multiple barriers</i> <i>Scenario analysis</i> Model abstraction Demonstration of the overall performance objective

\*Subissues relevant to the NFE PMR are shown in italics

The definition of the NFE includes the in-drift environment and the immediately surrounding host rock. This PMR describes models used to evaluate the rock part of the NFE, and the EBS PMR (CRWMS M&O 2000g) describes models used to evaluate the in-drift part of the NFE.

The ENFE KTI (NRC 1999a) subissues are addressed in various PMRs. Table 4-2 provides a correlation between the ENFE KTI subissues and the PMRs that address them. The remainder of this chapter and Appendix D of this PMR provide detailed explanations describing how the acceptance criteria relevant to the Near-Field Environment PMR have been addressed.

Table 4-2. PMRs Related to ENFE Issue Resolution Status Report/Key Technical Issue Subissues

NRC Key Technical Issue - Evolution of the Near-Field Environment Subissues	Process Model Reports Addressing Subissue
Effects of Coupled THC Processes on Seepage and Flow	Unsaturated Zone Flow and Transport Engineered Barrier System Degradation, Flow and Transport Near Field Environment
Effects of Coupled THC Processes on the Waste Package Chemical Environment	Engineered Barrier System Degradation, Flow and Transport Near Field Environment
Effects of Coupled THC effects on the Chemical Environment for Radionuclide Release	Unsaturated Zone Flow and Transport Engineered Barrier System Degradation, Flow and Transport
Effects of Coupled THC Processes on Radionuclide Transport Through Engineered and Natural Barriers	Unsaturated Zone Flow and Transport Engineered Barrier System Degradation, Flow and Transport Near Field Environment
Coupled THC Processes Affecting Potential Nuclear Criticality in the Near-Field	Criticality is addressed in a Topical Report and supporting documents

## 4.2.1 Evolution of the Near-Field Environment

The objective of the ENFE KTI (NRC 1999a) is to assess all aspects of the evolution of the near-field geochemical environment that have the potential to affect performance of the proposed repository. The near-field geochemistry will be perturbed from ambient conditions by variations in temperature and pressure associated with the heat production of the waste, introduction of foreign materials into the mountain, variations in fluid flow, and consequent chemical reactions. Coupled thermal-hydrologic-chemical (THC) and thermal-chemical processes can cause changes in parameter values and conceptual models used in various modules of performance assessment computer codes. The consequent effects on performance from the ENFE are expressed as the results of coupled processes.

### 4.2.1.1 ENFE IRSR Subissue 1

This subissue is entitled "*The Effects of Coupled THC Processes on Seepage and Flow.*" The acceptance criteria in this section are designed to ensure that coupled THC effects on the quantity and chemistry of seepage into drifts are adequately estimated and that they are appropriately considered in assessments of repository performance. Important factors affecting seepage and flow include: groundwater flux, fracture density and physical properties, presence or absence of fracture coatings, rock heterogeneity, moisture content, existence of fast pathways, and fluid-density gradients.

Chapter 3 of this PMR describes the process-level models, model abstractions and supporting analyses that address the near-field environment processes. Section 3.3 describes the models used to evaluate the potential effects of coupled THC processes on permeability and porosity within the NFE, which are then used in evaluations of UZ flow and transport. Temporal and spatial variations of properties or conditions used were consistent with the Unsaturated Zone Flow and Transport (UZ F&T) PMR (CRWMS M&O 2000f). In addition, spatial and temporal variations in conditions that arise from the emplacement of waste and the EBS were considered. Sections 3.2.3 and 3.4 of this PMR describe the abstraction of the models used to evaluate the potential effects of coupled THC processes on properties within the NFE that might impact seepage chemistry and UZ flow and transport in TSPA.

Seepage and flow are also covered in the UZ F&T PMR (CRWMS M&O 2000f). The NFE PMR contributes information to the UZ F&T PMR (CRWMS M&O 2000f) relative to permanent changes to the permeability and porosity structure. Changes can occur due to mechanical closure or opening of fractures during the period when thermal processes might mobilize water. However, assessments of drip-shield lifetime (CRWMS M&O 2000o, Figure 3-84) indicate no seepage through the drip shield that would allow water to contact the waste packages for a period of time that exceeds the period during which thermal mobilization of water might occur. Therefore, mechanical impacts on flow of water during this period are not of primary importance.

THC couplings under consideration for the engineered systems are covered in the EBS PMR (CRWMS M&O 2000g), and the Waste Form Degradation (WFD) PMR (CRWMS M&O 2000ab). THC couplings for the natural system are covered by both the UZ F&T PMR (CRWMS M&O 2000f) and this PMR.

#### 4.2.1.2 ENFE IRSR Subissue 2

This subissue is entitled "*Effects of Coupled Thermal-Hydrologic-Chemical Processes on the Waste Package Chemical Environment.*" The acceptance criteria in this section are designed to ensure adequate consideration of coupled THC processes affecting the waste package chemical environment in the assessment of repository performance. The EBS PMR (CRWMS M&O 2000g) discusses work performed that is related to the majority of the acceptance criteria described in this subissue. The NFE PMR has only a secondary role in resolution of this issue. It addresses property changes that might impact the chemistry of water within the unsaturated zone that seeps into the drifts. These property changes are input to the unsaturated zone analyses. The results, the chemistry of water seeping into drifts, are input to the EBS PMR (CRWMS M&O 2000g).

THC interactions between the natural and engineered systems are primarily covered within the EBS and UZ F&T PMRs (CRWMS M&O 2000g and 2000f). The EBS and WPD PMRs (CRWMS M&O 2000g and 2000ac) determine the chemistry of fluids that result from THC couplings between the drift and waste package materials. They also provide the water chemistry information to the unsaturated zone to analyze effects on flow and transport. The EBS and WPD PMRs (CRWMS M&O 2000g and 2000ac) report the evaluations of the resulting chemistry, the waste package chemical environment, and report on the associated abstractions. They also provide the descriptions of assumptions, approximations, simplifications, and abstractions used in those assessments. The UZ F&T PMR (CRWMS M&O 2000f) provides the descriptions of models used in establishing seepage water chemistry, and reports the seepage-water chemistry that is used as input to the EBS and WP models.

Section 3.3 of this PMR addresses models used to evaluate the potential effects of coupled THC processes on near-field chemical properties. These models provide the framework (or inputs) for the UZ F&T and EBS PMRs (CRWMS M&O 2000f and 2000g) to evaluate THC coupled processes at the DS, predict flow and transport behavior for specified thermal-loading conditions, and predict the chemistry of waters and gases entering the emplacement drifts. Sections 3.2.3 and 3.4 describe the abstraction of the models used to evaluate the potential effects of coupled THC processes on changes in mineralogy and deposition of salts.

#### 4.2.1.3 ENFE IRSR Subissue 3

This subissue is entitled "*The Effects of Coupled Thermal-Hydrologic-Chemical Processes on the Chemical Environment for Radionuclide Release.*" The acceptance criteria in this section are designed to ensure adequate evaluation of the chemical environment for radionuclide release and ensure that coupled THC processes affecting this chemical environment have been appropriately considered in the assessment of repository performance.

Slow rate of release of radionuclides from the waste form has been identified as a key factor for meeting the objective of acceptably low annual doses to a person living near the site (NRC 2000). Radionuclide release rates and solubility limits constitute one of the NRC key elements of subsystem abstraction for a performance assessment. Radionuclide release from waste forms and from the EBS will depend on the chemical environment, which will be

conditioned by coupled THC processes. The chemical environment for radionuclide release must be adequately evaluated and coupled THC processes must be appropriately considered.

Acceptance criteria addressed by this subissue are described by the EBS and WFD PMRs (CRWMS M&O 2000g, 2000ab, and 2000ac). There are no models of coupled effects on radionuclide release covered in this PMR.

#### **4.2.1.4 ENFE IRSR Subissue 4**

This subissue is entitled "*The Effects of Coupled Thermal-Hydrologic-Chemical Processes on Radionuclide Transport through Engineered and Natural Barriers.*" The acceptance criteria in this section are designed to ensure adequate evaluation of the effects of coupled THC processes on the transport of radionuclides through engineered and natural barriers, and ensure that these effects have been appropriately considered in the assessment of repository performance. Radionuclide concentration-reduction during transport through engineered and natural barriers is considered a key performance attribute of the proposed repository (NRC 2000). Distribution of mass flux between fracture and matrix, and retardation of radionuclides in fractures in the UZ and in the SZ constitute three of the NRC key elements of subsystem abstraction for performance assessment. Coupled THC processes affect each of these abstractions.

Radionuclide transport issues are reported primarily in the UZ F&T PMR (CRWMS M&O 2000f). The EBS, WFD, and WPD PMRs (CRWMS M&O 2000g, 2000ab, and 2000ac) provide input to UZ analyses relative to the chemistry of water, and the amount and form of radionuclides released from the drifts. As such, this subissue is discussed principally in the UZ F&T PMR (CRWMS M&O 2000f) with some discussion in the EBS, WFD, and WPD PMRs.

The NFE PMR discusses issues of precipitation and dissolution of minerals within the fracture system of the near-field, which could affect transport of radionuclides through this region. The calculation of these effects remains to be completed. The effects of the effluent chemistry, as described in the EBS, WFD, and WPD PMRs, are included in UZ transport calculations described in the UZ F&T PMR.

#### **4.2.2 Thermal Effects on Flow (TEF)**

The objective of the TEF KTI (NRC 1999b) is the estimation of temperature, moisture content, and humidity at the waste package surface, and estimation of temperature and thermally driven water flux with respect to the transport of radionuclides from failed waste packages. Redistribution of moisture driven by heat may result in extended periods of dryness in the proposed repository. Redistribution of moisture driven by heat could result in channeling moisture toward the waste package. It is necessary to understand the spatial and temporal effects of the thermal load on liquid-phase and gas-phase fluxes, and resultant effects on temperature and relative humidity of the waste package environment at the proposed repository, to have confidence in predictions of containment and long-term waste isolation.

#### 4.2.2.1 TEF IRSR Subissue 1

This subissue relates to the sufficiency of DOE's thermohydrologic testing program to provide information used to verify conceptual models that DOE will use to evaluate thermally-driven flow in the near field. Subissue 1 asks, "Is the U.S. Department of Energy Thermohydrologic testing program, including performance confirmation testing, sufficient to evaluate the potential for thermal reflux to occur in the near-field?" The acceptance criteria in this section are designed to critically evaluate the sufficiency of the thermohydrologic testing program to provide information needed to verify conceptual models used to predict thermally driven flow in the near-field (NRC 1999b).

Section 3.6 of this PMR describes the thermal tests, including the Single Heater Test (SHT), the DST, and the LBT. These tests were designed specifically to test thermal-hydrological (TH) process models. The LBT and DST were based on the VA design, and therefore tested reflux for that design. While repository design changes have occurred, this testing remains applicable to testing the conceptual and numerical models that describe refluxing. As described in Section 3.6, a specific goal of the LBT was observation of condensate refluxing above a boiling zone. Also, the Updated In Situ Thermal Testing Program Strategy (CRWMS M&O 1997c) states that the LBT was intended to address the need for information on drainage and reflux by fracture flow. The LBT has been completed and the results, including refluxing of condensates, are described in Section 3.6.1.1 of this PMR.

#### 4.2.2.2 TEF IRSR Subissue 2

This subissue relates to the sufficiency of DOE's thermohydrologic modeling approach (process-level models) to predict thermally-driven flow in the near-field. Subissue 2 asks, "*Is the U.S. Department of Energy thermohydrologic modeling approach sufficient to predict the nature and bounds of thermal effects on flow in the near-field?*" The acceptance criteria in this section are designed to critically evaluate the sufficiency of the thermohydrologic modeling approach (process-level models) to predict thermally-driven flow in the near-field (NRC 1999b).

This PMR provides input to coupled process-induced changes in the parameters used in those analyses. Sections 3.2.3, 3.3, 3.4, and 3.5 address the drift-scale coupled-process models and abstractions used to evaluate those parameter changes. TH analysis and modeling in this PMR are described in Sections 3.2.3 and 3.6 and the supporting *Thermal Test AMR* (CRWMS M&O 2000a). This subissue is also addressed in the UZ F&T and EBS PMRs (CRWMS M&O 2000f and 2000g).

#### 4.2.3 Repository Design and Thermal-Mechanical Effects

The primary issue of the Repository Design and Thermal-Mechanical Effects (RDTME) KTI (NRC 1999c) is the adequacy of design, construction, and operation of the geologic repository operations area, including seals for the shafts and boreholes, to meet the preclosure and postclosure performance objectives, taking into consideration the long-term thermal-mechanical (TM) processes.

Consideration of the time-dependent TM coupled response of a jointed rock mass is central to repository design and necessary for performance assessment (PA) at the Yucca Mountain site.

Consequently, that is the focus of both the preclosure and postclosure elements of this KTI. Design for adequate postclosure performance requires an understanding of the TM response of the jointed rock mass over an anticipated compliance period of 10,000 yr. Long-term TM response is anticipated to influence hydrological properties in the vicinity of the emplacement drifts, waste package degradation, radionuclide release within the EBS, performance of seals, and flow into and out of the emplacement drifts.

The RDTME IRSR Subissue 3 has three important components: (i) stability of the underground excavations with regard to safety during the preclosure period, waste retrievability, and potential adverse effects on emplaced wastes; (ii) effect of seismically induced rockfall with respect to waste package performance; and (iii) changes in emplacement-drift geometries and hydrological properties surrounding emplacement drifts due to TM perturbation of the rock mass. All of these components have broad design and performance implications.

Section 3.5 of this PMR describes the results of thermal-hydrological-mechanical (THM) calculations performed to estimate bounds on changes in fracture permeability in rock surrounding emplacement drifts. The results of these calculations are input to UZ F&T PMR (CRWMS M&O 2000f). Drift stability, rock fall and drift geometries are all covered in the EBS PMR (CRWMS M&O 2000g). This PMR considers changes in rock-mass properties, specifically hydrologic properties, as a result of THM.

#### **4.2.4 Total System Performance Assessment and Integration (TSPAI)**

The objective of the TSPA KTI (NRC 2000) is to describe an acceptable methodology for conducting performance assessments of repository performance and using these assessments to demonstrate compliance with the overall performance objective and requirements for multiple barriers. The acceptance criterion applicable to this PMR is described in the following section.

##### **4.2.4.1 TSPA IRSR Subissue 1**

This subissue focuses on the demonstration of multiple barriers and includes: (i) identification of design features of the EBS and natural features of the geologic setting that are considered barriers important to waste isolation; (ii) descriptions of the capability of barriers designed to isolate waste; and (iii) identification of degradation, deterioration, or alteration processes of engineered barriers that would adversely affect the performance of natural barriers. Acceptance criteria addressing multiple barriers will be developed and issued in Revision 3 of the TSPA IRSR.

Subissue 1 also addresses transparency and traceability of the analyses. The acceptance criteria describe staff's expectation of the contents of DOE's TSPA and the supporting documents. They focus on those aspects of the TSPA that will allow for an independent analysis of the results.

This PMR was carefully structured to be complete, clear, and consistent. Reviews of this document included checks for completeness, clarity and consistency. Descriptions are provided of process models and, if appropriate, model abstractions including summaries of data and assumptions used to construct models. The PMR and supporting AMRs provide descriptions of the basis for decisions and assumptions made during the abstraction process. In addition, data

and parameters used in the development of the AMRs are clearly identified and details regarding the pedigree of data are provided.

#### **4.2.4.2 TSPA IRSR Subissue 2**

This subissue focuses on the attributes of an acceptable methodology for identifying, screening, and selecting features, events and processes (FEPs) for inclusion in the total system performance assessment (TSPA). FEPs that could affect future system performance are used to formulate scenarios. This includes construction of scenario classes, assignment of probabilities to scenario classes, and their incorporation into the TSPA. This is a key factor in ensuring completeness of the TSPA. The acceptance criteria described in this subissue are applicable to every PMR that contains an AMR describing FEPs.

As described in Section 2.5, a systematic method was applied to identify and screen FEPs for NFE. FEPs have been identified and grouped into two broad categories of primary and secondary FEPs. The primary FEPs capture the issues associated with the secondary FEPs. The FEPs are further divided into “included” and “excluded” FEPs. Included FEPs are those directly represented in TSPA models and process models that support the TSPA.

INTENTIONALLY LEFT BLANK

## 5. SUMMARY AND CONCLUSIONS

The NF is the part of the UZ that is subjected to the influence of heat from waste such that significant alterations of the hydrological, mechanical, and mineralogical properties may occur. Physically, the NF includes the emplacement drift and the engineered components in the drift that are normally called the EBS. In the process model reports (PMRs), the EBS is treated separately from the NF. In terms of the thermal-hydrological-chemical-mechanical (THCM) processes of a potential repository, the EBS, the NF, and the unsaturated zone (UZ) are intimately coupled. The UZ will provide the initial and boundary conditions for the NF. The NF in turn provides boundary conditions, such as the impacts on seepage of water into the drift, to the EBS. On the other hand, the EBS provides the heat source to the NF. During the heating phase of a repository, the NF will affect the UZ by moving moisture into it. And during the heating phase, convection cells may connect the EBS, the NF and the UZ together. During the cooling phase, the UZ may feed some of the moisture back to the NF. The thermal-hydrological-chemical conditions within the EBS are strongly influenced by the NF. The introduced materials and their corrosion products in the EBS can chemically change the transport properties in the NF. And the transport of any radionuclides that may be released from waste packages, from the EBS to the accessible environment, will pass through the NF. The relationship among the PMRs that deal with those three components of a repository is discussed in the sections below.

### 5.1 THE UZ FLOW AND TRANSPORT INPUTS AND THE NFE MODELS

There are two AMRs in this PMR that dealt with flow and transport modeling. Those AMRs are the *Thermal Test AMR* (CRWMS M&O 2000a) and the *THC Process AMR* (CRWMS M&O 2000b). Both AMRs used the DK model with the active-fracture submodel, as described in the Conceptual and Numerical Models for UZ Flow and Transport AMR (CRWMS M&O 2000h). The DS property set developed in the UZ F&T was used throughout the analyses (CRWMS M&O 2000f, Section 3.6.4.1). The AMRs that feed this PMR and the UZ F&T PMR use the same geologic framework, infiltration rates, and the climate states in modeling the THC processes. There was minor difference in treating the initial water-saturation condition in the rock mass of the DST among the two model analyses in the *Thermal Test AMR*, with the NUFT analysis using the measured 92 percent as the initial water saturation of the tsw34 (CRWMS M&O 2000a, Table 4-3), and the TOUGH2 analysis using a 1-D column model to calculate the initial water saturation in the tsw34 (94 to 95 percent) (CRWMS M&O 2000a, p. 50).

### 5.2 THE REPOSITORY DESIGN INPUTS AND THE NFE PMR

The TTH AMR and the DST part of the DSCP AMR deal with analysis of the thermal field test results, therefore no repository design inputs were considered in the models. The THC Seepage part of the DSCP AMR took repository design inputs in its model. Among the design inputs, two time-periods of the repository design were considered: (1) a 50-yr. preclosure period during which 70 percent of the heat released by the waste packages is removed by ventilation, and during which there is no drip shield and backfill, and (2) a postclosure period following the preclosure period and extending to 100,000 years, during which a drip shield and backfill are installed above the waste packages, and no heat is removed by ventilation. Other design inputs of the TSPA-SR, Rev. 0, Basecase design were incorporated (CRWMS M&O 2000b, p. 27 and Figure 1).

### 5.3 THE EBS INPUTS AND THE NFE PMR

At the current stage of the coupling between this PMR and the EBS PMR, it is mostly forward coupling. The AMRs, especially the Water Distribution and Removal AMR (CRWMS M&O 2000u), the Physical and Chemical Environment AMR (CRWMS M&O 2000v), and the Thermohydrology AMR (CRWMS M&O 2000k), of the EBS PMR modeled the NFE in order to calculate the THC within the EBS. The inputs from the NFE TH model were included in those AMRs. The EBS AMRs include calculated in-drift processes to determine environmental conditions at the engineered barriers. These calculations included components of the EBS, such as the drip shield, backfill, invert, and waste packages; the emplacement drift layouts in a repository; waste package layout within an emplacement drift; and heat output of waste packages. These components were also used to determine the heat source for the NFE models.

A back-coupling from the EBS PMR to the NFE PMR would require considering the effect of the TMHC conditions in the EBS on the THC in the NF. For example, corrosion products from the introduced materials, including the waste packages, in the EBS may change the hydrological and chemical properties of the rock mass below the invert of a drift. Another example is water that seeps from the crown of a drift and flows through components in the EBS may have very different chemical properties than the water in the rock mass above the drift. This water may enter the rock mass below the drift via the drift invert. Those back-couplings from the EBS to the NFE have not been established. It is possible that the effect of back-coupling on the NFE is secondary.

### 5.4 VALIDITY OF COUPLED PROCESS MODELS FOR THE NEAR-FIELD ENVIRONMENT

The NFE evolves in response to highly coupled THCM processes. These processes are often coupled in complex ways that include back-coupling of process interactions. The interactions are largely caused by the introduction of heat to the system by the emplacement of waste. Therefore, the coupling of processes that contribute to the evolution of the NFE, and thus the NFE, are dependent on the design and operational features of the repository. The analyses summarized in this PMR were performed using the EDA-II design. The analyses were performed by considering coupling between processes such as thermal-hydrological, without including full or direct coupling of all of the THCM processes within the same model. The results of the TH, THC, and THM models will be summarized in this section. In addition, although a rigorous evaluation of the fully coupled THCM processes is not available, a discussion included presenting the synthesis of fully coupled THCM that can be derived from the TH, THC, and THM evaluations. Finally, this section discusses the level of confidence that has been established for the models, as well as the conclusions based on those models. This latter discussion will rely on the results of ongoing in situ thermal tests, and their use for model validation and property-set determinations, as reported in this PMR.

To support the following discussion, the interaction-matrix approach is used to conceptually identify the coupling of processes in the NFE. This approach assists in discussing the results of the models and shows how those results were extended to consider THCM implications. The interaction matrix shown on Figure 5-1 identifies the key components of the NFE process models (thermal-hydrologic-chemical-mechanical), along the diagonal, and the interactions of processes

are shown off-diagonal. Along the left-hand side of this matrix are examples of the types of property inputs needed by the models and along the top are examples of the site characteristics needed by the models. This matrix does not attempt to show all components and all couplings, rather it focuses on the key parameters, components, and processes that are discussed in this PMR. Forward-coupling is shown to the right of the diagonal, and back-coupling is shown to the left of the diagonal.

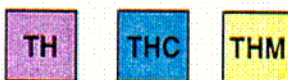
Because TH couplings are the basis for all of the other couplings, the TH model results will be discussed first. The major issues that are addressed by the TH part of the NFE PMR are the temperatures and moisture-distribution changes (saturation and water movement) within the NFE.

As shown on the interaction matrix, Figure 5-2, the first part of the TH model is the determination of the thermal response. As noted in the matrix, the thermal response model determines temperatures based on inputs of design and repository information, along with the thermal properties coupled with the hydrologic model, which determines moisture distributions based on the thermal input. As shown in the interaction matrix, the TH model includes a forward-coupling from the thermal response to the moisture conditions and then is back-coupled to the thermal response. This coupling is actually included in a single TH model and associated codes. However, it is shown explicitly here to distinguish it from the thermal response models that consider only conductive heat transfer.

The TH model temperature predictions for the NFE, at about 600 years after emplacement and for the mean-infiltration case, are summarized in Figures 3-7 through 3-11 (Multi-scale TH model without backfill), and in Figure 3-28 (THC model with backfill). The temperatures at 600 years in Figure 3-28 represent maximum temperatures because assumed climate change results in infiltration increases after 600 yr. Waste heat decreases with time. The maximum temperature for the crown of the drift occurs at about 100 yr.

TH models predict above-boiling temperatures extending approximately 10 meters into the rock of the NFE. Temperatures are elevated to approximately 90°C, extending about 30 meters above the drift. The temperature distributions are not symmetrical around the drift. The boiling temperature only extends above the drift about 5 meters, but extends below the drift nearly 13 meters. This is illustrative of the interactive coupling between the effects of waste placement in the drift, and of the effects of hydrologic response on the temperatures. (Two detailed models were used in the NFE to determine the TH response. These were the TH models included in the multi-scale abstraction and the TH parts of the THC models. The THC model did not consider the details of convection, radiation etc. within the drifts. The abstraction models were based on the multi-scale models that included these details. The multi-scale models are described within the EBS PMR. The TH results of the two model approaches were compared in Section 3.2.3.4 and found to be fairly consistent).

	Repository config., operation sequence, waste heat output	Ambient flow conditions (flow)	Ambient RH gas/barometric pressures	Ambient water chemistry, mineralogy	Fracture characteristics and mineralogy	Fracture characteristics and mineralogy	Fracture geometries, rock units, in situ stress
Heat transfer properties (conduction heat of vaporization, etc.)	<b>Thermal response</b>	Temperatures with time	Thermodynamics of vapor				
Hydrologic properties (porosity, permeability, etc.)	• Latent heat • Heat pipes	<b>Hydrologic response</b>	• Vaporization • Mobilization • Saturation	Saturation condensate/vapor			Water contribution to crack growth
Gas partial pressures, thermodynamic properties			<b>Relative humidity</b>		Vapor/rock interactions	Vapor/rock/solid interactions	
Thermodynamic properties data base (equilibrium, & kinetics)			Vapor partial pressure	<b>Water chemistry responses</b>	Evolved NF chemistry	• Reaction thermodyn. • Solubility • Precipitation • Carbonation	
Thermodynamic properties data base (equilibrium, & kinetics)	Altered flow paths	Changed hydrologic properties (altered flow paths)	Changed hydrologic properties		<b>Dissolution precipitation</b>	• Dehydration • Rock-water interactions (kinetics)	• Healing of fractures • Changes water avail. for cracking
Thermodynamic properties data base (equilibrium, & kinetics)	Thermal conductivity changes	Water release/consumpt. in reactions	Partial pressure (salts)	• Altered minerals • Rock-water interactions	• Fracture/pore plugging • Fracture healing • Colloid transport	<b>Mineralogy changes and salt deposition</b>	Volume changes (phase transform and mineral changes)
Rock & fracture properties (e.g. strength, stiffness)		Permeability changes			• Closing/opening fractures • Microcracks • Coalescence flow path	• Stress impacts • Mineral phase • Microcracks (new surfaces)	<b>Mechanical responses</b>



Source: Modified from Wilder 1997, Figure 1-5

Figure 5-1. Interaction Matrix Showing Coupling of NFE Processes

C-79

	Repository config., operation sequence, waste heat output	Ambient flow conditions (flow)	Ambient RH gas/barometric pressures	Ambient water chemistry, mineralogy	Fracture characteristics and mineralogy	Fracture characteristics and mineralogy	Fracture geometries, rock units, in situ stress
Heat transfer properties (conduction heat of vaporization, etc.)	<b>Thermal response</b>	Temperatures with time	Thermodynamics of vapor				
Hydrologic properties (porosity, permeability, etc.)	• Latent heat • Heat pipes	<b>Hydrologic response</b>	• Vaporization • Mobilization • Saturation	Saturation condensate/vapor			Water contribution to crack growth
Gas partial pressures, thermodynamic properties			<b>Relative humidity</b>		Vapor/rock interactions	Vapor/rock/solid interactions	
Thermodynamic properties data base (equilibrium, & kinetics)			Vapor partial pressure	<b>Water chemistry responses</b>	Evolved NF chemistry	• Reaction thermodyn. • Solubility • Precipitation • Carbonation	
Thermodynamic properties data base (equilibrium, & kinetics)	Altered flow paths	Changed hydrologic properties (altered flow paths)	Changed hydrologic properties		<b>Dissolution precipitation</b>	• Dehydration • Rock-water interactions (kinetics)	• Healing of fractures • Changes water avail. for cracking
Thermodynamic properties data base (equilibrium, & kinetics)	Thermal conductivity changes	Water release/consumpt. in reactions	Partial pressure (salts)	• Altered minerals • Rock-water interactions	• Fracture/pore plugging • Fracture healing • Colloid transport	<b>Mineralogy changes and salt deposition</b>	Volume changes (phase transform and mineral changes)
Rock & fracture properties (e.g. strength, stiffness)		Permeability changes			• Closing/opening fractures • Microcracks • Coalescence flow path	• Stress impacts • Mineral phase • Microcracks (new surfaces)	<b>Mechanical responses</b>

TH

THC

THM

Source: Modified from Wilder 1997, Figure 4-1

Figure 5-2. Interaction Matrix Showing TH Coupling

C-50

The TH model is also used to determine the hydrologic response to the thermal regime. The elevated temperatures cause redistribution of moisture such that the saturation within both fractures and matrix are changed within the NFE. The NFE model predictions for 600 years, as shown on Figure 3-28, define a zone where saturation is decreased from the original ambient saturation. A zone of 10 percent or less saturation extends for approximately 20 m below the drift and 18 m horizontally from the drift. This zone extends less than 10 m above the drift.

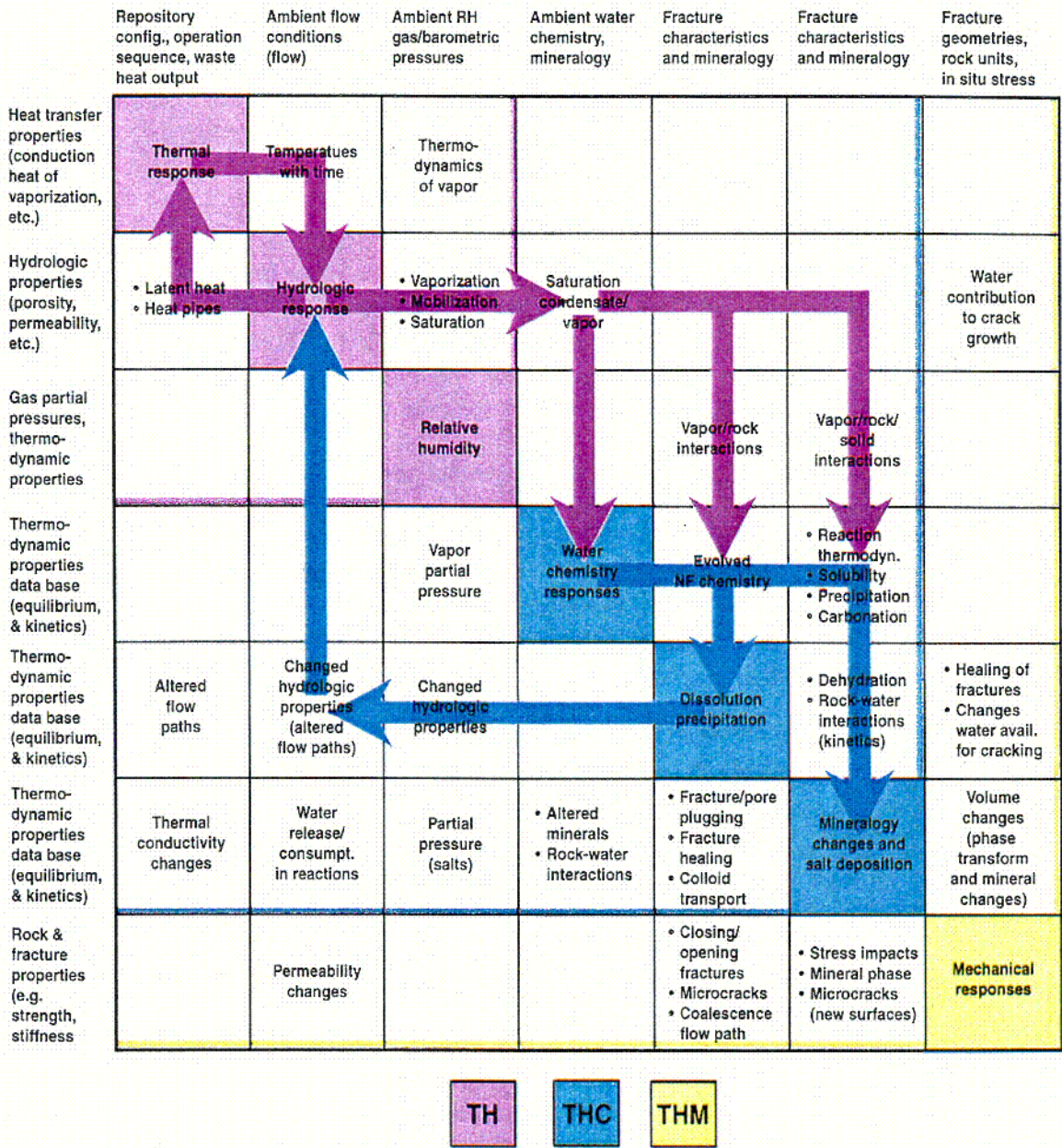
On the TH interaction matrix (Figure 5-2), the back-coupling indicates that the effects of latent heat and heat-pipes, and of saturation changes (not shown on the figure) are fed back into the thermal model. One of the TH characteristics of the coupling is the difference between thermal conductivity of saturated and dry rock; this coupling is reflected in the forward- and back-coupling shown on the interaction matrix.

The third diagonal entry (RH) on the TH interaction matrix (Figure 5-2) is not covered within the NF PMR, but is part of the TH model shared by the NFE and EBS PMRs. It will not be discussed here.

The next coupled model is the THC model. The major issues that are addressed in the THC model for the NFE are changes in hydrologic properties due to dissolution or precipitation of minerals, or due to rock-water interaction, and deposition of salts or other minerals that might impact the chemistry of percolating water.

As noted on the THC interaction matrix (see Figure 5-3), the water chemistry must first be determined. To determine the evolving water chemistry, the ambient chemistry must first be determined. The chemistry of percolating (ambient) water is determined and reported within the UZ F&T PMR (CRWMS M&O 2000f). This ambient chemistry determination is fed from that PMR to the NFE and EBS PMRs and associated AMRs water chemistry is determined by the THC model, as reported in the Drift Scale Coupled Process Model AMR (CRWMS M&O 2000b). As noted in Section 3.3.2.4, the THC model uses as an input the ambient water chemistry determined in the UZ F&T PMR studies. The model also uses geochemical properties databases of thermodynamic and kinetic or rate properties for chemical species. From these inputs, coupled with the temperature and saturation conditions determined in the TH submodels, the THC model calculates the evolution of water chemistry with time.

The chemistry, as calculated, is then abstracted along with TH and other coupled processes as reported within the Abstraction of DSCP AMR (CRWMS M&O 2000b). The results of these analyses are reported in Table 3-11 for the four time periods considered (0-50 years, 50-1,000 years, 1,000-2,000 years, and 2,000-10,000 years). As can be observed, the constituents in the water at the drift-wall decrease over the period from 50 to 1,000 yr. This may be partially an artifact of drying of this region that removes the water. Most of the chemical constituents return to values that are similar to those prior to closure of the repository at 50 yr. This implies that there are not long-term perturbations in water chemistry, with the possible exception of the bicarbonate ion ( $\text{HCO}_3^-$ ) and Silica ( $\text{SiO}_2$ ). Figure 3-29 shows that there is a significant drop in  $\text{CO}_2$  concentrations in fractures during drying. The THC seepage simulations indicate that there may be an increase in  $\text{CO}_2$  gas and carbonate concentrations around the drift during rewetting. The pH of the water drops during the period from closure until around 10,000 years, when the pH begins to slowly return to higher values.



Source: Modified from Wilder 1997, Figure 4-9

Figure 5-3. Interaction Matrix Showing THC Coupling

The issue of changes to hydrologic properties (due to the next diagonal element, dissolution and precipitation, on the interaction matrix [Figure 5-3]) was determined in the THC model based on the interaction of constituents in the water with the rock and in response to temperatures. Specifically, the models determined dissolution and precipitation of minerals that would change the porosity and permeability of the fracture system. The temperature-dependent solubilities of calcite and silica, in particular, are of interest.

The model results indicate that fracture porosity changes primarily due to calcite precipitation and that the change is relatively small (less than 1 percent of the initial porosity). Calcite deposition is expected to occur over wider zones than silica deposition. Therefore, a decrease of porosity due to calcite is not likely to occur in a very narrow zone. These analyses, and a cubic law to relate aperture to permeability, suggest that reduction in permeability due to mineral deposition within fractures would be negligible, less than the range of permeability within YM.

The back-coupling for changes in hydrologic properties are shown on the interactive matrix (Figure 5-3) in the changed hydrologic properties that feed to the hydrologic response model, which forward-feeds volume of water to the dissolution and precipitation model and back-feeds to the thermal response model. As can be seen, the coupling becomes much more involved. The THC model accounts for this coupling by off-line feedback between mineral dissolution and precipitation, and porosity, permeability and capillary pressure changes. It was noted that silica precipitation is subordinate to calcite.

The final aspect of concern for the NFE is that of the geomechanical responses and how these couple to other processes within the NFE. The THM coupled model essentially uses thermal response models to determine the temperatures with time. Those temperatures are then coupled to rock deformation and resulting stress responses. On the THM interaction matrix (Figure 5-4) this is the box at the upper right-hand corner. Although other geomechanical coupling (i.e., water impacts on crack growth) exist, they were considered of secondary importance to the deformations. Based on the calculated deformations, impacts on permeability were assessed. After 55 years, representing the highest heating gradient period, it was found that permeability increases of about 40 percent might be experienced above the drifts, due to normal deformations that would be expected to be reversible as the rock cooled, and increases from 3 to 6.5 times pre-heat values due to shear displacements. There are no established constitutive relationships to combine the effects of decreased permeability from both types of deformations. The increases will be at least equal to those related to the shear deformations. After 1,000 years, the permeability increases, due to normal deformations, to approximately twice the pre-emplacment value in the regions above the drifts, and to about a 40 percent increase in the pillar areas. However, there is projected to be about an order of magnitude increase in permeability above and below the drift due to shear displacements at 1,000 yr.

The back-coupling of these permeability changes into the NFE models should be as shown on the interaction matrix. However, the models are not fully coupled at this time. Back-coupling could be assessed by inputting the results into the property sets used in the hydrologic model and then repeating the calculations. This has not been done to date.

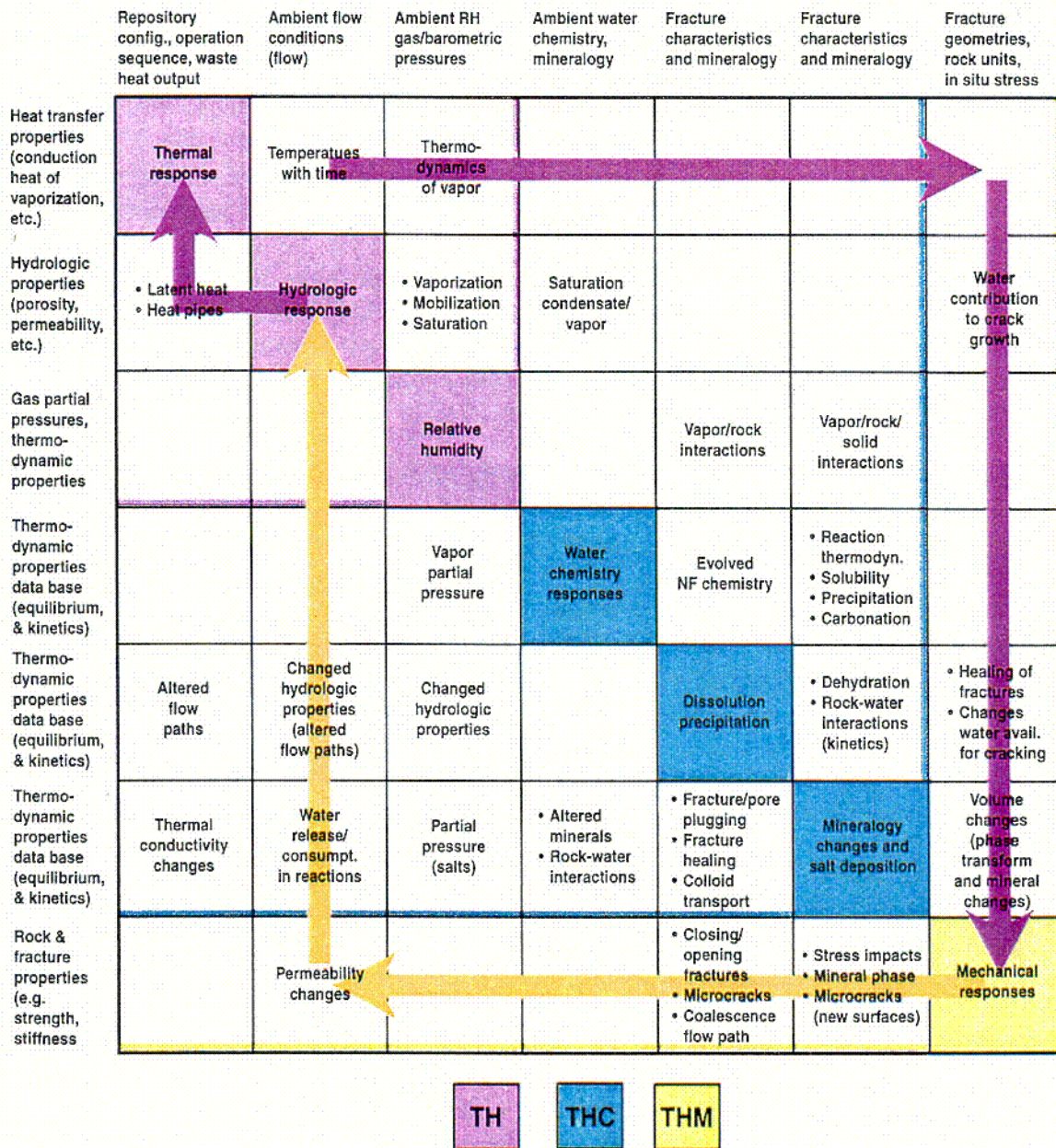


Figure 5-4. Interaction Matrix Showing THM Coupling

*C. 82*

The THCM responses can be assessed to some degree by comparison to the results of the THC model. The THC model includes the backfeeds from the C to the TH models. The results of the THC model indicate a small decrease in permeability (about 3 percent) above the drifts. This is of similar magnitude, but opposite direction, as the projected increases (about 40 percent) from the normal-deformation geomechanical responses. Thus, for regions above the drift, it can be concluded that the coupled effects, if including the normal-deformation components, would cancel-out. However, it is not known whether the much larger increased permeability from the shear deformations would then cause sufficient differences in the TH responses that the THC responses would be impacted. As shown in Figures 3-40 and 3-41, the regions of maximum potential for THM permeability enhancement are zones extending about 10 m above and below the drifts, with less of a potential increase along a horizontal plane extending through the drift centerline. The very minimal changes from THC (see Figure 3-33) indicate less than 1 percent decrease in permeability in a horizontal region about 15 to 18 m above the drift.

While these changes may suggest the potential for focusing flow towards the drifts, the heterogeneity of permeability is greater than the range of change projected and, furthermore, the fracture permeability is sufficient to support drainage through the pillar areas. Therefore, although there is still some uncertainty, it is not suggested by these analyses that restrictions to downward percolation would cause diversion from the pillar regions of the repository. Percolation from the regions above the drifts would continue regardless of any changes in permeability from the THM and THC effects. Extension of both simulations and testing to the lower tsw35 hydrogeologic unit (Tptpl) in which most emplacement drifts will be located is ongoing.

## 5.5 MODEL CONFIDENCE

The TH model capabilities to accurately predict temperatures have consistently been demonstrated, at least for the overall temperature fields that develop. This demonstration has included both laboratory and field studies. When temperatures are below boiling, the conduction only models are appropriate and the physics is well understood. Confidence in temperature predictions beyond the zone of boiling is quite high, with the principal uncertainty related to the property determinations of thermal conductivity and the natural heterogeneity of the system. When hydrological processes are considered (either boiling or convective movement of moisture that impacts heat) confidence is reduced. The major issues are not the physical understanding of the hydrological parameters; the issues are the property uncertainty (thermal conductivities of wet and dry rock are different), the heterogeneity of the ambient system, and the potential heterogeneity of thermal responses. For instance, the amount of drying that occurs is a function of the porosity and permeability of the rock matrix, and of the fracture spacing and connectivity, all of which can vary spatially. Since no model will be able to fully or directly account for this heterogeneity, a statistical approach will be needed. To date, the TH models have been quite accurate in predictions of TH responses in the thermal tests, with local spatial and temporal exceptions. Therefore, confidence in the TH model predictions of temperature is considered quite high.

The TH model predictions of hydrologic responses (second diagonal box on interaction matrix, Figure 5-4) is also relatively high. In addition to the heterogeneity issues, there are some uncertainties in the range of hydrologic properties. For instance, the imbibition curves show

hysteresis for wetting versus drying cycles. As noted in Section 2.4, there are different views as to the applicability of the van Genuchten model and the AFM, which could be viewed as conceptual uncertainty. However, in spite of these uncertainties, the TH models have generally accurately predicted both the magnitude and trends in hydrologic responses of field tests, such as the SHT, LBT, and DST. Therefore, while confidence is not as high for the hydrologic response parts of the TH models as for the temperature response parts, the confidence is nonetheless high, particularly in the tsw34 hydrogeologic unit (Ttpmn) in which the DST is being conducted.

As the THC interaction matrix (Figure 5-3) illustrates, the THC models are coupled to the TH models. As a result, the uncertainties for the THC models include not only the uncertainties of the chemical parts, but the uncertainties already discussed for the TH models. There are additional uncertainties related to the input data, as well as the geochemical models. As noted in Section 2.4, there are limited thermodynamic data available on chemical species at high concentrations and elevated temperatures. This introduces uncertainties for the model analyses that apply to regions close to the boiling or evaporation fronts. In the areas where the TH models predict saturations that exceed 10-20 percent, the ionic concentration due to water removal should not be a problem. The natural heterogeneity of the mineralogy may cause local uncertainties. Likewise, the effects of engineered heterogeneities, especially repository edge effects, may impact the thermal regime, which would couple to create some uncertainties.

The THC responses in field studies have not been as widely studied as the TH responses. However, there has been agreement between model predictions and measurements in the DST. For instance, in the DST, the simulations of CO<sub>2</sub> concentrations have the same trend as the measured concentrations. This indicates that the process model is reflecting the physical processes appropriately. The magnitudes of the simulated values did not match as well, which probably reflects not only the difficulties in accurately accounting for heterogeneity but also the challenges in obtaining accurate measurements. The water-chemistry simulations indicated lowered pH in the region of the highest gas-phase CO<sub>2</sub> concentrations (Section 3.3.3.3). This shift in pH is similar, both temporally and spatially, to that measured from water collected from boreholes in the DST. Further, chloride concentrations from water collected from those boreholes was 5 to 10 times more dilute than the pore water, which was also predicted by the models. In addition, trends of other species, such as Ca and Si, were similar in model results and measurements. Samples are not available for direct comparison of mineralogical changes predicted to those observed. However, trends in water chemistry provide evidence of the mineralogy trends. The chemistry determined from water samples from boreholes in the DST show decreasing Ca with temperatures, and the pH and silica concentrations are suggestive of calcite precipitation, as was simulated.

Thus, there is confidence in the THC model ability to predict the responses, although there is less confidence in the magnitudes predicted. The confidence in the THC results is somewhat less than that for the TH-only models.

The THM models are less mature than the TH or THC models. There are limited data available to build confidence in these models, since most of the data are from laboratory studies. Therefore, the projections from the THM models must be considered as giving trends and identifying areas of potential impacts, but the magnitudes of the projections cannot be given very high confidence. The primary effect of the uncertainty in THM model response is a potential

variability in fracture permeability, with an increase of up to an order of magnitude in an already large value. The consequence of such a permeability increase on seepage is expected to be small due to the high initial permeability. Therefore, because the primary THM coupling effect is through permeability changes, the effect of THM uncertainty on overall performance is not expected to be significant.

Uncertainties and limitations have been described in each of the AMRs that support the NFE PMR. The specific uncertainties are listed in Table 3-1. These uncertainties are related to thermal test measurements, property inputs, conceptual flow models, and boundary conditions that vary both in time and space. A discussion of the most important uncertainties, and how they affect TSPA, are discussed with potential advice to TSPA as to how these can be accommodated in the models that provide the abstractions.

There are measurement uncertainties associated with measurements of temperature and liquid saturation acquired from the LBT, SHT, and DST. The quantitative analysis of measured uncertainty is a function of the instrumentation and how it is used to measure a specific quantity. Uncertainty in measurements involves more than just the instrument, and therefore assessment of uncertainty must be based on the experience of those who design experiments and specify the instrumentation with which to take measurements.

The measured results (e.g., temperature at some radial distance from the heat source) are compared to TH model simulations, which try to characterize the processes initiated by heat. Uncertainties also exist in the model simulations. The important ones include property specifications, boundary conditions, and the conceptual flow models used to approximate the processes caused by thermal perturbation. These directly impact TSPA specifically, since it must provide an abstraction, to a total system model, of data obtained from a repository heating model that provides information over large space dimensions and long time intervals. The thermal tests provide information over a variety of different spatial scales for various lengths of time (both much less than that of the potential repository itself). However, the measured thermal tests provide TSPA the ability to test (against a controlled thermal perturbation) the thermal and inverse-modeled hydrologic property sets and the conceptual flow models used in the process models that are the basis of the abstractions.

The advice provided to TSPA resulting from the thermal tests is an analysis of different hydrologic property sets and conceptual flow models. A number of property sets and flow models are compared to measured data, because of the inherent uncertainty contained in each. Ranges of results are obtained from the TH simulations and compared to experimentally measured results of temperature and liquid saturation. An assessment is made as to the best fluid processes initiated by a controlled thermal perturbation (e.g., LBT, SHT, and DST), and hence should be applied to the TSPA models used to approximate repository heating. The result is the following: TSPA can build confidence in the property sets and conceptual flow models used in the TH models for abstraction, since they have been tested and verified against a quantifiable and understood thermal transient.

The process models discussed in the NFE PMR contain many of the uncertainties previously described (e.g., conceptual flow model, hydrologic properties, etc.). These uncertainties are characterized and understood by comparison to measured TH results from the LBT, SHT, and

DST. Many of the process models also contain potential limitations based on the assumptions applied to the inherent processes they characterize. The THC DS model contains uncertainties associated with:

- thermodynamic and kinetic parameters used to describe precipitation and dissolution
- reaction processes for dissolved solutes that occur at elevated temperatures
- fracture and matrix mineralogy
- initial water and gas chemistry
- reactive mineral surface area
- correlation used to modify permeability change as a function of porosity change
- water and gas composition changed by infiltration flux

These model limitations and uncertainties are evaluated with THC model comparisons to the measure data from (pH and aqueous carbonate) the DST. It was shown that the less complex geochemical system used as input in the THC model is supported by the measured results of the DST. Since this is the case, confidence is built in the model such that many of the uncertainties listed above produce water and gas compositions obtained by a model that are reasonably supported by an experiment. Therefore, the advice to TSPA is that the THC process-level model contains inherent uncertainties and limitations in the processes that it described, yet it reasonably approximates the measured results of an experiment that establishes a controlled heat input into a geologic formation. The same geologic formation that will house part of the repository wastes. However, TSPA must not only apply the THC model to present-day infiltration rate conditions at the location of the thermal tests, but also apply its results to different repository locations, infiltration rates, and future climate states. These, at this time, have no experimental backing associated with model confidence building. Since the DST model has been benchmarked with a degree of success against an evolving and understood heating process (the DST), its results are extended to other repository locations, infiltration fluxes, and future climate states. These results are uncertain due to the uncertainties mentioned above and how they may be different for other locations or geologic sub-units; however, the uncertainty in water and gas composition is quantified for varying infiltration flux and future climate states, and found to be usually less than an order-of-magnitude different than the expected-value case. Therefore, it is reasonable to apply the expected-value water and gas composition abstraction over the entire infiltration flux scenario (low, mean, and high).

One final assessment is required to advise TSPA as to the potential changes in fracture flow properties as a result of the reactive-transport processes that, at elevated temperatures and in the presence of water, initiate precipitation or dissolution of minerals in a geologic system. TSPA abstracts from a variety of process-level models. Some contain the coupled process of reactive transport with thermal-hydrology, others do not. Since TSPA abstracts from both model types, an assessment is required to determine whether the simplified models (TH-only) may inherently be neglecting processes that should be included. The evaluation considers both state and flow variables that are typically used to describe the performance of a geologic repository. Based on these comparisons and the calculation that reactive transport does not appreciably change the TH results that would be obtained from a TH-only model, it is recommended that TSPA select the process model that fits their needs. If the in-drift or near-field host rock thermodynamic and fracture-flow environment is to be determined without specification of a geochemical boundary

condition, it is recommended that a TH-only model be applied. It is computationally less rigorous and results in approximately the same TH response as obtained from a model that includes more processes in its formulation. If geochemical boundary conditions are needed, a fully coupled model must be applied to the abstraction.

## 5.6 CONCLUSION

Although there are uncertainties and issues of heterogeneities in properties, the overall binary coupling between thermal, hydrological, chemical, and mechanical processes in the near-field environment is understood, as discussed above. Ternary coupling among these processes has been investigated experimentally and computationally with good agreement. Simultaneous coupling of all four types of processes has not yet been addressed, but multiple combinations of ternary couplings have been investigated. Based on these considerations, THCM processes are not inconsistent with the treatment of repository performance in TSPA. Ranges of parameters are used in TSPA to account for uncertainty and investigate the sensitivity to specific processes and events. Ongoing work will further reduce these uncertainties and increase confidence in coupled-process models that must predict responses over geologic time scales.

Table 3-1 identifies uncertainties associated with TH, THC and model abstractions. The TH model uncertainties can best be addressed by use of conservative parameter values to bound the natural heterogeneity. The model uncertainty is within acceptable bounds, based on comparisons with field tests (Section 3.6). It appears that use of multiple models, perhaps with more representative grids to represent drifts, will address the model uncertainties. The uncertainties regarding property sets for Tptpl cannot be resolved until property data and testing within the Tptpl is performed. Lacking that information, use of properties from the Ttpmn for the entire repository footprint is the most defensible approach, since the property sets have been tested against field results.

In summary, the treatment of coupled processes in TSPA is considered adequate for its intended use for site recommendation.

## 6. REFERENCES

### 6.1 DOCUMENTS CITED

- Ahola, M.P.; Chowdhury, A.H.; Hsiung, S.M.; and Philip, J. 1994a. "Comparison of Coupled Thermal-Mechanical-Hydrological Analyses of a Fractured Rock Mass." *High Level Radioactive Waste Management, Proceedings of the Fifth Annual International Conference, Las Vegas, Nevada, May 22-26, 1994*. 4, 2492-2499. La Grange Park, Illinois: American Nuclear Society. TIC: 210984.
- Ahola, M.P.; Ofoegbu, G.I.; Chowdhury, A.H.; and Hsiung, S-M. 1994b. *Thermo-Hydro-Mechanical Coupled Modeling: Big-Ben Experiment, TC3 DECOVALEX - Phase III*. CNWRA 94-021. San Antonio, Texas: Center for Nuclear Waste Regulatory Analyses. TIC: 215628.
- Albin, A.L.; Singleton, W.L.; Moyer, T.C.; Lee, A.C.; Lung, R.C.; Eatman, G.L.W.; and Barr, D.L. 1997. *Geology of the Main Drift - Station 28+00 to 55+00, Exploratory Studies Facility, Yucca Mountain Project, Yucca Mountain, Nevada*. Milestone SPG42AM3. Denver, Colorado: Bureau of Reclamation and U.S. Geological Survey. ACC: MOL.19970625.0096.
- Baca, R.G. and Magnuson, S.O. 1990. *Independent Verification and Benchmark Testing of the UNSAT-H Computer Code, Version 2.0*. EGG-BEG-8811. Idaho Falls, Idaho: EG&G Idaho. TIC: 247840.
- Bandis, S.C.; Lumsden, A.C.; and Barton, N.R. 1983. "Fundamentals of Rock Joint Deformation." *International Journal of Rock Mechanics and Mining Sciences & Geomechanics Abstracts*, 20, (6), 249-268. Oxford, United Kingdom: Pergamon Press. TIC: 224201.
- Barton, C.A.; Hickman, S.; Morin, R.; Zoback, M.D.; Finkbeiner, T.; Sass, J.; and Benoit, D. 1997. "Fracture Permeability and Its Relationship to In Situ Stress in the Dixie Valley, Nevada, Geothermal Reservoir." *Proceedings from Twenty-Second Workshop on Geothermal Reservoir Engineering, January 27-29, 1997*. Pages 210-215. Stanford, California: Stanford University. TIC: 237673.
- Barton, N.R.; Bandis, S.; and Bakhtar, K. 1985. "Strength, Deformation, and Conductivity Coupling of Rock Joints." *International Journal of Rock Mechanics and Mining Sciences and Geomechanics Abstracts*, 22, (3), 121-140. New York, New York: Pergamon Press. TIC: 217135.
- Bear, J. 1988. *Dynamics of Fluids in Porous Media*. New York, New York: Dover Publications. TIC: 217568.
- Berge, P.A.; Wang, H.F.; and Blair, S.C. 1998. *Estimated Bounds on Rock Permeability Changes from THM Processes*. UCRL-ID-131492. Livermore, California: Lawrence Livermore National Laboratory. ACC: MOL.19981109.0302.

Bish, D.L. 1995. "Thermal Behavior of Natural Zeolites." *Natural Zeolites '93: Occurrence, Properties, Use, Proceedings of the 4th International Conference on the Occurrence, Properties, and Utilization of Natural Zeolites, June 20-28, 1993, Boise, Idaho*. Ming, D.W. and Mumpton, F.A., eds. Pages 259-269. Brockport, New York: International Committee on Natural Zeolites. TIC: 243086.

Bish, D.L. and Aronson, J.L. 1993. "Paleogeothermal and Paleohydrologic Conditions in Silicic Tuff from Yucca Mountain, Nevada." *Clays and Clay Minerals*, 41, (2), 148-161. Long Island City, New York: Pergamon Press. TIC: 224613.

Bish, D.L.; Carey, J.W.; Levy, S.S.; and Chipera, S.J. 1996. *Mineralogy-Petrology Contribution to the Near-Field Environment Report*. Milestone Report LA3668. Los Alamos, New Mexico: Los Alamos National Laboratory. ACC: MOL.19971111.0588.

Blair, S.C. and Berge, P.A. 1995. *Uniaxial Compression Behavior of Small Blocks of Welded Tuff*. UCRL-JC-122733. Livermore, California: Lawrence Livermore National Laboratory. ACC: MOL.19960501.0273.

Blair, S.C. and Berge, P.A. 1997. *Geomechanical Properties of Topopah Spring Tuff at the 0.5-m Scale: Preliminary Results of Compression Tests at Elevated Temperature*. UCRL-ID-125089. Livermore, California: Lawrence Livermore National Laboratory. TIC: 236600.

Blair, S.C. and Wood, S.A. 1998. "Geomechanical Observations During the Large Block Test." *High-Level Radioactive Waste Management, Proceedings of the Eighth International Conference Las Vegas, Nevada, May 11-14, 1998*. Pages 769-771. La Grange Park, Illinois: American Nuclear Society. TIC: 237082.

Blair, S.C.; Berge, P.A.; and Wang, H.F. 1997. *Bounding Models for Estimating Changes in Fracture Permeability Due to Thermo-Mechanical Stresses in Host Rock Surrounding the Repository, 1: Permeability Changes Estimated for the Heated Drift Test*. Milestone SPLF2M4. Livermore, California: Lawrence Livermore National Laboratory. ACC: MOL.19980107.0411.

Blair, S.C.; Kelly, J.M.; Pine, O.; Pletcher, R.; and Berge, P.A. 1996. *Effect of Radiation on the Mechanical Properties of Topopah Spring Tuff*. UCRL-ID-122899. Livermore, California: Lawrence Livermore National Laboratory. ACC: MOL.19961021.0132.

Bodvarsson, G.S.; Bandurraga, T.M.; and Wu, Y.S., eds. 1997. *The Site-Scale Unsaturated Zone Model of Yucca Mountain, Nevada, for the Viability Assessment*. LBNL-40376. Berkeley, California: Lawrence Berkeley National Laboratory. ACC: MOL.19971014.0232.

Borgesson, L. and Hernelind, J. 1995. *DECOVALEX I - Test Case 3: Calculation of the Big Ben Experiment - Coupled Modelling of the Thermal, Mechanical and Hydraulic Behaviour of Water-Unsaturated Buffer Material in a Simulated Deposition Hole*. SKB Technical Report 95-29. Stockholm, Sweden: Swedish Nuclear Fuel and Waste Management Company. TIC: 224376.

Brookins, D.G. 1984. *Geochemical Aspects of Radioactive Waste Disposal*. New York, New York: Springer-Verlag. TIC: 206675.

Brookins, D.G. 1986. "Natural Analogues for Radwaste Disposal: Elemental Migration in Igneous Contact Zones." *Chemical Geology*, 55, 337-344. Amsterdam, The Netherlands: Elsevier Science Publishers B.V. TIC: 246170.

Budnitz, B.; Ewing, R.C.; Moeller, D.W.; Payer, J.; Whipple, C.; and Witherspoon, P.A. 1999. *Peer Review of the Total System Performance Assessment-Viability Assessment Final Report*. Las Vegas, Nevada: Total System Performance Assessment Peer Review Panel. ACC: MOL.19990317.0328.

Buscheck, T.A. and Nitao, J.J. 1993. "Repository-Heat-Driven Hydrothermal Flow at Yucca Mountain, Part I: Modeling and Analysis." *Nuclear Technology*, 104, (3), 418-448. La Grange Park, Illinois: American Nuclear Society. TIC: 224039.

Buscheck, T.A. and Nitao, J.J. 1994. *The Impact of Buoyant, Gas-Phase Flow and Heterogeneity on Thermal-Hydrological Behavior at Yucca Mountain*. UCRL-JC-115351. Livermore, California: Lawrence Livermore National Laboratory. ACC: NNA.19940524.0012.

Buscheck, T.A.; Nitao, J.J.; and Chesnut, D.A. 1992. "The Impact of Episodic Nonequilibrium Fracture-Matrix Flow on Geological Repository Performance." *Proceedings of the Topical Meeting on Nuclear Waste Packaging, FOCUS '91, September 29-October 2, 1991, Las Vegas, Nevada*. Pages 312-323. La Grange Park, Illinois: American Nuclear Society. TIC: 231173.

Buscheck et al. 1997a. Not Used.

Buscheck et al. 1997b. Not Used.

Buscheck, T.A.; Shaffer, R.J.; Lee, K.H.; and Nitao, J.J. 1997c. *Analysis of Thermal-Hydrological Behavior During the Heating Phase of the Single-Heater Test at Yucca Mountain*. Supplemental Submission to Deliverable SP9266M4. Livermore, California: Lawrence Livermore National Laboratory. ACC: MOL.19980109.0241.

Buscheck, T.A.; Shaffer, R.J.; and Nitao, J.J. 1997d. *Pretest Thermal-Hydrological Analysis of the Drift-Scale Thermal Test at Yucca Mountain*. Livermore, California: Lawrence Livermore National Laboratory. ACC: MOL.19980507.0359.

Buscheck, T.A.; Nitao, J.J.; and Ramspott, L.D. 1997e. "Near-Field Thermal-Hydrological Behavior for Alternative Repository Designs at Yucca Mountain." *Scientific Basis for Nuclear Waste Management XX, Symposium held December 2-6, 1996, Boston, Massachusetts*. Gray, W.J. and Triay, I.R., eds. 465, 1029-1036. Pittsburgh, Pennsylvania: Materials Research Society. TIC: 238884.

Carey, J.W. and Bish, D.L. 1996. "Equilibrium in the Clinoptilolite-H<sub>2</sub>O System." *American Mineralogist*, 81, 952-962. Washington, D.C.: Mineralogical Society of America. TIC: 233145.

Carey, J.W.; Chipera, S.J.; Vaniman, D.T.; and Bish, D.L. 1997. *Three-Dimensional Mineralogic Model of Yucca Mountain, Nevada, Rev. 1.1*. Deliverable SP32B5M4. Draft R0. [Los Alamos, New Mexico]: Los Alamos National Laboratory. ACC: MOL.19980520.0170.

Chan, T.; Khair, K.; Jing, L.; Ahola, M.; Noorishad, J.; and Vuillod, E. 1995. "International Comparison of Coupled Thermo-Hydro-Mechanical Models of a Multiple-Fracture Bench Mark Problem: DECOVALEX Phase I, Bench Mark Test 2." *International Journal of Rock Mechanics and Mining Sciences & Geomechanics Abstracts*, 32, (5), 435-452. Oxford, United Kingdom: Elsevier Science. TIC: 235730.

Cohon, J.L. 1999. Comments on the Process for Selecting the Repository Design "Letter from J.L. Cohon (U.S. Nuclear Waste Technical Review Board) to L.H. Barrett (DOE/OCRWM), July 9, 1999." ACC: MOL.20000412.0786.

Cohon, J.L. 2000. Comments from the Nuclear Waste Technical Review Board January 2000 Meeting "Letter from J.L. Cohon (U.S. Nuclear Waste Technical Review Board) to I. Itkin (DOE/OCRWM), March 20, 2000." ACC: MOL.20000412.0787.

Crowe, B.; Self, S.; Vaniman, D.; Amos, R.; and Perry, F. 1983. "Aspects of Potential Magmatic Disruption of a High-Level Radioactive Waste Repository in Southern Nevada." *Journal of Geology*, 91, (3), 259-276. Chicago, Illinois: University of Chicago Press. TIC: 216959.

CRWMS M&O 1996. *Test Design, Plans and Layout Report for the ESF Thermal Test*. BAB000000-01717-4600-00025 REV 01. Las Vegas, Nevada: CRWMS M&O. ACC: MOL.19970114.0166.

CRWMS M&O 1997a. *Single Heater Test Status Report*. BAB000000-01717-5700-00002 REV 01. Las Vegas, Nevada: CRWMS M&O. ACC: MOL.19980416.0696.

CRWMS M&O 1997b. *Drift Scale Test Design and Forecast Results*. BAB000000-01717-4600-00007 REV 01. Las Vegas, Nevada: CRWMS M&O. ACC: MOL.19980710.0155.

CRWMS M&O 1997c. *Updated In Situ Thermal Testing Program Strategy*. B00000000-01717-5705-00065 REV 01. Las Vegas, Nevada: CRWMS M&O. ACC: MOL.19990526.0296.

CRWMS M&O 1998a. *Near-Field/Altered Zone Coupled Effects Expert Elicitation Project*. Las Vegas, Nevada: CRWMS M&O. ACC: MOL.19980729.0638.

CRWMS M&O 1998b. "Thermal Hydrology." Chapter 3 of *Total System Performance Assessment-Viability Assessment (TSPA-VA) Analyses Technical Basis Document*. B00000000-01717-4301-00003 REV 01. Las Vegas, Nevada: CRWMS M&O. ACC: MOL.19981008.0003.

CRWMS M&O 1998c. "Near-Field Geochemical Environment." Chapter 4 of *Total System Performance Assessment-Viability Assessment (TSPA-VA) Analyses Technical Basis Document*. B00000000-01717-4301-00004 REV 01. Las Vegas, Nevada: CRWMS M&O. ACC: MOL.19981008.0004.

CRWMS M&O 1999a. *License Application Design Selection Report*. B00000000-01717-4600-00123 REV 01 ICN 01. Las Vegas, Nevada: CRWMS M&O. ACC: MOL.19990908.0319.

CRWMS M&O 1999b. *Work Package Planning Summary for the Near Field Environment Process Model Report FY 00 WP #1401213NM1 and 891213NU1 Revision 00*. WPP-MGR-MD-000024. Las Vegas, Nevada: CRWMS M&O. ACC: MOL.19991021.0080.

CRWMS M&O 1999c. *Final Report Total System Performance Assessment Peer Review Panel*. Las Vegas, Nevada: CRWMS M&O. ACC: MOL.19990528.0155.

CRWMS M&O 1999d. *Single Heater Test Final Report*. BAB000000-01717-5700-00005 REV 00 ICN 1. Las Vegas, Nevada: CRWMS M&O. ACC: MOL.20000103.0634.

CRWMS M&O 2000a. *Thermal Tests Thermal-Hydrological Analysis/Model Report*. ANL-NBS-TH-000001 REV 00. Las Vegas, Nevada: CRWMS M&O. ACC: MOL.20000505.0231.

CRWMS M&O 2000b. *Drift-Scale Coupled Processes (DST and THC Seepage) Models*. MDL-NBS-HS-000001 REV 00. Las Vegas, Nevada: CRWMS M&O. ACC: MOL.19990721.0523.

CRWMS M&O 2000c. *Abstraction of Drift-Scale Coupled Processes*. ANL-NBS-HS-000029 REV 00. Las Vegas, Nevada: CRWMS M&O. ACC: MOL.20000525.0371.

CRWMS M&O 2000d. *Calculation of Permeability Change Due to Coupled Thermal-Hydrological-Mechanical Effects*. CAL-NBS-MD-000002 REV 00. Las Vegas, Nevada: CRWMS M&O. ACC: MOL.20000711.0192.

CRWMS M&O 2000e. *Features, Events and Processes in Thermal Hydrology and Coupled Processes*. ANL-NBS-MD-00004 REV 00. Las Vegas, Nevada: CRWMS M&O. ACC: MOL.20000602.0053.

CRWMS M&O 2000f. *Unsaturated Zone Flow and Transport Model Process Model Report*. TDR-NBS-HS-000002 REV 00. Las Vegas, Nevada: CRWMS M&O. ACC: MOL.20000320.0400.

CRWMS M&O 2000g. *Engineered Barrier System Degradation, Flow, and Transport Process Model Report*. TDR-EBS-MD-000006 REV 00. Las Vegas, Nevada: CRWMS M&O. ACC: MOL.20000324.0558.

CRWMS M&O 2000h. *Conceptual and Numerical Models for UZ Flow and Transport*. MDL-NBS-HS-000005 REV 00. Las Vegas, Nevada: CRWMS M&O. ACC: MOL.19990721.0526.

CRWMS M&O 2000i. *Site Recommendation Subsurface Layout*. ANL-SFS-MG-000001 REV 00. Las Vegas, Nevada: CRWMS M&O. ACC: MOL.20000908.0276.

CRWMS M&O 2000j. Not Used.

CRWMS M&O 2000k. *Multiscale Thermohydrologic Model*. ANL-EBS-MD-000049 REV 00. Las Vegas, Nevada: CRWMS M&O. ACC: MOL.20000609.0267.

CRWMS M&O 2000l. *Abstraction of Drift Seepage*. ANL-NBS-MD-000005 REV 00. Las Vegas, Nevada: CRWMS M&O. ACC: MOL.20000322.0671.

CRWMS M&O 2000m. *Abstraction of NFE Drift Thermodynamic Environment and Percolation Flux*. ANL-EBS-HS-000003 REV 00. Las Vegas, Nevada: CRWMS M&O. ACC: MOL.20000504.0296.

CRWMS M&O 2000n. *Calibrated Properties Model*. MDL-NBS-HS-000003 REV 00. Las Vegas, Nevada: CRWMS M&O. ACC: MOL.19990721.0520.

CRWMS M&O 2000o. *Waste Package Degradation Process Model Report*. TDR-WIS-MD-000002 REV 00 ICN 01. Las Vegas, Nevada: CRWMS M&O. ACC: MOL.20000620.0346.

CRWMS M&O 2000p. *Natural Analogues for the Unsaturated Zone*. ANL-NBS-HS-000007 REV 00. Las Vegas, Nevada: CRWMS M&O. ACC: MOL.19990721.0524.

CRWMS M&O 2000q. *UZ Flow Models and Submodels*. MDL-NBS-HS-000006 REV 00. Las Vegas, Nevada: CRWMS M&O. ACC: MOL.19990721.0527.

CRWMS M&O 2000r. *Analysis of Geochemical Data for the Unsaturated Zone*. ANL-NBS-HS-000017 REV 00. Las Vegas, Nevada: CRWMS M&O. ACC: MOL.20000725.0453.

CRWMS M&O 2000s. *Repository Safety Strategy: Plan to Prepare the Postclosure Safety Case to Support Yucca Mountain Site Recommendation and Licensing Considerations*. TDR-WIS-RL-000001 REV 03. Las Vegas, Nevada: CRWMS M&O. ACC: MOL.20000119.0189.

CRWMS M&O 2000t. *Mountain-Scale Coupled Processes (TH) Models*. MDL-NBS-HS-000007 REV 00. Las Vegas, Nevada: CRWMS M&O. ACC: MOL.19990721.0528.

CRWMS M&O 2000u. *Water Distribution and Removal Model*. ANL-EBS-MD-000032 REV 00. Las Vegas, Nevada: CRWMS M&O. ACC: MOL.20000504.0303.

CRWMS M&O 2000v. *Physical and Chemical Environment Abstraction Model*. ANL-EBS-MD-000046 REV 00. Las Vegas, Nevada: CRWMS M&O. ACC: MOL.20000523.0155.

CRWMS M&O 2000w. *Development of Numerical Grids for UZ Flow and Transport Modeling*. ANL-NBS-HS-000015 REV 00. Las Vegas, Nevada: CRWMS M&O. ACC: MOL.19990721.0517.

CRWMS M&O 2000x. *Near-Field Environment Process Model Report(PMR)*. TDP-NBS-MD-000011 REV 00. Las Vegas, Nevada: CRWMS M&O. ACC: MOL.20000310.0353.

CRWMS M&O 2000y. *Integrated Site Model Process Model Report*. TDR-NBS-GS-000002 REV 00 ICN 01. Las Vegas, Nevada: CRWMS M&O. ACC: MOL.20000121.0116.

CRWMS M&O 2000z. *Performance Confirmation Plan*. TDR-PCS-SE-000001 REV 01. Las Vegas, Nevada: CRWMS M&O. ACC: MOL.20000302.0312.

CRWMS M&O 2000aa. *Subsurface Facility System Description Document*. SDD-SFS-SE-000001 REV 00. Volume I. Las Vegas, Nevada: CRWMS M&O. ACC: MOL.20000221.0712.

CRWMS M&O 2000ab. *Waste Form Degradation Process Model Report*. TDR-WIS-MD-000001 REV 00. Las Vegas, Nevada: CRWMS M&O. ACC: MOL.20000403.0495.

CRWMS M&O 2000ac. *Drift Degradation Analysis*. ANL-EBS-MD-000027 REV 00. Las Vegas, Nevada: CRWMS M&O. ACC: MOL.20000107.0328.

CRWMS M&O 2000ad. *Emplacement Drift System Description Document* SDD-EDS-SE-000001 REV 00. Las Vegas, Nevada: CRWMS M&O. ACC: MOL.20000121.0119.

CRWMS M&O 2000ae. *Backfill Emplacement System Description Document*. SDD-BES-SE-000001 REV 00. Las Vegas, Nevada: CRWMS M&O. ACC: MOL.20000210.0074.

CRWMS M&O 2000af. *Subsurface Ventilation System Description Document*. SDD-SVS-SE-000001 REV 00. Las Vegas, Nevada: CRWMS M&O. ACC: MOL.20000217.0221.

CRWMS M&O 2000ag. *Ground Control System Description Document*. SDD-GCS-SE-000001 REV 00. Las Vegas, Nevada: CRWMS M&O. ACC: MOL.20000221.0711.

Daily, W.; Lin, W.; and Buscheck, T. 1987. "Hydrological Properties of Topopah Spring Tuff: Laboratory Measurements." *Journal of Geophysical Research*, 92, (B8), 7854-7864. Washington, D.C.: American Geophysical Union. TIC: 226512.

DOE (U.S. Department of Energy) 1988. *Site Characterization Plan Yucca Mountain Site, Nevada Research and Development Area, Nevada*. DOE/RW-0199. Nine volumes. Washington, D.C.: U.S. Department of Energy, Office of Civilian Radioactive Waste Management. ACC: HQO.19881201.0002.

DOE (U.S. Department of Energy) 1998. *Total System Performance Assessment*. Volume 3 of *Viability Assessment of a Repository at Yucca Mountain*. DOE/RW-0508. Washington, D.C.: U.S. Department of Energy, Office of Civilian Radioactive Waste Management. ACC: MOL.19981007.0030.

DOE (U.S. Department of Energy) 2000. *Quality Assurance Requirements and Description*. DOE/RW-0333P, Rev. 9. Washington, D.C.: U.S. Department of Energy, Office of Civilian Radioactive Waste Management. ACC: MOL.19991028.0012.

Ehrlich, R.; Etris, E.L.; Brumfield, D.; Yuan, L.P.; and Crabtree, S.J. 1991. "Petrography and Reservoir Physics III: Physical Models for Permeability and Formation Factor." *AAPG Bulletin*, 75, (10), 1579-1592. Tulsa, Oklahoma: American Association of Petroleum Geologists. TIC: 246294.

Esaki, T.; Du, S.; Mitani, Y.; Ikusada, K.; and Jing, L. 1999. "Development of a Shear-Flow Test Apparatus and Determination of Coupled Properties for a Single Rock Joint." *International Journal of Rock Mechanics and Mining Sciences*, 36, 641-650. New York, New York: Elsevier Science. TIC: 247483.

Flint, A.L.; Hevesi, J.A.; and Flint, L.E. 1996. *Conceptual and Numerical Model of Infiltration for the Yucca Mountain Area, Nevada*. Milestone 3GUI623M. Denver, Colorado: U.S. Geological Survey. ACC: MOL.19970409.0087.

Geller J.T.; Su G.; and Pruess K. 1996. *Preliminary Studies of Water Seepage Through Rough-Walled Fractures*. LBNL-38810. [Berkeley, California]: Lawrence Berkeley National Laboratory. ACC: MOL.20000705.0112.

Green, R.; Martin, R.; Svedeman, S.; and Dodge, F.T. 1991. "Nonisothermal Laboratory and Numerical Experiments Results." *Proceedings of Workshop V: Flow and Transport Through Unsaturated Fractured Rock - Related to High-Level Radioactive Waste Disposal, Held at Radisson Suite Hotel, Tuscon, Arizona, January 7-10, 1991*. Evans, D.D. and Nicholson, T.J., eds. NUREG/CP-0040, 161-168. Washington, D.C.: U.S. Nuclear Regulatory Commission. TIC: 207128.

Hardin, E.L. 1998. *Near-Field/Altered-Zone Models Report*. UCRL-ID-129179 DR. Livermore, California: Lawrence Livermore National Laboratory. ACC: MOL.19980504.0577.

Hardin, E.L. and Chesnut, D.A. 1997. *Synthesis Report on Thermally Driven Coupled Processes*. Milestone SPL8BM4. Livermore, California: Lawrence Livermore National Laboratory. ACC: MOL.19980107.0356.

Harrison-Giesler, D.J.; Morissette, R.P.; and Jardine, L.J. 1991. *Yucca Mountain Site Characterization Project Waste Package Plan*. UCRL-JC-106161. Livermore, California: Lawrence Livermore National Lab. ACC: NNA.19920529.0030.

Haukwa, C.B.; Wu, Y.S.; and Bodvarsson, G.S. 1999. "Thermal Loading Studies Using the Yucca Mountain Unsaturated Zone Model." *Journal Of Contaminant Hydrology*, 38, (1-3), 217-255. New York, New York: Elsevier Science Publishers. TIC: 244160.

Ho, C.K. 1997. "Models of Fracture-Matrix Interactions During Multiphase Heat and Mass Flow in Unsaturated Fractured Porous Media." *Proceedings of the ASME Fluids Engineering Division, November 16-21, 1997, Dallas, Texas*. FED-Vol. 244. Pages 401-412. New York, New York: American Society of Mechanical Engineers. TIC: 241082.

Ho, C.K. and Francis, N.D. 1998. "Coupled Thermo-Hydro-Mechanical Simulations of the Potential Repository at Yucca Mountain." *High-Level Radioactive Waste Management, Proceedings of the Eighth International Conference, Las Vegas, Nevada, May 11-14, 1998*. Pages 113-115. La Grange Park, Illinois: American Nuclear Society. TIC: 237082.

Hughson, D. and Green, R. 1999. *Evaluation of Thermal-Hydrological Model Concepts, Data, and U.S. Department of Energy Thermal Test Results-Status Report*. San Antonio, Texas: Center for Nuclear Waste Regulatory Analyses. TIC: 247537.

Israelsson, J. 1995. *DECOVALEX I - Bench-Mark Test 3: Thermo-Hydro-Mechanical Modelling*. SKB Technical Report 95-30. Stockholm, Sweden: Swedish Nuclear Fuel and Waste Management Company. TIC: 223944.

Itasca Consulting Group 1996. *FLAC, Fast Lagrangian Analysis of Continua, Version 3.3*. Four Volumes. Minneapolis, Minnesota: Itasca Consulting Group. TIC: 236418; 236419; 236420; 236421.

Itasca Consulting Group 1998. *3DEC, 3 Dimensional Distinct Element Code, User's Guide, (Version 2.00)*. Minneapolis, Minnesota: Itasca Consulting Group. TIC: 247503.

Jiao, Y. and Hudson, J.A. 1995. "The Fully-Coupled Model for Rock Engineering Systems." *International Journal of Rock Mechanics and Mining Sciences & Geomechanics Abstracts*, 32, (5), 491-512. Oxford, United Kingdom: Elsevier Science. TIC: 235731.

Jing, L.; Tsang, C.F.; and Stephansson, O. 1995. "DECOVALEX - An International Co-Operative Research Project on Mathematical Models of Coupled THM Processes for Safety Analysis of Radioactive Waste Repositories." *International Journal of Rock Mechanics and Mining Sciences & Geomechanics Abstracts*, 32, (5), 389-398. Oxford, United Kingdom: Elsevier Science. TIC: 235918.

Johnson, J.W.; Knauss, K.G.; Glassley, W.E.; DeLoach, L.D.; and Thompson, A.F.B 1998. "Reactive Transport Modeling of Plug-Flow Reactor Experiments: Quartz and Tuff Dissolution at 240°C." *Journal of Hydrology*, 209, 81-111. Amsterdam, The Netherlands: Elsevier Science. TIC: 240986.

Jury, W.A.; Gardner, W.R.; and Gardner, W.H. 1991. *Soil Physics*. 5th Edition. New York, New York: John Wiley & Sons. TIC: 241000.

Keenan, J.H.; Keyes, F.G.; Hill, P.G.; and Moore, J.G. 1969. *Steam Tables, Thermodynamic Properties of Water Including Vapor, Liquid, and Solid Phases*. New York, New York: John Wiley & Sons. TIC: 246766.

Klavetter, E.A. and Peters, R.R. 1986. *Estimation of Hydrologic Properties of an Unsaturated, Fractured Rock Mass*. SAND-84-2642. Albuquerque, New Mexico: Sandia National Laboratories. TIC: 202727.

Kneafsey, T.J. and Pruess, K. 1997. *Preferential Flow Paths and Heat Pipes: Status Report Second Quarter FY 1997*. Milestone SPL6A3M4. Berkeley, California: Lawrence Berkeley National Laboratory. ACC: MOL.19971125.0196.

Kneafsey, T.J. and Pruess, K. 1998. "Laboratory Experiments on Heat-Driven Two-Phase Flows in Natural and Artificial Rock Fractures." *Water Resources Research*, 34, (12), 3349-3367. Washington, D.C.: American Geophysical Union. TIC: 247468.

Kotra, J.P.; Lee, M.P.; Eisenberg, N.A.; and DeWispelare, A.R. 1996. *Branch Technical Position on the Use of Expert Elicitation in the High-Level Radioactive Waste Program*. NUREG-1563. Washington, D.C.: U.S. Nuclear Regulatory Commission. TIC: 226832.

Krumhansl, J.L. and Stockman, H.W. 1988. "Site Selection Criteria and Preliminary Results from the Valles Caldera Natural Analog Study." *Proceedings of Workshop IV on Flow and Transport Through Unsaturated Fractured Rock-Related to High Level Radioactive Waste Disposal, December 12-15, 1998 Tucson, Arizona*. Pages 249-276. Tucson, Arizona: University of Arizona. TIC: 247519.

Kwicklis, E.M. and Healy, R.W. 1993. "Numerical Investigation of Steady Liquid Water Flow in a Variably Saturated Fracture Network." *Water Resources Research*, 29, (12), 4091-4102. Washington, D.C.: American Geophysical Union. TIC: 226993.

Lasaga, A.C. 1998. *Kinetic Theory in the Earth Sciences*. Princeton, New Jersey: Princeton University Press. TIC: 246279.

LBNL (Lawrence Berkeley National Laboratory) 1999. *Software Code: TOUGHREACT V2.2*. V2.2. SUN. STN: 10154-2.2-00. URN-0365.

LBNL 2000. *Software Code: TOUGH2 V1.4*. V1.4. STN: 10007-1.4-01.

LLNL (Lawrence Livermore National Laboratory) 1999. *Software code: NUFT*. V3.0.1s. Sun SPARC, UNIX OS. 10130-3.0.1s-00. URN-0394.

LLNL 1999. *Software code, MSTHAC*. V6.2. STN: 10290-6.2-00. URN-0455.

Lee, K.H.; Kulshrestha, A.; and Nitao, J.J. 1993. *Interim Report on Verification and Benchmark Testing of the NUFT Computer Code, October 1993*. UCRL-ID-113521. Livermore, California: Lawrence Livermore National Laboratory. TIC: 235555.

Levy, S.S.; Fabryka-Martin, J.T.; Dixon, P.R.; Liu, B.; Turin, H.J.; and Wolfsberg, A.V. 1997. "Chlorine-36 Investigations of Groundwater Infiltration in the Exploratory Studies Facility at Yucca Mountain, Nevada." *Scientific Basis for Nuclear Waste Management XX, Symposium held December 2-6, 1996, Boston, Massachusetts*. Gray, W.J. and Triay, I.R., eds. 465, 901-908. Pittsburgh, Pennsylvania: Materials Research Society. TIC: 238884.

Lichtner, P.C. and Seth, M. 1996. "Multiphase-Multicomponent Nonisothermal Reactive Transport in Partially Saturated Porous Media." *Proceedings of the 1996 International Conference on Deep Geological Disposal of Radioactive Waste, September 16-19, 1996, Winnipeg, Manitoba, Canada*. Toronto, Ontario, Canada: Canadian Nuclear Society. TIC: 233923.

Lichtner, P.C.; Keating, G.; and Carey, B. 1999. *A Natural Analogue for Thermal-Hydrological-Chemical Coupled Processes at the Proposed Nuclear Waste Repository at Yucca Mountain, Nevada*. LA-13610-MS. Los Alamos, New Mexico: Los Alamos National Laboratory. TIC: 246032.

Lin, W. and Daily, W. 1988. *Hydrological Properties of Topopah Spring Tuff Under a Thermal Gradient Laboratory Results*. UCRL-96926. Livermore, California: Lawrence Livermore National Laboratory. ACC: NN1.19881027.0006.

Lin, W. and Daily, W.D. 1989. *Laboratory Study of Fracture Healing in Topopah Spring Tuff- Implications for Near Field Hydrology*. Livermore, California: Lawrence Livermore National Laboratory. ACC: NNA.19900711.0241.

Lin, W. and Roberts, J. 1996. "Laboratory-Determined Hydrologic Properties and Processes." Chapter 2 of *Near-Field and Altered-Zone Environment Report*. Wilder, D.G., ed. UCRL-LR-124998. Volume II. Livermore, California: Lawrence Livermore National Laboratory. ACC: MOL.19961212.0122.

Lin, W.; Wilder, D.; Blair, S.; Daily, W.; Gdowski, G.; Glassley, W.; Lee, K.; Meike, A.; Ramirez, A.; Roberts, J.; Ruddle, D.; Wagoner, J.; Watwood, D.; Williams, T.; and Carlson, R. 1998a. "The Large Block Test of the Exploratory Studies Facility Thermal Tests." *High-Level Radioactive Waste Management, Proceedings of the Eighth International Conference, Las Vegas, Nevada, May 11-14, 1998*. Pages 49-51. La Grange Park, Illinois: American Nuclear Society. TIC: 237082.

Lin, W.; Roberts, J.J.; and Wildenschild, D. 1998b. *A Report on Laboratory Scale Thermally-Coupled Processes Experiments*. UCRL-ID-129843. Livermore, California: Lawrence Livermore National Laboratory. ACC: MOL.19981123.0401.

Lin, W.; Roberts, J.J.; Glassley, W.E.; and Ruddle, D. 1995. *The Effect of Rock-Water Interaction on Permeability*. UCRL-JC-119574. Livermore, California: Lawrence Livermore National Laboratory. ACC: MOL.19960416.0275.

- Liu, H.H.; Doughty, C.; and Bodvarsson, G.S. 1998. "An Active Fracture Model for Unsaturated Flow and Transport in Fractured Rocks." *Water Resources Research*, 34, (10), 2633-2646. Washington, D.C.: American Geophysical Union. TIC: 243012.
- Mack, M.G.; Brandshaug, T.; and Brady, B.H. 1989. *Rock Mass Modification Around a Nuclear Waste Repository in Welded Tuff*. NUREG/CR-5390. Washington, D.C.: U.S. Nuclear Regulatory Commission. TIC: 229166.
- Manteufel, R.D.; Ahola, M.P.; Turner, D.R.; and Chowdhury, A.H. 1993. *A Literature Review of Coupled Thermal-Hydrologic-Mechanical-Chemical Processes Pertinent to the Proposed High-Level Nuclear Waste Repository at Yucca Mountain*. NUREG CR-6021. Washington, D.C.: U.S. Nuclear Regulatory Commission. TIC: 207771.
- Martin, R.J.; Noel, J.S.; Boyd, P.J.; and Price, R.H. 1997. *Creep Properties of the Paintbrush Tuff Recovered from Borehole USW NRG-7/7A: Data Report*. SAND95-1759. Albuquerque, New Mexico: Sandia National Laboratories. ACC: MOL.19971017.0661.
- Matyskiela, W. 1997. "Silica Redistribution and Hydrologic Changes in Heated Fractured Tuff." *Geology*, 25, (12), 1115-1118. Boulder, Colorado: Geological Society of America. TIC: 236809.
- Millard, A.; Durin, N.; Stietel, A.; Thoraval, A.; Vuillod, E.; Baroudi, H.; Plas, F.; Bougnoux, A.; Vouille, G.; Kobayashi, A.; Hara, K.; Fujita, T.; and Ohnishi, Y. 1995. "Discrete and Continuum Approaches to Simulate the Thermo-Hydro-Mechanical Couplings in a Large, Fractured Rock Mass." *International Journal of Rock Mechanics and Mining Sciences & Geomechanics Abstracts*, 32, (5), 409-414. Oxford, United Kingdom: Elsevier Science. TIC: 235740.
- Mohanty, S.; Chowdhury, A.H.; Hsiung, S-M.; and Ahola, M.P. 1994a. *Single Fracture Flow Behavior of Apache Leap Tuff Under Normal and Shear Loads*. San Antonio, Texas: Center for Nuclear Waste Regulatory Analyses. TIC: 247817.
- Mohanty, S.; Pickens, A.; and Kana, D. 1994b. "Single-Fracture Permeability Under Normal and Shear Displacement of Natural Rock Joint." *EOS Transactions*, 75, (44), 258. Washington, D.C.: American Geophysical Union. TIC: 247737.
- Murphy, W.M. and Pabalan, R.T. 1994. *Geochemical Investigations Related to the Yucca Mountain Environment and Potential Nuclear Waste Repository*. NUREG/CR-6288. San Antonio, Texas: Southwest Research Institute. TIC: 227032.
- Nataraja, M.S. and Brandshaug, T. 1992. *Staff Technical Position on Geologic Repository Operations Area Underground Facility Design - Thermal Loads*. NUREG-1466. Washington, D.C.: U.S. Nuclear Regulatory Commission. ACC: NNA.19921030.0049.

Nguyen, T.S. and Selvadurai, A.P.S. 1995. "Coupled Thermal-Mechanical-Hydrological Behaviour of Sparsely Fractured Rock: Implications for Nuclear Fuel Waste Disposal." *International Journal of Rock Mechanics Mining Sciences and Geomechanics Abstracts*, 32, (5), 465-479. Oxford, United Kingdom: Elsevier Science. TIC: 235741.

Nicholl, M.J.; Glass, R.J.; and Wheatcraft, S.W. 1994. "Gravity-Driven Infiltration Instability in Initially Dry Nonhorizontal Fractures." *Water Resources Research*, 30, (9), 2533-2546. Washington, D.C.: American Geophysical Union. TIC: 243493.

Nitao, J.J. 1993. "The NUFT Code for Modeling Nonisothermal, Multiphase, Multicomponent Flow and Transport in Porous Media." *Eos*, 74, (43), 313. Washington, D.C.: American Geophysical Union. TIC: 226135.

Nitao, J.J. and Buscheck, T.A. 1996. "Discrete-Fracture Modeling of Thermal-Hydrological Processes at Yucca Mountain and the LLNL G-Tunnel Heater Test." *Scientific Basis for Nuclear Waste Management XIX, Symposium held November 27-December 1, 1995, Boston, Massachusetts*. Murphy, W.M. and Knecht, D.A., eds. 412, 747-758. Pittsburgh, Pennsylvania: Materials Research Society. TIC: 233877.

Nitsche, H. 1991. "Basic Research for Assessment of Geologic Nuclear Waste Repositories: What Solubility and Speciation Studies of Transuranium Elements Can Tell Us." *Scientific Basis for Nuclear Waste Management XIV, Symposium held November 26-29, 1990, Boston, Massachusetts*. Abrajano, T., Jr. and Johnson, L.H., eds. 212, 517-529. Pittsburgh, Pennsylvania: Materials Research Society. TIC: 203656.

NRC (U.S. Nuclear Regulatory Commission) 1998. *Issue Resolution Status Report Key Technical Issue: Total System Performance Assessment and Integration*. Rev. 1. Washington, D.C.: U.S. Nuclear Regulatory Commission. ACC: MOL.19990105.0083.

NRC 1999a. *Issue Resolution Status Report Key Technical Issue: Evolution of the Near-Field Environment*. Rev. 2. Washington, D.C.: U.S. Nuclear Regulatory Commission. ACC: MOL.19990810.0640.

NRC 1999b. *Issue Resolution Status Report Key Technical Issue: Thermal Effects on Flow*. Rev. 2. Washington, D.C.: U.S. Nuclear Regulatory Commission. ACC: MOL.19991021.0156.

NRC 1999c. *Issue Resolution Status Report Key Technical Issue: Repository Design and Thermal-Mechanical Effects*. Rev. 02. Washington, D.C.: U.S. Nuclear Regulatory Commission. ACC: MOL.20000306.0670.

NRC 1999d. Minutes, Nuclear Regulatory Commission Meeting, Rockville, Maryland, March 16 and 17, 1999. Rockville, Maryland: U.S. Nuclear Regulatory Commission. ACC: MOL.19990406.0198.

NRC (U.S. Nuclear Regulatory Commission) 2000. *Issue Resolution Status Report Key Technical Issue: Total System Performance Assessment and Integration*. Rev. 2. Washington, D.C.: U.S. Nuclear Regulatory Commission. TIC: 247614.

NWTRB (U.S. Nuclear Waste Technical Review Board) 1992. Minutes, NWTRB Full Board Meeting, Denver, Colorado, July 7-8, 1992. TIC: 210563.

Olsson, W.A. and Brown, S.R. 1993. "Hydromechanical Response of a Fracture Undergoing Compression and Shear." *International Journal of Rock Mechanics, Mining Sciences & Geomechanics Abstracts*, 30, (7), 845-851. New York, New York: Pergamon Press. TIC: 234100.

Olsson, W.A. and Brown, S.R. 1994. *Mechanical Properties of Seven Fractures from Drillholes NRG-4 and NRG-6 at Yucca Mountain, Nevada*. SAND94-1995. Albuquerque, New Mexico: Sandia National Laboratories. ACC: MOL.19941007.0081.

Paperiello, C.J. 1999. "U.S. Nuclear Regulatory Commission Staff Review of the U.S. Department of Energy Viability Assessment for a High-Level Radioactive Waste Repository at Yucca Mountain, Nevada." Letter from C.J. Paperiello (NRC) to L.H. Barrett (DOE), June 2, 1999, with enclosures, "U.S. Nuclear Regulatory Commission's Staff Evaluation of U.S. Department of Energy's Viability Assessment" and Letter from B.J. Garrick (NRC Advisory Committee on Nuclear Waste) to S.A. Jackson (NRC), dated April 8, 1999. ACC: HQO.19990811.0007; HQO.19990811.0008.

Pruess, K. 1987. *TOUGH User's Guide*. NUREG/CR-4645. Washington, D.C.: U.S. Nuclear Regulatory Commission. TIC: 217275.

Pruess, K. 1991. *TOUGH2-A General-Purpose Numerical Simulator for Multiphase Fluid and Heat Flow*. LBL-29400. Berkeley, California: Lawrence Berkeley Laboratory. ACC: NNA.19940202.0088.

Pruess, K. 1997. "On Vaporizing Water Flow in Hot Sub-Vertical Rock Fractures." *Transport in Porous Media*, 28, (3), 335-372. Boston, Massachusetts: Kluwer Academic Publishers. TIC: 238922.

Pruess, K.; Tsang, Y.W.; and Wang, J.S.Y. 1984. *Numerical Studies of Fluid and Heat Flow Near High-Level Nuclear Waste Packages Emplaced in Partially Saturated Fractured Tuff*. LBL-18552. Berkeley, California: Lawrence Berkeley Laboratory. TIC: 211033.

Pruess, K.; Wang, J.S.Y.; and Tsang, Y.W. 1990. "On Thermohydrologic Conditions Near High-Level Nuclear Wastes Emplaced in Partially Saturated Fractured Tuff: 1. Simulation Studies with Explicit Consideration of Fracture Effects." *Water Resources Research*, 26, (6), 1235-1248. Washington, D.C.: American Geophysical Union. TIC: 221923.

Ramirez, A.L., ed. 1991. *Prototype Engineered Barrier System Field Test (PEBSFT) Final Report*. UCRL-ID-106159. Livermore, California: Lawrence Livermore National Laboratory. ACC: NNA.19910711.0047.

Raven, K.G. and Gale, J.E. 1985. "Water Flow in a Natural Rock Fracture as a Function of Stress and Sample Size." *International Journal of Rock Mechanics and Mining Sciences & Geomechanics Abstracts*, 22, (4), 251-261. Oxford, United Kingdom: Pergamon Press. TIC: 235724.

Reed, M.H. 1982. "Calculation of Multicomponent Chemical Equilibria and Reaction Processes in Systems Involving Minerals, Gases, and an Aqueous Phase." *Geochimica et Cosmochimica Acta*, 46, (4), 513-528. New York, New York: Pergamon Press. TIC: 224159.

Rehbinder, G. 1995. "Analytical Solutions of Stationary Coupled Thermo-Hydro-Mechanical Problems." *International Journal of Rock Mechanics and Mining Sciences & Geomechanics Abstracts*, 32, (5), 453-463. Oxford, United Kingdom: Elsevier Science. TIC: 235725.

Roberts, J.J. and Lin, W. 1997. "X-Ray Radiography of Fracture Flow and Matrix Imbibition in Topopah Spring Tuff Under a Thermal Gradient." *International Journal of Rock Mechanics and Mining Sciences*, 34, (3/4), 482. [New York, New York]: Elsevier Science. TIC: 237400.

Rosenberg, N.D.; Knauss, K.G.; and Dibley, M.J. 1999. *Evaporation of J13 Water: Laboratory Experiments and Geochemical Modeling*. UCRL-ID-134852. Livermore, California: Lawrence Livermore National Laboratory. TIC: 246322.

Sagar, B.; Bagtzoglou, A.C.; Green, R.T.; and Stothoff, S.A. 1995. "Measurement and Modeling of Flow Through Unsaturated Heterogeneous Rock in the Context of Geologic Disposal of Nuclear Waste." *Proceedings of the ASME Heat Transfer and Fluids Engineering Divisions: Presented at the 1995 ASME International Mechanical Engineering Congress and Exposition, November 12-17, 1995, San Francisco, California*. HTD Vol. 321, FED Vol. 233, 271-284. New York, New York: American Society of Mechanical Engineers. TIC: 247816.

Slider, H.C. 1976. *Practical Petroleum Reservoir Engineering Methods, An Energy Conservation Science*. Tulsa, Oklahoma: Petroleum Publishing Company. TIC: 247798.

Sonnenthal, E.; Spycher, N.; Apps, J.; and Simmons, A. 1998. *Thermo-Hydro-Chemical Predictive Analysis for the Drift-Scale Heater Test*. Milestone SPY289M4. Version 1.1. Berkeley, California: Lawrence Berkeley National Laboratory. ACC: MOL.19981130.0132.

Sonnenthal, E.L. and Bodvarsson, G.S. 1999. "Constraints on the Hydrology of the Unsaturated Zone at Yucca Mountain, NV from Three-Dimensional Models of Chloride and Strontium Geochemistry." *Journal of Contaminant Hydrology*, 38, (1-3), 107-156. New York, New York: Elsevier Science B.V. TIC: 244160.

Steefel, C.I. and Lasaga, A.C. 1994. "A Coupled Model for Transport of Multiple Chemical Species and Kinetic Precipitation/Dissolution Reactions with Application to Reactive Flow in Single Phase Hydrothermal Systems." *American Journal of Science*, 294, (5), 529-592. New Haven, Connecticut: Kline Geology Laboratory, Yale University. TIC: 235372.

Steeffel, C.I. and Lichtner, P.C. 1998. "Multicomponent Reactive Transport in Discrete Fractures: I. Controls on Reaction Front Geometry." *Journal of Hydrology*, 209, 186-199. New York, New York: Elsevier Science B.V. TIC: 247524.

Stephansson, O. 1995. "Introduction." *International Journal of Rock Mechanics and Mining Sciences & Geomechanics Abstracts*, 32, (5), 387. Oxford, United Kingdom: Elsevier Science. TIC: 236217.

Stockman, H.; Krumhansl, J.; Ho, C.; and McConnell, V. 1994. *The Valles Natural Analogue Project*. NUREG/CR-6221. Washington, D.C.: U.S. Nuclear Regulatory Commission. TIC: 246123.

Tsang, Y.W. and Birkholzer, J.T. 1999. "Predictions and Observations of the Thermal-Hydrological Conditions in the Single Heater Test." *Journal of Contaminant Hydrology*, 38, 385-425. New York, New York: Elsevier Science B.V. TIC: 244160.

Tsang, Y.W.; Apps, J.; Birkholzer, J.T.; Freifeld, B.; Hu, M.Q.; Peterson, J.; Sonnenthal, E.; and Spycher, N. 1999. *Single Heater Test Borehole Perspective*. LBNL-42537. Berkeley, California: Lawrence Berkeley National Laboratory. ACC: MOL.20000331.0665.

Wildenschild, D.; Roberts, J.J.; Hardin, E.; and Lin, W. 1998. *Experimental Tests of Enhancement of Thermal Vapor Diffusion in Topopah Spring Tuff*. UCRL-JC-128747. Livermore, California: Lawrence Livermore National Laboratory. ACC: MOL.19990118.0060.

Wilder, D.G. 1997. *Technical Bases for EBS Design*. Volume I of *Near-Field and Altered-Zone Environment Report*. UCRL-LR-107476, Rev. 1. Livermore, California: Lawrence Livermore National Laboratory. ACC: MOL.19980107.0365.

Wilder, D.G. and Yow, J.L., Jr. 1987. *Geomechanics of the Spent Fuel Test - Climax*. UCRL-53767. Livermore, California: Lawrence Livermore National Laboratory. ACC: NNA.19900110.0337.

Wilder, D.G., ed. 1993. *Preliminary Near-Field Environment Report*. UCRL-LR-107476. Two volumes. Livermore, California: Lawrence Livermore National Laboratory. ACC: NNA.19920501.0002.

Wilder, D.G., ed. 1996. *Volume II: Near-Field and Altered-Zone Environment Report*. UCRL-LR-124998. [Livermore, California]: Lawrence Livermore National Laboratory. ACC: MOL.19961212.0121; MOL.19961212.0122.

Wilder, D.G.; Lin, W.; Blair, S.C.; Buscheck, T.; Carlson, R.C.; Lee, K.; Meike, A.; Ramirez, A.L.; Wagoner, J.L.; and Wang, J. 1997. *Large Block Test Status Report*. UCRL-ID-128776. Livermore, California: Lawrence Livermore National Laboratory. ACC: MOL.19980508.0727.

Wilkins, D.R. and Heath, C.A. 1999. "Direction to Transition to Enhanced Design Alternative II." Letter from D.R. Wilkins (CRWMS M&O) and C.A. Heath (CRWMS M&O) to Distribution, June 15, 1999, LV.NS.JLY.06/99-026, with enclosures, "Strategy for Baselineing EDA II Requirements" and "Guidelines for Implementation of EDA II." ACC: MOL.19990622.0126; MOL.19990622.0127; MOL.19990622.0128.

WoldeGabriel, G.; Keating, G.N.; and Valentine, G.A. 1999. "Effects of Shallow Basaltic Intrusion into Pyroclastic Deposits, Grants Ridge, New Mexico, USA." *Journal of Volcanology and Geothermal Research*, 92, ([3]), 389-411. [New York, New York]: Elsevier Science B.V. TIC: 246037.

Wollenberg, H.A. and Flexser, S. 1986. "Contact Zones and Hydrothermal Systems as Analogues to Repository Conditions." *Chemical Geology*, 55, 345-359. Amsterdam, The Netherlands: Elsevier Science Publishers B.V. TIC: 246171.

Wruck, D.A. and Palmer, C.E.A. 1997. *Analysis of Elevated Temperature Data for Thermodynamic Properties of Selected Radionuclides*. Milestone SPL4B2M4. Livermore, California: Lawrence Livermore National Laboratory. ACC: MOL.19980109.0250.

Wu, Y-S.; Haukwa, C.; and Bodvarsson, G.S. 1999. "A Site-Scale Model for Fluid and Heat Flow in the Unsaturated Zone of Yucca Mountain, Nevada." *Journal of Contaminant Hydrology*, 38, (1-3), 185-215. New York, New York: Elsevier. TIC: 244160.

Xu, T. and Pruess, K. 1998. *Coupled Modeling of Non-Isothermal Multi-Phase Flow, Solute Transport and Reactive Chemistry in Porous and Fractured Media: 1. Model Development and Validation*. LBNL-42050. Berkeley, California: Lawrence Berkeley National Laboratory. TIC: 243735.

Xu, T.; Pruess, K.; and Brimhall, G. 1998. *An Improved Equilibrium-Kinetics Speciation Algorithm for Redox Reactions in Variably Saturated Subsurface Flow Systems*. LBNL-41789. Berkeley, California: Lawrence Berkeley National Laboratory. TIC: 240019.

Yunker, J.L. 1999. "Question from Nuclear Waste Technical Review Board Regarding Variable Hydrologic Properties in Subunits of Potential Repository Emplacement Horizon." Letter from J.L. Yunker (M&O) to Dr. S.J. Brocoum and R.E. Spence (DOE), May 11, 1999, LV.NS.JLY.05/99-020, with enclosure. ACC: MOL.19990520.0184.

Zimmerman, R.W. and Bodvarsson, G.S. 1996. "Effective Transmissivity of Two-Dimensional Fracture Networks." *International Journal of Rock Mechanics and Mining Sciences & Geomechanics Abstracts*, 33, (4), 433-438. Oxford, United Kingdom: Pergamon Press. TIC: 245649.

Zyvoloski, G.; Dash, Z.; and Kelkar, S. 1992. *FEHMN 1.0: Finite Element Heat and Mass Transfer Code*. LA-12062-MS, Rev. 1. Los Alamos, New Mexico: Los Alamos National Laboratory. ACC: NNA.19910625.0038.

Zyvoloski, G.A.; Robinson, B.A.; Dash, Z.V.; and Trease, L.L. 1997. *User's Manual for the FEHM Application – A Finite-Element Heat- and Mass-Transfer Code*. LA-13306-M. Los Alamos, New Mexico: Los Alamos National Laboratory. TIC: 235999.

## 6.2 CODES, STANDARDS, REGULATIONS, AND PROCEDURES

64 FR 46976. 40 CFR 197: Environmental Radiation Protection Standards for Yucca Mountain, Nevada; Proposed Rule. Readily Available

64 FR 67054. 10 CFR Parts 960 and 963. Office of Civilian Radioactive Waste Management; General Guidelines for the Recommendation of Sites for Nuclear Waste Repositories; Yucca Mountain Site Suitability Guidelines. Readily Available

64 FR 8640. Disposal of High Level Radioactive Wastes in a Proposed Geologic Repository at Yucca Mountain. Readily Available

AP-2.13Q, Rev. 0, ICN 1. *Technical Product Development Planning*. Washington, D.C.: U.S. Department of Energy, Office of Civilian Radioactive Waste Management. ACC: MOL.19991115.0230.

AP3.10Q, Rev 2, ICN 2. *Analyses and Models*.

AP-3.11Q, Rev. 1, ICN 2. *Technical Reports*. Washington, D.C.: U.S. Department of Energy, Office of Civilian Radioactive Waste Management. ACC: MOL.20001026.0083.

AP-3.12Q, Rev 0, ICN 2. *Calculations*. Las Vegas, Nevada: ACC: MOL.20000620.0068.

AP-3.15Q, Rev. 2, ICN 0. *Managing Technical Product Inputs*. Washington, D.C.: U.S. Department of Energy, Office of Civilian Radioactive Waste Management. ACC: MOL.20001109.0051.

AP-SIII.2Q, Rev 0, ICN 2. *Procedure for Qualification of Unqualified Data and the Documentation of Rationale for Accepted Data*. Las Vegas, Nevada. ACC: MOL.20000217.0150.

QAP-2-0, Rev. 5. *Conduct of Activities*. Las Vegas, Nevada: CRWMS M&O. ACC: MOL.19980826.0209.

## 6.3 SOURCE DATA, LISTED BY DATA TRACKING NUMBER

LL000314304242.094. NUFT Calculation LBT Sensitivity Calcs. Submittal date: 03/28/2000.

LL000509112312.003. TSPA-SR Multiscale TH Results (E0120) Mean Calculations Using Drift Scale Property Set. Submittal date: 05/18/2000.

LL970803004244.036. Data on Temperature of the Large Block Test (LBT). Submittal date: 08/08/1997.

LL970803104244.037. Data on Displacement of the Large Block Test (LBT).  
Submittal date: 08/08/1997.

LL980913304244.072. Data Submission Report for Electrical Resistance Tomography Results  
Obtained During the Large Block Test FY98. Submittal date: 09/24/1998.

LL980919304244.075. Neutron Logging Activities at the Large Block Test (LBT).  
Submittal date: 09/30/1998.

LL990702804244.100. Borehole and Pore Water Data. Submittal date: 7/13/1999.

LL990708904243.033. Drift Scale Test (DST) Neutron Logging Data Report.  
Submittal date: 07/29/1999.

MO9807DSTSET01.000. Drift Scale Test (DST) Temperature, Power, Current, Voltage Data  
for November 7, 1997 through May 31, 1998. Submittal date: 07/09/1998.

MO9810DSTSET02.000. Drift Scale Test (DST) Temperature, Power, Current, Voltage Data  
for June 1 through August 31, 1998. Submittal date: 10/09/1998.

MO9906DSTSET03.000. Drift Scale Test (DST) Temperature, Power, Current, and Voltage  
Data for September 1, 1998 through May 31, 1999. Submittal date: 06/08/1999.

INTENTIONALLY LEFT BLANK

**APPENDIX A**  
**STATUS OF TH MODELS IMPLEMENTED BY THE NUFT COMPUTER CODE**



## A.1 TH MODEL TESTING USING NUFT

NUFT is an integrated suite of software for numerical solution of a conceptual model of thermal and isothermal flow and transport in porous media, with application to subsurface contaminant transport problems. The code simulates the coupled transport of heat and multiple multicomponent fluid phases in porous and fractured media. The medium may be modeled as a single porous continuum, an equivalent porous continuum, or multiple continua consisting of porous and fractured media. Components may be volatile. Grid systems may be Cartesian or cylindrical, with one, two, or fully three-dimensional configurations possible. The active fracture concept (Liu et al. 1998) is one of the options available for handling fluid flow with the DKM.

A validation test plan was prepared as is required by the Software Activity Plan for qualification and certification of NUFT Version 3.0s. The Integration Test Case Suite consists of twenty-seven test cases. The cases are identified as *bmrk001* through *bmrk018*, *vsam1* through *vsam6*, and *verif01* through *verif03*. The problems are one-, two-, or fully three-dimensional, solved using the Cartesian coordinate system. The code was tested by benchmarking against NUFT 2.0s or by comparison with analytical solutions. All benchmarking problems were earlier benchmarked against the VTOUGH code.

The test cases are generally two-phase and two-component problems that may be thermal or isothermal. The phases are liquid and gas, and the components are water and air. Air is treated as a pseudo-component with averaged properties. In some problems, it was necessary to isolate a physical process for examination by turning off other processes. For example, vapor diffusion and liquid flow are turned-off to examine code performance in modeling gas flow driven by pressure gradients. In other problems, multiple processes are addressed.

The goal with *bmrk001* through *bmrk017* is to test the TH model's treatment of specific hydrologic and thermal processes that are central to nuclear-waste isolation at Yucca Mountain. In some cases, a single process is isolated and examined, while in others, two or three process are examined. All *bmrk* problems are 1-D.

The code's restart capability is tested using *bmrk018*. This test case is identical to *bmrk001*, except that execution is stopped at an earlier time and a restart file printed. The restart file is then used to prescribe initial conditions for a restart run.

The *vsam* test cases for NUFT, *vsam1* through *vsam6*, are one- and two-dimensional problems taken from the TOUGH manual. These problems were used in testing the TOUGH code, and later, in the qualification of VTOUGH and NUFT 2.0. Like the *bmrk* problems, the *vsam* problems examine many of the thermo-hydrologic processes that are important to nuclear waste disposal at the proposed repository site in Yucca Mountain. However, *vsam2* through *vsam6* address more practical problems that examine multiple interacting processes, in 1-D and 2-D. As with the *bmrks*, the code was tested by benchmarking against NUFT 2.0s.

The capability of NUFT to accurately solve three-dimensional problems was tested using *verif01*. This test problem addresses heat conduction in a rectangular parallel pipe. The numerical solution was compared with an analytical solution.

Radiant heat transfer was included in *verif03* and the NUFT nested-mesh option in *verif02*. Active fracture simulation is addressed in *verif04*, evaporative flux in *verif05*, and the dual permeability option is tested in *verif06*.

## A.2 HISTORICAL TH MODEL TESTING

Lee et al. (1993) presented preliminary verification and benchmark testing of NUFT. In this initial phase of model testing, seven one-dimensional fluid flow and thermal energy transport problems were solved. The primary objective was to examine model applicability for general field and laboratory problems.

The term "verification" implies checking of the governing equations of the mathematical model to ensure that they have been properly programmed, and that the numerical solution algorithm works as intended. Code verification was performed by making direct comparisons between NUFT simulation results and known analytical or semi-analytical solutions of appropriate problems.

Analytical and semi-analytical solutions are available for only a limited range of problems of interest, often with highly simplifying assumptions. Therefore, verification does not necessarily imply a fully debugged code, but suggests that the main program of the code and its frequently used subroutines are functioning adequately.

In order to test the performance of the code on real or hypothetical field and laboratory problems for which analytical solutions were not available, code calculations were directly compared with well-established codes that had been previously tested. Benchmarking is used here to imply this kind of code-to-code comparison using test problems that are more realistic and are of practical interest. A relative or comparative validity is established if the results of such a code intercomparison show some acceptably low deviation. Through benchmarking, the credibility of a well-established code in solving some specific type of problem can be transferred to another code.

The test problems were selected from a report on the verification and benchmark testing of the UNSAT-H computer code (Baca and Magnuson 1990).

The test problems are classified as isothermal and thermal. The seven problems solved comprise four isothermal and three thermal problems. A brief description of each of them follows:

1. VI-1. Philips Solution for a Vertical Column. This first isothermal test case is a verification problem addressing vertical unsaturated flow in a laboratory soil column. It requires simulation of the rapid movement of a wetting front driven by gravity and capillary forces. This test is a direct check of the computational accuracy of the code in the solution of Richardss equation.
2. BI-1. Vertical Flow in a Laboratory Soil Column with Ponding. This is a benchmark problem addressing vertical flow in a relatively dry laboratory soil column under ponded conditions. The problem is similar to VI-1, except a constant ponding height is maintained at the upper boundary. This problem tests the capability of the model to handle strong nonlinearities and high-pressure gradients. The NUFT simulation

results are compared with the results from three other codes: INSAT-H, FLASH, and TOUGH.

3. BI-2. Infiltration in a Stratified Vadose Zone. This benchmark problem addresses infiltration in a thick, relatively dry, multilayered vadose zone located in a semiarid environment. The simulation deals with moisture movement through desiccated soils of highly variable hydrologic properties. It is assumed that the system is initially at steady state, receiving recharge at a constant rate. The recharge rate is then drastically reduced, and the response of the system, as it adjusts to the new recharge rate and eventually approaches a new steady state, is simulated. This type of problem is usually difficult to solve numerically, and provides a good test of the code's numerical solution technique. NUFT is benchmarked against UNSAT-H.
4. BI-3. Partially Saturated Flow in Basalt. This problem requires simulation of unsaturated flow through a layered field site. The site considered is the vadose zone beneath the Radioactive Waste Management Complex of the Idaho National Environmental and Engineering Laboratory. The geology consists of surficial sediments underlain by flows of vesicular and massive basalt (Baca and Magnuson 1990). This test case will evaluate the model performance in simulating flow at field site using data obtained from laboratory and field measurements. NUFT is benchmarked against UNSAT-H.
5. VT-1. Heat Conduction with Sinusoidal Boundary Conditions. This nonisothermal problem presents a direct test of the ability of the code to solve the energy equation for purely conductive heat transfer with a time-varying temperature boundary condition. The system is a homogeneous soil column at a uniform initial temperature and a sinusoidal boundary temperature. Fluid flow is turned-off to prevent convective heat transfer. The problem simulates the temperature distribution observed in soil, including diurnal temperature fluctuations. Simulation results from NUFT are compared with the closed-form analytical solution.
6. VT-2. Heat Conduction with Constant Heat Flux. This problem tests the ability of the code to solve the energy equation for purely conductive heat transfer with a constant heat-flux boundary condition. As with VT-1, the system is a homogeneous soil column at a uniform initial temperature, with fluid flow turned-off to prevent convection. NUFT results are compared with the closed-form analytical solution.
7. BT-1. Thermal History of a Vadose Zone. This verification problem is based on field studies of soil temperatures at Idaho National Environmental and Engineering Laboratory (Baca and Magnuson 1990). The objective is to simulate the soil temperature history. The geology consists of surficial sediments and basalts. The system is simplified to two soil layers, each with homogeneous thermal properties. The surface boundary condition reflects seasonal temperature changes. The simulation results from NUFT are compared to results from UNSAT-H.

In this initial phase of verification and benchmark testing, the NUFT code was used to solve seven 1-D unsaturated-flow and heat-transfer problems. Three verification and four

benchmarking problems were solved. Verification was performed by making direct comparisons between NUFT simulation results and known analytical or semianalytical solutions. Benchmark testing was done by comparing NUFT simulation results with the results from well-established and previously tested codes, using field and laboratory problems for which analytical solutions are not available.

In the verification testing, agreement was observed between NUFT results and the analytical solutions. In the benchmark testing, results of code intercomparison were satisfactory.

From these testing results, it was concluded that the TH model and NUFT code were ready for application to the types of unsaturated-flow and heat-transport problems addressed here. Additional code testing is ongoing including, multidimensional problems with chemical-transport.

**APPENDIX B**

**ISSUES IDENTIFIED BY REVIEW GROUPS,  
AND PMR APPROACH FOR RESOLUTION**



## APPENDIX B

### 7. ISSUES IDENTIFIED BY REVIEW GROUPS, AND PMR APPROACH FOR RESOLUTION

This appendix was developed from a review of the TSPA Peer Review Panel (Budnitz et al. 1999), the NF/AZ Coupled Effects Expert Elicitation (CRWMS M&O 1998a) and correspondence and reports of the Nuclear Waste Technical Review Board and the NRC's Advisory Committee for Nuclear Waste.

Source	Description of Issue	PMR Approach
<p>Performance Assessment Peer Review Panel (PA PRP) (Budnitz 1999)</p>	<p>Concerning coupled processes and the data and models that support them, the Panel believes that it may be beyond the capabilities of current analytical methodologies to analyze system of such scales and complexity. For this reason, the effects of coupled processes can probably be best dealt with through a combination of bounding analyzes and engineered features designed to minimize the effects of such processes.</p>	<p>The EDA-II design provides for minimization of the effects through reduction in temperatures of the drift wall.</p> <p>The effects of coupled processes are modeled, as discussed in part, in Section 3.3 and 3.4 of this PMR based on ranges of properties and climates. Section 3.3 describes the models used to evaluate the potential effects of coupled THC processes on permeability and porosity within the NF. Section 3.4 describes the abstraction of the models used to evaluate the potential effects of coupled THC processes on UZ flow and transport. The confidence in coupled-process models is based on on-going field tests, which indicate that these models are generally appropriate.</p> <p>The effects of coupled processes are also described in other PMRs. The THC couplings under consideration for the engineered systems are included in the EBS Degradation, Flow, and Transport PMR (CRWMS M&amp;O 2000g), the Waste Package Degradation PMR (CRWMS M&amp;O 2000o), and the Waste Form Degradation PMR (CRWMS M&amp;O 2000ab). THC couplings for the natural system are included in both the UZ F&amp;T PMR (CRWMS M&amp;O 2000f) and this PMR.</p>
<p>PA PRP (Budnitz 1999)</p>	<p>The coupled effects and their absence from the TSPA-VA are a significant cause of concern to the Panel. In the opinion of the Panel, the assumptions made in the TSPA-VA that the effects of THC activities will be short-lived and can be neglected are not warranted.</p>	<p>The effects of coupled processes are modeled, in part, in Section 3.3 and 3.4 of this PMR. Section 3.3 describes the models used to evaluate the potential effects of coupled THC processes on permeability and porosity within the NF. Section 3.4 of this PMR describes the abstraction of the models used to evaluate the potential effects of coupled THC processes on UZ flow and transport. The conclusions from these analyses were that THC effects for the EDA II design were not significant and therefore, can be neglected regardless of their duration.</p> <p>The effects of coupled processes are also described in other PMRs. The THC couplings under consideration for the engineered systems are included in the EBS Degradation, Flow, and Transport PMR (CRWMS M&amp;O 2000g), the Waste Package Degradation PMR (CRWMS M&amp;O 2000o), and the Waste Form Degradation PMR (CRWMS M&amp;O 2000ab). THC couplings for the natural system are included in both the UZ F&amp;T PMR (CRWMS M&amp;O 2000f) and this PMR.</p>

**APPENDIX B**  
**ISSUES IDENTIFIED BY REVIEW GROUPS, AND PMR APPROACH FOR RESOLUTION (Continued)**

Source	Description of Issue	PMR Approach
PA PRP (Budnitz 1999)	The Panel believes that there are some complicating factors in analyzing the thermal processes that need further attention. The Panel suggested testing the abstraction methodology against the DST.	One of the objectives of the DST, as discussed in detail in the <i>Thermal Test AMR</i> , was to evaluate the impact of differing property sets and their impact on model results. Section 3.6 of this PMR describes the thermal tests, including the SHT, LBT, and the DST. Section 3.4 describes the abstraction of the models used to evaluate the potential effects of coupled THC processes on unsaturated zone flow and transport. The <i>Thermal Test AMR</i> (CRWMS M&O 2000q, Chapter 1) describes how a comparative analysis is performed of measurements from the thermal tests to results from the numerical simulations. These form the bases for the conclusions presented in the AMR.
PA PRP (Budnitz 1999)	Although the effects of thermal-mechanical interactions have not been included in the TSPA-VA, the Panel believes that they cannot be neglected.	This PMR considers changes in hydrological properties because of THM. Section 3.5 of this PMR describes the results of THM calculations performed to estimate bounds on changes in fracture permeability in rock surrounding emplacement drifts. The results of these calculations are input to the UZ F&T PMR (CRWMS M&O 2000f).
PA PRP (Budnitz 1999)	A substantial part of fundamental scientific work on the relevant geochemical processes and conditions remains to be done. The Panel emphasizes their concern that this work be completed; however, given the magnitude of the experimental programs required, they suspect much will be lacking at the time of LA.	Design changes implemented after TSPA-VA and incorporated in the EDA II design include reduced temperatures in the rock, a drip shield, different waste package design/materials, and a different ground support system. This reduces the need for studies, although it does not eliminate it. Furthermore, as described below, field studies continue. Section 3.6 of this PMR describes the thermal tests, including the SHT, the DST, and the LBT. The thermal testing program is designed for a duration that extends beyond the LA submittal date. This is required because of the temporal and geometrical scales needed to be somewhat representative of the repository conditions. However, the testing program will be sufficiently complete to allow testing of the conceptual and numerical models of the thermal heating period and with information from LBT and SHT, the cool down period can be represented, although testing will be incomplete. DOE is in the process of designing a Performance Confirmation program that will allow additional testing and model confidence-building to occur throughout the licensing process.

**APPENDIX B**  
**ISSUES IDENTIFIED BY REVIEW GROUPS, AND PMR APPROACH FOR RESOLUTION (Continued)**

Source	Description of Issue	PMR Approach
PA PRP (Budnitz et al. 1999)	Given this level of complexity, the Project staff should consider the degree to which they can expect to successfully model the NFE. There is considerable experience within the geochemical community in modeling equally complex systems (e.g., geothermal systems, natural analogue studies, studies of trace element behavior in natural systems). Even if critical parameters were well defined (e.g., incoming gas and water compositions); it would still be a formidable task to model the NFGE.	<p>Design changes implemented after TSPA-VA and incorporated in the EDA II design include reduced temperatures in the rock, a drip shield, different waste package design/materials, and a different ground support system (CRWMS M&amp;O 1999a, Table 603; and Wilkins and Heath 1999). This reduces the need for studies, although it does not eliminate it. Furthermore, field studies continue. The effects of coupled processes are modeled, in part, in Sections 3.3 and 3.4 of this PMR. Section 3.3 addresses models used to evaluate the potential effects of coupled THC processes on UZ flow and transport. Section 3.4 describes the abstraction of the models used to evaluate the potential effects of coupled THC processes on UZ flow and transport. These models provide the framework to evaluate THC coupled processes at DS, predict flow and transport behavior for specified thermal loading conditions, and predict the chemistry of waters and gases entering the emplacement drifts.</p> <p>The effects of coupled processes are also described in other PMRs. The THC couplings under consideration for the engineered systems are described in the EBS Degradation, Flow, and Transport PMR (CRWMS M&amp;O 2000g), the Waste Package Degradation PMR (CRWMS M&amp;O 2000o), and the Waste Form Degradation PMR (CRWMS M&amp;O 2000ab). THC couplings for the natural system are described in both the UZ F&amp;T PMR (CRWMS M&amp;O 2000f) and this PMR.</p>
TSPA-VA (CRWMS M&O 1998b, Volume 3, Section 6.5)*	Conceptual model of flow Differences have been found between results using the DK flow model and the equivalent-continuum flow model. The DK model allows for greater mobility of water in fractures, which has a great effect on modeled condensate build-up and drainage. A related flow issue, which could be important to thermal hydrology, is channelized flow, especially in discrete fractures. Such flow could greatly increase the spatial variability in the results by increasing the range of water flow rates contacting individual waste packages.	A description and treatment of DK models and ECMs is provided in the <i>Thermal Test AMR</i> (CRWMS M&O 2000q). As described in that AMR, flow of liquid, gas, and heat in the rocks for the model domain occurs in both the fractures and rock-matrix of the model domain. The fractures and rock-matrix are conceptualized as two separate, overlapping continua. This conceptual model is referred to as the DK model. The assumption that the fractures form a continuum for flow is consistent with fracture-mapping data, borehole videos, and interference air-permeability data obtained from the DST test block. An AFM has been incorporated to address issues of channelized flow. The UZ F&T PMR (CRWMS M&O 2000f) and EBS Degradation, Flow, and Transport PMRs (CRWMS M&O 2000g) include detailed descriptions of the conceptual flow models and their justifications. The thermal testing program provides data from which to determine model appropriateness. In general, it is found that the DK model, which includes an AFM, is able to match the field results. The DK model represents the trends of the processes occurring in the host rock during a thermal perturbation better than the ECM using the same hydrological properties.

\* The VA synthesized issues raised by internal and external parties, without attribution of the source of each issue

**APPENDIX B**  
**ISSUES IDENTIFIED BY REVIEW GROUPS, AND PMR APPROACH FOR RESOLUTION (Continued)**

Source	Description of Issue	PMR Approach
TSPA-VA (CRWMS M&O 1998b, Volume 3, Section 6.5)*	<p>Coupled processes</p> <p>A potentially important shortcoming of the thermal-hydrological calculations is the lack of coupling to thermal-mechanical and thermal-chemical processes. These issues have been addressed to a limited extent (see Section 3.3.1), but the full range of possible (or even likely) behaviors has not been analyzed. The Near Field Environment Expert Elicitation will aid in considering these issues, but it was not completed until after the TSPA-VA analyses were finished. Therefore, implementing the recommendations from the expert elicitation remains to be done.</p>	<p>Design changes implemented after TSPA-VA and incorporated in the EDA II design include reduced temperatures in the rock, a drip shield, different waste package design/materials, and a different ground support system. This reduces the need for studies, although it does not eliminate it. Furthermore, field studies continue.</p> <p>The coupling of THC to TM and TC processes has been investigated and is described in Chapter 3 of this PMR. The <i>Thermal Test AMR</i> (CRWMS M&amp;O 2000q) describes both the DST and LBT. The purpose of the DST is to evaluate coupled thermal, hydrological, chemical, and mechanical processes that take place in unsaturated, fractured tuff over a range of temperatures from approximately 25°C to nearly 100°C. The scale of the DST allows investigation of the NFE and associated coupled thermal, hydrological, chemical, and mechanical processes on an emplacement-drift scale. In addition, the objective of the LBT was to create a planar, horizontal region of boiling in fractured-welded Topopah Spring tuff, to observe coupled THMC behavior in a block representative of the repository horizon rock.</p> <p>See Section 2.4.5 of this PMR for a summary of the NFE expert elicitation. Recommendations from the NF expert elicitation were not used directly, because the expert-elicitation recommendations were already bounded by the NF seepage abstraction.</p>
TSPA-VA (CRWMS M&O 1998b, Volume 3, Section 6.5)*	<p>Thermal alterations of hydrological properties</p> <p>Thermal alterations of flow and thermal-hydrological-chemical or thermal-hydrological-mechanical alterations of hydrological properties are potentially important. In the current TSPA structure, these effects fall under the thermal-hydrology component, but thermal-hydrological effects could be more closely coupled with mountain-scale UZ flow and transport, if necessary.</p>	<p>The UZ F&amp;T PMR (CRWMS M&amp;O 2000f) addresses the effects of coupled THC on seepage and flow. In addition, Section 3.3 of this PMR addresses models used to evaluate the potential effects of coupled THC processes on UZ flow and transport.</p>

\* The VA synthesized issues raised by internal and external parties, without attribution of the source of each issue

**APPENDIX B**  
**ISSUES IDENTIFIED BY REVIEW GROUPS, AND PMR APPROACH FOR RESOLUTION (Continued)**

Source	Description of Issue	PMR Approach
TSPA-VA (CRWMS M&O 1998b, Volume 3, Section 6.5)*	<p>Thermal response of different hydrogeologic units</p> <p>The single heater test and the heated drift test are both located in the Topopah Spring middle nonlithophysal hydrogeologic unit. However, in the current repository design most of the emplacement drifts are in the Topopah Spring lower lithophysal unit, with some drifts in the middle nonlithophysal unit and others in the lower nonlithophysal unit. Confidence in the models would be enhanced by obtaining thermal response data in the other two units.</p>	<p>The Project has never maintained that the thermal testing program in the Topopah Spring middle nonlithophysal hydrogeologic unit was totally representative of the entire repository horizon (Yunker 1999). Nonetheless, the thermal testing program in the Topopah Spring middle Nonlithophysal hydrogeologic unit provides significant benefit to understanding coupled processes and thermal-mechanical properties of the Topopah Spring welded tuff.</p> <p>The recent completion of the ECRB cross drift through the Lower Lithophysal hydrogeologic unit offers the capability to extend thermal testing to the rock type in which most repository drifts will be located. The NWTRB recently questioned the general applicability of results from the DST. In response to these questions, several lines of evidence were reviewed and analyzed (Yunker 1999). It was concluded that the hydrological properties in all three subunits of the Topopah Spring welded tuff are sufficient to induce drainage of moisture flux that would be mobilized by the thermal pulse in a design concept that maintains pillars that are below boiling. The <i>Thermal Test AMR</i> (CRWMS M&amp;O 2000q) describes the thermal tests. As described in that AMR, although the DST block is located in the Topopah Spring middle nonlithophysal stratigraphic unit (tsw34) at Yucca Mountain, stratigraphic units both above and below tsw34 are also included in the model domain of the DST.</p>
TSPA-VA (CRWMS M&O 1998b, Volume 3, Section 6.5)*	<p>Thermal-mechanical-chemical coupling</p> <p>Coupled models would benefit from incorporation of more details of drift materials, both their physical-mechanical evolution and chemically-induced changes to the hydrological properties of the engineered materials. These aspects would improve the description of water flow and radionuclide transport pathways and allow for development of more specific NFGE scenarios.</p>	<p>The THC couplings under consideration for the engineered systems are addressed in the EBS Degradation, Flow, And Transport PMR (CRWMS M&amp;O 2000g), the Waste Package Degradation PMR (CRWMS M&amp;O 2000o), and the Waste Form Degradation PMR (CRWMS M&amp;O 2000ab). THC couplings for the natural system are addressed in both the UZ F&amp;T PMR (CRWMS M&amp;O 2000f) and the NFE PMR. However, design changes have mitigated many of the concerns related to drift and engineered materials. The drift design no longer uses concrete liners and invert materials, and therefore the evolution of water chemistry associated with cementaceous materials is mitigated.</p>

\* The VA synthesized issues raised by internal and external parties, without attribution of the source of each issue

**APPENDIX B**  
**ISSUES IDENTIFIED BY REVIEW GROUPS, AND PMR APPROACH FOR RESOLUTION (Continued)**

Source	Description of Issue	PMR Approach
TSPA-VA (CRWMS M&O 1998b, Volume 3, Section 6.5)*	<p>Conceptual model of the NFGE</p> <p>The updated NFGE model could consider such topics as:</p> <p>Heterogeneity of water composition flowing through the fracture system and interacting with the drift environment</p> <p>Explicit CO<sub>2</sub> evolution from water and minerals coupled to the gas flow in the thermal-hydrological system</p> <p>Explicit coupling of flow and geochemical reactions</p>	<p>Section 3.3 of this PMR addresses models used to evaluate the potential effects of coupled THC processes on UZ flow and transport. This includes a complete description of the pertinent description of the mineral-water processes in the host rock and their effect on the NFE. The model is used to evaluate the effects of mineral dissolution and precipitation, the effects of CO<sub>2</sub> exsolution and transport in the region surrounding the drift, the potential for forming calcite, silica or other mineral assemblage "precipitation caps", and the resulting changes to porosity, permeability and seepage. Water chemistry evaluation and the heterogeneity of water composition flowing through the fracture system and interacting with the drift environment are addressed in Section 3.3.4.</p> <p>These topics are also addressed in the UZ F&amp;T PMR (CRWMS M&amp;O 2000f) and EBS Degradation, Flow, And Transport PMR (CRWMS M&amp;O 2000g).</p>
TSPA-VA (CRWMS M&O 1998b, Volume 3, Section 6.5)*	<p>Consideration of All Significant Features and Processes in the Performance Assessment</p> <p>Modeling assumptions should be consistent across different process models, unless there is a defensible technical rationale.</p>	<p>The AMRs that document assumptions have been subjected to thorough interdisciplinary reviews to help ensure consistency among assumptions made in more than one document about a given parameter. In addition, the PMRs that summarize and integrate the results of the AMRs have been subjected to a review by a single review team, one of whose main objectives is to identify inconsistencies among the PMRs.</p>
NF Expert Elicitation (CRWMS M&O 1998a)	<p>Thermal-Mechanical</p> <p>Assess the mechanical stability of the host rock in the NFE, where rock-mass failure can cause linear collapse, leading to rockfall into the emplacement drifts. Describe the processes in the thermal evolution of the repository, that will contribute to NF mechanical stability, both during the period of increasing or stable elevated temperature, and during cool down. Consider changes, if any, that would occur solely from thermal and thermal-mechanical causes.</p>	<p>This issue is discussed in the EBS Degradation, Flow, and Transport PMR (CRWMS M&amp;O 2000g). Furthermore, design changes, specifically the addition of a drip shield and potential changes regarding backfill and drift orientation, minimize these impacts. This PMR considers changes in rock mass properties, specifically hydrological properties, because of THM. Section 3.5 of the NFE PMR describes the results of THM calculations performed to estimate bounds on changes in fracture permeability in rock surrounding emplacement drifts. The results of these calculations are input to UZ F&amp;T PMR (CRWMS M&amp;O 2000f). The results will also be input to the EBS Degradation, Flow, and Transport PMR (CRWMS M&amp;O 2000g) for evaluation of impact on drift stability.</p>

\* The VA synthesized issues raised by internal and external parties, without attribution of the source of each issue

**APPENDIX B**  
**ISSUES IDENTIFIED BY REVIEW GROUPS, AND PMR APPROACH FOR RESOLUTION (Continued)**

Source	Description of Issue	PMR Approach
<p>NFEE (CRWMS M&amp;O 1998a)</p>	<p><b>Thermal-Hydrological-Chemical</b></p> <p>Assess the impact of dissolution and precipitation in reflux zones, on fracture porosity and permeability above the emplacement drifts, and in pillars between drifts where drainage occurs in thermal-hydrological simulations conducted for the TSPA-VA base case. Describe the changes, if any, that would occur solely from these chemical causes, both during the period of maximum thermal-hydrological activity before the reflux zone begins to contract, and during the cool down.</p> <p>Assess the impact of mineral alteration (to secondary forms with different physical hydrological properties) on fracture porosity and permeability above the emplacement drifts and along pathways where drainage occurs in thermal-hydrological simulations conducted for the TSPA-VA base case. Describe the changes if any, that would occur solely both during the period of maximum thermal-hydrological activity before the reflux zone begins to contract, and during cool down.</p> <p>Assess changes in fracture-matrix coupling that may result from reflux activity. Describe the location, intensity, and irreversibility of such changes.</p> <p>Assess multiple effects from dissolution and alteration, and from thermal and thermal-mechanical processes, on the porosity, permeability, and mechanical stability of fracture pathways for drainage below the emplacement drifts.</p> <p>Assess the durability of any fracture porosity and permeability changes caused by dissolution and precipitation, or by mineral alteration, as the host rock cools. Consider redissolution of precipitates and mechanical adjustment of the rock mass during cooling. Identify any processes that are likely to dominate the long-term hydrological response of the rock mass.</p>	<p>These issues are addressed in both the UZ F&amp;T PMR (CRWMS M&amp;O 2000f) and this PMR. Section 3.3 of this PMR addresses models used to evaluate the potential effects of coupled THC processes on hydrological properties while the UZ F&amp;T PMR (CRWMS M&amp;O 2000f) addresses impact of these changes on UZ flow and transport. These models provide the framework to evaluate THC coupled processes at DS, predict flow and transport behavior for specified thermal-loading conditions, and predict the chemistry of waters and gases entering the emplacement drifts. This includes a complete, pertinent description of the mineral-water processes in the host rock and their effect on the NFE. The model is used to evaluate the effects of mineral dissolution and precipitation, the effects of CO<sub>2</sub> exsolution and transport in the region surrounding the drift, the potential for forming calcite, silica or other mineral assemblage "precipitation caps", and the resulting changes to porosity, permeability and seepage. Dissolution and precipitation are the primary impacts on FMXs.</p> <p>Section 3.5 of this PMR addresses models used to evaluate TM effects on permeability.</p>

**APPENDIX B**  
**ISSUES IDENTIFIED BY REVIEW GROUPS, AND PMR APPROACH FOR RESOLUTION (Continued)**

Source	Description of Issue	PMR Approach
NFEE (CRWMS M&O 1998a)	Uncertainties in the near field need to be addressed.	<p>THC couplings for the natural system are addressed in both the UZ F&amp;T PMR (CRWMS M&amp;O 2000f) and this PMR. The THC couplings under consideration for the engineered systems are addressed in the EBS Degradation, Flow, and Transport PMR (CRWMS M&amp;O 2000g), the Waste Package Degradation PMR (CRWMS M&amp;O 2000o), and the Waste Form Degradation PMR (CRWMS M&amp;O 2000ab). The UZ F&amp;T PMR addresses the effects of coupled THC on seepage and flow. Section 3.3 of this PMR addresses the drift-scale coupled process models used to evaluate the potential effects of coupled THC processes on properties within the NFE, which are then used in evaluations of UZ flow and transport. Temporal and spatial variations of properties or conditions used in this PMR were consistent with the UZ F&amp;T PMR (CRWMS M&amp;O 2000f). In addition, this PMR considered spatial and temporal variations in conditions that arise from the emplacement of waste and the EBS. This information was based on the multi-scale abstraction reported in the EBS Degradation, Flow, and Transport PMR (CRWMS M&amp;O 2000g), as well as in the <i>THC Abstraction AMR</i> (CRWMS M&amp;O 2000c) and the <i>NFE FEPs AMR</i> (CRWMS M&amp;O 2000e) that support this PMR.</p>
NFEE (CRWMS M&O 1998a)	NF chemical effects on the flow regime are not addressed in the PA and neither are temporal changes in NF chemistry.	<p>Section 3.3 of this PMR describes the models used to evaluate the potential effects of coupled THC processes on permeability and porosity within the NF. Section 3.4 describes the abstraction of the models used to evaluate the potential effects of coupled THC processes on UZ flow and transport. Temporal and spatial variations of properties or conditions used in this PMR were consistent with the UZ F&amp;T PMR (CRWMS M&amp;O 2000f). In addition, this PMR considered spatial and temporal variations in conditions that arise from the emplacement of waste and the EBS.</p> <p>THC couplings for the natural system are addressed in both the UZ F&amp;T PMR (CRWMS M&amp;O 2000f) and this PMR. The THC couplings under consideration for the engineered systems are addressed in the EBS Degradation, Flow, and Transport PMR (CRWMS M&amp;O 2000g), the Waste Package Degradation PMR (CRWMS M&amp;O 2000o), and the Waste Form Degradation PMR (CRWMS M&amp;O 2000ab). The UZ F&amp;T PMR (CRWMS M&amp;O 2000f) addresses the effects of coupled THC on seepage and flow.</p> <p>Results of THC analyses indicate that impact on flow is likely not to be significant. Section 3.3 of this PMR describes the models used to evaluate the potential effects of coupled THC processes on permeability and porosity in the NF. Section 3.4 describes the abstraction of the models used to evaluate the potential effects of coupled THC processes on UZ flow and transport. Temporal and spatial variations of properties or conditions used in this PMR were consistent with the UZ F&amp;T PMR (CRWMS M&amp;O 2000f). In addition, this PMR considered spatial and temporal variations in conditions that arise from the emplacement of waste and the EBS.</p>

**APPENDIX B**  
**ISSUES IDENTIFIED BY REVIEW GROUPS, AND PMR APPROACH FOR RESOLUTION (Continued)**

Source	Description of Issue	PMR Approach
NRC Letter dated June 2, 1999 (Paperiello 1999)	The data and models used in the VA to calculate the quantity and chemistry of water dripping on waste packages are inadequate to describe the process and extent of potential dripping under ambient and thermally-altered conditions.	The UZ F&T PMR (CRWMS M&O 2000f) addresses the effects of coupled THC on seepage and flow. The EBS Degradation, Flow, and Transport PMR (CRWMS M&O 2000g) describes the potential for seepage to contact waste packages. Section 3.3 of this PMR addresses the drift-scale coupled process models used to evaluate the potential effects of coupled THC processes on properties within the NFE, which are then used in evaluations of UZ flow and transport. The parameter values used in this PMR were the values either provided by the UZ F&T AMRs (CRWMS M&O 2000f) or used in their evaluations.
NRC Comments on TSPA-VA (Paperiello 1999)	The importance of characterizing the thermal perturbations to UZ flow fields during the heating phase and considering coupled thermal-hydrological-chemical-mechanical processes in PAs was raised in letters to DOE.	Section 3.3 of this PMR addresses the drift-scale coupled process models used to evaluate the potential effects of coupled THC processes on properties within the NFE, which are then used in evaluations of unsaturated zone flow and transport. The parameter values used in this PMR were the values either provided by the UZ F&T AMRs (CRWMS M&O 2000f) or used in their evaluations.  Section 3.6 of this PMR describes the thermal tests, including the Single Heater Test, the DST, and the LBT. The <i>Thermal Test AMR</i> (CRWMS M&O 2000a, Chapter 1) describes how the properties (and conceptual flow models) used to estimate in-drift thermodynamic environment and flow processes are compared to experimentally determined thermal-hydrological results.

**APPENDIX B**  
**ISSUES IDENTIFIED BY REVIEW GROUPS, AND PMR APPROACH FOR RESOLUTION (Continued)**

Source	Description of Issue	PMR Approach
<p>NRC Letter dated June 2, 1999 (Paperiello 1999)</p>	<p>Another issue is the appropriate role of data collected during performance confirmation, relative to data available at the time of construction authorization.</p>	<p>Section 3.6 of this PMR describes the thermal tests, including the SHT, the DST, and the LBT. The thermal testing program is designed for a duration that extends beyond the LA submittal date. This is required because of the temporal and geometrical scales needed to be somewhat representative of the repository conditions. However, data available at the time of construction authorization should be sufficiently complete to allow testing of the conceptual and numerical models of the thermal heating period. With the information from LBT and SHT, the cool down period can also be represented, although testing will be incomplete. DOE is in the process of designing a Performance Confirmation program that will allow additional testing and model confidence building to occur throughout the licensing process.</p>
<p>NRC Meeting 3/16/99 (NRC 1999d)</p>	<p>The DOE recognizes the chemical complexity of the near field, but the VA provides inadequate treatment of it. The chemical complexity of the NF needs to be addressed.</p>	<p>The effects of coupled processes are modeled, in part, in Section 3.2 and 3.3 of this PMR. Section 3.3 describes the models used to evaluate the potential effects of coupled THC processes on permeability and porosity within the NF. Section 3.4 of this PMR describes the abstraction of the models used to evaluate the potential effects of coupled THC processes on UZ flow and transport.</p> <p>The effects of coupled processes are also described in other PMRs. The THC couplings under consideration for the engineered systems are addressed in the EBS Degradation, Flow, and Transport PMR (CRWMS M&amp;O 2000g), the Waste Package Degradation PMR (CRWMS M&amp;O 2000o), and the Waste Form Degradation PMR (CRWMS M&amp;O 2000ab). THC couplings for the natural system are addressed by both the UZ F&amp;T PMR (CRWMS M&amp;O 2000f) and this PMR.</p> <p>The NFE THC models are being improved to reduce uncertainty in water chemistry and effects on hydrological properties that can affect seepage.</p>

**APPENDIX C**  
**NEAR-FIELD ENVIRONMENT FEATURES, EVENTS, AND PROCESSES**



## APPENDIX C

### NEAR-FIELD ENVIRONMENT FEATURES, EVENTS, AND PROCESSES

This appendix lists NFE FEPs. The process for developing and screening the FEPs is described in Section 2.5 of this PMR.

FEP Number	FEP Name and Description	Screening Decision	Screening Basis	PMR
1.1.02.00.00	Excavation/Construction. Excavation-related effects include changes to rock properties.	Fracture effects included/ chemistry effects excluded	Meets all criteria/low consequence	EBS UZ F&T
1.1.02.02.00	Effects of pre-closure ventilation. Controls the extent of the boiling front. Condensation of moisture as a result of ventilation onto a waste package should not occur during the preclosure period since the ventilation air is expected to be relatively dry and the air-flow rate will be high.	Include	Meets all criteria	EBS
1.2.02.01.00	Fractures. Generation of new fractures and re-activation of preexisting fractures may significantly change the flow and transport paths. Newly formed and reactivated fractures typically result from thermal, seismic, or tectonic events.	Exclude	Low consequence to dose (TBV)	UZ F&T SZ DE
2.1.08.01.00	Increased unsaturated water flux at the repository. Extremely rapid influx could reduce temperatures below the boiling point during part or all of the thermal period.	Include climate change/ exclude water quenching waste package	Meets all criteria/Low consequence to dose	UZ F&T EBS
2.1.08.02.00	Enhanced influx (Philip's drips). A mechanism for focusing unsaturated flow to an underground opening and producing local saturation.	Include	Meets all criteria	UZ F&T EBS
2.1.08.03.00	Repository dryout due to waste heat. The zone of reduced saturation migrates outward during the heating phase (about the first 1,000 years) and then migrates back to the containers as heat diffuses throughout the mountain and the radioactive sources decay.	Include	Meets all criteria	NFE UZ F&T
2.1.08.10.00	Desaturation or dewatering of the repository. "Dewatering" of rock at Yucca Mt occurs because of ventilation and because of repository heating. The UZ is unsaturated and "resaturation" (reentry of water to an equilibrium partial saturation) has a meaning different from that for a repository beneath the water table.	Include	Meets all criteria	NFE UZ F&T

**APPENDIX C**  
**NEAR-FIELD ENVIRONMENT FEATURES, EVENTS, AND PROCESSES (Continued)**

FEP Number	FEP Name and Description	Screening Decision	Screening Basis	PMR
2.1.08.11.00	<p>Resaturation of the repository.</p> <p>During resaturation (and sealing) of the repository, flow directions are different and the hydraulic conductivity is different. The conceptual flow models used in the process level thermal-hydrological models allowed rock matrix and fracture elements to resaturate as the repository cooled.</p>	Include	Meets all criteria	EBS
2.1.09.01.00	<p>Carrier plume forms in reestablishment of flow system and carries signature of repository (temp, pH, and solutes).</p> <p>It is likely that the flow system is reestablished before radionuclides are mobile. This reestablished flow system, which can be a locally saturated system (fracture flow) or a UZ flow system, carries the signature of the repository (e.g., pH, T, dissolved constituents, etc) and is termed the carrier plume</p>	Include	Meets all criteria	EBS
2.1.09.12.00	<p>Rind (altered-zone) formation in waste, EBS, and adjacent rock.</p> <p>Thermal-chemical processes alter the rock forming the drift walls mineralogically. These alterations have hydrological, thermal and mineralogic properties different from the current country rock.</p>	Included in THC model, but Excluded from TH models	Low consequence to dose	EBS
2.1.11.01.00	<p>Heat output/temperature in waste and EBS.</p> <p>Decay heat is a major issue in design. High loading density is intended to be part of the waste isolation scheme. Temperatures in the waste and EBS will vary through time.</p>	Include	Meets all criteria	EBS WF
2.1.11.02.00	<p>Non-uniform heat distribution/edge effects in repository.</p> <p>Temperature inhomogeneities in the repository lead to localized accumulation of moisture. Uneven heating and cooling at repository edges lead to non-uniform thermal effects during both the thermal peak and the cool-down period.</p>	Include/exclude TM effects	Meets all criteria/TM low consequence to dose (TBV)	NFE UZ F&T
2.2.01.01.00	<p>Excavation and construction-related changes in the adjacent host rock.</p> <p>Stress relief, leading to dilation of joints and fractures, is expected in an axial zone of up to one diameter width surrounding the tunnels.</p>	Exclude	Low Consequence to dose (TBV)	UZ F&T

**APPENDIX C**  
**NEAR-FIELD ENVIRONMENT FEATURES, EVENTS, AND PROCESSES (Continued)**

FEP Number	FEP Name and Description	Screening Decision	Screening Basis	PMR
2.2.01.02.00	<p>Thermal and other waste and EBS-related changes in the adjacent host rock.</p> <p>Changes in host-rock properties result from thermal effects or other factors related to emplacement of the waste and EBS, such as mechanical or chemical effects of backfill. Properties that may be affected include rock strength, fracture spacing and block size, and hydrological properties such as permeability.</p>	Exclude	Low consequence to dose (TBV)	
2.2.01.03.00	<p>Changes in fluid saturations in the excavation disturbed zone.</p> <p>During repository construction and operation, the near-field will partially desaturate, and the local hydrological regime may be disturbed. After backfilling, groundwater reenters host rock zones that were partially desaturated during the operational phase.</p>	Exclude	Low consequence to dose	
2.2.06.01.00	<p>Changes in stress (due to thermal, seismic, or tectonic effects) change porosity and permeability of rock.</p> <p>Even small changes in the fracture openings can cause large changes in permeability. The rock deforms according to the rock stress field. Changes in the groundwater flow and in the temperature field can change the stress acting on the rock, which in turn, can change the groundwater flow. However, it is estimated that the overall dose will not be sensitive to these permeability and flow path changes.</p>	Exclude	Low consequence to dose	DE
2.2.07.10.00	<p>Condensation zone forms around drifts.</p> <p>Repository design will affect the scale at which condensation caps form (over waste packages, over panels, or over the entire repository), and the extent to which "shedding" will occur as water flows from the region above one drift to the region above another drift or into the rock between drifts.</p>	Include	Meets all criteria	UZ F&T
2.2.07.11.00	<p>Return flow from condensation cap/resaturation of dryout zone.</p> <p>When the rocks have cooled enough, there is a return flow toward the drifts from the condensation cap as a plume of unsaturated flow.</p>	Include	Included in process models used in TSPA	UZ F&T

**APPENDIX C**  
**NEAR-FIELD ENVIRONMENT FEATURES, EVENTS, AND PROCESSES (Continued)**

FEP Number	FEP Name and Description	Screening Decision	Screening Basis	PMR
2.2.08.03.00	<p>Geochemical interactions in geosphere (dissolution, precipitation, weathering and effects on radionuclide transport).</p> <p>Effects on hydrological flow properties of the rock, radionuclide solubilities, sorption processes, and colloidal transport are relevant. Kinetics of chemical reactions should be considered in the context of the time scale of concern.</p>	Include	Meets all criteria	UZ F&T SZ
2.2.08.04.00	<p>Redissolution of precipitates directs more corrosive fluids to container.</p> <p>This FEP concerns chemical precipitation plugging pores during heating and dissolution of the plugs during cooldown. When the pores open, the corrosive water is released and drains into the drift.</p>	Include	Meets all criteria	EBS UZ F&T
2.2.10.04.00	<p>Thermal-mechanical alteration of fractures near repository.</p> <p>Heat from the waste causes thermal expansion of the surrounding rock, generating compressive stresses near the drifts and extensional stresses away from them. The zone of compression migrates with time.</p>	Exclude	Low consequence to dose (TBV)	UZ F&T
2.2.10.05.00	<p>Thermal-mechanical alteration of rocks above and below the repository.</p> <p>Thermal-mechanical compression at the repository produces tension-fracturing in the PTn and other units above the repository. These fractures alter UZ flow between the surface and the repository. Extreme fracturing may propagate to the surface, affecting infiltration. Thermal fracturing in rocks below the repository affects flow and radionuclide transport to the saturated zone.</p>	Exclude	Low consequence to dose (TBV)	UZ F&T
2.2.10.06.00	<p>Thermal-chemical alteration (solubility speciation, phase changes, precipitation and dissolution).</p> <p>Changes in the groundwater temperature in the far-field, if significant, may change the solubility and speciation of certain radionuclides. This would have the effect of altering radionuclide transport processes. Relevant processes include volume effects associated with silica phase changes, precipitation and dissolution of fracture-filling minerals (including silica and calcite), and alteration of zeolites and other minerals to clays.</p>	Exclude except for THC input to some geo-chemical models	Low consequence to dose (TBV)	UZ F&T SZ

**APPENDIX C**  
**NEAR-FIELD ENVIRONMENT FEATURES, EVENTS, AND PROCESSES (Continued)**

FEP Number	FEP Name and Description	Screening Decision	Screening Basis	PMR
2.2.10.10.00	<p>Two-phase buoyant flow and heat pipes.</p> <p>A heat-pipe consists of a system for transferring energy between a hot and a cold region, using the heat of vaporization and movement of the vapor as the transfer mechanism. Two-phase circulation continues until the heat source is too weak to provide thermal gradients required to drive it. Alteration of the rock adjacent to the drift produces may include dissolution that can maintain the permeability necessary to support circulation.</p>	Include	Meets all criteria	UZ F&T
2.2.10.12.00	<p>Geosphere dryout due to waste heat.</p> <p>Repository heat evaporates water near the drifts. The zone of reduced saturation migrates outward during the heating phase (about the first 1,000 years) and then migrates back to the containers as heat diffuses throughout the mountain and the radioactive sources decay. The extent and degree of dry-out depends on design and on the loading strategy for emplacement.</p>	Include	Meets all criteria	NFE UZ F&T
2.2.10.13.00	<p>Density-driven groundwater flow (thermal).</p> <p>The distribution of temperature within the crystalline basement is expected to be correlated with a distribution of groundwater density. Variations in density provide a driving force for groundwater flow. Density-driven flow is expected at Yucca Mountain, but with heat supplied by the repository. Based on the geothermal gradient and depth to the basement rocks, there is not likely to be any significant thermal contribution from the deep rocks.</p>	Include	Meets all criteria	SZ

INTENTIONALLY LEFT BLANK

**APPENDIX D**

**ISSUE RESOLUTION STATUS REPORTS, SUBISSUES,  
TECHNICAL ACCEPTANCE CRITERIA, AND PMR APPROACH**



## APPENDIX D

**ISSUE RESOLUTION STATUS REPORTS, SUBISSUES,  
TECHNICAL ACCEPTANCE CRITERIA, AND PMR APPROACH**

This appendix was developed from an analysis of the NRC's KTIs for the ENFE (NRC 1999a), Thermal Effects on Flow (NRC 1999b), Repository Design and Thermal-Mechanical Effects (NRC 1999c), and Total System Performance Assessment and Integration (NRC 2000). The table shows the location in YMP PMRs where each acceptance criterion applicable to the NFE is addressed.

NRC Acceptance Criteria	PMR Approach and Section Reference
<b>IRSR: EVOLUTION OF THE NEAR-FIELD ENVIRONMENT</b>	
<b>SUBISSUE 1 - EFFECTS OF COUPLED THC PROCESSES ON SEEPAGE AND FLOW</b>	
<b>Data and Model Justification Acceptance Criteria</b>	
<p>1 - Available data relevant to both temporal and spatial variations in conditions affecting coupled THC effects on seepage and flow were considered.</p>	<p>Section 3.3 of the NFE PMR describes the models used to evaluate the potential effects of coupled THC processes on permeability and porosity within the NFE. The <i>THC Process AMR</i> (CRWMS M&amp;O 2000b) describes how available data relevant to both temporal and spatial variations in conditions affecting coupled THC effects are considered. In addition, Section 3.10 of the UZ F&amp;T PMR (CRWMS M&amp;O 2000f) documents the abstraction of coupled THC effects for TSPA, based on the process modeling results presented in the same section.</p>
<p>2 - DOE's evaluation of coupled THC processes properly considered site characteristics in establishing initial and boundary conditions for conceptual models and simulations of coupled processes that may affect seepage and flow.</p>	<p>Section 3.3 of the NFE PMR describes the models used to evaluate the potential effects of coupled THC processes on permeability and porosity within the NFE. This information is contained in the <i>THC Process AMR</i> (CRWMS M&amp;O 2000b) that describes how available data relevant to both temporal and spatial variations in conditions affecting coupled THC effects are considered. In addition, the UZ F&amp;T PMR (CRWMS M&amp;O 2000f) summarizes available data used to establish initial and boundary conditions for the evaluation of THC effects on seepage and flow in the near field.</p>

NRC Acceptance Criteria	PMR Approach and Section Reference
<p>5 - If the testing program for coupled THC processes on seepage and flow is not complete at the time of LA, or if sensitivity and uncertainty analyses indicate additional data are needed, DOE will identify specific plans to acquire the necessary information as part of the performance confirmation program.</p>	<p>All of the information needed to support the LA will be complete prior to the LA. Arguments presented in the LA will be based on testing and analysis conducted before LA and considered in the licensing review. Testing contained in the performance confirmation program is confirmatory. The performance confirmation program addresses coupled THC effects associated with the rock mass cooling response, coupled process testing, and seepage testing under heated environments during the pre-emplacment period. Longer term testing for seepage and NF THC testing and monitoring around selected emplacement drifts and under simulated postclosure conditions is also addressed. Testing of the in-drift environments is included as well. See the Performance Confirmation Plan (CRWMS M&amp;O 2000z, Sections 5.3.1.2, 5.3.1.4, 5.3.1.5, 5.3.2, and Appendix G).</p>
<p>Acceptance Criteria within this sub-element addressed by other PMRs include:</p> <p>3 – UZ F&amp;T, EBS</p> <p>4 – UZ F&amp;T</p>	<p>See Table 4.3-1 of the UZ F&amp;T PMR and Appendix A of the EBS PMR (CRWMS M&amp;O 2000f and 2000g) for additional information regarding these acceptance criteria.</p>
<p><b>Data Uncertainty and Verification Acceptance Criteria</b></p>	
<p>1 - Reasonable or conservative ranges of parameters or functional relations were used to determine effects of coupled THC processes on seepage and flow. Parameter values, assumed ranges, probability distributions, and bounding assumptions are technically defensible and reasonably account for uncertainties.</p>	<p>Section 3.3 of this PMR addresses the DSCP models used to evaluate the potential effects of coupled THC processes on properties in the NFE, which are then used in evaluating UZ flow and transport. The parameter values used in this PMR were the values either provided by the UZ F&amp;T AMRs or used in their evaluations. Section 3.10.3 of the UZ F&amp;T PMR (CRWMS M&amp;O 2000f) discusses ranges in the characteristics of the natural system that were used to evaluate the effects of THC processes on seepage and flow, and the rationale for these ranges.</p>
<p>2 - Uncertainty in data due to both temporal and spatial variations in conditions affecting coupled THC effects on seepage and flow were considered.</p>	<p>Section 3.3 of this PMR addresses the DSCP models used to evaluate the potential effects of coupled THC processes on properties in the NFE, which are then used in evaluations of UZ flow and transport. Temporal and spatial variations of properties or conditions used were consistent with the UZ F&amp;T PMR (CRWMS M&amp;O 2000f). In addition, spatial and temporal variations in conditions that arise from the emplacement of waste and the EBS were considered. This information was based on the multi-scale abstraction reported here, as well as in the <i>THC Abstraction AMR</i> (CRWMS M&amp;O 2000c) and the <i>NFE FEPs AMR</i> (CRWMS M&amp;O 2000e) that support this PMR. Section 3.10.6 of the UZ F&amp;T PMR (CRWMS M&amp;O 2000f) discusses the uncertainty in data affecting THC coupled processes on seepage and flow.</p>

NRC Acceptance Criteria	PMR Approach and Section Reference
4 - The initial conditions, boundary conditions, and computational domain used in sensitivity analyses involving coupled THC effects on seepage and flow were consistent with available data.	Sensitivity analyses will be included in TSPA-SR.
5 - DOE's performance confirmation program should assess whether the natural system and engineered materials are functioning as intended and anticipated with regard to coupled THC effects on seepage and flow.	All of the information needed to support the LA will be complete prior to the LA. Arguments presented in the LA will be based on testing and analysis conducted before LA and considered in the licensing review. Testing contained in the performance confirmation program is confirmatory. The performance confirmation program addresses coupled THC effects associated with the rock mass cooling response, coupled process testing, and seepage testing under heated environments during the pre-emplacment period. Longer term testing for seepage and NF THC testing and monitoring around selected emplacement drifts and under simulated postclosure conditions is also addressed. Testing of the in-drift environments is included as well. See the Performance Confirmation Plan (CRWMS M&O 2000z, Sections 5.3.1.2, 5.3.1.4, 5.3.1.5, 5.3.2, and Appendix G).
Acceptance Criteria in this sub-element addressed by other PMRs include:  3 - UZ F&T	See Table 4.3-1 of the UZ F&T PMR (CRWMS M&O 2000f) for additional information regarding this acceptance criterion.
<b>Model Uncertainty Acceptance Criteria</b>	
1 - Appropriate models, tests, and analyses were used that are sensitive to the THC couplings under consideration for both natural and engineering systems, as described in the following examples. The natural-setting data indicate processes that should be evaluated include the precipitation of calcite or calcium-silica-hydrate phases along fracture surfaces as a result of migration of a hyperalkaline fluid that could affect hydraulic properties.	The DS THC models considered a large group of minerals, including calcite and hydrous calcium alumino-silicates, such as zeolites and smectite that occur naturally in the fracture and matrix. These are listed in Table 3-11 of Section 3.4 of this PMR and in the DS THC AMR (CRWMS M&O 2000b). The THC couplings under consideration for the engineered systems are also addressed in the EBS PMR (CRWMS M&O 2000g) and the Waste Form (WF) Degradation PMR (CRWMS M&O 2000ab). THC couplings for the natural system are addressed by both the UZ F&T PMR (CRWMS M&O 2000f) and the NFE PMR. However, much of this issue has been mitigated by design changes, which no longer incorporate use of concrete liners and invert materials. Thus, the major potential source of hyperalkaline fluids no longer exists. The UZ F&T and EBS PMRs (CRWMS M&O 2000f and 2000g) also discuss aspects of this Acceptance Criterion.

NRC Acceptance Criteria	PMR Approach and Section Reference
<p>3 - Alternative modeling approaches consistent with available data and current scientific understanding were investigated, and their results and limitations were appropriately considered.</p>	<p>Section 3.4 of this PMR describes the abstraction of the models used to evaluate the potential effects of coupled THC processes on properties within the NFE that might impact UZ flow and transport. The <i>THC Abstraction AMR</i> (CRWMS M&amp;O 2000c) describes how a comparison of the thermal hydrologic variables, obtained from a DS THC model that implemented two different geochemical systems, was performed. The comparison highlighted that the differences in mineralogy only weakly influence the overall TH response of the geologic system.</p> <p>Model approaches and alternative model approaches for THC impacts on flow and transport are discussed in Section 3.10.7 of the UZ F&amp;T PMR (CRWMS M&amp;O 2000f). This acceptance criterion is also discussed in the EBS PMR (CRWMS M&amp;O 2000g, Sections 3.1.1 and 3.1.2).</p>
<p>Acceptance Criteria in this subelement addressed by other PMRs include:</p> <p>2 - UZ F&amp;T, EBS</p> <p>4 - UZ F&amp;T, EBS</p>	<p>See Table 4.3-1 of the UZ F&amp;T and Appendix A of the EBS PMR (CRWMS M&amp;O 2000f and 2000g) for additional information regarding these acceptance criteria.</p>
<p><b>Model Verification Acceptance Criteria</b></p>	
<p>1 -The mathematical models for coupled THC effects on seepage and flow are consistent with conceptual models based on inferences about NFE, field data and natural alteration observed at the site, and expected engineered materials.</p>	<p>The mathematical models for coupled THC processes on seepage and flow are consistent with conceptual models and were developed based on data collected from the site, including the area around the in-situ thermal tests and borehole data. Section 3.3 and 3.4 of this PMR describes the process-level models, model abstractions, and supporting analyses that address the NFE processes. The <i>THC Process AMR</i> and <i>THC Abstraction AMR</i> (CRWMS M&amp;O 2000b and 2000c) that support development of this section describe the inputs and assumptions that underlie the modeling.</p> <p>Section 3.10 of the UZ F&amp;T PMR (CRWMS M&amp;O 2000f) summarizes the mathematical models used to evaluate coupled THC effects on seepage and flow. Rev. 0 of this PMR addresses the effects of THC on property sets. However, back-coupling with EBS PMR (CRWMS M&amp;O 2000g) to consider expected engineered materials impacts on NFE properties was not included. Therefore, the effects of flow out of the drifts were not addressed in Rev. 0 of the NFE PMR.</p> <p>This acceptance criterion is also discussed in Appendix A of the EBS PMR (CRWMS M&amp;O 2000g).</p>

NRC Acceptance Criteria	PMR Approach and Section Reference
<p>3 - Abstracted models for coupled THC effects on seepage and flow were based on the same assumptions and approximations shown to be appropriate for closely analogous natural or experimental systems. Abstracted model results were verified through comparison to outputs of detailed process models and empirical observations. Abstracted model results are compared with different mathematical models to judge robustness of results.</p>	<p>Section 3.4 of this PMR describes the abstraction of the models used to evaluate the potential effects of coupled THC processes on NFE properties, which were considered in the UZ flow and transport PMR. The <i>THC Abstraction AMR</i> (CRWMS M&amp;O 2000c) provides detailed descriptions of the inputs and assumptions used in the model abstraction. Chapter 5 of this PMR states that the assumptions described in detail in the <i>THC Process AMR</i> (CRWMS M&amp;O 2000b) are applied in the <i>THC Abstraction AMR</i>. The process-level model evaluation describes assumptions that are appropriate, because they are based on the calculation of mineral water reactions, the transport of aqueous and gaseous species, and the conceptual models that are used to describe the chemical and physical systems. It also provides a comparison of thermal-hydrologic variables obtained from a DS THC model that implemented two different geochemical systems. A comparison across process-level models (TH-only and THC) is also described in the AMR. In addition, results from a 2-D, DS, TH-only model are compared to the TH results of the 2-D DS THC model described in the <i>THC Process AMR</i> (CRWMS M&amp;O 2000b). Finally, the DS THC model TH results were compared to the multiscale TH model results in order to determine the extent of edge effects. These comparisons demonstrate robustness of results. Section 3.6 of this PMR discusses the validation of NFE models.</p> <p>Models with accompanying assumptions and approximations used to evaluate impacts of THC on seepage and flow are discussed primarily in the UZ F&amp;T PMR (CRWMS M&amp;O 2000f). Abstractions in the UZ F&amp;T PMR (CRWMS M&amp;O 2000f, Section 3.10) were derived from the underlying process models described in the UZ F&amp;T PMR (CRWMS M&amp;O 2000f). This acceptance criterion is also discussed in Appendix A of the EBS PMR (CRWMS M&amp;O 2000g).</p>
<p>Acceptance Criteria within this sub-element addressed by other PMRs include: 2 - UZ F&amp;T, EBS</p>	<p>See Table 4.3-1 of the UZ F&amp;T PMR and Appendix A of the EBS PMR (CRWMS M&amp;O 2000f and 2000g) for additional information regarding this acceptance criterion.</p>

NRC Acceptance Criteria	PMR Approach and Section Reference
<b>Integration Acceptance Criteria</b>	
<p>1 - DOE has considered all the relevant FEP. The abstracted models adequately incorporated design features, physical phenomena, and couplings, and used consistent and appropriate assumptions throughout.</p>	<p>Section 2.5 of this PMR describes the treatment and documentation of primary FEPs affecting thermal hydrology and coupled process phenomena that impact the NFE. This section describes the process used to ensure that FEPs are categorized as either included or excluded. Included FEPs are directly represented in the process models and abstractions and are discussed in the PMR sections corresponding to the specific models. Section 3.4 describes the abstraction of the models used to evaluate the potential effects of coupled THC processes on UZ flow and transport. The <i>THC Abstraction AMR</i> (CRWMS M&amp;O 2000c) provides descriptions of the inputs and assumptions used in the model abstraction.</p> <p>The UZ F&amp;T PMR (CRWMS M&amp;O 2000f) contains a discussion of FEPs impacting seepage and flow. This acceptance criterion is also discussed in Appendix A of the EBS PMR (CRWMS M&amp;O 2000g).</p>
<p>2 - Models reasonably accounted for known temporal and spatial variations in conditions affecting coupled THC effects on seepage and flow.</p>	<p>Sections 3.3 and 3.4 of this PMR describes the process-level models, model abstractions and supporting analyses that address the NFE processes. The <i>THC Process AMR</i> and <i>THC Abstraction AMR</i> (CRWMS M&amp;O 2000b and 2000c) that support development of this section describe the inputs and assumptions that underlie the modeling. The DS THC used average conditions and temperature profiles for seven cases to address the variation in natural system effects.</p> <p>The UZ F&amp;T PMR (CRWMS M&amp;O 2000f) and ISM PMR (CRWMS M&amp;O 2000y) discuss the spatial variations in properties and conditions that occur in the natural system that have impact on the NF. This acceptance criterion is also discussed in Appendix A of the EBS PMR (CRWMS M&amp;O 2000g).</p>

NRC Acceptance Criteria	PMR Approach and Section Reference
<p>3 - Not all THC couplings may be determined to be important to performance, and DOE may adopt assumptions to simplify PA analyses. If potentially important couplings are neglected, DOE should provide a technical basis for doing so. The technical basis could include activities, such as independent modeling, laboratory or field data, or sensitivity studies.</p>	<p>Section 2.1 of this PMR describes the process of analysis used to determine which couplings need to be considered in PA, and which were excluded, and the technical justification for that determination. Section 2.1 identifies and describes the weak couplings as second or third order effects for the NF processes. Weak coupled processes may be neglected in the initial calculations as second or third order effects this reduces the computer computational effort required to compute coupled problems. Sections 3.3 and 3.4 describe the process level models, model abstractions and supporting analyses that address the NFE processes. The <i>THC Process AMR</i> and <i>THC Abstraction AMR</i> (CRWMS M&amp;O 2000b and 2000c) that support development of this section describe the inputs and assumptions that underlie the modeling. Detailed descriptions and justification are provided for the basis for each assumption. The Repository Safety Strategy (RSS) describes the factors that contribute strongly to performance (CRWMS M&amp;O 2000s). Coupled processes are described in the RSS as factors that do not contribute strongly to performance.</p> <p>It should also be noted that Section 2.5 of this PMR describes the FEPs included in this PMR. The <i>NFE FEPs AMR</i> (CRWMS M&amp;O 2000e) supporting this section provides documentation and justification for screening arguments and TSPA dispositions. Documentation includes a statement of the screening decision for each FEP. Justification is provided for each excluded FEP, including the criterion on which it was excluded and the technical basis for the screening argument.</p> <p>The coupling of THC to seepage and flow is described in the UZ F&amp;T PMR (CRWMS M&amp;O 2000f). This acceptance criterion is also discussed in Appendix A of the EBS PMR (CRWMS M&amp;O 2000g).</p>

NRC Acceptance Criteria	PMR Approach and Section Reference
<p>4 - Where simplifications for modeling coupled THC effects on seepage and flow were used for PA analyses instead of detailed process models, the bases used for modeling assumptions and approximations were documented and justified.</p>	<p>This PMR addresses the process of changes to properties that would need to be considered within the UZ F&amp;T PMR (CRWMS M&amp;O 2000f). Sections 3.3 and 3.4 describe the process-level models, model abstractions and supporting analyses that address the NFE processes. The <i>THC Process AMR</i> and <i>THC Abstraction AMR</i> (CRWMS M&amp;O 2000b and 2000c) that support development of this section describe the inputs and assumptions that underlie the modeling. Detailed descriptions and justifications are provided for the basis for each assumption. In addition, the <i>THC Abstraction AMR</i> (CRWMS M&amp;O 2000c) provides explanations, documentation and justification for simplifications used in the abstractions described in that AMR.</p> <p>Modeling of seepage and flow, as well as abstractions of those models, is discussed in the UZ F&amp;T PMR (CRWMS M&amp;O 2000f). The UZ F&amp;T PMR (CRWMS M&amp;O 2000f, Section 3.10.11) documents the basis for the abstraction of coupled THC effects on seepage and flow. This acceptance criterion is also discussed in Appendix A of the EBS PMR (CRWMS M&amp;O 2000g).</p>
<b>Programmatic Acceptance Criteria</b>	
<p>1 - Data and models were collected, developed, and documented under acceptable quality assurance (QA) procedures.</p>	<p>Activities associated with development of this PMR and its related AMRs were determined to be subject to the quality assurance program as described in the Quality Assurance Requirements and Description (QARD) (DOE 2000) document. As such, collection of related data, development of analyses and models, and use and validation of software is subject to the requirements of procedures developed to implement quality assurance program requirements.</p>
<p>2 - Deficiency reports concerning data quality on issues related to coupled THC effects on seepage and flow were closed.</p>	<p>The NFE PMR has been prepared according to AP-3.10Q and AP-3.15Q to address quality assurance deficiency issues. At the current time, the data used for the analyses and models are obtained from controlled sources that are undergoing qualification, and will be closed after completion of data qualification entries.</p> <p>This acceptance criterion is also discussed in Appendix A of the EBS PMR (CRWMS M&amp;O 2000g).</p>

NRC Acceptance Criteria	PMR Approach and Section Reference
3 - If used, expert elicitations were conducted and documented in accordance with the guidance in NUREG-1563 (Kotra et al. 1996) or other acceptable approaches.	Expert elicitations regarding seepage and flow were conducted in both the UZ and NF aspects. Expert elicitations associated with development of this PMR were determined to be subject to the quality assurance program as described in the QARD (DOE 2000) document. Appendix C of the QARD and implementing procedures for expert elicitation were developed using the guidance provided in NUREG-1563 (Kotra et al. 1996). Section 2.4.5 of this PMR addresses expert elicitation regarding parts of the elicitation that relate to the NFE. Refer to that section for a description of how expert elicitation was used. For a complete discussion, refer to the UZ F&T PMR (CRWMS M&O 2000f).
<b>SUBISSUE 2 – EFFECTS OF COUPLED THC PROCESSES ON THE WASTE PACKAGE CHEMICAL ENVIRONMENT</b>	
<b>Data and Model Justification Acceptance Criteria</b>	
Acceptance Criteria in this subelement addressed by other PMRs include: 1 – EBS 2 – EBS 3 – EBS 4 – EBS 5 – EBS 6 – EBS 7 – EBS	See Appendix A of the EBS PMR (CRWMS M&O 2000g) for additional information regarding these acceptance criteria.
<b>Data Uncertainty and Verification Acceptance Criteria</b>	
1 – EBS 2 – EBS 3 – EBS 4 – EBS 5 – EBS	See Appendix A of the EBS PMR (CRWMS M&O 2000g) for additional information regarding these acceptance criteria.

NRC Acceptance Criteria	PMR Approach and Section Reference
<b>Model Uncertainty Acceptance Criteria</b>	
<p>1 - Appropriate models, tests, and analyses were used that are sensitive to the THC couplings under consideration for both natural and engineering systems as described in the following examples. The effects of THC coupled processes that may occur in the natural setting or due to interactions with engineered materials or their alteration products include the TH effects on gas and water chemistry.</p>	<p>The THC interactions between the natural and engineered systems are primarily addressed in the EBS and UZ F&amp;T PMRs (CRWMS M&amp;O 2000g and 2000f). This PMR addresses property changes that might impact the chemistry of water in the UZ that seeps into the drifts. These property changes are input to the UZ analyses. The results, the chemistry of the water seeping into drifts, are then input to the EBS PMR (CRWMS M&amp;O 2000g). The EBS and WPD PMRs (CRWMS M&amp;O 2000g and 2000ac) report the evaluations of the resulting chemistry.</p> <p>Likewise, the WP and EBS PMRs (CRWMS M&amp;O 2000o and 2000g) determine the chemistry of fluids that result from THC couplings between the drift and waste package materials. They also provide the water chemistry information to the UZ to determine its effect on flow and transport. In this PMR, no analyses were made of the impact of chemistry of water exiting drifts on the hydrologic and chemical properties of the NF. The effects of the effluent chemistry are included in UZ transport calculations described in the UZ F&amp;T PMR (CRWMS M&amp;O 2000f).</p> <p>Section 3.3 addresses models used to evaluate the potential effects of coupled THC processes on NF chemical properties. These models provide the framework (or inputs) for UZ and EBS to evaluate THC coupled processes at DS, predict flow and transport behavior for specified thermal-loading conditions, and predict the chemistry of waters and gases entering the emplacement drifts.</p>

NRC Acceptance Criteria	PMR Approach and Section Reference
<p>3 - DOE provided a reasonable description of the mathematical models included in its analyses of coupled THC effects on waste package chemical environment. The description should include a discussion of alternative modeling approaches not considered in its final analysis and the limitations and uncertainties of the chosen model.</p>	<p>The EBS PMR (CRWMS M&amp;O 2000g) and the WPD PMR (CRWMS M&amp;O 2000o) report the efforts to evaluate waste package chemical environment. The EBS PMR (CRWMS M&amp;O 2000g, Section 3.1.2) presents alternative models for fully coupled THC modeling and also discusses modeling limitations and uncertainties. The UZ F&amp;T PMR (CRWMS M&amp;O 2000f) provides the descriptions of models used in establishing seepage-water chemistry and reports seepage-water chemistry that is used as input to the EBS and Waste Package models. The NFE PMR provides an assessment of the changes in mineralogy and deposition of salts etc. that would affect the seepage-water chemistry.</p> <p>Section 3.3 of this PMR addresses models used to evaluate the potential effects of coupled THC processes on mineralogy and/or salt depositions within the NF zone. Section 3.4 describes the abstraction of the models used to evaluate the potential effects of coupled THC processes on those chemical factors. The <i>THC Abstraction AMR</i> (CRWMS M&amp;O 2000c) describes how the abstraction results in a number of simplified time-histories of mineral alterations or formations and/or depositions.</p>
<p>Acceptance Criteria in this sub-element addressed by other PMRs include:</p> <p>2 - EBS</p>	<p>See Appendix A of the EBS PMR (CRWMS M&amp;O 2000g) for additional information regarding this acceptance criterion.</p>

NRC Acceptance Criteria	PMR Approach and Section Reference
<b>Model Verification Acceptance Criteria</b>	
<p>3 - Abstracted models for coupled THC effects on waste package chemical environment were based on the same assumptions and approximations shown to be appropriate for closely analogous natural or experimental systems. Abstracted model results were verified through comparison to outputs of detailed process models and empirical observations. Abstracted model results are compared with different mathematical models to judge robustness of results.</p>	<p>The EBS and WPD PMRs (CRWMS M&amp;O 2000g and 2000ac) report the waste package chemical environment and report on the associated abstractions. The EBS and WPD PMRs (CRWMS M&amp;O 2000g and 2000ac) provide the descriptions of assumptions, approximations simplifications and abstractions used in those assessments. The UZ F&amp;T PMR (CRWMS M&amp;O 2000f) reports similar information for models used to determine seepage-water chemistry. The NFE PMR provides the description of assumptions and approximations used in models to assess the changes in mineralogy and deposition of salts etc. that would effect the seepage-water chemistry.</p> <p>Section 3.4 describes the abstraction of the models used to evaluate the potential effects of coupled THC processes on changes in mineralogy and deposition of salts etc. The <i>THC Abstraction AMR</i> (CRWMS M&amp;O 2000c) provides detailed descriptions of the inputs and assumptions used in the model abstraction. It also provides a comparison of thermal-hydrologic variables obtained from a DS THC model that implemented two different geochemical systems. A comparison across process-level models (TH-only and THC) is also described in the AMR. In addition, results from 2-D, DS, TH-only models are compared to the TH results of the 2-D DS THC model described in the <i>THC Process AMR</i> (CRWMS M&amp;O 2000b). Finally, the DS THC model TH results were compared to the multiscale TH model in order to determine the extent of edge effects.</p>
<p>Acceptance Criteria in this subelement addressed by other PMRs include:</p> <p>1 - EBS</p> <p>2 - EBS</p>	<p>See Appendix A of the EBS PMR (CRWMS M&amp;O 2000g) for additional information regarding this acceptance criterion.</p>
<b>Integration Acceptance Criteria</b>	
<p>1 - DOE has considered all the relevant FEP. The abstracted models adequately incorporated important design features, physical phenomena, and couplings, and used consistent and appropriate assumptions throughout.</p>	<p>The determination of features, events and processes important to an assessment of the waste package chemical environment is contained in the EBS and WPD PMRs (CRWMS M&amp;O 2000g and 2000ac). No evaluation of these FEPs was made as part of this PMR.</p>

NRC Acceptance Criteria	PMR Approach and Section Reference
<p>3 - Not all THC couplings may be determined to be important to performance, and DOE may adopt assumptions to simplify performance assessment analyses. If potentially important couplings are neglected, DOE should provide a technical basis for doing so. The technical basis can include activities such as independent modeling, laboratory or field data, and sensitivity studies.</p>	<p>The determination of which THC couplings were to be considered and how to address them was made in the EBS and WPD PMRs (CRWMS M&amp;O 2000g and 2000ac).</p> <p>This PMR considered couplings that impacted changes in physical and chemical parameters of the NF. As such, it merely discussed those couplings that impacted the NF directly. Chapter 3 describes the process level models, model abstractions and supporting analyses that address the NF environment processes. The AMRs that support development of this section describe the inputs and assumptions that underlie the modeling. Detailed descriptions and justifications are provided for the basis for each assumption.</p>
<p>4 - Where simplifications for modeling coupled THC effects on Waste Package chemical environment were used for performance assessment analyses instead of detailed process models, the bases used for modeling assumptions and approximations were documented and justified.</p>	<p>This PMR had no direct feeds to performance assessment in this aspect. The EBS and WPD PMRs (CRWMS M&amp;O 2000g and 2000ac) discuss the performance assessment efforts for this aspect.</p>
<p>Acceptance Criteria in this subelement addressed by other PMRs include:</p> <ul style="list-style-type: none"> <li>1 - EBS</li> <li>2 - EBS</li> <li>3 - EBS</li> <li>4 - EBS</li> </ul>	<p>See Appendix A of the EBS PMR (CRWMS M&amp;O 2000g) for additional information regarding this acceptance criterion.</p>
<p><b>Programmatic Acceptance Criteria</b></p>	
<p>Acceptance Criteria in this subelement addressed by other PMRs include:</p> <ul style="list-style-type: none"> <li>1 - EBS</li> <li>2 - EBS</li> <li>3 - EBS</li> </ul>	<p>See Appendix A of the EBS PMR (CRWMS M&amp;O 2000g) for additional information regarding these acceptance criteria.</p>

NRC Acceptance Criteria	PMR Approach and Section Reference
<b>SUBISSUE 3 - EFFECTS OF COUPLED THC PROCESSES ON THE CHEMICAL ENVIRONMENT FOR RADIONUCLIDE RELEASE</b>	
<b>Data and Model Justification Acceptance Criteria</b>	
Acceptance Criteria in this subelement addressed by other PMRs include: 1 – WF and EBS 2 – WF and EBS 3 – WF and EBS 4 – WF and EBS 5 – WF and EBS 6 – WF and EBS 7 – WF and EBS	See Table 4.2-1 of the WFD PMR and Appendix A of the EBS PMR (CRWMS M&O 2000ab and 2000g) for additional information regarding these acceptance criteria.
<b>Data Uncertainty and Verification Acceptance Criteria</b>	
Acceptance Criteria within this sub-element addressed by other PMRs include: 1 – WF and EBS 2 – WF and EBS 3 – WF and EBS 4 – WF and EBS 5 – WF and EBS	See Table 4.2-1 of the WFD PMR and Appendix A of the EBS PMR (CRWMS M&O 2000ab and 2000g) for additional information regarding these acceptance criteria.
<b>Model Uncertainty Acceptance Criteria</b>	
Acceptance Criteria in this subelement addressed by other PMRs include: 1 – WF and EBS 2 – WF and EBS 3 – WF and EBS	See Table 4.2-1 of the WFD PMR and Appendix A of the EBS PMR (CRWMS M&O 2000ab and 2000g) for additional information regarding these acceptance criteria.

NRC Acceptance Criteria	PMR Approach and Section Reference
<b>Model Verification Acceptance Criteria</b>	
Acceptance Criteria in this subelement addressed by other PMRs include: 1 – WF and EBS 2 – WF and EBS 3 – WF and EBS	See Table 4.2-1 of the WFD PMR and Appendix A of the EBS PMR (CRWMS M&O 2000ab and 2000g) for additional information regarding these acceptance criteria.
<b>Integration Acceptance Criteria</b>	
Acceptance Criteria in this subelement addressed by other PMRs include: 1 – WF and EBS 2 – WF and EBS 3 – WF and EBS 4 – WF and EBS	See Table 4.2-1 of the WFD PMR and Appendix A of the EBS PMR (CRWMS M&O 2000ab and 2000g) for additional information regarding these acceptance criteria.
<b>Programmatic Acceptance Criteria</b>	
Acceptance Criteria in this sub-element addressed by other PMRs include: 1 – WF and EBS 2 – WF and EBS 3 – WF and EBS	See Table 4.2-1 of the WFD PMR and Appendix A of the EBS PMR (CRWMS M&O 2000ab and 2000g) for additional information regarding these acceptance criteria.

NRC Acceptance Criteria	PMR Approach and Section Reference
<b>SUBISSUE 4 - EFFECTS OF COUPLED THC PROCESSES ON RADIONUCLIDE TRANSPORT THROUGH ENGINEERED AND NATURAL BARRIERS</b>	
<b>Data and Model Justification Acceptance Criteria</b>	
<p>1 - Available data relevant to both temporal and spatial variations in conditions affecting coupled THC effects on transport of radionuclides in the near-field were considered.</p>	<p>Radionuclide transport issues are reported in the UZ F&amp;T PMR (CRWMS M&amp;O 2000f). The UZ F&amp;T PMR (CRWMS M&amp;O 2000f, Section 3.10) describes how relevant data were incorporated into the modeling. The EBS, WF, and WPD PMRs (CRWMS M&amp;O 2000g, 2000ab, and 2000ac) provided input to UZ analyses relative to the chemistry of water and the amount and form of radionuclides released from the drifts. As such, this subissue is discussed principally in the UZ F&amp;T PMR (CRWMS M&amp;O 2000f) with some discussion in the other listed PMRs. There was no discussion within this PMR of this subissue.</p>
<p>2 - DOE's evaluation of coupled THC processes properly considered site characteristics in establishing initial and boundary conditions for conceptual models and simulations of coupled processes that may affect radionuclide transport in the near field.</p>	<p>The evaluation of coupled THC processes in the UZ F&amp;T PMR (CRWMS M&amp;O 2000f, Section 3.10) considered site characteristics in establishing initial and boundary conditions for conceptual models and simulation of coupled processes. This PMR calculated THC effects that could affect transport, but application of the results has not been completed. The chemistry of the effluent, as described in the EBS, WP, and WFD PMRs, is considered in transport by the UZ F&amp;T PMR.</p>
<p>7 - If the testing program for coupled THC processes on the chemical environment for radionuclide release from the EBS is not complete at the time of LA, or if sensitivity and uncertainty analyses indicate additional data are needed, DOE has identified specific plans to acquire the necessary information as part of the performance confirmation program.</p>	<p>All of the information needed to support the LA will be complete prior to the LA. Arguments presented in the LA will be based on testing and analysis conducted before LA and considered in the licensing review. Testing contained in the performance confirmation program is confirmatory. The performance confirmation program addresses coupled THC effects associated with the rock mass cooling response, coupled process testing, and seepage testing under heated environments during the pre-emplacment period. Longer term testing for seepage and NF THC testing and monitoring around selected emplacement drifts and under simulated postclosure conditions is also addressed. Testing of the in-drift environments is included as well. See the Performance Confirmation Plan (CRWMS M&amp;O 2000z, Sections 5.3.1.2, 5.3.1.4, 5.3.1.5, 5.3.2, and Appendix G).</p>

NRC Acceptance Criteria	PMR Approach and Section Reference
<p>Acceptance Criteria in this subelement addressed by other PMRs include:</p> <p>3 – EBS, UZ F&amp;T</p> <p>4 – EBS</p> <p>5 – EBS</p> <p>6 – EBS, UZ F&amp;T</p>	<p>See Appendix A EBS PMR and Table 4.3-1 of the UZ F&amp;T PMR (CRWMS M&amp;O 2000g and 2000f) for additional information regarding these acceptance criteria.</p>
<b>Data Uncertainty and Verification Acceptance Criteria</b>	
<p>Acceptance Criteria in this subelement addressed by other PMRs include:</p> <p>1 – EBS, UZ F&amp;T</p> <p>2 – EBS, UZ F&amp;T</p> <p>3 – EBS, UZ F&amp;T</p> <p>4 – EBS, UZ F&amp;T</p> <p>5 – EBS, UZ F&amp;T</p>	<p>See Appendix A of the EBS PMR and Table 4.3-1 of the UZ F&amp;T PMR (CRWMS M&amp;O 2000g and 2000f) for additional information regarding these acceptance criteria.</p>
<b>Model Uncertainty Acceptance Criteria</b>	
<p>1 - Appropriate models, tests, and analyses were used that are sensitive to the THC couplings under consideration for both natural and engineering systems as described in the following examples. The effects of THC coupled processes that may occur in the natural setting or due to interactions with engineered materials or their alteration products include the precipitation and dissolution of oxides and hydroxides on fracture surfaces, illitization of smectite, and recrystallization of zeolites to analcime, which could affect sorption characteristics.</p>	<p>The UZ F&amp;T PMR (CRWMS M&amp;O 2000f) reports the issues related to zeolites and other minerals related to sorption characteristics. The NFE PMR discusses issues of precipitation and dissolution appropriate to the NF minerals within the fracture system of the NF. The effects of NF property changes on transport remain to be evaluated. The effluent chemistry, described in the EBS, WP, and WFD PMRs, is considered in the UZ F&amp;T PMR.</p>
<p>Acceptance Criteria in this subelement addressed by other PMRs include:</p> <p>2 – EBS, UZ F&amp;T</p> <p>3 – EBS, UZ F&amp;T</p>	<p>See Appendix A of the EBS PMR and Table 4.3-1 of the UZ F&amp;T PMR (CRWMS M&amp;O 2000g and 2000f) for additional information regarding these acceptance criteria.</p>

NRC Acceptance Criteria	PMR Approach and Section Reference
<b>Model Verification Acceptance Criteria</b>	
Acceptance Criteria in this subelement addressed by other PMRs include: 1 – EBS, UZ F&T 2 – EBS, UZ F&T 3 – EBS, UZ F&T	See Appendix A of the EBS PMR and Table 4.3-1 of the UZ F&T PMR (CRWMS M&O 2000g and 2000f) for additional information regarding these acceptance criteria.
<b>Integration Acceptance Criteria</b>	
Acceptance Criteria in this subelement addressed by other PMRs include: 1 – EBS, UZ F&T 2 – EBS, UZ F&T 3 – EBS, UZ F&T 4 – EBS, UZ F&T	See Appendix A of the EBS PMR and Table 4.3-1 of the UZ F&T PMR (CRWMS M&O 2000g and 2000f) for additional information regarding these acceptance criteria.
<b>Programmatic Acceptance Criteria</b>	
Acceptance Criteria in this subelement addressed by other PMRs include: 1 – EBS, UZ F&T 2 – EBS, UZ F&T 3 – EBS, UZ F&T	See Appendix A of the EBS PMR and Table 4.3-1 of the UZ F&T PMR (CRWMS M&O 2000g and 2000f) for additional information regarding these acceptance criteria.
<b>SUBISSUE 5 - COUPLED THC PROCESSES AFFECTING POTENTIAL NUCLEAR CRITICALITY IN THE NEAR-FIELD</b>	
Subissue 5 acceptance criteria are not addressed in PMRs. Criticality is addressed in a Topical Report and in supporting documents.	

<b>IRSR: THERMAL EFFECTS ON FLOW</b>	
<b>SUBISSUE 1 - IS THE U.S. DEPARTMENT OF ENERGY TH TESTING PROGRAM, INCLUDING PERFORMANCE CONFIRMATION TESTING, SUFFICIENT TO EVALUATE THE POTENTIAL FOR THERMAL REFLUX TO OCCUR IN THE NEAR FIELD?</b>	
<b>Programmatic Acceptance Criteria</b>	
<p>1 - DOE's thermohydrologic testing program was developed under acceptable quality assurance procedures (QAP). Data were collected and documented under purview of these procedures.</p>	<p>Activities associated with development of this PMR and its related AMRs were determined to be subject to the quality assurance program as described in the QARD (DOE 2000) document. As such, collection of related data, development of analyses and models, and use and validation of software is subject to the requirements of procedures developed to implement quality assurance program requirements. The NFE PMR provides input on changed conditions that could impact flow. This subissue is also addressed in the EBS PMR (CRWMS M&amp;O 2000g), with supporting information from the NFE PMR.</p>
<p>2 - Expert elicitation may be used for, but not necessarily limited to, assessing if conceptual models bound the range of thermally driven refluxing expected at YM, in addition to thermohydrologic testing to provide conservative bounds to estimates. All expert elicitation are conducted and documented in accordance with NUREG -1563 (Kotra et al. 1996) or other acceptable approaches.</p>	<p>This PMR provides input on changed conditions that could impact flow. Therefore, this subissue is mainly addressed in the UZ F&amp;T PMR (CRWMS M&amp;O 2000f), with supporting information from this PMR. Expert elicitation associated with development of this PMR were determined to be subject to the quality assurance program as described in the QARD (DOE 2000) document. Appendix C of the QARD and implementing procedures for expert elicitation were developed using the guidance provided in NUREG-1563 (Kotra et al. 1996). Section 2.4.5 addresses expert elicitation. Refer to that section for a description of how expert elicitation was used.</p>

<b>IRSR: THERMAL EFFECTS ON FLOW</b>	
<b>SUBISSUE 1 - IS THE U.S. DEPARTMENT OF ENERGY TH TESTING PROGRAM, INCLUDING PERFORMANCE CONFIRMATION TESTING, SUFFICIENT TO EVALUATE THE POTENTIAL FOR THERMAL REFLUX TO OCCUR IN THE NEAR FIELD?</b>	
<b>Technical Acceptance Criterion 1</b>	
<p>1 - Thermohydrologic tests are designed and conducted with the explicit objective of testing conceptual and numerical models so that critical thermohydrologic processes can be observed and measured.</p>	<p>TH processes affecting flow and transport are in the UZ F&amp;T PMR (CRWMS M&amp;O 2000f). This PMR reports the in situ and field thermohydrologic testing. The EBS PMR (CRWMS M&amp;O 2000g) reports quarter-scale testing at the Atlas Test Facility. Associated laboratory testing is reported in each of these PMRs.</p> <p>In this PMR, Section 3.6 describes the thermal tests, including the (SHT), the DST, and the (LBT). These tests were designed specifically to test the TH processes. While subsequent repository design changes have occurred, this testing remains applicable to testing the conceptual and numerical models. The <i>Thermal Test AMR</i> (CRWMS M&amp;O 2000a) describes how the properties (and conceptual flow models) used to estimate in-drift thermodynamic environment and flow processes are compared to experimentally determined thermal-hydrologic results. The thermal tests provide measured temperature and liquid-saturation data obtained from a known thermal perturbation. These data help make it possible to assess whether the hydrologic properties developed for ambient conditions alone can also reproduce the extent of the transient flow processes driven by a thermal perturbation.</p>
<p>2 - Thermohydrologic tests are designed and conducted with explicit consideration of TH, thermal-chemical, and hydrologic-chemical couplings.</p>	<p>This PMR reports the in situ and field thermohydrologic testing. The EBS PMR (CRWMS M&amp;O 2000g) reports quarter-scale testing at the Atlas Test Facility. Associated laboratory testing is reported within each of these PMRs.</p> <p>Section 3.6 describes the thermal tests, including the LBT and the DST. Section 6.1 of the <i>Thermal Test AMR</i> describes the objectives of the LBT. The objective of the LBT was to create a planar, horizontal region of boiling in a block of fractured TSW, to observe coupled thermal-hydrological-mechanical-chemical (THMC) behavior in a representative rock unit. The heating duration of the test was designed to provide a sufficient length of time for THC processes to develop.</p> <p>The <i>THC Process AMR</i> (CRWMS M&amp;O 2000b) describes the DST. The purpose of the DST is to evaluate the coupled thermal, hydrological, chemical, and mechanical processes that take place in unsaturated, fractured tuff over a range of temperatures from approximately 25°C to nearly 200°C.</p>

<b>IRSR: THERMAL EFFECTS ON FLOW</b>	
<b>SUBISSUE 1 - IS THE U.S. DEPARTMENT OF ENERGY TH TESTING PROGRAM, INCLUDING PERFORMANCE CONFIRMATION TESTING, SUFFICIENT TO EVALUATE THE POTENTIAL FOR THERMAL REFLUX TO OCCUR IN THE NEAR FIELD?</b>	
<p>3 - Thermohydrologic tests are designed and conducted at different scales to discern scale effects on observed phenomena.</p>	<p>The testing program discussed in Section 3.6 was designed to continue the testing at different scales. The scale dimension was extended from laboratory scale (core samples) to bench scale (small block tests) to the LBT and SHT and then to the large scale DST. Section 3.6 provides a description of the thermal tests. The SHT, DST, and LBT are all different scale tests. The SHT is a small to intermediate sized field test. The DST is geometrically more complex and larger scale than the SHT or LBT. The scale of the DST allows investigation of the NFE and associated coupled thermal, hydrological, chemical, and mechanical processes on an emplacement-drift scale. The size of the LBT was chosen so that the block of rock to be heated was large enough to contain several fractures, but small enough so that boundary conditions and rock heterogeneity could be adequately controlled and/or characterized.</p> <p>This subissue is also addressed in the EBS PMR (CRWMS M&amp;O 2000g)</p>
<p>4 - Thermohydrologic tests are designed and conducted for temperature ranges expected under repository operating conditions.</p>	<p>The DST was designed to be consistent with the designs being considered. Section 3.6 describes the thermal tests, including the DST. As described in Section 3.6 of this PMR and in the <i>THC Process AMR</i> (CRWMS M&amp;O 2000b, Section 6.2), the purpose of the DST is to evaluate the coupled thermal, hydrological, chemical, and mechanical processes that take place in unsaturated, fractured tuff over a range of temperatures from approximately 25°C to nearly 200°C. The planned temperatures for the DST are consistent with an 85 MTU thermal load. Current design decisions may lower the driftwall peak temperatures. However, the overall rock temperatures are expected to be representative, unless there is a significant lowering of the MTU loading in the repository.</p> <p>This subissue is also addressed in the EBS PMR (CRWMS M&amp;O 2000g)</p>

<b>IRSR: THERMAL EFFECTS ON FLOW</b>	
<b>SUBISSUE 1 - IS THE U.S. DEPARTMENT OF ENERGY TH TESTING PROGRAM, INCLUDING PERFORMANCE CONFIRMATION TESTING, SUFFICIENT TO EVALUATE THE POTENTIAL FOR THERMAL REFLUX TO OCCUR IN THE NEAR FIELD?</b>	
<p>5 - Thermohydrologic tests are designed and conducted to determine if water refluxes back to the heaters during either the heating or cool-down phases of the tests.</p>	<p>Two of the field tests reported in this PMR were specifically designed to look at reflux issues. The LBT was designed to maximize the conditions under which refluxing could occur. The temperatures were maintained at the surface to a point that would allow for condensation within the rock, and the heater temperatures were maintained above boiling. The wing heaters in the DST were also designed to create conditions that would be favorable to condensate buildup (or more correctly to create a thermal barrier that could potentially impair condensate drainage, and thus allow for both reflux and "thermal perching" of condensate) by creating a horizontal plane above the boiling point approximately 1/3 of the way up on the block and by maintaining below boiling temperatures on the top of the block.</p> <p>Section 3.6 describes the thermal tests, including the DST and LBT. The LBT was an integrated test and many different types of data were collected. A specific goal of the LBT was observation of condensate refluxing above a boiling zone. Also, the <i>Updated In Situ Thermal Testing Program Strategy</i> (CRWMS M&amp;O 1997c) states that the LBT was intended to address the need for information on drainage/reflux by fracture flow.</p> <p>This subissue is also addressed in the EBS PMR (CRWMS M&amp;O 2000g)</p>
<p>7 - Thermohydrologic tests are designed and conducted to account for all mass and energy losses/gains in the model system.</p>	<p>As discussed in Section 3.6, the LBT had controlled or monitored side boundaries to account for all mass and energy losses/gains. These boundaries consisted of an impermeable membrane glued to the side-rock surface to prevent loss of water mass through the sides, with insulation and heat-flux monitoring outside the membrane to account for the energy losses/gains. Further, there was a temperature control system installed at the top of the block to maintain constant surface temperature. The power input from this system was monitored. There were no controls on water mass-movement through the top and bottom of the block, although measurements were made below the block.</p> <p>As also discussed in Section 3.6, the DST was heavily monitored to account for mass and energy losses within the measurement sections. There was only partial control or accounting for energy losses from the ends, as discussed in the <i>Thermal Test AMR</i> (CRWMS M&amp;O 2000a). Evaluation of impacts of heat and moisture losses in the DST concludes that test is acceptable and heat losses do not invalidate the test.</p> <p>This subissue is also addressed in the EBS PMR (CRWMS M&amp;O 2000g)</p>

<b>IRSR: THERMAL EFFECTS ON FLOW</b>	
<b>SUBISSUE 1 - IS THE U.S. DEPARTMENT OF ENERGY TH TESTING PROGRAM, INCLUDING PERFORMANCE CONFIRMATION TESTING, SUFFICIENT TO EVALUATE THE POTENTIAL FOR THERMAL REFLUX TO OCCUR IN THE NEAR FIELD?</b>	
8 - Thermohydrologic tests are designed and conducted such that the model environment is sufficiently characterized so that the level of uncertainty in property values does not result in unacceptable uncertainty in thermal test interpretation.	One of the objectives of the DST was to evaluate the impact of different property sets and their impact on model results. Section 3.6 describes the thermal tests, including the SHT, LBT and the DST. Chapter 1 of the <i>Thermal Test AMR</i> describes how a comparative analysis is performed of measurements from the thermal tests to results from the numerical simulations. These form the bases for the conclusions presented in the AMR. Section 6.2 of the <i>Thermal Test AMR</i> describes the results of the comparative analyses in sufficient detail to conclude that the environment is sufficiently characterized, so that the level of uncertainty in property values does not result in unacceptable uncertainty in thermal-test interpretation. Evaluation of impacts of heat and moisture losses in the DST concludes that losses do not invalidate the test.
9 - Thermohydrologic tests are designed and conducted such that accuracy in the measurement of the test environment saturation is sufficient to discern the relative ability of different conceptual models to represent the TH processes in heated partially saturated, fractured porous media.	Section 3.6 of this PMR describes the thermal tests, including the SHT, the DST, and the LBT. The <i>Thermal Test AMR</i> (CRWMS M&O 2000a) compares model results using a number of property sets to measured temperature and liquid saturation data obtained from a known thermal perturbation for comparison. The AMR provides a comparison of simulated and measured water saturation distributions to determine the accuracy of NFE and EBS TH models. The LBT and DST were performed at saturation ranges that are representative of that expected for the repository (from nearly 95% for DST to near-total desaturation or dryout).
<b>Technical Acceptance Criterion 2</b>	
Thermohydrologic test results from other sites and programs have been analyzed and applied, as appropriate, to the Yucca Mountain site.	Section 3.6 of this PMR addresses thermohydrologic test results from G-Tunnel, an unsaturated site similar to Yucca Mountain in rock type (welded tuff, Grouse Canyon) and initial saturation (approximately 85%).

<b>IRSR: THERMAL EFFECTS ON FLOW</b>	
<b>SUBISSUE 1 - IS THE U.S. DEPARTMENT OF ENERGY TH TESTING PROGRAM, INCLUDING PERFORMANCE CONFIRMATION TESTING, SUFFICIENT TO EVALUATE THE POTENTIAL FOR THERMAL REFLUX TO OCCUR IN THE NEAR FIELD?</b>	
<b>Technical Acceptance Criterion 3</b>	
If the thermohydrologic testing program is not complete at the time of LA submittal, DOE has explained why the testing program does not need to be completed for the LA and identified specific plans for completion of the testing program as part of the performance confirmation program.	All of the information needed to support the LA will be complete prior to the LA. Arguments presented in the LA will be based on testing and analysis conducted before LA and considered in the licensing review. Testing contained in the performance confirmation program is confirmatory. The performance confirmation program addresses thermal-hydrologic effects on unsaturated zone flow and seepage into emplacement drifts during the pre-emplacment period, including assessment of the thermal hydrologic response of rock mass and cooling and seepage testing under heated environments. Longer term testing for seepage and NF THC testing and monitoring around selected emplacement drifts and under simulated postclosure conditions is also addressed. Testing of the in-drift environments is included as well. See the Performance Confirmation Plan (CRWMS M&O 2000z, Sections 5.3.1.2, 5.3.1.4, 5.3.1.5, 5.3.2, and Appendix G).
<b>SUBISSUE 2 - IS THE U.S. DEPARTMENT OF ENERGY TH MODELING APPROACH SUFFICIENT TO PREDICT THE NATURE AND BOUNDS OF THERMAL EFFECTS ON FLOW IN THE NEAR FIELD?</b>	
<b>Programmatic Acceptance Criteria</b>	
1 - DOE's thermohydrologic modeling analyses were developed and documented under acceptable QA procedures.	Activities associated with development of this PMR and its related AMRs were determined to be subject to the quality assurance program as described in the QARD (DOE 2000) document. As such, collection of related data, development of analyses and models, and use and validation of software is subject to the requirements of procedures developed to implement quality assurance program requirements. TH modeling is contained in this PMR scope (Sections 3.2, 3.3, 3.4, and 3.6) and two of its supporting AMRs, <i>Thermal Test AMR</i> and <i>THC Abstraction AMR</i> (CRWMS M&O 2000a and 2000c). This subissue is also addressed in the EBS PMR (CRWMS M&O 2000g).

<b>IRSR: THERMAL EFFECTS ON FLOW</b>	
<b>SUBISSUE 1 - IS THE U.S. DEPARTMENT OF ENERGY TH TESTING PROGRAM, INCLUDING PERFORMANCE CONFIRMATION TESTING, SUFFICIENT TO EVALUATE THE POTENTIAL FOR THERMAL REFLUX TO OCCUR IN THE NEAR FIELD?</b>	
<p>2 - Expert elicitation may be used for, but not necessarily limited to, selecting a conceptual model and its parameters. All expert elicitation are conducted and documented in accordance with NUREG-1563 (Kotra et al. 1996) or other acceptable approaches</p>	<p>TH modeling is contained in this PMR scope (Sections 3.2, 3.3, 3.4, and 3.6) and two of its supporting AMRs, <i>Thermal Test AMR</i> and <i>THC Abstraction AMR</i> (CRWMS M&amp;O 2000a and 2000c). This subissue is also addressed in the UZ F&amp;T and EBS PMRs (CRWMS M&amp;O 2000f and 2000g). Expert elicitations were determined to be subject to the quality assurance program as described in the QARD (DOE 2000) document. Appendix C of the QARD and implementing procedures for expert elicitation were developed using the guidance provided in NUREG-1563 (Kotra et al. 1996).</p> <p>Section 2.4.5 addresses expert elicitation. Refer to that section for a description of how expert elicitation was used.</p>
<b>Technical Acceptance Criterion 1</b>	
<p>1 - Sufficient data are available to adequately define relevant parameters, parameter values, and conceptual models. Specifically, DOE should demonstrate that uncertainties and variabilities in parameter values are accounted for using defensible methods. The technical bases for parameter ranges, probability distributions or bounding values used are provided. Parameter values (single values, ranges, probability distributions, or bounding values) are derived from site-specific data or an analysis is included to show the assumed parameter values lead to a conservative effect on performance.</p>	<p>TH modeling is contained in this PMR scope (Sections 3.2, 3.3, 3.4, and 3.6) and two of its supporting AMRs, <i>Thermal Test AMR</i> and <i>THC Abstraction AMR</i> (CRWMS M&amp;O 2000a and 2000c). This subissue is also addressed in the UZ F&amp;T and EBS PMRs (CRWMS M&amp;O 2000f and 2000g). This PMR provides input to coupled-process-induced changes in the parameters used in those analyses. Section 3.3 addresses the drift-scale coupled-process models and abstractions used to evaluate those parameter changes.</p>
<p>2 - Sufficient data are available to adequately define relevant parameters, parameter values, and conceptual models. Specifically, DOE should demonstrate that analyses are consistent with site characteristics in establishing initial conditions, boundary conditions, and computational domains for conceptual models evaluated.</p>	<p>TH modeling is contained within this PMR scope (Sections 3.2, 3.3, 3.4, and 3.6) and two of its supporting AMRs, <i>Thermal Test AMR</i> and <i>THC Abstraction AMR</i> (CRWMS M&amp;O 2000a and 2000c). This subissue is also addressed in the UZ F&amp;T and EBS PMRs (CRWMS M&amp;O 2000f and 2000g). This PMR provides input to coupled-process-induced changes in the parameters used in those analyses. Section 3.3 addresses the coupled process models and abstractions used to evaluate parameter changes within the NF that might effect the results of the TH analyses.</p>

<b>IRSR: THERMAL EFFECTS ON FLOW</b>	
<b>SUBISSUE 1 - IS THE U.S. DEPARTMENT OF ENERGY TH TESTING PROGRAM, INCLUDING PERFORMANCE CONFIRMATION TESTING, SUFFICIENT TO EVALUATE THE POTENTIAL FOR THERMAL REFLUX TO OCCUR IN THE NEAR FIELD?</b>	
<b>Technical Acceptance Criterion 3</b>	
Coupling of processes has been evaluated using a methodology in accordance with NUREG-1466 (Nataraja and Brandshaug, 1992) or other acceptable methodology. Coupled processes may be uncoupled, if it is shown that the uncoupled model results bound the predictions of the fully-coupled model results.	<p>TH modeling is contained within this PMR scope (Sections 3.2, 3.3, 3.4, and 3.6) and two of its supporting AMRs, <i>Thermal Test AMR</i> and <i>THC Abstraction AMR</i> (CRWMS M&amp;O 2000a and 2000c). This subissue is also addressed in the UZ F&amp;T and EBS PMRs (CRWMS M&amp;O 2000f and 2000g). This PMR discusses the evaluation of coupled process effects on the conditions or parameters (e.g., porosity and permeability) that are input to the TH models.</p> <p>This acceptance criterion is also addressed by the EBS PMR (CRWMS M&amp;O 2000g). See Appendix A of the EBS PMR for additional discussion.</p>
<b>Technical Acceptance Criterion 4</b>	
The dimensionality of models, which include heterogeneity at appropriate scales and significant process couplings, may be reduced, if shown that the reduced dimension model bounds the predictions of the full dimension model.	<p>TH modeling is contained in this PMR scope (Sections 3.2, 3.3, 3.4, and 3.6) and two of its supporting AMRs, <i>Thermal Test AMR</i> and <i>THC Abstraction AMR</i> (CRWMS M&amp;O 2000a and 2000c). This subissue is also addressed in the UZ F&amp;T and EBS PMRs (CRWMS M&amp;O 2000f and 2000g). See Table 4.3-1 and Appendix A of the referenced PMRs for additional discussion.</p>
<b>Technical Acceptance Criterion 5</b>	
ECMs are acceptable for the rock matrix and small discrete features, if it can be demonstrated that water in small discrete features is in continuous hydraulic equilibrium with matrix water. Significant discrete features, such as fault zones, should be represented separately unless it can be shown that inclusion in the ECM produces a conservative effect on calculated overall performance.	<p>TH modeling is contained within this PMR scope (Sections 3.2, 3.3, 3.4, and 3.6) and two of its supporting AMRs, <i>Thermal Test AMR</i> and <i>THC Abstraction AMR</i> (CRWMS M&amp;O 2000a and 2000c). This subissue is also addressed in the UZ F&amp;T and EBS PMRs (CRWMS M&amp;O 2000f and 2000g). This PMR discusses issues dealing with THC effects on properties or with model confidence building. Chapter 3 addresses process models and abstractions. As described in that section, ECM models are not used in DS THC models. The only models used are DK models.</p> <p>This acceptance criterion is also addressed by the US F&amp;T and EBS PMRs (CRWMS M&amp;O 2000f and 2000g). See Table 4.3-1 and Appendix A of the referenced PMRs for additional discussion.</p>

<b>IRSR: THERMAL EFFECTS ON FLOW</b>	
<b>SUBISSUE 1 - IS THE U.S. DEPARTMENT OF ENERGY TH TESTING PROGRAM, INCLUDING PERFORMANCE CONFIRMATION TESTING, SUFFICIENT TO EVALUATE THE POTENTIAL FOR THERMAL REFLUX TO OCCUR IN THE NEAR FIELD?</b>	
<b>Technical Acceptance Criterion 7</b>	
Results of process-level models have been verified by demonstrated consistency with results/observations from field-scale, thermohydrologic test. In particular, sufficient physical evidence should exist to support the conceptual models used to predict thermally driven flow in the near field.	<p>Chapter 3 addresses process model confidence building or verification through comparisons with field tests. As described in that section, the DST THC model, constructed for the DST, is used to predict THC processes prior to and during the DST. Measured data from the DST are used to evaluate the conceptual and numerical models. Results from DST THC simulations were compared to measured gas-phase CO<sub>2</sub> concentrations, and the chemistry of waters collected from hydrology boreholes during the test. The results of these comparisons provide indication of consistency with results and observations from field-scale thermal tests.</p> <p>This acceptance criterion is also addressed by the UZ F&amp;T and EBS PMRs (CRWMS M&amp;O 2000f and 2000g). See Table 4.3-1 and Appendix A of the referenced PMRs for additional discussion.</p>

<b>IRSR: REPOSITORY DESIGN AND THERMO-MECHANICAL EFFECTS</b>	
<b>SUBISSUE 3: THERMAL-MECHANICAL EFFECTS ON UNDERGROUND FACILITY DESIGN AND PERFORMANCE</b>	
<b>Component 1: Thermal-Mechanical Effects on Design of the Underground Facility</b>	
<p>7 - The thermal-mechanical design and analyses make use of appropriate constitutive models that represent jointed rock mass behavior under prolonged heated conditions. These models are tested as appropriate (verified, validated, and calibrated) to the extent practicable before the submittal of the LA. (For those aspects of the models for which long-term experimental data are needed, continued verification and validation during performance confirmation are considered acceptable as long as detailed plans and procedures for such continued activities are found in the LA.)</p>	<p>All of the information needed to support the LA will be complete prior to the LA. Arguments presented in the LA will be based on testing and analyses conducted before LA and considered in the licensing review. Testing contained in the performance confirmation program is confirmatory. The performance confirmation program addresses thermal-mechanical effects on the rock mass during the pre-emplacment period. Additional longer-term measurements associated with rock mass monitoring are identified for selected emplacement drifts during the pre-closure period and are included in testing of the proposed simulation of the postclosure environment. See the Performance Confirmation Plan (CRWMS M&amp;O 2000z, Sections 5.3.1.5, 5.3.2, and Appendix G).</p>
<p>8 - Both drift- and repository-scale models of the underground facility are used in thermal-mechanical analyses to establish the intensity and distribution of ground movement (rock deformations, collapse, and other changes that may affect the integrity or geometrical configuration of openings within the underground facility). The number and variety of models permit the examination of conditions along drift-parallel and drift-normal directions.</p>	<p>This is addressed in the EBS PMR (CRWMS M&amp;O 2000g).</p>
<p>10 - Time sequences of thermal loading used in thermal-mechanical design and analyses are clearly defined.</p>	<p>This is reported in the EBS PMR (CRWMS M&amp;O 2000g). For purposes of THC and the THM calculation in this PMR, related to hydrology, the thermal loading and repository design inputs are provided in Sections 3.2, 3.3 and 3.5, 3.6. NFE and EBS TH calculations currently assume simultaneous emplacement of all waste, and run cases for various preclosure periods ranging from the first to last drift preclosure heat duration.</p>

<b>IRSR: REPOSITORY DESIGN AND THERMO-MECHANICAL EFFECTS</b>	
<b>SUBISSUE 3: THERMAL-MECHANICAL EFFECTS ON UNDERGROUND FACILITY DESIGN AND PERFORMANCE</b>	
<b>Component 3: Thermal-Mechanical Effects on Flow into Emplacement Drifts</b>	
1 - Approved quality assurance, control procedures, and standards, were applied to collection, development, and documentation of data, methods, models, and codes.	Activities associated with development of this PMR and its related AMRs were determined to be subject to the quality assurance program as described in the QARD (DOE 2000) document. As such, collection of related data, development of analyses and models, and use and validation of software is subject to the requirements of procedures developed to implement quality assurance program requirements. However, this subissue is primarily addressed in the EBS PMR (CRWMS M&O 2000g).
2 - If used, expert elicitation is conducted and documented in accordance with NUREG-1563 or other acceptable approaches.	This subissue is primarily addressed in the EBS PMR (CRWMS M&O 2000g). Expert elicitations were determined to be subject to the quality assurance program as described in the QARD (DOE 2000) document. Appendix C of the QARD and implementing procedures for expert elicitation were developed using the guidance provided in NUREG-1563 (Kotra et al. 1996).
4 - Changes in hydrological properties (e.g., fracture porosity and permeability) due to thermally induced ground movements are estimated taking into account the uncertainties in the context of their impacts on performance.	Section 3.5 describes the results of THM calculations performed to estimate bounds on changes in fracture porosity and permeability in rock surrounding emplacement drifts. Ongoing work is expected to reduce uncertainties in THM results.

<b>IRSR: TOTAL SYSTEM PERFORMANCE ASSESSMENT AND INTEGRATION</b>	
<b>SUBISSUE 1 – SYSTEM DESCRIPTION AND DEMONSTRATION OF MULTIPLE BARRIERS</b>	
<b>Transparency and Traceability of the Analysis</b>	
<b>TSPA Documentation Style, Structure, and Organization</b>	
Criterion T1 - Documents and reports are complete, clear, and consistent.	The NFE PMR was carefully structured to be complete, clear, and consistent. Reviews of the draft document included checks for completeness, clarity and consistency.
Criterion T2 - Information is amply cross-referenced.	The NFE PMR and supporting AMRs contain ample references to data sources, codes, assumptions, and conclusions.
<b>Features, Events, and Processes Identification and Screening</b>	
Criterion T1 - The screening process by which FEPs were included or excluded from the TSPA is fully described.	Section 2.5 of this PMR summarizes the FEPs process. Appendix C of this PMR presents the results for the NFE FEPs including excluded and included FEPs and the rationale for these decisions.
Criterion T2 - Relationships between relevant FEPs are fully described.	Section 2.5 of this PMR describes the relationship between primary and secondary FEPs. The NFE FEPs AMR (CRWMS M&O 2000e) provides additional documentation.
<b>Abstraction Methodology</b>	
Criterion T1 - The levels and method(s) of abstraction are described starting from assumptions defining the scope of the assessment down to assumptions concerning specific processes and the validity of given data.	For each model in the NFE PMR, descriptions are provided of process models and, if appropriate, model abstractions. The description includes a summary of data and assumptions used to construct models. The AMRs describing the models and the abstracted models provide additional details regarding data and assumptions.
Criterion T2 - A mapping (e.g., a road map diagram, a traceability matrix, a cross-reference matrix) is provided to show what conceptual features (e.g., patterns of volcanic events) and processes are represented in the abstracted models, and by what algorithms.	The NFE PMR and supporting AMRs provide descriptions of the basis for the decisions and assumptions that were made during the abstraction process.
Criterion T3 - An explicit discussion of uncertainty is provided to identify which issues and factors are of most concern or are key sources of disagreement among experts.	The NFE PMR provides a discussion of uncertainties and limitations for the major process models included in the report. The AMRs describing the abstracted models provide additional details regarding uncertainties and limitations.

<b>Data Use and Validity</b>	
Criterion T1 - The pedigree of data from laboratory tests, natural analogs, and the site is clearly identified.	Section 1.5 of this PMR describes the quality assurance requirements applied to the development of this PMR. Chapter 4 of the AMRs describing the models clearly identifies data and parameters used in the development of the AMRs and provides additional details regarding pedigree of data.
Criterion T2 - Input parameter development and basis for their selection is described.	The NFE PMR discusses input parameter development and the basis for using the parameters. Chapter 4 of the AMRs describing the models provide additional details regarding input parameter development and the basis for input selection.
Criterion T3 - A thorough description of the method used to identify performance confirmation program parameters [has been developed].	The Performance Confirmation Plan (CRWMS M&O 2000z) specifically addresses the methodology for identifying and selecting parameters that are important to performance based upon TSPA sensitivity analyses and the repository safety strategy. Methods used to collect information for each parameter will be described by the performance confirmation plan or relevant supporting documents to support the LA. Performance confirmation test selection and rationale is also described in the plan based upon the significance of the parameter being measured, and the ability of the test to distinguish construction, emplacement, or time dependent changes in the parameter significant to performance.
<b>Assessment Results</b>	
Criterion T1 - PA results (i.e., the peak expected annual dose within the compliance period) can be traced back to applicable analyses that identify the FEPs, assumptions, input parameters, and models in the PA.	The TSPA-SR summarizes features, processes, conceptual models, and their implementation into the TSPA. This discussion will be based in part on information provided by the NFE PMR.
Criterion T2 - The PA results include a presentation of intermediate results that provide insight into the assessment (e.g., results of intermediate calculations of the behavior of individual barriers)	TSPA-SR provides performance analysis results for the total system and will include intermediate results for the components of the system.
<b>Code Design and Data Flow</b>	
Criterion T1 - The flow of information (input and output) between the various modules is clearly described.	TSPA-SR provides a description of information flow between component models including couplings between information and data, conceptual and process-level models, and abstracted models.
Criterion T2 - Supporting documentation (e.g., user's manuals, design documents) clearly describes code structure and relationships between modules.	TSPA-SR describes the TSPA code and provides a reference to supporting documentation such as the user's guide.

<b>SUBISSUE 2 - SCENARIO ANALYSIS</b>	
<b>Identification of an Initial Set of Processes and Events</b>	
1 - DOE has identified a comprehensive list of processes and events that: (1) are present or might occur in the Yucca Mountain region and (2) includes those processes and events that have the potential to influence repository performance.	Section 2.5 describes the FEPs in this PMR. The <i>NFE FEPs AMR</i> (CRWMS M&O 2000e) supporting this section provides a list of the processes and events applicable to this PMR. The AMR provides a description of the screening arguments and dispositions for the FEPs and has been thoroughly reviewed by subject matter experts. In addition, the AMR describes development of the FEPs database, including a description of the FEPs process in sufficient detail to demonstrate the comprehensiveness of the database.
<b>Classification of Processes and Events</b>	
1 - DOE has provided adequate documentation identifying how its initial list of processes and events has been grouped into categories.	Section 2.5 of this PMR describes the FEPs in this PMR. The <i>NFE FEPs AMR</i> (CRWMS M&O 2000e) supporting this section provides documentation and justification for screening arguments and TSPA dispositions. Documentation is maintained of all mapping of FEPs into primary and secondary categories. For comprehensiveness, traceability is maintained from the secondary to the related primary FEPs. The AMR also describes development of the FEPs database, including identifying and classifying relevant FEPs.
2 - Categorization of processes and events is compatible with the use of categories during the screening of processes and events.	Section 2.5 describes the FEPs applicable to this PMR. The <i>NFE FEPs AMR</i> (CRWMS M&O 2000e) supporting this section provides documentation and justification for screening arguments and TSPA dispositions. Documentation is maintained of all mapping of FEPs into primary and secondary categories. The PMRs and AMRs describe the categorization of processes and events in sufficient detail to determine that events are not narrowly defined and that the categorization of processes and events is compatible with the use of categories during the screening of processes and events.
<b>Screening of Processes and Events</b>	
1 - Categories of processes and events that are not credible for the Yucca Mountain repository because of waste characteristics, repository design, or site characteristics are identified and sufficient justification is provided for DOE's conclusions.	Section 2.5 describes the FEPs in this PMR. The <i>NFE FEPs AMR</i> (CRWMS M&O 2000e) supporting this section provides documentation and justification for screening arguments and TSPA dispositions. Documentation includes a statement of the screening decision for each FEP. Justification is provided for each excluded FEP, including the criterion on which it was excluded and the technical basis for the screening argument.

<p>2 - The probability assigned to each category of processes and events not screened based on criterion T1 or criterion T2 is consistent with site information, well documented, and appropriately considers uncertainty.</p>	<p>Section 2.5 describes the FEPs in this PMR. The <i>NFE FEPs AMR (CRWMS M&amp;O 2000e)</i> supporting this section provides documentation and justification for screening arguments and TSPA dispositions. Probability estimates for FEPs are based on technical analysis of the past frequency of similar events consistent with site information, well documented, and which appropriately considered uncertainty.</p>
<p>3 - DOE has demonstrated that processes and events screened from the PA on the basis of their probability of occurrence, have a probability of less than one chance in 10,000 of occurring over 10,000 years.</p>	<p>Section 2.5 describes the FEPs in this PMR. The <i>NFE FEPs AMR (CRWMS M&amp;O 2000e)</i> supporting this section provides documentation and justification for screening arguments and TSPA dispositions. Justification is provided for each excluded FEP, including the criterion on which it was excluded and the technical basis for the screening argument. For excluded FEPs, documentation includes the criterion on which it was excluded and the technical basis for the screening argument. The probability assigned to FEPs may be one of the screening criteria. FEPs may be excluded from the TSPA only if they can be shown to have a probability of occurrence of less than one chance in 10,000 of occurring over 10,000 years (proposed 10 CFR 63.114) (64 FR 8460).</p>
<p>4 - DOE has demonstrated that categories of processes and events omitted from the PA on the basis that their omission would not significantly change the calculated expected annual dose, do not significantly change the calculated expected annual dose.</p>	<p>Section 2.5 describes the FEPs in this PMR. The <i>NFE FEPs AMR (CRWMS M&amp;O 2000e)</i> supporting this section provides documentation and justification for screening arguments and TSPA dispositions. For omitted categories, documentation includes the criterion on which it was excluded and the technical basis for the screening argument.</p>
<p><b>Formation of Scenarios</b></p>	
<p>1 - DOE has provided adequate documentation identifying: (1) whether processes and events have been addressed through consequence model abstraction or scenario analysis and (2) how the remaining categories of processes and events have been combined into scenario classes.</p>	<p>TSPA provides documentation and justification for screening arguments and TSPA dispositions. FEPs that have not been excluded are identified as either expected FEPs or disruptive FEPs. Expected FEPs will be included in the TSPA nominal scenario, which is simulated by the base case model described in the TSPA documentation. Disruptive scenarios are constructed from expected FEPs and combinations of disruptive FEPs. Section 2.5 describes the FEPs addressed in this PMR. The PMRs provide descriptions of process-level models, model abstractions, and supporting analyses in sufficient detail to conclude that processes and events have been addressed through consequence model abstraction or scenario analysis and that the remaining categories of processes and events have been combined into scenario classes.</p>

2 - The set of scenario classes is mutually exclusive and complete.	TSPA provides documentation and justification for screening arguments and TSPA dispositions. In addition, TSPA describes development of the FEPs database, including a description of the construction and screening of scenarios. Taken together, the entire set of PMRs and TSPA will provide NRC staff with sufficient documentation to evaluate whether the set of scenario classes is mutually exclusive and complete, and whether expected FEPs are addressed either through model abstraction or through incorporation into scenarios.
<b>Screening of Scenario Classes</b>	
1 - Scenario classes that are not credible for the Yucca Mountain repository because of waste characteristics, repository design, or site characteristics, individually or in combination, are identified and sufficient justification is provided for DOE's conclusions.	TSPA provides justification for screening arguments and TSPA dispositions. Scenarios are screened using the same regulatory, probability, and consequence criteria used for screening individual FEPs. Documentation of this process includes identification of any scenarios that have been screened from the analysis and the technical basis for that screening decision.
2 - The probability assigned to each scenario class is consistent with site information, well documented, and appropriately considers uncertainty.	TSPA provides justification for screening arguments and TSPA dispositions. Probability estimates for scenario classes are based on analyses similar to probabilities assigned for individual FEPs.
3 - Scenario classes that combine categories of processes and events may be screened from the PA on the basis of their probability of occurrence, provided: (i) the probability used for screening the scenario class is defined from combinations of initiating processes and events and (ii) DOE has demonstrated that they have a probability of less than one chance in 10,000 of occurring over 10,000 years.	TSPA provides justification for excluding scenario classes. The probability assigned to scenario classes is one of the screening criteria. Scenario classes may be excluded from the TSPA only if they can be shown to have a probability of occurrence of less than one chance in 10,000 of occurring over 10,000 years (64 FR 67054). Justification is provided for each excluded scenario class, including the criterion on which it was excluded and the technical basis for the screening argument. In addition, the <i>NFE FEPs AMR (CRWMS M&amp;O 2000e)</i> describes the development of the FEPs database, including a description of screening and specifying scenarios for TSPA analysis.
4 - Scenario classes may be omitted from the performance assessment on the basis that their omission would not significantly change the calculated expected annual dose, provided DOE has demonstrated that excluded categories of processes and events would not significantly change the calculated expected annual dose.	TSPA provides justification for excluding scenario classes. For excluded scenario classes, documentation includes the criterion on which it was excluded and the technical basis for the screening argument. In addition, the <i>NFE FEPs AMR (CRWMS M&amp;O 2000e)</i> describes the development of the FEPs database, including a description of screening and specifying scenarios for TSPA analysis.